frontiers | Research Topics

The discovery of bioactive natural products: The isolation and structural elucidation, genome mining, OSMAC strategy, and biotransformation

Edited by
Ling Liu, Dewu Zhang, Fushuang Li and Kalindi Morgan

Published in
Frontiers in Microbiology

ISSN 1664-8714
ISBN 978-2-8325-3275-1
DOI 10.3389/978-2-8325-3275-1

About Frontiers

Frontiers is more than just an open access publisher of scholarly articles: it is a pioneering approach to the world of academia, radically improving the way scholarly research is managed. The grand vision of Frontiers is a world where all people have an equal opportunity to seek, share and generate knowledge. Frontiers provides immediate and permanent online open access to all its publications, but this alone is not enough to realize our grand goals.

Frontiers journal series

The Frontiers journal series is a multi-tier and interdisciplinary set of open-access, online journals, promising a paradigm shift from the current review, selection and dissemination processes in academic publishing. All Frontiers journals are driven by researchers for researchers; therefore, they constitute a service to the scholarly community. At the same time, the *Frontiers journal series* operates on a revolutionary invention, the tiered publishing system, initially addressing specific communities of scholars, and gradually climbing up to broader public understanding, thus serving the interests of the lay society, too.

Dedication to quality

Each Frontiers article is a landmark of the highest quality, thanks to genuinely collaborative interactions between authors and review editors, who include some of the world's best academicians. Research must be certified by peers before entering a stream of knowledge that may eventually reach the public - and shape society; therefore, Frontiers only applies the most rigorous and unbiased reviews. Frontiers revolutionizes research publishing by freely delivering the most outstanding research, evaluated with no bias from both the academic and social point of view. By applying the most advanced information technologies, Frontiers is catapulting scholarly publishing into a new generation.

What are Frontiers Research Topics?

Frontiers Research Topics are very popular trademarks of the *Frontiers journals series*: they are collections of at least ten articles, all centered on a particular subject. With their unique mix of varied contributions from Original Research to Review Articles, Frontiers Research Topics unify the most influential researchers, the latest key findings and historical advances in a hot research area.

Find out more on how to host your own Frontiers Research Topic or contribute to one as an author by contacting the Frontiers editorial office: frontiersin.org/about/contact

The discovery of bioactive natural products: The isolation and structural elucidation, genome mining, OSMAC strategy, and biotransformation

Topic editors

Ling Liu — Institute of Microbiology, Chinese Academy of Sciences (CAS), China

Dewu Zhang — Institute of Medicinal Biotechnology, Chinese Academy of Medical Sciences, China

Fushuang Li — Whitehead Institute for Biomedical Research, Massachusetts Institute of Technology, United States

Kalindi Morgan — University of Northern British Columbia Canada, Canada

Citation

Liu, L., Zhang, D., Li, F., Morgan, K., eds. (2023). *The discovery of bioactive natural products: The isolation and structural elucidation, genome mining, OSMAC strategy, and biotransformation*. Lausanne: Frontiers Media SA.

doi: 10.3389/978-2-8325-3275-1

Table of contents

frontiers | Frontiers in Microbiology

TYPE Editorial
PUBLISHED 03 August 2023
DOI 10.3389/fmicb.2023.1253850

OPEN ACCESS

EDITED AND REVIEWED BY
Biswarup Mukhopadhyay,
Virginia Tech, United States

*CORRESPONDENCE
Dewu Zhang
✉ zhangdewuever@163.com
Kalindi Morgan
✉ kalindi.morgan@unbc.ca
Ling Liu
✉ liul@im.ac.cn

RECEIVED 06 July 2023
ACCEPTED 27 July 2023
PUBLISHED 03 August 2023

CITATION
Zhang D, Morgan K and Liu L (2023) Editorial: The discovery of bioactive natural products: the isolation and structural elucidation, genome mining, OSMAC strategy, and biotransformation.
Front. Microbiol. 14:1253850.
doi: 10.3389/fmicb.2023.1253850

Editorial: The discovery of bioactive natural products: the isolation and structural elucidation, genome mining, OSMAC strategy, and biotransformation

Dewu Zhang[1]*, Kalindi Morgan[2]* and Ling Liu[3]*

[1]Institute of Medicinal Biotechnology, Chinese Academy of Medical Sciences and Peking Union Medical College, Beijing, China, [2]Department of Chemistry and Biochemistry, University of Northern British Columbia, Prince George, BC, Canada, [3]Institute of Microbiology, Chinese Academy of Sciences, Beijing, China

KEYWORDS

natural products, structure elucidation, genome mining, OSMAC strategy, bioactivity

Editorial on the Research Topic
The discovery of bioactive natural products: the isolation and structural elucidation, genome mining, OSMAC strategy, and biotransformation

Natural products play a highly significant role in the drug discovery and development process, which are massively important in medical and clinical applications. From 1981 to 2020, a total of 1,394 small molecule drugs have been approved, among them 441 (32%) were direct or derived from natural products (Newman and Cragg, 2020). Microorganisms have provided abundant sources of natural products which have been developed as commercial products for human medicine, animal health, and plant crop protection. Back in 1928, Alexander Fleming discovered penicillin from fungus *Peniciliium notatum*, which began the microbial drug era (Tan and Tatsumura, 2015). Subsequently, an increasing number of microbial drugs have been discovered, such as lovastatin, vancomycin, erythromycin, polymyxin, abamectin, and etc. Nowadays, microbial drugs have become an indispensable part of protecting human health. However, ever-increasing risks of human, animal, and plant disease and growing drug resistance require more bioactive natural products to be discovered, in order to produce relevant therapeutic drugs.

In fact, traditional isolation and structure elucidation of natural products from microorganisms are still an important approach to discover drug leading compounds, which led to the discovery of a huge amount of bioactive natural products. Recently, with the rapid development of tools for whole genome sequencing and bioinformatics analyses, it further broadens our horizons for the discovery of new bioactive compounds (Hautbergue et al., 2018).

The overall goal of this Research Topic is to propose classical and advanced strategies for the discovery of bioactive natural products, including genome-mining, one strain many compounds (OSMAC) strategy, and etc. A total of thirteen papers by 121 authors were published to represent the latest research progress in their field, which helps the field in its' understanding of these most intriguing topics.

Liu et al. reported the discovery of novel antidiabetic compounds from the fungus *Penicillium* sp. HFF16. The researchers expanded the prenylated indole-terpenoids encindolene family with the elucidation of encindolenes I–L. The isolated compounds showed inhibitory effects on glucagon-induced hepatic glucose output and decreased intracellular cAMP levels in primary hepatocytes. These findings were significant for the development of new drugs against diabetes as they provided potential candidates for suppressing the hepatic glucagon response. Song et al. isolated the twenty secondary metabolites including seven new compounds from endophytic fungus *Fusarium decemcellulare* F25. Some of them exhibited antifungal activities against plant pathogen *Colletotrichum musae* ACCC 31244. Schneider et al. investigated the structures and biological activities of suomilides, a class of highly modified non-ribosomal peptides produced by cyanobacteria *Nostoc* sp. KVJ20. The researchers isolated and determined the chemical structures of four new suomilides, studied secondary metabolite expression patterns under various growth conditions, and proposed a biosynthetic gene cluster for the production of the suomilides. The study contributed to the understanding of the biosynthesis of suomilides and expanded the knowledge of cyanobacterial secondary metabolites. Wu et al. presented the isolations and structure elucidations of five new dimeric tetrahydroxanthone derivatives and four known dimeric tetrahydroxanthone analogs from the marine-derived fungus *Aspergillus aculeatinus* WHUF0198, and some of them displayed cytotoxic and antibacterial activities.

Yu et al. reported the discovery and biosynthesis of macrophasetins from the plant pathogen fungus *Macrophomina phaseolina*. The authors mined a PKS-NRPS and LLDAse encoding gene cluster from fungus *M. phaseolina* using bioinformatics analysis prediction and heterologous expression, and characterized the cluster to be responsible for the biosynthesis of novel 3-decalinoyltetramic acids (DTAs), macrophasetins. The DTA biosynthesis pathway were also investigated, and the results further validated the accuracy of the bioinformatics prediction. The findings set a good example to mine novel natural products from fungi by the combination of bioinformatics prediction and heterologous expression. Wang Z.-J. et al. exploited an efficient heterologous system based on streamlined *Burkholderia thailandensis* E264. The disorazol and rhizoxin biosynthetic gene clusters were expressed successfully with this host, and the yield of the heterologous product, disorazol F_2, was improved 96-fold by promoter substitution and insertion. This heterologous expression system provided another choice for the exploration of natural products from different phylogenetic taxa.

Qu et al. investigated the bioactivities and metabolomics of *Cordyceps gunnii* under different culture conditions. Five different solid media were used to culture the *C. gunnii* mycelium, and the extracts were assayed for various biological activities and analyzed using untargeted metabolomics. The results showed significant differences in activities and metabolites among the extracts from different culture conditions. This study provided a basis for further OSMAC applications to macrofungal species, contributing to the field of macrofungal secondary metabolite research. Wang Y. et al. reported the metabolomic profiles of the fermentation in co-culture of *Eurotium amstelodami* and *Bacillus licheniformis*. The results revealed that the co-culture combination of *E. amstelodami* and *Bacillus* species could significantly improve antibacterial activity against *Staphylococcus aureus*. Metabolomics data further indicated that abundant and various secondary metabolites were significantly enhanced in co-culture. This is the first metabolomics-based report of metabolite profiles of *E. amstelodami*. This study provided novel insights into the selection of good co-culture combinations, as well as activation of silent microbial secondary metabolite biosynthetic gene clusters. Lu et al. found a marine fungus *Penicillium mallochii* ACD-5 from sea cucumber with high potential in alkaloids production by *in situ* colony assay, TLC chemical colorization, and LC-MS/MS based metabolomics profiling. Using comprehensive metabolic annotation strategy, three chlorinated azaphilone alkaloids were obtained from *P. mallochii* ACD-5, and one of them showed remarkable anti-neuroinflammatory activity in liposaccharide induced BV-2 cells.

Duan et al. investigated the genome, transcriptome, and metabolome analysis of edible fungus *Dictyophora indusiata* (DI). Authors firstly created DI reference genome and identified 19,909 coding genes. Subsequent transcriptome and metabolome analyses of the five tissues of the DI fruiting bodies and mycelium indicated the mechanism underlying DI fruiting body differentiation, and also identified 728 metabolites. Meanwhile, the authors confirmed the significance of tryptophan metabolism and metabolite synthesis related genes in regulating fruiting body formation. This study expanded the understanding of resource development and application for DI.

Zhang et al. studied the molecular mechanism GylR-mediated regulation of glycerol metabolism in *Streptomyces clavuligerus* NRRL 3585. Authors identified the effector molecules and binding sequences of GylR, and further identified a minimal essential operator site (a core 18-bp sequence motif) of GylR-like regulators. The findings provided new basic elements for the development and application of glycerol-inducible regulatory tools for microbial metabolic engineering and synthetic biology research.

Morgan reviewed the use of nitrogen-15 in bacterial and fungal natural product discovery and biosynthetic characterization. Nitrogen-15 is an important element in various bioactive and structurally intriguing natural products, including alkaloids, non-ribosomal peptides, and hybrid natural products. The article highlighted the detection of nitrogen-15 at natural abundance using nuclear magnetic resonance and mass spectrometry techniques. It also explored the use of nitrogen-15 stable isotope feeding for biosynthetic characterization. The article provided insights into the role of nitrogen-15 in natural product discovery and characterization. Ren et al. reviewed the discovery and excavation of lichen bioactive natural products. The authors summarized the lichen-derived bioactive metabolites and highlighted the application of OSMAC, molecular network, and genome mining-based strategies in lichen-forming fungi, which offer great help to discover numerous novel secondary metabolites with various biological activities.

Overall, the works presented in this Research Topic provide an overview of some of traditional and latest strategies for the discovery of bioactive natural products. In order to cope with the growing risk of disease, it is necessary to further explore bioactive components with multiple pharmacological activities. However,

the research and development of most of natural products is only in preliminary *in vitro* experimental stage. So, the more in-depth pharmacological experiments for natural products need to be carried out for natural product research. We sincerely hope that this Research Topic can increase awareness and serve as forward-looking guide in the field of microbial natural products.

Author contributions

DZ: Writing—original draft, Writing—review and editing, Funding acquisition. KM: Writing—original draft, Writing—review and editing. LL: Funding acquisition, Writing—original draft, Writing—review and editing.

Funding

DZ acknowledges support from the National Natural Science Foundation of China (82073744) and CAMS Innovation Fund for Medical Sciences (2021-I2M-1-055). LL acknowledges support from the National Natural Science Foundation of China (32022002 and 21977113).

Acknowledgments

Great thanks to all the contributing authors, reviewers, and the Frontiers in Microbiology development team, whose efforts lead to the success of this Research Topic.

Conflict of interest

The authors declare that the research was conducted in the absence of any commercial or financial relationships that could be construed as a potential conflict of interest.

Publisher's note

References

Hautbergue, T., Jamin, E. L., Debrauwer, L., Puel, O., and Oswald, I. P. (2018). From genomics to metabolomics, moving toward an integrated strategy for the discovery of fungal secondary metabolites. *Nat. Prod. Rep.* 35, 147–173. doi: 10.1039/C7NP00032D

Newman, D. J., and Cragg, G. M. (2020). Natural products as sources of new drugs over the nearly four decades from 01/1981 to 09/2019. *J. Nat. Prod.* 83, 770–803. doi: 10.1021/acs.jnatprod.9b01285

Tan, S. Y., and Tatsumura, Y. (2015). Alexander Fleming (1881–1955): discoverer of penicillin. *Singapore Med. J.* 56, 366–367. doi: 10.11622/smedj.2015105

frontiers | Frontiers in Microbiology

TYPE Original Research
PUBLISHED 14 November 2022
DOI 10.3389/fmicb.2022.1056392

OPEN ACCESS

EDITED BY
Ling Liu,
Institute of Microbiology (CAS), China

REVIEWED BY
Yiguang Zhu,
Chinese Academy of Sciences (CAS), China
Dewu Zhang,
Chinese Academy of Medical Sciences, China

*CORRESPONDENCE
Huai Dong Zhang
zhanghuaidong@fjnu.edu.cn
Man Cheng Tang
tmc19@163.com
Li Li
lili@fjnu.edu.cn

†These authors have contributed equally to this work

SPECIALTY SECTION
This article was submitted to Microbial Physiology and Metabolism, a section of the journal Frontiers in Microbiology

RECEIVED 28 September 2022
ACCEPTED 17 October 2022
PUBLISHED 14 November 2022

CITATION
Yu C, Chen L, Gao YL, Liu J, Li PL, Zhang ML, Li Q, Zhang HD, Tang MC and Li L (2022) Discovery and biosynthesis of macrophasetins from the plant pathogen fungus *Macrophomina phaseolina*. *Front. Microbiol.* 13:1056392. doi: 10.3389/fmicb.2022.1056392

Discovery and biosynthesis of macrophasetins from the plant pathogen fungus *Macrophomina phaseolina*

Cui Yu[1†], Lin Chen[2,3†], Yang Le Gao[1], Jia Liu[1], Pei Lin Li[1], Ming Liang Zhang[1], Qin Li[1], Huai Dong Zhang[1*], Man Cheng Tang[2,3*] and Li Li[1*]

[1]Engineering Research Center of Industrial Microbiology (Ministry of Education) and College of Life Sciences, Fujian Normal University, Fuzhou, China, [2]State Key Laboratory of Microbial Metabolism, Joint International Research Laboratory of Metabolic and Developmental Sciences, School of Life Sciences and Biotechnology, Shanghai Jiao Tong University, Shanghai, China, [3]Zhangjiang Institute for Advanced Study, Shanghai Jiao Tong University, Shanghai, China

3-Decalinoyltetramic acids (DTAs) are a class of natural products with chemical diversity and potent bioactivities. In fungal species there is a general biosynthetic route to synthesize this type of compounds, which usually features a polyketide synthase-nonribosomal peptide synthetase (PKS-NRPS) and a lipocalin-like Diels-Alderase (LLDAse). Using a synthetic biology approach, combining the bioinformatics analysis prediction and heterologous expression, we mined a PKS-NRPS and LLDAse encoding gene cluster from the plant pathogenic fungus *Macrophomina phaseolina* and characterized the cluster to be responsible for the biosynthesis of novel DTAs, macrophasetins. In addition, we investigated the biosynthesis of these compounds and validated the accuracy of the phylogeny-guided bioinformatics analysis prediction. Our results provided a proof of concept example to this approach, which may facilitate the discovery of novel DTAs from the fungal kingdom.

KEYWORDS

3-Decalinoyltetramic acid, bioinformatics analysis, *Macrophomina phaseolina*, heterologous expression, genome mining

Introduction

3-Decalinoyltetramic acids (DTAs) are a class of natural products isolated from various organisms, which feature a tetramate (pyrrolidine-2,4-dione) unit connected to a decalin fragment with multiple chiral centers (Figure 1A; Schobert and Schlenk, 2008; Jiang et al., 2020). Due to their structural complexity and potent bioactivity, this group of compounds has been attracting a great deal of attention for their chemical synthesis and biosynthesis (Yin et al., 2013; Kauhl et al., 2016; Li et al., 2017; Kato et al., 2018; Kauhl et al., 2018; Fan et al., 2019; Tan et al., 2019; Chi et al., 2021). Recent biosynthetic studies have revealed that there is a general route to biosynthesize this type of compounds in fungi (Mo and Gulder, 2021). The carbon backbone is derived from a bimodular megasynthase, known as

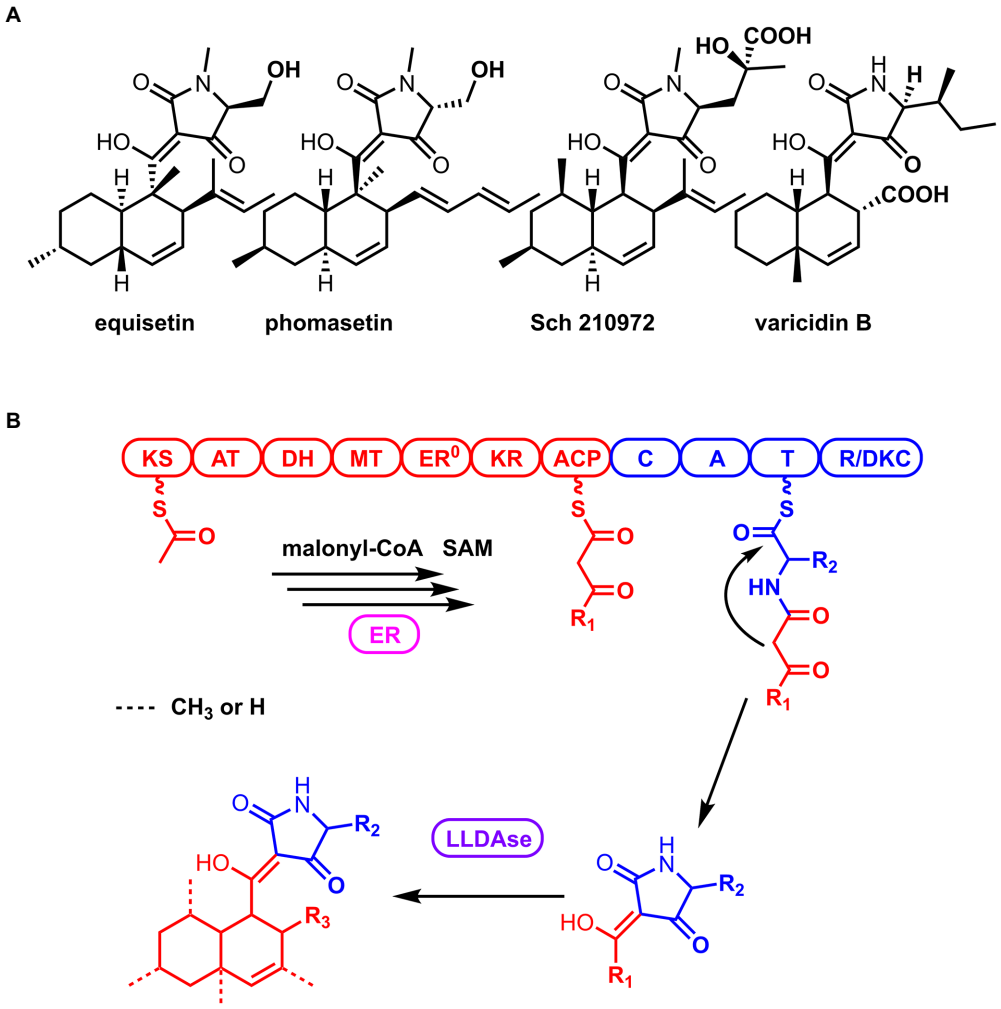

FIGURE 1
Structures of the representative 3-Decalinoyltetramic acids (DTAs; **A**) and the general biosynthetic route of DTAs in fungi **(B)**.

polyketide synthase (PKS)-nonribosomal peptide synthetase (NRPS), assembly line (Figure 1B). The PKS module is typically a highly reducing PKS that iteratively synthesize the polyketide portion. And its dissociated enoylreductase (ER) partner catalyzes the selective enoylreduction during different cycles to furnish the diene and dienophile that is ready for the decalin construction. The NRPS module selectively activates a specific amino acid (AA) and catalyzes the condensation of this activated amino acid and the mature polyketide to form an amide bond. Then the product of the assembly line is released by the C-terminal reductase/Dieckmann cyclase (R/DKC) domain, through Dieckmann cyclization to generate the tetramic acid. The decalin moiety is constructed off the assembly line through intramolecular Diels-Alder (IMDA) reaction that catalyzed by a lipocalin-like Diels-Alderase (LLDAse) in a regioselective and stereoselective manner. Other tailoring modifications, such as methylation and hydroxylation, further diverse the chemical structures. Recent genome sequencing efforts have identified that fungi encodes a significant number of biosynthetic gene clusters (BGCs) containing PKS-NRPS and LLDAse encoding genes. However, many of them have not been exploited or characterized to target DTAs.

Macrophomina phaseolina is known as a plant pathogenic fungus, which is capable of causing disease in more than 500 different plants including economically important crops (Kaur et al., 2012; Ijaz et al., 2013; Degani et al., 2020). This fungal species mainly causes severe charcoal rot, which is thought to be the second crucial soybean disease in the United States (Luna et al., 2017). Recent studies revealed that this fungal species is also a potential rich resource for structurally diverse bioactive metabolites, evidenced by the fact that there are more than 40 genes encoding PKSs, NRPSs, and their hybrids in its genome (Islam et al., 2012). Novel compounds have been reported from *M. phaseolina* in the past few years, exemplified by the dipeptide serine-glycine-betaine (Singh et al., 2021), the macrolide phaseolide A (Morishita et al., 2020), and the phytotoxic cyclopentenones phaseocyclopentenones (Masi et al., 2021). Recently, we also reported the discovery of novel polyketide-amino acid hybrid compounds from *M. phaseolina*

through genome mining (Gao et al., 2021). However, to date, no compounds belonging to the DTA family has been reported from this species.

To facilitate the discovery of novel bioactive secondary metabolites from fungal species, a set of new methods have been developed in recent years, including heterologous expression and transcription factor activation (Bauman et al., 2021). Most of these methods are focusing on the rapid discovery of novel natural products from diverse fungal species without accurate structural prediction, which means some of the natural products produced are known ones. Recently, Oikawa group reported the phylogeny-based bioinformatics analysis of fungal PKS-NRPS containing BGCs and linked a given BGC to a particular family of natural products (Minami et al., 2020). Inspired by their work, we reasoned that a synthetic biology approach combining bioinformatics prediction and heterologous expression is a promising way to mine novel DTAs from fungal species with improved accuracy. Here, we reported the discovery and biosynthesis of novel DTAs, macrophasetins, from *M. phaseolina* as a proof of concept to this approach.

Materials and methods

Strains, plasmids, and cultivation conditions

Macrophomina phaseolina MS6 was cultivated in PDA (potato dextrose agar, BD) or PDB (potato dextrose broth, BD) at 28°C (Gao et al., 2021). *Escherichia coli* DH5α were grown in Luria-Bertani media at 37°C for the standard DNA manipulation. *Saccharomyces cerevisiae* BJ5464-NpgA (*MATα ura3-52 his3-Δ200 leu2-Δ1 trp1 pep4::HIS3 prb1 Δ1.6R can1 GAL*) was used for expression plasmids construction (Wang et al., 2020). *Aspergillus nidulans* A1145 was cultured at 30°C in CD media (1% glucose, 5% 20× nitrate salts, 0.1% trace elements, and 2% agar for solid media) and used as the host of heterologous expression (Li et al., 2018). Plasmids pYTU, pYTP, and pYTR were used as heterologous expression vectors (Li et al., 2016).

Bioinformatics analysis

Phylogenetic analysis was conducted using maximum likelihood method with MEGA 6 (Tamura et al., 2013). The Phyre2 web portal was used for protein modeling, prediction and analysis (Kelly et al., 2015). The three-dimensional structures of MpsD based on the template CghA (PDB ID: 6KAW) was selected. The protein was 3-D protonated and energy minimized using default parameters of MOE 2014 (Molecular Operating Environment, version 2014.0901). The MMFF94 (Wahl et al., 2019) force field was applied to minimize the initial structures to yield the lowest energy 3D conformation. The binding site was determined based on the PLB (Propensity for Ligand Binding) score in the Site Finder module. Besides, the structure of **2** was constructed by ChemDraw software and then optimized with MOE. MOE-docking was employed to investigate the binding modes of MpsD and compound **2**. The best poses were kept for binding mode analysis.

Heterologous expression of *mps* in *Aspergillus nidulans*

Vectors of pYTU, pYTP, and pYTR were digested with *Pac*I and *Swa*I (New England Biolabs) for the expression plasmids construction. The genes in the *mps* cluster were amplified by PCR with Q5 High-Fidelity DNA polymerases (New England Biolabs) and cloned into vectors by recombination in yeast. The *mps* genes were amplified using PCR with the genomic DNA of *M. phaseolina* as the template. The *mpsA* was obtained in three pieces using primers UmpsAF1/R1, UmpsAF2/R2 and UmpsAF3/R3; the amyB promoter was amplified from pYTP with primers of AmyB-pYTU-F/R; *mpsG* was obtained by PCR with primers of UmpsGF/R. The five DNA fragments and pYTU digested with *Pac*I and *Swa*I were co-transformed into *S. cerevisiae* BJ5464-NpgA for assembly, leading to plasmid pYL081. The *mpsD* and *mpsF* were also amplified using the primers of PmpsDF/R and RmpsFF/R, respectively, and cloned into pYTP and pYTR by yeast homologous recombination, leading to pYL082 and pYL083. Yeast transformation was performed using Frozen-EZ Yeast Transformation II Kit (Zymo Research). The primers used for the heterologous expression are listed in Supplementary Table S1. The maps of pYL081, 082 and 083 were shown in Supplementary Figure S1.

The DNA transformation of *A. nidulans* A1145 was carried out as described by Li et al. (2016). The liquid CD-ST media (1 L: 20 g Starch, 20 g Peptone, 50 ml 20× Nitrate salts, 1 ml Trace elements, pH 6.5) was used for the production of secondary metabolites in heterologous expression.

Characterization of compounds produced by heterologous expression

A. nidulans harboring *mps* genes were grown in CD-ST for 5 days and then extracted with ethyl acetate twice. The organic phase was dried by speed Vacuum and dissolved in methanol for analysis. LC–MS analyses were performed on Thermo Scientific U3000/LCQ Fleet with Phenomenex Luna C18 column (3 μm, 2.0 × 150 mm). LC analyses were achieved with a linear gradient of 5–95% CH_3CN-H_2O in 30 min followed by 95% CH_3CN for 5 min with a flow rate of 0.25 ml/min. For isolation of compounds, ethyl acetate extract from 10 L culture was evaporated by Buchi Rotavapor and the crude extracts were injected to Combi-Flash system (Teledyne Isco) with a reversed-phase C18 column for initial separation. Fractions containing the target compounds were used for further purification by HPLC with a C18 column of Phenomenex Luna (5 μm, 10 × 250 mm). 1D and 2D NMR spectra

were obtained on Bruker AVANCE III HD 600 MHz NMR spectrometer to elucidate the chemical structures of compounds.

X-ray single-crystal diffraction for 3

X-ray single-crystal diffraction was performed on an Oxford Gemini S Ultra single-crystal diffractometer. A suitable crystal was selected and subjected to λ(MoKα) = 0.71073 Å at 273.15 K. The structure was determined using the direct method with Olex2 and refined with full-matrix least-squares calculations on F2 using Olex2.

Results and discussion

Bioinformatics analysis and product prediction of the *mps* cluster

Using the PKS-NRPS Fsa1 and LLDAse Fsa2 as the search query (Kato et al., 2015), we identified a compact BGC, *mps* cluster, from the genome of *M. phaseolina* (Figure 2A). The *mps* cluster encodes a PKS-NRPS (*mpsA*, MPH_07623), a putative LLDAse (*mpsD*, MPH_07627), a cytochrome P450 (*mpsF*, MPH_07629), a trans-acting ER (*mpsG*, MPH_07630), and two putative transcription factors (*mpsB*, MPH_07625 and *mpsE*, MPH_07628) together with a putative transporter (*mpsC*, MPH_07626). To explore the unknown natural product encoded by the *mps* gene cluster, we first did the bioinformatics analysis of the biosynthetic genes to predict the potential structure to assess whether it's a novel DTA.

We first analyzed the PKS-NRPS MpsA to predict the linear backbone of the final product. This enzyme contains 10 domains, which are, from the *N*-terminal to the *C*-terminal, ketosynthase (KS), acyltransferase, dehydratase, methyltransferase (MT), ketoreductase, acyl carrier protein, condensation, adenylation (A), peptide carrier protein, and R/DKC domains. For the polyketide portion, since the KS domain iteratively functions in each polyketide chain elongation step, we hypothesized that the closer the phylogenetic relationship of the KS domain the closer the structure of the polyketide chain produced by the PKS portion. Therefore, we constructed a phylogenetic tree of the KS domains identified from the reported fungal PKS-NRPS proteins by using the KS domain of CazM (Winter et al., 2015), a non-reducing PKS, as a root. As shown in Figure 2B, the structures of the polyketide products produced by different fungal PKS-NRPSs indeed showed correlation to the phylogenetic relationship of the KS domains. As the KS domain of MpsA is phylogenetically close to the KS domain of CghG (Sato et al., 2015), a PKS-NRPS from the Sch 210972 biosynthetic pathway, we proposed that the structure of the polyketide chain produced by MpsA is an octaketide with four olefinic bonds, similar to the polyketide chain produced by CghG. Furthermore, the MT domain of MpsA is also phylogenetically close to the MT domain of CghG (Figure 2B). Therefore, we proposed that the polyketide chain produced by MpsA would contain the similar methylation pattern as in Sch 210972.

Next, we analyzed the A domain of the NRPS portion, which is responsible for the AA activation and loading. Because the substrate specificity of A domains is dedicated by the AA residues surrounding the active site pocket (known as 10 AA code; Stachelhaus et al., 1999; Challis et al., 2000), we then did the sequence alignment of MpsA A domain with other fungal PKS-NRPS A domains, and identified the 10 AA code of MpsA A domain (Supplementary Table S6). However, compared to the known 10 AA code of other fungal NRPS A domains, the specific AA substrate of MpsA A domain could not be concluded. Therefore, to predict the AA substrate, a homology model of MpsA A domain was constructed using the structure of PheA (Conti et al., 1997; PDB ID: 1AMU) as a guide. When docking different AAs into the active site pocket we found that L-alanine is the probable substrate of MpsA A domain (Figure 2B).

Then, the bioinformatics analysis of the terminal R/DKC domain of MpsA was carried out, which is responsible for the product release from PKS-NRPS assembly line. Phylogenetic analysis revealed that the R/DKC domains from fungal PKS-NRPSs were separated into two groups (Figure 2B). The R/DKC domains catalyzing the Dieckmann cyclization to release the product as a tetramic acid fall into one group. And the R/DKC domains catalyzing the reduction release then followed by Knoevenagel condensation to yield a pyrrolinone product falling into the other group. The MpsA R domain phylogenetically falls into the group of R/DKC domains catalyzing the formation of a tetramic acid. Therefore, combined the analysis results of different domains of MpsA, we proposed that the linear product of MpsA could be the tetramic acid **1** (Figure 2D).

Last, we analyzed the enzymes involved in the post modification steps off the PKS-NRPS assembly line. Phylogenetic analysis of the reported LLDAses identified from different fungal species showed that they also clade into two groups. Group 1 LLDAses catalyze the IMDA reaction on tetramic acid substrates. Group 2 LLDAses catalyze the IMDA reaction on pyrrolinone substrates. The putative LLDAse MpsD clades in the group 1 LLDAses, suggesting it acts on a tetramic acid substrate which is consistent with the product prediction of MpsA. To further predict the product of MpsD, a homology model of MpsD was constructed using the structure of CghA (Sato et al., 2021; PDB ID: 6KAW) as a guide (Figure 2C). Docking studies with different IMDA reaction products of **1** were carried out. The results showed that the best matching product is **2** (structure shown in Figure 2D), which is the endo IMDA reaction product of **1** and contains a *trans* decalin ring. However, due to the diverse functions of P450s and limited structural information of fungal P450s, the function of P450 MpsF could not be precisely predicted. Since MpsF is phylogenetically close to PoxM (Sato et al., 2017; Supplementary Figure S21), a P450 from the oxaleimide biosynthetic pathway, we proposed that MpsF might catalyze the hydroxylation on **2**.

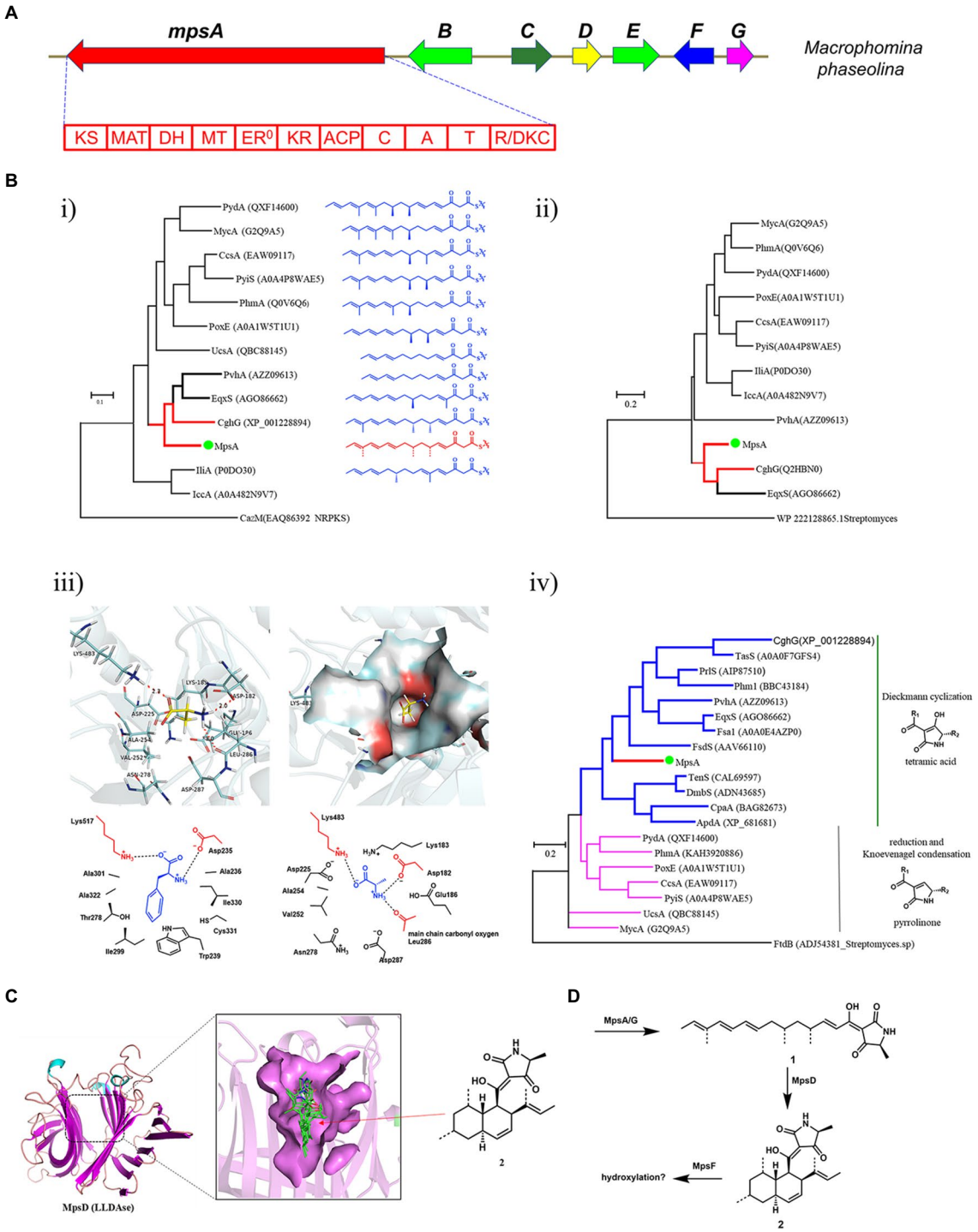

FIGURE 2
Bioinformatics analysis of the *mps* cluster. **(A)** The *mps* cluster identified from *M. phaseolina*. *mpsA* encodes PKS-NRPS, *mpsB* encodes transcription factor, *mpsC* encodes transporter, *mpsD* encodes LLDAse, *mpsE* encodes transcription factor, *mpsF* encodes cytochrome P450, *mpsG* encodes trans-acting ER. **(B)** Bioinformatics analysis of the domains identified from MpsA. (i) The phylogenetic tree of KS domains; (ii) The phylogenetic tree of MT domains; (iii) Structure-based prediction of the substrate of MpsA A domain; (iv) The phylogenetic tree of R/DKC domains. **(C)** Structure-based prediction of the product of MpsD. **(D)** The predicted metabolites encoded by *mps* cluster.

Based on the bioinformatics analysis results of the biosynthetic enzymes, we predicted the unknown natural product encoded by the *mps* cluster is a hydroxylated derivative of DTA **2** (Figure 2D). After searching in the compound databases, such as SciFinder, we did not find a known natural product with the same structural scaffold of **2**,

suggesting the metabolite encoded by *mps* cluster could be a novel DTA.

Heterologous expression of the *mps* cluster and characterization of the products

To explore the natural product encoded by the *mps* cluster, we introduced all the four biosynthetic genes, *mpsA*, *mpsD*, *mpsF* and *mpsG*, into the heterologous expression host *Aspergillus nidulans* (Li et al., 2016) on three vectors. Compared to the extract of the control strain harboring three empty vectors, three new metabolites (the major two are **3** and **5**, the minor one is **4**) were accumulated in the extract of *A. nidulans* expressing *mpsADFG* (Figure 3A, trace iii). Of which, **3** and **4** showed the same molecular weight (MW) of 357, and **5** showed the MW of 373 (Supplementary Figure S2). These compounds were isolated and characterized by 1D and 2D NMR spectroscopy to be DTAs (Supplementary Tables S2–S4; Supplementary Figures S3–S20), which is consistent with the bioinformatics analysis results of *mps* cluster.

For instance, the ^{1}H NMR spectrum of **3** showed five methyl groups [δ_H 0.95 (d, J=7.2 Hz), 1.33 (d, J=6.9 Hz), 1.47 (overlapped), 1.48 (brs), and 1.51 (s)], two olefinic protons [δ_H 5.23 (s), and 5.10 (d, J=6.5 Hz)], and a series of aliphatic multiplets. The ^{13}C NMR of **3** combined with DEPT experiment resolved 22 carbon signals

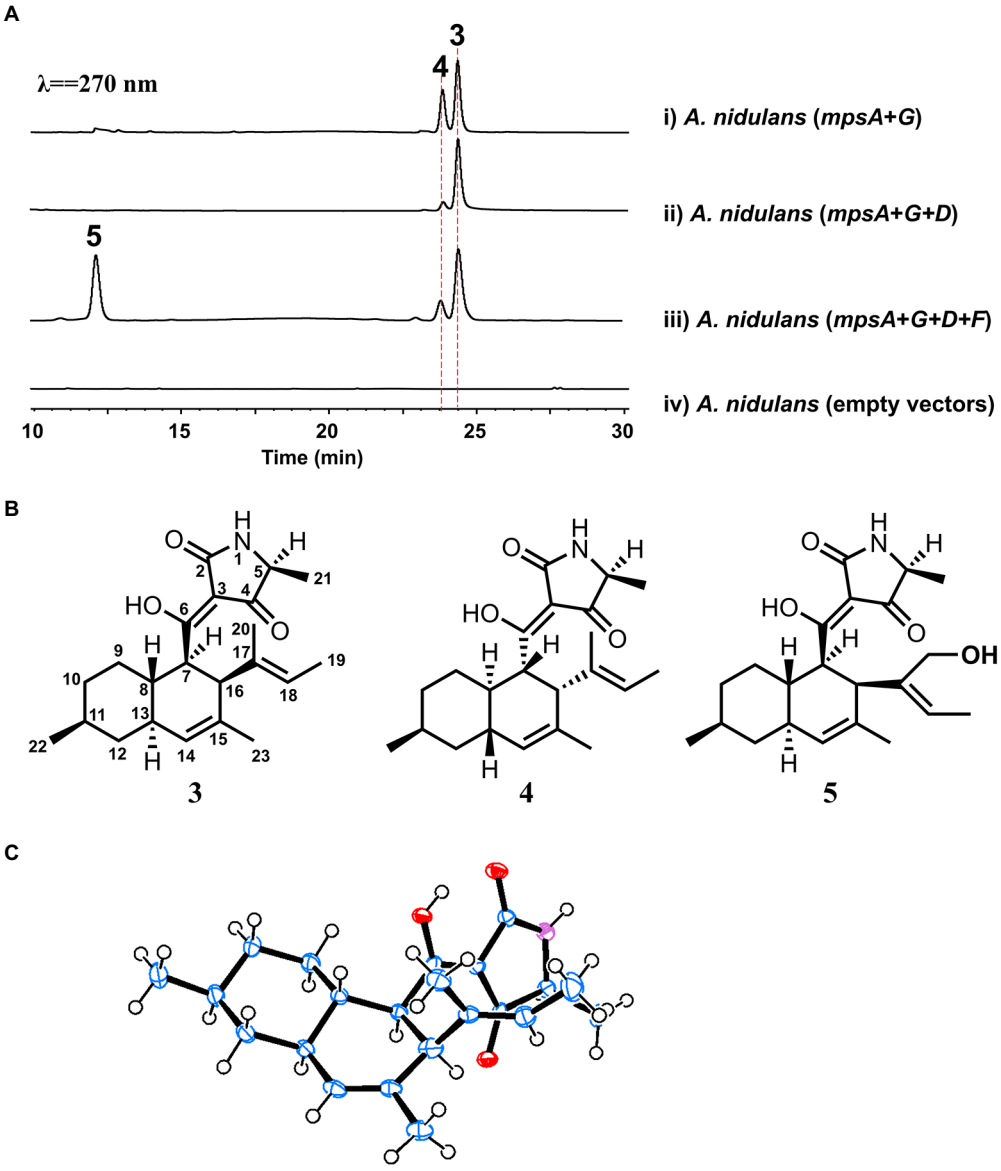

FIGURE 3
Biosynthesis of macrophasetins. **(A)** Metabolites analysis of heterologous reconstitution of the *mps* cluster in *A. nidulans*. The traces are HPLC with λ=270nm. **(B)** The structures of the characterized compounds. **(C)** Crystal structure of **3**.

attributable to a ketocarbonyl (δ_C 195.7), an amide carbonyl (δ_C 175.4), three sp^2 quaternary carbons (δ_C 101.2, 133.1 and 134.9), two sp^2 methines (δ_C 123.3 and 128.4), an oxygenated sp^2 quaternary carbons (δ_C 191.7), five methyls, three sp^3 methylenes, and six sp^3 methines (one ammoniated; Supplementary Table S2). As five of eight indices of hydrogen deficiency (IHDs) were accounted for by two carbonyls and three double bonds, the remaining three IHDs required that **3** was tricycle. Above information was similar to those of equisetin (Yin et al., 2013), except for the replacement of an oxygenated methylene and nitrogen methyl in equisetin by a methyl and proton in **3**, respectively. Detailed 2D NMR analyses (^{1}H–^{1}H COSY, HSQC and HMBC) permitted the establishment of the gross structure of **3** as depicted in Figure 3B.

Based on NOESY, the decalin rings in these three compounds (**3**–**5**) are all in *trans* configuration. In addition, we obtained an X-ray crystal structure of **3** (Figure 3C, CCDC 2210452), which allowed us to confirm the absolute stereochemistry of these three compounds. As for compound **3**, the absolute configuration is 5*S*, 7*R*, 8*S*, 11*S*, 13*S*, 16*S*. As shown in Figure 3B, **3** and **5** shared the same scaffold, the difference is that in **5** there is an additional hydroxyl group at C20. While, in compound **4**, the stereochemistry of the decalin ring is different from **3** and **5**. After searching in the compound databases, all the three compounds are novel DTAs, named macrophasetin A (**3**), B (**4**), and C (**5**). Both **3** and **5** exhibited antimicrobial activities against *Bacillus subtilis*, inhibiting the growth of *B. subtilis* at the concentration of 10 μg/ml (Supplementary Table S5). These results confirmed our hypothesis that the *mps* cluster could encode novel DTAs. Combined the results from the structural elucidation and the cluster bioinformatics analysis, we proposed that **5** is the end product of *mps* cluster.

Biosynthesis of macrophasetins

To further validate the proposal and investigate the biosynthesis of macrophasetins, the heterologous expression of combinations of *mps* cluster genes was carried out. When the PKS-NRPS MpsA and its associated enoylreductase partner MpsG were co-expressed in *A. nidulans*, the expected linear tetramic acid product **6** (structure shown in Figure 4) was not detected from the extracts of the co-expression strain, instead of the decalin-containing compounds **3** and **4** (Figure 3A, trace i). We proposed that the formation of **3** and **4** resulted from the spontaneous non-enzymatic IMDA reaction of **6**. However, the results still validated the predicted function of MpsA and MpsG, since the structure of **6** is almost identical to the predicted tetramic acid **1**. The only difference is the position of one methyl group, in compound **1** the methyl group attached to carbon 9 while in **6** it attached to carbon 15. This result further proofed our hypothesis that the closer the phylogenetic relationship of PKS domains the closer the structure of their synthesized polyketides.

When MpsA/G and the putative LLDAse MpsD were co-expressed in *A. nidulans*, **3** was detected from the extract of co-expression strain as the major product (Figure 3A, trace

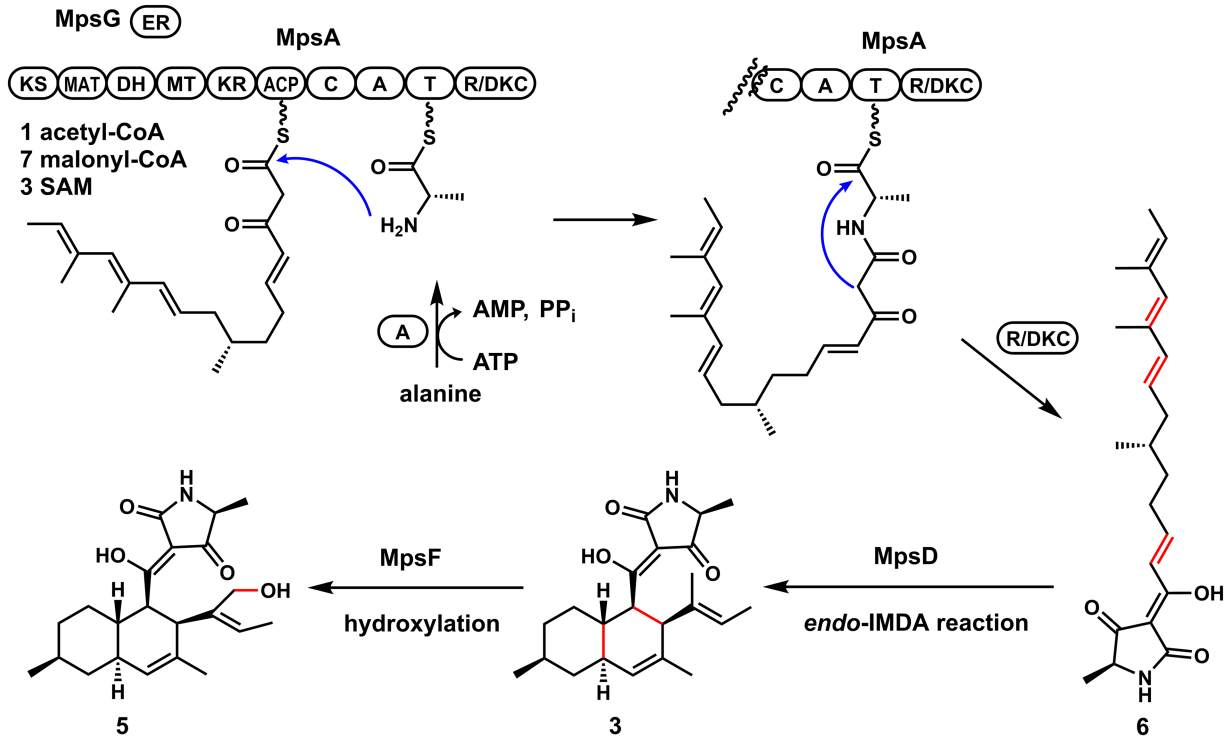

FIGURE 4
The proposed biosynthetic pathway of macrophasetins.

ii). Though a little amount of **4** was still detected, the ratio of **3**/**4** changed a lot compared to the co-expression strain of MpsA/G. Therefore, the proposed function of MpsD was confirmed to be a DAse catalyzing the *endo*-IMDA reaction of the linear substrate **6** just as predicted. In addition, since the production of **5** was not detected from the strain expressing MpsA/D/G, we concluded that **5** is the end product of the *mps* cluster. And the function of the P450 MpsF was validated to be a hydroxylase catalyzing the hydroxylation on **3** at C20 position.

Based on these findings, we proposed the biosynthetic pathway of macrophasetins. As shown in Figure 4, the PKS-NRPS MpsA together with its associated enoylreductase partner MpsG incorporate one unit of acetyl-CoA, seven units of malonyl-CoA, and one unit of L-alanine to assemble the backbone of macrophasetins to afford the linear tetramic acid intermediate **6**. Without the LLDAse MpsD, **6** can undergo the non-enzymatic IMDA reaction to generate both **3** and **4**. Catalyzed by MpsD, **6** is thoroughly converted to **3** *via* the *endo*-IMDA reaction in a regioselective and stereoselective manner. Finally, the P450 MpsF catalyzes the hydroxylation at C20 to yield the end product **5**.

Conclusion

In summary, guided by the bioinformatics analysis prediction, we mined a biosynthetic gene cluster from the plant pathogenic fungus *M. phaseolina*, which was characterized to be responsible for the biosynthesis of novel DTAs. We also investigated the biosynthesis of these DTAs, and validated the accuracy of the bioinformatics prediction. Our results provide a successful example to the proof of concept that combining phylogeny-guided bioinformatics prediction and heterologous expression is a powerful approach to mine novel DTAs from fungal species, which may facilitate the novel natural products discovery.

Data availability statement

The datasets presented in this study can be found in online repository. The name of the repository is the Cambridge Crystallographic Data Centre and the accession number is 2210452. The X-ray data of 3 has been deposited to CCDC and released. You can find the information via this link https://www.ccdc.cam.ac.uk/structures/Search?Ccdcid=2210452&DatabaseToSearch=Published.

Author contributions

LL, MT, and HZ conceived and designed the experiments. CY, LC, YG, JL, PL, MZ, and QL performed the experiments. LC, CY, MT, and LL analyzed the data. CY, MT, and LL interpreted the results. MT and LL wrote the manuscript. All authors contributed to the article and approved the submitted version.

Funding

This work was supported by the National Key R&D Program of China under Grant nos. 2021YFA0910501 and 2018YFA0901900, the National Natural Science Foundation of China under Grant nos. 31870039 and 32170069, and the Natural Science Foundation of Fujian Province under Grant no. 2021J01173.

Conflict of interest

The authors declare that the research was conducted in the absence of any commercial or financial relationships that could be construed as a potential conflict of interest.

Publisher's note

Supplementary material

The Supplementary material for this article can be found online at: https://www.frontiersin.org/articles/10.3389/fmicb.2022.1056392/full#supplementary-material

References

Bauman, K. D., Butler, K. S., Moore, B. S., and Chekan, J. R. (2021). Genome mining methods to discover bioactive natural products. *Nat. Prod. Rep.* 38, 2100–2129. doi: 10.1039/D1NP00032B

Challis, G. L., Ravel, J., and Townsend, C. A. (2000). Predictive, structure-based model of amino acid recognition by nonribosomal peptide synthetase adenylation domains. *Chem. Biol.* 7, 211–224. doi: 10.1016/S1074-5521(00)00091-0

Chi, C., Wang, Z., Liu, T., Zhang, Z., Zhou, H., Li, A., et al. (2021). Crystal structures of Fsa2 and Phm7 catalyzing [4 + 2] Cycloaddition reactions with reverse Stereoselectivities in Equisetin and Phomasetin biosynthesis. *ACS Omega* 6, 12913–12922. doi: 10.1021/acsomega.1c01593

Conti, E., Stachelhaus, T., Marahiel, M. A., and Brick, P. (1997). Structural basis for the activation of phenylalanine in the non-ribosomal biosynthesis of gramicidin S. *EMBO J.* 16, 4174–4183. doi: 10.1093/emboj/16.14.4174

Degani, O., Dor, S., Abraham, D., and Cohen, R. (2020). Interactions between Magnaporthiopsis maydis and *Macrophomina phaseolina*, the causes of wilt diseases in maize and cotton. *Microorganisms* 8:249. doi: 10.3390/microorganisms8020249

Fan, Y., Zhang, D., Tao, X., Wang, Y., Liu, J., Li, L., et al. (2019). Biosynthetic hypothesis-guided discovery and Total syntheses of PKS-NRPS hybrid metabolites from endophytic fungus *Periconia* species. *Org. Lett.* 21, 1794–1798. doi: 10.1021/acs.orglett.9b00371

Gao, Y., Xie, M., Yu, C., Zhang, M., Huang, J., Li, Q., et al. (2021). Heterologous expression of Macrollins from Phytopathogenic *Macrophomina phaseolina* revealed a cytochrome P450 Monooxygenase in the biosynthesis of *β*-hydroxyl Tetramic acid. *J. Agric. Food Chem.* 69, 15175–15183. doi: 10.1021/acs.jafc.1c05304

Ijaz, S., Sadaqat, H. A., and Khan, M. N. (2013). A review of the impact of charcoal rot (*Macrophomina phaseolina*) on sunflower. *J. Agric. Sci.* 151, 222–227. doi: 10.1017/S0021859612000512

Islam, M. S., Haque, M. S., Islam, M. M., Emdad, E. M., Halim, A., Hossen, Q. M. M., et al. (2012). Tools to kill: genome of one of the most destructive plant pathogenic fungi *Macrophomina phaseolina*. *BMC Genomics* 13:493. doi: 10.1186/1471-2164-13-493

Jiang, M., Chen, S., Li, J., and Liu, L. (2020). The biological and chemical diversity of Tetramic acid compounds from marine-derived microorganisms. *Mar. Drugs* 18:114. doi: 10.3390/md18020114

Kato, N., Nogawa, T., Hirota, H., Jang, J. H., Takahashi, S., Ahn, J. S., et al. (2015). A new enzyme involved in the control of the stereochemistry in the decalin formation during equisetin biosynthesis. *Biochem. Biophys. Res. Commun.* 460, 210–215. doi: 10.1016/j.bbrc.2015.03.011

Kato, N., Nogawa, T., Takita, R., Kinugasa, K., Kanai, M., Uchiyama, M., et al. (2018). Control of the Stereochemical course of [4+2] Cycloaddition during *trans*-Decalin formation by Fsa2-family enzymes. *Angewandte Chem. Int.* 57, 9754–9758. doi: 10.1002/anie.201805050

Kauhl, U., Andernach, L., and Opatz, T. (2018). Total synthesis of *epi*-Trichosetin. *J. Organomet. Chem.* 83, 15170–15177. doi: 10.1021/acs.joc.8b02450

Kauhl, U., Andernach, L., Weck, S., Sandjo, L. P., Jacob, S., Thines, E., et al. (2016). Total synthesis of (−)-Hymenosetin. *J. Organomet. Chem.* 81, 215–228. doi: 10.1021/acs.joc.5b02526

Kaur, S., Dhillon, G. S., Brar, S. K., Vallad, G. E., Chand, R., and Chauhan, V. B. (2012). Emerging phytopathogen *Macrophomina phaseolina*: biology, economic importance and current diagnostic trends. *Crit. Rev. Microbiol.* 38, 136–151. doi: 10.3109/1040841X.2011.640977

Kelly, L. A., Mezulis, S., Yates, C. M., Wass, M. N., and Sternberg, M. J. (2015). The Phyre2 web portal for protein modeling, prediction and analysis. *Nat. Protoc.* 10, 845–858. doi: 10.1038/nprot.2015.053

Li, L., Tang, M. C., Tang, S., Gao, S., Soliman, S., Hang, L., et al. (2018). Genome mining and assembly-line biosynthesis of the UCS1025A Pyrrolizidinone family of fungal alkaloids. *J. Am. Chem. Soc.* 140, 2067–2071. doi: 10.1021/jacs.8b00056

Li, L., Yu, P. Y., Tang, M. C., Zou, Y., Gao, S. S., Hung, Y. S., et al. (2016). Biochemical characterization of a eukaryotic decalin-forming Diels-Alderase. *J. Am. Chem. Soc.* 138, 15837–15840. doi: 10.1021/jacs.6b10452

Li, X., Zheng, Q., Yin, J., Liu, W., and Gao, S. (2017). Chemo-enzymatic synthesis of equisetin. *Chem. Commun.* 53, 4695–4697. doi: 10.1039/C7CC01929G

Luna, M. P. R., Mueller, D., Mengistu, A., Singh, A. K., Hartman, G. L., and Wise, K. A. (2017). Advancing our understanding of charcoal rot in soybeans. *J. Int. Pest Manag.* 8, 1–8. doi: 10.1093/jipm/pmw020

Masi, M., Sautua, F., Zatout, R., Castaldi, S., Arrico, L., Isticato, R., et al. (2021). Phaseocyclopentenones a and B, phytotoxic penta- and tetrasubstituted cyclopentenones produced by *Macrophomina phaseolina*, the causal agent of charcoal rot of soybean in Argentina. *J. Nat. Prod.* 84, 459–465. doi: 10.1021/acs.jnatprod.0c01287

Minami, A., Ugai, T., Ozaki, T., and Oikawa, H. (2020). Predicting the chemical space of fungal polyketides by phylogeny-based bioinformatics analysis of polyketide synthase-nonribosomal peptide synthetase and its modification enzymes. *Sci. Rep.* 10:13556. doi: 10.1038/s41598-020-70177-w

Mo, X., and Gulder, T. A. M. (2021). Biosynthetic strategies for tetramic acid formation. *Nat. Prod. Rep.* 38, 1555–1566. doi: 10.1039/D0NP00099J

Morishita, Y., Sonohara, T., Taniguchi, T., Adachi, K., Fujita, M., and Asai, T. (2020). Synthetic-biology-based discovery of a fungal macrolide from *Macrophomina phaseolina*. *Org. Biomol. Chem.* 18, 2813–2816. doi: 10.1039/D0OB00519C

Sato, M., Dander, J. E., Sato, C., Hung, Y. S., Gao, S. S., Tang, M. C., et al. (2017). Collaborative biosynthesis of Maleimide- and Succinimide-containing natural products by fungal Polyketide Megasynthases. *J. Am. Chem. Soc.* 139, 5317–5320. doi: 10.1021/jacs.7b02432

Sato, M., Kishimoto, S., Yokoyama, M., Jamieson, C. S., Narita, K., Maeda, N., et al. (2021). Catalytic mechanism and *endo*-to-*exo* selectivity reversion of an octalin-forming natural Diels-Alderase. *Nat. Cat.* 4, 223–232. doi: 10.1038/s41929-021-00577-2

Sato, M., Yagishita, F., Mino, T., Uchiyama, N., Patel, A., Chooi, Y. H., et al. (2015). Involvement of Lipocalin-like CghA in Decalin-forming Stereoselective Intramolecular [4+2] Cycloaddition. *ChemBioChem* 16, 2294–2298. doi: 10.1002/cbic.201500386

Schobert, R., and Schlenk, A. (2008). Tetramic and tetronic acids: an update on new derivatives and biological aspects. *Bioorg. Med. Chem.* 16, 4203–4221. doi: 10.1016/j.bmc.2008.02.069

Singh, G., Singh, J., Singamaneni, V., Singh, S., Gupta, P., and Katoch, M. (2021). Serine-glycine-betaine, a novel dipeptide from an endophyte *Macrophomina phaseolina*: isolation, bioactivity and biosynthesis. *J. Appl. Microbiol.* 131, 756–767. doi: 10.1111/jam.14995

Stachelhaus, T., Mootz, H. D., and Marahiel, M. A. (1999). The specificity-conferring code of adenylation domains in nonribosomal peptide synthetases. *Chem. Biol.* 6, 493–505. doi: 10.1016/S1074-5521(99)80082-9

Tamura, K., Stecher, G., Peterson, D., Filipski, A., and Kumar, S. (2013). MEGA6: molecular evolutionary genetics analysis version 6.0. *Mol. Biol. Evol.* 30, 2725–2729. doi: 10.1093/molbev/mst197

Tan, D., Jamieson, C. S., Ohashi, M., Tang, M. C., Houk, K. N., and Tang, Y. (2019). Genome-mined Diels-Alderase catalyzes formation of the *cis*-Octahydrodecalins of Varicidin a and B. *J. Am. Chem. Soc.* 141, 769–773. doi: 10.1021/jacs.8b12010

Wahl, J., Freyss, J., von Korff, M., and Sander, T. (2019). Accuracy evaluation and addition of improved dihedral parameters for the MMFF94s. *J. Chem.* 11:53. doi: 10.1186/s13321-019-0371-6

Wang, X., Gao, Y.-L., Zhang, M.-L., Zhang, H.-D., Huang, J.-Z., and Li, L. (2020). Genome mining and biosynthesis of the acyl-CoA:cholesterol acyltransferase inhibitor beauveriolide I and III in *Cordyceps militaris*. *J. Biotechnol.* 309, 85–91. doi: 10.1016/j.jbiotec.2020.01.002

Winter, J. M., Cascio, D., Dietrich, D., Sato, M., Watanabe, K., Sawaya, M. R., et al. (2015). Biochemical and structural basis for controlling chemical modularity in fungal Polyketide biosynthesis. *J. Am. Chem. Soc.* 137, 9885–9893. doi: 10.1021/jacs.5b04520

Yin, J., Kong, L., Wang, C., Shi, Y., Cai, S., and Gao, S. (2013). Biomimetic synthesis of equisetin and (+)-fusarisetin a. *Chem. Eur. J.* 19, 13040–13046. doi: 10.1002/chem.201302163

frontiers | Frontiers in Microbiology

TYPE Original Research
PUBLISHED 17 November 2022
DOI 10.3389/fmicb.2022.1073243

OPEN ACCESS

EDITED BY
Dewu Zhang,
Chinese Academy of Medical Sciences, China

REVIEWED BY
Xianpu Ni,
Shenyang Pharmaceutical University, China
Xiao Liu,
Beijing University of Chinese Medicine, China

*CORRESPONDENCE
Youming Zhang
zhangyouming@sdu.edu.cn
Xiaoying Bian
bianxiaoying@sdu.edu.cn
Xiaokun Xu
xuxiaokun313@163.com

†These authors have contributed equally to this work

SPECIALTY SECTION
This article was submitted to Microbial Physiology and Metabolism, a section of the journal Frontiers in Microbiology

RECEIVED 18 October 2022
ACCEPTED 28 October 2022
PUBLISHED 17 November 2022

CITATION
Wang Z-J, Liu X, Zhou H, Liu Y, Zhong L, Wang X, Tu Q, Huo L, Yan F, Gu L, Müller R, Zhang Y, Bian X and Xu X (2022) Engineering of *Burkholderia thailandensis* strain E264 serves as a chassis for expression of complex specialized metabolites.
Front. Microbiol. 13:1073243.
doi: 10.3389/fmicb.2022.1073243

Engineering of *Burkholderia thailandensis* strain E264 serves as a chassis for expression of complex specialized metabolites

Zong-Jie Wang[1†], Xiaotong Liu[1†], Haibo Zhou[1†], Yang Liu[1], Lin Zhong[1,2], Xue Wang[1], Qiang Tu[1,2], Liujie Huo[1], Fu Yan[1], Lichuan Gu[1], Rolf Müller[3], Youming Zhang[1,2*], Xiaoying Bian[1*] and Xiaokun Xu[1*]

[1]Helmholtz International Lab for Anti-infectives, Shandong University-Helmholtz Institute of Biotechnology, State Key Laboratory of Microbial Technology, Shandong University, Qingdao, China, [2]CAS Key Laboratory of Quantitative Engineering Biology, Shenzhen Institute of Synthetic Biology, Shenzhen Institute of Advanced Technology, Chinese Academy of Sciences, Shenzhen, China, [3]Department of Microbial Natural Products, Helmholtz Institute for Pharmaceutical Research, Helmholtz Centre for Infection Research and Department of Pharmacy at Saarland University, Saarbrücken, Germany

Heterologous expression is an indispensable approach to exploiting natural products from phylogenetically diverse microbial communities. In this study, we constructed a heterologous expression system based on strain *Burkholderia thailandensis* E264 by deleting efflux pump genes and screening constitutive strong promoters. The biosynthetic gene cluster (BGC) of disorazol from *Sorangium cellulosum* So ce12 was expressed successfully with this host, and the yield of its product, disorazol F_2, rather than A_1, was improved to 38.3mg/L by promoter substitution and insertion. In addition to the disorazol gene cluster, the BGC of rhizoxin from *Burkholderia rhizoxinica* was also expressed efficiently, whereas no specific peak was detected when shuangdaolide BGC from *Streptomyces* sp. B59 was transformed into the host. This system provides another option to explore natural products from different phylogenetic taxa.

KEYWORDS

***Burkholderia*, chassis, heterologous expression, disorazol, rhizoxin**

Introduction

Natural products and their derivatives are important sources of new drugs (Newman and Cragg, 2020). With the development of next-generation sequencing technologies, an increasing amount of genomic data is available in public databases, and bioinformatic analysis has indicated that most of them are unexplored (Paoli et al., 2022). More than 99% of microbial organisms are currently unculturable (Pace, 1997); therefore, exploiting these treasures has attracted the interest of researchers worldwide. Heterologous expression has been confirmed as an effective strategy for obtaining natural products from slow-growing or even unculturable organisms, as well as poorly explored organisms, due to the lack of

efficient genetic manipulation tools (Huo et al., 2019; Paoli et al., 2022).

Disorazols are a class of macrocyclic polyketides discovered in the myxobacterial strain *S. cellulosum* So ce12 (Jansen, 1994), and the flagship compound, disorazol A_1, can inhibit the proliferation of different cancer cell lines at close to picomolar levels by interfering with microtubular dynamics (Elnakady et al., 2004; Menchon et al., 2018). The disorazol gene cluster was identified in So ce12 by transposon mutagenesis (Carvalho et al., 2005; Kopp et al., 2005). It is composed of four clustered genes (*disABCD*) and unidentified genes encoding tailoring enzymes responsible for epoxidation and methylation, which may lie outside of the biosynthetic gene cluster (BGC). Among them, *disABC* encode hybrid *trans*-AT PKS/NRPS megaenzymes, and *disD* encodes a separate protein that contains an acyl transferase domain and a possible oxidoreductase domain (Figure 1A). In our previous study, the disorazol BGC cloned in a bacterial artificial chromosome library was reconstructed by Red/ET-mediated recombineering (Zhang et al., 1998) and expressed in the model myxobacterium *Myxococcus xanthus* DK1622, considering the difficulties of culture and genetic manipulation of the original producer (Tu et al., 2016). However, this heterologous host grows relatively slowly and the yield remains quite low (<1 mg/L).

To overcome this problem, the strains from Burkholderiales with high GC content and abundant secondary metabolites (Kunakom and Eustáquio, 2019) can be used to express the disorazol gene cluster, which was inspired by the success of employing *Schlegelella brevitalea* DSM 7029 (Tang et al., 2019) as an efficient heterologous host to produce myxobacteria-derived epothilones, vioprolides and myxochelins (Bian et al., 2017; Yan et al., 2018; Liu J. et al., 2021). *Burkholderia thailandensis* E264, isolated from rice fields in Thailand, is a low virulence member of genus *Burkholderia* compared with *B. pseudomallei*, and *B. mallei*. Although a few infection cases caused by *B. thailandensis* in immunocompromised patients were reported (Brett et al., 1998; Glass et al., 2006; Chang et al., 2017), it is extensively studied as a model organism of the factors controlling virulence or as a producer of secondary metabolites, such as the metabolite bactobolin produced by a hybrid PKS-NRPS gene cluster (Duerkop et al., 2009; Seyedsayamdost et al., 2010), thailandamide biosynthesized through PKS (Nguyen et al., 2008), and the acyldepsitripeptide histone deacetylase inhibitor burkholdac catalyzed by NRPS (Biggins et al., 2011). Abundant secondary metabolites indicated that it could provide abundant substrates for expressing heterologous BGCs. In addition to possessing huge biosynthetic potential, strain E264 also has a fast growth rate, which makes it more suitable as a heterologous host (Mao et al., 2017; Liu et al., 2022). However, as a member of the genus *Burkholderia*, the intrinsic multidrug-resistance of the wild-type strain E264 makes genetic manipulation difficult, which partially results from the resistance-nodulation-division family efflux pumps (Biot et al., 2011, 2013).

In this study, we first deleted multidrug-resistance genes and obtained several antibiotic-sensitive mutants. The native potent promoters in strain E264 were screened by transcriptome analysis and evaluated *in vivo* by cloning them into a promoterless luciferase reporter vector. Selected promoters were used to improve the yields of disorazol in this heterologous host. Finally, the heterologous expression system was used to express the gene clusters from other phylogenetic taxa. The BGC of rhizoxin cloned by Red/ET-mediated direct cloning (Fu et al., 2012) was expressed successfully, whereas no specific peak was detected in the fermentation of the heterologous host containing shuangdaolide BGC cloned by direct cloning from *Streptomyces* sp. B59.

Results

Improved characteristics of engineered strain E264

During the course of expressing the disorazol gene cluster, *B. thailandensis* E264 showed better performance than the well-studied host DSM 7029 (Bian et al., 2017; Yan et al., 2018; Liu J. et al., 2021) in terms of growth rate and production. To facilitate genetic manipulation, three efflux pumps in strain E264, AmrAB-OprA (abbreviated as A), BpeAB-OprB (B), and BpeEF-OprC (C) (Biot et al., 2011, 2013), were inactivated by homologous recombination combined with *pheS* counterselection mediated seamless gene deletions (Barrett et al., 2008), and mutants with one, two, or three pump knockouts were obtained. Antibiotic susceptibility determined by the disc diffusion test was shown in tables S4 and S5. For most antibiotics, the mutant with one pump knockout (E264ΔA, E264ΔB, or E264ΔC) showed improved antibiotic sensitivity compared to the wild-type, suggesting that they are involved in multidrug resistance. Therefore, the mutant with three pump knockouts (E264ΔBAC) was constructed and used to express gene clusters or characterize promoters in subsequent experiments.

Compared with the wild-type, E264ΔBAC was more sensitive to the tested antibiotics, except ampicillin (Figure 2A, Table 1). The minimum inhibitory concentrations (MIC) of the tested antibiotics against mutant E264ΔBAC were much lower than the concentrations used to select transformants (Supplementary Table S6). The MIC value (<7.5 μg/ml) of kanamycin against the mutant was much lower than the concentration (300 μg/ml) used to select transformants of the wild type (Kang et al., 2011). The MIC values of tetracycline, chloramphenicol, and erythromycin are lower than 0.6, 1.9, and 3.1 μg/ml, respectively. The antibiotic-sensitive mutant E264ΔBAC facilitates the genetic engineering of this potential heterologous host with low-concentration antibiotics as a selectable marker. In addition, the growth rate of the mutant E264ΔBAC was not affected by engineering, and the growth curve of the mutant was similar to that of the wild-type strain E264, except that the maximum OD600 was slightly lower (Figure 2B).

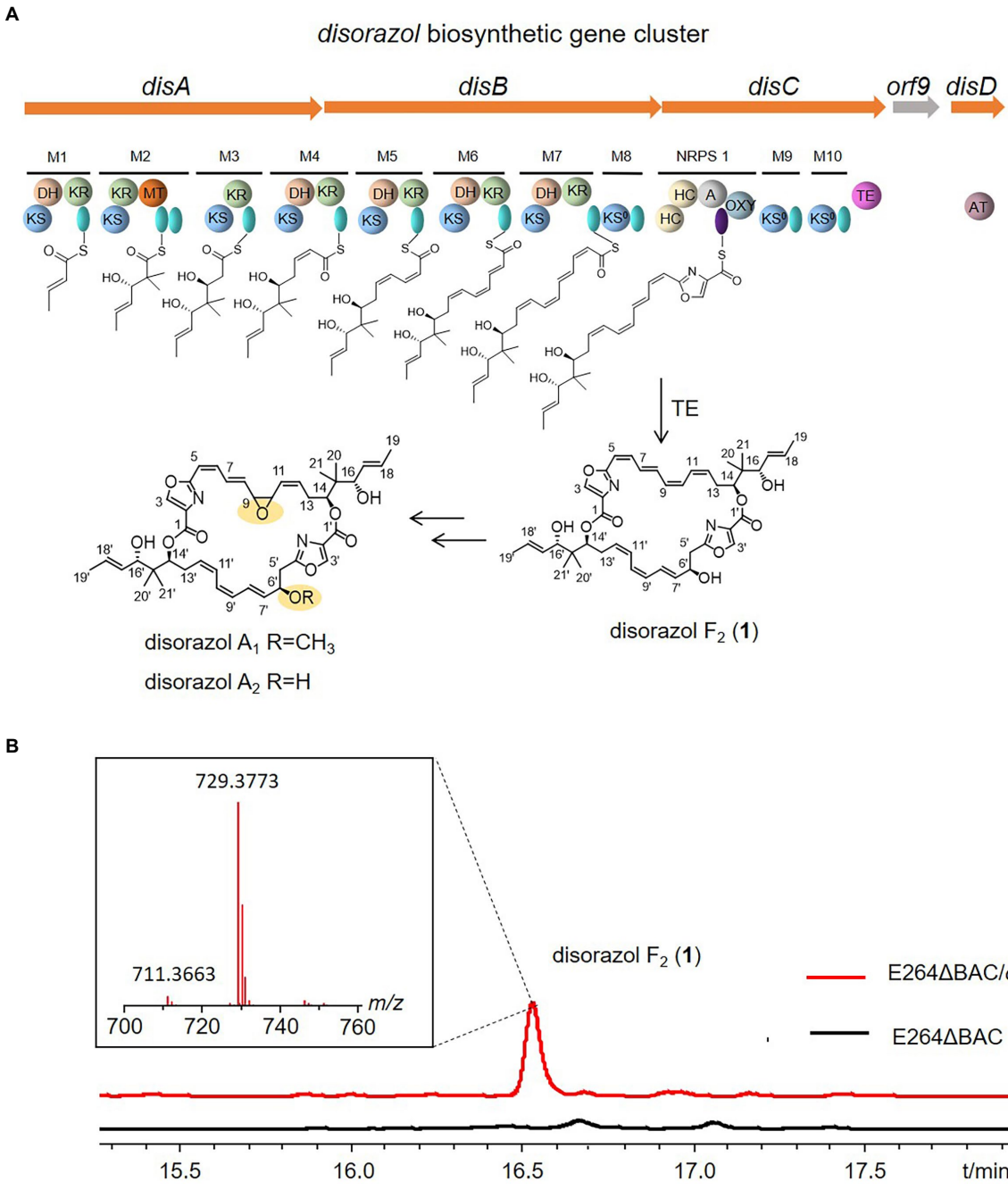

FIGURE 1
Domain organization of the disorazole biosynthetic gene cluster from *Sorangium cellulosum* So ce12 **(A)**, and disorazol F_2 produced by E264ΔBAC/*dis* **(B)**. KS: ketosynthase, AT: acyl transferase, green oval: acyl carrier protein (ACP), HC: condensation/heterocyclization, A: adenylation, purple oval: peptidyl carrier protein (PCP), OXY: oxygenase, KR: ketoreductase, DH: dehydratase, MT: C-methyltransferase, TE: thioesterase,

Production of disorazol in E264ΔBAC

After obtaining the mutant, the plasmid p15A-dis (Supplementary Figure S1; Tu et al., 2016) was introduced into the mutant E264ΔBAC *via* conjugation mediated by the donor strain *Escherichia coli* WM3064 (Dehio and Meyer, 1997). A specific peak at *m/z* 729.4 was observed in the crude extract of the mutant with the disorazol gene cluster, and the area of the specific peak produced by mutant E264ΔBAC was much higher than that of *S. brevitalea* DSM 7029, which we used for heterologous expression of *cis*-PKS-derived epothilone (Figure 1B and Supplementary Figure S2; Bian et al., 2017), suggesting that E264 is more suitable for expressing this *trans*-AT PKS gene cluster. However, the molecular weight of the product (**1**) was different from that of disorazol A_1 (Figure 1B). The

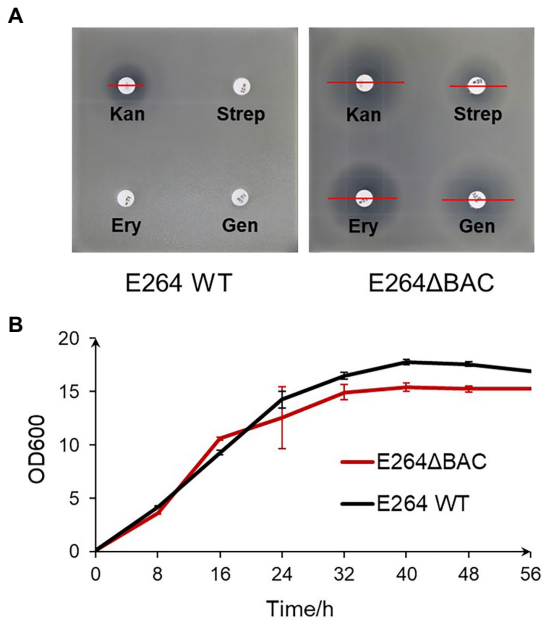

FIGURE 2
Characteristics of engineered strain E264. **(A)** Antibiotic sensibility test of mutant E264ΔBAC compared with wild-type strain E264. Kan, kanamycin 30μg/disc; Strep, streptomycin 10μg/disc; Ery, erythromycin 15μg/disc; Gen, gentamicin 10μg/disc. **(B)** Growth curves of both wild-type strain E264 and mutant E264ΔBAC.

TABLE 1 The growth of mutant E264ΔBAC under different concentration of antibiotics.

Antibiotics	Concentration/μg·ml^{-1}					
Streptomycin	50	25	12.5	6.3	3.1	1.6
Gentamicin	10	5	2.5	1.3	0.6	
Tetracycline	10	5	2.5	1.3	0.6	
Apramycin	25	12.5	6.3	3.1	1.6	0.8
Kanamycin	30	15	7.5	3.8	1.9	0.9
Chloramphenicol	30	15	7.5	3.8	1.9	0.9
Erythromycin	25	12.5	6.3	3.1	1.6	0.8
Spectinomycin	100	50	25	12.5	6.3	3.1

0.05 < OD600 < 0.1 | 0.1 < OD600 < 0.5 | 0.5 < OD600 < 1.0 | OD600 > 1. The grey shade represents the OD600 in different concentration of antibiotic.

molecular formula of **1** was predicted to be $C_{42}H_{52}N_2O_9$ based on HR-ESIMS (*m/z* 729.3773 $[M+H]^+$, calcd 729.3746; Figure 1B), which is consistent with disorazol F_2. Furthermore, the ^1H and ^{13}C NMR spectra of **1** confirmed that the product is disorazol F_2 (**1**) (Supplementary Table S7, Supplementary Figures S3 and S4; Jansen, 1994). Compared to disorazol A_1, the epoxide at C-9/C-10 in **1** was replaced by a double bond, and the hydroxyl group at C-6′ was not methylated (Figure 1A).

The heterologous expression of disorazol in a phylogenetically distant relative of the myxobacterial strain *S. cellulosum* could exclude the influence of homologous genes in the previously reported myxobacterial host *M. xanthus* DK1622 (Tu et al., 2016) and facilitate the elucidation of its biosynthetic pathway. The *orf9* encoding a ubiquinone biosynthesis protein Coq4 is not necessary for disorazol production (Tu et al., 2016). The product produced by the heterologous host *B. thailandensis* E264 is disorazol F_2 rather than A_1 or A_2 produced by original producer So ce12 or myxobacterial host DK1622, indicating that the epoxidation and methylation of disorazols may be catalyzed by enzymes encoded by genes located outside of the gene cluster. Another debate regarding disorazols is the installation of a hydroxyl group at C-6. Theoretically, the DH7 domain could catalyze the elimination of hydroxyl groups at C-6 and C-6′ and form symmetrical macrodiolide products; however, most natural disorazols are unsymmetrical owing to the presence of the hydroxyl group at C-6′. The product obtained from E264ΔBAC::Ptet-*dis* is disorazol F_2, an unsymmetrical macrodiolide, which suggests that the hydroxyl group at C-6′ is not installed during post-PKS modification.

Yield improvement of disorazol F_2

Initially, the yield of disorazol F_2 (**1**) was less than 0.4 mg/L. To improve the yield of F_2 (**1**), we first characterized potent native promoters in E264. Fifty native promoters with high expression levels at different phases of growth in M9 broth were selected based on the data of transcriptome analysis. However, the data of transcriptome may be affected by sample processing procedures, such as liquid nitrogen freezing, we further characterized the promoters *in vivo* by a luciferase assay to obtain a series of potent constitutive promoters of E264 (Supplementary Figure S5, Supplementary Table S8; Ouyang et al., 2020). To avoid possible positional effects, an *attB* site, the attachment site of site-specific recombination, was integrated into the locus of operon BpeEF-OprC, resulting in the mutant E264ΔBAC::*attB*. The potent promoters P11 (promoter of a hypothetical protein), P17 (promoter of a radical SAM protein), P33 (promoter of a hypothetical protein), P35 (promoter of a peroxiredoxin), P44 (promoter of a membrane protein), and P46 (promoter of a DUF4148 domain-containing protein) were employed to promote the expression of the disorazol gene cluster, resulting in a significant increase in yield (Figure 3A). Among them, the optimal promoter, P46, resulted in an approximately 23-fold increase in the average yield of disorazol F_2 (**1**) to 9.3 mg/L. Promoters P17 and P44 showed similar effects, which led to an obvious increase in yield to 7.5 and 8.6 mg/L, respectively. Other promoters also improved the yields by 1.5-fold to 6.5-fold. To further improve the yield, promoters P46, P44, P17, and P46 were inserted upstream of genes *disA*, *disB*, *disC*, and *disD* using the RedEx method (Supplementary Figure S6; Song et al., 2020), which generated mutants 1P (P46), 2P (P46 + P44), 3P (P46 + P44 + P17), and 4P

(P46 + P44 + P17 + P46; Figure 3B). The yield of disorazol F_2 (**1**) showed a positive correlation with the number of promoters, which reached to 38.3 mg/L in mutant 4P-*dis*, 96-fold higher than that of E264ΔBAC::Ptet-*dis*. The significantly improved efficiency of heterologous expression encouraged us to express BGCs from other phylogenetical taxa.

Expression of BGCs from other phylogenetical taxa

In addition to the gene cluster from myxabacteria, the BGCs of rhizoxin (rhi) from *Burkholderia rhizoxinica* (Partida-Martinez and Hertweck, 2007) and shuangdaolide (sdl; Supplementary Figure S7) from *Streptomyces* sp. B59 (Liu Y. et al., 2021) were transferred to E264ΔBAC::*attB*. No specific peak was detected in the crude extract of E264ΔBAC::*attB*/sdl, whereas a series of specific peaks were observed in the fermentation product of E264ΔBAC::*attB*/rhi, whose molecular weights were consistent with the reported rhizoxins (Figure 4). Specific peaks a and b with a high proportion were detected at *m/z* 628.3 with t_R = 13.4 min and at *m/z* 642.3 with t_R = 14.8 min. Based on HRMS, the molecular formula of the compound in peak a was established as $C_{35}H_{49}NO_9$ (*m/z* 628.3483 $[M + H]^+$, calcd 628.3482), which is identical to that of rhizoxins M_1, Z_2, and S_2; peak b may contain rhizoxin M_2 or Z_2 ($C_{36}H_{51}NO_9$, *m/z* 642.3636 $[M + H]^+$, calcd 642.3637). In addition to the major peaks, we also observed some specific peaks in a relatively low proportion of the fermentation product of E264ΔBAC::*attB*/rhi. Their MS/MS spectra were similar to peaks a and b, and HRMS suggested that they were also related to known rhizoxins (Supplementary Table S9). The BGC of rhizoxin from closely related species was expressed successfully in the host based on strain E264, and the potential of this heterologous expression system still needs to be further developed.

Cytotoxicity test of disorazol F_2 (1)

Owing to the low yield of the original producer So ce12, the cytotoxicity of disorazol F_2 has never been reported in previous studies. In this study, the cytotoxicity of disorazol F_2 (**1**) was evaluated against three human cancer cell lines (HepG2, HCT116, and A549; Table 2). Although one-two orders of magnitude weaker than epoxide disorazols A_1 and A_2 (Tu et al., 2016), disorazol F_2 still exhibited potent activity against the tested cell lines with IC_{50} values ranging from 0.25 to 3.11 nM, one to three orders of magnitude stronger than clinically used doxorubicin or vincristine. The cytotoxicity assay compared with previously reported data (Irschik et al., 1995; Elnakady et al., 2004; Hopkins and Wipf, 2009; Tu et al., 2016) suggested that the activity of disorazols is affected by the epoxide at C-9/C-10, which suggests the tailoring enzyme of the disorazol pathway is still a significant task.

Discussion

Disorazols are a family of natural products with nanomolar cytotoxicity. However, the difficulties in culture and genetic manipulation of the original producer have limited further study. The heterologous expression system developed in this study efficiently overcomes these problems. This provides a powerful tool for illuminating this fantastic pathway. Heterologous expression in strain E264 indicated that the enzymes catalyzed

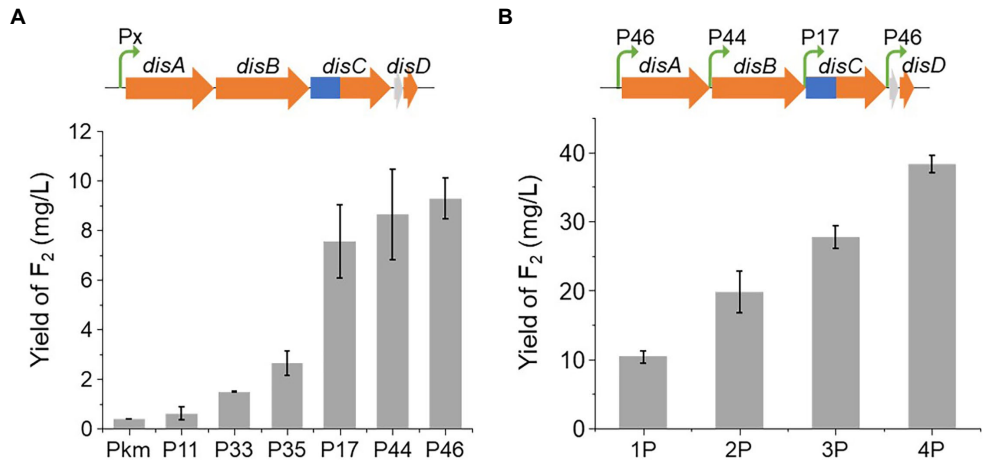

FIGURE 3
The yield of disorazol F_2 produced by E264ΔBAC with different promoter strategies. **(A)** The yields of F_2 (**1**) in E264ΔBAC::attB/dis from cluster expression promoted by different promoters (Px). **(B)** The yields of F_2 (**1**) in E264ΔBAC::attB/dis driven by different numbers of promoters.

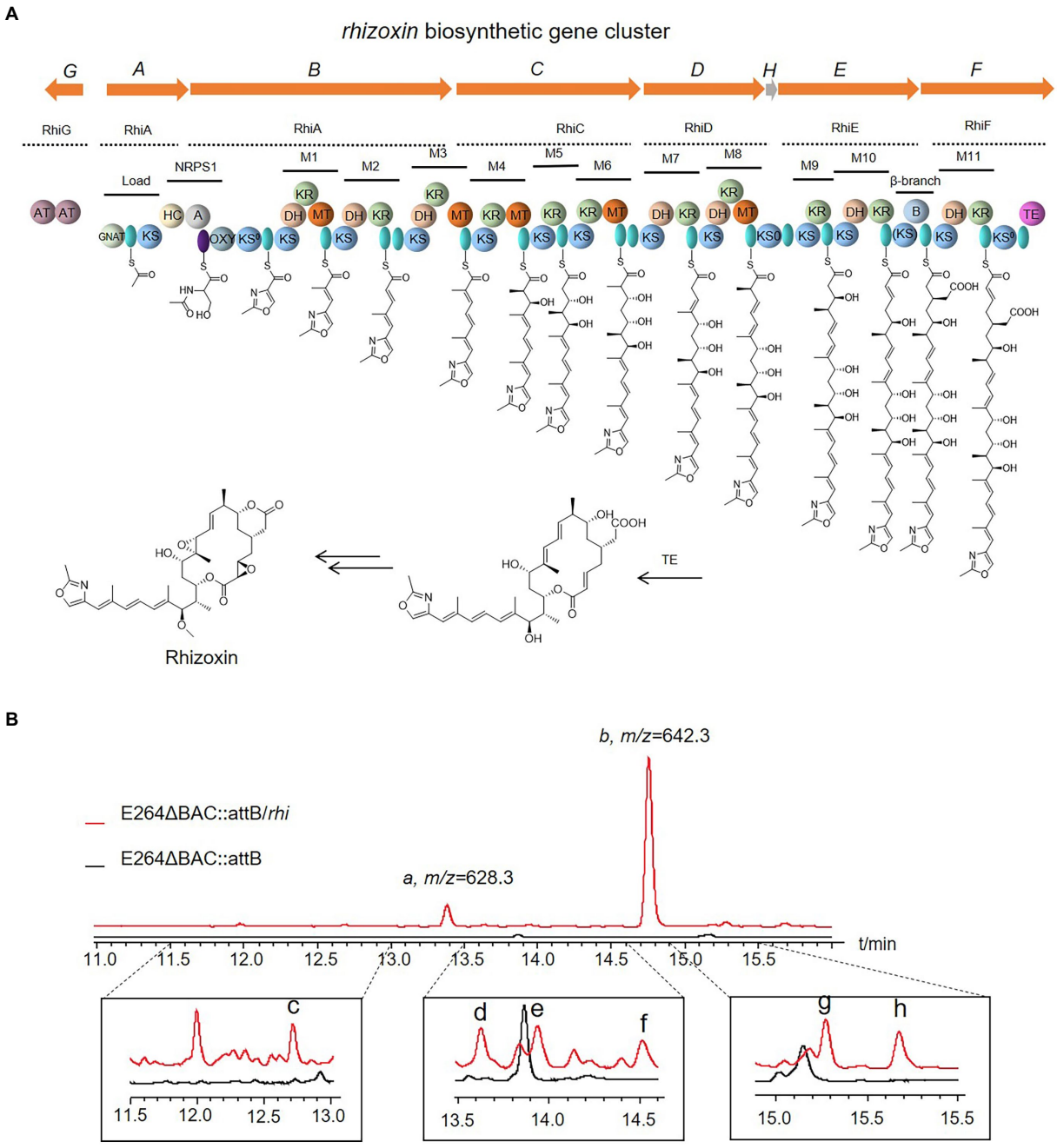

FIGURE 4
Organization of the rhizoxin (*rhi*) biosynthesis gene cluster and model for rhizoxin biosynthesis **(A)**, and the fermentation products of E264ΔBAC::attB/rhi **(B)**. GNAT: N-acetyltransferase; KS: ketosynthase, AT: acyl transferase, green oval: ACP, HC: condensation/heterocyclization, A: adenylation, purple oval: PCP, OXY: oxygenase, KR: ketoreductase, DH: dehydratase, MT: C-methyltransferase, TE: thioesterase, B: unknown domain possibly involved in β-branching.

epoxidation and methylation outside of the gene cluster. The gene cluster of disorazol also possesses some interesting characteristics unusual in classical PKS, such as a missing loading domain in module 1 and repeated ACP domains in module 2, as well as these 'redundant' domains in genes *disB* and *disC*. These interesting points may be elucidated in the near future by expressing domain (s) inactivation or deletion of the disorazol gene cluster with an efficient heterologous host.

This heterologous expression system also provides a platform for producing unnatural disorazol by PKS engineering. Natural

TABLE 2 Activity of disorazol F_2 (1) against human cancer cell lines (IC_{50}, nM).

Compounds	HepG2	HCT116	A549
F_2 (**1**)	0.25 ± 0.01	3.11 ± 0.10	2.74 ± 0.56
Vincristine	6.62 ± 0.48	50.05 ± 3.68	44.28 ± 4.55
Doxorubicin	830 ± 119	793 ± 90	919 ± 35

IC_{50} values are calculated from three independent biological replicates.

products are designed to help producers occupy an ecological niche rather than to help people cure diseases. Therefore, it is effective to improve drug properties of them by increasing structural diversity (Floss, 2006). We believe that an increasing number of disorazol derivatives will be generated using this platform, which will promote drug development in this fantastic family.

Finally, myxobacteria are becoming an important source of natural products for drug discovery and still possess enormous biosynthetic potential (Weissman and Müller, 2010; Bader et al., 2020). The gene cluster of epothilone, a marketed anti-cancer drug isolated from *Sorangium cellulosum*, was successfully expressed in strain DSM 7029 with higher yields after multiple medium optimization and genome engineering (Bian et al., 2017; Yu et al., 2020). The heterologous expression system based on strain E264 provides another choice for the exploration of natural products from myxobacteria.

In addition to the advantages mentioned above, some problems must be addressed in this heterologous expression system. First, although strain E264 have been extensively studied in lab, as a class II opportunistic pathogen, potential risks need to be evaluated to ensure safety during large-scale fermentation. Additional measures, such as appropriate containment, are needed to ensure safety, which will significantly increase costs in industrial production. To overcome this problem, the construction of attenuated mutants through genetic engineering may be feasible. Secondly, this study obtained disorazol F_2 rather than A_1, which might leave the real "natural products" in the process of expressing other gene clusters. This problem needs to be addressed in other systems. Finally, the expression of shuangdaolide in the host failed, which may have resulted from their phylogenetic relationships. This result indicates that various hosts are required to express gene clusters from different taxa.

In summary, we developed an efficient heterologous expression system based on streamlined *B. thailandensis* E264, in which the disorazol gene cluster was expressed successfully. The yield of the heterologous product, disorazol F_2, was improved 96-fold using promoter substitution and insertion. The expression of the rhizoxin gene cluster from *Burkholderia rhizoxina* was also successful, whereas no specific peak was detected in the fermentation of the host containing the shuangdaolide gene cluster. Furthermore, the safety and compatibility of the heterologous expression system should be improved.

Materials and methods

Bacterial strains

Burkholderia thailandensis E264 was purchased from German collection of microorganisms and cell cultures GmbH (DSMZ) and was cultured in low-salt Luria-Bertani medium (1% tryptone, 0.5% yeast extract, 0.1% NaCl) at 37°C. The markerless mutants of strain E264 were established as described in section construction of deletion mutants. *Escherichia coli* GB05-red was used for mediating homologous recombination between a linear and circular DNA molecular (LCHR) while *E. coli* GB05-dir mediating linear plus linear recombination (LLHR). *Escherichia coli* GB05-dir-gyrA462 or GB05-red-gyrA462 were used for constructing plasmids with counterselectable marker CcdB. *Escherichia coli* WM3064 was employed as a conjugal donor (Dehio and Meyer, 1997). Unless otherwise specified, the strains of *Escherichia coli* were cultured under the same conditions with strain E264. Tetracycline (Tet) was added to a final concentration of 50 μg/ml for selective growth of wild type strain of *B. thailandensis* E264. For mutant E264ΔBAC, antibiotics were added to final concentrations of 30 μg/ml kanamycin (Kan) or 5 μg/ml gentamicin (Genta) as required, for strains of *E. coli*, the concentrations were 30 μg/ml Kan, 100 μg/ml ampicillin (Amp) or 15 μg/ml chloramphenicol (Cm).

Construction of deletion mutants

The genomic DNA (gDNA) of strain E264 was isolated using phenol – chloroform – isoamyl alcohol mixture (Wang et al., 2020). To obtain markerless mutants, genetic tools developed by Barrett *et al* were modified and applied in this study (Barrett et al., 2008). Briefly, about 1 kb regions upstream and downstream of targeted genes amplified by PCR using PrimeSTAR® HS DNA polymerase with GC buffer were cloned into vector pBR322-amp-tet-pheS (linearized with restriction enzymes *Xab*I and *Nco*I) by strain GB05-dir. The plasmids with homology arms were introduced into strain E264 by natural transformation (Garcia, 2017), and correct clones verified by colony PCR were cultured in LSLB without antibiotic for 12 h to eliminate selection marker. The overnight cultures were centrifuged and washed twice with liquid M9G medium (M9 medium of Sangon, Shanghai supplemented with 20 mM Glucose), then 50 μl cell suspensions were plated on M9G plates supplementing with 0.1% 4-Chloro-D, L-phenylalanine (Sigma-Aldrich) to screen the recombinants with selection marker deletion. Markerless mutants were further verified by colony PCR. To generate mutant E264ΔBAC::*attB*, the sequence of *attB* (GGGTGCCAGGGCGTGCCCTTGGGCTC CCCGGGCGCGTA) was inserted between the homology arms of pBR322-Amp-Tet-pheS-oprC through oligonucleotide synthesis, and the plasmid was introduced into mutant E264ΔBA followed by selection and counterselection successively.

Antibiotic sensitivity test

To make test plates, the overnight cultures (200 µl) of strain E264 or E264ΔBAC were mixed with 50 ml melted LSLB agar medium. Then, the paper discs containing different antibiotics (HangweiTM, Hangzhou) were placed on the media. The plates were cultured at 37°C overnight to measure the diameter of inhibition zone.

Plasmids construction for promoter characterization

The amp-ccdB cassette flanked with two restriction enzyme *Nde*I sites and about 40 bp homology arms was amplified from plasmid p15A-amp-ccdB using primers amp-ccdB-P11-F/R (Wang et al., 2018), the PCR product and plasmid p15A-genta-int-attP-P11-firefly (Ouyang et al., 2020) were electroporated into *E. coli* GB05-red-gyrA462 expressed recombinases Redα/Redβ, which resulted in plasmid p15A-genta-int-attP-amp-ccdB-firefly. Colonies growth on plates supplemented with Amp and Genta were transferred into 1.8 ml fresh LB broth with appropriate antibiotics and incubated at 37°C overnight. The plasmid DNA was extracted from the overnight culture and confirmed by restriction analysis.

Promoter Px was amplified using primers PX-F/R with 40 bp homology arms, and plasmid p15A-genta-int-attP-amp-ccdB-firefly was linearized with restriction endocuclease *Nde*I. The products of PCR and restriction enzyme digestion were electroporated into *E. coli* GB05-dir expressed recombinases RecE/RecT, which resulted in plasmid p15A-genta-int-attP-Px-firefly.

Luciferase assay

Plasmids with different promoters located upstream of luciferase gene were introduced into E264ΔBAC::*attB* by conjugation mediated by WM3064 (Dehio and Meyer, 1997), The expression levels of report gene in transformants were detected by Luciferase Assay System of Promega Corporation. Briefly, 20 µl cell lysates prepared according the instruction were mixed with 100 µl of Luciferase Assay Reagent, and the light produced by the mixture was quantified by GloMaxTM 96 Microplate Luminometer of Promega Corporation.

Reconstruction of disorazol gene cluster

Cloning vector BAC-cm flanked with *Pac*I/*Hpa*I sites and homology arms was amplified by PCR from plasmid pBeloBAC11 (digested with *Bam*HI and *Hin*dIII) using primers bac-dis-F/R. The products of PCR and plasmid p15A-dis (Tu et al., 2016) linearized with *Xba*I were electroporated into *E. coli* GB05-dir, which resulted in plasmid pBAC-cm-dis.

Plasmid p15A-genta-int-attP-Px-firefly was linearized with *Mfe*I, then cassette p15A-genta-int-attP-Px with homology arms was amplified by PCR using primers Px-dis-F/R. The PCR product and linearized plasmid pBAC-cm-dis (digested with *Pac*I and *Hpa*I) were assembled by LLHR mediated by GB05-dir, which resulted in plasmid p15A-genta-int-attP-Px-dis.

To construct plasmids with multiple promoters and improve the yield of disorazol, the strategy of RedEx was employed (Song et al., 2020). Breifly, plasmid p15A-genta-int-attP-P46-dis was electroporated into *E. coli* GB05-red-gyrA462, then the cassette 2P-amp-ccdB, dis (17985–18044)-*Pac*I-amp-ccdB-*Pac*I-dis (18015–18044)-P44-dis (18053–18110; the first nucleotide of *disA* was designated as 1), generated by fusion PCR was electroporated into *E. coli* GB-red-gyrA462 with plasmid p15A-genta-int-attP-P46-dis. The cassette 2P-amp-ccdB was inserted upstream of *disB* through LCHR mediated by recombinases Redα/Redβ which resulted in plasmid p15A-genta-int-attP-2P-dis-amp-ccdB. The plasmid p15A-genta-int-attP-2P-dis-amp-ccdB was digested with *Pme*I, and 100 ng linearized plasmid DNA was treated with 0.2 U T4pol (New England BioLabs) in a 20 µl reaction at 25°C for 30 min, 75°C for 20 min, 50°C for 20 min and then held at 4°C in a thermocycler. The reaction mixture was electroporated into *E. coli* GB2005 cells after desalting treatment. The recombinant p15A-genta-int-attP-2P-dis (2 promoters) with promoter P44 inserting upstream *disB* was identified with *Kpn*I/*Pme*I restriction analysis.

Utilizing the strategy of RedEX, promoter P17 was inserted upstream of gene *disC* and P46 was inserted upstream of gene *disD* successively, which resulted in plasmid p15A-genta-int-attP-3P-dis (3 promoters) and p15A-genta-int-attP-4P-dis (4 promoters), respectively.

Metabolite extraction, HPLC, and LC–MS analyses

Single colonies were inoculated into 2 ml Eppendorf tubes containing 1.8 ml LB broth supplemented with appropriate antibiotics and incubated at 37°C overnight with shaking at 900 rpm. The seed cultures (1%, v/v) were transferred into 50 ml M9 broth in 250 ml Erlenmeyer flask and incubated at 30°C with shaking at 200 rpm for 24 h before 2% XAD-16 resin was added, then the incubation was continued for another 48 h. The resin was collected by centrifugation and resuspended with 50 ml of methanol. The mixtures were shaken at 30°C, 200 rpm for 2 h. The methanol was removed by evaporation *in vacuo*, and residues were dissolved with 1 ml of methanol. After filtering with 0.22 µm membrane, the crude extracts were analyzed by UPLC-MS (UltiMate 3,000 UPLC system combined with Bruker amazon SL Ion Trap mass spectrometer). The C18 column (2.1 × 100 mm. 2.2 µm, Thermo) was utilized to analyze the crude extracts at a 0.3 ml/min flow rate using the following program:

0–3 min 5% solvent B; 3–22 min, 5 95% with linear gradient; then, 22–25 min, 5% solvent B (Solvent A, Milli Q water supplemented with 0.1% formic acid; Solvent B, acetonitrile supplemented with 0.1% formic acid). Mass spectra were acquired in positive ion mode.

Isolation of disorazol F_2 (1)

The crude extract from 10 L culture of E264ΔBAC::Ptet/*dis* was fractionated with Sephadex LH-20 column (GE Healthcare) chromatography using MeOH as a mobile phase. Fractions containing F_2 (**1**) were combined and further purified by semipreparative reverse-phase HPLC (Agilent ZORBAX SB-C18 column, 250 × 9.4 mm, 5 μm; gradient elution 0–2 min, 64% ACN; 2–17 min, 64–90% ACN; 17–22 min, 95% ACN, 22–25 min, 64% ACN; 2.5 ml/min). Finally, 1.5 mg of disorazol F_2 (**1**) was obtained with retention time at 15.1 min.

Quantitative analysis of disorazol F_2 (1)

The standard curve of disorazol F_2 (**1**) was established by measuring the area of absorption spectrum at UV 280 nm containing 0.05, 0.1, 0.2, 0.5 and 1.0 mg/ml disorazol F_2 (**1**). The yield of disorazol F_2 (**1**) was determined by reference to the standard curve.

Data availability statement

The datasets presented in this study can be found in online repositories. The accession number for the RNA-Seq data in this paper is GEO: PRJNA889572.

Author contributions

XX, XB, YZ, and Z-JW: designed research. XX, Z-JW and XL: performed research. HZ, YL, LZ, XW, QT, LH, FY, LG, RM, XB, and YZ: analyzed data. Z-JW, XX, HZ, and XB: wrote the paper. All authors contributed to the article and approved the submitted version.

Funding

This work was supported by the National Key R&D Program of China (2021YFC2100500, 2019YFA0905700, 2019YFA09004000), the National Natural Science Foundation of China (32161133013, 32070060, 32100052, and 32170038), the Shandong Provincial Natural Science Foundation of China (ZR2019JQ11, ZR2019ZD18, and ZR2019ZD30), the 111 project (B16030), Youth Interdisciplinary Innovative Research Group of SDU (2020QNQT009), and the China Postdoctoral Science Foundation (2020M682169).

Acknowledgments

The authors thank Haiyan Sui, Xiangmei Ren, Zhifeng Li, Jingyao Qu, and Jing Zhu of the State Key Laboratory of Microbial Technology of Shandong University for their help and guidance within NMR, LC, and HPLC-HRMS.

Conflict of interest

The authors declare that the research was conducted in the absence of any commercial or financial relationships that could be construed as a potential conflict of interest.

Publisher's note

Supplementary material

The Supplementary material for this article can be found online at: https://www.frontiersin.org/articles/10.3389/fmicb.2022.1073243/full#supplementary-material

References

Bader, C. D., Panter, F., and Müller, R. (2020). In depth natural product discovery—myxobacterial strains that provided multiple secondary metabolites. *Biotechnol. Adv.* 39:107480. doi: 10.1016/j.biotechadv.2019.107480

Barrett, A. R., Kang, Y., Inamasu, K. S., Son, M. S., Vukovich, J. M., and Hoang, T. T. (2008). Genetic tools for allelic replacement in *Burkholderia* species. *Appl. Environ. Microbiol.* 74, 4498–4508. doi: 10.1128/AEM.00531-08

Bian, X., Tang, B., Yu, Y., Tu, Q., Gross, F., Wang, H., et al. (2017). Heterologous production and yield improvement of epothilones in Burkholderiales strain DSM 7029. *ACS Chem. Biol.* 12, 1805–1812. doi: 10.1021/acschembio.7b00097

Biggins, J. B., Gleber, C. D., and Brady, S. F. (2011). Acyldepsipeptide HDAC inhibitor production induced in *Burkholderia thailandensis*. *Org. Lett.* 13, 1536–1539. doi: 10.1021/ol200225v

Biot, F. V., Lopez, M. M., Poyot, T., Neulat-Ripoll, F., Lignon, S., Caclard, A., et al. (2013). Interplay between three RND efflux pumps in doxycycline-selected strains of *Burkholderia thailandensis*. *PLoS One* 8:e84068. doi: 10.1371/journal.pone.0084068

Biot, F. V., Valade, E., Garnotel, E., Chevalier, J., Villard, C., Thibault, F. M., et al. (2011). Involvement of the efflux pumps in chloramphenicol selected strains of

Burkholderia thailandensis: proteomic and mechanistic evidence. *PLoS One* 6:e16892. doi: 10.1371/journal.pone.0016892

Brett, P. J., Deshazer, D., and Woods, D. E. (1998). *Burkholderia thailandensis* sp. nov., a *Burkholderia pseudomallei*-like species. *Int. J. Syst. Bacteriol.* 48 Pt 1, 317–320. doi: 10.1099/00207713-48-1-317

Carvalho, R., Reid, R., Viswanathan, N., Gramajo, H., and Julien, B. (2005). The biosynthetic genes for disorazoles, potent cytotoxic compounds that disrupt microtubule formation. *Gene* 359, 91–98. doi: 10.1016/j.gene.2005.06.003

Chang, K., Luo, J., Xu, H., Li, M., Zhang, F., Li, J., et al. (2017). Human infection with *Burkholderia thailandensis*, China, 2013. *Emerg. Infect. Dis.* 23, 1416–1418. doi: 10.3201/eid2308.170048

Dehio, C., and Meyer, M. (1997). Maintenance of broad-host-range incompatibility group P and group Q plasmids and transposition of Tn5 in *Bartonella henselae* following conjugal plasmid transfer from *Escherichia coli*. *J. bacteriol.* 179, 538–540. doi: 10.1128/jb.179.2.538-540.1997

Duerkop, B. A., Varga, J., Chandler, J. R., Peterson, S. B., Herman, J. P., Churchill, M. E. A., et al. (2009). Quorum-sensing control of antibiotic synthesis in *Burkholderia thailandensis*. *J. Bacteriol.* 191, 3909–3918. doi: 10.1128/JB.00200-09

Elnakady, Y. A., Sasse, F., Lunsdorf, H., and Reichenbach, H. (2004). Disorazol A1, a highly effective antimitotic agent acting on tubulin polymerization and inducing apoptosis in mammalian cells. *Biochem. Pharmacol.* 67, 927–935. doi: 10.1016/j.bcp.2003.10.029

Floss, H. G. (2006). Combinatorial biosynthesis-potential and problems. *J. Biotechnol.* 124, 242–257. doi: 10.1016/j.jbiotec.2005.12.001

Fu, J., Bian, X., Hu, S., Wang, H., Huang, F., Seibert, P. M., et al. (2012). Full-length rec E enhances linear-linear homologous recombination and facilitates direct cloning for bioprospecting. *Nat. Biotechnol.* 30, 440–446. doi: 10.1038/nbt.2183

Garcia, E. (2017). *Burkholderia thailandensis*: genetic manipulation. *Curr. Protoc. Microbiol.* 45:4C.2.1-4C.2.15. doi: 10.1002/cpmc.27

Glass, M. B., Gee, J. E., Steigerwalt, A. G., Cavuoti, D., Barton, T., Hardy, R. D., et al. (2006). Pneumonia and septicemia caused by *Burkholderia thailandensis* in the United States. *J. Clin. Microbio.* 44, 4601–4604. doi: 10.1128/jcm.01585-06

Hopkins, C. D., and Wipf, P. (2009). Isolation, biology and chemistry of the disorazoles: new anti-cancer macrodiolides. *Nat. Prod. Rep.* 26, 585–601. doi: 10.1039/b813799b

Huo, L., Hug, J. J., Fu, C., Bian, X., Zhang, Y., and Müller, R. (2019). Heterologous expression of bacterial natural product biosynthetic pathways. *Nat. Prod. Rep.* 36, 1412–1436. doi: 10.1039/c8np00091c

Irschik, H., Jansen, R., Gerth, K., Hofle, G., and Reichenbach, H. (1995). Disorazol a, an efficient inhibitor of eukaryotic organisms isolated from myxobacteria. *J. Antibiot. (Tokyo)* 48, 31–35. doi: 10.7164/antibiotics.48.31

Jansen, R. (1994). Disorazoles, highly cytotoxic metabolites from the sorangicin-producing bacterium *Sorangium cellulosum*, strain So ce 12. *Liebigs. Ann. Chem.* 1994, 759–773. doi: 10.1002/jlac.199419940802

Kang, Y., Norris, M. H., Wilcox, B. A., Tuanyok, A., Keim, P. S., and Hoang, T. T. (2011). Knockout and pullout recombineering for naturally transformable *Burkholderia thailandensis* and *Burkholderia pseudomallei*. *Nat. Protoc.* 6, 1085–1104. doi: 10.1038/nprot.2011.346

Kopp, M., Irschik, H., Pradella, S., and Müller, R. (2005). Production of the tubulin destabilizer disorazol in *Sorangium cellulosum*: biosynthetic machinery and regulatory genes. *Chembiochem* 6, 1277–1286. doi: 10.1002/cbic.200400459

Kunakom, S., and Eustáquio, A. S. (2019). Burkholderia as a source of natural products. *J. Nat. Prod.* 82, 2018–2037. doi: 10.1021/acs.jnatprod.8b01068

Liu, J., Wang, X., Dai, G., Zhang, Y., and Bian, X. (2022). Microbial chassis engineering drives heterologous production of complex secondary metabolites. *Biotechnol. Adv.* 59:107966. doi: 10.1016/j.biotechadv.2022.107966

Liu, Y., Zhou, H., Shen, Q., Dai, G., Yan, F., Li, X., et al. (2021). Discovery of polycyclic macrolide shuangdaolides by heterologous expression of a cryptic *trans*-AT PKS gene cluster. *Org. Lett.* 23, 6967–6971. doi: 10.1021/acs.orglett.1c02589

Liu, J., Zhou, H., Yang, Z., Wang, X., Chen, H., Zhong, L., et al. (2021). Rational construction of genome-reduced *Burkholderiales chassis* facilitates efficient heterologous production of natural products from proteobacteria. *Nat. Commun.* 12:4347. doi: 10.1038/s41467-021-24645-0

Mao, D., Bushin, L. B., Moon, K., Wu, Y., and Seyedsayamdost, M. R. (2017). Discovery of scm R as a global regulator of secondary metabolism and virulence in *Burkholderia thailandensis* E264. *Proc. Natl. Acad. Sci. U. S. A.* 114, E2920–e2928. doi: 10.1073/pnas.1619529114

Menchon, G., Prota, A. E., Lucena-Agell, D., Bucher, P., Jansen, R., Irschik, H., et al. (2018). A fluorescence anisotropy assay to discover and characterize ligands targeting the maytansine site of tubulin. *Nat. Commun.* 9:2106. doi: 10.1038/s41467-018-04535-8

Newman, D. J., and Cragg, G. M. (2020). Natural products as sources of new drugs over the nearly four decades from 01/1981 to 09/2019. *J. Nat. Prod.* 83, 770–803. doi: 10.1021/acs.jnatprod.9b01285

Nguyen, T., Ishida, K., Jenke-Kodama, H., Dittmann, E., Gurgui, C., Hochmuth, T., et al. (2008). Exploiting the mosaic structure of trans-acyltransferase polyketide synthases for natural product discovery and pathway dissection. *Nat. Biotechnol.* 26, 225–233. doi: 10.1038/nbt1379

Ouyang, Q., Wang, X., Zhang, N., Zhong, L., Liu, J., Ding, X., et al. (2020). Promoter screening facilitates heterologous production of complex secondary metabolites in Burkholderiales strains. *ACS Synth. Biol.* 9, 457–460. doi: 10.1021/acssynbio.9b00459

Pace, N. R. (1997). A molecular view of microbial diversity and the biosphere. *Science* 276, 734–740. doi: 10.1126/science.276.5313.734

Paoli, L., Ruscheweyh, H.-J., Forneris, C. C., Hubrich, F., Kautsar, S., Bhushan, A., et al. (2022). Biosynthetic potential of the global ocean microbiome. *Nature* 607, 111–118. doi: 10.1038/s41586-022-04862-3

Partida-Martinez, L. P., and Hertweck, C. (2007). A gene cluster encoding rhizoxin biosynthesis in "*Burkholderia rhizoxina*", the bacterial endosymbiont of the fungus *Rhizopus microsporus*. *Chembiochem.* 8, 41–45. doi: 10.1002/cbic.200600393

Seyedsayamdost, M. R., Chandler, J. R., Blodgett, J. A. V., Lima, P. S., Duerkop, B. A., Oinuma, K.-I., et al. (2010). Quorum-sensing-regulated bactobolin production by *Burkholderia thailandensis* E264. *Org. Lett.* 12, 716–719. doi: 10.1021/ol902751x

Song, C., Luan, J., Li, R., Jiang, C., and Wang, H. (2020). RedEx: a method for seamless DNA insertion and deletion in large multimodular polyketide synthase gene clusters. *Nucleic Acids Res.* 48:e130. doi: 10.1093/nar/gkaa956

Tang, B., Yu, Y., Liang, J., Zhang, Y., Bian, X., Zhi, X., et al. (2019). Reclassification of '*Polyangium brachysporum*' DSM 7029 as *Schlegelella brevitalea* sp. nov. *Int. J. Syst. Evol. Microbiol.* 69, 2877–2883. doi: 10.1099/ijsem.0.003571

Tu, Q., Herrmann, J., Hu, S., Raju, R., Bian, X., Zhang, Y., et al. (2016). Genetic engineering and heterologous expression of the disorazol biosynthetic gene cluster via red/ET recombineering. *Sci. Rep-UK* 6:21066. doi: 10.1038/srep21066

Wang, H., Li, Z., Jia, R., Yin, J., Li, A., Xia, L., et al. (2018). ExoCET: exonuclease *in vitro* assembly combined with RecET recombination for highly efficient direct DNA cloning from complex genomes. *Nucleic Acids Res.* 46:e28. doi: 10.1093/nar/gkx1249

Wang, Z. J., Zhou, H., Zhong, G., Huo, L., Tang, Y. J., Zhang, Y., et al. (2020). Genome mining and biosynthesis of primary amine-acylated desferrioxamines in a marine gliding bacterium. *Org. Lett.* 22, 939–943. doi: 10.1021/acs.orglett.9b04490

Weissman, K. J., and Müller, R. (2010). Myxobacterial secondary metabolites: bioactivities and modes-of-action. *Nat. Prod. Rep.* 27, 1276–1295. doi: 10.1039/c001260m

Yan, F., Auerbach, D., Chai, Y., Keller, L., Tu, Q., Hüttel, S., et al. (2018). Biosynthesis and heterologous production of vioprolides: rational biosynthetic engineering and unprecedented 4-methylazetidinecarboxylic acid formation. *Angew. Chem. Int. Ed. Engl.* 57, 8754–8759. doi: 10.1002/anie.201802479

Yu, Y., Wang, H., Tang, B., Liang, J., Zhang, L., Wang, H., et al. (2020). Reassembly of the biosynthetic gene cluster enables high epothilone yield in engineered *Schlegelella brevitalea*. *ACS Syn. Bio.* 9, 2009–2022. doi: 10.1021/acssynbio.0c00100

Zhang, Y., Buchholz, F., Muyrers, J. P., and Stewart, A. F. (1998). A new logic for DNA engineering using recombination in *Escherichia coli*. *Nat. Genet.* 20, 123–128. doi: 10.1038/2417

frontiers | Frontiers in Microbiology

TYPE Original Research
PUBLISHED 25 November 2022
DOI 10.3389/fmicb.2022.1078293

OPEN ACCESS

EDITED BY
Dewu Zhang,
Chinese Academy of Medical Sciences, China

REVIEWED BY
Guoqing Niu,
Southwest University, China
Chin-Yuan Chang,
National Chiao Tung University, Taiwan

*CORRESPONDENCE
Keqiang Fan
fankq@im.ac.cn

SPECIALTY SECTION
This article was submitted to Microbial Physiology and Metabolism, a section of the journal Frontiers in Microbiology

RECEIVED 24 October 2022
ACCEPTED 07 November 2022
PUBLISHED 25 November 2022

CITATION
Zhang C, Zhao Y, Li Z, Wang W, Huang Y, Pan G and Fan K (2022) Molecular mechanism of GylR-mediated regulation of glycerol metabolism in *Streptomyces clavuligerus* NRRL 3585. *Front. Microbiol.* 13:1078293. doi: 10.3389/fmicb.2022.1078293

Molecular mechanism of GylR-mediated regulation of glycerol metabolism in *Streptomyces clavuligerus* NRRL 3585

Chaobo Zhang[1,2], Youbao Zhao[1], Zilong Li[1], Weishan Wang[1,2], Ying Huang[1,2], Guohui Pan[1,2] and Keqiang Fan[1]*

[1]State Key Laboratory of Microbial Resources, Institute of Microbiology, Chinese Academy of Sciences, Beijing, China, [2]University of Chinese Academy of Sciences, Beijing, China

Glycerol is a readily available and low-cost simple polyol compound, which can be used as a carbon source for microorganisms to produce various value-added products. Understanding the underlying regulatory mechanism in glycerol metabolism is critical for making better use of glycerol for diverse applications. In a few reported *Streptomyces* strains, the glycerol utilization gene cluster (*glp* operon) was shown to be regulated by the IclR family transcriptional regulator GylR. However, the molecular regulatory mechanism mediated by GylR has not been fully elucidated. In this study, we first analyzed the available *Actinobacteria* genomes in the NCBI Genome database, and found that the *glp* operon-like gene clusters are conserved in *Streptomyces* and several other genera of *Actinobacteria*. By taking *Streptomyces clavuligerus* NRRL 3585 as a model system, we identified that GylR represses the expressions of *glp* operon and *gylR* by directly binding to their promoter regions. Both glycerol-3-phosphate and dihydroxyacetone phosphate can induce the dissociation of GylR from its binding sequences. Furthermore, we identified a minimal essential operator site (a palindromic 18-bp sequence) of GylR-like regulators in *Streptomyces*. Our study for the first time reported the binding sequences and effector molecules of GylR-like proteins in *Streptomyces*. The molecular regulatory mechanism mediated by GylR presumably exists widely in *Streptomyces*. Our findings would facilitate the design of glycerol utilization pathways for producing valuable products. Moreover, our study provided new basic elements for the development of glycerol-inducible regulatory tools for synthetic biology research in the future.

KEYWORDS

glycerol, metabolism, regulatory mechanism, sequence motif, *Streptomyces*, *Actinobacteria*

Introduction

Glycerol is a simple polyol compound existing widely in biological systems (Klein et al., 2017; Doi, 2019). In addition, glycerol is the main by-product of biodiesel production (da Silva et al., 2009; Poblete-Castro et al., 2020). These facts make glycerol as a relatively cheap and readily available substance. Glycerol has a number of industrial applications. It has been widely used in cosmetics and food industry due to its hygroscopic and other properties (Doi, 2019; Poblete-Castro et al., 2020). Furthermore, glycerol is an important substrate in biological industries as it can be converted into various value-added products, such as pharmaceuticals, resins, detergents, plastics and tobacco (Pagliaro et al., 2007; Poblete-Castro et al., 2020). In bacteria, glycerol can be metabolized mainly through two routes (Lin, 1976; Doi, 2019; Poblete-Castro et al., 2020). The first route involves the phosphorylation of glycerol to form glycerol-3-phosphate (G3P), and the subsequent oxidation of G3P to generate dihydroxyacetone phosphate (DHAP). In the other route, glycerol is firstly oxidized to dihydroxyacetone, which is then phosphorylated to afford DHAP. DHAP can be further channeled to downstream metabolic pathways like the glycolysis pathway. Thus it can be seen that glycerol can serve as a common precursor to biosynthesize various products. Usually, the genes encoding the enzymes for conversion of glycerol to DHAP are tightly controlled by different types of transcriptional regulators (Lin, 1976; Hindle and Smith, 1994; Bong et al., 2019; Poblete-Castro et al., 2020). Understanding the molecular regulatory mechanism of glycerol metabolism is critical for better use of glycerol to produce valuable products.

Streptomycetes are Gram-positive filamentous soil bacteria and are well known as prolific producers of a wide variety of natural products, including many antibacterial, anticancer, and immunosuppressive drugs (Kormanec et al., 2019; Lee et al., 2021). Glycerol can be used as a carbon source by streptomycetes to produce those valuable products, such as the clinically used beta-lactamase inhibitor clavulanic acid produced by *Streptomyces clavuligerus* NRRL 3585 (Saudagar et al., 2008; Guo et al., 2013; Shin et al., 2021). Until now, studies on the glycerol metabolism in streptomycetes have only been reported for *Streptomyces coelicolor* A3(2) (Smith and Chater, 1988a,b; Hindle and Smith, 1994; Lee et al., 2017) and *S. clavuligerus* NRRL 3585 (Baños et al., 2009), both of which contain a glycerol utilization gene cluster. In *S. coelicolor* A3(2), the glycerol utilization gene cluster consists of *gylR* and *gylCAB*, in which *gylCAB* corresponds to the *glp* operon (*glpF1K1D1*) in *S. clavuligerus* NRRL 3585 (Smith and Chater, 1988a,b; Baños et al., 2009). The three key glycerol utilization genes (*gylC/glpF1*, *gylA/glpK1*, and *gylB/glpD1*) encode a glycerol transporter, a glycerol kinase, and a FAD-dependent glycerol-3-phosphate dehydrogenase, respectively (Figure 1). Specifically, the transmembrane protein GylC/GlpF1 facilitates the uptake of glycerol into the cells, and then intracellular glycerol is phosphorylated by the kinase GylA/GlpK1 to form G3P, which is subsequently oxidized by the dehydrogenase GylB/GlpD1 to afford DHAP (Figure 1; Baños et al., 2009). Studies in *S. coelicolor* A3(2) suggested that GylR negatively regulates the transcription of the *glp* operon. G3P was proposed to be a true effector molecule of GylR, but there is a lack of experimental evidence (Seno and Chater, 1983; Seno et al., 1984). In *S. clavuligerus* NRRL 3585, similar results were observed. The *glp* operon is negatively regulated by GylR. As a member of the IclR family transcriptional regulators, GylR can directly bind to the promoter region of *glp* operon (Figure 1; Baños et al., 2009). *In vivo* studies have revealed that the expression of *glp* operon can be induced by the addition of glycerol during fermentation (Baños et al., 2009; Guo et al., 2013). Studies in non-*Streptomyces* strains, such as *Mycolicibacterium smegmatis* (previously known as *Mycobacterium smegmatis*), indicated that G3P rather than glycerol might bind to GylR-like proteins, and, as a result, regulate the *glp* operon (Bong et al., 2019). Despite the aforementioned studies, the exact binding sequences and the small molecule effectors of GylR-like proteins remain elusive in *Streptomyces*.

In this study, we first carried out a systematic bioinformatic analysis, which revealed that the *glp* operon is highly conserved in *Streptomyces* genomes, and the *glp* operon-like glycerol utilization gene clusters (minimally containing one set of clustered *glpF*, *glpK*, and *glpD* homologous genes) are present in many genera of the phylum *Actinobacteria*. The results implied a common metabolic pathway of glycerol in *Streptomyces*. Then, we took *S. clavuligerus* NRRL 3585 as a model system to further investigate the molecular mechanism of GylR-mediated regulation of glycerol metabolism. Our results showed that GylR negatively regulates the transcriptions of *gylR* and *glp* operon by directly binding to their promoter regions, and the exact binding sequences were identified to contain a conserved 18-bp sequence motif. In addition to G3P, DHAP was found to be another effector molecule that could cause the dissociation of GylR from its binding sequences. Our study for the first time identified the binding sequences and effector molecules of GylR-like proteins in *Streptomyces*, which further elucidated the molecular mechanism of GylR-mediated regulation of glycerol metabolism. The results would facilitate the design of glycerol utilization pathways, and provide valuable regulatory elements for synthetic biology research.

Materials and methods

Strains, plasmids, primers, and growth conditions

Bacterial strains and plasmids used in this study are listed in Supplementary Table 1 in the Supplementary material. Primers in this study are listed in Supplementary Table 2. *Escherichia coli* DH5α was used as a general host for propagating plasmids. *E. coli* ET12567 (pUZ8002) (Kieser et al., 2000) was used as a host for transferring DNA from *E. coli* to *Streptomyces* in intergeneric conjugation experiments. *E. coli* Rosetta (DE3) was used as a host for production of GylR protein. *S. clavuligerus* NRRL 3585 and its derived strains were grown on yeast extract-dextrose (YD) agar

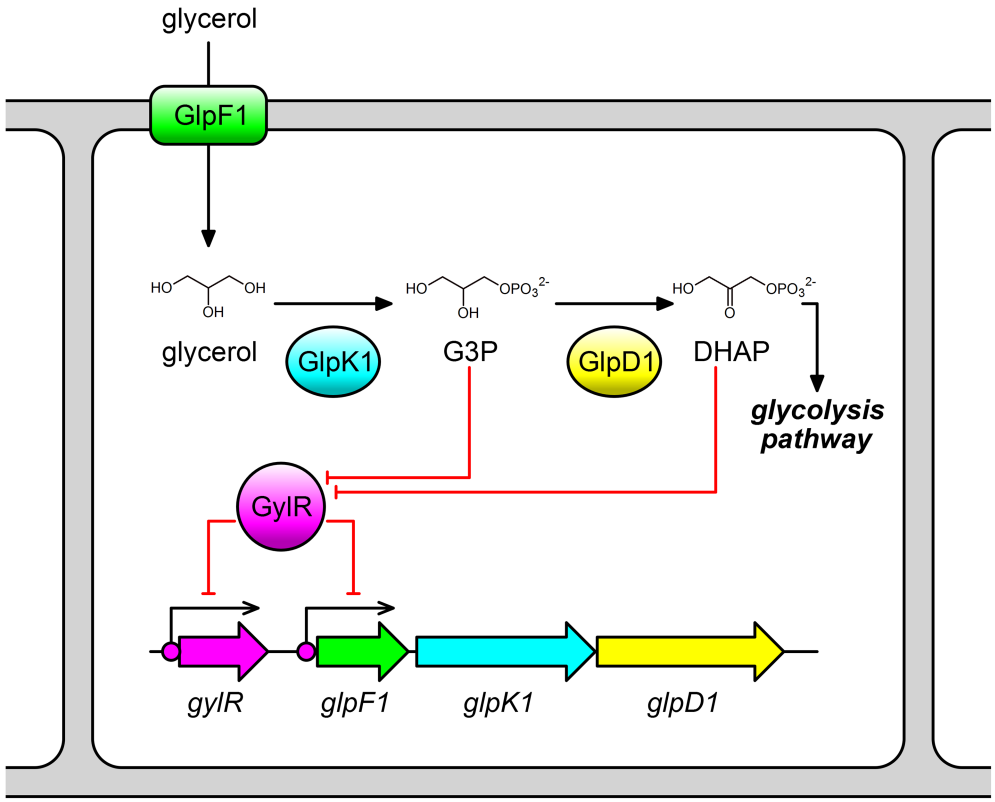

FIGURE 1
Schematic representation of GylR-mediated regulation on glycerol metabolism in *Streptomyces clavuligerus* NRRL 3585. The *glp* operon consisting of *glpF1*, *glpK1*, and *glpD1*, is negatively regulated by GylR. G3P and DHAP act as effector molecules that can bind to GylR and induce the dissociation of GylR from its binding sites. G3P, glycerol-3-phosphate; DHAP, dihydroxyacetone phosphate.

medium at 28°C (Xiang et al., 2009). The SA medium used for fermentation and RNA extraction is composed of 10 g/l soluble starch, 2 g/l L-asparagine, 21 g/l MOPS, 0.6 g/l $MgSO_4{\cdot}7H_2O$, and 0.1% (v/v) trace element solution ($FeSO_4{\cdot}7H_2O$, 1 mg/ml; $MnCl_2{\cdot}H_2O$, 1 mg/ml; $ZnSO_4{\cdot}7H_2O$, 1 mg/ml; $CaCl_2{\cdot}2H_2O$, 1.3 mg/ml; Guo et al., 2013). Antibiotics were used at the following concentrations unless otherwise specified: apramycin, 100 μg/ml; kanamycin, 50 μg/ml; chloramphenicol, 12.5 μg/ml; nalidixic acid, 25 μg/ml. General procedures for *E. coli* and *Streptomyces* manipulations were performed according to the standard protocols (Kieser et al., 2000).

Bioinformatic analyses

The completed genomes of the phylum *Actinobacteria* were downloaded from the NCBI Genome database (as of September 2022). The *glpF*, *glpK*, *glpD*, and *gylR* homologs were identified using standalone BLASTP program (Camacho et al., 2009) with the previously reported glycerol utilization genes in *S. clavuligerus* NRRL 3585 as query sequences (Baños et al., 2009). Protein sequence comparison was performed using EMBOSS 6.5.0 (Rice et al., 2000). DNA motif search and the data analysis were preformed using Python scripts. The conserved sequence motif logo was generated using MEME Suite 5.5.0 (Bailey et al., 2006). The information of all the identified homologs, including their GenBank accession numbers and sequences, was provided in Supplementary Sheet 1. The information of all the clustered homologs was provided in Supplementary Sheet 2. The information of all the DNA sequences corresponding to the conserved 18-bp sequence motif was provided in Supplementary Sheet 3.

Construction of the mutant strain *Streptomyces clavuligerus ΔgylR*

To construct a plasmid for inactivation of *gylR*, a 1,461-bp upstream DNA fragment was amplified with primers gylR-U-F and gylR-U-R, and a 1,469-bp downstream DNA fragment was amplified with primers gylR-D-F and gylR-D-R, using *S. clavuligerus* NRRL 3585 genomic DNA as the template. After digestion with appropriate enzymes (*Eco*RI and *Bam*HI for upstream fragment, *Bam*HI and *Hin*dIII for downstream fragment), the two fragments were inserted into *Eco*RI/*Hin*dIII-digested pKC1139 to generate pKC1139-gylR, which was verified

by DNA sequencing. The plasmid pKC1139-gylR was transformed into *E. coli* ET12567 (pUZ8002) and then introduced into *S. clavuligerus* NRRL 3585 by intergeneric conjugation. After several rounds of passaging the exconjugants on solid YD medium, apramycin sensitive colonies were screened by PCR using primers gylR-del-F and gylR-del-R to obtain the double-crossover mutants Δ*gylR* (Supplementary Figure 1).

RNA extraction and quantitative reverse transcription PCR

The transcriptional levels of the analyzed genes in *S. clavuligerus* NRRL 3585 and Δ*gylR* mutant strains were evaluated by quantitative reverse transcription PCR (RT-qPCR). Total RNAs were isolated from the cultures grown in SA media without or with 163 mM glycerol at 24 h as in previous studies (Baños et al., 2009; Guo et al., 2013). The RNA samples were treated with RQ1 RNase-free DNase (Promega) to remove genomic DNA. Synthesis of cDNA and subsequent RT-qPCR were performed according to the standard methods (Li et al., 2015), and transcription of the *hrdB* gene was used as the internal control.

Promoter activity assay

The green fluorescent protein (GFP) gene was amplified by PCR from pIJ-Potr using primer pair GFP-F and GFP-R (Wang et al., 2016). The PCR product was digested with *Spe*I and *Eco*RI, and then inserted into the corresponding sites of the integrative plasmid pSET152 to generate pSET152-GFP. The promoter region of *glp* operon (P*glp*) was amplified with primer pair Pglp-F and Pglp-R using *S. clavuligerus* NRRL 3585 genomic DNA as the template. The PCR product was digested with *Bam*HI and *Spe*I, and then inserted into pSET152-GFP. The resultant plasmid pSET152-Pglp-GFP was introduced into *S. clavuligerus* NRRL 3585 and Δ*gylR* mutant strains through conjugation to obtain WT-Pglp-GFP and Δ*gylR*-Pglp-GFP, respectively. As a control, the plasmid pSET152-GFP was transformed into *S. clavuligerus* NRRL 3585 to generate the recombinant strain WT-GFP. The above recombinant strains were cultivated in SA medium for 12 h. Then, 200 μl of cell culture was washed twice with pure water, and transferred into 96-well plates. The fluorescence intensities were recorded using a Synergy™ HT Multi-Mode Microplate Reader with an excitation at 489 nm and an emission at 512 nm for analysis. Pure water was used as a blank control. The biomass of *S. clavuligerus* strains were detected by the simplified diphenylamine colorimetric method (Zhao et al., 2013).

Overproduction and purification of GylR

The coding region of *gylR* was amplified by PCR from *S. clavuligerus* NRRL 3585 genomic DNA using primer pair gylR-F and gylR-R. The PCR product was digested with *Nde*I and *Xho*I and then inserted into the corresponding sites of pET-30a. The resultant plasmid pET30a-gylR was verified by DNA sequencing and subsequently introduced into *E. coli* Rosetta (DE3) for production of GylR. The *E. coli* Rosetta (DE3) harboring pET30a-gylR was cultured in LB supplemented with 50 μg/ml kanamycin at 37°C and 250 rpm until an OD_{600} of 0.6 was reached, at which time point 0.1 mM isopropyl-β-D-thiogalactopyranoside (IPTG) was added, and the strain culture was allowed to incubate at 30°C for 4 h. The cells were harvested, and resuspended in lysis buffer (20 mM Tris–HCl, pH 8.0, 500 mM NaCl, 5 mM imidazole, and 10% sorbitol).

The C-terminal His_6-tagged GylR was purified using nickel-nitrilotriacetic acid (Ni-NTA) agarose chromatography according to the manufacturer's protocol (Novagen) with glycerol in all the buffers being substituted by sorbitol. Of note, the elution buffer used for the purification of GylR contained 500 mM imidazole and 10% (w/v) sorbitol. As purified GylR was unstable and lost activity quickly, we used freshly purified GylR in all the assays in this study. The protein concentration was determined by using a bicinchoninic acid (BCA) protein assay kit (Novagen).

Size-exclusion chromatography assays

The polymerization state of GylR was analyzed by size-exclusion chromatography on a Shimadzu Prominence HPLC system using TSKgel G3000 SWxl column (7.8 × 300 mm, TOSOH Inc.) with an elution solvent of 0.1 M Na_2SO_4 (pH 6.7) and a flow rate of 0.5 ml/min as described previously (Pan et al., 2017). Bovine serum albumin, ovalbumin, and AlpJ were used as molecular weight standards.

Electrophoretic mobility shift assays

The electrophoretic mobility shift assays (EMSAs) were performed according to the protocol described previously (Wang et al., 2009). The DNA probes BS1 (upstream region of the coding sequence of *gylR*) and BS2 (upstream region of the coding sequence of *glpF1*) were amplified from *S. clavuligerus* NRRL 3585 genomic DNA with primer pairs BS1-F/BS1-R, and BS2-F/BS2-R, respectively. Other DNA probes were synthesized by Invitrogen. A typical 20 μl reaction mixture consisted of 10 ng/μl DNA probe, GylR (various concentrations), small molecules (glycerol or G3P or DHAP with different concentrations), 50 mM HEPES (pH 7.5), 1 mM dithiothreitol (DTT), 5 mM $MgCl_2$, 0.2 mg/ml bovine serum albumin (BSA), 2 mM EDTA and 5% sorbitol. After incubation at 25°C for 25 min, protein-bound DNA and free DNA were separated by electrophoresis on nondenaturing 6.0% (w/v) polyacrylamide gels with a running buffer (pH 7.5) containing 200 mM HEPES and 4 mM EDTA. Gels were stained with SYBR Gold. The concentrations of DNA probes were determined with a NanoVue Plus spectrophotometer.

DNase I footprinting assay

In order to determine the binding sites of GylR, labeled BS1 and BS2 probes were amplified by PCR with primer pairs FAM-gylR/HEX-gylR and FAM-glpF1/HEX-glpF1, respectively. A typical 50 µl reaction mixture contained 200 ng FAM/HEX-labeled DNA probe, 0–40 ng/µl GylR, 100 mM KCl, 20 mM HEPES (pH 7.5), 2 mM DTT, 5 mM $MgCl_2$, 0.5 mg/ml BSA, and 5% sorbitol. After incubation at 25°C for 25 min, 5.5 µl RQ1 RNase-free DNase I buffer and 0.375 U DNase I were added. The mixture was incubated at 25°C for an additional 80 s. Then, the reaction was stopped by addition of 10 µl stop solution (20 mM EGTA, pH 8.0) and 100 µl phenol-chloroform (1:1, v/v). Samples were analyzed by Genolab Biotech Co., Ltd.

Rapid amplification of 5′ cDNA ends (5′-RACE)

The transcription start points (tsp) of *gylR*, and *glp* operon were determined by using a FirstChoice RLM-RACE kit (Ambion) following the manufacturer's instructions. Total RNAs from *S. clavuligerus* NRRL 3585 were prepared as described above (Guo et al., 2013). Total RNAs (10 ng) were successively treated with calf intestine alkaline phosphatase (CIP), tobacco acid pyrophosphatase (TAP) and ligated with a 45-base 5′-RACE adapter at the 5′-end using T4 RNA ligase. Reverse transcription was performed using SuperScript III reverse transcriptase with the supplement of random decamers. PCR was first performed using a 5'-RACE outer primer and gene-specific outer primer with *Q5* DNA polymerase (New England Biolabs). This PCR product was used as the template of inner PCR using a 5′-RACE inner primer and a gene-specific inner primer. A 25 µl volume of each PCR reaction mixture was analyzed by 2% agarose gel electrophoresis. The product of inner PCR was sent for sequencing after gel purification.

Results

The distribution of *glp* operon-like glycerol utilization gene clusters in *Actinobacteria*

Previous studies strongly suggested that *glp* operon probably serves as a general pathway in glycerol metabolism in *Streptomyces* strains (Smith and Chater, 1988b; Hindle and Smith, 1994; Baños et al., 2009). Indeed, we found that the *glp* operon accompanied by *gylR* is highly conserved in the genus *Streptomyces*, as 441 out of 458 completed genomes of *Streptomyces* in the NCBI Genome database (as of Sep. 2022) each harbor a *glp* operon with an adjacent *gylR* homologous gene (Figure 2; Supplementary Sheets 1, 2). This encouraged us to further analyze the distribution of *glp* operon-like gene clusters (minimally containing one set of clustered *glpF*, *glpK*, and *glpD* homologous genes) in other genera of the phylum *Actinobacteria*. Therefore, we performed a systematic analysis of the remaining 3,112 completed genomes of *Actinobacteria* available in the NCBI Genome database (as of Sep. 2022). The *glpF*, *glpK*, *glpD*, and *gylR* homologous genes identified in each of the *Actinobacteria* genomes were shown in Supplementary Sheet 1. Overall, 1,517 out of 3,570 genomes each contain at least one set of *glpF*, *glpK*, and *glpD* homologous genes (not necessarily clustered). The bioinformatic analysis showed that the *glp* operon-like gene clusters often exist in *Kitasatospora* and *Streptacidiphilus*, the other two genera of the family Streptomycetaceae (Figure 2; Supplementary Sheet 2). In several genera of the family Pseudonocardiaceae, including *Saccharopolyspora*, *Saccharothrix*, *Saccharopolyspora*, *Actinoalloteichus*, and *Amycolatopsis*, almost every genome of them contains a gene cluster consisting of *glpFK* homologous genes, and an upstream *glpD* homolog (transcribed in the opposite direction). However, no *gylR* homolog was found around those gene clusters. Interestingly, over half of the *Amycolatopsis* genomes also contain another gene cluster. In each of these gene clusters, a *gylR* homolog and another *glpK* homolog are present upstream of the *glpFKD* homologous genes. Such a gene cluster is present in most of the genomes of *Pseudonocardia*, *Actinoplanes*, and *Actinomadura*. In the majority of *Nocardiopsis* genomes, a *gylR* homolog and *glpKFD* homologous genes were found clustered together. In most genomes of *Brevibacterium*, *Micrococcus*, *Rothia*, *Kocuria*, *Brachybacterium*, *Cellulomonas*, and *Cellulosimicrobium*, a gene cluster, in which a *glpD* homolog is located upstream of the *glpFK* homologous genes, was identified without *gylR* homologs nearby. In some other genera, such as *Corynebacterium*, *Rhodococcus*, *Mycolicibacterium*, and *Nocardia*, *glp* operon-like gene clusters were found in less than 50% analyzed genomes (Supplementary Sheet 2). Surprisingly, in the analyzed genomes of *Mycobacterium*, the *glpF*, *glpK* and *glpD* homologous genes were all found to be standalone proteins. It is worth pointing out again that the strain previously called *Mycobacterium smegmatis* (harboring a *glp* operon-like gene cluster) was renamed *Mycolicibacterium smegmatis* based on the updated taxonomy system of NCBI.

Overall, the results showed that *glp* operon-like gene clusters are present in many genera of *Actinobacteria*, and these clusters are likely to play important roles in the glycerol metabolism in *Actinobacteria*. It is obvious that *Actinobacteria* strains have evolved diverse *glp* operon-like gene clusters, which might be beneficial to different host strains for utilizing glycerol.

GylR represses the expression of *glp* operon and *gylR* itself

The above bioinformatic analysis further supported that *glp* operon together with *gylR* serves as an important general pathway in glycerol metabolism of *Streptomyces*. Here, we took *S. clavuligerus* NRRL 3585 as a model strain to further investigate

10.3389/fmicb.2022.1078293

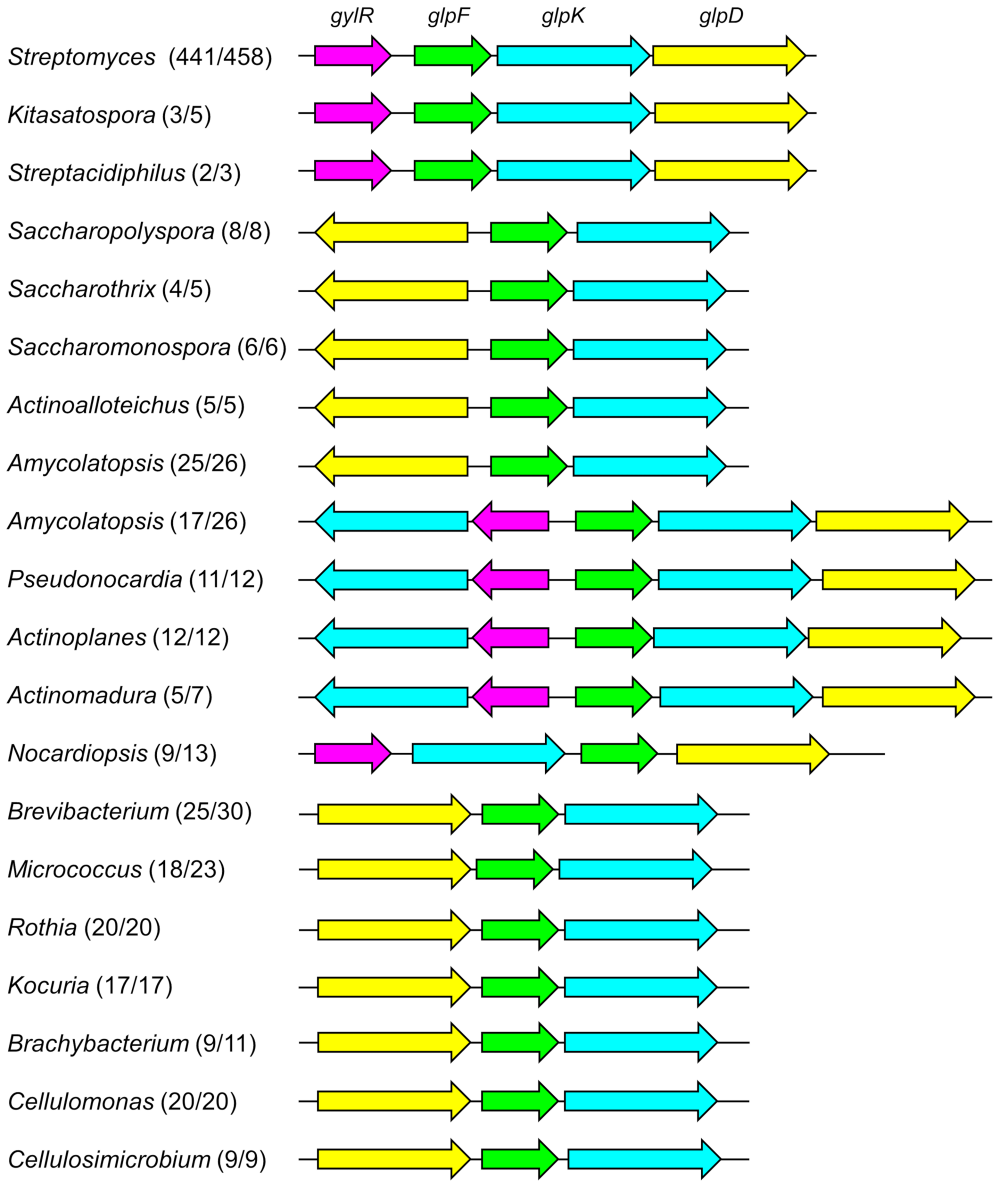

FIGURE 2
The distribution of *glp* operon-like gene clusters in analyzed genomes of the phylum *Actinobacteria*. The numbers after the name of each genus represented the frequency of *glp* operon-like gene clusters being identified, e.g., *Streptomyces* (441/458) denoted that 441 out 458 *Streptomyces* genomes each contains a *glp* operon-like gene cluster. The genera, in which less than 50% genomes harbor the *glp* operon-like gene clusters, were not included in this figure.

the molecular regulatory mechanism of GylR in glycerol metabolism. To better understand the regulatory role of GylR, we generated the mutant strain *S. clavuligerus* Δ*gylR* with a truncation in *gylR* gene (Supplementary Figure 1). For the wild-type (WT) strain NRRL 3585, the transcriptions of *glpF1, glpD1* and *glpK1* were at low levels at the absence of glycerol, while the addition of 163 mM glycerol to the SA medium significantly augmented the transcriptions of *glpF1, glpD1* and *glpK1* (Figure 3A). However, for the mutant strain Δ*gylR*, the transcriptions of the three genes were all at high levels with or without the addition of glycerol. In addition, we found that the transcription of *gylR* was also induced by glycerol in the WT strain, and the transcription of truncated *gylR* in Δ*gylR* was at a similarly high level regardless of whether glycerol was added or not (Figure 3A). These results showed that GylR is a repressor regulating the transcriptions of the *glp* operon, as well as *gylR* itself in *S. clavuligerus*, which was consistent with the previous reports in *S. clavuligerus* (Baños et al., 2009) and *S. coelicolor* (Smith and Chater, 1988b).

Furthermore, we analyzed the activity of P*glp* (a DNA fragment containing the promoter of *glp* operon) using green fluorescent protein (GFP) as a reporter. The reporter plasmid

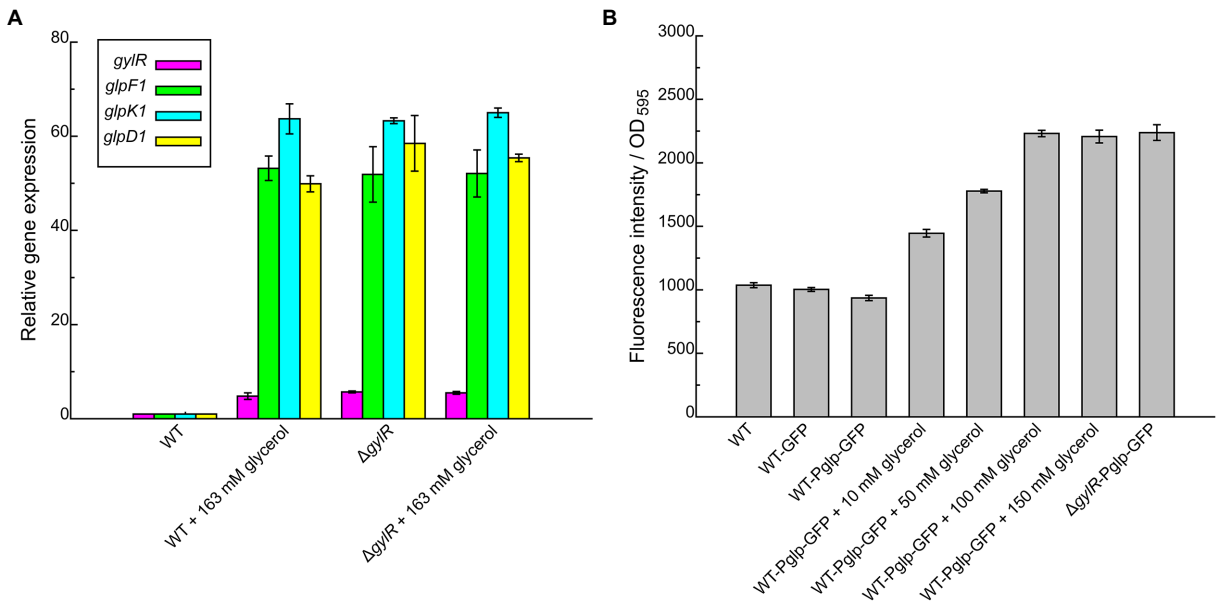

FIGURE 3
Transcriptional analysis of *gylR* and *glp* operon in *Streptomyces clavuligerus* NRRL 3585 and recombinant strains under different culture conditions. **(A)** RT-qPCR analysis of the transcriptional levels of *gylR*, *glpF1*, *glpK1*, and *glpD1* in *Streptomyces clavuligerus* NRRL 3585 (WT) and Δ*gylR* cultivated in SA medium or SA medium supplemented with 163mM glycerol. The *hrdB* gene (encoding the RNA polymerase principal sigma factor) was used as an internal control. The relative gene expression values in WT were arbitrarily assigned as 1. **(B)** Evaluation of the activities of *Pglp* (promoter region of *glp* operon) in WT and recombinant strains cultivated in SA medium or SA medium supplemented with different concentrations of glycerol. The fluorescence intensity of GFP and biomass (OD_{595}) were analyzed after 12h of cultivation. OD_{595} values were determined using the simplified diphenylamine colorimetric method (Zhao et al., 2013). Error bars represent standard deviations of three independent replicates.

pSET152-Pglp-GFP was constructed and transformed into the WT and Δ*gylR* strains, affording the recombinant strains WT-Pglp-GFP and Δ*gylR*-Pglp-GFP, respectively. A control plasmid pSET152-GFP was also constructed and transformed into WT to obtain the recombinant strain WT-GFP. We observed that, in comparison to that of WT-GFP, the transcription of *glp* operon in WT-Pglp-GFP was induced by glycerol in a concentration-dependent manner, and reached the maximum level when glycerol concentration was above 100 mM (Figure 3B). As expected, the transcription of *glp* operon in Δ*gylR*-Pglp-GFP was at a level comparable to the maximum level in the WT-Pglp-GFP strain induced by glycerol. These results further confirmed that GylR negatively regulates the expression of *glp* operon, and also implied that GylR serves as the main regulator of *glp* operon.

GylR directly binds to the promoter regions of *glp* operon and *gylR*

Although GylR was proposed to regulate the *glp* operon and *gylR* through binding to their promoter regions in *S. clavuligerus*, there is a lack of experimental evidences (Baños et al., 2009). We overproduced C-terminal His_6-tagged GylR in *E. coli* Rosetta (DE3) and purified it to homogeneity by Ni-NTA affinity chromatography (Supplementary Figure 2A). Size-exclusion chromatography analysis revealed that GylR forms a dimer under the tested conditions (Supplementary Figure 2B), which is reasonable as IclR family transcription factors typically bind to their target sequences as dimers or tetramers (Suvorova and Gelfand, 2021). Then, the electrophoretic mobility shift assay (EMSA) was carried out to determine the direct interactions between GylR and the promoter regions of *gylR* and *glp* operon. Two DNA fragments (BS1 and BS2) containing the promoters of *gylR* and *glp* operon, respectively, were used as DNA probes in the EMSA studies. As shown in Figures 4A,B, GylR could directly bind to both BS1 and BS2 in a concentration dependent manner. Together, the above results strongly supported that GylR negatively regulates the expression of *glp* operon and *gylR* through directly binding to their promoter regions.

Glycerol-3-phosphate and dihydroxyacetone phosphate are the effector molecules of GylR

To date, the effector molecules that could modulate the binding affinity of GylR to its target DNA regions have not been identified in streptomycetes. Previous preliminary studies in strains like *S. coelicolor* A3(2) and *Mycolicibacterium smegmatis* (Seno et al., 1984; Bong et al., 2019) inspired us to propose that the metabolites in the early stage of glycerol metabolic pathway might serve as the effector molecules of GylR in *S. clavuligerus* NRRL

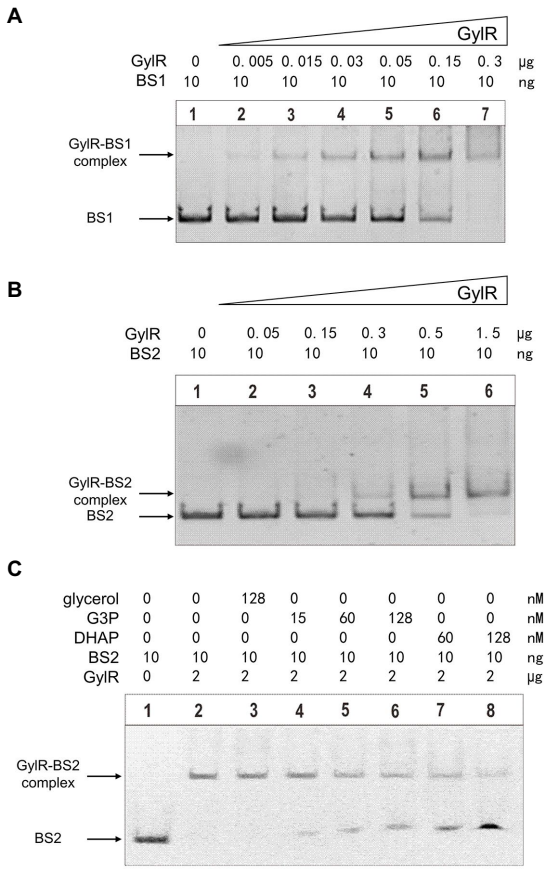

FIGURE 4
Binding of GylR to the promoter regions of *gylR* and *glp* operon, and identification of the effector molecules of GylR by EMSAs. **(A)** EMSAs of GylR binding to probe BS1 containing P*glp* (promoter of *glp* operon). **(B)** EMSAs of GylR binding to probe BS2 containing P*gyl* (promoter of *gylR*). **(C)** Effects of glycerol, G3P, and DHAP on GylR binding to BS2 by EMSAs.

3585. Therefore, we tested the effects of adding glycerol and its metabolites, G3P and DHAP, to the aforementioned EMSA reactions of GylR with the DNA probe BS2. The results showed that both G3P and DHAP were capable of inducing the dissociation of GylR from BS2, whereas glycerol could not induce the dissociation under tested conditions (Figure 4C). It is worth noting that DHAP was discovered for the first time as an effector molecule of GylR-like regulatory proteins.

Characterization of the binding sequences of GylR revealing a conserved sequence motif

To elucidate the exact binding sequences of GylR at the promoter regions of *gylR* and *glp* operon, DNase I footprinting experiments were carried out. The results revealed two protected regions including a region from position +11 to +57 (5′-TGGTCGACATCGACCAATGGTGTTCAGCATTGTCGAA TCGCAGTGGG-3′) relative to the transcription start point (tsp) of *gylR*, and the other region from position −17 to −63 (5′-AAACTGCCGTTCATCGGTCGGCATTGTCGAACACCTA CCGGAAATAC-3′) relative to the tsp. of the *glp* operon (Figure 5A). As shown in Figure 5B, the binding region upstream of *gylR* is located right after the −10 region of promoter P*gyl*, which implied that GylR represses *gylR* through impeding the transcription elongation. On the other side, the binding region upstream *glpF1* overlaps with the promoter P*glp*, suggesting that GylR inhibits the transcription of *glp* operon by hindering the binding of RNA polymerase to P*glp*.

Analysis of the two binding regions of GylR, and their homologous DNA regions upstream of *gylR* and *glpF1* homologs in representative *Streptomyces* strains including *S. coelicolor* A3(2), *Streptomyces albus* DSM 41398, and *Streptomyces avermitilis* MA-4680, suggested a relatively conserved 21-bp sequence region (5′-YGKTCRRCATTGYCGAAYVVS-3′; Figure 6A). Then, the corresponding 21-bp DNA probes were synthesized and tested in the EMSAs. The results showed that GylR could bind to all these 21-bp DNA probes (Figure 6A). To identify the minimal core DNA sequences that interact with GylR to form a complex, the 21-bp probe F1 (derived from BS2) was trimmed from two ends separately to afford a set of shortened DNA probes, which were tested in the subsequent EMSAs (Figures 6B,C). The results allowed us to narrow down to a minimum 18-bp palindromic DNA sequence F1-c (5′-GGTCGGCATTGTCGAACA-3′), which could be bound by GylR (Figure 6D). Then, the aforementioned 21-bp DNA probes were all shortened to 18-bp DNA probes, and the EMSA results showed that GylR was able to bind all these 18-bp DNA sequences (Figure 6D). Furthermore, homologous 18-bp DNA sequences were identified in the upstream regions of *gylR* and *glpF1* homologs in all the *Streptomyces* genomes harboring a *glp* operon (Supplementary Sheet 3). Analysis of these 18-bp DNA sequences led to the identification of an 18-bp sequence motif (Figure 6E). These results elucidated the detailed DNA binding sequences of GylR in *S. clavuligerus* NRRL 3585. Moreover, a core 18-bp sequence motif was identified to be bound by GylR-like regulators in *Streptomyces* based on experimental data and bioinformatic analysis. The molecular regulatory mechanism of GylR revealed by our study and previous reports presumably represents a general regulatory mechanism in glycerol metabolism in *Streptomyces*.

Discussion

Glycerol can be obtained from multiple paths, especially the growing biodiesel industry that produces glycerol as a main byproduct. The expanding production and reducing cost have made glycerol readily available for versatile applications, one of which is to use it as a carbon source for microorganisms to produce value-added products (da Silva et al., 2009; Guo et al., 2013; Poblete-Castro et al., 2020). As the fertile producers of natural product drugs, streptomycetes can metabolize glycerol

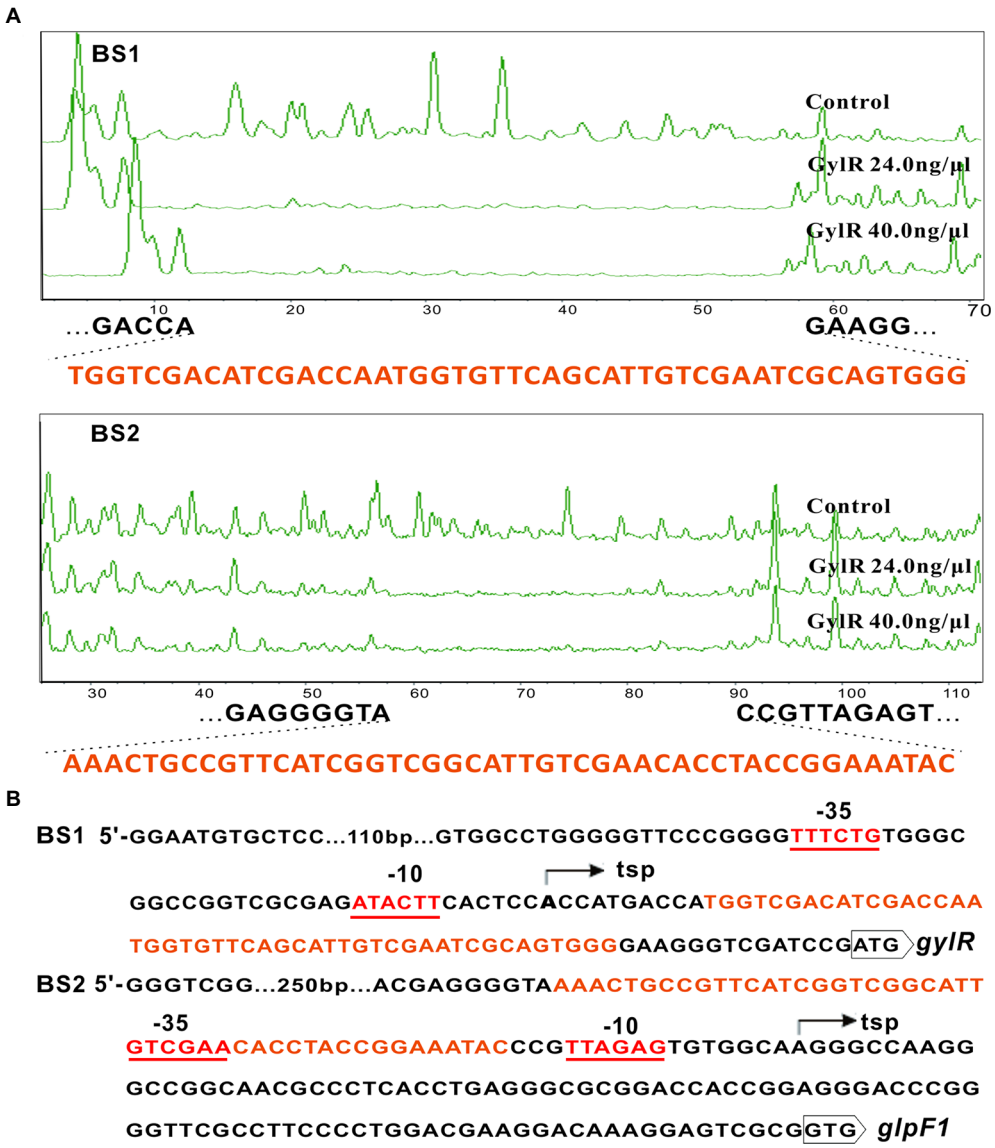

FIGURE 5
Identification of the binding sequences of GylR and the transcription start sites of *gylR* and *glpF1*. **(A)** DNase I footprinting assays of GylR with the probes BS1 and BS2. Footprints of GylR were shown between dashed lines. **(B)** Sequence analysis of BS1 and BS2. The identified binding sequences of GylR on BS1 and BS2 were shown in orange. The transcription start sites (tsp) of *gylR* and *glpF1* were determined and marked by bent arrows. The putative −10 and −35 regions of both promoters P*gyl* and P*glp* were underlined.

through the *glp* operon that is negatively regulated by GylR, as evident from previous studies in *S. coelicolor* A3(2) and *S. clavuligerus* NRRL 3585 (Smith and Chater, 1988b; Hindle and Smith, 1994; Baños et al., 2009). In this study, by analyzing all completed genomes of the phylum *Actinobacteria* available in the NCBI Genome database, we found that the *glp* operon-like glycerol utilization gene clusters are conserved in *Streptomyces* and several other genera of *Actinobacteria*, suggesting a common glycerol metabolic pathway in these microbes. Using *S. clavuligerus* NRRL 3585 as a model system, our *in vivo* data further confirmed that GylR represses the expression of *glp* operon and *gylR*, and the inhibition could be relieved upon addition of glycerol to the medium. Characterization of the effector molecules is important for fully understanding the mechanism of a regulatory protein. Prior to our research, there are only few studies on identifying the effectors of GylR-like regulators. In *S. coelicolor* A3(2), G3P was proposed to be an effector molecule of GylR based on *in vivo* study (Seno and Chater, 1983; Seno et al., 1984). In *Mycolicibacterium smegmatis*, *in vitro* data showed that G3P is an effector molecule of the GylR homolog, which positively regulates the *glp* operon-like gene cluster (Bong et al., 2019). In *E. coli* and *Pseudomonas* spp., the GlpR proteins regulating the glycerol utilization gene clusters show no significant sequence similarity to GylR, and G3P was

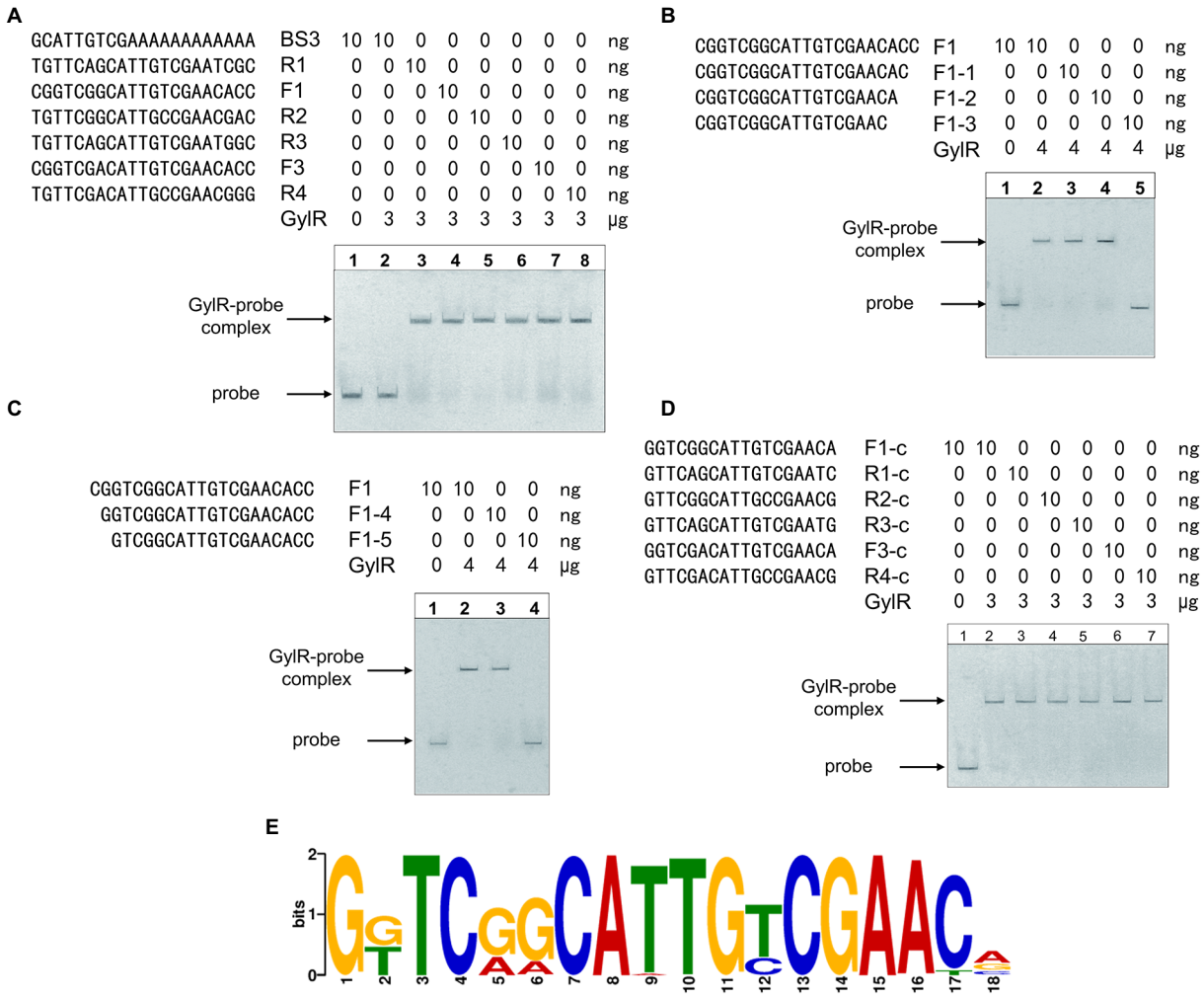

FIGURE 6
Identification of the core binding sequences of GylR revealing an 18-bp sequence motif. **(A)** EMSAs of GylR binding to the 21-bp DNA sequences from several representative *Streptomyces* strains. The DNA probes R1, R2, R3, and R4 referred to the corresponding 21-bp DNA sequences upstream of *gylR* homologs in *S. clavuligerus* NRRL 3585, *S. coelicolor* A3(2), *S. albus* DSM 41398, and *S. avermitilis* MA-4680, respectively. The DNA probes F1 and F3 referred to the corresponding 21-bp DNA sequences upstream of *glpF1* homologs in *S. clavuligerus* NRRL 3585, and *S. albus* DSM 41398, respectively. The corresponding 21-bp DNA sequences upstream of *glpF1* homologs in *S. coelicolor* A3(2) and *S. avermitilis* MA-4680 were identical to that of probe F1. The probe BS3 was used as a negative control. **(B)** EMSAs of GylR binding to trimmed F1 probes on the 3-prime end. **(C)** EMSAs of GylR binding to trimmed F1 probes on the 5-prime end. **(D)** EMSAs of GylR binding to the core 18-bp DNA sequences derived from the aforementioned representative 21-bp DNA sequences. F1-c, R1-c, R2-c, R3-c, F3-c, and R4-c referred to the core 18-bp DNA sequences derived from the probes F1, R1, R2, R3, F3, and R4, respectively. **(E)** The conserved 18-bp sequence motif bound by GylR-like proteins in *Streptomyces* strains. The 18-bp sequence motif was obtained by analyzing the putative binding sequences upstream of *gylR* homologs and *glpF1* homologs in available *Streptomyces* genomes with MEME Suite 5.5.0 (Bailey et al., 2006).

suggested to be an effector molecule of these GlpR proteins (Lin, 1976; Poblete-Castro et al., 2020). However, there is a lack of direct evidences of identifying the effector molecules of GylR-like regulators in *Streptomyces*. Our study provided direct evidences showing that both G3P and DHAP are effector molecules of GylR in *S. clavuligerus* NRRL 3585, while glycerol is not. DHAP is for the first time discovered as an effector molecule of GylR-like regulatory proteins. Previous study in *E. coli* suggested that DHAP might have weak interaction with GlpR (Larson et al., 1987). These findings further supported the feedback activation mechanism in the regulation of glycerol metabolism (Lin, 1976; Baños et al., 2009). Specifically, due to the tight control of GylR, the *glp* operon expressed at a very low level initially, which enabled the slow conversion of glycerol to G3P and DHAP. Once these effector molecules reached to concentrations that could induce the dissociation of GylR from the binding of *glp* operon, the glycerol metabolic pathway was fully activated.

We further revealed the binding sequences of GylR at the promoter regions of *glp* operon and *gylR*, which was not known previously. The results suggested that GylR inhibits the expression of *gylR* and *glp* operon through impeding the transcription

initiation and elongation, respectively. Based on experimental data and bioinformatic analysis, we were able to identify a palindromic 18-bp sequence motif important for the binding of GylR-like regulators in *Streptomyces*. It is worth noting that, the *glp* operon in *Streptomyces* could also be regulated by other proteins or pathways. In *S. coelicolor* A3(2), the *glp* operon is negatively regulated by the pleiotropic protein NdgR, the binding site of which does not overlap with the binding sequences of GylR (Lee et al., 2017). In addition, the *glp* operon in *S. coelicolor* A3(2) was reported to be subject to carbon catabolite repression (Smith and Chater, 1988a,b).

Glycerol-inducible regulatory elements have many applications in the metabolic engineering and synthetic biology research fields. The promoter of *glp* operon (P*glp*) has been successfully used to coordinate the glycerol utilization with natural product biosynthesis, leading to 3.2-fold enhanced clavulanic acid production in *S. clavuligerus* NRRL 3585 (Guo et al., 2013). A glycerol-inducible expression system based on the antiterminator protein GlpP and its target promoter PglpD was applied in the heterologous production of aspartase and nattokinase in *B. subtilis* (Han et al., 2022). Replacing the promoters of *zwf*, *pgi* and *pfk1* genes with the glycerol-inducible promoter pGUT1, resulting in significantly improved production of *myo*-inositol in *Pichia pastoris* (Zhang et al., 2022). Understanding the underlying molecular regulatory mechanisms in glycerol metabolism will lay a foundation for the design of efficient and simple glycerol-inducible regulatory tools.

In conclusion, by taking *S. clavuligerus* NRRL 3585 as a model system, we have identified the effector molecules and binding sequences of GylR, a key regulator in the glycerol metabolic pathway. Furthermore, we identified a core 18-bp sequence motif that is minimally required for the binding of GylR-like regulators in *Streptomyces*. These findings further revealed the molecular mechanism mediated by GylR in the regulation of glycerol metabolism. The information is of importance for the design of better glycerol utilization pathways that can improve utilization of glycerol to produce valuable products. Moreover, these findings would facilitate the development and application of glycerol-inducible regulatory elements for synthetic biology research in the future.

Data availability statement

The original contributions presented in the study are included in the article/Supplementary material, further inquiries can be directed to the corresponding author.

Author contributions

YZ, KF, and GP conceived and designed the project. CZ and YZ performed the experiments. KF carried out the bioinformatics analyses. CZ, KF, and GP analyzed the data and wrote the manuscript with the input of all authors. YH, WW, and ZL provided key suggestions and revised the manuscript. All authors contributed to the article and approved the submitted version.

Funding

This work was supported by the National Key R&D Program of China (2021YFC2100600 and 2020YFA0907700), and the National Natural Science Foundation of China (32070067).

Acknowledgments

We thank Yihua Chen (Institute of Microbiology, Chinese Academy of Sciences) for the insightful comments and suggestions on the preparation of the manuscript. This manuscript is dedicated to the memory of our beloved mentor Keqian Yang.

Conflict of interest

The authors declare that the research was conducted in the absence of any commercial or financial relationships that could be construed as a potential conflict of interest.

Publisher's note

Supplementary material

The Supplementary material for this article can be found online at: https://www.frontiersin.org/articles/10.3389/fmicb.2022.1078293/full#supplementary-material

References

Bailey, T. L., Williams, N., Misleh, C., and Li, W. W. (2006). MEME: discovering and analyzing DNA and protein sequence motifs. *Nucleic Acids Res.* 34, W369–W373. doi: 10.1093/nar/gkl198

Baños, S., Pérez-Redondo, R., Koekman, B., and Liras, P. (2009). Glycerol utilization gene cluster in Streptomyces clavuligerus. *Appl. Environ. Microbiol.* 75, 2991–2995. doi: 10.1128/AEM.00181-09

Bong, H.-J., Ko, E.-M., Song, S.-Y., Ko, I.-J., and Oh, J.-I. (2019). Tripartite regulation of the glpFKD operon involved in glycerol catabolism by GylR, Crp, and SigF in mycobacterium smegmatis. *J. Bacteriol.* 201:e00511. doi: 10.1128/JB.00511-19

Camacho, C., Coulouris, G., Avagyan, V., Ma, N., Papadopoulos, J., Bealer, K., et al. (2009). BLAST+: architecture and applications. *BMC Bioinform.* 10:421. doi: 10.1186/1471-2105-10-421

Da Silva, G. P., Mack, M., and Contiero, J. (2009). Glycerol: a promising and abundant carbon source for industrial microbiology. *Biotechnol. Adv.* 27, 30–39. doi: 10.1016/J.BIOTECHADV.2008.07.006

Doi, Y. (2019). Glycerol metabolism and its regulation in lactic acid bacteria. *Appl. Microbiol. Biotechnol.* 103, 5079–5093. doi: 10.1007/S00253-019-09830-Y

Guo, D., Zhao, Y., and Yang, K. (2013). Coordination of glycerol utilization and clavulanic acid biosynthesis to improve clavulanic acid production in Streptomyces clavuligerus. *Sci. China Life Sci.* 56, 591–600. doi: 10.1007/s11427-013-4507-z

Han, L., Chen, Q., Luo, J., Cui, W., and Zhou, Z. (2022). Development of a glycerol-inducible expression system for high-yield heterologous protein production in Bacillus subtilis. *Microbiol. Spectr.* 10:e0132222. doi: 10.1128/SPECTRUM.01322-22

Hindle, Z., and Smith, C. P. (1994). Substrate induction and catabolite repression of the Streptomyces coelicolor glycerol operon are mediated through the GylR protein. *Mol. Microbiol.* 12, 737–745. doi: 10.1111/j.1365-2958.1994.tb01061.x

Kieser, T., Bibb, M. J., Buttner, M. J., Chater, K. F., and Hopwood, D. A. (2000). *Practical Streptomyces Genetics*. Norwich: The John Innes Foundation.

Klein, M., Swinnen, S., Thevelein, J. M., and Nevoigt, E. (2017). Glycerol metabolism and transport in yeast and fungi: established knowledge and ambiguities. *Environ. Microbiol.* 19, 878–893. doi: 10.1111/1462-2920.13617

Kormanec, J., Rezuchova, B., Homerova, D., Csolleiova, D., Sevcikova, B., Novakova, R., et al. (2019). Recent achievements in the generation of stable genome alterations/mutations in species of the genus Streptomyces. *Appl. Microbiol. Biotechnol.* 103, 5463–5482. doi: 10.1007/s00253-019-09901-0

Larson, T. J., Ye, S. Z., Weissenborn, D. L., Hoffmann, H. J., and Schweizer, H. (1987). Purification and characterization of the repressor for the sn-glycerol 3-phosphate regulon of Escherichia coli K12. *J. Biol. Chem.* 262, 15869–15874.

Lee, B. R., Bhatia, S. K., Song, H. S., Kim, J., Kim, W., Park, H., et al. (2017). The role of NdgR in glycerol metabolism in *Streptomyces coelicolor*. *Bioprocess Biosyst. Eng.* 40, 1573–1580. doi: 10.1007/S00449-017-1813-Z

Lee, N., Hwang, S., Kim, W., Lee, Y., Kim, J. H., Cho, S., et al. (2021). Systems and synthetic biology to elucidate secondary metabolite biosynthetic gene clusters encoded in *Streptomyces genomes*. *Nat. Prod. Rep.* 38, 1330–1361. doi: 10.1039/d0np00071j

Li, S., Wang, W., Li, X., Fan, K., and Yang, K. (2015). Genome-wide identification and characterization of reference genes with different transcript abundances for *Streptomyces coelicolor*. *Sci. Rep.* 5:15840. doi: 10.1038/srep15840

Lin, E. C. (1976). Glycerol dissimilation and its regulation in bacteria. *Annu. Rev. Microbiol.* 30, 535–578. doi: 10.1146/ANNUREV.MI.30.100176.002535

Pagliaro, M., Ciriminna, R., Kimura, H., Rossi, M., and della Pina, C. (2007). From glycerol to value-added products. *Angew. Chem. Int. Ed. Engl.* 46, 4434–4440. doi: 10.1002/ANIE.200604694

Pan, G., Gao, X., Fan, K., Liu, J., Meng, B., Gao, J., et al. (2017). Structure and function of a C-C bond cleaving oxygenase in atypical angucycline biosynthesis. *ACS Chem. Biol.* 12, 142–152. doi: 10.1021/acschembio.6b00621

Poblete-Castro, I., Wittmann, C., and Nikel, P. I. (2020). Biochemistry, genetics and biotechnology of glycerol utilization in pseudomonas species. *Microb. Biotechnol.* 13, 32–53. doi: 10.1111/1751-7915.13400

Rice, P., Longden, I., and Bleasby, A. (2000). EMBOSS: the European molecular biology open software suite. *Trends Genet.* 16, 276–277. doi: 10.1016/s0168-9525(00)02024-2

Saudagar, P. S., Survase, S. A., and Singhal, R. S. (2008). Clavulanic acid: a review. *Biotechnol. Adv.* 26, 335–351. doi: 10.1016/j.biotechadv.2008.03.002

Seno, E. T., Bruton, C. J., and Chater, K. F. (1984). The glycerol utilization operon of Streptomyces coelicolor: genetic mapping of gyl mutations and the analysis of cloned gylDNA. *Mol. Gen. Genet.* 193, 119–128. doi: 10.1007/BF00327424

Seno, E. T., and Chater, K. F. (1983). Glycerol catabolic enzymes and their regulation in wild-type and mutant strains of *Streptomyces coelicolor* A3(2). *J. Gen. Microbiol.* 129, 1403–1413. doi: 10.1099/00221287-129-5-1403

Shin, C. H., Cho, H. S., Won, H. J., Kwon, H. J., Kim, C. W., and Yoon, Y. J. (2021). Enhanced production of clavulanic acid by improving glycerol utilization using reporter-guided mutagenesis of an industrial *Streptomyces clavuligerus* strain. *J. Ind. Microbiol. Biotechnol.* 48:kuab004. doi: 10.1093/JIMB/KUAB004

Smith, C. P., and Chater, K. F. (1988a). Cloning and transcription analysis of the entire glycerol utilization (gylABX) operon of Streptomyces coelicolor A3(2) and identification of a closely associated transcription unit. *Mol. Gen. Genet.* 211, 129–137.

Smith, C. P., and Chater, K. F. (1988b). Structure and regulation of controlling sequences for the Streptomyces coelicolor glycerol operon. *J. Mol. Biol.* 204, 569–580.

Suvorova, I. A., and Gelfand, M. S. (2021). Comparative analysis of the IclR-family of bacterial transcription factors and their DNA-binding motifs: structure, positioning, co-evolution, regulon content. *Front. Microbiol.* 12:675815. doi: 10.3389/FMICB.2021.675815

Wang, L., Tian, X., Wang, J., Yang, H., Fan, K., Xu, G., et al. (2009). Autoregulation of antibiotic biosynthesis by binding of the end product to an atypical response regulator. *Proc. Natl. Acad. Sci. U. S. A.* 106, 8617–8622. doi: 10.1073/pnas.0900592106

Wang, W., Yang, T., Li, Y., Li, S., Yin, S., Styles, K., et al. (2016). Development of a synthetic oxytetracycline-inducible expression system for Streptomycetes using de novo characterized genetic parts. *ACS Synth. Biol.* 5, 765–773. doi: 10.1021/acssynbio.6b00087

Xiang, S., Li, J., Yin, H., Zheng, J., Yang, X., Wang, H.-B., et al. (2009). Application of a double-reporter-guided mutant selection method to improve clavulanic acid production in *Streptomyces clavuligerus*. *Metab. Eng.* 11, 310–318. doi: 10.1016/j.ymben.2009.06.003

Zhang, Q., Wang, X., Luo, H., Wang, Y., Wang, Y., Tu, T., et al. (2022). Metabolic engineering of Pichia pastoris for myo-inositol production by dynamic regulation of central metabolism. *Microb. Cell Factories* 21:112. doi: 10.1186/S12934-022-01837-X

Zhao, Y., Xiang, S., Dai, X., and Yang, K. (2013). A simplified diphenylamine colorimetric method for growth quantification. *Appl. Microbiol. Biotechnol.* 97, 5069–5077. doi: 10.1007/s00253-013-4893-y

frontiers | Frontiers in Microbiology

TYPE Original Research
PUBLISHED 12 January 2023
DOI 10.3389/fmicb.2022.1076577

OPEN ACCESS

EDITED BY
Kalindi Morgan,
University of Northern British Columbia, Canada

REVIEWED BY
Fengyu Du,
Qingdao Agricultural University, China
Feng Ge,
Kunming University of Science and Technology, China
Xian-Wen Yang,
State Oceanic Administration, China

*CORRESPONDENCE
Pei-Ji Zhao
✉ pjzhao@ynu.edu.cn

†These authors have contributed equally to this work and share first authorship

SPECIALTY SECTION
This article was submitted to Microbial Physiology and Metabolism, a section of the journal Frontiers in Microbiology

RECEIVED 21 October 2022
ACCEPTED 23 December 2022
PUBLISHED 12 January 2023

CITATION
Qu S-L, Xie J, Wang J-T, Li G-H, Pan X-R and Zhao P-J (2023) Activities and metabolomics of *Cordyceps gunnii* under different culture conditions. *Front. Microbiol.* 13:1076577. doi: 10.3389/fmicb.2022.1076577

Activities and metabolomics of *Cordyceps gunnii* under different culture conditions

Shuai-Ling Qu†, Juan Xie†, Jun-Tao Wang, Guo-Hong Li, Xue-Rong Pan and Pei-Ji Zhao*

State Key Laboratory for Conservation and Utilization of Bio-Resources in Yunnan, School of Life Sciences, Yunnan University, Kunming, Yunnan, China

Many active metabolites have been identified from various species of the fungal genus *Cordyceps*. A predominant species of this genus is *Cordyceps gunnii*, but there are limited reports on the active ingredients from this species. This study aimed to conduct activity assays and metabolome analysis on extracts of *C. gunnii* obtained under different culture conditions. Five different solid media were selected to culture the mycelium of *C. gunnii* and the metabolites were extracted with organic solvents; concurrently, the wild stroma and host complexes of *C. gunnii* were extracted by ethyl acetate. Extracts were subsequently assayed for various biological activities and were analyzed by untargeted metabolomics. There were significant differences in the activities and metabolites of *C. gunnii* extracts from different culture conditions and from wild stroma and host complexes. The extracts of stroma and host complexes and mycelia cultured on WGA medium for 21days exhibited similar effective inhibitory activity against five cell lines. A total of 51 metabolites were annotated and included various structural types. The literatures indicate that most of the identified compounds have a variety of different biological activities. These findings provide the basis for further systematic excavation of *C. gunnii* and improved utilization of this fungal species.

KEYWORDS

***Cordyceps gunnii*, different growing conditions, untargeted metabolome, cytotoxic activity, nematocidal activity**

1. Introduction

Cordyceps is a genus of fungi that are parasitic on insects, fungi, or plant bodies. According to the latest data from MycoBank,[1] *Cordyceps* is the most abundant and diverse genus in the family Clavellaceae, and 630 species have been identified, with more than 130 of these species reported in China (Olatunji et al., 2018). Fungi of the genus *Cordyceps* (including stroma and host complexes, fruit body and mycelium) produce numerous secondary metabolites and have a variety of biological activities (Qu et al., 2022).

1 https://www.Mycobank.org

Cordyceps gunnii (heterotypic synonym: *Paecilomyces gunnii*), originally discovered in Tasmania, Australia, was first isolated and identified in China in Duyun county of Guizhou Province (Liang, 1983), and its activity and metabolites have attracted constant attention. Aqueous and alcoholic extracts of *C. gunnii* mycelium markedly reduced writhing times in mice using pain models of acetic acid-induced writhing and hot-plate tests in mice with intragastric administration and hypodermic injection (Chen et al., 2009). Se-polysaccharide obtained from selenium-enriched mycelia of *C. gunnii* exhibited anti-tumor activity within ovarian tumor model rats modeled with SK-OV-3 cells (Sun et al., 2018), while polysaccharides from *C. gunnii* mycelia showed immunomodulatory activity *via* the TLR4/NF-κB signaling pathway (Meng et al., 2019). Three novel macrocyclic tetrameric lactams—gunnilactams A, B, and C—were obtained from the submerged fermentation broth of *C. gunnii*, and gunnilactam A showed selective moderate cytotoxic activity against C42B cells (human prostate cancer) with an IC_{50} value of 5.4 μM (Zheng et al., 2017). However, some studies have reported that extracts from the mycelium of *C. gunnii* have no apparent activity. For example, Meng et al. (2012) found that water extracts and ethyl acetate extracts of *C. gunnii* cultured in potato-dextrose-broth (PDB) did not exhibit obvious activity against BEL-7402 cells and COLO205 cells.

In addition, different fermentation conditions had significant effects on the content and anti-tumor activity of polysaccharide from *C. gunnii* (Liu et al., 2019). In 2002, Zeeck coined the term OSMAC (One Strain Many Compounds) to describe the approach of modifying fermentation conditions to increase the types and abundance of microbial metabolites (Bode et al., 2002), and there has been some successful research using this strategy. For example, Paranagama et al. (2007) found that culture conditions affected the metabolite production of the fungi *Paraphaeosphaeria quadriseptata* and *Chaetomium chiversii*. The main reason for this may be that the metabolic biosynthesis genes are expressed differently under different growth conditions (Scherlach and Hertweck, 2009). As part of our ongoing search for undescribed active compounds from microorganisms, a series of novel active compounds were obtained from different fungi (Pu et al., 2021; Liu et al., 2022).

In the present work, five different solid media were selected to culture the mycelium of *C. gunnii* according to the literature and our preliminary experiments, and the metabolites were extracted with organic solvents; simultaneously, the metabolites of the wild stroma and host complexes of *C. gunnii* were extracted with ethyl acetate. The extracts were assayed for various activities and analyzed by untargeted metabolomics.

2. Materials and methods

2.1. Experimental strain and culture conditions

Cordyceps gunnii YMF1.00003 is preserved in the State Key Laboratory of Conservation and Utilization of Biological Resources in Yunnan and was identified as *Cordyceps gunnii* after internal transcribed spacer (ITS) identification (GenBank accession no. OP474063). Stroma and host complexes of *C. gunnii* were purchased from Shiqian County of Guizhou Province, and the ITS of the stroma was sequenced and identified (GenBank accession no. OP558778). *Meloidogyne javanica* was obtained from the roots of tomatoes grown in E'shan County in Yunnan Province. Eggs of *M. javanica* were acquired according to Liu et al. (2022). Briefly, *M. javanica* egg masses were handpicked from tomato root galls, surface-sterilized in 1% NaClO solution for 4 min, rinsed three times with distilled water (dH_2O), placed in a Petri dish with water, and incubated in the dark at 25°C to prepare second-stage juveniles (J2s). The newly hatched J2s were collected daily. The nematode concentration was adjusted to 2×10^4 nematodes/mL according to experimental needs.

Based on the literatures and our previous preliminary experiments, we selected nutrient-rich media, including various carbon sources, organic nitrogen sources, coenzymes and trace elements; and tried to make significant differences in the composition of these media. Finally, five media [CMA (20.0 g maize, 10.0 g glucose, 0.4 g peptone, 1.0 g VB, 1 l water); YMG (4.0 g yeast extract, 20.0 g glucose, 1 l water); PDA (200.0 g potato, 20.0 g glucose, 1 l water); GPY (20.0 g glucose, 6.0 g peptone, 10.0 g yeast paste, 1 l water); WGA (30.0 g wheat bran, 20.0 g glucose, 1.5 g KH_2PO_4, 1.5 g $MgSO_4$, 1 l water)] were used to optimize culture conditions for mycelia of *C. gunnii*. Briefly, 200 ml each solid medium was divided into six Petri dishes. Then, the mycelium of *C. gunnii* is inoculated into each Petri dish and cultivated at 28°C for 14 or 21 days, respectively. The cultures were extracted exhaustively three times by EtOAc/MeOH/AcOH (80:15:5, by vol.). The soaking solution was obtained by filtration (repeated three times) and was evaporated under reduced pressure at 45°C to obtain the infusion. These extracts were named as CMA14, CMA21, YMG14, YMG21, PDA14, PDA21, GPY14, GPY21, WGA14, and WGA21, respectively. The stroma and host complexes of *C. gunnii* were cut and immersed in ethyl acetate organic solvent for 3 days, then filtrated to obtain the immersion solution (repeated three times); this extract was named CG. Finally, the extract was dried under reduced pressure at 45°C. All extracts were assayed for various biological activities and were analyzed by liquid chromatography-mass spectrometry (LC–MS).

2.2. 3-(4,5-dimethylthiazol-2-yl)-5-(3-carboxymethoxyphenyl)-2-(4-sulfophenyl)-2H-tetrazolium (MTS) method for cytotoxic activity

All extracts (100 μg/ml) were evaluated for their cytotoxicity activity by 3-(4,5-dimethylthiazol-2-yl)-2,5 diphenyl tetrazolium bromide (MTT) method. The MTT method was used for the bioassays was conducted as described in the literature (Su et al., 2013). Five cell lines were selected for testing (leukemia cell line HL-60, hepatocarcinoma cell line SMMC-7721, lung adenocarcinoma cell line A549, breast cancer cell line

MDA-MB-231, and colon cancer cell line SW480). Taxol was used as a positive control. All experiments were performed in triplicate, and the data are expressed as means ± standard deviation (SD) of three independent experiments.

2.3. Assay for protective effect against corticosterone-induced oxidative stress

Poorly differentiated PC12 cells were maintained in DMEM medium supplemented with 10% fetal bovine serum (FBS), penicillin (100 U/ml), and streptomycin (100 μg/ml), and were incubated at 5% CO_2 and 37°C. Subsequently, the cells were divided into the following groups: Blank group (contains PC12 cells and DMSO at a final concentration of 0.1%); NC group (contains PC12 cells, a final concentration of 150 μM corticosterone (CORT), and a final concentration of 0.1% DMSO); DIM group [contains PC12 cells, a final concentration of 10 μM desipramine (DIM), a final concentration of 150 μM CORT, and a final concentration of 0.1% DMSO]; Each extracts group (contains PC12 cells, a final concentration of 150 μM CORT, and 20 μg/ml extract). Briefly, poorly differentiated PC12 cells were seeded in 96-well culture plates at a density of 1×10^4 cells/well. After 24 h, samples were added to the wells according to the previously described groups and were incubated for 48 h. MTS solution was then added to each well and the absorbance was measured at 492 nm using a Thermo Multiskan FC. Each group included three repetitions (Jiang et al., 2014).

2.4. Assay for nematocidal activity against *Meloidogyne javanica*

The tested extracts were dispersed in MeOH. Two hundred *M. javanica* J2s (100 μl) were added to each sample, and the final concentration of the tested compounds was set at 10 mg/ml. The total and dead nematode numbers were enumerated every 24 h (Huang et al., 2020); nematodes were considered dead if they were flat or cracked. Subsequently, nematode mortality was calculated. Avermectin was used as a positive control, and test solution without compound was used as a negative control. Three replicates were conducted for each test.

2.5. Metabolomic data acquisition and statistical analysis

Untargeted LC–MS metabolomics was performed on a Dionex UltiMate 3,000 LC system coupled with a Q-Exactive Orbitrap MS (Thermo, San Jose, CA, United States). All samples were separated on an Agilent Zorbax Eclipse Plus C18 (50 × 2.1 μm; Agilent Technologies, CA, United States) with a particle size of 1.8 μm at an LC flow rate of 300 μl/min and a column temperature of 40°C. Mobile phase A comprised water containing 0.5% formic acid, and mobile phase B comprised 0.5% formic acid in methanol. The extracts were prepared separately by dissolving in chromatographic methanol to a concentration of 10 mg/ml, filtering three times, placing at 4°C overnight, and then setting aside as samples for LC–MS detection. The 30-min gradient for positive electrospray ionization (ESI) mode was set as: 0–3 min, 1% solvent B; 3–20 min, 1–99% solvent B; 22–25 min, 99% solvent B; and 25–30 min, 1% solvent B. The injection volume was 5 μl, and each sample was injected in triplicate. The injection order was randomized, and the group information was blinded for LC–MS analysis. The instrument settings included a capillary temperature of 350°C, sheath gas flow rate of 35 (arbitrary units), auxiliary gas flow rate of 10 (arb), spray voltage of 4.0 kV, full MS resolution of 70,000, and MS/MS resolution of 17,500. Each sample was prepared in biological triplicate. The LC–MS instrument was controlled using Thermo Scientific Xcalibur 4.1 software.

The raw data file was analyzed using Compound Discoverer (CD version 3.3, Thermo Fisher Scientific) software for metabolomics data analysis. A blank sample was used for background subtraction and noise removal during the pre-processing step. The data were analyzed in 11 groups (CG, CMA-14, CMA-21, YMG-14, YMG-21, PDA-14, PDA-21, GPY14, GPY21, WGA-14, and WGA-21). For analysis of the data on metabolite variation in the nine groups, simple univariate statistical analyses were carried out on $\log_2$-transformed data using a paired *t*-test. Volcano plots were created using these data, with a threshold of $p < 0.05$ and absolute $\log_2$ fold-change of >1 set for defining a notable change in compound abundance among all samples. All components among were searched against an accurate mass database consisting of known fungal metabolites using a mass tolerance of 10 ppm. The database was prepared using SciFinder, and additional fungal natural products were identified in the literatures. Meanwhile, other potential compound identifications were obtained by comparing the MS/MS scan with the MZCloud, ChemSpider, and MZvault libraries. To confirm and evaluate intact mass-based identifications, manual analyses of fragmentation data were performed as described below. All compounds tentatively identified *via* accurate intact mass were confirmed using accurate mass, tandem MS (MS^2) data. To ensure that low-quality spectra were not included, MS^2 spectra containing fewer than five peaks at >1% relative abundance were excluded from the analysis. Additionally, spectra containing more than 100 peaks at >1% abundance were included only if >20% of the peaks appeared in the higher m/z half of the spectrum. Both general fragmentation rules and fragmentation library modes were used. When published fragmentation data were available, a comparison was also performed to further confirm identifications.

3. Results and discussion

3.1. Stroma and host complex and culture status of *Cordyceps gunnii*

In the stroma and host complex, the host was white, gray to brown (dried specimen), without hyphae on the surface; the

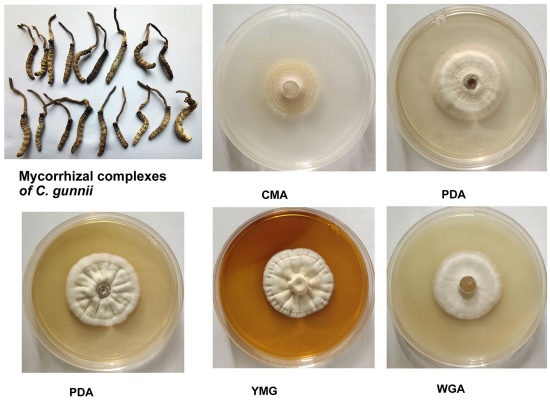

FIGURE 1
Appearance of solid-state fermentation cultures of *Cordyceps gunnii* after 21days on different media, and stroma and host complexes of *C. gunnii*.

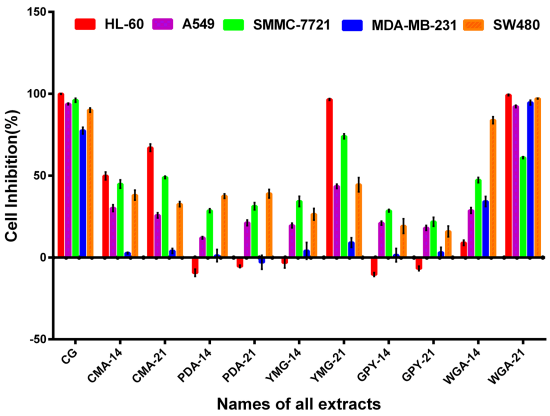

FIGURE 2
The cytotoxic activity of the crude extract.

stroma was single, yellow to brown, and rose from the head of the host (Figure 1). Colony diameters were 21–23 mm and 22–27 mm on CMA after incubation at 28°C for 14 and 21 days, respectively. The colonies were dense, white at first, then turning pale to light yellow. Colonies on PDA were circular, white, reverse yellow and attained diameters of 20–26 and 29–33 mm at 28°C after 14 and 21 days, respectively. Synnemata emerged from the surface and in the margin of the colony and were pale yellow to yellow. Colonies grown on YMG and GPY were radiological with diameters the same as those on PDA, and were dense and white to pale yellow. Colonies grown on WGA were circular, white, and attained diameters of 20–22 and 26–30 mm after growth at 28°C for 14 and 21 days, respectively.

To quantify the various extracts in different medium, culture and extraction was performed. Hundred milliliter of each of the five media (GPY, CMA, YMG, WGA, and PDA) divided into 5 Petri dishes plates, respectively; then the mycelium was inoculated on the media and incubated for 14 or 21 days, respectively. After 21 days of mycelium growth, the weights of the five extracts GPY-21, CMA-21, YMG-21, WGA-21, and PDA-21 were 346, 286, 191, 390, and 193 mg, respectively.

3.2. Cytotoxic activity of extracts

The cytotoxic activity of the extracts of *C. gunnii* cultured under different conditions was examined against five human cancer cell lines (HL-60, A549, SMMC-7721, MDA-MB-231, and SW480). All extracts were tested at a concentration of 100 μg/ml, and Taxol was used as a positive control. As shown in Figure 2, the cytotoxic activity of the extracts from different culture conditions and stroma and host complexes exhibited significant differences. The CG group, extracted from stroma and host complexes of *C. gunnii*, showed strong inhibitory activity against the five tumor cell lines. The extracts from the mycelium of *C. gunnii* cultured for only 14 days had no significant cytotoxic activity at the tested concentrations except that WGA-14 group showed selective inhibition of the SW480 cell line. However, the cytotoxic activity of the extracts from mycelium cultured for 21 days was very different. Among them, WGA-21 group had marked inhibitory activity against all five cell lines, which was almost similar to the CG group. YMG-21 group was the most effective extract in HL-60 and SMMC-7721 cells, while the CMA-21 group exhibited certain inhibitory activity on HL-60 cells.

3.3. Protective activity of extracts against neural cell damage induced by corticosterone

CORT-induced PC12 cell damage is used as an *in vitro* experimental model for depression studies. All extracts were evaluated for their protective activities against PC12 cell injury induced by CORT. After adding the extracts for 48 h, the absorbance of each well was measured by the MTS method and the cell survival rate was calculated. None of the 11 extracts had any apparent protective effect on corticosterone-induced nerve cell damage at the concentration of 20 μg/ml (Supplementary Figure S1).

3.4. Nematocidal activity of extracts against *Meloidogyne javanica*

The nematocidal activity of the crude extracts of *C. gunnii* was assayed against *M. javanica* by counting the number of dead nematodes at 12, 24, 48, 72, and 96 h in the presence of 10 mg/ml crude extracts. None of the extracts showed significant activity. The highest nematocidal activity was observed with the extract from CMA medium (Figure 3), but the mortality was only 18.38% at 96 h. In addition, the GPY extract showed a paralyzing effect on *M. javanica* at 24 h, with 20–30% nematodes in a state

of paralysis; however, at subsequent time points those nematodes were restored.

3.5. Untargeted metabolomics analysis of extracts

To determine whether metabolites and metabolic pathways in *C. gunnii* were changed under different culture conditions, the extract samples were subjected to LC–MS untargeted metabolomics. Quantitative analysis of low-molecular-weight metabolites can reveal the relative relationship between changes and metabolites, and may indicate the reasons for differences in activity in the extracts from different culture media. Extracted metabolites were analyzed in positive ion modes as described in the section "Materials and Methods." Loading data for Principal Component Analysis (PCA) was derived from all metabolites identified by Compound Discoverer 3.3 after LC–MS analysis and their peak area tendencies. The first and second principal components (PC1 and PC2) explained 49% of the overall variance. CG was significantly separated from all other samples in PC1 (29.7%) and PC2 (19.3%) (Figure 4A). CMA-21 was clearly separated from WGA-21 and other samples. Furthermore, the separation degree of WGA-21 and CMA-21 was relatively close to CG, while other samples (CMA-14, YMG-14, YMG-21, PDA-14, PDA-21, and WGA-14) showed no obvious separation. This result highlights the significant differences in the major metabolites produced by *C. gunnii* under different culture conditions. Referring to the results of the activity assays, subsequent work focused on identifying differences in the compounds produced in WGA-21 and CG.

Combining all the analyzed extracts, 4,382 unique molecular species were detected using UPLC-HR-ESI-MS. The high-resolution MS signals from different isotopes and adduct peaks were combined so that the vast majority of molecular species represented individual metabolites produced by the corresponding strain. We aimed to determine the differences in secondary metabolites between CG and WGA groups, and data were displayed as a volcano plot for visualization. Using significance cutoffs of a false discovery rate (FDR)-adjusted *p*-value (<0.05) and a fold-change difference > 1, 886 metabolites were upregulated in the CG group, while 879 metabolites were upregulated in the WGA group (Figure 4B). To determine the structures of the upregulated compounds, a structural library containing 249 metabolites from the genus *Cordyceps* was assembled after removing common steroids and fatty acids (Olatunji et al., 2018; Qu et al., 2022).

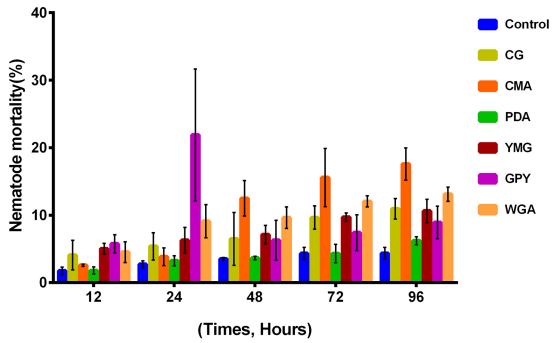

FIGURE 3
Nematocidal activity of the crude extracts of *C. gunnii*.

The complete masses of upregulated compounds were used to search the structural library and other libraries (MZCloud, ChemSpider, and MZvault). When searching these databases with a mass tolerance of 10 ppm, 51 annotations were verified (Table 1). The 51 identified compounds include various structural types such as non-ribosomal peptide synthetase (NRPS), polyketides (PKS), terpenes, and nucleosides. Among the 51 compounds, 19 were unique to the WGA group, 18 were unique to the CG group, and the other 14 compounds were present in the extracts of both WGA and CG groups. Most of these compounds were derived from the genus *Cordyceps* and other fungi, and a wide variety of activities have been reported. Furthermore, there were numerous metabolites with undefined structures that were significantly upregulated in the CG and WGA groups. The screening of culture conditions based on activity and metabolome is a powerful tool to facilitate exploration of the active metabolites of *Cordyceps*.

Of the 51 annotated compounds, many are reported to show a wide variety of biological activities. For example, two sesquiterpenoids, 3,4-diacetoxy-12,13-epoxy-9-trichothecene-15-ol and acetoxyscirpenediol, showed significant cytotoxic activity (Claridge et al., 1979; Nam et al., 2001); and simultaneously, this type of compound also has good nematicidal activity. Ovalicin and a related compound showed anti-angiogenic activity (Pillalamarri et al., 2019) and cytotoxicity (Chang et al., 2013). Opaliferin exhibited slight cytotoxicity (Grudniewska et al., 2014). In addition, cordycepin is the most famous active metabolite from *Cordyceps*, and has a wide spectrum of activities (Qu et al., 2022). Amdoxovir is a nucleoside compound with significant antiviral properties (Quan and Peters, 2004). Annotation of these compounds in the metabolome can appropriately help explain the activity of the extracts. In addition, because the compound(s) in the crude extracts have some cytotoxic activity, some experiments can only be performed with a lower concentration of the extract, resulting in the inability to obtain improved experimental results. For example, the protective activity of corticosterone against neural cell damage requires the testing sample to not have obvious cytotoxic activity.

With the rapid development of sequencing technology, increasing numbers of complete microbial genomes have been reported. Analysis of most of the reported fungal genome data revealed that a large number of secondary metabolic gene clusters were silent (or weakly expressed) under experimental culture conditions, and the corresponding metabolites could not be isolated and identified (Brakhage and Schroeckh, 2011; Keller,

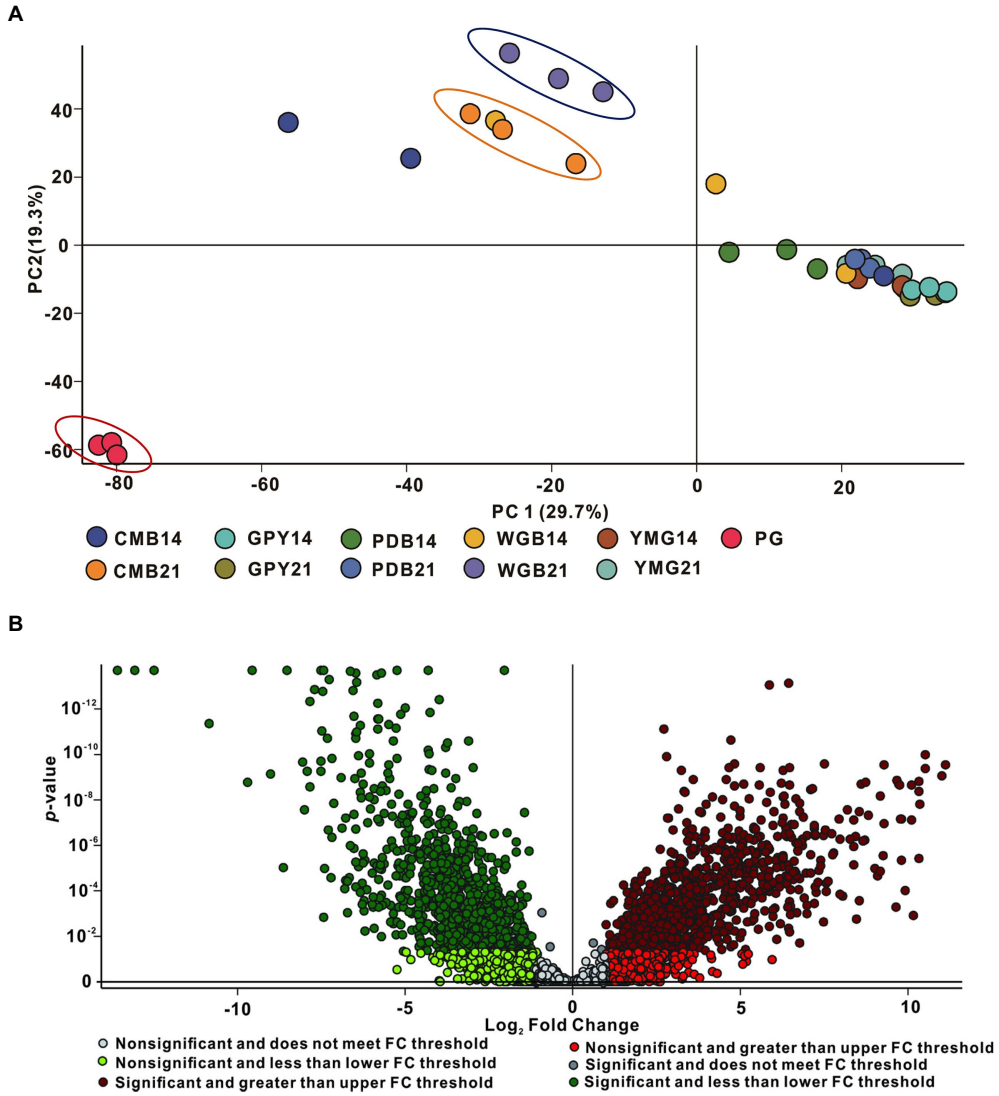

FIGURE 4
Principal component analysis (PCA) and volcano plot of all samples. **(A)** PCA of all extracts. **(B)** The volcano plot of CG group vs. WGA group.

2019; Lei and Zhao, 2019). The culture conditions of microorganisms are known to be critical for the quantity and abundance of secondary metabolites in microbial fermentation studies. In recent years, through the OSMAC strategy, a series of compounds with novel structures and multiple activities have been isolated and identified from fungi. After screening the medium of *Stereum hirsutum*, four sesquiterpene and amino acid hybrid quaternary ammonium salts, stereumamides A–D, were identified from the fermentation products. These compounds have certain antibacterial activity (Duan et al., 2018). Meng et al. (2016) obtained the diketopiperazine compounds spirobrocazine A and brocazine G from the marine endophyte *Penicillium brocae* MA-231, and brocazine G has strong anti-*Staphylococcus aureus* activity [minimum inhibitory concentration (MIC) 0.25 μg/ml] and cytotoxic activity (IC_{50} of 664 and 661 nM against cell lines A2780 and A2780 CisR, respectively). Wakefield and colleagues co-cultured marine-derived *Aspergillus fumigatus* MR2012 with *Streptomyces leeuwenhoekii* strain C34 and strain C58, respectively, and found that the metabolites changed significantly. Among the co-cultured metabolites of *Aspergillus fumigatus* MR2012 and *Streptomyces leeuwenhoekii* C34, two novel compounds—luteoride D and pseurotin G—were isolated and identified. In addition, a lasso peptide (chaxapeptin), which was not detected in *Streptomyces leeuwenhoekii* C34, was also isolated under co-cultivation conditions (Wakefield et al., 2017). Another study used a similar approach to rapidly search for anti-COVID-19 natural products. The soybean-associated endophytic fungi *Aspergillus terreus* was cultured and screened in five media, and a total of 18 compounds were identified through metabolome analysis. Multivariate analysis subsequently showed that *Aspergillus terreus* was more suitable for producing metabolites growing in PDB and modified PDB, and molecular docking

TABLE 1 Known compounds confidently identified from extracts of the WGA and CG groups.

Identified metabolites	m/z	Formula	Ion mode	Cal. mass	Delta mass (ppm)	Distribution
GameXPeptide F	615.4199	$C_{33}H_{54}N_6O_5$	$[M+H]^+$	615.4229	−4.79	Both
Pestalotiopin B	544.3611	$C_{32}H_{49}NO_6$	$[M+H]^+$	544.3633	−4.46	Both
Fumosoroseain A	498.3766	$C_{28}H_{52}NO_6$	$[M+H]^+$	498.3789	−2.24	WGA
Me lucidenate N	475.3035	$C_{28}H_{43}O_6$	$[M+H]^+$	475.3054	−1.75	CG
Certonardosterol J	463.3767	$C_{29}H_{51}O_4$	$[M+H]^+$	463.3782	−1.45	CG
3,5-Dihydroxy-14,15-epoxyergosta-7,22-diene-6-one	443.3136	$C_{28}H_{42}O_4$	$[M+H]^+$	443.3156	−2.02	CG
27-*O*-methylasporyzin C	436.3194	$C_{29}H_{42}NO_2$	$[M+H]^+$	436.321	−1.96	WGA
4′-Hydroxylisoflavone-7-*O*-*β*-4″-methoxylglucopyranoside	431.1316	$C_{18}H_{18}N_6O_7$	$[M+H]^+$	430.131	0.66	WGA
7-Ketositosterol	429.3709	$C_{29}H_{49}O_2$	$[M+H]^+$	429.3727	−1.84	CG
Ergosterol peroxid	429.3343	$C_{28}H_{45}O_3$	$[M+H]^+$	429.3363	−2.04	WGA
3-Hydroxy-5,9-epoxy-7,22-dien-6-one-ergosta	427.3194	$C_{28}H_{43}O_3$	$[M+H]^+$	427.3207	−1.26	CG
3-Oxoergosta-1,4,22-trien-26-oic acid	425.3031	$C_{28}H_{41}O_3$	$[M+H]^+$	425.3031	2.31	Both
*N*6-(Glycyl-L-glutaminyl)-D-lysyl-D-alanine	425.2126	$C_{16}H_{30}N_6O_6Na$	$[M+Na]^+$	425.2119	0.66	CG
Dihydrobrassicasterol	423.3605	$C_{30}H_{47}O$	$[M+H]^+$	423.3621	−1.59	Both
Glycoasperfuran	417.1525	$C_{18}H_{21}N_6O_6$	$[M+H]^+$	417.1517	0.79	WGA
N-oleoyl-L-glutamine	411.3237	$C_{23}H_{43}N_2O_4$	$[M+H]^+$	411.3258	1.93	CG
Campesterol	401.3718	$C_{28}H_{49}O$	$[M+H]^+$	401.3778	−6	WGA
Ergosta-5,7,22,24 (28)-tetraen-3-ol	395.3290	$C_{28}H_{43}O$	$[M+H]^+$	394.3308	−1.8	CG
Ergosta-4,6,8 (14),22E-tetraen-3-one	393.3137	$C_{28}H_{41}O$	$[M+H]^+$	393.3152	−1.48	CG
12-(3-adamantan-1-ylureido)dodecanoic acid	393.3135	$C_{23}H_{41}N_2O_3$	$[M+H]^+$	393.3112	2.31	CG
Cordypyrone B	379.1898	$C_{22}H_{28}O_4Na$	$[M+Na]^+$	379.188	1.77	WGA
Opaliferin	375.1429	$C_{18}H_{24}O_7Na$	$[M+Na]^+$	375.1414	1.48	WGA
3,4-Diacetoxy-12,13-epoxy-9-trichothecene-15-ol	367.1714	$C_{19}H_{27}O_7$	$[M+H]^+$	366.1751	−3.68	Both
Cordypyrone A	363.1945	$C_{22}H_{28}O_3Na$	$[M+H]^+$	363.1931	1.47	CG
4-Acetoxyscirpene-3,15-diol	325.1611	$C_{17}H_{25}O_4$	$[M+H]^+$	325.1646	−3.42	Both
Palythinol	325.1244	$C_{14}H_{22}O_7Na$	$[M+H]^+$	325.1258	−1.41	WGA
Ovalicin	319.1507	$C_{16}H_{24}O_5Na$	$[M+H]^+$	319.1516	−0.15	Both
Annullatin C	317.1712	$C_{17}H_{26}O_4Na$	$[M+H]^+$	317.1723	−1.09	CG
Cordycepone	311.1249	$C_{17}H_{20}O_4Na$	$[M+H]^+$	311.1254	−0.44	CG
2′-Deoxy-5′-uridylic acid	311.0635	$C_9H_{16}N_2O_8P$	$[M+H]^+$	311.0639	−0.36	CG
Lupinic acid	307.1505	$C_{13}H_{19}N_6O_3$	$[M+H]^+$	307.1513	0.98	Both
Mesterolone	305.2462	$C_{20}H_{33}O_2$	$[M+H]^+$	305.2473	−1.31	CG
Paecilomycine B	305.1347	$C_{15}H_{22}O_5Na$	$[M+Na]^+$	305.1359	−1.27	Both
Annullatin B	301.1783	$C_{17}H_{26}O_3Na$	$[M+Na]^+$	300.1774	0.87	Both
Annullatin A	299.1605	$C_{17}H_{24}O_3Na$	$[M+Na]^+$	299.1594	−1.31	Both
2-Amino-2′-*O*-methyladenosine	297.1318	$C_{11}H_{17}N_6O_4$	$[M+H]^+$	297.1306	1.22	CG
2′-Amino-2′-deoxyguanosine	283.1162	$C_{10}H_{14}N_6O_4$	$[M+H]^+$	283.1149	1.32	WGA
Paecilomycine A	267.1578	$C_{15}H_{22}O_4$	$[M+H]^+$	267.1591	−1.32	WGA
Amdoxovir	253.1035	$C_9H_{12}N_6O_3$	$[M+H]^+$	253.1044	−0.83	WGA
Cordycepin	252.107	$C_{10}H_{14}N_5O_3$	$[M+H]^+$	252.1091	−2.17	WGA

(Continued)

TABLE 1 (Continued)

Identified metabolites	m/z	Formula	Ion mode	Cal. mass	Delta mass (ppm)	Distribution
Cyclo(L-Phe-L-Pro)	245.1273	$C_{14}H_{17}N_2O_2$	$[M+H]^+$	245.1285	−1.18	Both
Lumichrome	243.0866	$C_{12}H_{10}N_4O_2$	$[M+H]^+$	243.0877	−1	WGA
8-(Hydroxyethylamino)adenine	227.1244	$C_8H_{13}N_6O_2$	$[M+H+MeOH]^+$	227.1251	−0.76	CG
2,6-Diamino-9-(2-hydroxyethoxymethyl)purine	225.1087	$C_8H_{13}N_6O_2$	$[M+H]^+$	225.1095	−0.7	CG
Cephalosporolide C	217.1061	$C_{10}H_{17}O_5$	$[M+H]^+$	217.1071	−0.93	WGA
Cyclo(Leu-Pro)	211.1430	$C_{11}H_{19}N_2O_2$	$[M+H]^+$	211.1414	−1.1	Both
2,6-Dihydroxypseudooxynicotine	211.1068	$C_{10}H_{15}N_2O_3$	$[M+H]^+$	211.1077	−0.94	WGA
Cepharosporolide E	199.0956	$C_{10}H_{15}O_4$	$[M+H]^+$	199.0965	−0.93	WGA
4,7-Dihydroxyoct-2-enoic acid	197.0799	$C_8H_{14}O_4Na$	$[M+Na]^+$	197.0784	1.5	WGA
Cyclo(valyl-prolyl)	197.1275	$C_{10}H_{17}N_2O_2$	$[M+H]^+$	197.1285	−0.75	Both
Suspensolide	195.1371	$C_{12}H_{19}O_2$	$[M+H]^+$	195.138	−0.86	WGA

studies revealed that the metabolites aspergillide B1 and 3α-hydroxy-3,5-dihydromonacolin L may have high inhibitory activity against COVID-19 (El-Hawary et al., 2021).

4. Conclusion

Genomic data of *C. gunnii* has not yet been reported or released; therefore it is currently impossible to analyze potential secondary metabolites of this fungal species through genomic analysis. Early folk use of the stroma and host complexes of *C. gunnii*, so we look forward to find the active ingredients of *C. gunnii* by comparing the activities and metabolites of the mycelium under different cultural conditions with the active and metabolic components of *C. gunnii* in the wild. The activity and metabolome data of each extract varied significantly, among which the activities (cytotoxic and nematicidal activities) and metabolome data from WGA extract and wild *C. gunnii* were more similar. In addition to the compounds we annotated, a large number of unknown metabolites were produced under different growth and cultural conditions of *C. gunnii,* suggesting that the metabolites of this entomogenous fungus have the potential to be further explored.

Data availability statement

The original contributions presented in the study are included in the article/Supplementary material, further inquiries can be directed to the corresponding author.

Author contributions

P-JZ and G-HL: conceptualization and writing – review and editing. P-JZ, S-LQ, and JX: methodology. P-JZ and X-RP: software. P-JZ: validation and funding acquisition. P-JZ and S-LQ: data curation. S-LQ, JX, and J-TW: writing—original draft preparation. All authors have read and agreed to the published version of the manuscript.

Funding

This research was funded by the National Natural Science Foundation of China (32270132 and 31970060) and Yunnan Science and Technology Special Project (202102AA100013 and 202001BB050061).

Conflict of interest

The authors declare that the research was conducted in the absence of any commercial or financial relationships that could be construed as a potential conflict of interest.

Publisher's note

Supplementary material

The Supplementary material for this article can be found online at: https://www.frontiersin.org/articles/10.3389/fmicb.2022.1076577/full#supplementary-material

References

Bode, H. B., Bethe, B., Hofs, R., and Zeeck, A. (2002). Big effects from small changes: possible ways to explore nature's chemical diversity. *Chembiochem* 3, 619–627. doi: 10.1002/1439-7633(20020703)3:7<619::AID-CBIC619>3.0.CO;2-9

Brakhage, A. A., and Schroeckh, V. (2011). Fungal secondary metabolites - strategies to activate silent gene clusters. *Fungal Genet. Biol.* 48, 15–22. doi: 10.1016/j.fgb.2010.04.004

Chang, Y. C., Deng, T. S., Pang, K. L., Hsiao, C. J., Chen, Y. Y., Tang, S. J., et al. (2013). Polyketides from the littoral plant associated fungus *Pseudallescheria boydii*. *J. Nat. Prod.* 76, 1796–1800. doi: 10.1021/np400192q

Chen, X. R., Zhu, G. S., Liu, Z. Y., Yang, X. S., Liang, B., Xu, Q. M., et al. (2009). Study on analgesic effect of mycelia extract from *Paecilomyces gunnii*. *Guizhou Agric. Sci.* 37, 52–54.

Claridge, C. A., Schmitz, H., and Bradner, W. T. (1979). Antitumor activity of some microbial and chemical transformation products of anguidine (4,15-diacetoxyscirpene-3-ol). *Cancer Chemother. Pharmacol.* 2, 181–182. doi: 10.1007/BF00258292

Duan, Y. C., Feng, J., Bai, N., Li, G. H., Zhang, K. Q., and Zhao, P. J. (2018). Four novel antibacterial sesquiterpene-α-amino acid quaternary ammonium hybrids from the mycelium of mushroom *Stereum hirsutum*. *Fitoterapia* 128, 213–217. doi: 10.1016/j.fitote.2018.05.026

El-Hawary, S. S., Mohammed, R., Bahr, H. S., Attia, E. Z., El-Katatny, M. H., Abelyan, N., et al. (2021). Soybean-associated endophytic fungi as potential source for anti-COVID-19 metabolites supported by docking analysis. *J. Appl. Microbiol.* 131, 1193–1211. doi: 10.1111/jam.15031

Grudniewska, A., Hayashi, S., Shimizu, M., Kato, M., Suenaga, M., Imagawa, H., et al. (2014). Opaliferin, a new polyketide from cultures of entomopathogenic fungus *Cordyceps* sp. NBRC 106954. *Org. Lett.* 16, 4695–4697. doi: 10.1021/ol502216j

Huang, D., Yu, C., Shao, Z. Z., Cai, M. M., Li, G. Y., Zheng, L. Y., et al. (2020). Identification and characterization of nematicidal volatile organic compounds from deep-sea *Virgibacillus dokdonensis* MCCC 1A00493. *Molecules* 25:744. doi: 10.3390/molecules25030744

Jiang, B. P., Liu, Y. M., Le, L., Li, Z. Y., Si, J. Y., Liu, X. M., et al. (2014). Cajaninstilbene acid prevents corticosterone-induced apoptosis in PC12 cells by inhibiting the mitochondrial apoptotic pathway. *Cell. Physiol. Biochem.* 34, 1015–1026. doi: 10.1159/000366317

Keller, N. P. (2019). Fungal secondary metabolism: regulation, function and drug discovery. *Nat. Rev. Microbiol.* 17, 167–180. doi: 10.1038/s41579-018-0121-1

Lei, H. M., and Zhao, P. J. (2019). Advances in research on mining fungal secondary metabolites. *Sci. Sin. Vitae* 49, 865–873. doi: 10.1360/SSV-2019-0091

Liang, Z. Q. (1983). A description of *Cordyceps gunnii* in China. *Acta Mycol. Sin.* 2, 258–259. doi: 10.13346/j.mycosystema.1983.04.011

Liu, R., Bao, Z. X., Li, G. H., Li, C. Q., Wang, S. L., Pan, X. R., et al. (2022). Identification of nematicidal metabolites from *Purpureocillium lavendulum*. *Microorganisms* 10:1343. doi: 10.3390/microorganisms10071343

Liu, X. C., Li, H. R., Kang, T., Zhu, Z. Y., Liu, Y. L., Sun, H. Q., et al. (2019). The effect of fermentation conditions on the structure and anti-tumor activity of polysaccharides from *Cordyceps gunnii*. *RSC Adv.* 9, 18205–18216. doi: 10.1039/c9ra01202h

Meng, M., Wang, H. Y., Li, Z. B., Guo, M. Z., and Hou, L. H. (2019). Protective effects of polysaccharides from *Cordyceps gunnii* mycelia against cyclophosphamide-induced immunosuppression to TLR4/TRAF6/NF-kappa B signalling in BALB/c mice. *Food Funct.* 10, 3262–3271. doi: 10.1039/c9fo00482c

Meng, L. H., Wang, C. Y., Mándi, A., Li, X. M., Hu, X. Y., Kassack, M. U., et al. (2016). Three diketopiperazine alkaloids with spirocyclic skeletons and one bisthiodiketopiperazine derivative from the mangrove-derived endophytic fungus *Penicillium brocae* MA-231. *Org. Lett.* 18, 5304–5307. doi: 10.1021/acs.orglett.6b02620

Meng, Z. B., Wen, T. C., and Kang, J. C. (2012). Anti-tumor activity of extracts of *Cordyceps gunnii* (Berk.) Berk. *J. Guizhou Norm. Colle.* 28, 38–40. doi: 10.13391/j.cnki.issn.1674-7798.2012.06.006

Nam, K. S., Jo, Y. S., Kim, Y. H., Hyun, J. W., and Kim, H. W. (2001). Cytotoxic activities of acetoxyscirpenediol and ergosterol peroxide from *Paecilomyces tenuipes*. *Life Sci.* 69, 229–237. doi: 10.1016/s0024-3205(01)01125-0

Olatunji, O. J., Tang, J., Tola, A., Auberon, F., Oluwaniyi, O., and Ouyang, Z. (2018). The genus Cordyceps: an extensive review of its traditional uses, phytochemistry and pharmacology. *Fitoterapia* 129, 293–316. doi: 10.1016/j.fitote.2018.05.010

Paranagama, P. A., Wijeratne, E. M., and Gunatilaka, A. A. (2007). Uncovering biosynthetic potential of plant-associated fungi: effect of culture conditions on metabolite production by *Paraphaeosphaeria quadriseptata* and *Chaetomium chiversii*. *J. Nat. Prod.* 70, 1939–1945. doi: 10.1021/np070504b

Pillalamarri, V., Arya, T., Haque, N., Bala, S. C., Marapaka, A. K., and Addlagatta, A. (2019). Discovery of natural product ovalicin sensitive type 1 methionine aminopeptidases: molecular and structural basis. *Biochem. J.* 476, 991–1003. doi: 10.1042/BCJ20180874

Pu, X. J., Hu, Q. Y., Li, S. S., Li, G. H., and Zhao, P. J. (2021). Sesquiterpenoids and their quaternary ammonium hybrids from the mycelium of mushroom *Stereum hirsutum* by medium optimization. *Phytochemistry* 189:112852. doi: 10.1016/j.phytochem.2021.112852

Qu, S. L., Li, S. S., Li, D., and Zhao, P. J. (2022). Metabolites and their bioactivities from the genus *Cordyceps*. *Microorganisms* 10:1489. doi: 10.3390/microorganisms10081489

Quan, D. J., and Peters, M. G. (2004). Antiviral therapy: nucleotide and nucleoside analogs. *Clin. Liver Dis.* 8, 371–385. doi: 10.1016/j.cld.2004.02.012

Scherlach, K., and Hertweck, C. (2009). Triggering cryptic natural product biosynthesis in microorganisms. *Org. Biomol. Chem.* 7, 1753–1760. doi: 10.1039/b821578b

Su, J., Zhao, P., Kong, L., Li, X., Yan, J., Zeng, Y., et al. (2013). Trichothecin induces cell death in NF-κB constitutively activated human cancer cells via inhibition of IKKβ phosphorylation. *PLoS One* 8:e71333. doi: 10.1371/journal.pone.0071333

Sun, H. Q., Zhu, Z. Y., Tang, Y. L., Ren, Y. Y., Song, Q. Y., Tang, Y., et al. (2018). Structural characterization and antitumor activity of a novel se-polysaccharide from selenium enriched *Cordyceps gunnii*. *Food Funct.* 9, 2744–2754. doi: 10.1039/c8fo00027a

Wakefield, J., Hassan, H. M., Jaspars, M., Ebel, R., and Rateb, M. E. (2017). Dual induction of new microbial secondary metabolites by fungal bacterial co-cultivation. *Front. Microbiol.* 8:1284. doi: 10.3389/fmicb.2017.01284

Zheng, Y. B., Zhang, J. Y., Wei, L. F., Shi, M. M., Wang, J. F., and Huang, J. Z. (2017). Gunnilactams A-C, macrocyclic tetralactams from the mycelial culture of the entomogenous fungus *Paecilomyces gunnii*. *J. Nat. Prod.* 80, 1935–1938. doi: 10.1021/acs.jnatprod.7b00060

frontiers | Frontiers in Microbiology

TYPE Original Research
PUBLISHED 26 January 2023
DOI 10.3389/fmicb.2023.1080743

OPEN ACCESS

EDITED BY
Dewu Zhang,
Institute of Medicinal Biotechnology, Chinese Academy of Medical Sciences, China

REVIEWED BY
Xueqin Lv,
Jiangnan University, China
Moshe Shemesh,
Agricultural Research Organization (ARO), Israel

*CORRESPONDENCE
Chuanbo Zhang
✉ zhangchuanbo2004@163.com

†These authors have contributed equally to this work and share first authorship

SPECIALTY SECTION
This article was submitted to Microbial Physiology and Metabolism, a section of the journal Frontiers in Microbiology

RECEIVED 26 October 2022
ACCEPTED 10 January 2023
PUBLISHED 26 January 2023

CITATION
Wang Y, Chen Y, Xin J, Chen X, Xu T, He J, Pan Z and Zhang C (2023) Metabolomic profiles of the liquid state fermentation in co-culture of *Eurotium amstelodami* and *Bacillus licheniformis*. *Front. Microbiol.* 14:1080743. doi: 10.3389/fmicb.2023.1080743

Metabolomic profiles of the liquid state fermentation in co-culture of *Eurotium amstelodami* and *Bacillus licheniformis*

Yunsheng Wang†, Yincui Chen†, Jiankang Xin, Xianjing Chen, Tingyan Xu, Jiefang He, Zhangxu Pan and Chuanbo Zhang*

Laboratory of Microbial Resources and Industrial Application, College of Life Sciences, Guizhou Normal University, Guiyang, China

As an important source of new drug molecules, secondary metabolites (SMs) produced by microorganisms possess important biological activities, such as antibacterial, anti-inflammatory, and hypoglycemic effects. However, the true potential of microbial synthesis of SMs has not been fully elucidated as the SM gene clusters remain silent under laboratory culture conditions. Herein, we evaluated the inhibitory effect of *Staphylococcus aureus* by co-culture of *Eurotium amstelodami* and three *Bacillus* species, including *Bacillus licheniformis*, *Bacillus subtilis,* and *Bacillus amyloliquefaciens*. In addition, a non-target approach based on ultra-performance liquid chromatography time-of-flight mass spectrometry (UPLC-TOF-MS) was used to detect differences in extracellular and intracellular metabolites. Notably, the co-culture of *E. amstelodami* and *Bacillus* spices significantly improved the inhibitory effect against *S. aureus*, with the combination of *E. amstelodami* and *B. licheniformis* showing best performance. Metabolomics data further revealed that the abundant SMs, such as Nummularine B, Lucidenic acid E2, Elatoside G, Aspergillic acid, 4-Hydroxycyclohexylcarboxylic acid, Copaene, and Pipecolic acid were significantly enhanced in co-culture. Intracellularly, the differential metabolites were involved in the metabolism of amino acids, nucleic acids, and glycerophospholipid. Overall, this work demonstrates that the co-culture strategy is beneficial for inducing biosynthesis of active metabolites in *E. amstelodami* and *B. licheniformis*.

KEYWORDS

***Eurotium amstelodami*, *Bacillus licheniformis*, co-culture, metabolomic profiles, secondary metabolism**

1. Introduction

Secondary metabolites (SMs), produced by microorganisms, are a class of low molecular weight compounds associated with a variety of biological activities. These SMs are also important sources of lead molecules in drug discovery (Chiang et al., 2009; Baral et al., 2018; Linnakoski et al., 2018; Chen et al., 2021; Wang G. et al., 2022). Since the isolation and wide use of Penicillin from *Penicillium* spp. (Fleming, 2001), researchers have isolated and identified a number of SMs with medicinal value from different microbial species. For instance, SMs isolated from *Actinomycetes* species have been important sources of antibiotics for clinical use (Shivlata and Satyanarayana, 2015). Lovastatin, a SM derived from *Aspergillus terreus* and *Monascus ruber*, is a common type of drug which is clinically prescribed to treat high cholesterol (Panda et al., 2010; Guo and Wang, 2014). In recent years, genomic sequencing and annotation data have suggested

the presence of unexpectedly abundant putative SM biosynthetic gene clusters in microbial genomes (Geib and Brock, 2017; Figueiredo et al., 2021). However, previous studies have confirmed that the gene clusters for SMs are silent or exhibit very low expression levels under normal laboratory culture conditions (Chiang et al., 2011; Brakhage, 2013; Ancheeva et al., 2018), resulting in a large gap between discovered SMs and genome capability.

Microbial co-culture typically involves the cultivation of two or more strains (including fungi-fungi, fungi-bacterial, and bacterial-bacterial) in one culture vessel (Mantravadi et al., 2019), and is considered to be an excellent strategy for increasing the content and variety of SMs (Bertrand et al., 2014; Caudal et al., 2022). In the competition for living space and nutrients, microorganisms are constantly interacting with each other, which can activate the expression SM encoding gene clusters (Costa et al., 2019). Fumicyilne A was a novel SM obtained by co-culture of the soil-derived bacterium *Streptomyces rapamycinicus* and *Aspergillus fumigatus*, the production of Fumicyilne A might be attributed to the activation of the biosynthetic pathway of silent terpenoids in *A. fumigatus* (König et al., 2013). Similarly, Sung and colleagues (Sung et al., 2017) found that co-culture of Marine-Derived *Streptomyces* spp. and human pathogens resulted in enhanced production of three antibiotics, including Granaticin, Granatomycin D, and Dihydrogranaticin B. However, the use of co-culture in the activation of silent SM genes remains mostly accidental. Further, this process lacks reproducibility and predictability, which poses a significant challenge in future co-culture strategies for mining SMs.

Eurotium amstelodami is a filamentous fungus classified under the Phylum Ascomycota. Previous reviews and studies have shown that *E. amstelodami* can produce abundant useful SMs (Slack et al., 2009), such as Neoechinulin A, Neoechinulin B, Epiheveadride, Flavoglaucin, Auroglaucin, Isotetrahydroauroglaucin, Echinulin, Preechinulin, and Neoechinulin E. Additionally, Asperflavin, a SM isolated from marine-derived *E. amstelodami* inhibits the production of pro-inflammatory cytokines, including TNF-α, IL-1β, and IL-6 (Yang et al., 2017), which may be potentially promising lead molecules for preventing and treating inflammatory diseases. These data support the hypothesis that *E. amstelodami* is a rich resource for mining novel SMs. Similarly, *Bacillus* species are common gram-positive bacterium detected in the air (Premkrishnan et al., 2021), water (Mothe and Sultanpuram, 2016), soil (Lim et al., 2016), and fermented foods (Wu et al., 2022). Various *Bacillus* members (e.g., *Bacillus licheniformis*, *Bacillus subtilis*, and *Bacillus amyloliquefaciens*) are extensively used in the production of bioinsecticides and antibiotics due to their ability to synthesize a number of metabolites with biological activity (Xu et al., 2014; Yang et al., 2016; Shahzad et al., 2017; Mohamad et al., 2018), indicating a great potential for SM synthesis.

Many co-culture experiments involving two or more microorganisms isolated from the same habitats [e.g., soil (Wang et al., 2021), plant endophyte (Li H. T. et al., 2020), the ocean (Bao et al., 2017), and fermentation food (Liu Z. et al., 2022)] seem to show excellent effects on the induction and synthesis of SMs. In this case, microbes living and reproducing in the same ecological environment may compete for similar resources, including living space and nutrients, resulting in generating of some new compound molecules to improve viability (Knowles et al., 2022). In this work, we established a co-culture system for *E. amstelodami* and three *Bacillus* species (*B. amyloliquefaciens*, *B. licheniformis*, and *B. subtilis*) isolated from the Maotai-flavor Daqu (saccharification fermentation agent for liquor fermentation) and evaluated the inhibitory effect of different co-culture combinations on *Staphylococcus aureus*. Moreover, the metabolites (extracellular and intracellular) from the pure-culture and co-culture of *E. amstelodami* and *B. licheniformis* were analyzed and identified using a non-targeted metabolomics approach. Furthermore, we propose a potential mechanism behind the enhanced inhibition of *S. aureus* during the co-culture process.

2. Materials and methods

2.1. Strains and cultivation

Eurotium amstelodami GZ23, *B. licheniformis* GZ241, *B. subtilis* GZ237, and *B. amyloliquefaciens* GZ121 were isolated from Maotai-flavor Daqu produced in Renhuai City, Guizhou Province, China. According to our previous study (Wang Y. et al., 2022), *E. amstelodami* was grown on high-concentration sodium chloride MYA solid medium (malt extract 20 g, yeast extract powder 5 g, agar powder 15 g, sucrose 30 g, NaCl 170 g and water 1,000 ml) at 37°C to induce a conidia production, the appropriate concentration of conidia of *E. amstelodami* was adjusted to 1×10^6 spore/mL by a blood count plate before inoculation. *Bacillus* species were inoculated in 150 ml LB liquid medium (Lysogeny Broth: 10 g/l NaCl, 5 g/l yeast extract, 10 g/l tryptone) at 37°C and 180 rpm/min for 12 h, and the cell concentration was adjusted to 1×10^8 CFU/ml. To prepare the test bacteria, *S. aureus* ATCC 25923 was inoculated into 5 ml LB liquid medium and incubated overnight at 37°C while shaking at 180 rpm until a concentration of 1×10^6 CFU/ml was reached.

2.2. Co-culture conditions

A liquid co-culture system of *E. amstelodami* and *Bacillus* spices was established. In brief, conidia of *E. amstelodami* were inoculated in 150 ml of MYA liquid medium at a volume ratio of 1:4, and cultured at 30°C on a rotary shaker at 180 rpm for 3 day. Then, the pre-cultured *Bacillus* species were added to MYA medium in the same proportion and the cultivations were continued for 7 day. For pure culture, *E. amstelodami* and *Bacillus* species were grown in 150 ml MYA liquid medium at the same inoculation ratio and incubated at 30°C for 10 day and 7 day by shaking at 180 rpm/min, respectively.

2.3. Antibacterial activity assay

Antibacterial activity tests were performed according to Zhang X. et al. (2022) with minor modifications. Briefly, the fermentation supernatant was collected and filtered using a 0.22 μm filter membrane to remove bacteria at the end of the cultivation. Subsequently, *S. aureus* test solution (10 μl) and 100 μl of LB liquid medium were seeded into 96-well plates, followed by addition of 80 μl of fermentation supernatant. Following incubation for 10 h at 37°C, the uninoculated sterilized MYA medium served as control. The optical density of all wells was measured using a microplate reader at 600 nm. All experiments were performed in triplicate. Antibacterial activity was calculated as a percentage as follows: Inhibition rate (%) = (*S. aureus* OD_{600} in the control – *S. aureus* OD_{600} in the test)/*S. aureus* OD_{600} in the control × 100.

2.4. Growth monitoring

At the end of fermentation, the pure culture broths of *E. amstelodami* or *B. licheniformis* were centrifuged at 5000 × g at 4°C for 5 min, and the supernatants were discarded. Next, cells or mycelia were harvested and washed three times with sterile water and subsequently dried at 100°C in an oven to a constant dry weight. For co-culture, the mycelia of *E. amstelodami* were separated using Whatman no.1 filter paper (Sigma-Aldrich, Darmstadt, Germany) and then washed three times in sterile distilled water. Meanwhile, due to the small size of *B. licheniformis* cells, they can easily pass through the filter paper during the filtration process and were collected after a similar centrifugation procedure to remove the supernatants. All samples were oven dried at a constant temperature before dry weight was measured. All treatments were carried out in triplicate.

2.5. Microscopic analysis

The ultrastructure of *E. amstelodami* and *B. licheniformis* during co-culture and pure culture was observed by scanning electron microscopy (SEM). Simply, the cultures were fixed in 5% (v/v) glutaryl glycol for 12 h at 4°C, and the excess fixative was drained off. Cells were then washed three times with phosphate buffer solution and ethanol gradient dehydration (30, 50, 70, 90 and 100% (v/v)) was performed for 10 min, followed by drying with a critical point dryer (CPD300, Leica Microsystems, Wetzlar, Germany). The samples were coated with carbon (Bal-Tec Sputter Coater SCD 005, Bal-Tec GmbH, Witten, Germany) and examined using a scanning electron microscope (UHR Nova NanoSEM 230, FEI Company, Hillsboro, OR, United States).

2.6. Metabolomic analysis

2.6.1. Preparation of extracellular metabolome samples

The fermentation broths were centrifuged at 5,000 × g (10 min, 4°C) after cultivation and the supernatant was collected, followed by drying with LGJ-18A freeze dryer (Shanghai Hefan Instrument Co., Ltd.) to obtain a dried power, which was then stored at-80°C for subsequent analysis.

2.6.2. Preparation of intracellular metabolome samples

Pure culture fermentations broths of *E. amstelodami* and *B. licheniformis* were centrifuged at 5,000 × g for 10 min at 4°C, then the supernatants were discarded, and cell pellets were washed three times with deionized water. As for the co-culture, the mycelia of *E. amstelodami* were separated by Whatman no.1 filter paper and then washed three times in sterile distilled water. Lastly, cells of *B. licheniformis* were collected by centrifugation in a frozen centrifuge. All samples were stored at-80°C for later use.

2.6.3. Metabolomic detection

At the time of use, the frozen sample was ground to a fine powder in liquid nitrogen. The sample powder (50 mg) was accurately weighed into a 2 ml centrifuge tube and then thoroughly mixed with a 400 µl solution (methanol: acetonitrile = 1:1 (v:v), containing 0.02 mg/ml internal standard (L-2-chlorophenylalanine)) by using a vortex mixer. Subsequently, the mixture was fully ground using a frozen tissue lapping apparatus Wonbio-96c (containing a grinding bead with a diameter of 6 mm), followed immediately by low-temperature extraction (40 kHz, 5°C). The sample was placed at-20°C for 30 min and centrifuged for 15 min (13,000 g, 4°C). The supernatants were then transferred into the injection vials for analysis.

The extracted samples were analyzed on a UHPLC-triple TOF system from AB SCIEX coupled with a Triple TOF 5600 system. At 40°C, 10 µl of each sample were injected onto an ACQUITY UPLC HSS T3 column (2.1 × 100 mm, 1.8 µm particle size; Waters, Milford, United States) with a flow rate of 0.40 ml/min, and the total separation time for chromatographic analysis was set as 16 min. Analysis was performed following chromatographic conditions: phase A: 95% water +5% acetonitrile (0.1% formic acid in water), phase B: 47.5% acetonitrile +47.5% isopropanol +5% water (0.1% formic acid in water), *t*: 0–5 min 100% A, 0.5–2.5 min 75% A, 2.5–13 min 0% A, 13–16 min 0%A. We have previously reported the optimization of the UHPLC conditions and mass spectrometry parameters (Wang Y. et al., 2022). Further, the raw data were imported into the metabolomics software, Progenesis QI (Waters Corporation, Milford, United States), for processing and identification of characteristic peaks. The MS and MS/MS mass spectrometry information were matched to the metabolic database with the MS mass error set to less than 10 ppm, and the metabolites were identified according to the matching of secondary mass spectrometry. The main databases used were http://www.hmdb.ca, http://metlin.scripps.edu, as well as other public databases.

2.7. MS/MS molecular networking

The Global Social Molecular Network for Natural Products (GNPS[1]), a web-based mass spectrometry ecosystem for storing, analyzing, and sharing MS/MS spectral data, allows for visualization of datasets from different users and comparisons to all publicly available reference spectra, thereby enabling annotation of known molecules and discovery of putative analogs (Wang et al., 2016). In this study, the original disembarking data of metabolic profiling were processed in MS convert (version 3.0.10051, Vanderbilt University, Nashville, TN, USA) and uploaded separately to the GNPS platform using WinSCP software (version 5.17.3) to create a molecular network of extracellular metabolites. The main parameters for creating a classical molecular network were: Precursor ion mass tolerance of 2.0 Da and fragment ion tolerance of 0.5 Da. Edges were filtered by setting the default GNPS minimum cosine score above 0.7 and more than 6 matched peaks. Network topK of 10, minimum matched fragment ions of 2, and more than 6 matched peaks. To enhance the chemical structural information in the molecular network, the molecular networks were then performed with the MolNetEnhancer workflow, and Cytoscape software (v3.8.2) was used to visualize the interaction network.

The molecular network job (in the positive ion mode) is available at https://gnps.ucsd.edu/ProteoSAFe/status.jsp?task=cae28240c12549fcb7d50715dcc31eed.

1 https://gnps.ucsd.edu/

The molecular network job (in the negative ion mode) is available at https://gnps.ucsd.edu/ProteoSAFe/status.jsp?task=81b0246e0f404468996ba0e9a58eba4e.

MolNetEnhancer network job (in the positive ion mode) is available at https://gnps.ucsd.edu/ProteoSAFe/status.jsp?task=5d47c651ac394eb6b90f6b1ac4e3af9c.

MolNetEnhancer network job (in the negative ion mode) is available at https://gnps.ucsd.edu/ProteoSAFe/status.jsp?task=32c528365e0145a5a7b6c6b2ae41f36b.

2.8. Statistical analysis

All experiments were performed in triplicate, and the obtained data were presented as the mean ± standard deviation. Statistical computation and plotting were conducted using Microsoft Excel 2022 and GraphPad Prism 8.0.2, respectively. The significant differences in antibacterial effects between different treatments were analyzed by one-way analysis of variance with Duncan's test ($p < 0.05$). For UPLC-TOF-MS analysis, principal component analysis (PCA) and partial least squares discriminant analysis (PLS-DA) were performed by using ropes (R packages) version 1.6.2. Student's t-test was used to analyze significant differences between groups. The differential metabolites between groups were identified according to the value (value >1) of variable importance in the projection (VIP), *t*-test analysis ($p < 0.05$) for the fold change (FC) analysis (FC >=1.5 or <= 0.67). Pathway enrichment analysis of the differential metabolites was performed based on the Kyoto Encyclopedia of Genes and Genomes (KEGG) database.

3. Results

3.1. Co-culture resulted in an increased antibacterial activity

This work evaluated the effect of liquid co-culture of *E. amstelodami* and three *Bacillus* species on antibacterial activity against *S. aureus*. As shown in Table 1, we observed that the cell free culture supernatant of all strains [*E. amstelodami* (20.11%), *B. licheniformis* (3.18%), *B. subtilis* (53.83%), and *B. amyloliquefaciens* (85.89%)] exhibited inhibition on *S. aureus* in pure culture. Interestingly, co-culture of *E. amstelodami* and *Bacillus* species improved the antibacterial activity against *S. aureus*, compared to pure coculture. Among them, the co-culture combination of *E. amstelodami* with *B. licheniformis* (76.71%) showed the most significant improvement in antibacterial activity, which was 3.81-fold and 24.12-fold higher than *E. amstelodami* and *B. licheniformis* pure culture, respectively. These data suggest that the co-culture strategy significantly changes the components in the liquid medium, including the degradation and transformation of some substances. As the co-culture combination of *E. amstelodami* and *B. licheniformis* showed excellent effect, we chose the combination of these two microorganisms for further analysis.

TABLE 1 Co-culture and pure culture of *E. amstelodami* and *Bacillus* species showed different inhibition effects on *S. aureus*.

Treatment	Inhibition rate (%)[a]
E. amstelodami pure culture	20.11 ± 0.04d
B. licheniformis pure culture	3.18 ± 0.01e
B. subtilis pure culture	53.83 ± 0.04c
B. amyloliquefaciens pure culture	85.89 ± 0.03a
Co-culture of *E. amstelodami* and *B. licheniformis*	76.71 ± 0.04b
Co-culture of *E. amstelodami* and *B. subtilis*	82.26 ± 0.01a
Co-culture of *E. amstelodami* and *B. amyloliquefaciens*	90.21 ± 0.01a

Data were reported as the mean value ± standard. [a]Different letters in the same column indicated significant differences between treatments, $p < 0.05$, $n = 3$.

3.2. The interaction between *Eurotium amstelodami* and *Bacillus licheniformis*

Here, SEM was used to study the morphological characteristics of *E. amstelodami* and *B. licheniformis* during co-culture. As shown in Figures 1A,B, no significant differences in the cell morphology of *E. amstelodami* were observed between co-culture and pure culture, and similar results were obtained in *B. licheniformis* (Figure 1C). Interestingly, we found that *E. amstelodami* and *B. licheniformis* were tightly entwined together during co-culture, and few cells of individual *B. licheniformis* were present in the fermentation broth. In addition, the dry weight of *E. amstelodami* was significantly decreased by 2.75 times during co-culture compared to pure culture (Figure 1D). Conversely, *B. licheniformis* appeared to be unaffected (Figure 1E), indicating that *B. licheniformis* inhibited the growth of *E. amstelodami* during the co-culture process.

3.3. Extracellular metabolomic analysis of co-cultures

To decipher the mechanism behind the improvement of antibacterial activity against *S. aureus* due to co-culture, we performed metabolomic analysis for detection the extracellular metabolic differences of *E. amstelodami* and *B. licheniformis* between co-culture and pure culture. PCA analysis is an unsupervised multivariate statistical analysis method, which can reflect the overall differences and the degree of variation between the samples of each group. As shown in Figure 2A, the PCA score plots exhibited a great separation trend in extracellular metabolomic profiles among *E. amstelodami* pure culture (LA), *B. licheniformis* pure culture (LB), and co-culture (LAB), and the first and second principal components explained 45.50 and 30.00% of the total variability, respectively. To achieve and maximize distinction from different groups, the samples were grouped using a supervised partial least square discriminant analysis (PLS-DA). As shown in Figures 2B, a total of 9 samples from the 3 groups were within 95% confidence intervals. LA, LB, and LAB groups were greatly separated, and the reproducibility of samples between groups was excellent, indicating that metabolic profiles of *E. amstelodami* and *B. licheniformis* changed during co-culture. The R2X(*cum*), R2Y(*cum*), and Q2(*cum*) values obtained from PLS-DA were 0.662, 0.747, and 0.571, respectively, suggesting the model was reliable and with good prediction ability.

Based on the results of PLS-DA model, the differential extracellular metabolite features between groups were selected using a combination of VIP value >1.0, value of p ($p <= 0.05$) and fold change (FC >=1.5 or FC <=0.67). A total of 316 significantly different extracellular metabolites were found between *E. amstelodami* co-culture and pure culture (162 up-regulated and 254 down-regulated metabolites;

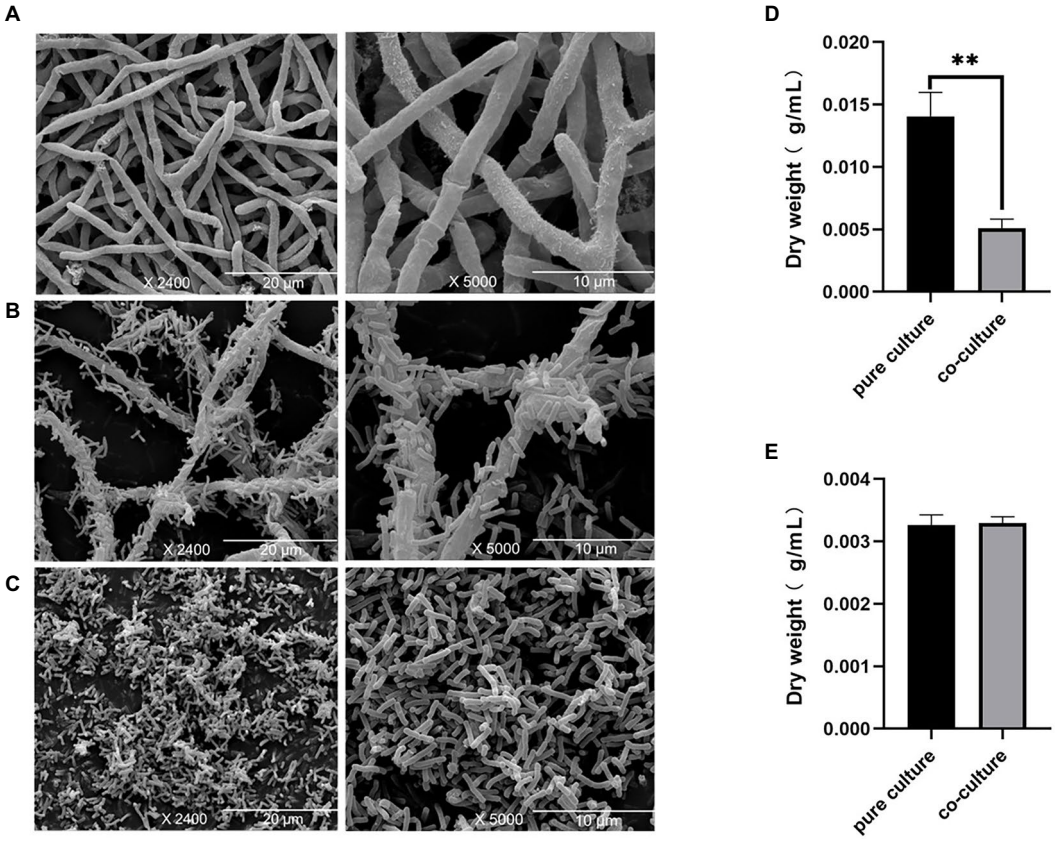

FIGURE 1
Scanning electron microscopy of *Eurotium amstelodami* mycelia in pure culture **(A)**, co-cultures **(B)** and *Bacillus licheniformis* pure culture **(C)**. Dried mycelial and cells weight of *E. amstelodami* **(D)** and *B. licheniformis* **(E)**. Data are reported as the mean value ± standard deviation of three replicates, Statistical significance (Student's t-test) is indicated as follows: *p<0.05.

Supplementary Table S1). At the same time, a total of 250 significantly different extracellular metabolites were obtained in *B. licheniformis* (154 up-regulated and 96 down-regulated metabolites; Supplementary Table S2). Next, we screened for the metabolites that were only overexpressed in the co-culture group. The screening criteria included (i) high contribution to sample classification in PLS-DA (VIP score > 1.5); (ii) the fold change between groups (*E. amstelodami* co-culture vs. pure culture and *B. licheniformis* co-culture vs. pure culture) was larger than 1.5; (iii) statistically significant change in the pairwise comparison between groups (*E. amstelodami* co-culture vs. pure culture and *B. licheniformis* co-culture vs. pure culture) was smaller than 0.05 (*value of p* in Student's t-test). Finally, 53 metabolites were obtained to construct the heatmap (Figure 2C; Supplementary Table S3). We found that the contents of various amino acids, peptides, and analogs were induced to be highly expressed, including Capryloylglycine, Leucyl-Cystein, Glutamylthreonine, Prolylphenylalanine, Tyrosyl-Histidine, Pentosidine, and Hydroxyprolyl-Tyrosine. Notably, a variety of biologically active SMs were also identified, including Nummularine B, Lucidenic acid E2, Elatoside G, Aspergillic acid, 4-Hydroxycyclohexylcarboxylic acid, Copaene, and Pipecolic acid.

3.4. Intracellular metabolomic analysis of co-cultures

The PCA score plots exhibited a good separation trend in intracellular metabolomic profiles among *E. amstelodami* pure culture (SA), *E. amstelodami* co-culture (SCA), *B. licheniformis* pure culture (SB), and *B. licheniformis* co-culture (SCB), and the first and second principal components explained 45.50 and 20.90% of the total variability (Figure 3A), respectively. As shown in Figure 3B, the intracellular metabolites of *E. amstelodami* between pure culture and co-culture were clearly distinguished in the PLS-DA model, and the reproducibility of the samples between groups was excellent. The R2X(*cum*), R2Y(*cum*), and Q2(*cum*) values obtained from PLS-DA were 0.662, 0.747, and 0.571, respectively, indicating that the model was reliable and had good prediction ability, and similar results were obtained in *B. licheniformis* (Figure 3C). These data indicated that the intracellular metabolites also dramatically changed during the co-culture of *E. amstelodami* and *B. licheniformis*.

A total of 397 significantly different intracellular metabolites were selected between *E. amstelodami* co-culture and pure culture (161 up-regulated and 224 down-regulated metabolites; Figure 4A; Supplementary Table S4). We found that a large number of up-regulated metabolites were annotated as amino acids, peptides, and analogs, including Capryloylglycine, Tyrosyl-Histidine, Prolylphenylalanine, Allysine, Citrulline, Glycyl-Arginine, Tyrosyl-Proline, Lysyl-Arginine, and Tyrosyl-Isoleucine. Interestingly, the contents of abundant terpenoid were enhanced during the co-culture process, such as Oleoside dimethyl ester, Cyclopassifloside II, Oleoside 11-methyl ester, (4R,6S)-p-Menth-1-ene-4,6-diol 4-glucoside, Citronellyl beta-sophoroside, 6beta-Hydroxy-3-oxo-12-oleanen-28-oic acid, 10-Hydroxymelleolide, and Ganoderic acid I. In addition, several other types of SMs (e.g., Tryptophanol, Torvoside E, Glycitin, Cholic acid

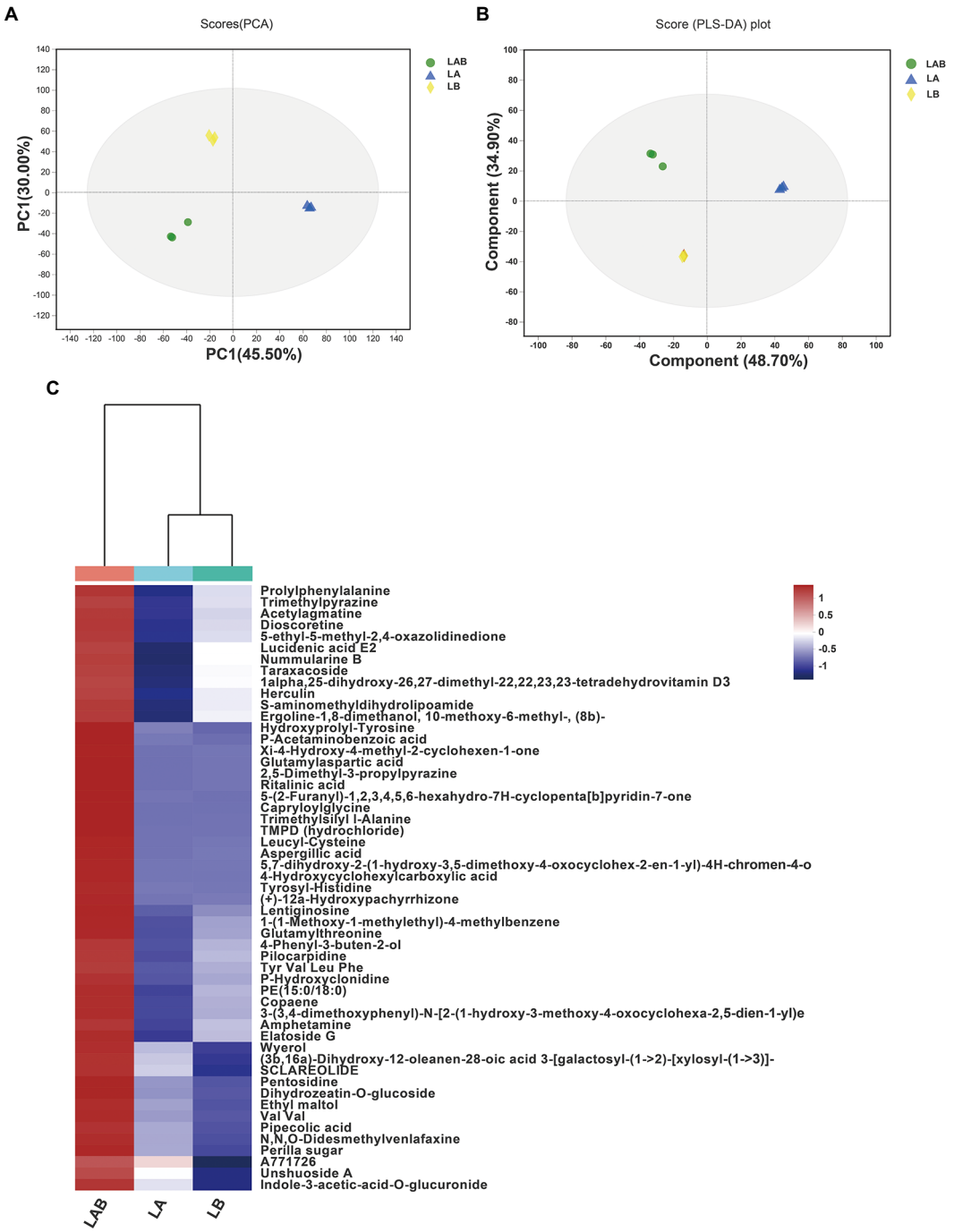

FIGURE 2
Principal components analysis (PCA) score plots of extracellular metabolites **(A)**. Partial least squares discriminant analysis (PLS-DA) score plots of extracellular metabolites **(B)**. Hierarchical clustering analysis (HCA) of the 59 extracellular metabolites only overexpressed in co-culture group and represented on a heatmap **(C)**. (LA, extracellular metabolites of *E. amstelodami* pure culture; LB, extracellular metabolites of *B. licheniformis* pure culture; LAB, extracellular metabolites of co-culture).

glucuronide, and Norharman) were also enhanced in co-culture. Among the downregulated metabolites, various metabolites were annotated as fatty acids and conjugates, such as Palmitoleic acid, Floionolic acid, Pentadecanoic acid, 2-Isopropylmalic acid, Cyclohexaneundecanoic acid, 13-hydroxyoctadecanoic acid, and 2-Hydroxy-22-methyltetracosanoic acid. We further used the KEGG database for functional pathway enrichment analysis of differentially expressed metabolites. The results showed that the different metabolites were mainly involved in biosynthesis of cofactors (map01240), lysine degradation (map00310), purine metabolism (map00230), ABC transporters (map02010), pyrimidine metabolism (map00240), and tryptophan metabolism (map00380), which were related to the primary metabolism of microorganisms (Figure 4C).

A total of 330 significantly different intracellular metabolites were screened between *B. licheniformis* co-culture and pure culture (203 up-regulated and 127 down-regulated metabolites; Figure 4B;

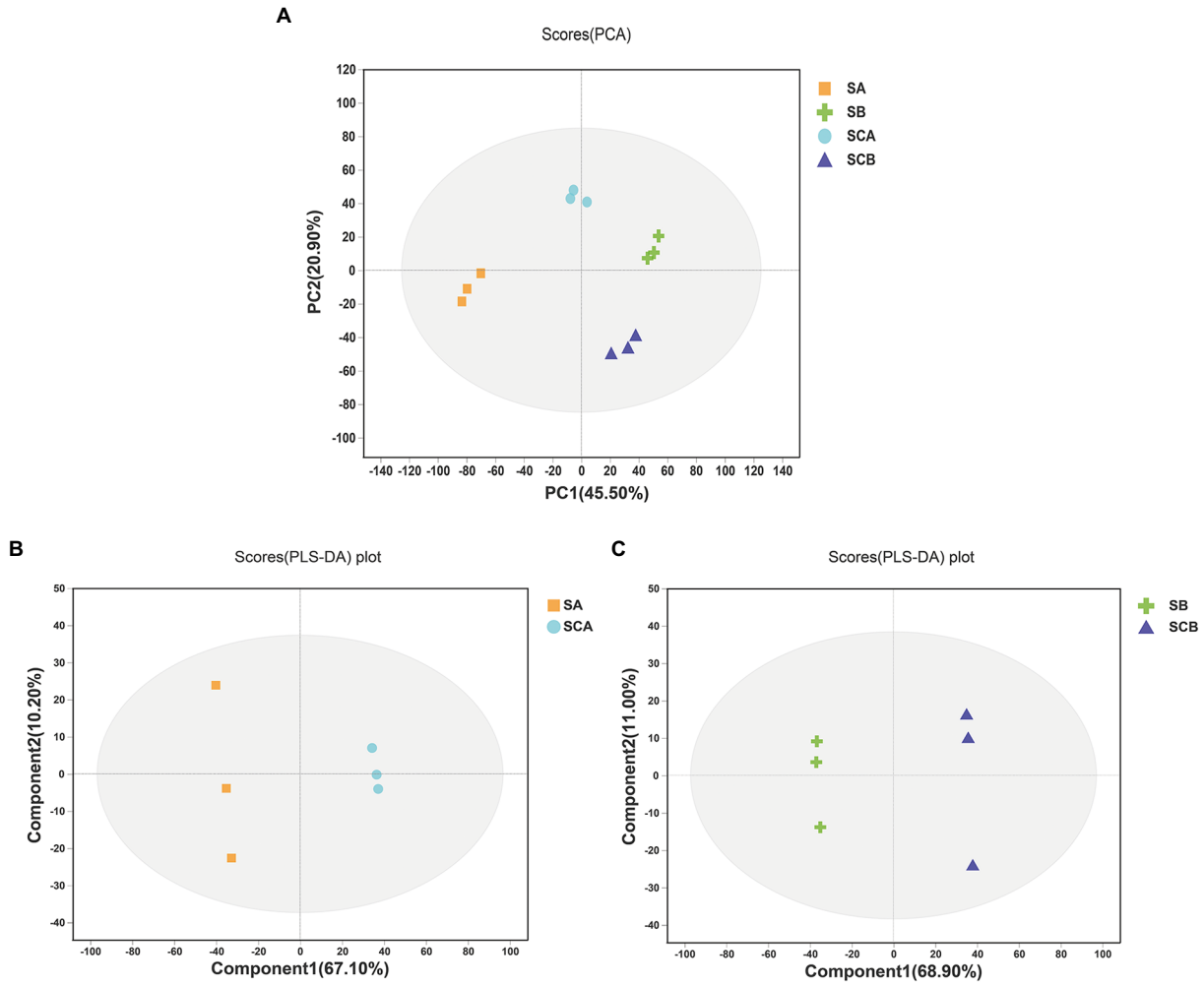

FIGURE 3
PCA score plots of intracellular metabolites **(A)**. PLS-DA score plots of intracellular metabolites between *E. amstelodami* pure culture and co-culture**(B)**. PLS-DA score plots of intracellular metabolites between *B. licheniformis* pure culture and co-culture **(C)**. (SA, intracellular metabolites of *E. amstelodami* pure culture; SCA, intracellular metabolites of *E. amstelodami* co-culture; SB, intracellular metabolites of *B. licheniformis* pure culture; SCB, intracellular metabolites of *B. licheniformis* co-culture).

Supplementary Table S5). Compared to pure culture, a large number of amino acids, peptides, and analogs such as Asparaginyl-Histidine, Glycylproline, Isoleucylproline, L-Alloisoleucine, Leucyl-Cysteine, Pantetheine, Saccharopine, and Acetyl-L-tyrosine were enhanced in co-culture. Additionally, some fatty acyls and conjugates were highly expressed, including 6-(2-Hydroxyethoxy)-6-oxohexanoic acid, S-3-oxodecanoyl cysteamine, Mevalonic acid, 3,4-Methyleneadipic acid, 2-Isopropylmalic acid, and 1-Pentadecanecarboxylic acid. However, the contents of several fatty acyls and conjugates were also decreased during the co-culture process, including Floionolic acid, 2-Hydroxy-22-methyltetracosanoic acid, Physapubescin, Dodecanoylcarnitine, Sorbitan laurate, and Hexadecanedioic acid, suggesting that *B. licheniformis* required significant fatty acid metabolism in response to competition for space and nutrients in broth co-culture. The main KEGG functional pathways enriched in differential metabolites were biosynthesis of cofactors (map01240), ABC transporters (map02010), purine metabolism (map00230), glycerophospholipid metabolism (map00564), cysteine and methionine metabolism (map00270), was well as pantothenate and CoA biosynthesis (map00770; Figure 4D).

3.5. Molecular networking analysis

To further explore the chemical space of the extracellular metabolites produced during co-culture of *E. amstelodami* and *B. licheniformis*, we uploaded the extracellular MS–MS data to the GNPS platform for classical molecular network construction. A total of 3,787 spectra were obtained in MN, of which 457 (12.07%) consensus spectra (green node) were obtained in the *E. amstelodami* pure culture, 527 (13.92%) consensus spectra (blue nodes) were obtained for *B. licheniformis* pure culture, and 604 (15.95%) consensus spectra (red nodes) were obtained for co-culture group in the positive ionization mode. Additionally, 218 putative annotated compounds were obtained by automatic annotation of GNPS (Supplementary Table S6). Here, the MolNetEnhancer tool was used to enhance chemical structural information. As shown in Figure 5A, molecular networks of the fractions revealed the presence of clusters related to different chemical classes. The co-culture of *E. amstelodami* and *B. licheniformis* resulted in the accumulation of various metabolites in different molecular families, such as Glycerophosphoethanolamine families, including PE-AEG (o-17:0/17:1) and PE (16:1/16:1;

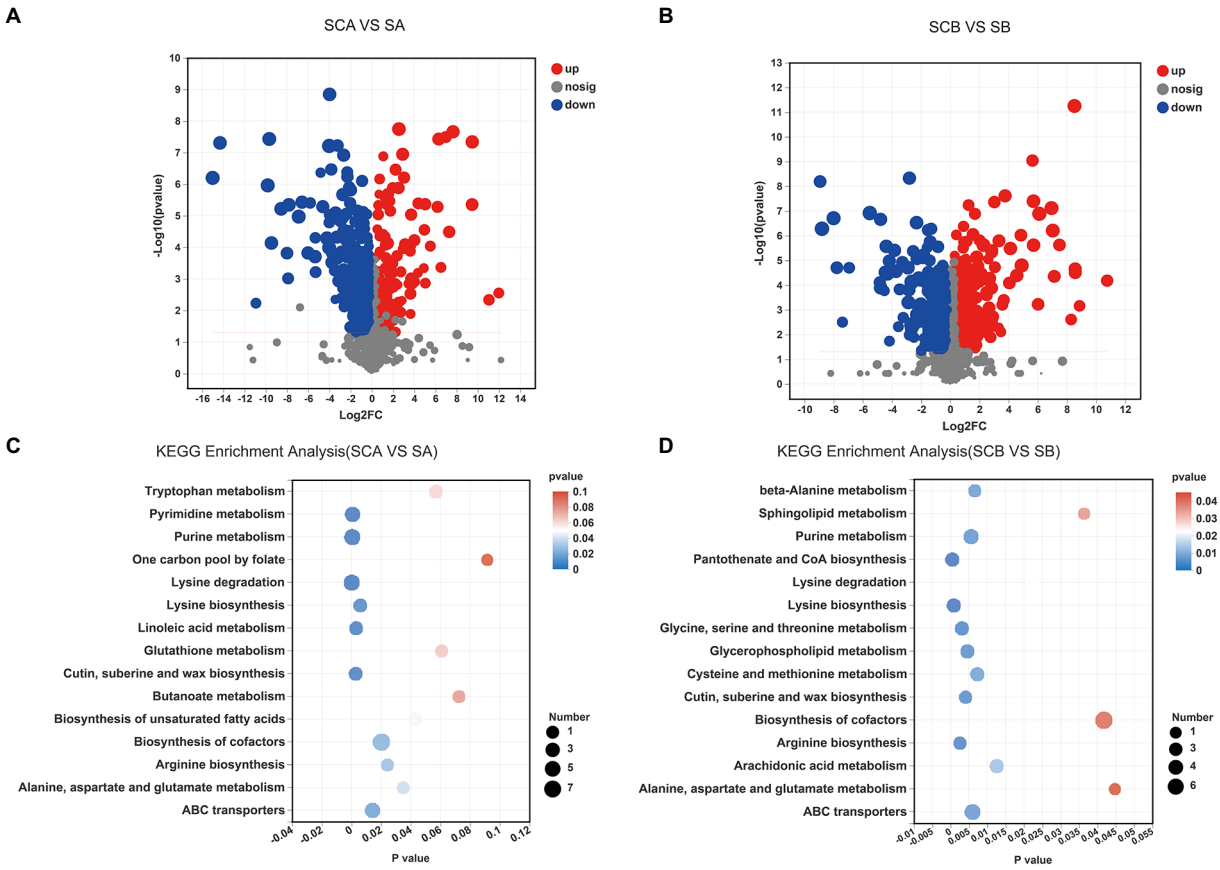

FIGURE 4
Volcano plot displaying the differences in intracellular metabolic profiles between pure culture and co-culture of *E. amstelodami* **(A)** and *B. licheniformis* **(B)**. Pathway analysis for intracellular metabolites of *E. amstelodami* **(C)**, *B. licheniformis* **(D)** pure culture and co-cultures.

Figure 5B); Styrenes families (a putative compound was annotated as Yohimbine; Figure 5C), and amino acids, peptides, and analogs (Figure 5D). In addition, a putative molecular family of flavonoid glycosides was annotated (Figure 5E), which exhibited no significant differences between the co-culture and pure culture group. Furthermore, Figure 5F showed a putative flavoglaucin that was detected only in the co-culture group, indicating that it was induced by co-culture.

In the negative ionization mode, A total of 4,530 spectra were obtained in MN, of which 698 (15.41%) consensus spectra were obtained in the *E. amstelodami* pure culture, 702 (15.50%) consensus spectra were obtained for *B. licheniformis* pure culture, and 741 (16.36%) consensus spectra were obtained in co-culture group. Additionally, 99 putative annotated compounds were obtained by automatic annotation of GNPS (Supplementary Table S7), less than those annotated in the positive ionization mode. As shown in Supplementary Figure S1B, a putative molecular family of benzodiazeines was annotated (Figure 5E), which exhibited no significant differences between the co-culture and pure culture group. Similarly, we observed that a putative molecular family of Glycerophosphoethanolamines (4 compounds were annotated, including PE (17:0/0:0), PE (18:2/0:0), PE (15:0/15:0) and PE (15:0/18:2)) were enhanced in the co-culture group (Supplementary Figure S1C), as well as several unannotated molecular families (Supplementary Figure S1D–E). In addition, a molecular family of Anthraquinones were identified in the *E. amstelodami* pure culture group but not in the other groups (Supplementary Figure S1F), indicating that co-culture might inhibit the production of these compounds. Interestingly, Supplementary Figure S5G showed a putative phytoceramide C2 that was detected only in the co-culture group, indicating that some new SMs were produced.

3.6. Co-culture affected both primary and secondary metabolism

We summarized the changes of some intracellular and extracellular metabolites as well as metabolic pathways during co-culture of *E. amstelodami* and *B. licheniformis*. As shown in Figure 6, compared with pure culture, we found that many primary metabolites involved in amino acid metabolism and nucleic acid metabolism (pyrimidine metabolism and purine metabolism) were greatly down-regulated in *E. amstelodami*, such as oratidine, uridine, uracil, pesudouridine, inosine, guanine, guanosine, hypoxanthine, and urate, indicating that its primary metabolism was weakened. However, opposite results were obtained in *B. licheniformis*. Compared to pure culture, we observed that multiple metabolites involved in purine metabolism and pantothenate and CoA biosynthesis pathways were significantly up-regulated, including xanthylic acid, xanthosine, urcial, L-aspartic acid, and xanthine, suggesting the vigorous and active metabolism of *B. licheniformis*. Additionally, some important intermediate metabolites enriched in the glycerophospholipid metabolic pathway were differentially expressed in *B. licheniformis*. Taken together, these data suggest that co-culture

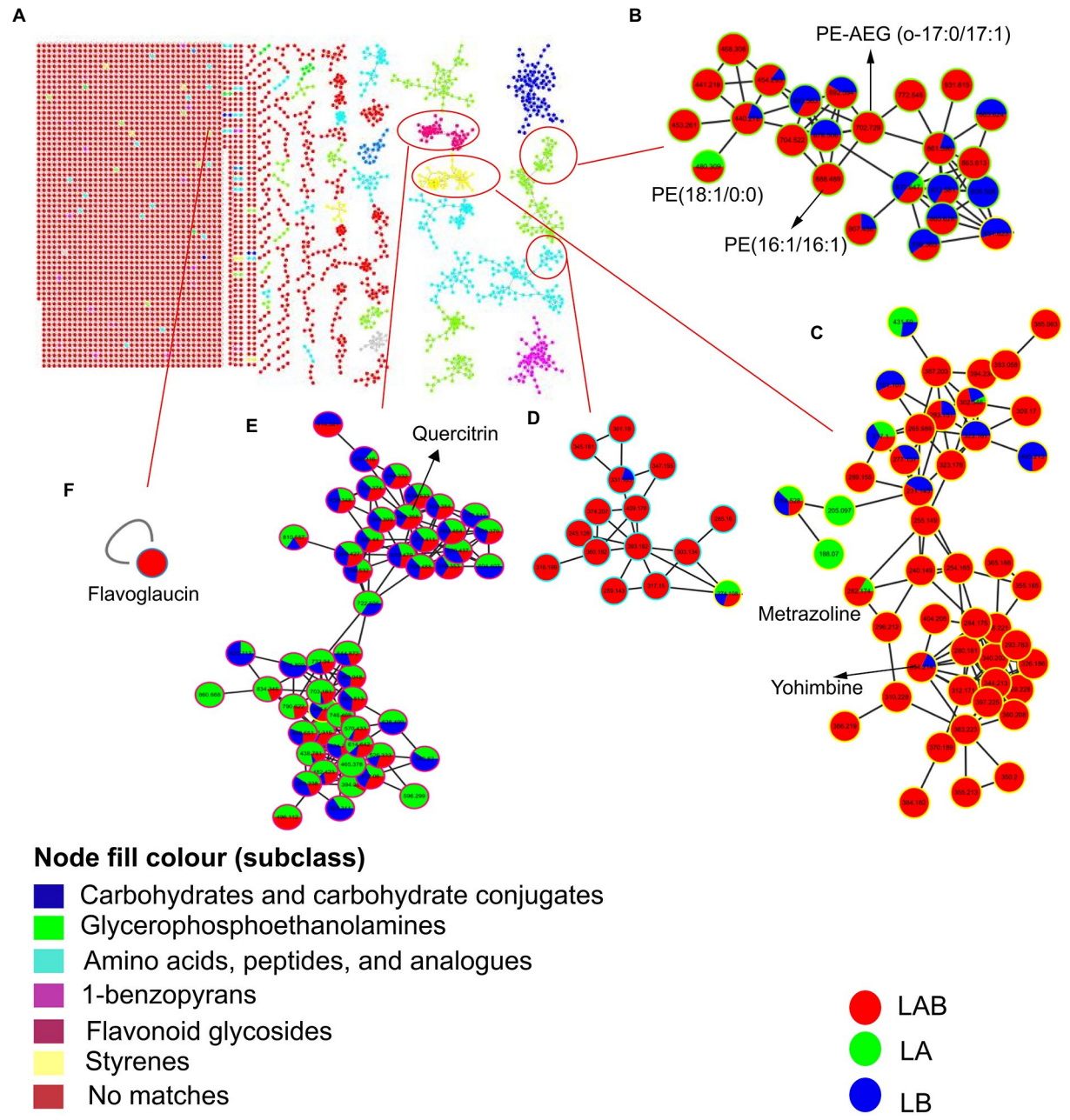

FIGURE 5
Molecular network of the MS/MS spectra for extracellular extracts of *E. amstelodami*, *B. licheniformis* pure culture and co-cultures in positive ion mode **(A)**. Chemical classification was achieved by MolNetEnhancer at the subclass level, **(B–E)** shows clusters of glycerophosphoethanolamines, styrenes, amino acids, peptides, and analogs and flavonoid glycosides, respectively. **(F)** Shows a putative flavoglaucin. Nodes represent parent ions and edge thickness corresponds to the cosine score, which represents the degree of similarity between the connected nodes. Pie ratio was determined according to scan number of spectra.

conditions impact primary metabolism of these two microorganisms, resulting in large amounts of SMs being induced extracellularly.

4. Discussion

Our results showed that the co-culture of *E. amstelodami* and *Bacillus* species significantly improves the inhibitory effect against *S. aureus* and different co-culture combination showed different improvement effects. Many studies have demonstrated that *B. amyloliquefaciens* can produce a wide variety of SMs with desirable antibacterial activity (Shahzad et al., 2018; Mullins et al., 2020). Here, we observed that *B. amyloliquefaciens* pure cultures exhibited excellent inhibition of *S. aureus*,which was consistent with previous reports (Arguelles-Arias et al., 2009; Du et al., 2022). However, the co-culture combination of *E. amstelodami* and *B. amyloliquefaciens* achieved an impressive inhibition rate of 90.21%, it seems that the improvement was not significant compared to the pure cultures. Interestingly, the most significant improvement was observed in the co-culture of *E. amstelodami* and *B. licheniformis*, indicating that several silenced

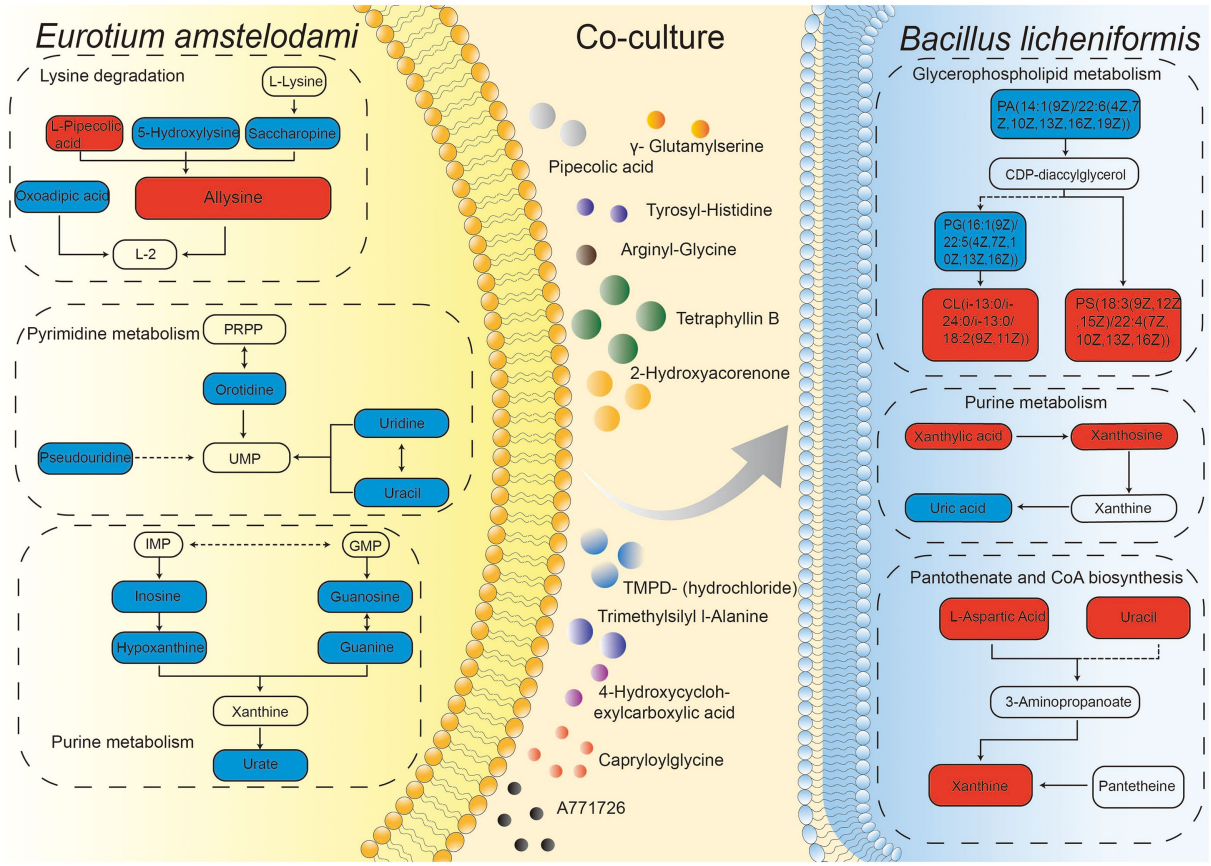

FIGURE 6
Integration map of some metabolic pathways for intracellular and extracellular metabolites of *E. amstelodami* and *B. licheniformis* co-cultures.

gene clusters encoding for SMs in *E. amstelodami* or *B. licheniformis* were activated, thereby enhancing antibacterial activity. The phenomenon of enhanced antibacterial activity caused by microbial co-culture with *Bacillus* species had been demonstrated in a number of studies. Li T. T. et al. (2020) found that the co-culture of *Trichoderma atroviride* and *B. subtilis* exhibited improved antifungal activity against *Fusarium graminearum*, which is the causal agent of *Fusarium* head blight in many cereal crops. Similarly, the co-culture combination of *Aspergillus sydowii* and *B. subtilis* has been shown to significantly increase inhibitory activity against *S. aureus* (Sun et al., 2022). In recent years, many research reported that *Bacillus* species was an ideal strain for establishing co-culture systems, on the one hand, *Bacillus* species, as a representative of biocontrol microorganisms, the co-culture of *Bacillus* species and other biocontrol microorganisms exhibited stronger inhibition of plant pathogenic microorganisms and promoted plant growth (Karuppiah et al., 2019; Liu H. et al., 2022), on the other hand, the co-culture of *Bacillus* species and other microorganisms could markedly increase the production of SMs contained multibiological activity (Sun et al., 2022; Zhang X. F. et al., 2022). However, due to the randomness of microbial co-culture as well as the structural complexity of SMs, many potentially promising microbial co-culture combinations remain undiscovered. Here, we propose a strategy to screen co-culture microbial combinations by targeting the improvement of antibacterial activity. Interestingly, studies have shown that changes in state of the medium (i.e., solid or liquid), composition (i.e., carbon source and nitrogen source) and culture conditions (i.e., temperature, culture length, and pH), or the addition of some trace elements might lead to improved antibacterial activity (Boruta et al., 2020; Boruta, 2021; Gao et al., 2021; Sun et al., 2022), which provided new strategies to further explore valuable SMs of the co-culture of *E. amstelodami* and *Bacillus* species.

There are three mechanisms of activating silenced gene clusters when microorganisms coexist in the same environment: (1) small-molecule secretion induced by one strain can be used as a precursor or substrate to induce the production of new SMs by another strain; (2) exogenous molecules act as a form of chemical defense to produce antibiotics or signaling molecules involved in competition between different strains; (3) direct contact activates silenced gene clusters between opposing strains resulting in the production of related SMs (Okada and Seyedsayamdost, 2017; Peng et al., 2021). In this work, the micrographs impressively demonstrated an intimate interaction between *B. licheniformis* and *E. amstelodami* in the co-culture. It is possible that this physical contact mimics the interaction pattern of the two microbes in their natural habitat. Similar results were reported previously for the co-culture of *Aspergillus oryzae* and *Zygosaccharomyces rouxii* (Liu Z. et al., 2022). Our finding was also supported by the study of Schroeckh and colleagues (Schroeckh et al., 2009) that a distinct physical contact between *Aspergillus nidulans* and actinomycetes leaded to the activation of a cryptic polyketide synthase. Interestingly, the dry weight of the mycelia significantly decreased in the co-culture of *E. amstelodami*, whereas *B. licheniformis* was unaffected. This was likely due to constant competition for nutrients

and space during co-culture (Bovio et al., 2019; Liu Z. et al., 2022), and *E. amstelodami* seems to be a weak competitor. Notably, members of *Bacillus* species are well-known producers of lipopeptides that can inhibit the growth of some fungi (Hossain et al., 2016; Lax et al., 2019). We speculated that *B. licheniformis* produced lipopeptides that inhibited the growth of *E. amstelodami*, which merits further investigation.

Since microbial co-culture involves interactions between different species or the same species but different strains, as well as formed metabolites that are more complex and diverse (Adnani et al., 2015). These data underscore the importance of efficient detection methods of metabolites in co-culture. In the current study, UHPLC-QTOF-MS/MS was used to accurately detect the differences in metabolites (intracellular and extracellular) between *E. amstelodami* and *B. licheniformis* in co-and pure culture. Based on the PCA and PLS-DA results, intracellular and extracellular metabolites were clearly separated between the different groups. Similar findings were confirmed in a variety of microbial co-culture combinations (Oppong-Danquah et al., 2018; Detain et al., 2022), indicating that co-culture results in significant changes in compound diversity. This conclusion was confirmed by differential metabolite screening. The content of a large number of biologically active SMs, including Nummularine B, Lucidenic acid E2, Elatoside G, Aspergillic acid, 4-Hydroxycyclohexylcarboxylic acid, Copaene, and Pipecolic acid, were significantly increased in the co-culture group. Importantly, Nummularine B, a cyclic peptide alkaloid, exhibited effective inhibitory effects on porcine epidemic diarrhea virus (PEDV) (Kang et al., 2015). Lucidenic acid E2 is a triterpenoid, which widely exists in *Ganoderma lucidum* and shows certain anti-tumor effects (Iwatsuki et al., 2003; Che et al., 2017). Elatosides G, a saponin, was found to exhibit potent hypoglycemic activity in the oral glucose tolerance test in rats (Yoshikawa et al., 1995). Aspergillic acid, a derivative of natural pyrazines, is an antibiotic substance produced by *Aspergillus flavus* (Woodward 1947). Copaene is a tricyclic sesquiterpene, which has been shown to increase antioxidation in human lymphocyte cultures (Türkez et al., 2014). Pipecolic acid is an important precursor of a number of useful microbial SMs, and Piperinic acid-derived fractions have been proposed as an essential bioactivity of certain microbial natural products in pharmaceutical applications (He, 2006). Ulteriorly, several typical molecular clusters of SMs were identified based on a molecular network tool in GNPS, including flavonoid glycosides, anthraquinones and harmala alkaloids. Interestingly, several compounds, which were only annotated or had relatively high content in co-culture, such as PE-AEG (o-17:0/17:1), PE (16:1/16:1), yohimbine, flavoglaucin, and phytoceramide C2. Flavoglaucin is an antioxidant produced by molds used in fermented foods (Miyake et al., 2010). Notably, we found a large number of unannotated molecular families both in the co-culture and pure culture, indicating a tiny fraction of this vast chemical space had been discovered. Although current research revealed that a large number of SMs were induced during co-culture process, the specific SMs that play an inhibitory role remain unknow. In the future, the isolation of SMs may be exciting and interesting to know which compounds exert antimicrobial effects and understand their production mechanisms.

Amino acid metabolism plays an important biological function in microbial growth and in the synthesis of SMs (El Hajj Assaf et al., 2020; Subba et al., 2022). We found that the content of amino acids and derivatives were significantly increased in the fermentation broth during the process of co-culture, such as allysine, leucyl-lysine, prolylphenylalanine, trimethylsilyl L-alanine and arginyl-glutamine. According to Wu et al., co-culture of *B. amyloliquefaciens* ACCC11060 and *Trichoderma asperellum* GDFS1009 resulted in a significant enhancement of amino acids (Wu et al., 2018), including d-aspartic acid, L-allothreonine, L-glutamic acid, L-histidine, L-isoleucine, L-leucine, L-proline, and L-serine, which was quite similar to our result. Further, this provides a theoretical basis for exploring the production of large amounts of amino acids by microbial fermentation.

Nucleic acid (purine metabolism and pyrimidine metabolism) metabolism plays an important role in the synthesis of microbial genetic material, energy supply, metabolic regulation, and as messenger molecules, as well as in the formation of coenzymes (Rang et al., 2020). Here, we observed that several important intermediate metabolites were dramatically decreased in *E. amstelodami* co-cultures, indicating that the nucleotide metabolism of *E. amstelodami* was attenuated, this was consistent with our observation that the growth of *E. amstelodami* decreased.

Glycerophospholipids are important components of cell membranes (Sohlenkamp and Geiger, 2016; Qian et al., 2022). Previous studies have shown that glycerophospholipid metabolism plays an especially important role in the response to extracellular stress (Lopalco et al., 2017; Zai et al., 2017). Here, many important intermediate metabolites of glycerophospholipid metabolic were differentially expressed in the co-culture process (both *E. amstelodami* and *B. licheniformis*), suggesting that these two microbes activated the glycerophospholipid metabolic pathway in coping with co-culture stress.

In summary, the co-culture combination of *E. amstelodami* and Bacillus species could significantly improve antibacterial activity against *S. aureus*. Here, we demonstrate that the co-culture strategy successfully induced a large number of biologically active SMs. To the best of our knowledge, this is the first metabolomics-based report of metabolite profiles of *E. amstelodami*. These results provide novel insights into the selection of good co-culture combinations, as well as activation of microbial SM synthesis silencing gene clusters.

Data availability statement

The original contributions presented in the study are included in the article/Supplementary material, further inquiries can be directed to the corresponding author.

Author contributions

CZ: conceptualization, supervision, revision, validation, and investigation. YW: experiment, software, and writing—original draft preparation. YW, YC, XC, JH, and JX: resources. YW, YC, and TX: data curation and project administration. YW and YC: data analysis. CZ and YW: visualization. All authors have read and agreed to the published version of the manuscript.

Funding

This study was supported by the National Natural Science Foundation of China (Nos. 31860438 and 81760688).

Conflict of interest

The authors declare that the research was conducted in the absence of any commercial or financial relationships that could be construed as a potential conflict of interest.

Publisher's note

All claims expressed in this article are solely those of the authors and do not necessarily represent those of their affiliated organizations, or those of the publisher, the editors and the reviewers. Any product that may be evaluated in this article, or claim that may be made by its manufacturer, is not guaranteed or endorsed by the publisher.

Supplementary material

The Supplementary material for this article can be found online at: https://www.frontiersin.org/articles/10.3389/fmicb.2023.1080743/full#supplementary-material

References

Adnani, N., Vazquez-Rivera, E., Adibhatla, S. N., Ellis, G. A., Braun, D. R., and Bugni, T. S. (2015). Investigation of interspecies interactions within marine Micromonosporaceae using an improved co-culture approach. *Mar. Drugs* 13, 6082–6098. doi: 10.3390/md13106082

Ancheeva, E., Daletos, G., and Proksch, P. (2018). Lead compounds from mangrove-associated microorganisms. *Mar. Drugs* 16:319. doi: 10.3390/md16090319

Arguelles-Arias, A., Ongena, M., Halimi, B., Lara, Y., Brans, A., Joris, B., et al. (2009). *Bacillus amyloliquefaciens* GA1 as a source of potent antibiotics and other secondary metabolites for biocontrol of plant pathogens. *Microb. Cell Factories* 8:63. doi: 10.1186/1475-2859-8-63

Bao, J., Wang, J., Zhang, X. Y., Nong, X. H., and Qi, S. H. (2017). New Furanone derivatives and alkaloids from the co-culture of marine-derived fungi *Aspergillus sclerotiorum* and *Penicillium citrinum*. *Chem. Biodivers.* 14:327. doi: 10.1002/cbdv.201600327

Baral, B., Akhgari, A., and Metsä-Ketelä, M. (2018). Activation of microbial secondary metabolic pathways: avenues and challenges. *Synth. Syst. Biotechnol.* 3, 163–178. doi: 10.1016/j.synbio.2018.09.001

Bertrand, S., Bohni, N., Schnee, S., Schumpp, O., Gindro, K., and Wolfender, J. L. (2014). Metabolite induction via microorganism co-culture: a potential way to enhance chemical diversity for drug discovery. *Biotechnol. Adv.* 32, 1180–1204. doi: 10.1016/j.biotechadv.2014.03.001

Boruta, T. (2021). A bioprocess perspective on the production of secondary metabolites by Streptomyces in submerged co-cultures. *World J. Microbiol. Biotechnol.* 37:171. doi: 10.1007/s11274-021-03141-z

Boruta, T., Marczyk, A., Rychta, K., Przydacz, K., and Bizukojc, M. (2020). Confrontation between *Penicillium rubens* and *Aspergillus terreus*: investigating the production of fungal secondary metabolites in submerged co-cultures. *J. Biosci. Bioeng.* 130, 503–513. doi: 10.1016/j.jbiosc.2020.06.012

Bovio, E., Garzoli, L., Poli, A., Luganini, A., Villa, P., Musumeci, R., et al. (2019). Marine fungi from the sponge *Grantia compressa*: biodiversity, Chemodiversity, and biotechnological potential. *Mar. Drugs* 17:220. doi: 10.3390/md17040220

Brakhage, A. A. (2013). Regulation of fungal secondary metabolism. *Nat. Rev. Microbiol.* 11, 21–32. doi: 10.1038/nrmicro2916

Caudal, F., Tapissier-Bontemps, N., and Edrada-Ebel, R. A. (2022). Impact of co-culture on the metabolism of marine microorganisms. *Mar. Drugs* 20:153. doi: 10.3390/md20020153

Che, X. Q., Li, S. P., and Zhao, J. (2017). Ganoderma triterpenoids from aqueous extract of *Ganoderma lucidum*. *Zhongguo Zhong Yao Za Zhi* 42, 1908–1915. doi: 10.19540/j.cnki.cjcmm.20170412.001

Chen, G., Wang, M., Ni, X., and Xia, H. (2021). Optimization of tetramycin production in *Streptomyces ahygroscopicus* S91. *J. Biol. Eng.* 15:16. doi: 10.1186/s13036-021-00267-4

Chiang, Y. M., Chang, S. L., Oakley, B. R., and Wang, C. C. (2011). Recent advances in awakening silent biosynthetic gene clusters and linking orphan clusters to natural products in microorganisms. *Curr. Opin. Chem. Biol.* 15, 137–143. doi: 10.1016/j.cbpa.2010.10.011

Chiang, Y. M., Lee, K. H., Sanchez, J. F., Keller, N. P., and Wang, C. C. (2009). Unlocking fungal cryptic natural products. *Nat. Prod. Commun.* 4, 1505–1510. doi: 10.1177/1934578X0900401113

Costa, J. H., Wassano, C. I., Angolini, C. F. F., Scherlach, K., Hertweck, C., and Pacheco Fill, T. (2019). Antifungal potential of secondary metabolites involved in the interaction between citrus pathogens. *Sci. Rep.* 9:18647. doi: 10.1038/s41598-019-55204-9

Detain, J., Rémond, C., Rodrigues, C. M., Harakat, D., and Besaury, L. (2022). Co-elicitation of lignocelluloytic enzymatic activities and metabolites production in an *Aspergillus-Streptomyces* co-culture during lignocellulose fractionation. *Curr. Res. Microb. Sci.* 3:100108. doi: 10.1016/j.crmicr.2022.100108

Du, H., Yao, W., Kulyar, M. F., Ding, Y., Zhu, H., Pan, H., et al. (2022). Effects of *Bacillus amyloliquefaciens* TL106 isolated from Tibetan pigs on probiotic potential and intestinal microbes in weaned piglets. *Microbiol. Spectr.* 10:e0120521. doi: 10.1128/spectrum.01205-21

El Hajj Assaf, C., Zetina-Serrano, C., Tahtah, N., Khoury, A. E., Atoui, A., Oswald, I. P., et al. (2020). Regulation of secondary metabolism in the *Penicillium* genus. *Int. J. Mol. Sci.* 21:9462. doi: 10.3390/ijms21249462

Figueiredo, S. A. C., Preto, M., Moreira, G., Martins, T. P., Abt, K., Melo, A., et al. (2021). Discovery of cyanobacterial natural products containing fatty acid residues*. *Angew. Chem. Int. Ed. Engl.* 60, 10064–10072. doi: 10.1002/anie.202015105

Fleming, A. (2001). On the antibacterial action of cultures of a penicillium, with special reference to their use in the isolation of *B. influenzae*. 1929. *Bull. World Health Organ.* 79, 780–790. PMID: 11545337

Gao, C. H., Cao, H., Cai, P., and Sørensen, S. J. (2021). The initial inoculation ratio regulates bacterial coculture interactions and metabolic capacity. *ISME J.* 15, 29–40. doi: 10.1038/s41396-020-00751-7

Geib, E., and Brock, M. (2017). ATNT: an enhanced system for expression of polycistronic secondary metabolite gene clusters in *Aspergillus niger*. *Fungal Biol. Biotechnol.* 4:13. doi: 10.1186/s40694-017-0042-1

Guo, C. J., and Wang, C. C. (2014). Recent advances in genome mining of secondary metabolites in *Aspergillus terreus*. *Front. Microbiol.* 5:717. doi: 10.3389/fmicb.2014.00717

He, M. (2006). Pipecolic acid in microbes: biosynthetic routes and enzymes. *J. Ind. Microbiol. Biotechnol.* 33, 401–407. doi: 10.1007/s10295-006-0078-3

Hossain, M. T., Khan, A., Chung, E. J., Rashid, M. H., and Chung, Y. R. (2016). Biological control of rice *Bakanae* by an endophytic *Bacillus oryzicola* YC7007. *Plant Pathol. J.* 32, 228–241. doi: 10.5423/ppj.oa.10.2015.0218

Iwatsuki, K., Akihisa, T., Tokuda, H., Ukiya, M., Oshikubo, M., Kimura, Y., et al. (2003). Lucidenic acids P and Q, methyl lucidenate P, and other triterpenoids from the fungus *Ganoderma lucidum* and their inhibitory effects on Epstein-Barr virus activation. *J. Nat. Prod.* 66, 1582–1585. doi: 10.1021/np0302293

Kang, K. B., Ming, G., Kim, G. J., Ha, T. K., Choi, H., Oh, W. K., et al. (2015). Jubanines F-J, cyclopeptide alkaloids from the roots of *Ziziphus jujuba*. *Phytochemistry* 119, 90–95. doi: 10.1016/j.phytochem.2015.09.001

Karuppiah, V., Vallikkannu, M., Li, T., and Chen, J. (2019). Simultaneous and sequential based co-fermentations of *Trichoderma asperellum* GDFS1009 and *Bacillus amyloliquefaciens* 1841: a strategy to enhance the gene expression and metabolites to improve the bio-control and plant growth promoting activity. *Microb. Cell Factories* 18:185. doi: 10.1186/s12934-019-1233-7

Knowles, S. L., Raja, H. A., Roberts, C. D., and Oberlies, N. H. (2022). Fungal-fungal co-culture: a primer for generating chemical diversity. *Nat. Prod. Rep.* 39, 1557–1573. doi: 10.1039/d1np00070e

König, C., Scherlach, K., Schroeckh, V., Horn, F., Nietzsche, S., Brakhage, A., et al. (2013). Bacterium induces cryptic meroterpenoid pathway in the pathogenic fungus *Aspergillus fumigatus*. *Chembiochem* 14, 938–942. doi: 10.1002/cbic.201300070

Lax, S., Cardona, C., Zhao, D., Winton, V. J., Goodney, G., Gao, P., et al. (2019). Microbial and metabolic succession on common building materials under high humidity conditions. *Nat. Commun.* 10:1767. doi: 10.1038/s41467-019-09764-z

Li, H. T., Liu, T., Yang, R., Xie, F., Yang, Z., Yang, Y., et al. (2020). Phomretones A–F, C12polyketides from the co-cultivation of *Phoma* sp. YUD17001 and *Armillaria* sp. *R. Soc. Chem. Adv.* 10, 18384–18389. doi: 10.1039/d0ra02524k

Li, T. T., Zhang, J. D., Tang, J. Q., Liu, Z. C., Li, Y. Q., Chen, J., et al. (2020). Combined use of *Trichoderma atroviride* CCTCCSBW0199 and brassinolide to control *Botrytis cinerea* infection in tomato. *Plant Dis.* 104, 1298–1304. doi: 10.1094/pdis-07-19-1568-re

Lim, K. B., Balolong, M. P., Kim, S. H., Oh, J. K., Lee, J. Y., and Kang, D. K. (2016). Isolation and characterization of a broad spectrum bacteriocin from *Bacillus amyloliquefaciens* RX7. *Biomed. Res. Int.* 2016:8521476. doi: 10.1155/2016/8521476

Linnakoski, R., Reshamwala, D., Veteli, P., Cortina-Escribano, M., Vanhanen, H., and Marjomäki, V. (2018). Antiviral agents from fungi: diversity, mechanisms and potential applications. *Front. Microbiol.* 9:2325. doi: 10.3389/fmicb.2018.02325

Liu, Z., Kang, B., Duan, X., Hu, Y., Li, W., Wang, C., et al. (2022). Metabolomic profiles of the liquid state fermentation in co-culture of *A. oryzae* and *Z. rouxii*. *Food Microbiol.* 103:103966. doi: 10.1016/j.fm.2021.103966

Liu, H., Li, T., Li, Y., Wang, X., and Chen, J. (2022). Effects of *Trichoderma atroviride* SG3403 and *Bacillus subtilis* 22 on the biocontrol of wheat head blight. *J. Fungi (Basel)* 8:1250. doi: 10.3390/jof8121250

Lopalco, P., Stahl, J., Annese, C., Averhoff, B., and Corcelli, A. (2017). Identification of unique cardiolipin and monolysocardiolipin species in *Acinetobacter baumannii*. *Sci. Rep.* 7:2972. doi: 10.1038/s41598-017-03214-w

Mantravadi, P. K., Kalesh, K. A., Dobson, R. C. J., Hudson, A. O., and Parthasarathy, A. (2019). The quest for novel antimicrobial compounds: emerging trends in research, development, and technologies. *Antibiotics (Basel)* 8:8. doi: 10.3390/antibiotics8010008

Miyake, Y., Ito, C., Tokuda, H., Osawa, T., and Itoigawa, M. (2010). Evaluation of flavoglaucin, its derivatives and pyranonigrins produced by molds used in fermented foods for inhibiting tumor promotion. *Biosci. Biotechnol. Biochem.* 74, 1120–1122. doi: 10.1271/bbb.90955

Mohamad, O. A. A., Li, L., Ma, J. B., Hatab, S., Xu, L., Guo, J. W., et al. (2018). Evaluation of the antimicrobial activity of endophytic bacterial populations from Chinese traditional medicinal plant licorice and characterization of the bioactive secondary metabolites produced by *Bacillus atrophaeus* against *Verticillium dahliae*. *Front. Microbiol.* 9:924. doi: 10.3389/fmicb.2018.00924

Mothe, T., and Sultanpuram, V. R. (2016). Production, purification and characterization of a thermotolerant alkaline serine protease from a novel species *Bacillus caseinilyticus*. *3 Biotech* 6:53. doi: 10.1007/s13205-016-0377-y

Mullins, A. J., Li, Y., Qin, L., Hu, X., Xie, L., Gu, C., et al. (2020). Reclassification of the biocontrol agents Bacillus subtilis BY-2 and Tu-100 as *Bacillus velezensis* and insights into the genomic and specialized metabolite diversity of the species. *Microbiology (Reading)* 166, 1121–1128. doi: 10.1099/mic.0.000986

Okada, B. K., and Seyedsayamdost, M. R. (2017). Antibiotic dialogues: induction of silent biosynthetic gene clusters by exogenous small molecules. *FEMS Microbiol. Rev.* 41, 19–33. doi: 10.1093/femsre/fuw035

Oppong-Danquah, E., Parrot, D., Blümel, M., Labes, A., and Tasdemir, D. (2018). Molecular networking-based metabolome and bioactivity analyses of marine-adapted fungi co-cultivated with phytopathogens. *Front. Microbiol.* 9:2072. doi: 10.3389/fmicb.2018.02072

Panda, B. P., Javed, S., and Ali, M. (2010). Production of Angkak through co-culture of *Monascus purpureus* and *Monascus ruber*. *Braz. J. Microbiol.* 41, 757–764. doi: 10.1590/s1517-83822010000300028

Peng, X.-Y., Wu, J.-T., Shao, C.-L., Li, Z.-Y., Chen, M., and Wang, C.-Y. (2021). Co-culture: stimulate the metabolic potential and explore the molecular diversity of natural products from microorganisms. *Mar. Life Sci. Technol.* 3, 363–374. doi: 10.1007/s42995-020-00077-5

Premkrishnan, B. N. V., Heinle, C. E., Uchida, A., Purbojati, R. W., Kushwaha, K. K., Putra, A., et al. (2021). The genomic characterisation and comparison of *Bacillus cereus* strains isolated from indoor air. *Gut. Pathog.* 13:6. doi: 10.1186/s13099-021-00399-4

Qian, W., Li, X., Liu, Q., Lu, J., Wang, T., and Zhang, Q. (2022). Antifungal and Antibiofilm efficacy of Paeonol treatment against biofilms comprising *Candida albicans* and/or *Cryptococcus neoformans*. *Front. Cell. Infect. Microbiol.* 12:884793. doi: 10.3389/fcimb.2022.884793

Rang, J., He, H., Yuan, S., Tang, J., Liu, Z., Xia, Z., et al. (2020). Deciphering the metabolic pathway difference between *Saccharopolyspora pogona* and *Saccharopolyspora spinosa* by comparative proteomics and METABONOMICS. *Front. Microbiol.* 11:396. doi: 10.3389/fmicb.2020.00396

Schroeckh, V., Scherlach, K., Nützmann, H. W., Shelest, E., Schmidt-Heck, W., Schuemann, J., et al. (2009). Intimate bacterial-fungal interaction triggers biosynthesis of archetypal polyketides in *Aspergillus nidulans*. *Proc. Natl. Acad. Sci. U. S. A.* 106, 14558–14563. doi: 10.1073/pnas.0901870106

Shahzad, R., Khan, A. L., Bilal, S., Asaf, S., and Lee, I. J. (2017). Plant growth-promoting endophytic bacteria versus pathogenic infections: an example of *Bacillus amyloliquefaciens* RWL-1 and *Fusarium oxysporum* f. Sp. lycopersiciin tomato. *Peer j* 5:e3107. doi: 10.7717/peerj.3107

Shahzad, R., Latif Khan, A., Ali, L., Bilal, S., Imran, M., Choi, K. S., et al. (2018). Characterization of new bioactive enzyme inhibitors from endophytic *Bacillus amyloliquefaciens* RWL-1. *Molecules* 23:114. doi: 10.3390/molecules23010114

Shivlata, L., and Satyanarayana, T. (2015). Thermophilic and alkaliphilic actinobacteria: biology and potential applications. *Front. Microbiol.* 6:1014. doi: 10.3389/fmicb.2015.01014

Slack, G. J., Puniani, E., Frisvad, J. C., Samson, R. A., and Miller, J. D. (2009). Secondary metabolites from *Eurotium* species, *Aspergillus calidoustus* and *A. insuetus* common in Canadian homes with a review of their chemistry and biological activities. *Mycol. Res.* 113, 480–490. doi: 10.1016/j.mycres.2008.12.002

Sohlenkamp, C., and Geiger, O. (2016). Bacterial membrane lipids: diversity in structures and pathways. *FEMS Microbiol. Rev.* 40, 133–159. doi: 10.1093/femsre/fuv008

Subba, P., Saha, P., Karthikkeyan, G., Biswas, M., Prasad, T. S. K., and Roy-Barman, S. (2022). Metabolite profiling reveals overexpression of the global regulator, MoLAEA leads to increased synthesis of metabolites in *Magnaporthe oryzae*. *J. Appl. Microbiol.* 132, 3825–3838. doi: 10.1111/jam.15518

Sun, Y., Shi, X., Xing, Y., Ren, X. X., Zhang, D. Y., Li, X., et al. (2022). Co-culture of *Aspergillus sydowii* and *Bacillus subtilis* induces the production of antibacterial metabolites. *Fungal Biol.* 126, 320–332. doi: 10.1016/j.funbio.2022.01.002

Sung, A. A., Gromek, S. M., and Balunas, M. J. (2017). Upregulation and identification of antibiotic activity of a marine-derived *Streptomyces* sp. via co-cultures with human pathogens. *Mar. Drugs* 15:250. doi: 10.3390/md15080250

Türkez, H., Celik, K., and Toğar, B. (2014). Effects of copaene, a tricyclic sesquiterpene, on human lymphocytes cells in vitro. *Cytotechnology* 66, 597–603. doi: 10.1007/s10616-013-9611-1

Wang, M., Carver, J. J., Phelan, V. V., Sanchez, L. M., Garg, N., Peng, Y., et al. (2016). Sharing and community curation of mass spectrometry data with global natural products social molecular networking. *Nat. Biotechnol.* 34, 828–837. doi: 10.1038/nbt.3597

Wang, Y., Chen, Y., Zhang, J., and Zhang, C. (2022). Overexpression of llm1 affects the synthesis of secondary metabolites of *Aspergillus cristatus*. *Microorganisms* 10:1707. doi: 10.3390/microorganisms10091707

Wang, K., Liu, N., Shang, F., Huang, J., Yan, B., Liu, M., et al. (2021). Activation of secondary metabolism in red soil-derived streptomycetes via co-culture with mycolic acid-containing bacteria. *Microorganisms* 9:2187. doi: 10.3390/microorganisms9112187

Wang, G., Ran, H., Fan, J., Keller, N. P., Liu, Z., Wu, F., et al. (2022). Fungal-fungal cocultivation leads to widespread secondary metabolite alteration requiring the partial loss-of-function VeA1 protein. *Sci. Adv.* 8:eabo6094. doi: 10.1126/sciadv.abo6094

Woodward, C. R. Jr. (1947). Production of aspergillic acid by surface cultures of *Aspergillus flavus*. *J. Bacteriol.* 54, 375–379. doi: 10.1128/jb.54.3.375-379.1947

Wu, Q., Ni, M., Dou, K., Tang, J., Ren, J., Yu, C., et al. (2018). Co-culture of bacillus amyloliquefaciens ACCC11060 and *Trichoderma asperellum* GDFS1009 enhanced pathogen-inhibition and amino acid yield. *Microb. Cell Factories* 17:155. doi: 10.1186/s12934-018-1004-x

Wu, Y., Tao, Y., Jin, J., Tong, S., Li, S., and Zhang, L. (2022). Multi-omics analyses of the mechanism for the formation of soy sauce-like and soybean flavor in *Bacillus subtilis* BJ3-2. *BMC Microbiol.* 22:142. doi: 10.1186/s12866-022-02555-5

Xu, H. M., Rong, Y. J., Zhao, M. X., Song, B., and Chi, Z. M. (2014). Antibacterial activity of the lipopetides produced by *Bacillus amyloliquefaciens* M1 against multidrug-resistant *Vibrio* spp. isolated from diseased marine animals. *Appl. Microbiol. Biotechnol.* 98, 127–136. doi: 10.1007/s00253-013-5291-1

Yang, X., Kang, M. C., Li, Y., Kim, E. A., Kang, S. M., and Jeon, Y. J. (2017). Asperflavin, an anti-inflammatory compound produced by a marine-derived fungus, *Eurotium amstelodami*. *Molecules* 22:1823. doi: 10.3390/molecules22111823

Yang, J., Zhu, X., Cao, M., Wang, C., Zhang, C., Lu, Z., et al. (2016). Genomics-inspired discovery of three antibacterial active metabolites, Aurantinins B, C, and D from compost-associated *Bacillus subtilis* fmb60. *J. Agric. Food Chem.* 64, 8811–8820. doi: 10.1021/acs.jafc.6b04455

Yoshikawa, M., Yoshizumi, S., Ueno, T., Matsuda, H., Murakami, T., Yamahara, J., et al. (1995). Medicinal foodstuffs. I. Hypoglycemic constituents from a garnish foodstuff "taranome," the young shoot of *Aralia elata* SEEM.: elatosides G, H, I, J, and K. *Chem. Pharm. Bull. (Tokyo)* 43, 1878–1882. doi: 10.1248/cpb.43.1878

Zai, X., Yang, Q., Yin, Y., Li, R., Qian, M., Zhao, T., et al. (2017). Relative quantitative proteomic analysis of *Brucella abortus* reveals metabolic adaptation to multiple environmental stresses. *Front. Microbiol.* 8:2347. doi: 10.3389/fmicb.2017.02347

Zhang, X., Han, J., Zheng, X., Yan, J., Chen, X., Zhou, Q., et al. (2022). Use of *Lactiplantibacillus plantarum* ZJ316 as a starter culture for nitrite degradation, foodborne pathogens inhibition and microbial community modulation in pickled mustard fermentation. *Food Chem. X* 14:100344. doi: 10.1016/j.fochx.2022.100344

Zhang, X. F., Li, Q. Y., Wang, M., Ma, S. Q., Zheng, Y. F., Li, Y. Q., et al. (2022). 2E,4E-Decadienoic acid, a novel anti-oomycete agent from coculture of *Bacillus subtilis* and *Trichoderma asperellum*. *Microbiol. Spectr.* 10:e0154222. doi: 10.1128/spectrum.01542-22

frontiers | Frontiers in Microbiology

TYPE Original Research
PUBLISHED 01 February 2023
DOI 10.3389/fmicb.2023.1127971

OPEN ACCESS

EDITED BY
Ling Liu,
Institute of Mssicrobiology (CAS),
China

REVIEWED BY
Tao Feng,
South-Central University for Nationalities,
China
Hui Cui,
Guangzhou University of Chinese Medicine,
China

*CORRESPONDENCE
Gang Li
✉ gang.li@qdu.edu.cn
Chunmao Yuan
✉ yuanchunmao01@126.com
Kang Zhou
✉ kangzhouzj@126.com

SPECIALTY SECTION
This article was submitted to
Microbial Physiology and Metabolism,
a section of the journal
Frontiers in Microbiology

RECEIVED 20 December 2022
ACCEPTED 17 January 2023
PUBLISHED 01 February 2023

CITATION
Song Z, Sun YJ, Xu S, Li G, Yuan C and
Zhou K (2023) Secondary metabolites from the
Endophytic fungi *Fusarium decemcellulare* F25
and their antifungal activities.
Front. Microbiol. 14:1127971.
doi: 10.3389/fmicb.2023.1127971

Secondary metabolites from the Endophytic fungi *Fusarium decemcellulare* F25 and their antifungal activities

Ziwei Song[1,2], Yan Jun Sun[3], Shuangyu Xu[4], Gang Li[3]*, Chunmao Yuan[4]* and Kang Zhou[1,2]*

[1]School of Pharmaceutical Sciences, Guizhou University, Guiyang, China, [2]Key Laboratory of Plant Resource Conservation and Germplasm Innovation in Mountainous Region, Ministry of Education, Guizhou University, Guiyang, China, [3]Department of Natural Medicinal Chemistry and Pharmacognosy, School of Pharmacy, Qingdao University, Qingdao, China, [4]State Key Laboratory of Functions and Applications of Medicinal Plants, Guizhou Medical University, Guiyang, China

Seven new compounds, including three isocoumarins (**1**–**3**), three pyrrolidinone derivatives (**8**–**10**), and one pentaene diacid (**15**), together with 13 known compounds, were isolated from the rice culture of the endophytic fungus *Fusarium decemcellulare* F25. Their structures and stereochemistry were established using HRESIMS, NMR, electronic circular dichroism (ECD) calculations, and single-crystal X-ray diffraction. The possible biosynthetic pathways for compounds **1–3** and **8**–**10** were proposed. The antifungal efficacies of compounds **1–20** were evaluated against *Colletotrichum musae*, and compounds **13**, **14**, and **17** exhibited inhibitory activities against *C. musae* with MIC values of 256, 64 and 128 μg/mL, respectively.

KEYWORDS

***Fusarium decemcellulare* F25, secondary metabolites, isocoumarins, pyrrolidinones, antifungal activities**

1. Introduction

Endophytic fungi are microorganisms that asymptomatically colonize living tissues of healthy plants (Li and Lou, 2018). Their complex interactions with the plant host, other organisms, and the external environment result in the production of secondary metabolites that are often characterized by diverse structures and biological activities (Zhang et al., 2006; Gao et al., 2018; Gupta et al., 2019).

Mahonia fortunei is a traditional Chinese medicinal plant, and its root, stem, and leave can be used as medicine for treating bacterial infection, pneumoconiosis, psoriasis, and cough (Zhang et al., 2015). Fungal endophytes from this medicinal plant have afforded many bioactive novel natural products, indicating that mining fungi from this host is an effective strategy for obtaining potential lead compounds (Li et al., 2015, 2016; Wang et al., 2019; Tian et al., 2021). Specifically, an antibacterial tetracyclic triterpenoid with a unique aromatic B-ring, and a cytochalasan with a new 6/6/5-fused tricyclic core skeleton were isolated from *M. fortunei*-derived endophytic fungi (Li et al., 2015; Wang et al., 2019).

In our continuous research on fungal endophytes from *M. fortunei*, endophytic *Fusarium decemcellulare* F25 was obtained. Study on secondary metabolites from *F. decemcellulare* is relatively less. Li et al. reported three cyclic pentapeptides and an antifungal cyclic lipopeptide from an endophytic fungus, *F. decemcellulare* LG53 (Li et al., 2016). The well-known shikimic acid can be produced by *F. decemcellulare* harboring in the fruits of the plant *Flacourtia inermis* (Qader et al., 2018). Under guidance of ^{1}H NMR, 12 polypropionate derivatives were isolated from a marine-derived fungus *F. decemcellulare* SYSUMS6716, and two compounds, decempyrones C and J,

exhibited potent anti-inflammatory activity and inhibitory activity against protein tyrosine phosphatase A (Guo et al., 2021).

In the specific ecological niche, endophytic fungi could coevolve with associated organisms, such as other endophytic fungi and environmental pathogens. This usually made fungal endophytes produce antifungal compounds for chemical defense (Li et al., 2015). Therefore, the antifungal activity of the ethyl acetate (EtOAc) extract of *F. decemcellulare* F25 was investigated. Its ethyl acetate extract showed a significant inhibition activity against *Colletotrichum musae* ACCC 31244, revealing the production of bioactive metabolites and being worth for chemical investigation.

Further isolation led to the identification of three new isocoumarins (**1**–**3**), three new pyrrolidinones (**8**–**10**), and one new pentaene diacid (**15**), together with 13 known compounds from the endophytic fungus *F. decemcellulare* F25 (Figure 1). Herein, we report their isolation, identification, and biological activity, together with the proposed biosynthetic pathway.

2. Materials and methods

2.1. General experimental procedures

Optical rotations were acquired on a JASCOP-1020 polarimeter. ECD data were measured on a Chirascan spectropolarimeter. IR spectra were measured on PerkinElmer infrared spectrophotometer. 1D and 2D NMR spectra were recorded on Bruker Avance 400 or 600 DRX spectrometers in acetone-d_6, methanol-d_4, DMSO-d_6 and chloroform-*d*. Column chromatography (CC) was performed on silica gel (200–300 mesh; Qingdao Marine Chemical Plant Branch., China), RP-C18 (ODS-A, 50 μm, YMC, Kyoto, Japan), or Sephadex LH-20 (100–200 mesh; Beijing Solarbio Technology Co., Ltd., China). Plates precoated with silica gel GF254 (Rushan, Shandong Sun Desiccant Co., Ltd.) were used for thin layer chromatography (TLC). An Agilent HPLC series 1260 and Shimadzu LC-20AR were used for analysis and isolation. For analysis, an Agilent Eclipse XDB-C18 column (4.6 × 150 mm, 5 μm) was used. The isolation was achieved on an Agilent semi-preparative Eclipse XDB-C18 column (9.4 × 250 mm, 5 μm). HPLC-MS data were acquired on an Agilent 1260 Series system coupled with an Agilent Accurate-Mass-Q-TOF MS 6520 system equipped with an Electrospray ionization (ESI) source.

2.2. Fungal material

The endophytic fungus *F. decemcellulare* F25 was isolated from the stem of the Chinese medicinal plant *M. fortunei* collected from Qingdao, People's Republic of China. The fungal strain was deposited in 20% glycerol at −80°C in the school of Pharmaceutical Sciences, Guizhou University, Guizhou, China. The endophytic fungus was identified as *F. decemcellulare* by the analysis of internal transcribed spacer (ITS) region of the rDNA (GenBank No. OQ001346).

2.3. Fermentation and extraction

The fungal strain *F. decemcellulare* F25 was cultured on potato dextrose agar (PDA) media for a week at 28 ± 2°C. A week-old culture plate was cut into small pieces under aseptic conditions, and were then inoculated into 394 flasks (300 mL) each containing 40 g of rice, 0.12 g of peptone, and 60 mL of water. The cultures were incubated at 28 ± 2°C for 40 days. Afterward, the whole cultures were extracted with ethyl acetate by sonication under ice bath conditions for three times. Then the EtOAc solution was collected and evaporated to dryness, affording 352.2 g of brown extracts. After suspension of the crude extract in water, petroleum ether and EtOAc were used to extract 294.6 g and 50.0 g of the corresponding organic phase, respectively.

2.4. Isolation and purification

The EtOAc extract was fractionated by column chromatography (CC) on ODS eluting with a gradient of acetonitrile (CH_3CN)/H_2O (0:100; 3:7; 5:5; 7:3; 100:0, *v/v*, each 8 L) to give eight fractions (Fr. A–Fr. H).

Fraction A was applied to semi-preparative HPLC to yield compounds **11** (t_R 22.1 min, 53.3 mg), **4** (t_R 38.2 min, 8.9 mg), **5** (t_R 39.1 min, 16.5 mg), **6** (t_R 40.3 min, 29.1 mg), and a mixture of **8** and **9** (t_R 29.2 min, 16.2 mg), eluting with a gradient of CH_3CN in H_2O from 40 to 65%. The above mixture was subjected to isolation on a chiral HPLC column to afford compounds **8** (t_R 25.1 min, 6.2 mg) and **9** (t_R 28.9 min, 5.9 mg). Fraction A (14.4 g) was also separated into 12 subfractions (A1 – A12) by CC on silica gel eluted by CH_2Cl_2/CH_3OH (1:0, 40:1, 30:1, 20:1, 10:1, 5:1 and 0:1, v/v, each 7 L). Subfraction A3 was purified by semi-preparative HPLC with a gradient elution from 30 to 85% CH_3CN in H_2O to afford compounds **1** (t_R 33.0 min, 11.5 mg) and **18** (t_R 12.6 min, 16.4 mg). Subfraction A6 was then applied to semi-preparative HPLC with a gradient from 30 to 55% CH_3CN in H_2O as eluent to obtain compound **19** (t_R 14.2 min, 25.3 mg). Compound **10** (t_R 33 min, 27.8 mg) was purified by semi-preparative HPLC, eluting with a gradient of CH_3CN in H_2O from 40 to 65% (v/v) as eluent from subfraction A7. Compound **2** (t_R 17.5 min, 10.1 mg) was obtained from subfraction A8 using semi-preparative HPLC with a gradient elution from 30 to 85% CH_3CN in H_2O. Subfrcation A9 was separated by semi-preparative HPLC with a gradient elution from 30 to 75% CH_3CN in H_2O to yield compound **3** (t_R 27.0 min, 10.6 mg).

Fraction C was fractionated by CC on Sephadex LH-20 eluting with CH_3OH/CH_2Cl_2 (1:1, v/v) to give five subfractions (C1–C5). Subfraction C3 was purified by semi-preparative HPLC with a gradient elution from 45 to 50% CH_3CN in H_2O with 0.1% trifluoroacetic acid (TFA) to afford compounds **15** (t_R 38.1 min, 7.5 mg) and **16** (t_R 37.5 min, 10.3 mg). Fraction C4 was subjected to semi-preparative HPLC with a gradient elution from 35 to 65% CH_3CN in H_2O to yield compound **7** (t_R 16.0 min, 2.0 mg).

Fraction D was purified by semi-preparative HPLC eluting with gradient from 60 to 70% CH_3CN in H_2O with 0.1% TFA to offer compound **17** (t_R 33.5 min, 6.3 mg). Compound **12** (t_R 27.2 min, 6.2 mg) was obtained from fraction F by semi-preparative HPLC eluting with a gradient elution from 50 to 100% CH_3CN in H_2O. Compounds **13** (t_R 19.3 min, 17.5 mg), **14** (t_R 22.0 min, 17.7 mg), and **20** (t_R 28.5 min, 13.1 mg) were obtained from fraction G using semi-preparative HPLC with a gradient elution from 75 to 100% CH_3CN in H_2O.

2.5. Spectroscopic data of compounds

Compound (**1**), yellowish solid; LC-UV (CH_3CN in H_2O) λ_{max}: 248, 330 nm; IR ν_{max}: 3319, 2942, 2832, 1677, 1020 cm^{-1}; ^1H NMR

10.3389/fmicb.2023.1127971

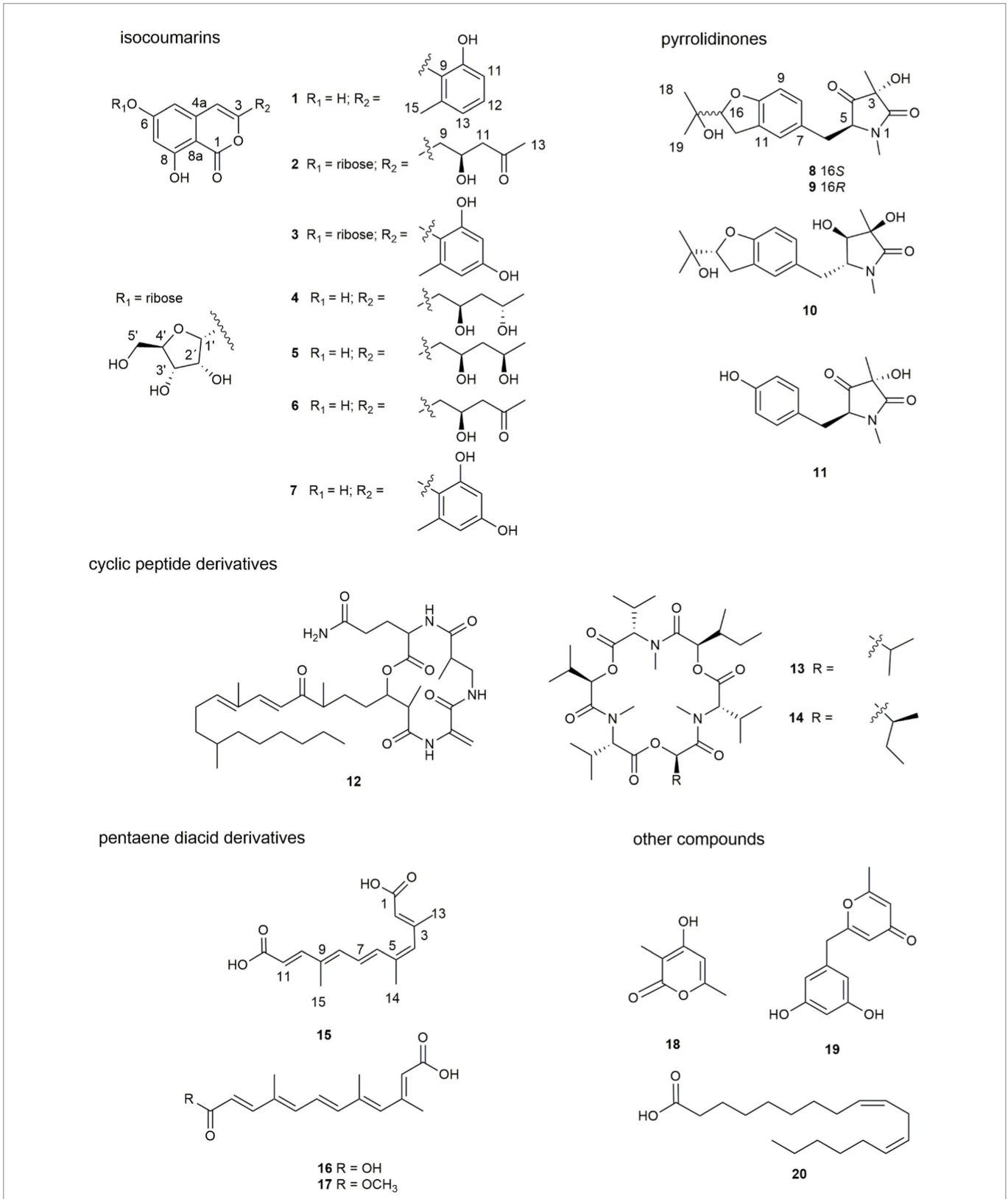

FIGURE 1
Structures of compounds **1**–**20**.

(DMSO-d_6, 400 MHz); and ^{13}C NMR (DMSO-d_6, 100 MHz) data, see Table 1; HRESIMS *m/z* 285.0762 $[M+H]^+$ (calcd. For $C_{16}H_{13}O_5$, 285.0757).

Compound (**2**), yellowish solid; $[\alpha]_D^{23}$ +51.6 (*c* 0.68, CH_3OH); LC-UV (CH_3CN in H_2O) λ_{max}: 244, 276, 330 nm; IR ν_{max}: 3330, 2925, 1681, 1642, 1625, 1572, 1357, 1237, 1163, 1018, 990 cm^{-1}; ^{1}H NMR (DMSO-d_6, 400 MHz); and ^{13}C NMR (DMSO-d_6,100 MHz) data, see Table 1; HRESIMS *m/z* 411.1289 $[M+H]^+$ (calcd. For $C_{19}H_{23}O_{10}$, 411.1286).

Compound (**3**), yellowish solid; $[\alpha]_D^{23}$ +63.2 (*c* 0.56, CH_3OH); LC-UV (CH_3CN in H_2O) λ_{max}: 204, 236, 336 nm; IR ν_{max}: 3310, 2917,

1678, 1616, 1570, 1505, 1470, 1400, 1158, 1024, 999 cm^{-1}; ^1H NMR (DMSO-d_6, 400 MHz); and ^{13}C NMR (DMSO-d_6,100 MHz) data, see Table 1; HRESIMS *m/z* 433.1133 $[M+H]^+$ (calcd. For $C_{21}H_{21}O_{10}$, 433.1129).

Compound (**8**), colorless oil; $[\alpha]_D^{24}$ -22.7 (*c* 0.59, CH_3OH); LC-UV (CH_3CN in H_2O) λ_{max}: 200, 230, 286 nm; IR ν_{max}: 3329, 2946, 2836, 1661, 1451, 1408, 1114, 1017 cm^{-1} ^1H NMR (DMSO-d_6, 400 MHz) and ^{13}C NMR (DMSO-d_6,100 MHz) data, see Supplementary Table 1; HRESIMS *m/z* 334,1,649 $[M+H]^+$ (calcd. For $C_{18}H_{24}NO_5$, 334.1649).

Compound (**9**), colorless oil; $[\alpha]_D^{24}$ +8.23 (*c* 0.61, CH_3OH); LC-UV (CH_3CN in H_2O) λ_{max}: 200, 230, 286 nm; IR ν_{max}: 3329, 2946, 2836, 1661, 1451, 1408, 1114, 1017 cm^{-1};^1H NMR (DMSO-d_6, 400 MHz); and ^{13}C NMR (DMSO-d_6,100 MHz) data, see Supplementary Table 1; HRESIMS *m/z* 334, 1,652 $[M+H]^+$ (calcd. For $C_{18}H_{24}NO_5$, 334.1649).

Compound (**10**), colorless oil; $[\alpha]_D^{23}$ -24.1 (*c* 2.25, CH_3OH); LC-UV (CH_3CN in H_2O) λ_{max}: 204, 228, 286 nm; IR ν_{max}: 3336, 3286, 2905, 1644, 1427, 1367, 1334, 1314, 1164, 1053, 1030 cm^{-1}; ^1H NMR (DMSO-d_6, 400 MHz); and ^{13}C NMR (DMSO-d_6,100 MHz) data, see Supplementary Table 1; HRESIMS *m/z* 336,1808 $[M+H]^+$ (calcd. For $C_{18}H_{26}NO_5$, 336.1805).

Compound (**15**), yellow powder; LC-UV (CH_3CN in H_2O) λ_{max}: 220, 280, 360 nm; IR ν_{max}: 3387, 2833, 1698, 1475, 1391, 1017 cm^{-1}; ^1H NMR (DMSO-d_6, 400 MHz); and ^{13}C NMR (DMSO-d_6,100 MHz) data, see Supplementary Table 2; HRESIMS *m/z* 263.1277 $[M+H]^+$ (calcd. For $C_{15}H_{19}O_4$, 263.1278).

TABLE 1 ^1H NMR (400 MHz, δ in ppm) and ^{13}C NMR Data (100 MHz, δ in ppm) of 1–3 (DMSO-d_6).

Position	1		2		3	
	δ_C, type	δ_H (*J* in Hz)	δ_C, type	δ_H (*J* in Hz)	δ_C, type	δ_H (*J* in Hz)
1	166.0, C		165.5, C		166,2, C	
3	150.8, C		154.9, C		151.7, C	
4	108.7, CH	6.69, s	105.9, CH	6.55, s	108.9, CH	6.67, s
4a	138.2, C		139.3, C		139.6, C	
5	103.3, CH	6.47,d (2.1)	103.3, CH	6.57, d (2.3)	103.8, CH	6.72, d (2.2)
6	165.7, C		164.2, C		164.3, C	
7	101.9, CH	6.38, d (2.1)	102.5, CH	6.64, d (2.3)	102.8, CH	6.61, d (2.2)
8	162.7, C		162.2, C		162.3, C	
8a	98.4, C		99.9, C		100.1, C	
9	120.0, C		40.9, CH_2	2.60, m	111.5, C	
10	155.9, C		64.6, CH	4.28, m	157.3, C	
11	113.0, CH	6.75, d (8.3)	50.3, CH_2	2.57, m	100.3, CH	6.23, d (2.2)
12	130.6, CH	7.18, t (8.3)	207.7, C		159.3,C	
13	120.6, CH	6.77, d (8.3)	30.5, CH_3	2.11, s	108.4,CH	6.19, d (2.2)
14	139.6, C				139.3, C	
15	19.5, CH_3	2.21, s			19.9, CH_3	2.12, s
1'			100.0, CH	5.74, d (4.4)	100.0, CH	5.76, d (4.5)
2'			71.5, CH	4.10, m	71.6, CH	4.11, m
3'			69.2, CH	3.96, m	69.3, CH	3.93, m
4'			86.7, CH	3.96, m	86.9, CH	3.98, m
5'			61.4, CH_2	3.48, m	61.5, CH_2	3.49, m

2.6. X-ray crystallographic analysis of compound 9

The crystal structure of compound **9** was obtained from the solution of CH_3OH. A suitable crystal were collected on a Bruker APEX-II CCD Venture diffractometer using graphite-monochromated Mo Kα radiation ($\lambda = 0.710\ 73$ Å) at 297 K. Absorption correction using equivalent reflctions was performed with the SADABS program. Crystallographic tables were constructed using Olex2 (Dolomanov et al., 2010). The structure was solved with the Shelxt software package (Sheldrick, 2015), and refined with the Shelxt refinement package using Least Squares minimization.

Crystal data for compound **9**: $C_{18}H_{25}NO_6$ ($M = 351.39$ g/mol): triclinic, space group P1, $a = 6.4597(7)$ Å, $b = 7.5258(7)$ Å, $c = 9.4129(7)$ Å, $\alpha = 95°$, $\beta = 100°$, $\gamma = 93°$, $V = 93.981(8)$ Å^3, $Z = 1$, $T = 297$ K, μ(Mo Kα) = 0.098 mm^{-1}, $F(000) = 188$, $\rho_{calc} = 1.311$ g/cm^3; of the 8,205 reflections measured ($4.44° \leq 2\Theta \leq 50.01°$), 2,823 were unique ($R_{int} = 0.0922$, $R_{sigma} = 0.0810$) which used in all calculations. The final R_1 was 0.0596 ($I > 2\sigma(I)$), and wR_2 was 0.1706 (all data).

2.7. Antifungal assay

Following our previously established methods (Wang et al., 2019; Tian et al., 2021), the crude extract of *F. decemcellulare* F25 was firstly evaluated for antifungal activity against five plant pathogens (*Colletotrichum musae* ACCC 31244, *Alternaria solani*, *Fusarium foetens*, *Fusarium mangiferae*, and *Lasiodiplodia pseudotheobromae*) by agar diffusion assay. The crude extract showed inhibitory activity against *C. musae* ACCC 31244, indicating the production of antifungal molecules. Further antifungal evaluation of pure compounds against *C. musae* ACCC 31244 was determined with the broth dilution method, and provided minimum inhibitory concentration (MIC) values. The cycloheximide was used as a positive control in parallel to reveal the comparative antifungal efficacy of compounds **1**–**20**.

3. Results and discussion

3.1. OSMAC screen and fermentation of *Fusarium decemcellulare* F25

The OSMAC (One Strain Many Compounds) approach refers to the activation of many silent gene clusters in microorganisms by altering the

culture environment of the strain. This strategy maximizes the biosynthetic capacity of a microorganism that produces structurally diverse and biologically active secondary metabolites. The *F. decemcellulare* F25 was cultured on four different solid media including rice-based, soybean-based, corn-based, and czapek-dox agar (CDA) culture. Remarkably, HPLC chromatograms showed a number of peaks in rice-based culture, suggesting that the rice medium strongly triggered the production of secondary metabolites (Supplementary Figure 1).

3.2. Screening of antifungal activities of crude extract

The antifungal activities of crude extracts were evaluated against five plant pathogens. Compared with the positive control drug cycloheximide, it was found that, at the concentration of 40 μg/paper disk, the crude extract of *F. decemcellulare* F25 showed antifungal activity against the fungal *C. musae* (Supplementary Figure 2). Considering the abundant secondary metabolites and the antifungal activity of *F. decemcellulare* F25, this strain F25 was further subjected to chemical investigation.

3.3. Structural characterization of these isolated compounds

Seven new compounds, including three isocoumarins (**1**–**3**), three pyrrolidinone derivatives (**8**–**10**), and one pentaene diacid (**15**), together with 13 known compounds, were isolated from the rice culture of the endophytic fungus *Fusarium decemcellulare* F25.

Compound **1** was obtained as a yellowish solid. Its molecular formula $C_{16}H_{12}O_5$ was established by the HRESIMS at *m/z* 285.0762 $[M+H]^+$ (calcd. For 285.0757), implying eleven degrees of unsaturation. The presence of hydroxyl and carbonyl groups were implied by IR absorption bands at 3319 and 1677 cm^{-1}, respectively. The ^1H and ^{13}C NMR data of **1** (Table 1) were highly similar to those of pleosporalone A (Cao et al., 2016), excepted for a proton at C-7 in **1** rather than a methyl group in pleosporalone A. In addition, the coupling constant between H-5 and H-7 ($J = 2.1$ Hz) proved that there is no methyl substitution at C-7 of **1**. The HMBC correlations (Figure 2) from H-5 (δ_H 6.47) to C-6 (δ_C 165.7), C-7 (δ_C 101.9), and C-8a (δ_C 98.4), and from H-7 (δ_H 6.38) to C-5 (δ_C 103.3), C-6 (δ_C 165.7), C-8 (δ_C 162.7), and C-8a (δ_C 98.4), together with the HSQC spectrum (δ_C/δ_H 101.9/6.38 and 103.3/6.47 ppm) further confirmed that there is a proton attached to C-7. Final detailed analysis of the HSQC and HMBC spectra allowed the assignment for all proton and carbon resonances of **1**. Thus, the structure of compound **1** was assigned completely.

Compound **2** was obtained as a yellowish solid. Its molecular formula $C_{19}H_{22}O_{10}$ was established by the HRESIMS at *m/z* 411.1289 $[M+H]^+$ (calcd for 411.1286), implying nine degrees of unsaturation. The presence of hydroxyl and carbonyl groups were shown by IR absorption bands at 3330, 1681 cm^{-1}, respectively. The attachment of sugar unit was determined to be ribose by comparison of ^1H and ^{13}C NMR data of compound **2** with those of daldiniside C. The coupling constant of the anomeric proton at δ_H 5.74 (1H, d, $J = 4.4$ Hz) indicated the ribose unit should be α-configured (Hu et al., 2014). Additionally, the pentose moiety was linked to C-6 proved by the correlation of H-1'/C-6 observed in the HMBC (Figure 2) experiment and H-1'/H-5, H-1'/H-7 in NOESY spectrum (Figure 3). The ^1H NMR and ^{13}C NMR data (Table 1) showed the presence of an isocoumarin unit in **2**, whose structure was the same as that of compound **6** ((−)-citreoisocoumarin)) (Yamamura et al., 1991) by comparison with spectroscopic data. Thus, the structure of compound **2** was established.

Compound **3** was obtained as a yellowish solid. Its molecular formula $C_{21}H_{20}O_{10}$ was established by the HRESIMS at *m/z* 433.1133 $[M+H]^+$ (calcd for 433.1129), implying 12 degrees of unsaturation. The presence of hydroxyl and carbonyl groups were shown by IR absorption bands at 3310, 1678 cm^{-1}, respectively. The ^1H and ^{13}C NMR data of aglycone in **3** (Table 1) were highly similar to those of polyisocoumarin

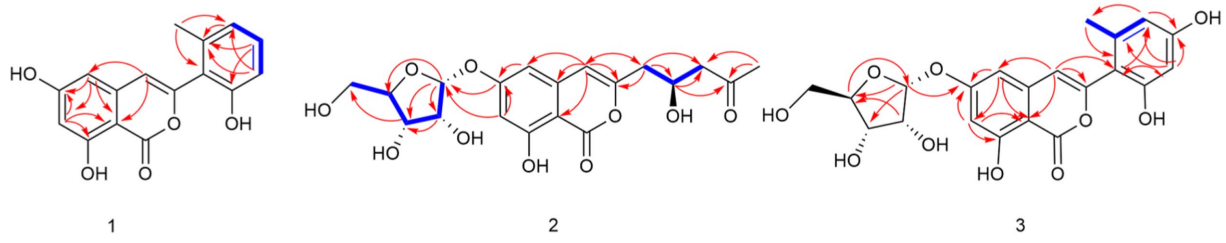

FIGURE 2
Key COSY (bold lines) and HMBC (arrows) correlations of compounds **1**–**3**.

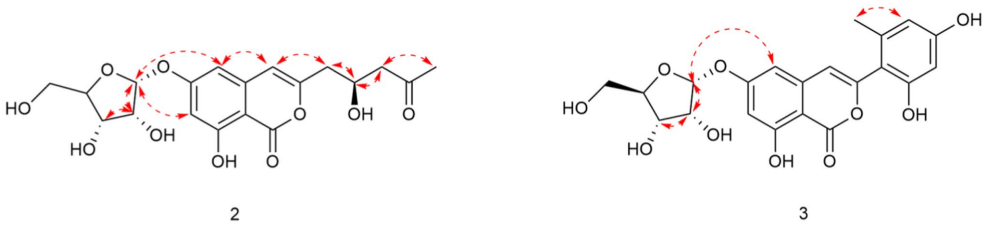

FIGURE 3
Key NOESY correlations of compounds **2** and **3**.

(Jiang et al., 2020), which was previously isolated from *Polygonum cuspidatum*. However, an α-ribose attached at the C-6 of **3** rather than a β-D-glucopyrancose at C-6 in polyisocoumarin. And the NMR data showed that compound **3** and compound **2** have the same ribose at C-6. Thus, the structure of compound **3** was assigned completely.

Compounds **8** and **9** were obtained as colorless oil. Their molecular formula $C_{18}H_{23}NO_5$ were established by the HRESIMS at *m/z* 334.1649 and 334.1652 $[M+H]^+$, respectively (calcd for 334.1649), implying eight degrees of unsaturation. The presence of hydroxyl and carbonyl groups were implied by IR absorption bands at 3329 and 1661 cm^{-1}, respectively. Detailed analysis of the ^1H and ^{13}C NMR data suggested that **8** possessed the same planar structure as that of rigidiusculamide C (Li et al., 2009). A comparison of the NMR data (Supplementary Table 1) of **8** and **9** suggested that they differed only in the substituent at C-16. Detailed analysis of the HSQC and HMBC spectra allowed the assignment for all proton and carbon resonances of **9**. The relative configuration of **9** was assigned by single-crystal X-ray diffraction as shown in Figure 4. To clarify the absolute configurations of **8** and **9**, ECD calculations were performed by the time dependent density functional theory-predicted curve calculated at the quantum mechanical level. The calculated electronic circular dichroism (ECD) curve of (3*S*, 5*S*, 16*S*)-**8** matched well with the **8** experimental ECD data, and the ECD curve of (3*S*, 5*S*, 16*R*)-**9** is in good agreement with the experimental ECD data of **9**. Therefore, the absolute configuration of compound **8** was determined as 3*S*, 5*S*, 16*S*, and the absolute configuration of compound **9** was 3*S*, 5*S*, 16*R* (Figure 5).

Compound **10** was obtained as a yellow oil. Its molecular formula $C_{18}H_{25}NO_5$ was established by the HRESIMS at *m/z* 336.1808 $[M+H]^+$ (calcd for 336.1805), implying seven degrees of unsaturation. The presence of hydroxyl and carbonyl groups were implied by IR absorption bands at 3336 and 1644 cm^{-1}, respectively. The NMR data (Supplementary Table 1) of **10** revealed highly similar identical structural features to those found in **8**, except that the C-4 ketone carbon was replaced by an oxygenated methine in **10**. And **10** has the same planar structure as rigidiusculamide D (Li et al., 2009). The NOESY correlation of CH_3 with H-4 indicates that 3-OH and 4-OH are located on the same face, whereas H-5 and H-4 placed on the opposite face of the ring supported by the absence of a NOESY correlation between H-5 and H-4. To determine the absolute configuration, the simulated electronic circular dichroism (ECD) spectra of **10** were obtained from the calculation of Gaussian 16 based on time-dependent density functional theory. The absolute configurations of C-3, C-4, C-5, and C-16 in **10** were deduced as 3*R*, 4*R*, 5*R*, and 16*S*, respectively, by comparing calculated ECD spectra with the experimental ECD spectrum (Figure 5).

Compound **15** was isolated as a yellow powder. Its molecular formula $C_{15}H_{18}O_4$ was established by the HRESIMS at *m/z* 263.1277 $[M+H]^+$ (calcd for 263.1278), implying seven degrees of unsaturation. The presence of hydroxyl and carbonyl groups were implied by IR absorption bands at 3387 and 1698 cm^{-1}, respectively. A comparison of NMR data (Supplementary Table 2) with those of nectriacid C (Cui et al., 2016) suggested that **15** possessed a closely similar structure as nectriacid C, except that there is no methoxy group (δ_H 3.74, δ_C 51.7) in **15**. Its NMR data suggested that **15** belonged to the pentaene diacid derivative. Thus, the structure of compound **15** was assigned completely.

The remaining 13 known compounds from the *F. decemcellulare* F25 were identified as 12-epicitreoisocoumarinol (**4**) (Cui et al., 2016), eoisocoumarinol (**5**) (Cui et al., 2016), (−)-citreoisocoumarin (**6**) (Yamamura et al., 1991; Ola et al., 2013), trichophenol A (**7**) (Liu et al., 2020), rigidiusculamide B (**11**) (Li et al., 2009), fusaristatins A (**12**) (Shiono et al., 2007), enniatin H (**13**) (Nilanonta et al., 2003), enniatin I (**14**) (Nilanonta et al., 2003), nectriacid A (**16**) (Cui et al., 2016), nectriacid B (**17**) (Cui et al., 2016), 4-hydroxy-3,6-dimethyl-2*H*-pyrane-2-one (**18**) (Hirota et al., 1999), macrocarpon C (**19**), (Ola et al., 2013), and α-linoleic acid (**20**) (Zeng et al., 2017) by comparison of their MS and NMR data with those reported in the literature.

3.4. Antifungal assays

Compounds **1**–**20** were assayed for their antifungal activities. The results showed that compounds **13**, **14**, and **17** exhibited inhibitory

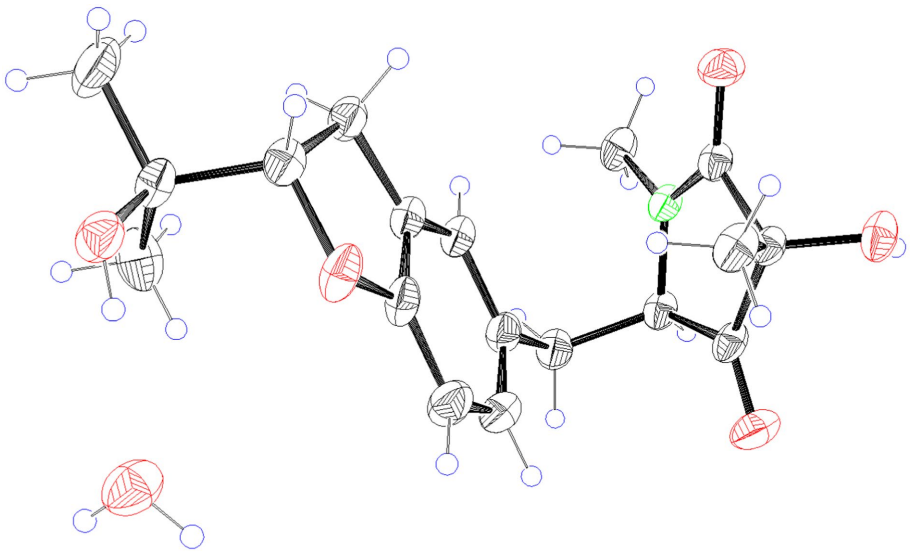

FIGURE 4
X-ray ORTEP drawing of compound **9**.

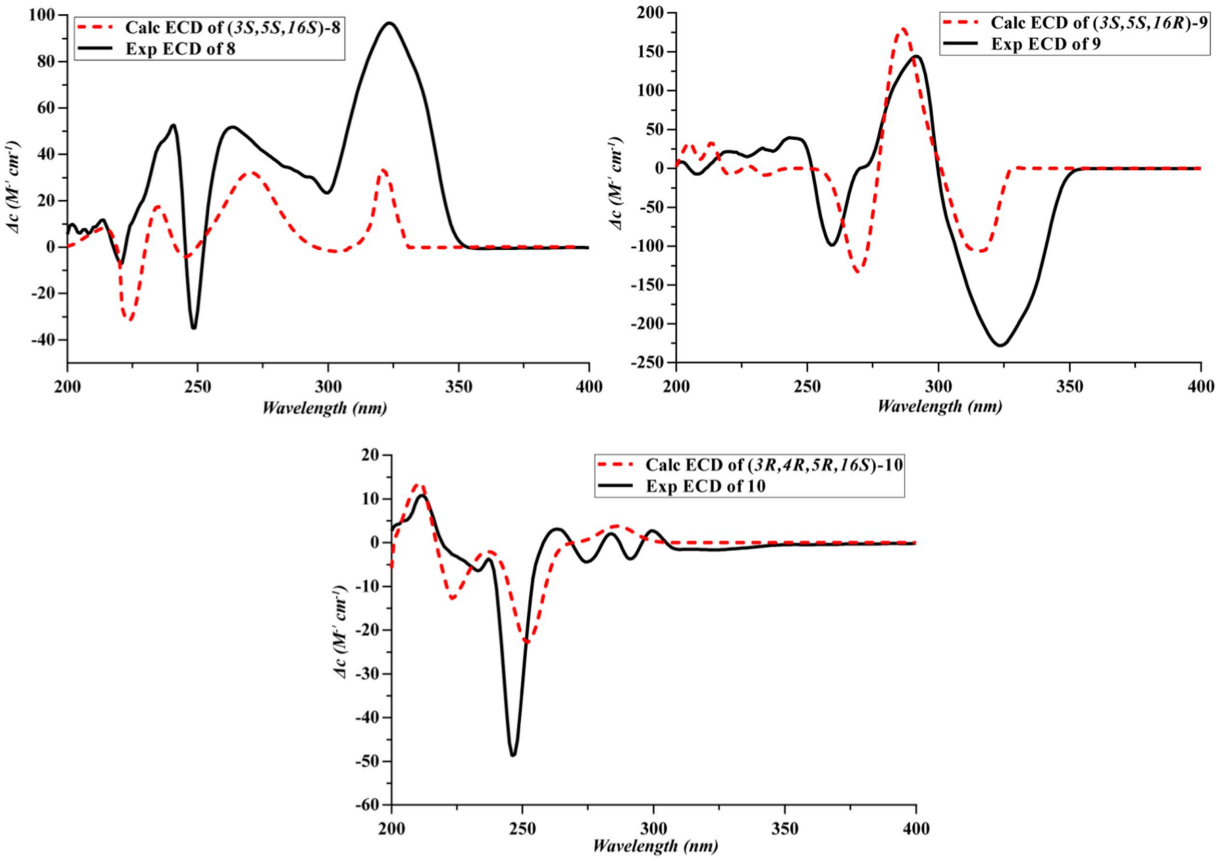

FIGURE 5
Experimental and calculated ECD spectra of **8**–**10**.

activities against the plant-pathogenic fungus *C. musae* ACCC31244 with MICs of 256, 64, and 128 μg/mL, respectively. The MIC of the positive control cycliheximide was 32 μg/mL.

3.5. Plausible biogenetic pathways

The biosynthetic pathways of compounds **1** and **3** (Scheme 1) start with condensation catalyzed by nonreducing polyketide synthase (nrPKS) of two acetyl-coenzyme A molecules and six malonyl-CoA molecules resulting in the formation of the intermediate **i** (Liu and Begley, 2020). Intermediate **i** was catalyzed by TE domains or spontaneous C-O bond closure to form intermediate **ii**. The isocoumarin **1** was derived from intermediate **ii** through methylation and dehydration, while, intermediate **ii** will create **3** by methylation and ribosylation. The biosynthetic pathway of **2** (Scheme 1) starts with condensation catalyzed by a modular (nrPKS) of one acetyl-coenzyme A molecule and six malonyl-CoA molecules resulting in the formation of the intermediate **iv**. Intermediate **iv** was catalyzed by thioesterase (TE) domains or spontaneous C−O bond closure to form intermediate **v**. A series of reductive modifications for this intermediate led to intermediate **vi**. Intermediate **vi** then underwent a ribosylation reaction to afford **2**.

As shown in Scheme 2, pyrrolidones originate from the cyclization of an amino acid and a polyketide (Royles, 1995; Li et al., 2009), leading to the formation of **11**. The pyrrolidones **8** and **9** were likely to be biogenetically derived from **11** through prenylation, oxidation, cyclization, and hydroxylation. The derivative **10** was formed from **8** or **9** through one-step hydrogenation.

4. Conclusion

In summary, the chemical investigation on the endophytic fungus *F. decemcellulare* F25 resulted in the isolation and identification of twenty secondary metabolites, including three new isocoumarin derivatives (**1**–**3**), three new pyrrolidinones (**8**–**10**), and one new pentaene diacid (**15**), together with thirteen known compounds. Compounds **13**, **14**, and **17** exhibited antifungal activities against plant pathogen *C. musae* ACCC31244. This study reveals the potential of endophytic fungi as a promising source of bioactive compounds.

Data availability statement

The datasets presented in this study can be found in online repositories. The names of the repository/repositories and accession number(s) can be found at: GenBank No. OQ001346 of ITS region of the rDNA in NCBI and Deposition Number 2232225 of X-ray crystallographic data in CCDC.

Author contributions

ZS and KZ: conception or design. KZ, ZS, YJS, GL, SX, and CY: acquisition, analysis, or interpretation of data. ZS, KZ, GL, and CY: drafting the work or revising and final approval of the manuscript. All authors have reviewed the manuscript. All authors contributed to the article and approved the submitted version.

10.3389/fmicb.2023.1127971

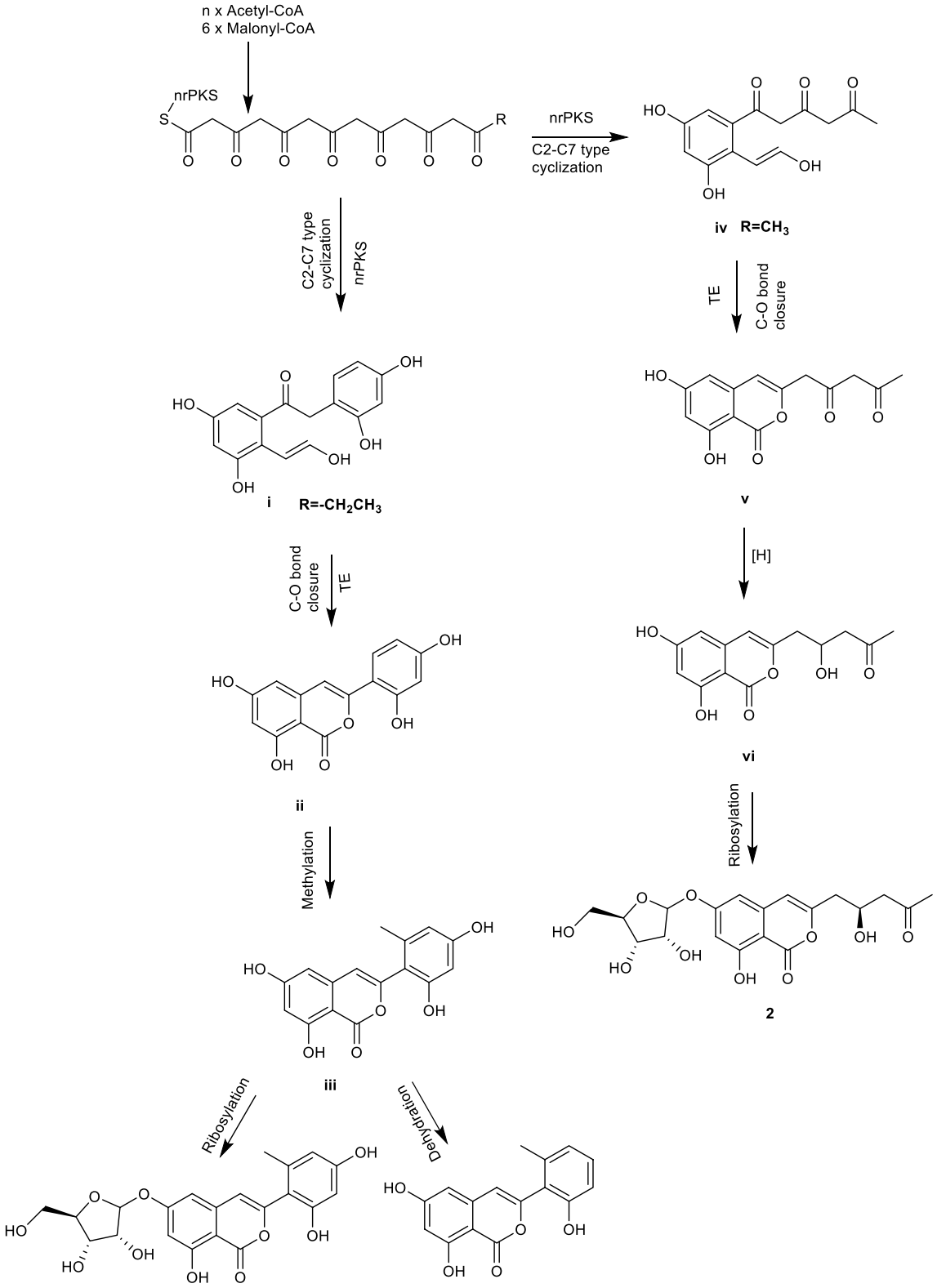

SCHEME 1
Plausible biogenetic pathways of compounds **1**–**3**.

Funding

We gratefully acknowledge the National Natural Science Foundation of China (grant nos. 22067002 and 82060635), the Science and Technology Foundation of Guizhou (grant no. J[2020]1Y049), and Guizhou University (grant no. (2018)04) for the financial supports.

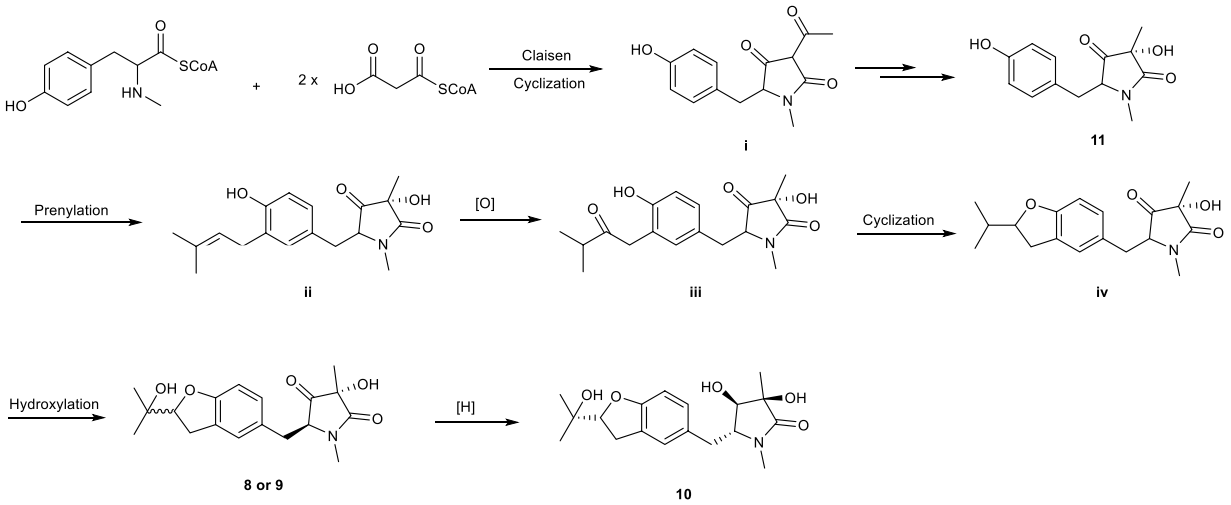

SCHEME 2
Plausible biogenetic pathways of compounds **8**–**10**.

Conflict of interest

The authors declare that the research was conducted in the absence of any commercial or financial relationships that could be construed as a potential conflict of interest.

Publisher's note

All claims expressed in this article are solely those of the authors and do not necessarily represent those of their affiliated organizations, or those of the publisher, the editors and the reviewers. Any product that may be evaluated in this article, or claim that may be made by its manufacturer, is not guaranteed or endorsed by the publisher.

Supplementary material

The Supplementary material for this article can be found online at: https://www.frontiersin.org/articles/10.3389/fmicb.2023.1127971/full#supplementary-material

References

Cao, F., Yang, J. K., Liu, Y. F., Zhu, H. J., and Wang, C. Y. (2016). Pleosporalone a, the first azaphilone characterized with aromatic A-ring from a marine-derived *Pleosporales* sp. fungus. *Nat. Prod. Res.* 30, 2448–2452. doi: 10.1080/14786419.2016.1198352

Cui, H., Liu, Y., Nie, Y., Liu, Z., Chen, S., Zhang, Z., et al. (2016). Polyketides from the mangrove-derived endophytic fungus *Nectria* sp. HN001 and their α-glucosidase inhibitory activity. *Mar. Drugs* 14, 1660–3397. doi: 10.3390/md14050086

Dolomanov, O. V., Bourhis, L. J., Gildea, R. J., Howard, J. A. K., and Puschmann, H. (2010). OLEX2: a complete structure solution, refinement and analysis program. *J. Appl. Cryst.* 42, 339–341. doi: 10.1107/S0021889808042726

Gao, H., Li, G., and Lou, H. X. (2018). Structural diversity and biological activities of novel secondary metabolites from endophytes. *Molecules* 23, 646–677. doi: 10.3390/molecules23030646

Guo, H., Wu, Q., Chen, D., Jiang, M., Chen, B., et al. (2021). Absolute configuration of polypropionate derivatives: Decempyrones A–J and their MptpA inhibition and anti-inflammatory activities. *Bioorg. Chem.* 115:105156. doi: 10.1016/j.bioorg.2021.105156

Gupta, S., Chaturvedi, P., Kulkarni, M. G., and Staden, J. V. (2019). A critical review on exploiting the pharmaceutical potential of plant endophytic fungi. *Biotechnol. Adv.* 39:107462. doi: 10.1016/j.bioteschadv.2019.107462

Hirota, A., Nemoto, A., Tsuchiya, Y., Hojo, H., and Abe, N. (1999). Isolation of a 2-pyrone compound as an antioxidant from a fungus and its new reaction product with 1, 1-diphenyl-2-picrylhydrazyl radical. *Biosci. Biotechnol. Biochem.* 63, 418–420. doi: 10.1271/bbb.63.418

Hu, Z. X., Xue, Y. B., Bi, X. B., Zhang, J. W., Luo, Z. W., Li, X. N., et al. (2014). Five new secondary metabolites produced by a marine-associated fungus, *Daldinia eschscholzii*. *Mar. Drugs* 12, 5563–5575. doi: 10.3390/md12115563

Jiang, J. S., Li, F. S., Feng, Z. M., Yang, Y. N., and Zhang, P. C. (2020). New phenolic glycosides from *Polygonum cuspidatum*. *J. Asian Nat. Prod. Res.* 22, 17–23. doi: 10.1080/10286020.2019.1646730

Li, G., Kusari, S., Golz, C., Strohmann, C., and Spiteller, M. (2016). Three cyclic pentapeptides and a cyclic lipopeptide produced by endophytic *Fusarium decemcellulare* LG53. *RSC Adv.* 6, 54092–54098. doi: 10.1039/C6RA10905E

Li, G., Kusari, S., Kusari, P., Kayser, O., and Spiteller, M. (2015). Endophytic *Diaporthe* sp. LG23 produces a potent antibacterial tetracyclic triterpenoid. *J. Nat. Prod.* 78, 2128–2132. doi: 10.1021/acs.jnatprod.5b00170

Li, J., Liu, S., Niu, S., Zhuang, W., and Che, Y. (2009). Pyrrolidinones from the ascomycete fungus *Albonectria rigidiuscula*. *J. Nat. Prod.* 72, 2184–2187. doi: 10.1021/np900619z

Li, G., and Lou, H. X. (2018). Strategies to diversify natural products for drug discovery. *Med. Res. Rev.* 38, 1255–1294. doi: 10.1002/med.21474

Liu, H. W., and Begley, T. P. (2020). *Comprehensive Natural Products III*. Oxford: Elsevier.

Liu, X. H., Hou, X. L., Song, Y. P., Wang, B. G., and Ji, N. Y. (2020). Cyclonerane sesquiterpenes and an isocoumarin derivative from the marine-alga-endophytic fungus *Trichoderma citrinoviride* A-WH-20-3. *Fitoterapia* 141:104469. doi: 10.1016/j.fitote.2020.104469

Nilanonta, C., Isaka, M., Chanphen, R., Thong-Orn, N., Tanticharoen, M., and Thebtaranonth, Y. (2003). Unusual enniatins produced by the insect pathogenic fungus *Verticillium hemipterigenum*: isolation and studies on precursor-directed biosynthesis. *Tetrahedron* 59, 1015–1020. doi: 10.1016/S0040-4020(02)01631-9

Ola, A. R. B., Thomy, D., Lai, D., Brötz-Oesterhelt, H., and Proksch, P. (2013). Inducing secondary metabolite production by the endophytic fungus *Fusarium tricinctum* through coculture with *Bacillus subtilis*. *J. Nat. Prod.* 76, 2094–2099. doi: 10.1021/np400589h

Qader, M. M., Kumar, N. S., Jayasinghe, L., and Fujimoto, Y. (2018). Shikimic acid production by *Fusarium decemcellulare*, an endophytic fungus isolated from *Flacourtia inermis* fruits. *J. Biol. Active Prod. Nat.* 8, 43–50. doi: 10.1080/22311866.2018.1426494

Royles, B. J. L. (1995). Naturally occurring tetramic acids: structure, isolation, and synthesis. *Chem. Rev.* 95, 1981–2001. doi: 10.1021/cr00038a009

Sheldrick, G. M. (2015). SHELXT–integrated space-group and crystal-structure determination. *Acta Cryst* 71, 3–8. doi: 10.1107/S2053273314026370

Shiono, Y., Tsuchinari, M., Shimanuki, K., Miyajima, T., Murayama, T., Koseki, T., et al. (2007). Fusaristatins a and B, two new cyclic lipopeptides from an endophytic *Fusarium* sp. *J. Antibiot.* 60, 309–316. doi: 10.1038/ja.2007.39

Tian, C., Gao, H., Peng, X. P., Li, G., and Lou, H. X. (2021). Fusidic acid derivatives from the endophytic fungus *Acremonium pilosum* F47. *J. Asian Nat. Prod. Res.* 23, 1148–1155. doi: 10.1080/10286020.2020.1866559

Wang, H. H., Li, G., Qiao, Y. N., Sun, Y., Peng, X. P., and Lou, H. X. (2019). Chamiside a, a cytochalasan with a tricyclic core skeleton from the endophytic fungus *Chaetomium nigricolor* F5. *Org. Lett.* 21, 3319–3322. doi: 10.1021/acs.orglett.9b01065

Yamamura, S., Lai, S., Shizuri, Y., Kawai, K., and Furukawa, H. (1991). Three new phenolic metalolites from *Penicillium* species. *Heterocycles* 32, 297–305. doi: 10.3987/COM-90-5639

Zeng, J. X., Bing, X. B., Ying, B. I., Wang, J., Ren, G., Wang, H. L., et al. (2017). Chemical constitutes from plantaginis semen(II). *Chin. J. Exp. Tradit. Med. Form.* 23, 81–84. doi: 10.13422 /j.cnki.syfjx.2017040081

Zhang, H. W., Song, Y. C., and Tan, R. X. (2006). Biology and chemistry of endophytes. *Nat. Prod. Rep.* 23, 753–711. doi: 10.1039/b609472b

Zhang, D., Tao, X., Chen, R., Liu, J., Li, L., Fang, X., et al. (2015). Pericoannosin a, a polyketide synthase-nonribosomal peptide synthetase hybrid metabolite with new carbon skeleton from the endophytic fungus *Periconia* sp. *Org. Lett.* 17, 4304–4307. doi: 10.1021/acs.orglett.5b02123

frontiers | Frontiers in Microbiology

TYPE Original Research
PUBLISHED 09 February 2023
DOI 10.3389/fmicb.2023.1137159

OPEN ACCESS

EDITED BY
Dewu Zhang,
Institute of Medicinal Biotechnology (CAMS), China

REVIEWED BY
Wanping Chen,
University of Göttingen, Germany
Mao Peng,
Westerdijk Fungal Biodiversity Institute, Netherlands

*CORRESPONDENCE
Zhendong Chen
✉ czd3808@gxaas.net
Zeping Wang
✉ yaheng830619@163.com

†These authors have contributed equally to this work

SPECIALTY SECTION
This article was submitted to Microbial Physiology and Metabolism, a section of the journal Frontiers in Microbiology

RECEIVED 04 January 2023
ACCEPTED 24 January 2023
PUBLISHED 09 February 2023

CITATION
Duan M, Long S, Wu X, Feng B, Qin S, Li Y, Li X, Li C, Zhao C, Wang L, Yan Y, Wu J, Zhao F, Chen Z and Wang Z (2023) Genome, transcriptome, and metabolome analyses provide new insights into the resource development in an edible fungus *Dictyophora indusiata*.
Front. Microbiol. 14:1137159.
doi: 10.3389/fmicb.2023.1137159

Genome, transcriptome, and metabolome analyses provide new insights into the resource development in an edible fungus *Dictyophora indusiata*

Mingzheng Duan[1,2†], Shengfeng Long[3†], Xiaojian Wu[3], Bin Feng[4], Sunqian Qin[4], Yijie Li[1], Xiang Li[1], Changning Li[1], Chenggang Zhao[3], Lingqiang Wang[2], Yong Yan[3], Jianming Wu[1], Falin Zhao[2], Zhendong Chen[3]* and Zeping Wang[1]*

[1]Sugarcane Research Institute, Guangxi Academy of Agricultural Sciences/Sugarcane Research Center, Chinese Academy of Agricultural Science/Key Laboratory of Sugarcane Biotechnology and Genetic Improvement (Guangxi), Ministry of Agriculture, Nanning, China, [2]Key Laboratory for Conservation and Utilization of Subtropical Agro-Bioresources, College of Agriculture, Guangxi University, Nanning, China, [3]Guangxi Academy of Agricultural Sciences, Nanning, China, [4]Laibin Branch of Guangxi Academy of Agricultural Sciences, Laihua Center, Laibin, China

Dictyophora indusiata (Vent. Ex Pers.) Fisch. (DI) is an edible and medicinal fungus widely used in East Asian countries. However, during DI cultivation, the formation of fruiting bodies cannot be regulated, which leads to yield and quality losses. The present study performed a combined genome, transcriptome, and metabolome analysis of DI. Using Nanopore and Illumina sequencing approaches, we created the DI reference genome, which was 67.32Mb long with 323 contigs. We identified 19,909 coding genes on this genome, of which 46 gene clusters were related to terpenoid synthesis. Subsequent transcriptome sequencing using five DI tissues (cap, indusia, mycelia, stipe, and volva) showed high expression levels of genes in the cap, indicating the tissue's importance in regulating the fruiting body formation. Meanwhile, the metabolome analysis identified 728 metabolites from the five tissues. Mycelium was rich in choline, while volva was rich in dendronobilin; stipe had monosaccharides as the primary component, and the cap was the main source of indole acetic acid (IAA) synthesis. We confirmed the importance of tryptophan metabolism for DI fruiting body differentiation based on KEGG pathway analysis. Finally, the combined multiomics analysis identified three new genes related to IAA synthesis of the tryptophan metabolic pathway in the cap, which may regulate DI fruiting body synthesis and improve DI quality. Thus, the study's findings expand our understanding of resource development and the molecular mechanisms underlying DI development and differentiation. However, the current genome is still a rough draft that needs to be strengthened.

KEYWORDS

widely-targeted metabolome, food chemistry, edible fungi, tryptophan, UPLC-ESI-MS/MS

1. Introduction

Edible and medicinal fungi are known for their nutritional and medicinal values and are consumed by people worldwide (Buckley, 2008; Lu et al., 2020). The edible and medicinal fungi promote human health and are considered functional foods (Hetland et al., 2008; Li et al., 2019; Krakowska et al., 2020). Among the many edible and medicinal fungi distributed worldwide, *Dictyophora indusiata* (DI, Phallaceae) is widely used in East Asian countries as both medicine and food (Wang et al., 2021). Currently, DI is known for two primary uses; the stipe is used as a delicacy and has various medicinal properties, such as antitumor effects, eye benefits, lipofuscin resistance, cardiovascular protective, antibiosis, mental tranquilization, immunomodulatory, and antioxidant activities (Liao et al., 2015; Liu et al., 2017; Wang Y. et al., 2019; Wang W. et al., 2019). It is also a good source of fungal polysaccharides (Liu et al., 2017; Wang W. et al., 2019) and bioactive compounds (Huang et al., 2011), which enhance human health.

DI has been domesticated and produced artificially in the south of China; however, there are many problems in its cultivation, resource utilization, and development. The short mature stage (few hours) of DI fruiting bodies demands prompt harvesting; delayed harvest causes autolysis of fruiting bodies, leading to wastage. The mature fruiting bodies comprise four tissues (Figure 1A). In south China, usually only the stipe has been consume, while the other three tissues (cap, indusia, and volva) get discarded, which leading to a considerable waste of resources. Wang et al. (2020, 2021), based on the transcriptome, proteome, and metabolome analyses, showed that the cell wall stress-dependent MAPK pathway and a few other unique proteins and metabolites play critical roles in the morphological development of DI. However, the formation of DI fruiting bodies is not entirely explored due to the lack of a reference genome. Meanwhile, the crucial tissue regulating fruiting body formation remains unclear, and the DI mycelium remains less exploited for medicinal use. Moreover, DI has various bioactive compounds, and the genome harbors numerous functional genes related to metabolites with medicinal properties; however, research in this field is less. Therefore, addressing these issues and improving our understanding will promote the economic value of DI.

In recent years, advanced omics technologies have been applied to study fungi. A combination of second-generation and third-generation sequencing technologies has been widely used to analyze the genome of edible and medicinal fungi, such as *Russula griseocarnosa*, *Agrocybe cylindracea*, *Hericium erinaceus*, *Auricularia heimuer*, and *Gloeostereum incarnatum* (Wang X. et al., 2019; Yuan et al., 2019; Gong et al., 2020; Liang et al., 2020; Yu et al., 2020). Transcriptomic studies revealed the fruiting body formation of edible and medicinal fungi, such as *Leucocalocybe mongolica*, *Lentinula edodes*, and the peach-shaped and mature fruiting bodies of DI (Yoo et al., 2019; Wang et al., 2020; Duan et al., 2021). Meanwhile, metabolomic studies characterized the edible and medicinal fungi and their diverse medicinal components, such as bioactive metabolites, antibiotics, and agrochemicals (Alberti et al., 2020). These earlier studies indicated that combining various "omics" technologies would help elucidate DI fruiting body differentiation and explore resource value.

Therefore, the present study investigated the molecular mechanism underlying DI fruiting body differentiation and the resource value of medicinal compounds and gene resources based on sequencing and UHPLC-ESI-MS/MS. We present a reference genome of DI based on

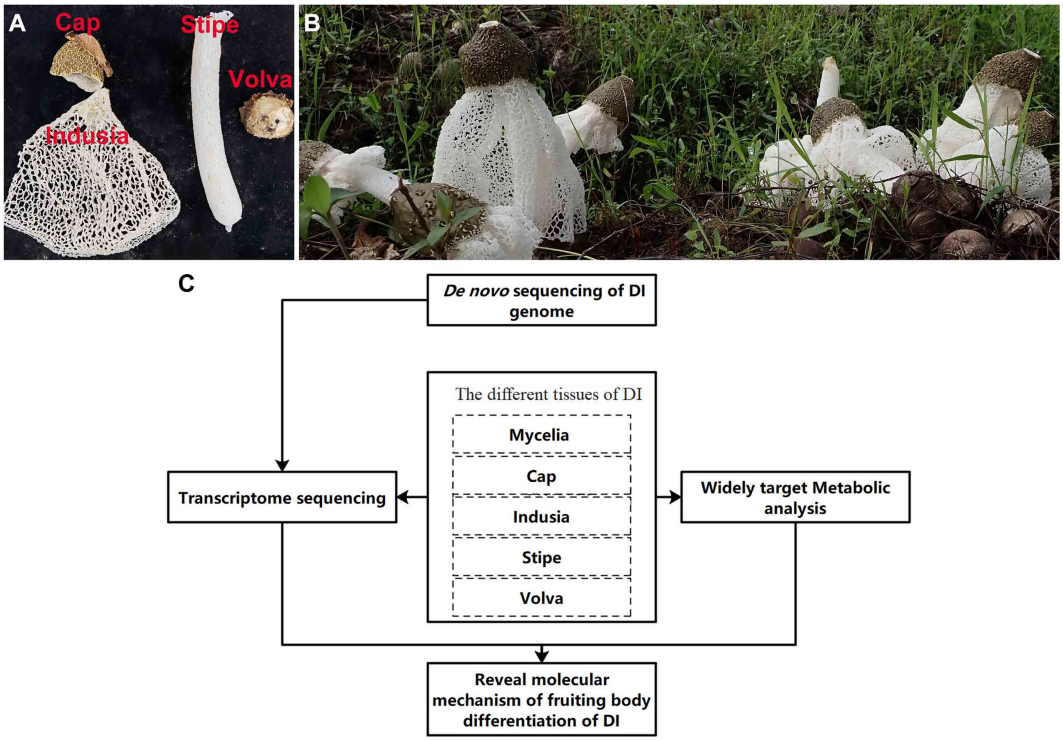

FIGURE 1
Apparent morphology of DI fruiting bodies and technical route of the study. **(A)** Different kinds of DI tissues used in this study. **(B)** Morphology of DI fruiting bodies at harvest. **(C)** The technical route of this study.

third-generation sequencing. Then, transcriptome sequencing was performed using five DI tissues (cap, indusia, mycelia, stipe, and volva) to identify the tissues with the most significant influence on fruiting body differentiation. Further, a widely-targeted metabolome analysis was performed to explore the medicinal value of these five DI tissues and the metabolic processes affecting the DI fruiting body differentiation. Finally, the functional gene resources associated with the high value metabolites in the DI genome were mined based on multi-omics association analysis. The findings of the study will lay a foundation for improving the quality and resource value of DI.

2. Results

2.1. *De novo* genome sequencing

2.1.1. Reference genome of *Dictyophora* genus

We constructed the reference genome of DI to advance our understanding of the molecular mechanisms underlying DI fruiting body development and differentiation. As shown in Table 1, third-generation nanopore sequencing combined with NGS sequencing generated a reference genome of 67.32 Mb (Strain ID: ZS). The genome had 216 contigs, a GC content of 44.05%, a contig N50 of 0.79 Mb, L50 of 20, and 19,909 genes. BUSCO analysis recovered 87.6% (254/290) of the core genes (Supplementary Table S1), indicating high integrity of the assembled genome.

2.1.2. Genome annotation based on public databases

We further annotated the DI genes using public databases. The predicted 19,909 genes of DI (Strain ZS; a total length of 31.88 Mb, 47.35% of the genomic size) showed an average gene length of 1,601 bp and an average GC content of 47.25%. We annotated these genes using the four public databases, GO (Gene Ontology), KOG (Eukaryotic Orthologous Groups), KEGG (Kyoto Encyclopedia of Genes and Genomes), and CAZyme (Carbohydrate-Active enzymes). The preliminary comparison showed the annotation of 39.63% (7,891), 16.98% (3,381), 51.22% (10199), and 4.14% (826) of genes in the GO, KOG, KEGG, and CAZyme databases, respectively. In the GO categories (Figure 2A), 3,815 genes enriched "metabolic process," the predominant term in the biological process category; 999 genes enriched "cell part," the predominant term in the cellular component category; 3,975 genes enriched "binding," the predominant term in the molecular function category. KOG annotation (Figure 2B) assigned 1,143 genes to the code class "S: Function unknown," which was the predominant class. The second most enriched code class was "U: Intracellular trafficking, secretion, and vesicular transport," with 270 genes. Meanwhile, KEGG annotation (Level 2) predominantly enriched "Transport and catabolism" with 690 genes (Figure 2C). The annotation based on CAZyme divided the genes into 910 gene families (Figure 2D), of which 135 belonged to AA (Auxiliary Activities), 126 to CBM (Carbohydrate-Binding Modules), 161 to CE (Carbohydrate Esterases), 319 to GH (Glycoside Hydrolases), 151 to GT (Glycosyl Transferases), and 18 to PL (Polysaccharide Lyases).

TABLE 1 Statistics of assembly of the DI genome.

Genome ID	ZS
Genome assembly size (Mb)	67.32
GC content (%)	44.05
Contigs	216
N50 (Mb)	0.79
L50	20
Largest contig (Mb)	3.39
Gene number	19,909
Nanopore sequencing coverage	181×
NGS sequencing coverage	176×

2.1.3. Secondary metabolism-associated genes of DI

Further annotations based on FCPD (Fungal cytochrome P450 database) and antiSMASH revealed genes associated with the secondary metabolites of DI. The FCPD pipeline identified 369 DI genes related to 41 of P450 gene families (Supplementary Table S2). Meanwhile, antiSMASH showed that 64 gene clusters of DI were associated with secondary metabolism synthesis (Supplementary Table S3). Among them, 64 gene clusters were related to the terpene class, and the remaining were associated with the synthesis of indole, T1PKS (Type I PKS: Polyketide synthase), NRPS (Non-ribosomal peptide synthetase cluster), siderophore, and NRPS-like (NRPS-like fragment) metabolites.

2.2. Transcriptome sequencing of five DI tissues

2.2.1. Sequencing analysis and differentially expressed genes (DEGs)

Further, to reveal the differences in gene expression patterns between different tissue types of DI, transcriptome sequencing was performed using different fruiting body tissues (cap, indusium, mycelium, stipe, and volva) and the dikaryotic mycelium as control. As shown in Table 2, a total of 109.15 GB of NGS data were generated, with an average of 6 GB per sample; the lowest Q30 value was 91.87% (Stipe3), and the total mapped rate of all samples was at least 95.8% (Volva1), indicating the high quality of the transcriptome data.

We then identified the DEGs (Figure 3). The violin plots showed higher expression levels of genes in cap and mycelia but lower in indusia and volva (Figure 3A); the expression of genes was moderate in the stipe. Venn diagram showed that 2,670 DEGs were shared between all tissues, while 4,687 were common between mycelia and cap; 64, 67, 189, 283, and 1,550 DEGs were unique to the indusia, volva, stipe, cap, and mycelia (Figure 3B). The correlation heat map showed high association in the expression pattern of DEGs between indusia and volva ($R = 0.69$; Figure 3C). The subsequent pairwise comparison of tissues revealed two expression patterns of DEGs (Figure 3D); one group showed significantly downregulated expression in all comparisons with mycelia (mycelia vs. indusia, cap, stipe, and volva; e.g., mycelia vs. indusia with 10,958 and 1,317 of downregulated and upregulated DEGs); another group had DEGs upregulated in cap compared with other tissues, except mycelia (stipe, indusia, and volva vs. cap). Another Venn diagram based on DEGs of different comparison groups showed that unique DEGs related to mycelia and cap were significantly higher than those between other tissues; mycelia vs. cap had 232 unique DEGs, but indusia vs. volva had only 5 unique DEGs (Figure 3E). Thus, the observations indicated that among all the five DI tissues, mycelium and cap were the most significantly active tissues with numerous DEGs, predominantly

10.3389/fmicb.2023.1137159

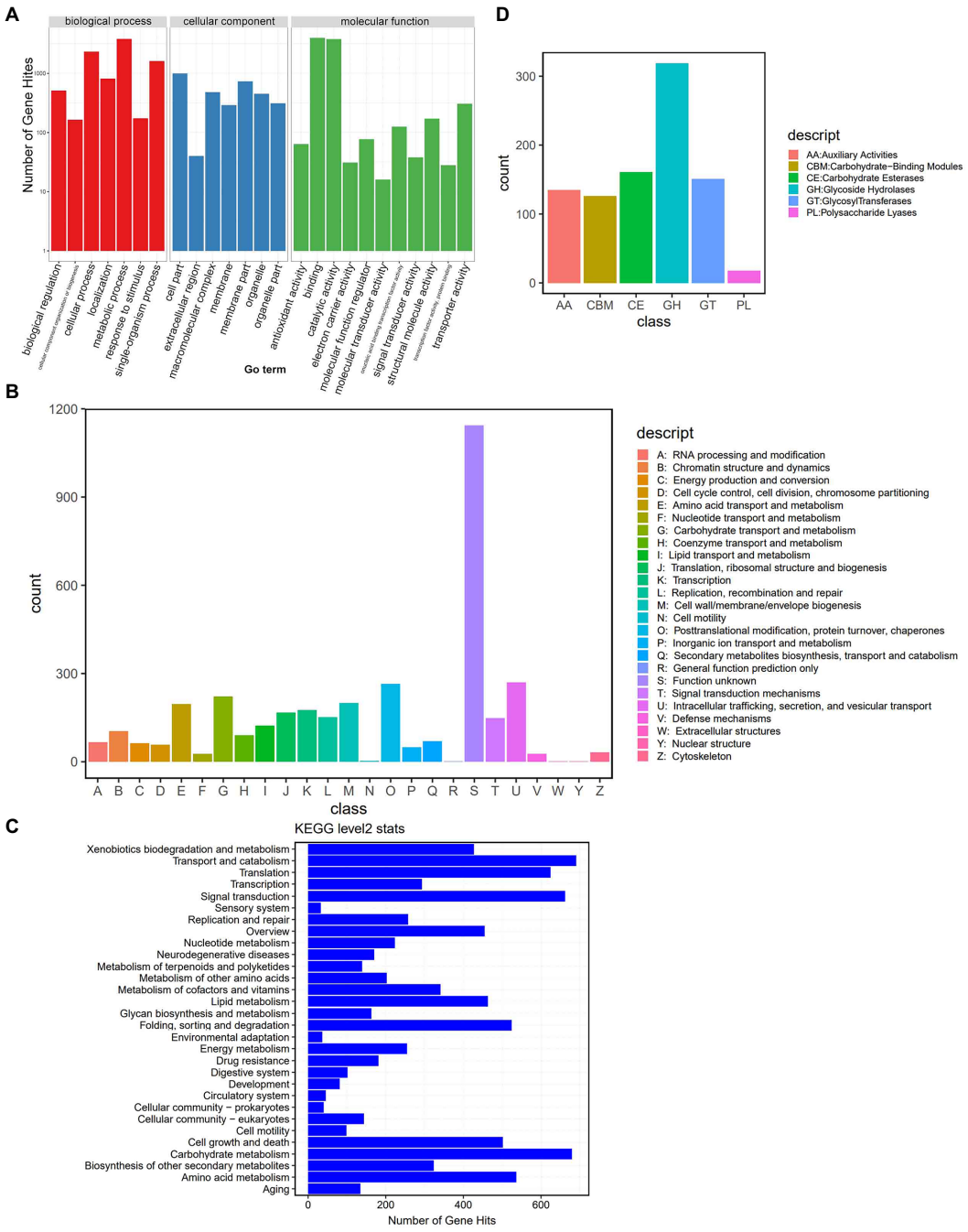

FIGURE 2
Genome annotation based on public databases. **(A)** GO annotation. The upper horizontal axis shows the three GO categories (Biological Process – BP, Cellular Component – CC, and Molecular Function – MF), the lower horizontal axis shows the subclassification of these three categories, and the vertical axis represents the number of gene hits. **(B)** KOG annotation. The horizontal axis shows the KOG classes, and the vertical axis represents the number of gene hits. **(C)** KEGG (Level 2) annotation. The horizontal axis represents the number of gene hits, and the vertical axis shows the classes. **(D)** CAZyme annotation. The horizontal axis shows the classes, and the vertical axis represents the number of gene hits.

upregulated genes, suggesting their leading role in the differentiation of DI fruiting bodies; this confirmed mycelium and cap as critical tissues for the differentiation of DI fruiting bodies.

2.2.2. Go and KEGG differential genes enrichment analysis

To further determine the functions of these DEGs, we performed enrichment analysis based on GO and KEGG databases (Figure 4; Supplementary Figure S1). GO annotation showed that "cellular process (GO:0009987)," "metabolic process (GO:0008152)," and "biological regulation (GO:0065007)" were the top three enriched terms in the biological process category; "binding (GO:0005488)" and "catalytic activity (GO:0003824)" were the two significantly enriched terms in molecular functions; "cellular anatomical entity (GO:0110165)" and "protein-containing complex (GO:0032991)" were the two significantly enriched terms in cellular component

10.3389/fmicb.2023.1137159

TABLE 2 Statistics of the transcriptome sequences from five DI tissues.

ID	Clean Data (GB)	Q30 (%)	Total Mapped (%)
Cap1	6.64	92.85%	96.36%
Cap2	6.41	92.61%	96.18%
Cap3	6.52	92.60%	96.42%
Indusia1	7.76	92.24%	95.93%
Indusia2	7.51	92.55%	96.46%
Indusia3	7.38	93.02%	96.39%
Mycelia1	6.97	92.44%	96.89%
Mycelia2	7.78	93.19%	97.06%
Mycelia3	6.74	92.62%	96.95%
Stipe1	6.93	93.05%	96.69%
Stipe2	7.75	92.89%	96.46%
Stipe3	7.63	91.87%	96.20%
Volva1	7.55	92.54%	95.80%
Volva2	7.51	92.64%	96.29%
Volva3	7.99	92.38%	96.08%

(Figure 4). Meanwhile, KEGG enrichment analysis showed global and overview map (ko01100) as the most significantly enriched pathway in all comparison groups and level 1 class of metabolism (Supplementary Figure S1). In the indusia vs. cap comparison, the Metabolic pathway (ko01100) had 1,538 DEGs, while the translation (ko00970) pathway was enriched with 462 DEGs. Meanwhile, the translation (ko00970), transport and catabolism (ko04138), signal transduction (ko04011), and aging (ko04213) pathways were the most enriched in the level 1 class of Genetic In-formation Processing, Cellular Processes, Environmental Information Processing, and Organismal Systems. We found that the DEGs expression trend in the above two databases was consistent with distribution of DEGs across different DI tissues (Figure 3), indicating the reliability of the annotation.

2.3. Widely-targeted metabolome analysis of five DI tissue

2.3.1. Metabolite composition

We performed a widely-targeted metabolome analysis based on the UPLC-ESI-MS/MS approach to determine the metabolic composition of different DI tissues. We determined the Z-scores to evaluate the categories and abundance of metabolites (Figure 5) and then analyzed the sample-sample correlation of metabolite distribution in the five tissues. As shown in Figure 5A, the cap, indusia, and stipe metabolites were highly correlated ($R > 0.67$). Further, based on public and commercial databases, 728 metabolites (grouped into ten classes), including 89 of alkaloids, 119 of amino acids and derivatives, 6 of flavonoids, 7 of lignans and coumarins, 130 of lipids, 71 of nucleotides and derivatives, 78 of organic acids, 109 of phenolic acids, 12 of terpenoids, and 107 of metabolites belong to others, were detected in the five DI tissues (Figure 5B). Detailed information on the metabolites is presented in Supplementary Table S4.

2.3.2. Differential metabolites

Furthermore, we compared the metabolite abundance among the five tissues and analyzed their distribution characteristics. K-means clustering was performed to group the metabolites based on the abundance in the different tissues (Figure 6A; Supplementary Table S5). A total of nine groups of metabolites were identified with specific expression trends. We identified 91 metabolites in mycelia (class 1), 138 in volva (class 4), 113 in indusia (class 2), 72 in cap (class 3), and 71 in stipe (class 6) with representative of the tissue types. Further, we analyzed the most abundant tissue-specific metabolites (Table 3). Choline, dibutyl phthalate*, and diisobutyl phthalate* were the top three tissue-specific metabolites in mycelia, 13(S)-HODE;13(S)-hydroxyoctadeca-9Z,11E-dienoic acid, 9S-Hydroxy-10E,12Z-octadecadienoic acid, and punicic acid (9Z,11E,13Z-octadecatrienoic acid) in volva, linoleic acid, D-Pantothenic acid, and naphthisoxazol A in indusial, succinyladenosine, isocitric acid, and quinic acid in the cap, and D-mannose*, inositol*, and D-glucose* in stipe. Furthermore, we analyzed the relationship between the differential metabolites in each tissue compared with mycelia to screen metabolites related to DI fruiting body differentiation. As shown in Figure 6B, mycelia vs. volva (52) had the maximum unique, differential metabolites compared with mycelia vs. cap (24), mycelia vs. stipe (15), and mycelia vs. indusia (21).

We then analyzed the distribution of terpenoid metabolites in DI in detail. As shown in Figure 7, 12 terpenoids were detected from the five DI tissue types. Among them, Dendronobilin I-iso1 and Mansonone N were the top two terpenoids in terms of intensity, with Dendronobilin I-iso1 mainly synthesized in volva and Mansonone N in mycelia.

2.3.3. Tryptophan metabolism of DI

Transcriptome analysis detected the highest abundance of DEGs in the cap and mycelia, suggesting that these two tissues were critical for DI fruiting body differentiation. Therefore, we conducted metabolic pathway enrichment analysis for the cap and mycelia based on the KEGG database. As shown in Figure 8, three pathways, including Tryptophan metabolism (ko00380), Amino sugar and nucleotide sugar metabolism (ko00520), and Pentose and glucuronate interconversions (ko00040), were significantly ($p < 0.05$) enriched in the cap vs. mycelia comparison group. We detected the highest enrichment intensity for Tryptophan metabolism, with the highest participation of metabolites. As shown in Figure 9, a large amount of L-Tryptophan was first synthesized and enriched in the cap, indusia, and stipe during mycelium differentiation into fruiting bodies, and most of the L-Tryptophan metabolized to tryptamine (Figures 9A,B). As Figure 9A, through a series of metabolic processes, tryptamine got metabolized to 3-indoleacetonitrile and then indole-3-acetic acid (IAA). Next, IAA got metabolized into a node metabolite anthranilic acid, which further converted into 2-aminophenol, 2-amino-3-methoxybenzoic acid, quinolinic acid, 2-picolinic acid, and 2-oxoadipic acid. Finally, 2-oxoadipic acid got metabolized *via* the next metabolic pathway of glycolysis (ko00010). Thus, these observations indicated that during the formation of DI fruiting bodies from mycelium, the metabolite L-tryptophan and the Tryptophan metabolism pathway play significant roles.

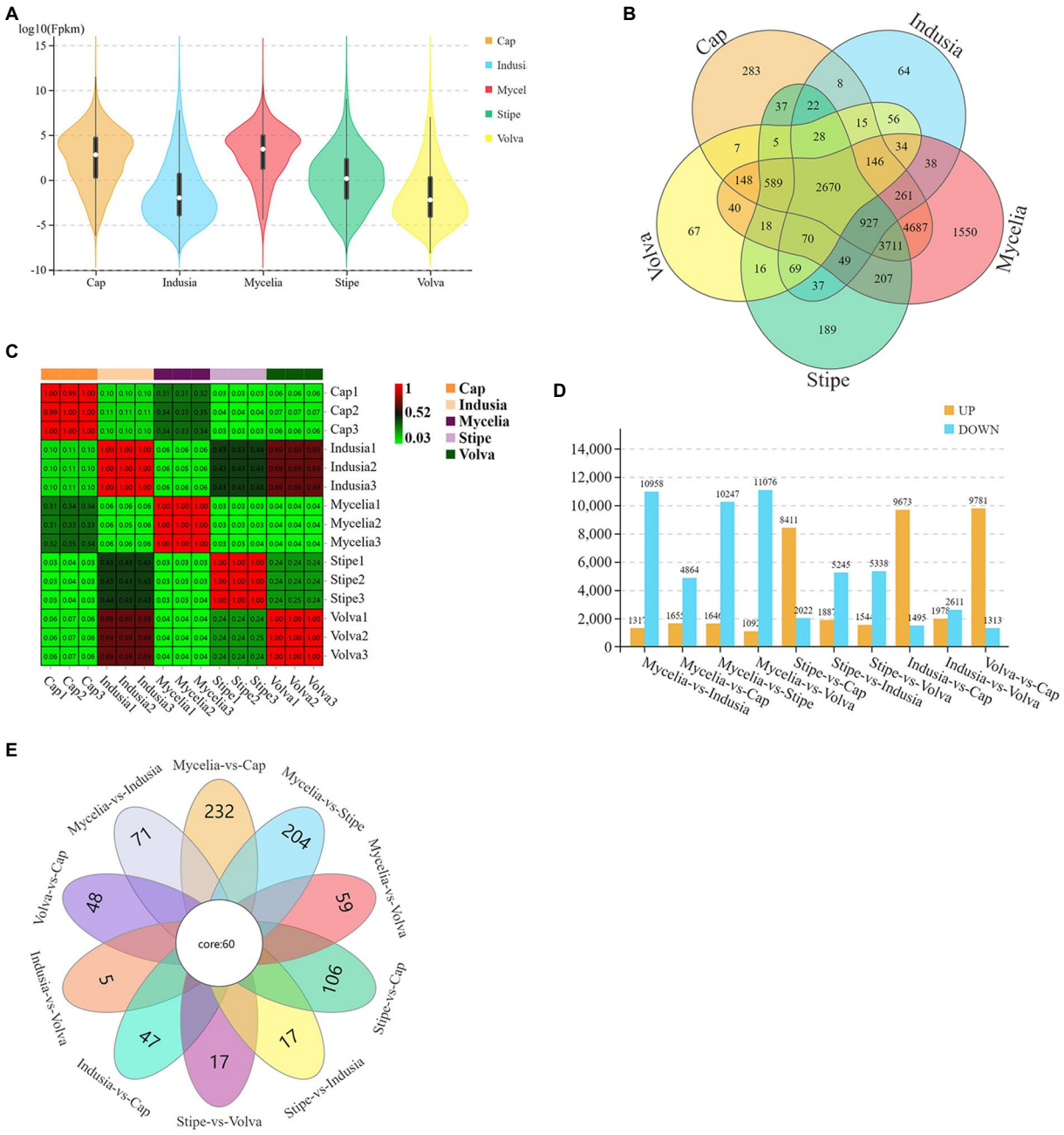

FIGURE 3
Distribution of DEGs across different DI tissues. **(A)** The violin plots display the gene expression intensity in five tissue types of DI. The curves represent the probability curve of the data distribution. The number of data points is positively correlated with the width of the probability curve. The upper and lower ends indicate the maximum and minimum values of nonoutliers, respectively. The upper and lower edges of the vertical line indicate the 75th and 25th percentiles of the data, respectively; the central dot indicates the median. The horizontal axis represents different tissues, and the vertical axis represents the log_{10}FPKM. **(B)** Venn diagram of DEGs in five tissues. Different colors represent different tissues. **(C)** Correlation heat map based on the expression of DEGs in five tissues. The abscissa and ordinate indicate the samples. The numbers in the grid are the Pearson correlation coefficient values. The different colors of the grid indicate different correlations. Red means a positive correlation; the darker the color, the stronger the correlation. **(D)** DEGs of each comparison group. The abscissa represents different comparison groups, and the ordinate represents the number of DEGs. **(E)** Venn diagram of DEGs of different comparison groups.

2.4. Combined multi-omics analysis

2.4.1. Transcriptome and metabolome correlation analysis

Furthermore, to understand the key genes and metabolites affecting DI fruiting body differentiation, we performed a correlation analysis based on the metabolome and transcriptome data and assessed the metabolite and gene expression similarity among the five tissue types. PCA based on mycelia's metabolome and transcriptome data showed significant differences; the mycelia appeared separated from the other four tissue types. The transcriptome PCA showed clustering of the stipe, volva, and indusia (Figure 10A); however, the cap appeared separated from these three tissues. The metabolome PCA showed that the volva was separated, while the indusia, cap, and stipe were clustered together

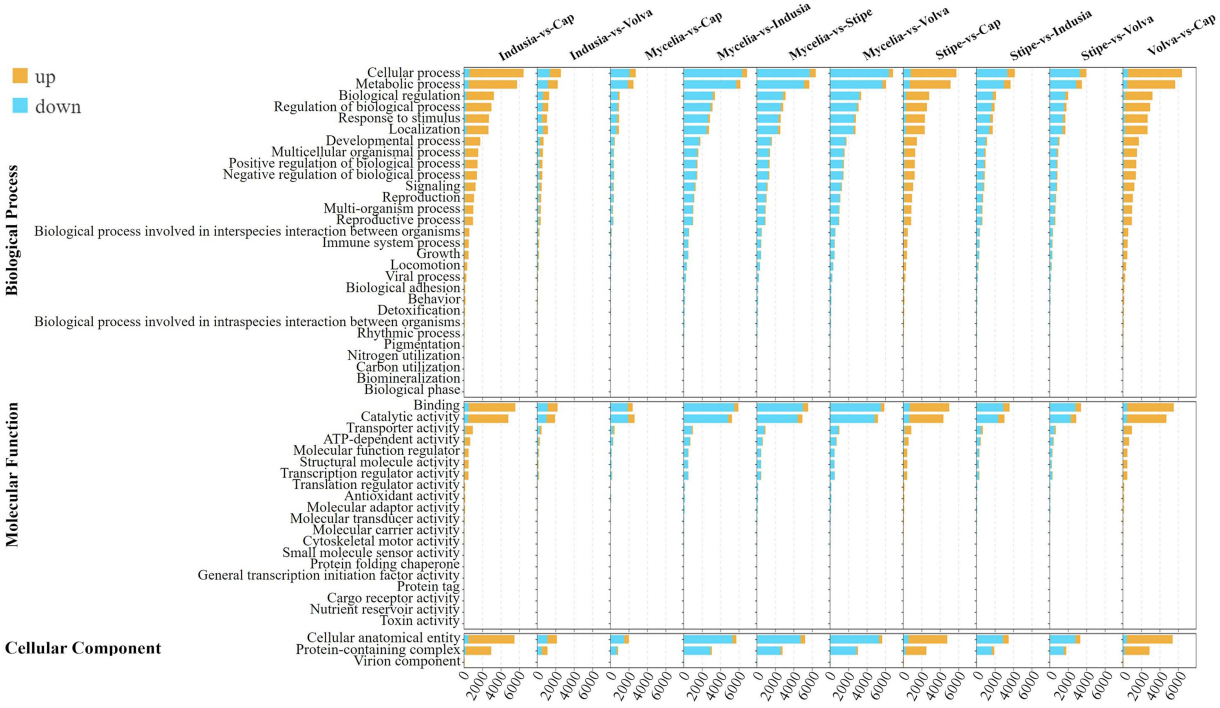

FIGURE 4
GO enrichment of the differentially expressed genes of different comparison groups. Different colors indicate the number of upregulated and downregulated genes in multiple comparison groups. In the upper left corner is the figure legend.

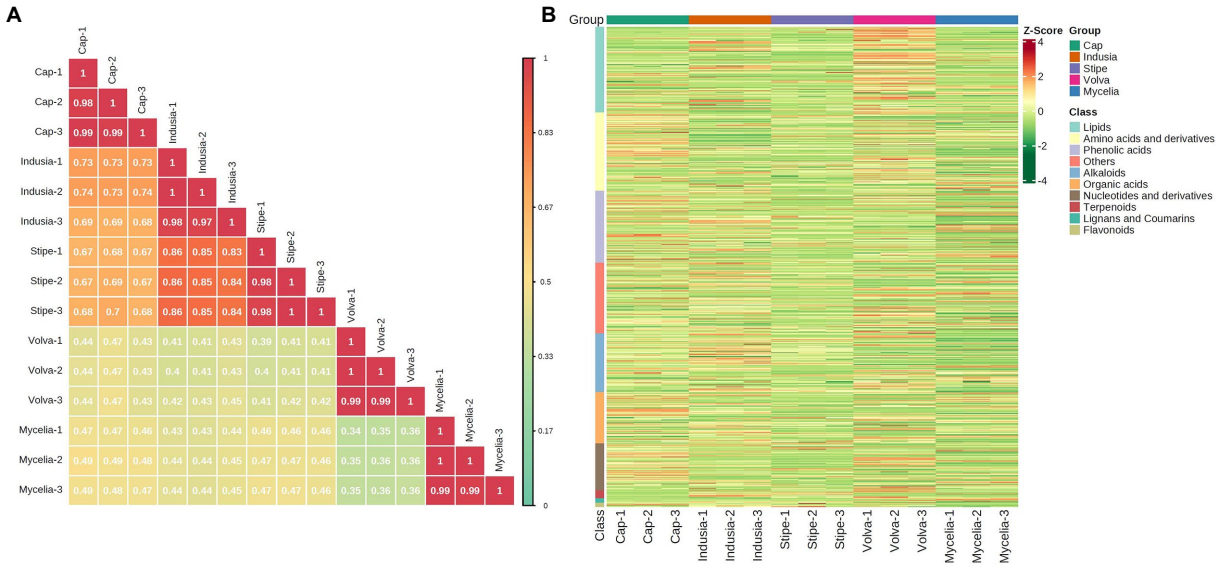

FIGURE 5
Metabolite composition of five DI tissues. **(A)** Pearson's correlation heat map. The longitudinal and diagonal lines show the sample names, and different colors represent the different Pearson correlation coefficients; the key is shown on the right side. **(B)** Clustering heat map of all metabolites. Each column represents a sample, and each row represents a metabolite class. A color bar represents the metabolite abundance. Different shades of red and green represent the upregulated and downregulated metabolites, respectively.

(Figure 10B). These results indicated that the metabolite accumulation and the transcriptome expression were not wholly consistent among the different DI tissue types.

We further identified the transcriptome and metabolome elements associated with fruiting body differentiation based on O2PLS analysis. We selected the top 10 genes and metabolites based on the loading value of expression of the DEGs and the differential metabolites (Figures 10C,D). Further annotation and abundance analysis of these genes and metabolites showed that most of these DEGs were homologous to the hypothetical protein from *Clathrus columnatus* and

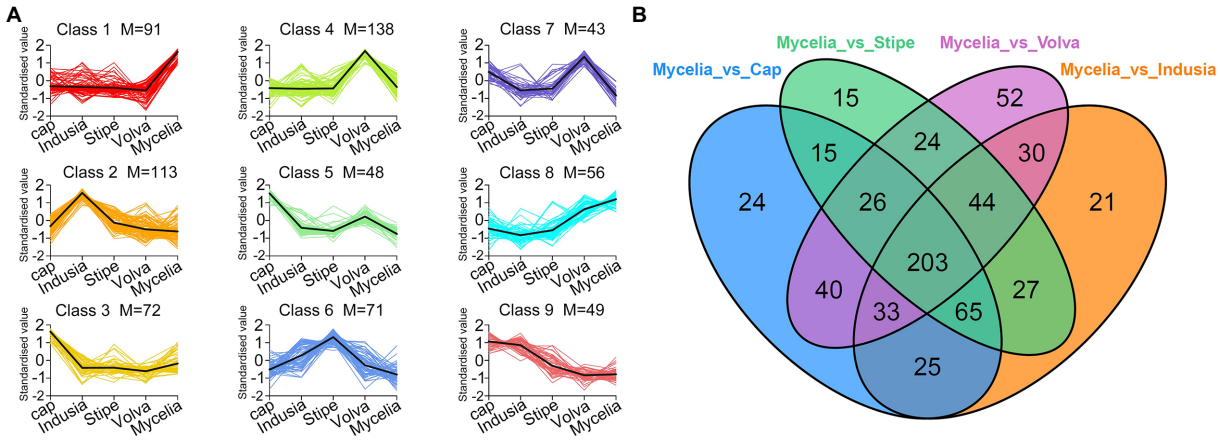

FIGURE 6
Analysis of the distribution characteristics of metabolites in different DI tissue types. **(A)** K-means clustering of metabolites of five DI tissue types. The abscissa represents the sample group, the ordinate represents standardized relative metabolite content, and the class represents the metabolite category number with the same trend in five DI tissue types. M represents the number of metabolites in this class. **(B)** Venn diagram shows differential metabolites of different comparison groups.

TABLE 3 Top three metabolites in the DI tissues.

Tissue	Class	Formula	Compounds	Class type
Mycelia	1	$C_5H_{14}NO^+$	Choline	Alkaloids
	1	$C_{16}H_{22}O_4$	Dibutyl phthalate*	Phenolic acids
	1	$C_{16}H_{22}O_4$	Diisobutyl phthalate*	Phenolic acids
Volva	4	$C_{18}H_{32}O_3$	13(S)-HODE;13(S)-Hydroxyoctadeca-9Z,11E-dienoic acid	Lipids
	4	$C_{18}H_{32}O_3$	9S-Hydroxy-10E,12Z-octadecadienoic acid	Lipids
	4	$C_{18}H_{30}O_2$	Punicic acid (9Z,11E,13Z-octadecatrienoic acid)	Lipids
Indusia	2	$C_{18}H_{32}O_2$	Linoleic acid	Lipids
	2	$C_9H_{17}NO_5$	D-Pantothenic Acid	Others
	2	$C_{11}H_9NO_2$	Naphthisoxazol A	Alkaloids
Cap	3	$C_{14}H_{17}N_5O_8$	Succinyladenosine	Nucleotides and derivatives
	3	$C_6H_8O_7$	Isocitric Acid	Organic acids
	3	$C_7H_{12}O_6$	Quinic Acid	Organic acids
Stipe	6	$C_6H_{12}O_6$	D-Mannose*	Others
	6	$C_6H_{12}O_6$	Inositol*	Others
	6	$C_6H_{12}O_6$	D-Glucose*	Others

*Indicates the metabolite presence of isomer.

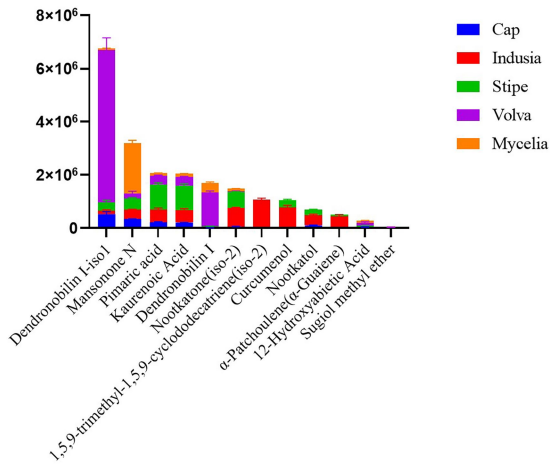

FIGURE 7
Distribution of terpenoids in different DI tissues. The abscissa represents the metabolite name, and the ordinate represents the peak area unit.

Sphaerobolus stellatus, except for MSTRG.18365, which may be involved in the synthesis of Proteophosphoglycan ppg4 (Supplementary Table S6). Meanwhile, the metabolites included four lipids (lysopc 17:1, lysope 17:1, lysope 17:1(2n isomer), and dihydrosphingosine-1-phosphate), three nucleotides and derivatives (2′-deoxyadenosine, 2′-deoxyuridine, and 2′-deoxyinosine), two phenolic acids (3,4-dihydroxybenzoic acid, protocatechuic acid* and 2,5-dihydroxybenzoic acid, gentisic acid*), and one organic acid (3-methyl-2-oxobutanoic acid, Supplementary Table S7).

2.4.2. Identification of tryptophan metabolism-associated genes in DI

We also performed a KEGG association analysis of transcriptome and metabolome data associated with the tryptophan metabolism pathway (ko00380) to identify the DEGs associated with tryptophan metabolism. KEGG enrichment analysis of the genes related to tryptophan metabolism in the cap vs. mycelia group showed that 50 were associated with the synthesis of 13 metabolites

10.3389/fmicb.2023.1137159

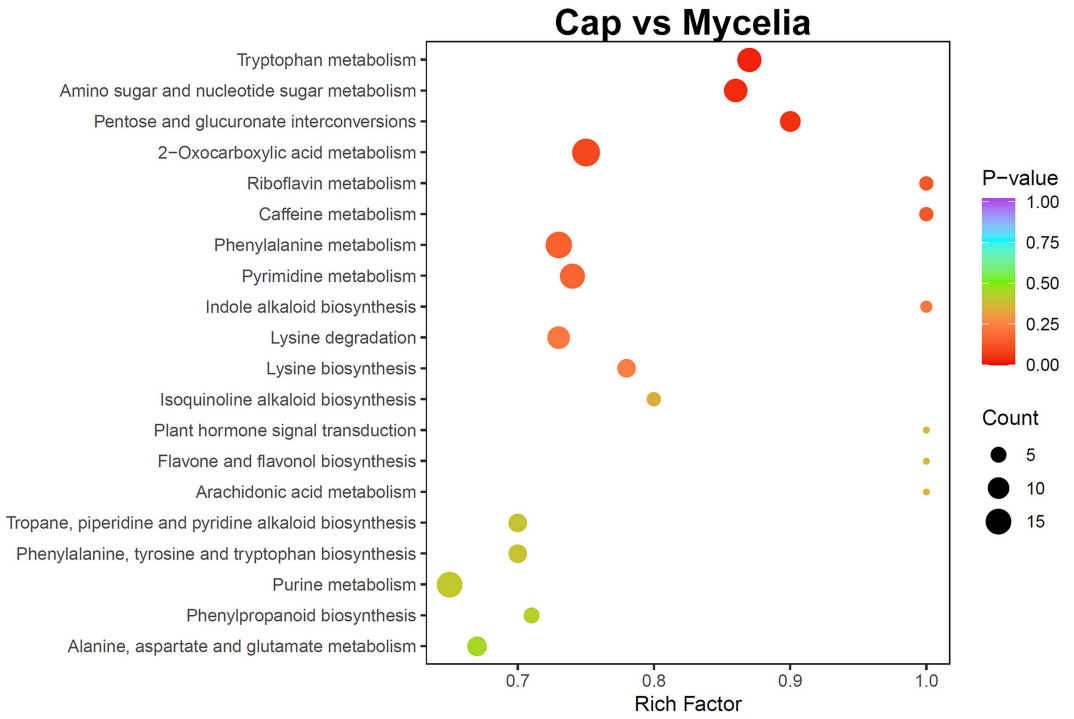

FIGURE 8
KEGG pathway enrichment analysis of the metabolome between cap and mycelia. The abscissa represents the rich factor of each pathway, and the ordinate represents the pathway name (sorted by value of *p*). The color of the dots reflects the value of *p*; the redder the dots, the more significant the enrichment. The dot size represents the number of differential metabolites enriched in the pathway.

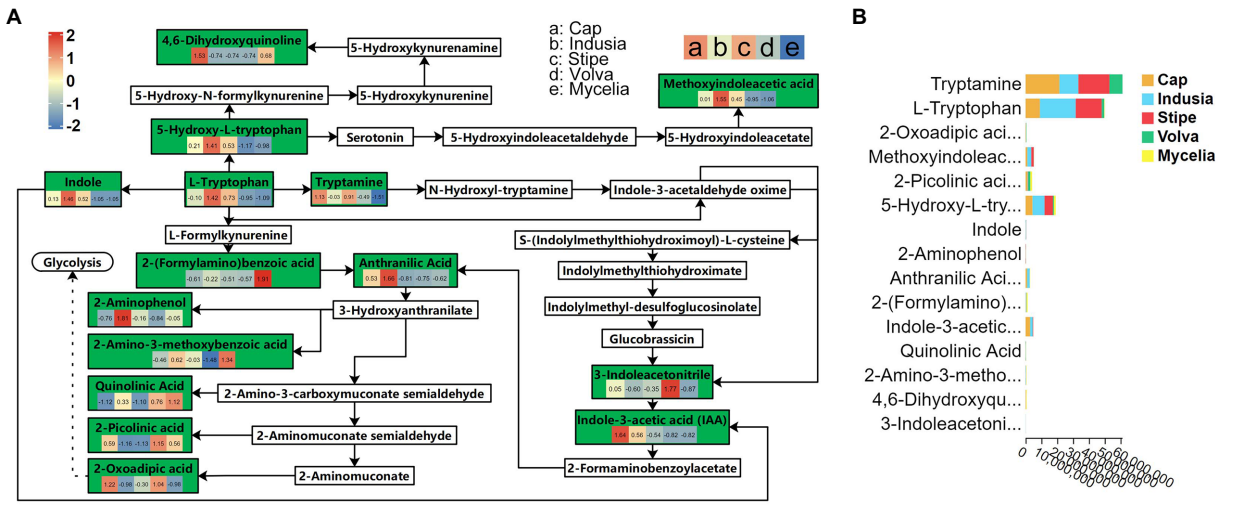

FIGURE 9
Tryptophan metabolism pathway (ko00380) in five DI tissues. **(A)** The boxes represent metabolites involved in the pathway. Green boxes represent the detected metabolites, and white boxes represent the undetected metabolites. The color (red to blue) key in the green boxes represents the relative abundance of the metabolite in different tissues (Evaluated by *z*-value, the key is shown in the upper left corner). The alphabets used for the tissues are shown in the upper right corner. The solid arrows represent the metabolic process, and the dashed arrows leading to glycolysis represent the processes in which some metabolites are ignored; metabolites eventually end up in glycolysis. **(B)** Relative abundance of metabolites of the ko00380 pathway in different DI tissues. The abscissa represents the peak area unit of the metabolite, and the ordinate represents different metabolites. Different colors in the stack diagram indicate different tissues shown in the legend in the upper right corner.

(Figure 10E, $p = 0.02$). Further, we classified the association between these 50 DEGs and 13 metabolites based on Pearson's correlation analysis. as shown in Figure 10F; Supplementary Table S8; 30 DEGs were significantly associated with four metabolites, including 2-(formylamino)benzoic, indole-3-acetic acid (IAA), uinolinic acid, and 2-amino-3-methoxybenzoic acid, of the tryptophan metabolism pathway. NR database-based annotation showed that most DEGs were homologous to the hypothesized proteins of *Clathrus columnatus*,

10.3389/fmicb.2023.1137159

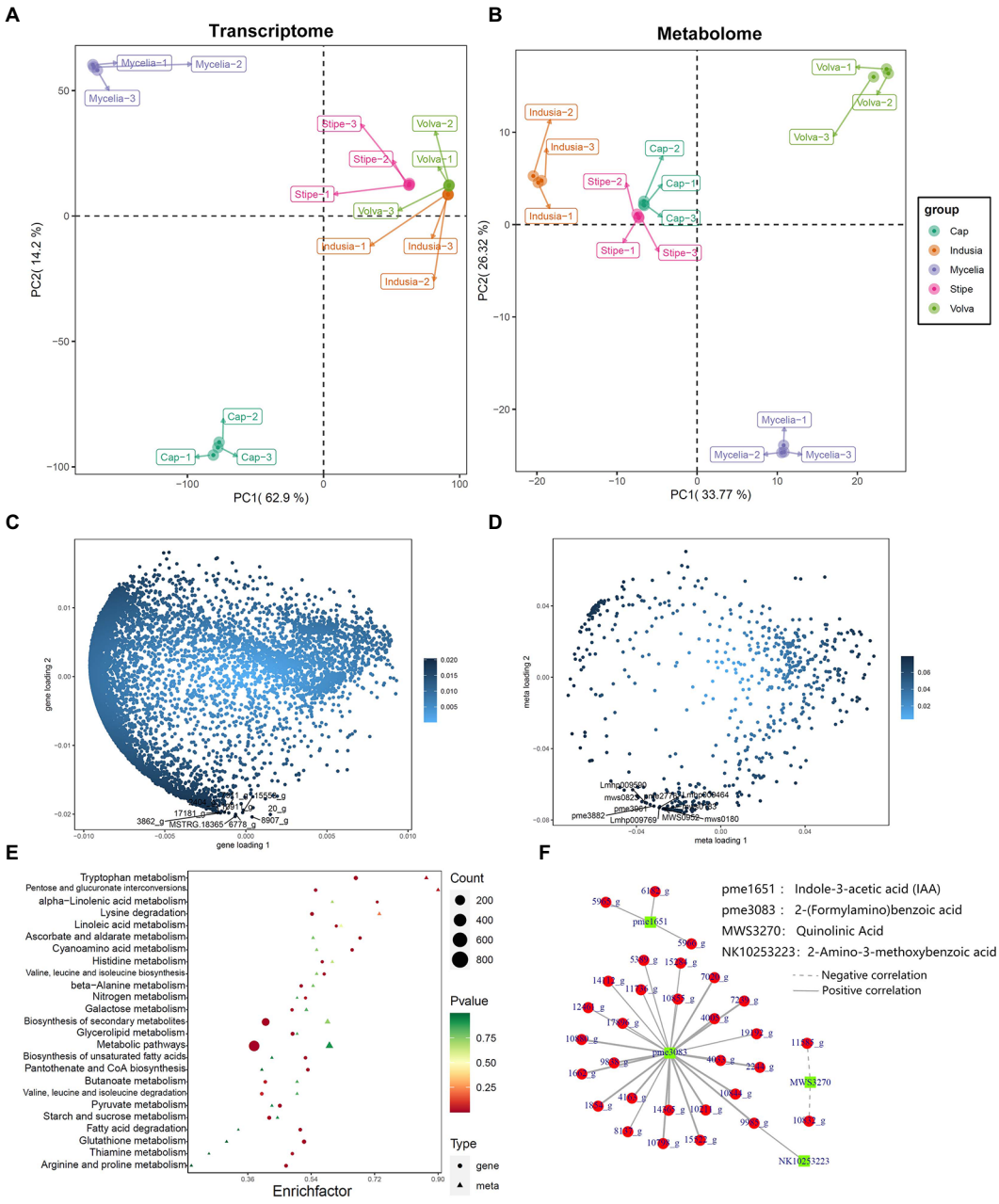

FIGURE 10
Correlation between metabolome and transcriptome of DI. **(A,B)** Metabolome and transcriptome PCA analysis. The abscissa represents PC1, and the ordinate represents PC2. **(C,D)** Metabolome and transcriptome O2PLS analysis. The abscissa represents the one-dimensional gene **(C)**/metabolite **(D)** loading value, and the ordinate represents the two-dimensional gene **(C)**/metabolite **(D)** loading value. **(E)** KEGG pathway enrichment analysis of DEGs and differential metabolites between cap and mycelia. The abscissa represents the corresponding enrichment factor of each pathway, and the ordinate represents the pathway name (sorted by value of *p*). The color of the dots and the triangles reflects the value of *p* of the genes and corresponding metabolites; the redder the dots/triangle, the more significant the enrichment. The size of the dot/triangle represents the number of differential genes and metabolites. Figure legend is shown on the right side. **(F)** Pearson correlation network between DEGs and metabolites. Red represents DEGs, and the green represents metabolites.

indicating that their gene functions have not been verified. In addition, among DEGs annotated as non-hypothetical proteins, we found that 11736_g (amidase signature do-main-containing protein), 14112_g (aldehyde dehydrogenase domain-containing protein), 14365_g (pyridoxal phosphate-dependent transferase), 17896_g (amidase signature domain-containing protein), 1854_g (pyridoxal phosphate-dependent transferase), 5389_g (FAD-binding domain-containing protein), and 7020_g (L-tyrosine:2-oxoglutarate aminotransferase) may be related to the synthesis of 2-(Formylamino)benzoic acid, and 5965_g (aldehyde dehydrogenase) may be associated with the synthesis of IAA.

2.4.3. Quantitative polymerase chain reaction validation

Finally, quantitative polymerase chain reaction (qPCR) (Figure 11) was performed for the five selected genes to verify the accuracy of the results of the combined multi-omics analysis presented in Figure 10.

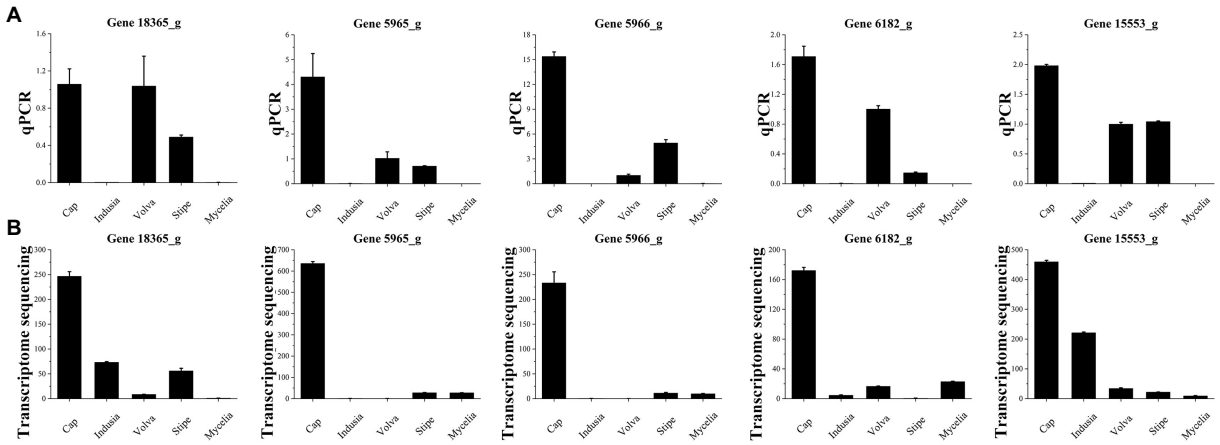

FIGURE 11
qPCR validation of five genes of five DI tissues identified from transcriptome sequencing. **(A)** Transcriptome sequencing results of the five genes in five DI tissues. The abscissa represents the tissues, and the ordinate represents FPKM expression levels. **(B)** qPCR analysis of the five genes in five DI tissues. The abscissa represents the tissues, and the ordinate represents the $2^{-\Delta\Delta Ct}$ values.

Among the five genes, three (5965_g, 5966_g, and 6182_g) were related to IAA synthesis (Figure 10F; Supplementary Table S8) and two (MSTRG.18365 and 15553_g) were identified based on O2PLS analysis (Figure 10C). We found that four out of the five genes (except for MSTRG.18365) showed an expression trend in qPCR consistent with the transcriptome data, with higher expression in the cap than the other four tissues. These observations indicate that our transcriptome data are reliable.

3. Discussion

DI is a delicious edible fungus widely cultivated artificially in east Asia. However, due to the lack of understanding of the molecular mechanisms underlying fruiting body formation, its cultivation and breeding are limited. Moreover, in many regions, such as south China, all DI fruiting bodies are discarded during harvest except the stipe, leading to largescale waste of resources. Therefore, the present study investigated the molecular background and metabolic process of DI fruiting body differentiation.

3.1. Genome of DI

Initially, we combined third-generation sequencing with high-throughput sequencing and assembled the DI reference genome, which could be used to understand the molecular details of DI. However, due to dualnucleated strain sequencing, the assembly was not ideal (N50 < 1 Mb). In contrast, recent studies that used similar sequencing strategies for mononuclear edible strains, such as *Leucocalocybe mongolica* (Duan et al., 2021), *Hericium erinaceus* (Gong et al., 2020), *Auricularia heimuer* (Yuan et al., 2019), and *Cordyceps guangdongensis* (Zhang et al., 2018), published genomes with N50 values above 1 Mb. Meanwhile, our assembly results are similar to the genome generated for *Russula griseocarnosa* (Yu et al., 2020) and *Agrocybe cylindracea* (Liang et al., 2020) based on third-generation sequencing and from dikaryotic mycelium or fruiting body (N50 < 1 Mb). Therefore, the present study still provides a reference genome of DI to assemble high quality genomes and data for understanding the developmental details. These observations suggest mononuclear diploid sequencing to obtain a more accurate reference genome. Taken together, the current genome is still a rough draft that needs to be strengthened. Therefore, we plan to further improve the assembly quality and gene annotation level of DI genomes by mononuclear sequencing in the future.

We further predicted 19,909 genes from the DI genome. Due to the largescale diversity in fungal species, our results of predicted genes did not match well with the public databases. Only a small fraction of predicted genes (39.63%) was annotated based on the GO database, consistent with the low annotation rate reported for other edible fungi, such as *Leucocalocybe mongolica* (65.98%) (Duan et al., 2021) and *Russula griseocarnosa* (22.63%) (Yu et al., 2020). These observations indicate space for future research on edible fungi, including DI. Further detailed analysis based on FCPD and antiSMASH annotations showed that 369 genes belonged to the P450 family and 64 belonged to the secondary metabolism gene cluster related to synthesizing secondary metabolites. These secondary metabolites, including the terpenes, have high medicinal value (Muszyńska et al., 2018), indicating significant potential for their application. Moreover, the genes associated with secondary metabolites have been annotated in the genomes of other edible fungi, including *Russula griseocarnosa* (Yu et al., 2020) and *Auricularia heimuer* (Yuan et al., 2019). Therefore, our study provides insights into the potential ability of DI to synthesize terpenes and a genetic basis for the biosynthesis of medicinal compounds.

3.2. Transcriptome sequencing reveals cap as critical tissues for DI fruiting body differentiation

In DI transcriptome studies, selecting an appropriate tissue representing the fruiting body is often challenging as the structure of the DI fruiting body is complex. Therefore, in this study, we divided DI into four tissue types. Moreover, our transcriptome study (section 3.2) proved that DEGs varied greatly among the different tissue types and identified a representative tissue, Cap, for DI fruiting body studies.

Our study found that the expression intensity of the DEGs in the comparison groups associated with cap or mycelia were significantly higher than the other tissues (Figure 3A), and these groups had significantly more common DEGs than the other groups (Figure 3B); the comparison groups associated with cap or mycelia has a significant number of DEGs (Figure 3D). The GO and KEGG enrichment analysis of DEGs between different tissue types showed the same functional DEG distribution trend (Figure 4; Supplementary Figure S1), confirming cap as the primary gene-expressing tissue during DI fruiting body formation. Earlier, Wang et al. (2020) identified 1954 unigenes across the developmental stages of DI *via* a *de novo* transcriptome study using peach-shaped and mature fruiting bodies. Meanwhile, we found far more DEGs in the cap of the DI fruiting body. Thus, the present study suggests that the cap is a tissue type that represents the expression pattern of DI fruiting bodies and plays a vital role in fruiting body differentiation.

3.3. Metabolome reveals novel resource value of DI tissues

The fruiting body of DI has a complex structure. Presently, the edible part of DI is the stipe, and the other four tissues are discarded. Therefore, we assessed the resource value of five DI tissues by analyzing the metabolite composition based on a widely-targeted metabolomic approach. We detected 729 metabolites from the five tissues, more than those (529) detected from the peach-shaped tissue of DI (Wang et al., 2021). In addition, we identified choline as the predominant metabolite in mycelia. Choline is essential for cell membranes' structural integrity and signaling functions (Zeisel, 2006; Wiedeman et al., 2018). Studies have also detected choline in other medicinal fungi, such as Morchella (Yang et al., 2021), *Poria cocos* (Sun, 2014), and *Sanghuangporus baumii* (Zheng et al., 2021); however, it is usually extracted from the fungal fruiting bodies, unlike mycelium in the present study. Thus, the present study's findings suggest that DI mycelium may be a potential raw material for extracting the medicinal ingredient after fermentation. We also found monosaccharides as the major metabolites in the primary edible tissue of DI, the stipe, suggesting presence of polysaccharides (Table 3). Polysaccharides are active components with antioxidant capacity and medicinal use (Liu et al., 2017). The present study also detected fungal polysaccharides as the main medicinal components of the edible fraction of DI, confirming the importance of DI stipe in exploiting fungal polysaccharides.

Additionally, we detected terpenoids in five tissue types of DI. Terpenoids are important medicinal components of higher fungi with promising economic value (Xiao and Zhong, 2016). Genome annotation based on the antiSMASH database identified 64 terpenoid synthesis related gene clusters (Supplementary Table S3), and metabolome analysis identified 12 kinds of terpenoids. Terpenoid biosynthetic genes and corresponding metabolites identified in the present study provide a reference for developing terpenoids from DI. Interestingly, we found that Dendronobilin I-iso1, the major terpenoid of DI, was mainly distributed in the volva but not in the stipe, the main edible part of DI. The sesquiterpenoid dendronobilin, a medicinal ingredient usually extracted from the Dendrobium genus and found in the traditional Chinese herbal medicine "Shi Hu," has antitumor, antimutagenic, and immunomodulatory activities (Zhang et al., 2007; Meng et al., 2017). Therefore, our study suggests the development of terpenoid components from DI volva, previously considered agricultural waste. Taken together, the present study proposes a novel value of DI and promotes the development of mycelia and volva as resources for medicinal use.

3.4. Tryptophan metabolism in regulating DI fruiting body differentiation

Understanding the factors controlling fruiting body formation helps improve the quality and yield of DI through manual intervention. The transcriptome study revealed that mycelia and cap are the key parts affecting DI fruiting body differentiation (Figure 3). Further comparative metabolome analysis (mycelia vs. cap) revealed the importance of tryptophan metabolism in regulating DI fruiting body differentiation (Figure 7). Earlier, Yan et al. found that in *Lentinula edodes*, tryptophan metabolism affects fruiting body development (Yan et al., 2021), while Kück et al. reported that disrupting the signaling of amino acids, including tryptophan, delayed *Sordaria macrospora* fruiting body development (Kück, 2005). Our study also found that glycolytic metabolism occurs post tryptophan metabolism in DI (Figure 9). Thus, we infer that tryptophan metabolism may help extract energy from the vegetative mycelia during fruiting body formation, and this hypothesis is worth testing in the future. Moreover, we found specific enrichment of IAA in the cap during DI tryptophan metabolism. The plant growth hormone IAA is classified as an indole derivative of the auxin family (Nutaratat et al., 2016). It is one of the metabolites produced by rhizobia to promote plant growth (Sun et al., 2018). Therefore, our study suggests that the cap of DI, so far used as agricultural waste, has the potential to be developed into fertilizer to promote plant growth, and this requires detailed investigation.

3.5. Metabolite synthesis related genes affect DI fruiting body differentiation

Multi-omics study revealed that the distribution of metabolites in DI tissues was not consistent with the trend observed in gene expression (Figures 10A,B), probably because gene expression is a phased event, while metabolites have the property of accumulation. However, we identified through O2PLS analysis that the top 10 metabolites and DEGs with the most significant influence correlated with each other (Figures 10C,D; Supplementary Tables S6, S7). However, little is known about the function of these metabolites and genes; therefore, we hope to elucidate their relationship with DI fruiting body differentiation in future studies. In addition, we found that four metabolites of the tryptophan metabolic pathway, including IAA, were associated with DEGs identified by transcriptome sequencing, which indicates novel ways to regulate IAA synthesis. We identified three novel genes (Figure 10F; 5965_g, 5966_g, and 6182_g) related to IAA synthesis. The genes 5966_g and 6182_g were annotated as hypothetical proteins in the NR database, indicating a novel pathway to regulate endogenous IAA synthesis in plants; however, this needs to be investigated using model crops, such as Arabidopsis. Meanwhile, the gene 5966_g is associated with aldehyde dehydrogenase. A previous study reported that an aldehyde dehydrogenase from the bacterial plant pathogen Pseudomonas syringae produces IAA (Koren et al., 2017), which also suggests the significance of our finding. These genes may be valuable resources for improving plant growth.

4. Materials and methods

4.1. Materials

The DI variety Gutian-1 obtained from the Guangxi Academy of Agricultural Sciences, Nanning City (Guangxi, China), was used in this study. The material used for *de novo* genome sequencing was derived from a binucleated mycelial strain of fruiting body of Gutian-1, named ZS. Materials of five tissue types (Figure 1A) used for transcriptome and metabolome analyses (Figure 1B) were obtained from the production site of Guangxi Dan Gui Xian Agricultural Technology Co. Ltd., Guilin City (Guangxi, China). All materials were frozen in liquid nitrogen immediately after sampling and stored in a freezer at-80°C since Aug. 2021.

4.2. Methods

As shown in Figure 1C, we performed *de novo* sequencing of the DI genome. Then, we performed transcriptome and metabolome analyses using the five DI tissues. Finally, based on the multi-omics approach, we elucidated the molecular mechanism of DI fruiting body differentiation and the metabolites of importance in the different tissues.

4.2.1. *De novo* genome sequencing

Genomic DNA was extracted from 0.1 g of ZS fresh mycelium using MabioFungal DNA Extraction Mini Kit B (Guangzhou, China), following the manufacturer's instructions. The next-generation sequencing (NGS) libraries were generated from the extracted genomic DNA using NEB Next® Ultra™ DNA Library Prep Kit for Illumina® (NewEngland Biolabs, USA), following the manufacturer's recommendations, and sequenced on a Novaseq6000 platform to obtain 150 bp paired-end reads. Meanwhile, genomic DNA was fragmented with g-TUBES (Covaris, USA) and end-repaired to prepare fragments with size >20 Kb. These DNA fragments were enriched by BluePippin size selection (Sage Science, USA), and the sequencing libraries were prepared using the SQK-LSK109 Sequencing Kit (Oxford Nanopore Technologies, Oxford Science Park, OX4 4DQ, UK), following the manufacturer's protocol. Finally, the libraries were sequenced on a Nanopore MinION platform at the Guangdong Magigene Biotechnology Co., Ltd. (China).

The Illumina raw data and Nanopore raw data were filtered by fastp (v0.21) (Chen et al., 2018) and quast (Gurevich et al., 2013), respectively, using default parameters. The filtered reads were assembled to generate contigs without gaps using Canu (v1.8) (Koren et al., 2017). The hierarchical genome assembly process (HGAP) pipeline was used to correct for random errors in the long seed reads (seed length threshold 6 Kb) by aligning shorter reads from the same library against them with Pilon (v1.23) (Walker et al., 2014). Then, we used SSPACE (v1.1) (Boetzer et al., 2011) with preassembled reads for the final *de novo* assembly. GeneMark-ES (v4.69) (Lomsadze et al., 2014) and Augustus (v2.7) (Stanke et al., 2008) were used to retrieve the related coding genes in the DI genome. BUSCO (v5.4.3) analysis was used to assess the genome integrity (Manni et al., 2021).

We then used both software and merged result from GeneMark-ES and Augustus to obtain the final list of coding genes. Then, the gene functional annotation was carried out using GO (Gene Ontology; (Gene Ontology Consortium, 2021), KEGG (Kyoto Encyclopedia of Genes and Genomes) (Kanehisa and Goto, 2000), and KOG (Eukaryotic Orthologous Groups) (Tatusov et al., 2003). Meanwhile, the secondary metabolism-associated gene clusters were identified using antiSMASH[1] (Blin et al., 2021) with the default parameters, and FCPD[2] (Park et al., 2008) with the parameters of e-value <1e-10 and identity >40%. The Carbohydrate-Active enzymes (CAZymes) were predicted for the genome using dbCAN (Yin et al., 2012), with an e-value ≤1e-5.

4.2.2. Transcriptome sequencing

Total RNA was extracted from 0.1 g of fresh DI tissues (stipe, cap, indusium, volva, and mycelium) using TRIzol reagent (Invitrogen, Carlsbad, CA, USA) according to the manufacturer's protocol and sequenced on an Illumina Novaseq6000 system at the Gene Denovo Biotechnology Co. Ltd. (Guangzhou, China).

The raw reads were filtered to obtain high-quality reads using fastp (v0.18.0), which removed reads containing adapters, more than 10% unknown nucleotides (N), and more than 50% low-quality bases (Q-value ≤20) (Chen et al., 2018). These filtered reads were then aligned to the reference genome generated in this study. An index of the reference genome was built, and paired-end clean reads were mapped to the reference genome using HISAT (v2.2.4) (Kim et al., 2015) with "-rna-strandness RF" and other default parameters. The mapped reads of each sample were assembled using StringTie (v1.3.1) (Pertea et al., 2015, 2016). An FPKM (fragment per kilobase of transcript per million mapped reads) value was calculated for each transcription region to quantify the expression of genes and variations among different comparison groups using RSEM (v1.3.3) (Li and Dewey, 2011). Finally, DESeq2 (v1.36) (Love et al., 2014) was used to analyze the differential expression of genes between two groups and(Li et al., 2021) between two samples. The genes with a false discovery rate (FDR) <0.05 and an absolute fold change ≥2 were identified as the differentially expressed genes (DEGs). Venn analysis was performed to compare the DEGs between the different comparison groups using the VennDiagram package (v1.6.16) in R (Chen and Boutros, 2011).

Further, GO (Gene Ontology Consortium, 2021) and KEGG (Kanehisa and Goto, 2000) enrichment analyses were performed for the DEGs. The DEGs associated with specific GO terms and KEGG pathways compared to the genome background were filtered using the FDR ≤ 0.05 threshold. Finally, the Pearson's correlation between DEGs of each tissue type was analyzed using the OmicShare tools[3] to assess the reliability of the experimental results and the operational stability. A correlation coefficient closer to 1 indicates better repeatability between two experiments. Meanwhile, the correlation coefficient between two replicas was calculated to evaluate the repeatability between samples.

4.2.3. Widely-targeted metabolome analysis

A widely-targeted metabolome analysis based on ultra-high-performance liquid chromatography-electrospray ionization-tandem mass spectrometry (UHPLC-ESI-MS/MS) was performed to identify the metabolites and their differences among the five tissues of DI at the Metware Biotechnology Co., Ltd. (Wuhan, China), as described earlier (Li et al., 2021). The DI different tissue samples were freeze-dried for 48 h and ground into powder. Approximately 100 mg of the powder was extracted with 70% aqueous methanol (0.6 ml), and the extract was analyzed on a UHPLC-ESI-MS/MS system (UHPLC, Shim-pack UFLC

1 antismash.secondarymetabolites.org
2 http://p450.riceblast.snu.ac.kr/index.php?a=view
3 https://www.omicshare.com/tools

SHIMADZU CBM30A system, Kyoto, Japan; MS, Applied Biosystems 4,500 Q TRAP, Framingham, MA, USA). Three biological replicates were maintained for each tissue. Meanwhile, all the sample extracts were mixed to prepare the quality control (QC) sample used to test the measurement accuracy after every six samples.

The qualitative analysis of the primary and secondary mass spectrometry data was performed using a self-built database MWDB (v2.0; Metware Biotechnology Co., Ltd. Wuhan, China) and the publicly available databases, such as MassBank[4], HMDB (Human Metabolome Database[5]), and METLIN[6]. Meanwhile, the quantitative analysis of the metabolites was performed using the multiple reaction monitoring mode (MRM) of triple quadrupole mass spectrometry. MultiQuant (v3.0.2) was used to access the mass spectrometry files and to integrate and correct the peaks. The area of each chromatographic peak represented the relative content of the metabolite; the mass spectra were integrated and corrected to determine the content of each metabolite in the different samples. Further, the levels of each metabolite in the various samples were compared based on the retention time and peak pattern.

The raw data were processed using the Analyst 1.6.3 software (AB Sciex, Framingham, MA, USA). The original abundance of the metabolites was log-transformed to normalize the data and decrease the variance. Principal component analysis (PCA), cluster analysis, and orthogonal projections to latent structures-discriminant analysis (OPLS-DA) were conducted for the metabolite data in R[7], following the previously described methods (Li et al., 2021). Variable importance in projection (VIP) values of all metabolites from the OPLS-DA were extracted using the first component. Finally, the differential metabolites among the pairwise comparisons of different DI tissue types (such as mycelia vs. cap) were screened based on the following criteria: (i) VIP ≥ 1 (high confidence in pairwise comparisons); (ii) a fold change ≥ 2 and ≤ 0.5. Further, KEGG annotation and metabolic pathway analysis were performed for the differential metabolites. A hypergeometric test was used to identify the significantly enriched pathways ($p < 0.05$).

4.2.4. Multi-omics analysis

Unsupervised principal component analysis (PCA) of transcriptome and metabolome data was performed using the statistics function prcomp within R[8] after scaling the data. Two-way orthogonal partial least square (O2PLS) analysis was also performed to screen the genes and metabolites with a strong influence on DI tissue differentiation with R (OmicsPLS v1.2.0) (Bouhaddani et al., 2018). Further, the correlation between the transcriptome and metabolome data was analyzed by calculating the Pearson correlation coefficient in R (v4.7, base package), and the correlation network of genes and metabolites was built in R (igraph v1.3.4[9]).

4.2.5. Quantitative polymerase chain reaction

Total RNA was extracted from five DI tissue types using TRIzol reagent (Section 2.2.2) and reverse transcribed (2 μg of RNA with an OD260/OD280 of 1.9–2.0) into cDNA using the iScript cDNA Synthesis Kit (Bio-Rad). Real-time quantitative PCR to validate the expression of five genes in the transcriptome data was performed with SYBR Green Master Mix (Thermo Fisher Scientific, MA, United States) on a QuantStudio™ Flex Real-Time PCR System, maintaining three technical repeats per sample. The housekeeping gene (reference genes) 5711_t was used to normalize mRNA expression levels, and the fold change in expression levels was defined using the $2^{-\Delta\Delta Ct}$ equation. The melting curve for each gene was generated to validate the specificity of the amplicon. The qPCR primers were designed using Primer Premier 5 and are listed in Supplementary Table S9.

5. Conclusion

The present study reveals the DI reference genome for further functional research. Transcriptome and metabolome analyses of the four tissues of the DI fruiting bodies and mycelium revealed the mechanism underlying DI fruiting body differentiation. However, future studies should aim to generate high-quality genomes by mononuclear sequencing. Our analysis also detected new metabolites from the mycelium (choline) and volva (dendronobilin) that expand the economic, medicinal, and agricultural values of DI. Additionally, unraveling the significance of tryptophan metabolism and novel genes related to IAA synthesis in regulating fruiting body formation proposes candidates for manipulating DI. The study thus raises new scientific questions on the developmental use of DI.

Data availability statement

The datasets presented in this study can be found in online repositories. The names of the repository/repositories and accession number(s) can be found at: https://www.ncbi.nlm.nih.gov/, PRJNA877048 and JAQFWX000000000.1.

Author contributions

MD, ZW, ZC, and LW contributed to conception and design of the study. MD, SL, XW, BF, SQ, YL, XL, CL, CZ, YY, JW, and FZ performed investigation. MD and SL performed the statistical analysis. MD wrote the first draft of the manuscript. All authors contributed to the article and approved the submitted version.

Funding

This work was jointly funded by the National Natural Science Foundation of China (grant number NNSFC 32260715), Central Government Guides Local Funds for Science and Technology Development (grant number GuiKe ZY21195033), Guangxi Major Science and Technology Project (grant number GuiKe AA22117004), Guangxi Science and Technology Base and Special Talent (grant number GuiKe AD20297130), Science and Technology Pioneer Special of Guangxi Academy of Agricultural Sciences (grant number

4 http://www.massbank.jp
5 http://www.hmdb.ca
6 http://metlin.scripps.edu/index.php
7 http://www.r-project.org/
8 www.r-project.org
9 https://CRAN.R-project.org/package=igraph, access on 2022.08.18

GuiNongKeMeng 202203-1-2), and Team Project for Guangx Academy of Agriculture Sciences (grant number Guinongke 2021YT004).

Acknowledgments

We thank TopEdit (www.topeditsci.com) for linguistic assistance during the preparation of this manuscript.

Conflict of interest

The authors declare that the research was conducted in the absence of any commercial or financial relationships that could be construed as a potential conflict of interest.

Publisher's note

Supplementary material

The Supplementary Material for this article can be found online at: https://www.frontiersin.org/articles/10.3389/fmicb.2023.1137159/full#supplementary-material

References

Alberti, F., Kaleem, S., and Weaver, J. A. (2020). Recent developments of tools for genome and metabolome studies in basidiomycete fungi and their application to natural product research. *Biology Open* 9. doi: 10.1242/bio.056010

Blin, K., Shaw, S., Kloosterman, A. M., Charlop-Powers, Z., van Wezel, G. P., Medema, M. H., et al. (2021). antiSMASH 6.0: improving cluster detection and comparison capabilities. *Nucleic Acids Res.* 49, W29–w35. doi: 10.1093/nar/gkab335

Boetzer, M., Henkel, C. V., Jansen, H. J., Butler, D., and Pirovano, W. (2011). Scaffolding pre-assembled contigs using SSPACE. *Bioinformatics* 27, 578–579. doi: 10.1093/bioinformatics/btq683

Bouhaddani, S. E., Uh, H. W., Jongbloed, G., Hayward, C., Klarić, L., Kiełbasa, S. M., et al. (2018). Integrating omics datasets with the OmicsPLS package. *BMC Bioinformatics* 19:371. doi: 10.1186/s12859-018-2371-3

Buckley, M. (2008). *American Academy of microbiology colloquia reports, the fungal kingdom: Diverse and essential roles in earth's ecosystem*., American Society for Microbiology., Washington, DC

Chen, H., and Boutros, P. C. (2011). VennDiagram: a package for the generation of highly-customizable Venn and Euler diagrams in R. *BMC Bioinformatics* 12:35. doi: 10.1186/1471-2105-12-35

Chen, S., Zhou, Y., Chen, Y., and Gu, J. (2018). fastp: an ultra-fast all-in-one FASTQ preprocessor. *Bioinformatics* 34, i884–i890. doi: 10.1093/bioinformatics/bty560

Duan, M., Bao, H., and Bau, T. (2021). Analyses of transcriptomes and the first complete genome of *Leucocalocybe mongolica* provide new insights into phylogenetic relationships and conservation. *Sci. Rep.* 11:2930. doi: 10.1038/s41598-021-81784-6

Gene Ontology Consortium (2021). The gene ontology resource: enriching a GOld mine. *Nucleic Acids Res.* 49, D325–d334. doi: 10.1093/nar/gkaa1113

Gong, W., Wang, Y., Xie, C., Zhou, Y., Zhu, Z., and Peng, Y. (2020). Whole genome sequence of an edible and medicinal mushroom, *Hericium erinaceus* (Basidiomycota, fungi). *Genomics* 112, 2393–2399. doi: 10.1016/j.ygeno.2020.01.011

Gurevich, A., Saveliev, V., Vyahhi, N., and Tesler, G. (2013). QUAST: quality assessment tool for genome assemblies. *Bioinformatics* 29, 1072–1075. doi: 10.1093/bioinformatics/btt086

Hetland, G., Johnson, E., Lyberg, T., Bernardshaw, S., Tryggestad, A. M., and Grinde, B. (2008). Effects of the medicinal mushroom *Agaricus blazei* Murill on immunity, infection and cancer. *Scand. J. Immunol.* 68, 363–370. doi: 10.1111/j.1365-3083.2008.02156.x

Huang, M., Chen, X., Tian, H., Sun, B., and Chen, H. (2011). Isolation and identification of antibiotic albaflavenone from *Dictyophora indusiata* (vent: Pers.). *J. Chem. Res.* 35, 659–660. doi: 10.3184/174751911X13202334527264

Kanehisa, M., and Goto, S. (2000). KEGG: Kyoto encyclopedia of genes and genomes. *Nucleic Acids Res.* 28, 27–30. doi: 10.1093/nar/28.1.27

Kim, D., Langmead, B., and Salzberg, S. L. (2015). HISAT: a fast spliced aligner with low memory requirements. *Nat. Methods* 12, 357–360. doi: 10.1038/nmeth.3317

Koren, S., Walenz, B. P., Berlin, K., Miller, J. R., Bergman, N. H., and Phillippy, A. M. (2017). Canu: scalable and accurate long-read assembly via adaptive k-mer weighting and repeat separation. *Genome Res.* 27, 722–736. doi: 10.1101/gr.215087.116

Krakowska, A., Zięba, P., Włodarczyk, A., Kała, K., Sułkowska-Ziaja, K., Bernaś, E., et al. (2020). Selected edible medicinal mushrooms from *Pleurotus* genus as an answer for human civilization diseases. *Food Chem.* 327:127084. doi: 10.1016/j.foodchem.2020.127084

Kück, U. (2005). A *Sordaria macrospora* mutant lacking the leu1 gene shows a developmental arrest during fruiting body formation. *Mol. Gen. Genomics.* 274, 307–315. doi: 10.1007/s00438-005-0021-8

Li, B., and Dewey, C. N. (2011). RSEM: accurate transcript quantification from RNA-Seq data with or without a reference genome. *BMC Bioinformatics* 12:323. doi: 10.1186/1471-2105-12-323

Li, X., He, Y., Zeng, P., Liu, Y., Zhang, M., Hao, C., et al. (2019). Molecular basis for *Poria cocos* mushroom polysaccharide used as an antitumour drug in China. *J. Cell. Mol. Med.* 23, 4–20. doi: 10.1111/jcmm.13564

Li, W., Wen, L., Chen, Z., Zhang, Z., Pang, X., Deng, Z., et al. (2021). Study on metabolic variation in whole grains of four proso millet varieties reveals metabolites important for antioxidant properties and quality traits. *Food Chem.* 357:129791. doi: 10.1016/j.foodchem.2021.129791

Liang, Y., Lu, D., Wang, S., Zhao, Y., and Hu, S. (2020). Genome assembly and pathway analysis of edible mushroom agrocybe cylindracea. *Genom. Proteom. Bioinformat.* 18, 341–351. doi: 10.1016/j.gpb.2018.10.009

Liao, W., Luo, Z., Liu, D., Ning, Z., Yang, J., and Ren, J. (2015). Structure characterization of a novel polysaccharide from *Dictyophora indusiata* and its macrophage immunomodulatory activities. *J. Agric. Food Chem.* 63, 535–544. doi: 10.1021/jf504677r

Liu, X., Chen, Y., Wu, L., Wu, X., Huang, Y., and Liu, B. (2017). Optimization of polysaccharides extraction from *Dictyophora indusiata* and determination of its antioxidant activity. *Int. J. Biol. Macromol.* 103, 175–181. doi: 10.1016/j.ijbiomac.2017.04.125

Lomsadze, A., Burns, P. D., and Borodovsky, M. (2014). Integration of mapped RNA-Seq reads into automatic training of eukaryotic gene finding algorithm. *Nucleic Acids Res.* 42:e119. doi: 10.1093/nar/gku557

Love, M. I., Huber, W., and Anders, S. (2014). Moderated estimation of fold change and dispersion for RNA-seq data with DESeq2. *Genome Biol.* 15:550. doi: 10.1186/s13059-014-0550-8

Lu, H., Lou, H., Hu, J., Liu, Z., and Chen, Q. (2020). Macrofungi: a review of cultivation strategies, bioactivity, and application of mushrooms. *Compr. Rev. Food Sci. Food Saf.* 19, 2333–2356. doi: 10.1111/1541-4337.12602

Manni, M., Berkeley, M. R., Seppey, M., Simão, F. A., and Zdobnov, E. M. (2021). BUSCO update: novel and streamlined workflows along with broader and deeper phylogenetic coverage for scoring of eukaryotic, prokaryotic, and viral genomes. *Mol. Biol. Evol.* 38, 4647–4654. doi: 10.1093/molbev/msab199

Meng, C.-W., He, Y.-L., Peng, C., Ding, X.-J., Guo, L., and Xiong, L. (2017). Picrotoxane sesquiterpenoids from the stems of *Dendrobium nobile* and their absolute configurations and angiogenesis effect. *Fitoterapia* 121, 206–211. doi: 10.1016/j.fitote.2017.07.017

Muszyńska, B., Grzywacz-Kisielewska, A., Kała, K., and Gdula-Argasińska, J. (2018). Anti-inflammatory properties of edible mushrooms: a review. *Food Chem.* 243, 373–381. doi: 10.1016/j.foodchem.2017.09.149

Nutaratat, P., Srisuk, N., Arunrattiyakorn, P., and Limtong, S. (2016). Indole-3-acetic acid biosynthetic pathways in the basidiomycetous yeast *Rhodosporidium paludigenum*. *Arch. Microbiol.* 198, 429–437. doi: 10.1007/s00203-016-1202-z

Park, J., Lee, S., Choi, J., Ahn, K., Park, B., Park, J., et al. (2008). Fungal cytochrome P450 database. *BMC Genomics* 9:402. doi: 10.1186/1471-2164-9-402

Pertea, M., Kim, D., Pertea, G. M., Leek, J. T., and Salzberg, S. L. (2016). Transcript-level expression analysis of RNA-seq experiments with HISAT, StringTie and Ballgown. *Nat. Protoc.* 11, 1650–1667. doi: 10.1038/nprot.2016.095

Pertea, M., Pertea, G. M., Antonescu, C. M., Chang, T. C., Mendell, J. T., and Salzberg, S. L. (2015). StringTie enables improved reconstruction of a transcriptome from RNA-seq reads. *Nat. Biotechnol.* 33, 290–295. doi: 10.1038/nbt.3122

Stanke, M., Diekhans, M., Baertsch, R., and Haussler, D. (2008). Using native and syntenically mapped cDNA alignments to improve de novo gene finding. *Bioinformatics* 24, 637–644. doi: 10.1093/bioinformatics/btn013

Sun, Y. (2014). Biological activities and potential health benefits of polysaccharides from *Poria cocos* and their derivatives. *Int. J. Biol. Macromol.* 68, 131–134. doi: 10.1016/j.ijbiomac.2014.04.010

Sun, S. L., Yang, W. L., Fang, W. W., Zhao, Y. X., Guo, L., and Dai, Y. J. (2018). The plant growth-promoting rhizobacterium *Variovorax boronicumulans* CGMCC 4969 regulates the level of Indole-3-acetic acid synthesized from Indole-3-acetonitrile. *Appl. Environ. Microbiol.* 84:e00298–18. doi: 10.1128/AEM.00298-18

Tatusov, R. L., Fedorova, N. D., Jackson, J. D., Jacobs, A. R., Kiryutin, B., Koonin, E. V., et al. (2003). The COG database: an updated version includes eukaryotes. *BMC Bioinformatics* 4:41. doi: 10.1186/1471-2105-4-41

Walker, B. J., Abeel, T., Shea, T., Priest, M., Abouelliel, A., Sakthikumar, S., et al. (2014). Pilon: an integrated tool for comprehensive microbial variant detection and genome assembly improvement. *PLoS One* 9:e112963. doi: 10.1371/journal.pone.0112963

Wang, Y., Lai, L., Teng, L., Li, Y., Cheng, J., Chen, J., et al. (2019). Mechanism of the anti-inflammatory activity by a polysaccharide from *Dictyophora indusiata* in lipopolysaccharide-stimulated macrophages. *Int. J. Biol. Macromol.* 126, 1158–1166. doi: 10.1016/j.ijbiomac.2019.01.022

Wang, W., Liu, H., Zhang, Y., Feng, Y., Yuan, F., Song, X., et al. (2019). Antihyperlipidemic and hepatoprotective properties of alkali-and enzyme-extractable polysaccharides by *Dictyophora indusiata*. *Sci. Rep.* 9:14266. doi: 10.1038/s41598-019-50717-9

Wang, X., Peng, J., Sun, L., Bonito, G., Wang, J., Cui, W., et al. (2019). Genome sequencing illustrates the genetic basis of the pharmacological properties of *Gloeostereum incarnatum*. *Genes* 10:188. doi: 10.3390/genes10030188

Wang, J., Wen, X., Yang, B., Liu, D., Li, X., and Geng, F. (2020). De novo transcriptome and proteome analysis of *Dictyophora indusiata* fruiting bodies provides insights into the changes during morphological development. *Int. J. Biol. Macromol.* 146, 875–886. doi: 10.1016/j.ijbiomac.2019.09.210

Wang, J., Wen, X., Zhang, Y., Zou, P., Cheng, L., Gan, R., et al. (2021). Quantitative proteomic and metabolomic analysis of *Dictyophora indusiata* fruiting bodies during post-harvest morphological development. *Food Chem.* 339:127884. doi: 10.1016/j.foodchem.2020.127884

Wiedeman, A. M., Barr, S. I., Green, T. J., Xu, Z., Innis, S. M., and Kitts, D. D. (2018). Dietary choline intake: current state of knowledge across the life cycle. *Nutrients* 10:1513. doi: 10.3390/nu10101513

Xiao, H., and Zhong, J. J. (2016). Production of useful Terpenoids by higher-fungus cell factory and synthetic biology approaches. *Trends Biotechnol.* 34, 242–255. doi: 10.1016/j.tibtech.2015.12.007

Yan, D., Gao, Q., Rong, C., Liu, Y., Song, S., Yu, Q., et al. (2021). Comparative transcriptome analysis of abnormal cap and healthy fruiting bodies of the edible mushroom *Lentinula edodes*. *Fungal Genet. Biol.* 156:103614. doi: 10.1016/j.fgb.2021.103614

Yang, Y., Yang, J., Wang, H., Jin, Y., Liu, J., Jia, R., et al. (2021). Analysis of primary metabolites of *Morchella* fruit bodies and mycelium based on widely targeted metabolomics. *Arch. Microbiol.* 204:98. doi: 10.1007/s00203-021-02612-z

Yin, Y., Mao, X., Yang, J., Chen, X., Mao, F., and Xu, Y. (2012). dbCAN: a web resource for automated carbohydrate-active enzyme annotation. *Nucleic Acids Res.* 40, W445–W451. doi: 10.1093/nar/gks479

Yoo, S. I., Lee, H. Y., Markkandan, K., Moon, S., Ahn, Y. J., Ji, S., et al. (2019). Comparative transcriptome analysis identified candidate genes involved in mycelium browning in Lentinula edodes. *BMC Genomics* 20:121. doi: 10.1186/s12864-019-5509-4

Yu, F., Song, J., Liang, J., Wang, S., and Lu, J. (2020). Whole genome sequencing and genome annotation of the wild edible mushroom, *Russula griseocarnosa*. *Genomics* 112, 603–614. doi: 10.1016/j.ygeno.2019.04.012

Yuan, Y., Wu, F., Si, J., Zhao, Y.-F., and Dai, Y.-C. (2019). Whole genome sequence of *Auricularia heimuer* (Basidiomycota, Fungi), the third most important cultivated mushroom worldwide. *Genomics* 111, 50–58. doi: 10.1016/j.ygeno.2017.12.013

Zeisel, S. H. (2006). Choline: critical role during fetal development and dietary requirements in adults. *Annu. Rev. Nutr.* 26, 229–250. doi: 10.1146/annurev.nutr.26.061505.111156

Zhang, C., Deng, W., Yan, W., and Li, T. (2018). Whole genome sequence of an edible and potential medicinal fungus, cordyceps guangdongensis. *G3* 8, 1863–1870. doi: 10.1534/g3.118.200287

Zhang, X., Liu, H.-W., Gao, H., Han, H.-Y., Wang, N.-L., Wu, H.-M., et al. (2007). Nine new sesquiterpenes from *Dendrobium nobile*. *Helv. Chim. Acta* 90, 2386–2394. doi: 10.1002/hlca.200790245

Zheng, N., Ming, Y., Chu, J., Yang, S., Wu, G., Li, W., et al. (2021). Optimization of extraction process and the antioxidant activity of phenolics from *Sanghuangporus baumii*. *Molecules* 26:3850. doi: 10.3390/molecules26133850

frontiers | Frontiers in Microbiology

TYPE Original Research
PUBLISHED 27 February 2023
DOI 10.3389/fmicb.2023.1138830

OPEN ACCESS

EDITED BY
Dewu Zhang,
Chinese Academy of Medical Sciences,
China

REVIEWED BY
Gang Li,
Qingdao University,
China
Li Li,
Fujian Normal University,
China

*CORRESPONDENCE
Kui Hong
✉ kuihong31@whu.edu.cn
Hongkai Bi
✉ hkbi@njmu.edu.cn
You-Sheng Cai
✉ cysh2002@whu.edu.cn

†These authors have contributed equally to this work

SPECIALTY SECTION
This article was submitted to Microbial Physiology and Metabolism, a section of the journal Frontiers in Microbiology

RECEIVED 06 January 2023
ACCEPTED 07 February 2023
PUBLISHED 27 February 2023

CITATION
Wu J, Shui H, Zhang M, Zeng Y, Zheng M, Zhu K-K, Wang S-B, Bi H, Hong K and Cai Y-S (2023) Aculeaxanthones A–E, new xanthones from the marine-derived fungus *Aspergillus aculeatinus* WHUF0198.
Front. Microbiol. 14:1138830.
doi: 10.3389/fmicb.2023.1138830

Aculeaxanthones A–E, new xanthones from the marine-derived fungus *Aspergillus aculeatinus* WHUF0198

Jun Wu[1,2†], Hua Shui[1†], Mengke Zhang[3], Yida Zeng[2], Mingxin Zheng[4], Kong-Kai Zhu[5], Shou-Bao Wang[6], Hongkai Bi[4*], Kui Hong[2*] and You-Sheng Cai[1,2*]

[1]Department of Nephrology, Zhongnan Hospital of Wuhan University, School of Pharmaceutical Sciences, Wuhan University, Wuhan, China, [2]Key Laboratory of Combinatorial Biosynthesis and Drug Discovery, Ministry of Education and School of Pharmaceutical Sciences, Wuhan University, Wuhan, China, [3]Department of Pharmacy, Renmin Hospital of Wuhan University, Wuhan, China, [4]Department of Pathogen Biology & Jiangsu Key Laboratory of Pathogen Biology & Helicobacter pylori Research Centre, Nanjing Medical University, Nanjing, China, [5]Advanced Medical Research Institute, Shandong University, Jinan, Shandong, China, [6]Beijing Key Laboratory of Drug Targets Identification and Drug Screening, Institute of Materia Medica, Chinese Academy of Medical Sciences and Peking Union Medical College, Beijing, China

Introdduction: Dimeric natural products are widespread in plants and microorganisms, which usually have complex structures and exhibit greater bioactivities than their corresponding monomers. In this study, we report five new dimeric tetrahydroxanthones, aculeaxanthones A–E (**4–8**), along with the homodimeric tetrahydroxanthone secalonic acid D (**1**), chrysoxanthones B and C (**2** and **3**), and 4–4′-secalonic acid D (**9**), from different fermentation batches of the title fungus.

Methods: A part of the culture was added to a total of 60 flasks containing 300 ml each of number II fungus liquid medium and culture 4 weeks in a static state at 28°C. The liquid phase (18 L) and mycelia was separated from the fungal culture by filtering. A crude extract was obtained from the mycelia by ultrasound using acetone. To obtain a dry extract (18 g), the liquid phase combined with the crude extract were further extracted by EtOAc and concentrated in vacuo. The MIC of anaerobic bacteria was examined by a broth microdilution assay. To obtain MICs for aerobic bacteria, the agar dilution streak method recommended in Clinical and Laboratory Standards Institute document (CLSI) M07-A10 was used. Compounds 1–9 was tested against the Bel-7402, A-549 and HCT-116 cell lines according to MTT assay.

Results and Discussion: The structures of these compounds were elucidated on the base of 1D and 2D NMR and HR-ESIMS data, and the absolute configurations of the new xanthones **4–8** were determined by conformational analysis and time-dependent density functional theory-electronic circular dichroism (TDDFT-ECD) calculations. Compounds 1–9 were tested for cytotoxicity against the Bel-7402, A549, and HCT-116 cancer cell lines. Of the dimeric tetrahydroxanthone derivatives, only compound 6 provided cytotoxicity effect against Bel-7402 cell line (IC50, 1.96 μM). Additionally, antimicrobial activity was evaluated for all dimeric tetrahydroxanthones, including four Gram-positive bacteria including Enterococcus faecium ATCC 19434, *Bacillus subtilis* 168, *Staphylococcus aureus* ATCC 25923 and MRSA USA300; four Gram-negative bacteria, including *Helicobacter pylori* 129, G27, as well as 26,695, and multi drug-resistant strain *H. pylori* 159, and one *Mycobacterium M. smegmatis* ATCC 607. However, only compound 1 performed activities against *H. pylori* G27, *H. pylori* 26695, *H. pylori*

129, *H. pylori* 159, *S. aureus* USA300, and *B. subtilis* 168 with MIC values of 4.0, 4.0, 2.0, 2.0, 2.0 and 1.0 μg/mL, respectively.

KEYWORDS

***Aspergillus aculeatinus*, dimeric tetrahydroxanthones, marine natural products, antimicrobial activity, cytotoxic activity**

Introduction

Dimeric natural products are widespread in plants and microorganisms, which usually have complex structures and exhibit greater bioactivities than their corresponding monomers (Wezeman et al., 2015; Cai et al., 2018; Lombe et al., 2019). In fungi and lichens, dimeric tetrahydroxanthones (synonyms ergochromes, ergopigments, ergoflavins, ergochrysins, secalonic acids) are important polyketides with diverse structures (Franck, 1969, 1980; Rezanka and Sigler, 2007; Deshmukh et al., 2009). The dimeric tetrahydroxanthones are usually classified as heterodimer and homodimer, with 2–2′, 2–4′, or 4–4′ linkage according to the structural differences of two monomers (Wezeman et al., 2015). The homodimers are composed of the same two chromanone lactone subunits (a γ-lactone moiety linked to a dihydrobenzopyranone) or two tetrahydroxanthone monomers, while the heterodimers consist of two different tetrahydroxanthone monomers and/or chromanone monomers or their derivatives (Zhang et al., 2008; El-Elimat et al., 2015). Due to their interesting chemical properties and a broad spectrum of bioactivities, for instance, antimicrobial, antiviral, anti-inflammatory, and antiparasitic activities as well as cytotoxicity (Cai et al., 2014; Wu et al., 2015; Luenne et al., 2021; Sadorn et al., 2021; Cao et al., 2022; Phang et al., 2022), dimeric tetrahydroxanthones have been extensively studied in chemical and pharmacological fields (Masters and Brase, 2012; Roensberg et al., 2013; Qin et al., 2015a; Qin and Porco, 2015; Xiao et al., 2017; Lv et al., 2021).

In the process of our ongoing screening for new biologically active natural products from marine-derived fungi, we discovered that the fungus *Aspergillus aculeatinus* WHUF0198 contained an assortment of chemically diverse metabolites revealed by LC-ESIMS (UV–vis) profiles, and displayed potent antibacterial and antitumor properties during our preliminary screening of bioassays. We previously reported one new norditerpene, one new indone, and one paraherquamide alkaloid, along with 13 known compounds from the culture of this fungus (Wu et al., 2021, 2022). In this study, we report five new dimeric tetrahydroxanthones, aculeaxanthones A–E (**4**–**8**), along with the homodimeric tetrahydroxanthone secalonic acid D (**1**), chrysoxanthones B and C (**2** and **3**), and 4–4′-secalonic acid D (**9**), from different fermentation batches of the title fungus. In contrast to the reported dimeric tetrahydroxanthones, compounds **4**–**8** have many kinds of dimeric patterns, covering the common 2–2′ linkage (**5**–**7**) and the less prevalent 2–4′ linkage (**4** and **8**). Employing NMR and ECD spectroscopy and TDDFT calculations, the absolute configurations of these tetrahydroxanthones were investigated. What's more, the cytotoxicity and antibacterial evaluation of all the isolates were also discussed herein.

Materials and methods

General experimental procedures

A PerkinElmer Model 341 polarimeter was applied to measure optical rotations. ECD spectra were acquired using a Chirascan V100 spectropolarimeter. NMR data were recorded at 400 or 600 MHz (Bruker AVANCE). HRESIMS spectra were obtained on a ThermoFisher mass spectrometer (LTQ Orbitrap XL). Size-exclusion chromatography was conducted with Sephadex LH-20. Column chromatography (CC) was applied using silica gel which was produced by Anhui Liangchen Co., Ltd.

Fungal material and mass culture

A specimen of *A. aculeatinus* was identified using the ITS sequences and the morphological characteristics (Wu et al., 2021). A voucher specimen (WHUF0198) has been preserved in School of Pharmaceutical Sciences, Wuhan University. The fungus was precultivated on number II fungus medium (Wu et al., 2022) and incubated at 28°C for a week. After that, a part of the culture was added to a total of 60 flasks containing 300 ml each of number II fungus liquid medium and culture 4 weeks in a static state at 28°C.

Extraction and isolation

The liquid phase (18 L) and mycelia was separated from the fungal culture by filtering. A crude extract was obtained from the mycelia by ultrasound using acetone. To obtain a dry extract (18 g), the liquid phase combined with the crude extract were further extracted by EtOAc and concentrated *in vacuo*. The dry extract was divided into six fractions (F1–F6) and a silica gel CC was applied to gain twenty-six fractions (F5a–F5z) as described earlier (Wu et al., 2022). F5n (125 mg), F5y (110 mg) and F5z (90 mg) was separated using a Sepex-C18 column (250 × 10 mm, 5 μm) with DAD detection and a flow rate of 3 ml/min to gain **2** (5 mg, 68% MeOH-H_2O, t_R 25.3 min), **8** (5 mg, MeCN/H_2O, 55:45, v/v, t_R 22.3 min) and **9** (2 mg, 75% MeOH-H_2O, t_R 24.2 min). F5i (400 mg) was separated using Sephadex LH-20 (MeOH-CH_2Cl_2 1:1) to yield ten fractions (F5i.1–F5i.10). F5i.5 (30 mg) was repurified by Sepex-C18 column with a shimodzu HPLC system (60–80% MeOH-H_2O) to yield **3** (2 mg, 3 ml/min, t_R 24.8 min), **4** (1 mg, 3 ml/min, t_R 26.5 min). F5i.3 (40 mg) was repurified by Sepex-C18 column (65–70% MeOH-H_2O over 28 min) to gain **5** (1 mg, 3 ml/min, t_R 25.6 min), **6** (2 mg, 3 ml/min, t_R 18.3 min) and **7** (1 mg, 3 ml/min, t_R 27.1 min) (Figure 1).

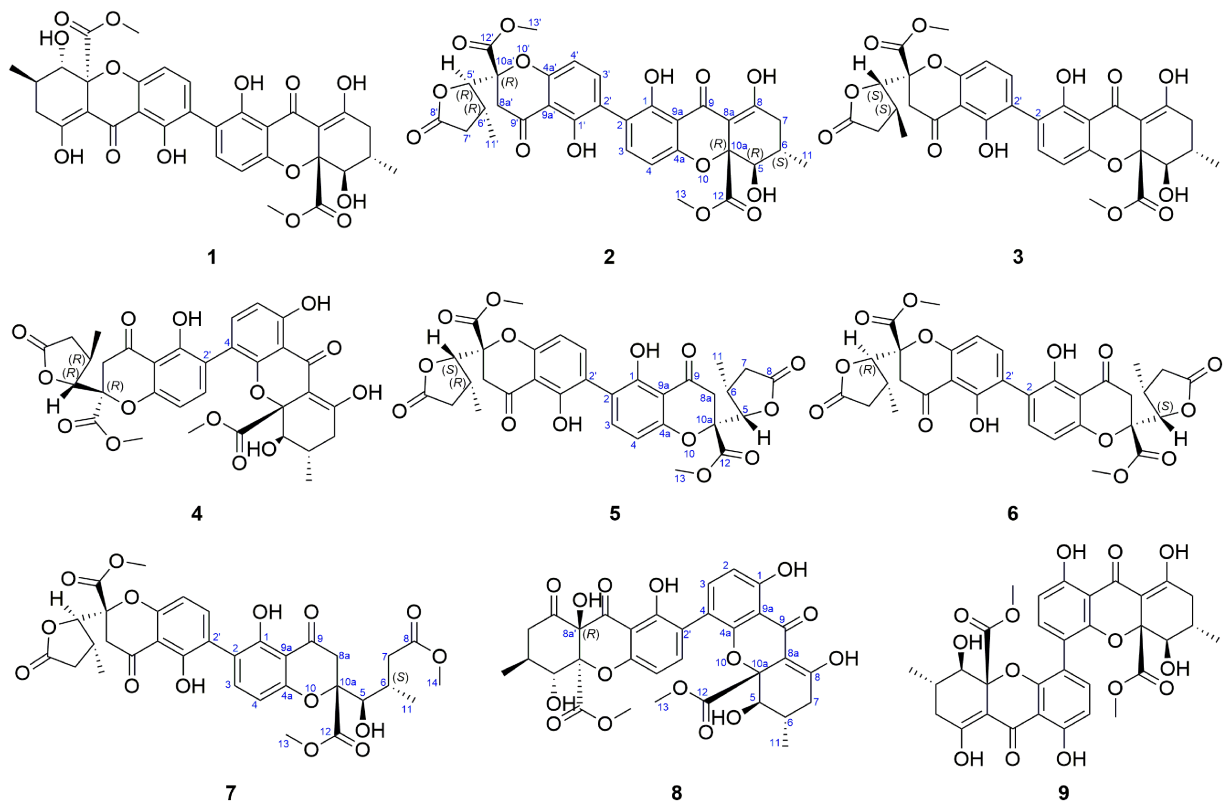

FIGURE 1
Structures of dimeric tetrahydroxanthones **1**–**9**.

Aculeaxanthone A (***4***): orange powder; $[\alpha]_D^{20}$ +272.5 (*c* 0.04, $CDCl_3$); ECD (1.5×10^{-4} M, MeOH), λ [nm] ($\Delta\varepsilon$) 292 (+1.68), 246 (−32.51), 223 (−48.65); ^1H and ^{13}C NMR ($CDCl_3$), see Table 1; HR-ESIMS (*m/z*): 661.1525 $[M+Na]^+$ (calcd for $C_{32}H_{30}O_{14}Na$, 661.1533).

Aculeaxanthone B (***5***): yellow powder; $[\alpha]_D^{20}$ −9 (*c* 0.03, MeOH); ECD (1.5×10^{-4} M, MeOH), λ [nm] ($\Delta\varepsilon$) 264 (−0.91), 223 (+6.02); ^1H and ^{13}C NMR ($CDCl_3$), see Table 2; HR-ESIMS (*m/z*): 661.1523 $[M+Na]^+$ (calcd for $C_{32}H_{30}O_{14}Na$, 661.1533).

Aculeaxanthone C (***6***): yellow powder; $[\alpha]_D^{20}$ −5 (*c* 0.067, MeOH); ECD (1.7×10^{-4} M, MeOH), λ [nm] ($\Delta\varepsilon$) 292 (+1.01), 246 (−0.36), 233 (+0.75), 213 (−0.83); ^1H and ^{13}C NMR ($CDCl_3$), see Table 2; HR-ESIMS (*m/z*): 661.1526 $[M+Na]^+$ (calcd for $C_{32}H_{30}O_{14}Na$, 661.1533).

Aculeaxanthone D (***7***): yellow powder; $[\alpha]_D^{20}$ +5 (*c* 0.02, MeOH); ECD (1.6×10^{-4} M, MeOH), λ [nm] ($\Delta\varepsilon$) 339 (+0.16), 244 (+0.47), 214 (−0.69); ^1H and ^{13}C NMR ($CDCl_3$), see Table 2; HR-ESIMS (*m/z*): 693.1789 $[M+Na]^+$ (calcd for $C_{33}H_{34}O_{15}Na$, 693.1795).

Aculeaxanthone E (***8***): yellow powder; $[\alpha]_D^{20}$ +28.5 (*c* 0.067, MeOH); ECD (1.7×10^{-4} M, MeOH), λ [nm] ($\Delta\varepsilon$) 379 (+6.18), 338 (−0.66), 295 (+0.03), 244 (−6.65), 220 (+0.81); ^1H and ^{13}C NMR ($CDCl_3$), see Table 1; HR-ESIMS (*m/z*): 677.1472 $[M+Na]^+$ (calcd for $C_{32}H_{30}O_{15}Na$, 677.1482).

Computational analysis

The conformational majorization of the stereoisomers was achieved using computational TDDFT calculations. To perform the conformational analysis, MMFF94 molecular mechanics was carried out. The ground-state geometries of those stereoisomers were further optimized using Gaussian 09 (Frisch et al., 2009). Vibrational evaluation was finished using TDDFT calculations at the B3LYP/6-311G (2d, p) level to determine minima. The Boltzmann distribution law (Eq. 1) was used to calculate the equilibrium populations at room-temperature. The overall theoretical ECD spectra were simulated with a Gaussian function and then acquired according to the Boltzmann weighting.

$$\frac{N_i}{N} = \frac{g_i e^{-\frac{E_i}{k_B T}}}{\sum g_i e^{-\frac{E_i}{k_B T}}} \quad (1)$$

In this case, N_i represents the number of conformers i with degeneracy g_i and energy E_i at temperature T, and k_B is Boltzmann constant.

TABLE 1 ^{1}H and ^{13}C NMR spectroscopic data for 4 and 8 ($CDCl_3$, TMS, δ ppm).

No.	4		8	
	δ_C	δ_H, J (Hz)	δ_C	δ_H, J (Hz)
1	161.7		158.4	
2	110.4	6.62 d (8.6)	107.7	6.63 d (8.5)
3	140.7	7.49 d (8.6)	140.3	7.47 d (8.5)
4	118.0		117.5	
4a	155.3		159.3	
5	76.9	3.85 d (11.3)	76.8	3.94 d (11.2)
6	29.3	2.40 m	29.2	2.42 dq (11.2, 6.2, 5.6)
7	36.4	2.73 dd (19.2, 6.3)	36.3	2.74 dd (19.2, 6.2)
		2.28 dd (19.2, 10.6)		2.32 dd (19.2, 10.7)
8	177.1		177.7	
8a	101.6		101.5	
9	-		187.1	
9a	107.3		106.9	
10a	85.0		84.8	
11	18.0	1.13 d (6.4)	18.0	1.18 d (6.4)
12	169.9		170.3	
13	53.7	3.79 s	53.3	3.73 s
1-OH		11.42 s		11.77 s
1′	159.6		157.3	
2′	118.0		118.8	
3′	141.6	7.90 d (8.5)	141.5	7.58 dd (8.5, 1.0)
4′	107.2	6.64 d (8.5)	107.1	6.69 dd (8.5, 1.0)
4a′	158.3		160.6	
5′	87.6	4.49 d (3.9)	74.0	4.50 d (10.7)
6′	30.2	2.89 s	32.0	2.09 m
7′	36.0	2.95 dd (17.5, 9.3)	43.4	2.92 dd (15.0, 12.7)
		2.26 dd (17.5, 4.4)		2.51 dd (15.0, 5.3)
8′	175.0		198.5	
8a′	39.9	3.23 d (17.0)	71.8	
		3.11 d (17.0)		
9′	193.8		191.6	
9a′	107.3		106.5	
10a′	84.1		89.4	
11′	20.9	1.32 d (6.8)	18.5	1.22 d (6.3)
12′	169.0		167.9	
13′	53.4	3.70 s	53.6	3.69 s
1′-OH		11.84 s		

Antibacterial assay

All the isolates were tested against Gram-positive bacteria including *Enterococcus faecium* ATCC 19434, *Bacillus subtilis* 168, *Staphylococcus aureus* ATCC 25923 and MRSA USA300, Gram-negative bacteria including *Helicobacter pylori* 129, G27, as well as 26695, and multi drug-resistant strain *H. pylori* 159, and one Mycobacterium *M. smegmatis* ATCC 607. The MIC of anaerobic bacteria was examined by a broth microdilution assay. Briefly, twofold serial dilutions of compounds **1**–**9** were prepared in 96-well microtiter plates. *H. pylori* liquid cultures was also diluted with BHI broth and was inoculated into each well to get a final concentration of 5×10^5 CFU/ml. After incubation in a microaerophilic atmosphere at 37°C for 72 h, the MIC was confirmed to be the lowest concentration which resulted in no turbidity. Metronidazole was used as a positive control. To obtain MICs for aerobic bacteria, the agar dilution streak method recommended in Clinical and Laboratory Standards Institute document (CLSI) M07-A10 was used. The broth was diluted with saline and applied to plates, delivering a final concentration of approximately 10^5 CFU/spot.

Cytotoxicity assay

Compounds **1**–**9** was tested against the Bel-7402, A-549 and HCT-116 cell lines according to MTT assay. All the isolates were dissovled and diluted using dimethyl sulfoxide (DMSO). Cells were seeded at 4000 cells in 96-well microplates and incubated for 24 h and spent with the isolates for 72 h. After that, each well was treat for 4 h with MTT reagent. By operating a microplate reader, absorbance at 570 nm was measured after replacing the medium with 100 µl of DMSO. All compounds were tested three times independently ($n=3$). 5-Fluorouracil was applied to positive control. Finally, the Logit method was applied to caculate IC_{50} values.

Results and discussion

Compounds **1**–**6** and **9** gave the same molecular formula of $C_{32}H_{30}O_{14}$, deduced by HR-ESIMS, providing 18 unsaturation degrees. Compounds **1**, **2**, **3** and **9** were determined to be secalonic acid D, chrysoxanthones B, C, and 4–4′-secalonic acid D, respectively, by detailed comparison of their specific rotation values and NMR data with literatures (El-Elimat et al., 2015; Qin et al., 2015b; Zhen et al., 2018). The absolute configurations of **2**, **3** and **9** were also confirmed by TDDFT-ECD calculation (Supplementary Figures S5, S9, S52).

Aculeaxanthone A (**4**) was obtained as an orange powder. Compound **4** provided the near-identical NMR data to those of **2**. The significant difference appeared in **4** was the HMBC correlations from the H-2 and hydroxyl proton 1-OH to C-9a, which suggested the C-4–C-2′ linkage for **4** instead of C-2–C-2′ linkage in **2**. The tetrahydroxanthone and the chromanone monomers in **4** connected with a C-4–C-2′ linkage was determined by the COSY correlations of H-2/H-3 instead of H-4/H-3, and HMBC correlations of H-3 with C-2′ and C-4a and H-3′ with C-4. The relative configuration of the two monomers in **4** was the same to those in **2**, as indicated by the coupling constants (Table 1) and the interpretation of the NOE signals, together with the biogenetic consideration. To confirm the absolute configuration of **4**, the calculated ECD spectrum of **4a** were acquired according to the TDDFT calculations (Grkovic et al., 2007; Bringmann et al., 2009). The Molecular Operating Environment (MOE) was performed to conduct the systematic conformational analysis for **4a** (5*R*, 6*S*, 10a*R*, 5'*R*, 6'*R*, 10a'*R*)

10.3389/fmicb.2023.1138830

TABLE 2 ^{1}H and ^{13}C NMR spectroscopic data for 5–7 ($CDCl_3$, TMS, δ ppm).

No.	5		6		7	
	δ_C	δ_H, J (Hz)	δ_C	δ_H, J (Hz)	δ_C	δ_H, J (Hz)
1	159.7		159.2		158.8	
2	117.4		117.4		117.4	
3	141.4	7.53 d (8.5)	141.2	7.52 d (8.6)	141.0	7.49 d (8.5)
4	107.3	6.64 d (8.5)	107.3	6.63 d (8.6)	107.1	6.61 d (8.5)
4a	158.4		158.4		158.8	
5	82.7	4.81 d (6.9)	82.7	4.81 d (6.8)	76.1	4.05 d (6.7)
6	33.5	2.99 *p* (7.7)	33.3	2.98 *p* (7.4)	30.3	2.38 m
7	36.5	2.71 dd (17.3, 8.3)	36.5	2.71 dd (17.3, 8.3)	39.6	2.60 q (9.1)
		2.49 dd (17.3, 8.0)		2.48 dd (17.3, 7.9)		2.39 dd (9.1, 5.9)
8	174.7		174.7		173.0	
8a	39.6	3.28 d (17.3) (17.3)	39.6	3.28 d (17.0) (17.0)	40.0	3.26 brs
		3.21 d		3.21 d		
9	194.1		194.1		195.8	
9a	107.1		107.1		107.5	
10a	84.3		83.9		86.9	
11	14.8	1.34 d (7.2)	14.8	1.34 d (7.2)	13.5	1.07 d (6.4)
12	169.1		169.1		170.4	
13	53.6	3.78 s	53.6	3.77 s	53.1	3.76 s
14					51.6	3.70 s
1-OH		11.92 s		11.91 s		12.01 s
5-OH						2.76 d (7.2)
1′	159.7		159.2		159.2	
2′	117.4		117.4		117.4	
3′	141.4	7.53 d (8.5)	141.2	7.52 d (8.6)	141.4	7.52 d (8.6)
4′	107.3	6.64 d (8.5)	107.3	6.63 d (8.6)	107.1	6.62 d (8.6)
4a′	158.4		158.4		158.8	
5′	82.7	4.81 d (6.9)	87.5	4.46 d (4.0)	87.4	4.46 d (3.9)
6′	33.5	2.99 p (7.7)	29.9	2.84 m	29.6	2.84 m
7′	36.5	2.71 dd (17.3, 8.3)	35.9	2.92 dd (17.8, 9.4)	35.8	2.92 dd (17.8, 9.3)
		2.49 dd (17.3, 8.0) 2.49 dd (17.3, 8.0)		2.24 dd (17.8, 4.6) 2.24 dd (17.8, 4.6)		2.24 dd (17.8, 4.5) 2.24 dd (17.8, 4.5)
8′	174.7		175.2		174.7	
8a′	39.6	3.28 d (17.3)	39.5	3.22 d (17.0)	39.3	3.21 d (17.0)
		3.21 d (17.3)		3.06 d (17.0)		3.06 d (17.0)
9′	194.1		194.1		194.1	
9a′	107.1		107.1		107.5	
10a′	84.3		83.9		84.3	
11′	14.8	1.34 d (7.2)	20.7	1.29 d (6.9)	20.6	1.29 d (6.9)
12′	169.1		168.7		168.7	
13′	53.6	3.78 s	53.6	3.77 s	53.5	3.77 s
1′-OH OH′		11.92 s				
5′-OH OH′				11.91 s		12.02 s

according to the Merck Molecular Force Field (MMFF). The lowest energy conformers were obtained after we reoptimize the designated stereoisomer according to TDDFT at the B3LYP/6-311G (2d, p) (Grimme, 2006) level. These were further filtered to gain the principal conformer on the base of the Boltzmann distribution. Finally, Gaussian broadening was used to provide the complete calculated ECD spectrum of **4a**. Obviously, the experimental and calculated ECD spectra for **4** was in great agreement (Figure 2), indicating that an 5*R*, 6*S*, 10a*R*, 5'*R*, 6'*R*, 10a'*R* absolute configuration could be assigned to **4**.

Compound **4** was found unstable in DMSO-d_6, consistent with the findings of Wu et al. (2015). Then the central chirality elements of **2** and **4** was assigned by chemical conversions. The conversion was monitored by ^{1}H-NMR spectra and the product was isolated using a shimodzu HPLC system. The Wessely-Moser rearrangement between **2** (2′–2 linkage) and **4** (2′–4 linkage) was represented in Figure 3, which further confirmed the absolute configuration of **4**.

Aculeaxanthone B (**5**) was acquired as a yellow powder. Its 1D NMR data displayed only half as many carbon resonances as expected, which were assigned as three carbonyls (δ_C 174.7, 194.1, and 169.1), six aromatic carbons (δ_C 159.7, 117.4, 141.4, 158.4, and 107.1), one nonprotonated sp^3 carbon linked to oxygen (δ_C 84.3), two

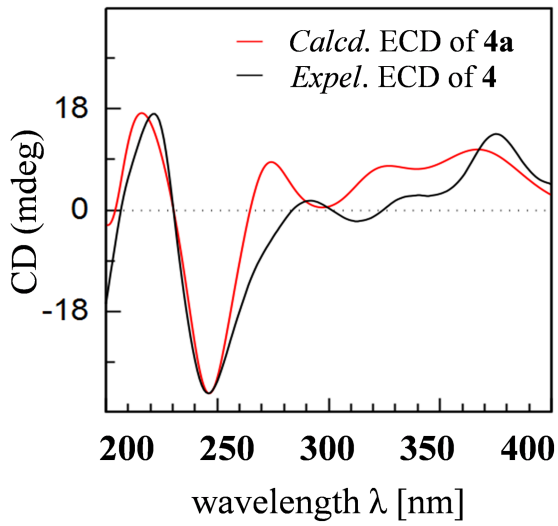

FIGURE 2
Experimental ECD spectrum of **4** and calculated ECD spectrum of **4a**.

10.3389/fmicb.2023.1138830

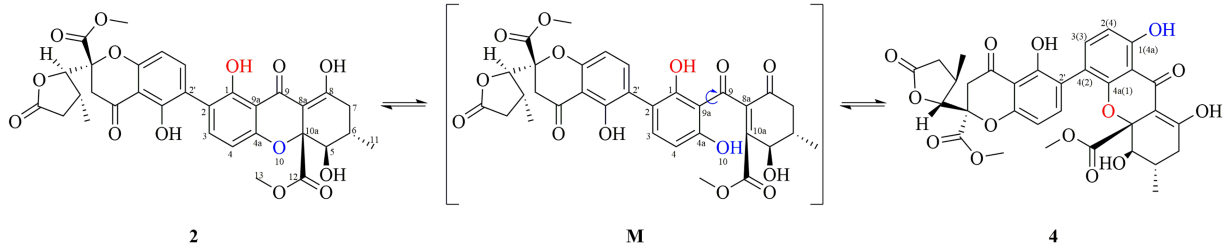

FIGURE 3
Proposed interconversion mechanism between **2** and **4**.

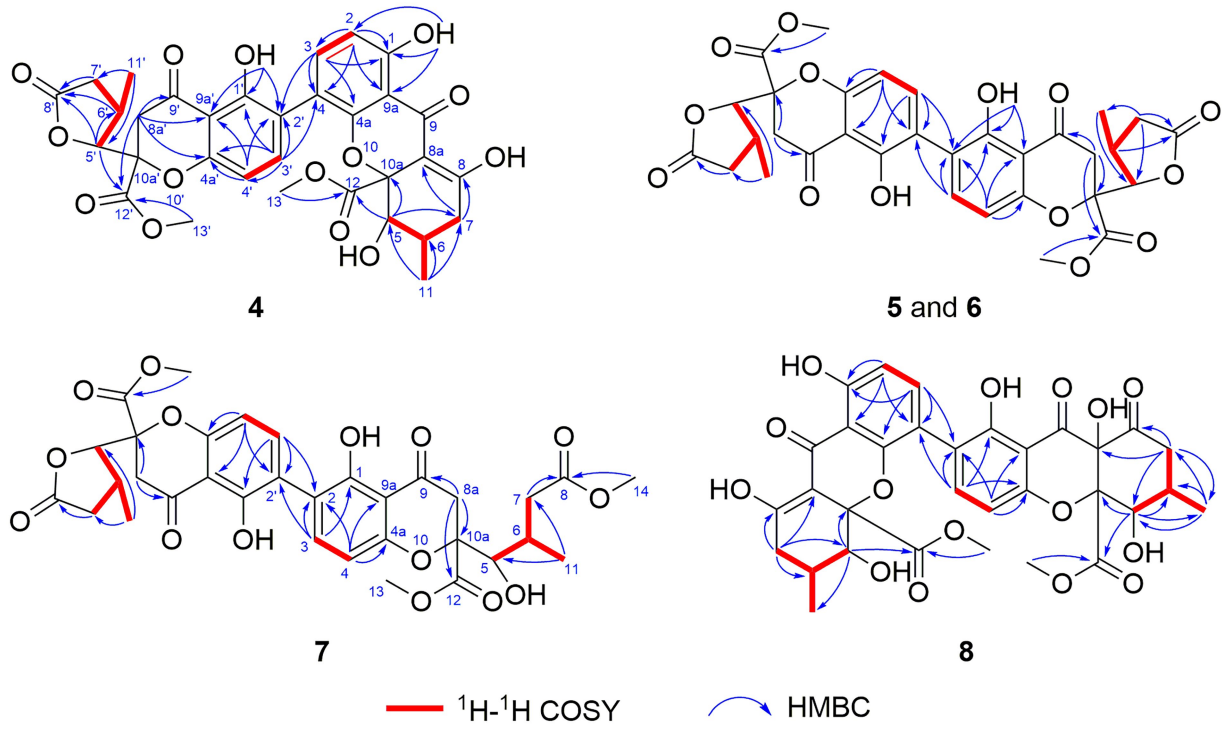

FIGURE 4
^{1}H-^{1}H COSY and HMBC correlations of **4**–**8**.

methines (δ_C 82.7 and 33.5), two methylenes (δ_C 36.5 and 39.6), one methyl (δ_C 14.8), and one methoxyl (δ_C 53.6). Analysis of ^{1}H NMR spectrum indicated one aromatic ring, two methylenes, one oxymethine, one methine, one methyl, and one methoxyl (Table 2). These evidence indicated that **5** must be a symmetric homodimer of two chromanone lactone monomers. The HMBC correlations of H-5 with C-10a and C-12 determined the connection between the lactone moiety and the chromanone monomeric unit (Figure 4). The 2–2′ linkage of **5** was established by the HMBC correlations of 1-OH with C-2 and C-9a, H-3 (H-3′) with C-1 (C-1′), C-4a (C-4a'), and C-2′ (C-2) (Figure 4). The NOESY spectrum was used to provide the relative configuration of **4** (Figure 5). The strong NOESY correlations from H-5 (H-5′) to H-6 (H-6′) and H_α-8a (H_α-8a') suggested that these protons provided the co-facial orientation, which was also determined by the evidence of the coupling constant ($^3J_{H\text{-}5,H\text{-}6} = 6.9$ Hz) with analogues in literatures (Zhang et al., 2008; El-Elimat et al., 2015; Wu et al., 2015). For 5*S*, 6*R*, 10a*R*, 5'*S*, 6'*R*, 10a'*R*, the experimental spectrum agreed well with the calculated one, which unequivocally assigns the absolute configuration of **5** (Figure 6).

Aculeaxanthone C (**6**) was also found to possess the identical molecular formula ($C_{32}H_{30}O_{14}$) to **2**–**5**, as suggested by the HR-ESIMS ions observed at *m/z* 661.1526 (calcd for $C_{32}H_{30}O_{14}Na^+$, 661.1533). A scrupulous analysis of the 1D NMR data of **6** and **5** (Table 2) indicated **6** to be a heterodimer of two different chromanone lactone monomers. Subtraction of the signals of aculeaxanthone B (**5**) subunit confirmed the near-identical remaining NMR data with those of the chromanone lactone of **2**. The relative configuration of one chromanone lactone in **6** was determined by the NOESY correlation of H-5/H-6 (Figure 5). The configuration of H-5′ and H-6′ in another chromanone lactone monomer was determined as the same as that of **2**, confirmed by the NOESY correlation of H-5′ with H-11′ (Figure 5). To establish the absolute configuration of **6**, the lowest energy conformer was calculated. Distinctly, the experimental ECD spectrum for **6** and the calculated one for **6a** can

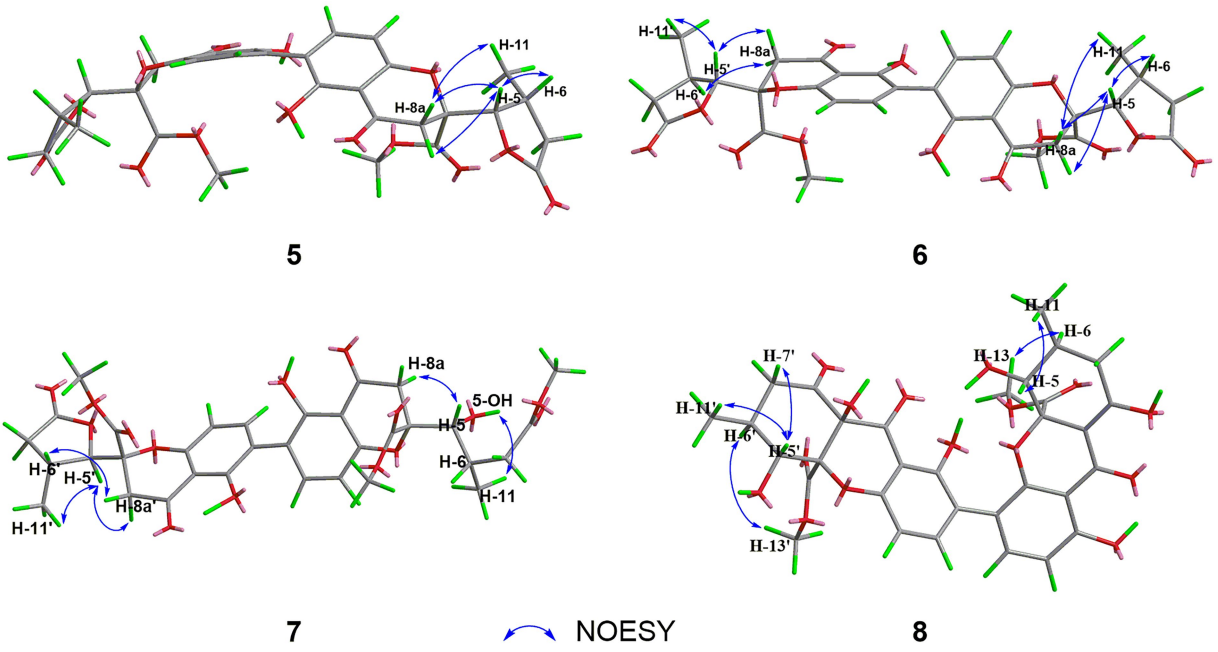

FIGURE 5
NOESY correlations of **5**–**8**.

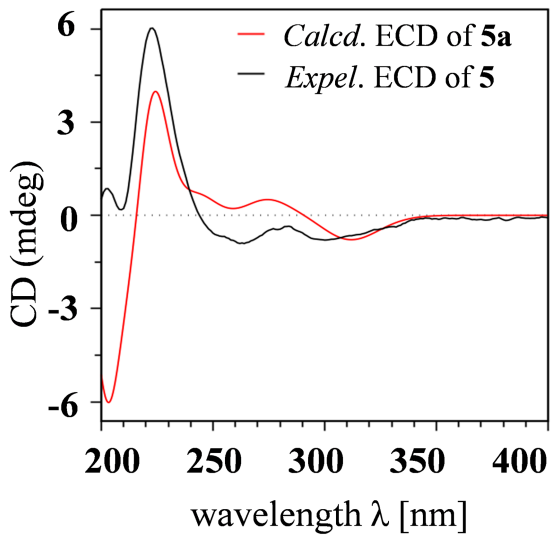

FIGURE 6
Experimental ECD spectrum of **5** and calculated ECD spectrum of **5a**.

be found a great fit (Figure 7). Finally, the 5*S*, 6*R*, 10a*R*, 5'*R*, 6'*R*, 10a'*R* configuration could be assigned to **6** (Figure 1).

Aculeaxanthone D (**7**) was derived as a yellow powder. Its molecular formula was deduced as $C_{33}H_{34}O_{15}$ from the HR-ESIMS ions at *m/z* $[M+Na]^+$ 693.1789, indicating that **7** presented one more carbon and one less unsaturation degree than compounds **1**–**6**. The 1D NMR data (Table 2) displayed that the chromanone lactone monomer of **7** was identical to that of **2** and **6**. Compound **7** was determined to possess 2–2′ linkage by the HMBC correlations from H-3 (δ_H 7.49) to C-2′ (δ_C 117.4) and H-3′ (δ_H 7.52) to C-2 (δ_C 117.4). The distinction difference was that a side chain in **7** replaced the cyclohexene moiety in **2**, determined by the HMBC correlations of the methoxyl H_3-14 (δ_H 3.70) with C-8 (δ_C173.0). The relative configurations of the chromanone monomer in **7** were identical to those in **2** and **6** from the NOESY correlations between H-5′ with H-11′(Figure 5), the chemical shifts, and biogenetic grounds. The anti relationship between H-5 with H-6 in **7** were proposed to be the same as those in **2**, deduced from the coupling constants ($^3J_{H\text{-}5,H\text{-}6}$ = 6.7 Hz) and biogenetic consideration. To gain the absolute configuration of **7**, the ECD spectrum for the lowest energy conform **7a** (5*R*, 6*S*, 10a*R*, 5'*R*, 6'*R*, 10a'*R*), was calculated and compared with the experimental one. Notably, the calculated ECD spectrum showed good fitting with the experimental one (Figure 7), determining that an 5*R*, 6*S*, 10a*R*, 5'*R*, 6'*R*, 10a'*R* absolute configuration could be defined to **7**.

The molecular formula of aculeaxanthone E (**8**) was assigned as $C_{32}H_{30}O_{15}$, 16 mass units greater than that of compounds **1**–**6**, according to its HR-ESIMS ion at *m/z* 677.1472 $[M+Na]^+$ (calcd for 677.1482). The ^{13}C NMR and HSQC spectra (Table 1) showed 32 signals corresponding to five carbonyls (δ_C 187.1, 170.3, 198.5, 191.6, and 167.9), two 1,2,3,4-substituted benzene rings, one double band (δ_C 177.7 and 101.5), three nonprotonated sp^3 carbons linked to oxygen (δ_C 84.8, 71.8, and 89.4), two oxymethines (δ_C 76.8 and 74.0), two methylenes (δ_C 36.3 and 43.4), two methoxyls (δ_C 53.3 and 53.6), two methines (δ_C 29.2 and 32.0), and two methyls (δ_C 18.0 and 18.5) (Table 1). Inspection of the 1D NMR data of **8** with those in earlier reported (Wang et al., 2018) suggested **8** to be a heterodimer of tetrahydroxanthone monomer and hexahydroxanthone monomer. Careful analysis of the 2D NMR spectra suggested that the tetrahydroxanthone monomer of **8** was identical to those of compounds **1**–**4**. Subtraction of the signals of the tetrahydroxanthone monomer indicated the similitube of the remaining NMR data with those of penibishexahydroxanthone A (Chen M. et al., 2019). The

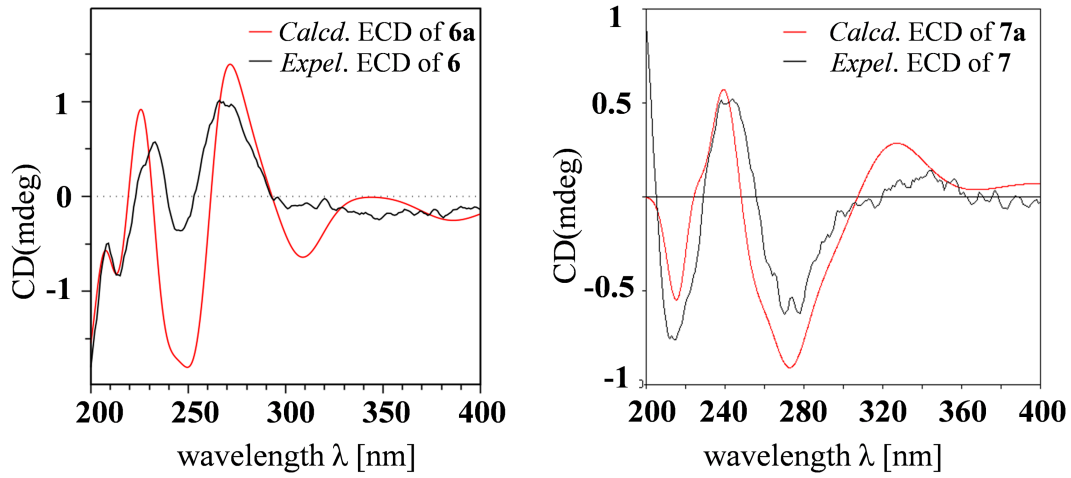

FIGURE 7
Experimental ECD spectra of **6** and **7** and calculated ECD spectra of **6a** and **7a**.

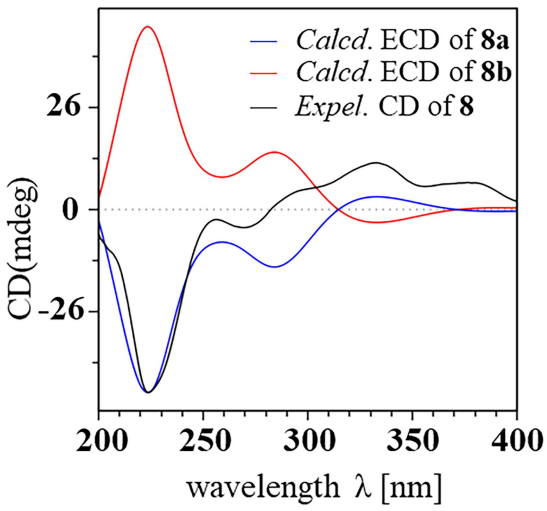

FIGURE 8
Experimental and calculated ECD spectra of compound **8**.

2–4′ linkage was determined by the HMBC correlations of H-3 with C-2′ and H-3′ with C-4 (Figure 4). Then, the planar structure of **8** as displayed in Figure 1. The tetrahydroxanthone monomer in **8** was easily determined to be identical to those of compounds **1**–**4** by the NOESY correlation from H-5 to H_3-11 (Figure 5), the large $^3J_{H\text{-}5,\ H\text{-}6}$ (11.2 Hz) value. The large $^3J_{H\text{-}5',H\text{-}6'}$ (10.7 Hz) value, strong NOESY correlation of H-5′ with H_3-11′, and the near-identical chemical shifts with those of penibishexahydroxanthone A suggested that the hexahydroxanthone monomer was identical to penibishexahydroxanthone A. To determine the absolute configuration of **8,** TDDFT-ECD spectra of **8a** (5*R*, 6*S*, 10a*S*, 5'*R*, 6'*S*, 8a'*R*, 10a'*S*) and **8b** (5*S*, 6*R*, 10a*R*, 5'*S*, 6'*R*, 8a'*S*, 10a'*R*) were calculated (Figure 8). After that, **8** was assigned as 5*R*, 6*S*, 10a*S*, 5'*R*, 6'*S*, 8a'*R*, 10a'*S*, as shown in Figure 1.

Compound **9** possessed the same molecular formula ($C_{32}H_{30}O_{14}$) as secalonic acid D (**1**) which was based on its HR-ESIMS analysis (*m/z* 661.1530; $[M+Na]^+$, calcd for 661.1533), suggesting it to be an isomer of **1**. Similar to **5**, **9** displayed half of the expected carbon signals, suggesting a structurally symmetrical. Careful analysis of the NMR spectra, **9** displayed identical 1D NMR data to those of 4–4′-secalonic acid D, 4–4′-secalonic acid A (Chen L. et al., 2019), and talaroxanthone (Koolen et al., 2013), suggesting that **9** shared the same planar structure and relative configurations as those compounds. Compound **9** was finally determined to be 4–4′-secalonic acid D by comparison their specific rotation values, of which the absolute configuration was further determined by the TDDFT-ECD calculation (Figure S52). However, after comparison of the 1 D NMR data of talaroxanthone with those of 4–4′-secalonic acid A, the structure of talaroxanthone should be revised to 4–4′-secalonic acid A (Koolen et al., 2013), due to their identical NMR data, particularly the large $^3J_{H\text{-}5,\ H\text{-}6}$ (12.0 Hz) value, and the specific rotation values (Koolen et al., 2013; Qin and Porco, 2015).

Compounds **1**–**9** were tested for cytotoxicity against the Bel-7402, A549, and HCT-116 cancer cell lines. Of the dimeric tetrahydroxanthone derivatives, only compound **6** provided cytotoxicity effect against Bel-7402 cell line (IC_{50}, 1.96 μM). Additionally, antimicrobial activity was evaluated for all dimeric tetrahydroxanthones, including four Gram-positive bacteria including *Enterococcus faecium* ATCC 19434, *B. subtilis* 168, *S. aureus* ATCC 25923 and MRSA USA300; four Gram-negative bacteria, including *H. pylori* 129, G27, as well as 26695, and multi drug-resistant strain *H. pylori* 159, and one Mycobacterium *M. smegmatis* ATCC 607. However, only compound **1** performed activities against *H. pylori* G27, *H. pylori* 26695, *H. pylori* 129, *H. pylori* 159, *S. aureus* USA300, and *B. subtilis* 168 with MIC values of 4.0, 4.0, 2.0, 2.0, 2.0 and 1.0 μg/ml, respectively.

Conclusion

In summary, five new dimeric tetrahydroxanthones (**4**–**8**) with a high degree of structural complexity and diversity were separated from the culture of the marine-derive fungus *A. aculeatinus*

WHUF0198. Compound **4** represented the chemical conversion product of **2**, indicating the possibility that some dimeric tetrahydroxanthones might produce spontaneously from the natural dimers in the process of the fermentation or extraction. Compounds **5** and **6** contained two chromanone monomers coupled by a 2–2′ linkage to form a symmetric homodimer and an asymmetric dimer, respectively. Compound **7** included a common chromanone lactone unit and a ring-opened tetrahydroxanthone monomer, which might derive from **2** instead of the methanolysis product of **6**. Thus, compound **8** represented the fifth dimeric hexahydroxanthones, of which the common tetrahydroxanthone monomer and the hexahydroxanthone monomer were connected by a 2–4′ linkage. Furthermore, the structure of talaroxanthone should be revised to 4–4′-secalonic acid A based on their identical NMR data and specific rotation values. The absolute configurations of all dimeric tetrahydroxanthones were determined by a combination of ECD calculation, chemical conversions, specific rotations, and biogenetic consideration. Compound **6** showed cytotoxicity effect against Bel-7402 cell line with an IC_{50} value of 1.96 μM, and compound **1** provided activities against *H. pylori* G27, *H. pylori* 26695, *H. pylori* 129, *H. pylori* 159, *S. aureus* USA300, and *B. subtilis* 168 with MIC values of 4.0, 4.0, 2.0, 2.0, 2.0 and 1.0 μg/ml, respectively.

Data availability statement

The original contributions presented in the study are included in the article/Supplementary material, further inquiries can be directed to the corresponding authors.

Author contributions

Y-SC, KH, and HB: conceptualization, methodology, and writing—review and editing. JW, HS, and K-KZ: data curation. Y-SC, HS, and MeZ: funding acquisition. K-KZ: software. JW, YZ, and HS: chemical investigation. MiZ, S-BW, and HB: bioactivity assays. KH: fungal resources. JW, HS, and Y-SC: data analysis. JW, MeZ, and HS: writing—original draft preparation. All authors contributed to the article and approved the submitted version.

Funding

This research was supported by the National Key Research and Development Program of China (no. 2021YFC2100600), the National Natural Science Foundation of China (nos. 81973201 and 82204225), the Natural Science Foundation of Hubei Province (nos. 2021CFB347 and 2021CFB061), and the Joint Fund of Health Commission of Hubei Province (no. WJ2019H024).

Acknowledgments

We are grateful to Shuai Ding for the cytotoxic activity test of compound **2**. We thank Ran Zhang from the Core Facility of Wuhan University for his assistance with NMR analysis.

Conflict of interest

The authors declare that the research was conducted in the absence of any commercial or financial relationships that could be construed as a potential conflict of interest.

The handling editor DZ declared a shared parent affiliation with the author S-BW at the time of review.

Publisher's note

All claims expressed in this article are solely those of the authors and do not necessarily represent those of their affiliated organizations, or those of the publisher, the editors and the reviewers. Any product that may be evaluated in this article, or claim that may be made by its manufacturer, is not guaranteed or endorsed by the publisher.

Supplementary material

The Supplementary material for this article can be found online at: https://www.frontiersin.org/articles/10.3389/fmicb.2023.1138830/full#supplementary-material

References

Bringmann, G., Bruhn, T., Maksimenka, K., and Hemberger, Y. (2009). The assignment of absolute stereostructures through quantum chemical circular dichroism calculations. *Eur. J. Org. Chem.* 2009, 2717–2727. doi: 10.1002/ejoc.200801121

Cai, S., King, J. B., Du, L., and Powell, D. R. (2014). Cichewicz, R H. bioactive sulfur-containing sulochrin dimers and other metabolites from an *Alternaria* sp. isolate from a Hawaiian soil sample. *J. Nat. Prod.* 77, 2280–2287. doi: 10.1021/np5005449

Cai, Y.-S., Sarotti, A. M., Zhou, T.-L., Huang, R., Qiu, G., Tian, C., et al. (2018). Flabellipparicine, a flabelliformide-apparicine-type bisindole alkaloid from *Tabernaemontana divaricata*. *J. Nat. Prod.* 81, 1976–1983. doi: 10.1021/acs.jnatprod.8b00191

Cao, H.-Y., Yi, C., Sun, S.-F., Li, Y., and Liu, Y.-B. (2022). Anti-inflammatory dimeric tetrahydroxanthones from an endophytic *Muyocopron laterale*. *J. Nat. Prod.* 85, 148–161. doi: 10.1021/acs.jnatprod.1c00878

Chen, M., Gui, Y., Zhu, H., Zhang, Z., and Lin, H.-W. (2019). Proangiogenic penibishexahydroxanthone a from the marine-derived fungus *Penicillium* sp. ZZ486A. *Tetrahedron Lett.* 60, 1393–1396. doi: 10.1016/j.phytochem.2018.04.021

Chen, L., Li, Y.-P., Li, X.-X., Lu, Z.-H., Zheng, Q.-H., and Liu, Q.-Y. (2019). Isolation of 4,4′-bond secalonic acid D from the marine-derived fungus *Penicillium oxalicum* with inhibitory property against hepatocellular carcinoma. *J. Antibiot.* 72, 34–44. doi: 10.1038/s41429-018-0104-5

Deshmukh, S. K., Mishra, P. D., Kulkarni-Almeida, A., Verekar, S., Sahoo, M. R., Periyasamy, G., et al. (2009). Anti-inflammatory and anticancer activity of ergoflavin isolated from an endophytic fungus. *Chem. Biodivers.* 6, 784–789. doi: 10.1002/cbdv.200800103

El-Elimat, T., Figueroa, M., Raja, H. A., Graf, T. N., Swanson, S. M., Falkinham, J. O. III, et al. (2015). Biosynthetically distinct cytotoxic polyketides from *Setophoma terrestris*. *Eur. J. Org. Chem.* 2015, 109–121. doi: 10.1002/ejoc.201402984

Franck, B. (1969). Structure and biosynthesis of the ergot pigments. *Angew. Chem. Int. Edit.* 8, 251–260. doi: 10.1002/anie.196902511

Franck, B. (1980). "The biosynthesis of the ergochromes" in *The Biosynthesis of Mycotoxins: A Study in Secondary Metabolism*. ed. P. S. Steyn (New York: Academic Press), 157–191.

Frisch, M. J., Trucks, G. W., Schlegel, H. B., Scuseria, G. E., Robb, M. A., Cheeseman, J. R., et al. (2009). *Investigation of Structural and Electronic Properties of [Tris (Benzene-1,2-Dithiolato) M] 3- (M = V, Cr, Mn, Fe and Co) Complexes: A Spectroscopic and Density Functional Theoretical Study. Gaussian 09, Revision A.02*, Gaussian, Inc., Wallingford, CT.

Grimme, S. (2006). Semiempirical GGA-type density functional constructed with a long-range dispersion correction. *J. Comput. Chem.* 27, 1787–1799. doi: 10.1002/jcc.20495

Grkovic, T., Ding, Y., Li, X. C., and Ferreira, D. (2007). Theoretical calculation of electronic circular dichroism of the rotationally restricted 3, 8′ -biflavonoid morelloflavone. *J. Org. Chem.* 72, 9010–9017. doi: 10.1021/jo801622n

Koolen, H. H. F., Menezes, L. S., Souza, M. P., Silva, F. M. A., Almeida, F. G. O., de Souza, A. Q. L., et al. (2013). Talaroxanthone, a novel xanthone dimer from the endophytic fungus *Talaromyces* sp. associated with duguetia stelechantha (Diels) R. *E. Fries. J. Brazil. Chem. Soc.* 24, 880–883. doi: 10.5935/0103-5053.20130104

Lombe, B. K., Feineis, D., and Bringmann, G. (2019). Dimeric naphthylisoquinoline alkaloids: polyketide-derived axially chiral bioactive quateraryls. *Nat. Prod. Rep.* 36, 1513–1545. doi: 10.1039/C9NP00024K

Luenne, F., Koehler, J., Stroh, C., Mueller, L., Daniliuc, C. G., Mueck-Lichtenfeld, C., et al. (2021). Insights into ergochromes of the plant pathogen *Claviceps purpurea*. *J. Nat. Prod.* 84, 2630–2643. doi: 10.1021/acssuschemeng.8b00102

Lv, X. J., Ding, F., Wei, Y. J., and Tan, R. X. (2021). Antiosteoporotic tetrahydroxanthone dimers from aspergillus brunneoviolaceus FB -2 residing in human gut. *Chin. J. Chem.* 39, 1580–1586. doi: 10.1002/cjoc.202100026

Masters, K.-S., and Brase, S. (2012). Xanthones from fungi, lichens, and bacteria: the natural products and their synthesis. *Chem. Rev.* 112, 3717–3776. doi: 10.1021/cr100446h

Phang, Y. L., Zheng, C., and Xu, H. (2022). Structural diversity and biological activities of caged Garcinia xanthones: recent updates. *Acta Mater. Med.* 22, 72–95. doi: 10.3390/molecules22122026

Qin, T., Iwata, T., Ransom, T. T., Beutler, J. A., and Porco, J. A. (2015a). Syntheses of dimeric tetrahydroxanthones with varied linkages: investigation of "shapeshifting" properties. *J. Am. Chem. Soc.* 137, 15225–15233. doi: 10.1021/jacs.5b09825

Qin, T., and Porco, J. A. (2015). Total syntheses of secalonic acids a and D. *Angew. Chem. Int. Edit.* 53, 3107–3110. doi: 10.1002/anie.201311260

Qin, T., Skraba-Joiner, S. L., Khalil, Z. G., Johnson, R. P., Capon, R. J., and Porco, J. A. (2015b). Atropselective syntheses of (−) and (+) rugulotrosin a utilizing point-to-axial chirality transfer. *Nat. Chem.* 7, 234–240. doi: 10.1038/nchem.2173

Rezanka, T., and Sigler, K. (2007). Hirtusneanoside, an unsymmetrical dimeric tetrahydroxanthone from the lichen *Usnea hirta*. *J. Nat. Prod.* 70, 1487–1491. doi: 10.1021/np070079m

Roensberg, D., Debbab, A., Mandi, A., Vasylyeva, V., Boehler, P., Stork, B., et al. (2013). Pro-apoptotic and immunostimulatory tetrahydroxanthonedimers from the endophytic fungus *Phomopsis longicolla*. *J. Org. Chem.* 78, 12409–12425. doi: 10.1016/j.tetlet.2015.03.126

Sadorn, K., Saepua, S., Boonyuen, N., Choowong, W., Rachtawee, P., and Pittayakhajonwut, P. (2021). Bioactive dimeric tetrahydroxanthones with 2,2′- and 4,4′-axial linkages from the entomopathogenic fungus *Aschersonia confluens*. *J. Nat. Prod.* 84, 1149–1162. doi: 10.1021/acs.jnatprod.0c01212

Wang, P., Luo, Y.-F., Zhang, M., Dai, J.-G., Wang, W.-J., and Wu, J. (2018). Three xanthone dimers from the Thai mangrove endophytic fungus *Phomopsis* sp. xy21. *J. Asian Nat. Prod. Res.* 20, 217–226. doi: 10.1016/j.fitote.2018.11.004

Wezeman, T., Braese, S., and Masters, K.-S. (2015). Xanthone dimers: a compound family which is both common and privileged. *Nat. Prod. Rep.* 32, 6–28. doi: 10.1039/C4NP00050A

Wu, J., Wang, F., He, L.-M., Zhou, S.-Y., Wang, S.-B., Jia, J., et al. (2022). Aculeaquamide a, cytotoxic paraherquamide from the marine fungus *Aspergillus aculeatinus* WHUF0198. *Nat. Prod. Res.* 36, 4388–4393. doi: 10.1080/14786419.2021.1998047

Wu, G., Yu, G., Kurtan, T., Mandi, A., Peng, J., Mo, X., et al. (2015). Versixanthones A-F, cytotoxic xanthone-chromanone dimers from the marine-derived fungus *Aspergillus* versicolor HDN1009. *J. Nat. Prod.* 78, 2691–2698. doi: 10.1021/acs.jnatprod.5b00636

Wu, J., Zhang, H., He, L.-M., Xue, Y.-Q., Jia, J., Wang, S.-B., et al. (2021). A new fusicoccane-type norditerpene and a new indone from the marine-derived fungus *Aspergillus aculeatinus* WHUF0198. *Chem. Biodivers.* 18:e2100562. doi: 10.1002/cbdv.202100562

Xiao, Z., Li, Y., and Gao, S. (2017). Total synthesis and structural determination of the dimeric tetrahydroxanthone ascherxanthone A. *Org. Lett.* 19, 1834–1837. doi: 10.1021/acs.orglett.7b00592

Zhang, W., Krohn, K., Zia-Ullah, , Florke, U., Pescitelli, G., Lorenzo, D. B., et al. (2008). New mono-and dimeric members of the secalonic acid family: blennolides A-G isolated from the fungus *Blennoria* sp. *Chem. Eur. J.* 14, 4913–4923. doi: 10.1002/chem.200800035

Zhen, X., Gong, T., Wen, Y.-H., Yan, D.-J., Chen, J.-J., and Zhu, P. (2018). Chrysoxanthones A–C, three new Xanthone–Chromanone heterdimers from sponge-associated *Penicillium chrysogenum* HLS111 treated with histone deacetylase inhibitor. *Mar. Drugs* 16:357. doi: 10.3390/md16100357

frontiers | Frontiers in Microbiology

TYPE Original Research
PUBLISHED 02 March 2023
DOI 10.3389/fmicb.2023.1099103

OPEN ACCESS

EDITED BY
Kalindi Morgan,
University of Northern British Columbia
Canada,
Canada

REVIEWED BY
Erwei Li,
Institute of Microbiology (CAS), China
Dewu Zhang,
Institute of Medicinal Biotechnology,
Chinese Academy of Medical Sciences,
China

*CORRESPONDENCE
Guojun Pan
gjpan@sdfmu.edu.cn

†These authors have contributed equally to this work

SPECIALTY SECTION
This article was submitted to
Microbial Physiology and Metabolism,
a section of the journal
Frontiers in Microbiology

RECEIVED 15 November 2022
ACCEPTED 06 February 2023
PUBLISHED 02 March 2023

CITATION
Liu X, Kong F, Xiao N, Li X, Zhang M, Lv F, Liu X, Kong X, Bi J, Lu X, Kong D, Hao G, Zhou L and Pan G (2023) Prenylated indole-terpenoids with antidiabetic activities from *Penicillium* sp. HFF16 from the rhizosphere soil of *Cynanchum bungei* Decne.
Front. Microbiol. 14:1099103.
doi: 10.3389/fmicb.2023.1099103

Prenylated indole-terpenoids with antidiabetic activities from *Penicillium* sp. HFF16 from the rhizosphere soil of *Cynanchum bungei* Decne

Xijin Liu[1†], Fandong Kong[2†], Na Xiao[3†], Xiaoyu Li[1], Mingyu Zhang[1], Fujin Lv[1], Xiaolin Liu[1], Xiangchuan Kong[1], Jing Bi[1], Xinyi Lu[1], Daqing Kong[1], Gangping Hao[1], Liman Zhou[2] and Guojun Pan[1*]

[1]College of Life Sciences, Shandong First Medical University & Shandong Academy of Medical Sciences, Tai'an, Shandong, China, [2]Key Laboratory of Chemistry and Engineering of Forest Products, State Ethnic Affairs Commission, Guangxi Key Laboratory of Chemistry and Engineering of Forest Products, Guangxi Collaborative Innovation Center for Chemistry and Engineering of Forest Products, School of Chemistry and Chemical Engineering, Guangxi Minzu University, Nanning, China, [3]State Key Laboratory of Crop Biology, College of Agronomy, Shandong Agriculture University, Tai'an, Shandong, China

Finding novel and effective suppression of hepatic glucagon response antidiabetic compounds is urgently required for the development of new drugs against diabetes. Fungi are well known for their ability to produce new bioactive secondary metabolites. In this study, four new prenylated indole-terpenoids (**1-4**), named encindolenes I-L, as well as a known analogue (**5**), were isolated from the fungus *Penicillium* sp. HFF16from the rhizosphere soil of *Cynanchum bungei* Decne. The structures of the compounds were elucidated by spectroscopic data and ECD analysis. In the antidiabetic activity assay, compounds **1-5** could inhibit glucagon-induced hepatic glucose output with EC_{50} values of 67.23, 102.1, 49.46, 25.20, and 35.96μM, respectively, and decrease the intracellular cAMP contents in primary hepatocytes.

KEYWORDS

fungus, *Penicillium* sp. HFF16, indole-terpenoids, Antidiabetic activity, *Cynanchum bungei* Decne

Introduction

The liver plays a major role in whole body glucose metabolism by maintaining a balance between glucose production and glucose storage (Lewis et al., 2021; Zhang et al., 2022). Excessive hepatic glucose production contributes substantially to diabetes, and it is proposed that suppression of hepatic glucose production may provide therapeutic advantages for the control of diabetes (Xiao et al., 2017; Liao et al., 2021). During fasting, hepatic gluconeogenesis is the primary source of glucagon-mediated endogenous glucose production (Unger and Cherrington, 2012). Glucagon, a pancreas-derived hormone induced by fasting, promotes gluconeogenesis through induction of intracellular cAMP production. Glucagon promotes hepatic gluconeogenesis through upregulation of cAMP/PKA signaling pathway and prevents hypoglycemia (Zhang et al., 2019). Therefore, finding novel and effective inhibition of glucagon-mediated gluconeogenesis bioactive compounds are urgently required. Fungal secondary

metabolites have been proven to be an important source of natural compounds with novel structures and unique activities, many of which contribute to drug discovery and are approved by the US Food and Drug Administration (Pan G. J. et al., 2021; Shankar and Sharma, 2022). The paxilline-type indole-diterpenoids are one of the largest classes of fungal indole-terpenoids (Kong et al., 2019), many of which have significant bioactivities. In our preliminary search for bioactive metabolites from *Penicillium* sp. HFF16, from the rhizosphere soil of *Cynanchum bungei* Decne from Mount Tai, China, nine new indole-terpenoids with weak anti-inflammatory activities and antidiabetic effects were investigated (Pan G. et al., 2021; Xiao et al., 2022). Considering such a significant work, *Penicillium*sp.HFF16 was re-fermented and chemical investigation on its extracts revealed another four new indole-terpenoids (**1**-**4**) (Figure 1). All of the compounds exhibited moderate antidiabetic effects on glucagon-stimulated cAMP accumulation and hepatic glucose output in primary hepatocytes. Herein, the isolation, structural elucidation, and bioactivities of these compounds were described.

Materials and methods

General experimental procedures

Optical rotations were measured on an Anton PaarMCP-100 digital polarimeter, and UV spectra were measured on a Beckman DU 640 spectrophotometer. ECD data were collected using a JASCO J-715 spectropolarimeter. NMR spectra were recorded on a Bruckmercury Plus-400 spectrometers with TMS as an internal standard. HRESIMS spectra were recorded with a Micromass Autospec-Uitima-TOF. Infrared (IR) spectra were obtained on a FTIR-650 spectrometer. Semi-preparative high-performance liquid chromatography (HPLC) was carried out using an ODS column (YMC-pack ODS-A, 10 × 250 mm, 5 μm, 4 mL/min). Thin-layer chromatography (TLC) and column chromatography (CC) were performed on plates precoated with silica gel GF_{254} (10–40 μm, Yantai Jiangyou Silicone Development Co. Ltd).

Fungal material and fermentation

The fungus *Penicillium* sp. HFF16 was isolated from the rhizosphere soil of *Cynanchum bungei* Decne, in Mount Tai, China in May 2020 and identified according to its morphological characteristics and ITS gene sequences (Pan G. et al., 2021). A reference culture of *Penicillium* sp. HFF16 maintained at -80°C is deposited in our laboratory. The isolate was cultured on the plates of PDA medium at 28°C for 4 days. Plugs of agar supporting mycelium growth were cut and transferred aseptically to the 10 × 250-mL Erlenmeyer flasks each containing 100 mL of liquid medium (potato 200 g, glucose 20 g per liter of tap water) and cultured at 28°C at 150 RPM for 3 days. The seed liquid was inoculated aseptically into the 200 × 1,000-mL Erlenmeyer flasks each containing rice medium (80 g rice, 100 mL of tap water) at 0.5–1% inoculation amount and incubated at room temperature under static conditions for 35 days.

Extraction and isolation

The cultures (16 kg) were then extracted into 50 L of ethyl acetate (EtOAc) by soaking overnight. The extraction repeated for three times. The combined EtOAc extracts were dried under vacuum to produce 52.1 g of extract. The EtOAc extract was subjected to a silica gel column-vacuum liquid chromatography column, eluting with a stepwise gradient of 0, 9, 11, 15, 20, 30, 50, and 100% EtOAc in petroleum ether (v/v), to give seven fractions (Fr. 1-7). Fraction 2 (17.2 g) was applied to ODS silica gel with gradient elution of CH_3OH (MeOH)-H_2O (1:5, 2:3, 3:2, 4:1, 1:0) to yield four subfractions (Fr. 2-1-Fr. 2-4). Fr. 2-1 (5.0 g) was applied to ODS silica gel with gradient elution of MeCN-H_2O (1,4, 2:3, 3:2, 7:3, 4:1, 9:1, 9.5:1, and 0) to yield six tertiary fractions (Fr. 2-1-1-Fr. 2-1-6). Fr. 2-1-3 (0.81 g) was purified using semi-prep HPLC (isocratic system 93.6% MeOH/H_2O, v/v) to yield nine fourthiary fractions (Fr. 2-1-3-1-Fr. 2-1-3-9). Fr. 2-1-3-8 (49 mg) was purified using semi-prep HPLC (isocratic system 90% MeCN/H_2O, v/v) to give compounds **1** (t_R10.1 min; 10 mg), **4** (t_R6.1 min; 11 mg), and **5** (t_R 8.1 min; 13 mg). Fr. 2-1-3-7 (62 mg) was

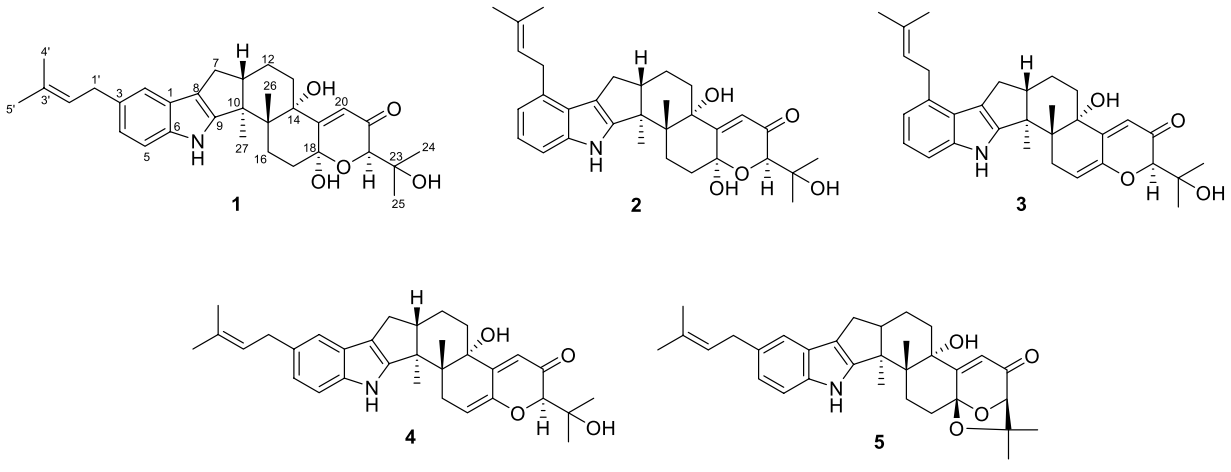

FIGURE 1
The chemical structures of compounds **1**-**5**.

10.3389/fmicb.2023.1099103

purified using semi-prep HPLC (isocratic system 90% MeCN/H_2O, v/v) to give compounds **3** (t_R5.8 min; 9 mg) and **2** (t_R9.9 min; 11 mg).

Encindolene I (***1***): white powder; [α]25 D-10 (*c* 0.1, MeOH); UV (MeOH) λ_{max} (log ε): 288 (2.96), 233 (3.47) nm;IR (KBr) ν_{max}: 3391, 2,961, 2,923, 1,667, 1,453, 1,260, 1,024 cm^{-1}; ECD (MeOH) λ_{max} 205 (−13.71), 229 (+4.43), 260 (+4.57), 325 (+6.60) nm. ^1H and ^{13}C NMR data, Tables 1, 2; HRESIMS *m/z*542.2862 $[M+Na]^+$ (calcd for $C_{32}H_{41}NO_5Na$, 542.2877).

Encindolene J (***2***): white powder; [α]25 D-11 (*c* 0.1, MeOH); UV (MeOH) λ_{max} (log ε): 283 (3.06), 231 (3.56) nm;IR (KBr) ν_{max}: 3453, 2,953, 2,921, 1,670, 1,453, 1,375, 1,172 cm^{-1}; ECD (MeOH) λ_{max} 207 (−26.39), 226 (+5.56), 248 (+10.57), 302 (+2.26) nm. ^1H and ^{13}C NMR data, Tables 1, 2; HRESIMS *m/z*542.2864 $[M+Na]^+$ (calcd for $C_{32}H_{41}NO_5Na$, 542.2877).

Encindolene K (***3***): white powder; [α]25 D + 354 (*c* 0.1, MeOH); UV (MeOH) λ_{max} (log ε): 283 (3.06), 231 (3.50) nm;IR (KBr) ν_{max}: 3427, 2,930, 1,660, 1,373, 1,298, 1,180 cm^{-1}; ECD (MeOH) λ_{max} 204 (−12.42), 223 (+4.43), 239 (−12.73), 325 (+18.33) nm. ^1H and ^{13}C NMR data, Tables 1, 2; HRESIMS *m/z*502.2947 $[M+H]^+$ (calcd for $C_{32}H_{40}NO_4$, 502.2952).

Encindolene L (***4***): white powder; [α]25 D + 52 (*c* 0.1, MeOH); UV (MeOH) λ_{max} (log ε): 288 (2.98), 233 (3.47) nm;IR (KBr) ν_{max}: 3428, 2,929, 2,923, 1,660, 1,451, 1,297, 1,179 cm^{-1}; ECD (MeOH) λ_{max} 207 (−8.98), 225 (+6.60), 242 (−10.71), 325 (+16.67) nm. ^1H and ^{13}C NMR data, Tables 1, 2; HRESIMS *m/z*502.2950 $[M+H]^+$ (calcd for $C_{32}H_{40}NO_4$, 502.2952).

TABLE 1 The ^{13}C NMR (100MHz) data of compounds, 1-4 in CD_3OD.

Position	1	2	3	4
	δ_C			
1	125.7, C	124.8, C	124.8, C	125.7, C
2	117.2, CH	132.7, C	132.7, C	117.2, CH
3	132.3, C	118.4, CH	118.4, CH	132.3, C
4	120.9, CH	120.3, CH	120.3, CH	120.9, CH
5	111.6, CH	109.7, CH	109.8, CH	111.6, CH
6	139.5, C	140.9, C	141.1, C	139.7, C
7	27.3, CH_2	29.4, CH_2	29.4, CH_2	27.3, CH_2
8	116.1, C	115.8, C	115.8, C	116.0, C
9	153.1, C	152.2, C	152.0, C	152.9, C
10	51.3, C	51.1, C	50.9, C	51.2, C
11	50.2, CH	50.5, CH	50.2, CH	50.0, CH
12	21.5, CH_2	21.5, CH_2	21.6, CH_2	21.7, CH_2
13	33.5, CH_2	33.7, CH_2	32.7, CH_2	32.7, CH_2
14	77.2, C	77.2, C	75.3, C	75.3, C
15	43.4, C	43.5, C	43.5, C	43.5, C
16	26.0, CH_2	26.0, CH_2	31.5, CH_2	31.5, CH_2
17	28.1, CH_2	28.1, CH_2	112.7, CH	112.7, CH
18	98.4, C	98.4, C	145.7, C	145.7, C
19	160.6, C	160.7, C	156.0, C	156.0, C
20	122.1, CH	122.1, CH	116.3, CH	116.3, CH
21	198.4, C	198.3, C	196.9, C	196.9, C
22	78.5, CH	78.6, CH	86.4, CH	86.4, CH
23	72.4, C	72.3, C	73.9, C	73.8, C
24	24.9, CH_3	24.9, CH_3	25.9, CH_3	25.9, CH_3
25	25.2, CH_3	25.2, CH_3	26.0, CH_3	26.0, CH_3
26	19.4, CH_3	19.3, CH_3	20.4, CH_3	20.4, CH_3
27	15.7, CH_3	15.6, CH_3	15.8, CH_3	15.9, CH_3
1'	34.8, CH_2	32.4, CH_2	32.4, CH_2	34.7, CH_2
2'	125.4, CH	124.8, CH	124.8, CH	125.4, CH
3'	131.1, C	131.2, C	131.2, C	131.0, C
4'	25.2, CH_3	25.2, CH_3	25.2, CH_3	25.2, CH_3
5'	17.1, CH_3	17.3, CH_3	17.3, CH_3	17.1, CH_3

Preparation of primary hepatocytes and cell viability assay

Primary hepatocytes were isolated from male C57BL/6J mice (Jinan Pengyue Experimental Animal Breeding Co. Ltd) by an improved two-step collagenase infusion (Xiao et al., 2017). All experiments and animal care conducted in accordance with the Provision and General Recommendation of Chinese Experimental Animals Administration Legislation and were approved by the Animal Ethics Committee of Shandong Agriculture University. Primary mouse hepatocytes were maintained in DMEM medium with 10% fetal bovine serum (FBS). After attachment, the cells incubated with 100 nM glucagon, as well as the tested compounds. After 24 h, MTT solution was added and incubated for 4 h. The purple crystals were dissolved with dimethylsulfoxide (DMSO) and the absorbance value was determined at 570 nm.

Hepatic glucose production and intracellular cAMP measurement

Primary hepatocytes on 48-well plates were maintained in DMEM (10% FBS) medium. After attachment, the media was replaced with Krebs-Ringer HEPES buffer to fast the cells for 2 h. Then, the cells were cultured with glucose out media supplemented with 10 mM pyruvate, 100 nM glucagon, or with metformin (1 mM) and the tested compounds (1, 20, 40, 80, and 160 μm). After 6 h, the cell supernatant was collected for glucose analysis. For intracellular cAMP measurement, primary hepatocytes were treated with the tested compounds in the presence or absence of 100 nM glucagon for 4 h. cAMP was calculated in primary hepatocytes with an ELISA kit. All data were expressed as the mean ± SD from at least three independent experiments.

Results and discussion

Structure elucidation of compounds

Compound **1** was assigned the molecular formula $C_{32}H_{41}NO_5$ by HRESIMS, with 13 degrees of double-bond equivalents. The ^{13}C and HSQC NMR spectra (Table 1) of **1** revealed a total of 32 carbons including eight aromatic carbons (three protonated) corresponding to one indole moiety, four olefinic carbons attributed to two double

TABLE 2 The ^{1}H NMR (400MHz) data of compounds, 1-4 in CD_3OD.

Position	1	2	3	4
	δ_H (*J* in Hz)			
2	7.09, s			7.07, s
3		6.70, d (7.8)	6.70, d (7.8)	
4	6.81, br d (8.1)	6.87, t (7.8)	6.87, t (7.8)	6.79, br d (8.3)
5	7.14, br d (8.1)	7.10, d (7.8)	7.12, d (7.8)	7.17, d (8.3)
7	2.35, dd (11.6, 11.6)	2.52, overlap	2.53, dd (13.0, 14.6)	2.35, overlap
	2.66, overlap	2.81, overlap	2.82, overlap	2.66, overlap
11	2.70, overlap	2.84, m	2.82, m	2.80, m
12	1.63, m	1.70, m	1.70, m	1.74, m
	2.01, m	2.04, m	2.10, m	2.06, m
13α	1.63, overlap	1.77, overlap	2.07, m	2.07, m
13β	1.60, overlap	1.70, overlap	1.98, m	1.97, m
16α	2.47, m	2.48, m	2.38, dd (17.7, 6.5)	2.38, overlap
16β	1.73, m	1.75, m	3.18, br d (17.7)	3.18, br d (17.7)
17α	2.53, m	2.55, m	5.75, m	5.75, m
17β	1.99, m	1.99, m		
20	5.80, s	5.87, s	5.96, s	5.95, s
22	4.05, s	4.07, s	4.12, s	4.12, s
24	1.31, s	1.32, s	1.32, s	1.32, s
25	1.30, s	1.31, s	1.26, s	1.26, s
26	0.85	1.02	1.09	1.07
27	1.28, s	1.32, s	1.35, s	1.35, s
1'	3.37, d (7.6)	3.57, m	3.56, m	3.36, d (7.6)
2'	5.38, br t (7.6)	5.36, br t (7.2)	5.36, br t (7.2)	5.36, br t (7.6)
4'	1.74, br s	1.74, br s	1.73, br s	1.74, br s
5'	1.75, br s	1.76, br s	1.76, br s	1.74, br s

bonds, four oxygenated sp^3 carbons with one protonated, two sp^3 quaternary carbons, six sp^3 methylenes, one sp^3 non-protonated methine, and six methyls. The presence of a prenyl group was demonstrated by HMBC correlations from the two methyls H_3-4′ and H_3-5′ (δ_H 1.74 and 1.75) to one olefinic quaternary carbon (δ_C 125.4) and one olefinic methine (δ_C 131.1) and COSY correlation between the olefinic proton H-2′ (δ_H 5.38) and the methylene protons H_2-1′ (δ_H 3.37). The above data were quite similar to those of the known compound 3-methyl-2-butenylpaspaline (**5**) (Cole et al., 1977), with the main differences being the chemical shifts for the two oxygenated carbons C-18 and C-22, which were δ_C 98.4 and 78.5 for **1** while 104.4 and 88.0 for **5** (Cole et al., 1977). These data, as well as the less of a H_2O in the molecule formula compared to that of **5** deduced from the HRESIMS data, suggested that the connection between C-18 and C-22 in **5** was cleaved through hydrolysis to afford **1**. The HMBC and COSY data (Figure 2) further confirmed this deduction. The relative configuration of **1** was assigned by the analysis of its ROESY spectrum (Figure 3). ROESY correlations of H-11/H_3-26/Hβ-13 suggested the same orientation of these protons and the trans-diaxial relationship of H_3-26 and OH-14, while correlation of H_3-27/Hα-16 indicated that these protons located at the face opposite to H_3-26. ROESY correlations of H_3-26/Hβ-17/H_3-25 suggested the same face of these protons, indicating the α orientation of OH-18 and H-22. The experimental ECD spectrum (Figure 4) of **1** showed negative Cotton effects (CEs) around 206, 239, and 373 nm, and positive ones around 228, 220, and 326 nm, respectively (Figure 4), which were very similar to those for encindolenes D and E (Pan G. et al., 2021), two analogs isolated from the same fungus. This led to the assignment of the absolute configurations of **1** as shown in Figure 1.

Compound **2** was obtained as a white powder, and its molecular formula was determined to be the same as that of **1** according to the HRESIMS data, with a molecule of H_2O less than **1**. The NMR data of **2** were also quite similar to those of **1**. The main differences between the ^{1}H NMR spectra of them were that signals attributed to a 1,2,3-trisubstituted benzene ring in **2** replaced those corresponding to a 1,2,6-trisubstituted benzene ring in **1**, indicating the location of the prenyl at C-2 or C-5 in **2**. HMBC correlations from the methylene protons of the prenyl group H_2-1′ to C-1, C-2, and C-3 in the indole group and COSY correlations of H-3/H-4/H-5 further confirmed this deduction. Their remaining substructures were determined to be identical according to the 2D NMR data. The relative configuration of **2** was deduced to be the same as that of **1** based on their similar NMR chemical shifts. ROESY correlations (Figure 3) of H-11/H_3-26/Hβ-17/H-24 (25) suggested the face of these protons. ROESY correlation (Figure 3) of H_3-27/Hα-16 indicated that these protons located at the face opposite to H_3-26. These data further confirming the above deduction. The absolute configurations of **2** were also assigned as shown in Figure 1 by a comparison of its ECD spectrum with that of **1** (Figure 4), which showed great similarity.

The molecular formula of compound **3** was established as $C_{32}H_{39}NO_4$ by HRESIMS, with one H_2O less compared to **1** and **2**. The NMR spectra of **3** were closely related to those of **2**, indicating that **3** was also a prenylated indole-diterpenoid. A comparison of the NMR data between **2** and **3** revealed the absence of the dioxygenated non-protonated carbon C-18 and a methylene and the presence of an additional trisubstituted double bond in **2** compared to **3**. COSY correlations of H_2-16 with the olefinic proton H-17 and HMBC correlation from H_2-16 to C-17 and C-18 suggested that dehydration occurred at C-17/C-18 in **2** to afford compound **3**. The relative configuration of **3** was proposed to be the same as that of **2** based on a biosynthetic consideration, which was further confirmed by NOESY correlations of H-11/H_3-26/Hβ-13 and H_3-27/Hα-16. The ECD spectra of **3** were quite similar to those of **1** and **2** (Figure 4), thus assigning their same absolute configurations for the chiral carbons C-10, C-11, C-14, C-15, C-22, and C-23.

The molecular formula of compound **4** was established to be the same as that of **3** by HRESIMS. Their NMR data were also quite similar. A comparison of the NMR data of **4** with those of **1** revealed that they bear the same 3-prenylated indole moiety. The remaining NMR data of **4** were nearly identical to those of **3**. The above data led to the determination of the structure of **4**, and the only difference between it and **3** was the location of the prenyl group,

10.3389/fmicb.2023.1099103

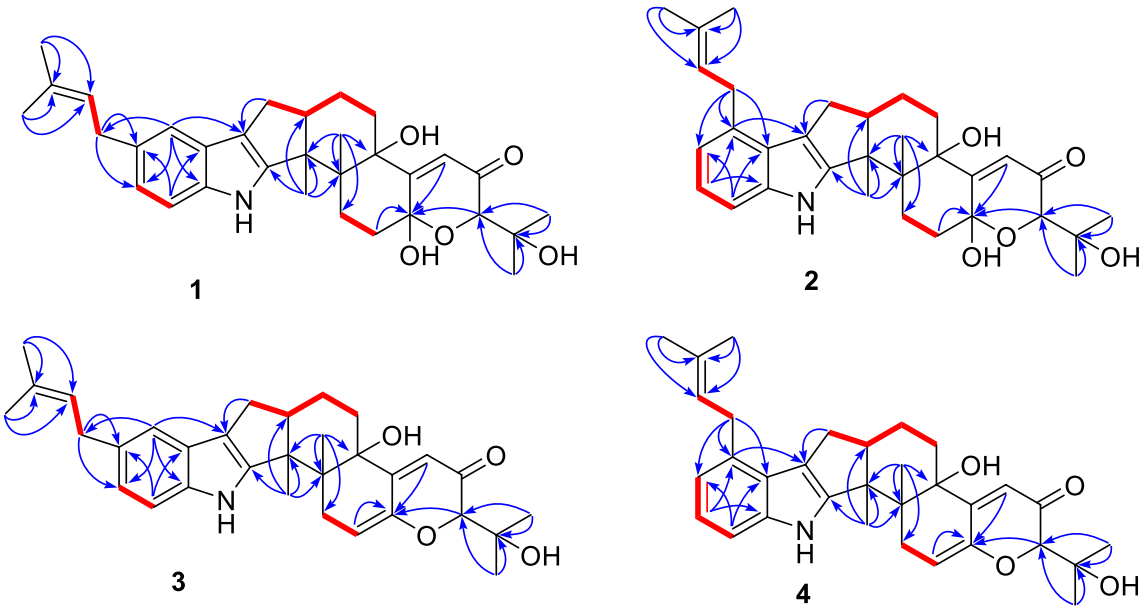

FIGURE 2
Selected HMBC and COSY correlations of compounds **1**-**4**.

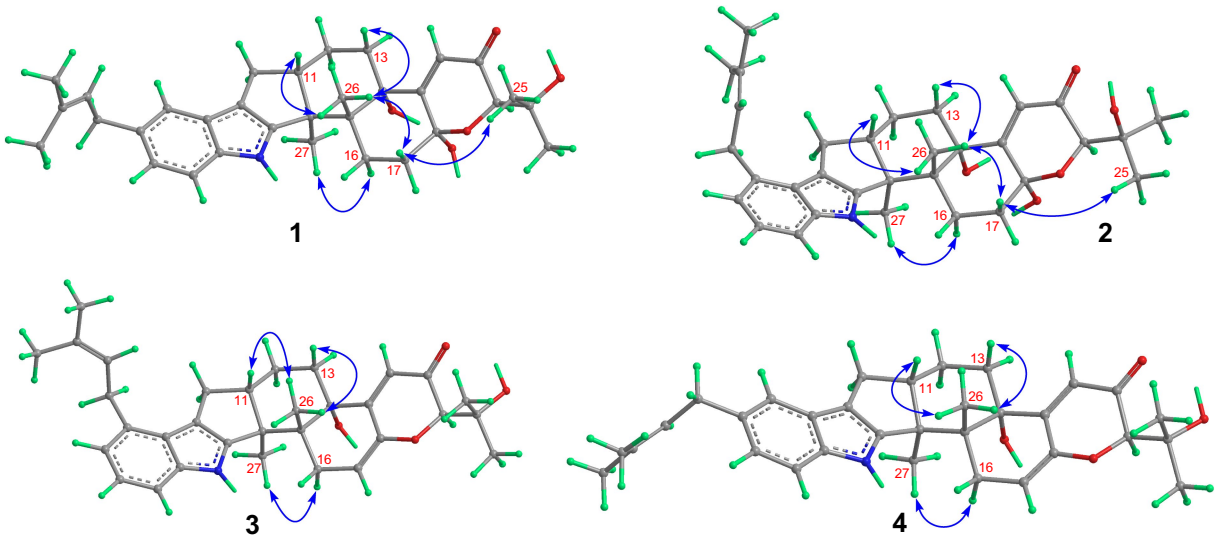

FIGURE 3
Selected ROESY correlations of compounds **1**-**4**.

which was C-2 in **4**. HMBC correlations from H_2-1′ to C-2, C-3, and C-4, as well as COSY correlations of H-4/H-5, further confirmed this deduction. The relative configuration of **4** was deduced to be the same as that of **3** by their similar NMR data (Tables 1, 2). ROESY correlations of H-11/H_3-26/Hβ-13 and H_3-27/Hα-16 further confirmed this deduction. The absolute configuration of **4** was also assigned to be the same as that of **3** by their similar ECD curves (Figure 4).

Compounds **1**-**5** are structurally closely related. Compounds **1** and **4** could be the dehydration products of **5**, while **2** and **3** could be the dehydration products of another known compound paspalitrem C. Therefore, it is necessary to define whether these compounds were artificial products due to acidic dehydration during the purification process and find the reaction conditions of mutual transformation between them to lay a foundation for the accumulation of these compounds. The experiment of mutual transformation between these compounds was performed. The results indicated that compound **5** could be converted to compounds **1** and **4** in 0.1% trifluoroacetic acid in methanol, and paspalitrem C, a previously isolated analog from the same fungus, can be converted to compounds **2** and **3** under the same conditions (Scheme 1). However, after the treatment of silica gel and C18,

there is no structural transformation, but in other strong acids such as hydrochloric acid and sulfuric acid, the compound is basically degraded without effective results. These results indicated that the production of compounds **1**-**4** is probably the result of enzyme catalysis, but it cannot exclude the possibility that compounds **1**-**4** may be artificial products from **5** and paspalitrem C due to the slightly acidic growth environment in the late stage of cultivation. These results also suggested that the absolute configurations of all the chiral carbon except for C-18 in **1**, **2**, and **5** were the same.

Until now, a total of 17 indole-terpenoids including compounds **1**-**5** and other twelve previously reported analogs such as encindolenes A-C, 18-O-methyl-encindolene A (Pan G. et al., 2021), encindolenes D-H (Xiao et al., 2022), paspalitrem C (Dorner et al., 1984), 7-methoxypaxilline (Ariantari et al., 2019), and 7-hydroxy-13-dehydroxypaxilline (Peter and Christopher, 1994) have been identified from *Penicillium* sp. HFF16, and the plausible biosynthetic pathway of the eight different skeletons was shown in Scheme 2. It was proposed that 7-hydroxy-13-dehydroxypaxilline was the main precursor of all the paxilline-type indole-terpenoids, which could undergo prenylation, dehydration, methoxylation, and cyclization occurred to afford the other analogs.

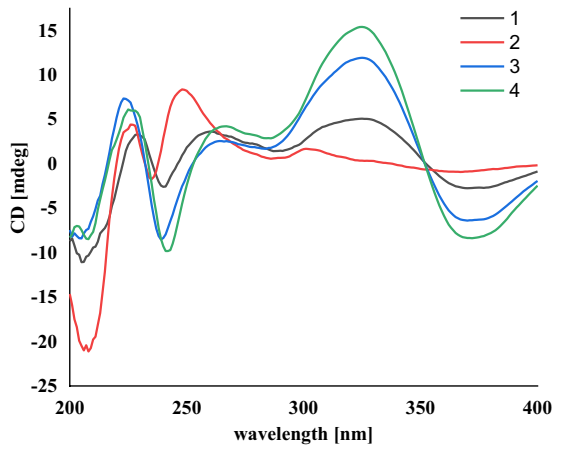

FIGURE 4
The experimental ECD spectra of compounds **1**-**4**.

Antidiabetic activity assay

All the compounds were evaluated for cell viability at a concentration of 160 μM, and with this result, all the tested compounds (cell viability >90%) were selected for subsequent glucose output inhibition experiment (Figure 5). Glucose output in response to all the nontoxic compounds was measured to assess the antidiabetic effects in hepatocytes. Glucagon promotes hepatic glycogenolysis and increases hepatic gluconeogenesis, and we showed that glucagon challenge increased hepatic glucose output. Compounds **1**-**5** inhibited hepatic glucose output and their EC_{50} values (67.23, 102.1, 49.46, 25.20, and 35.96 μM) were higher than that of the positive control metformin (EC_{50} = 5.09 μM). Cyclic AMP (cAMP) as an intracellular second messenger is crucial for glucagon-induced hepatic glucose production. Glucagon challenge increased intracellular cAMP content, while compounds **1**-**5** treatment suppressed cAMP accumulation in hepatocytes. The results suggested that tested compounds inhibited hepatic glucose output may be by suppression hepatic cAMP accumulation.

Conclusion

In our previous study, nine new indole-diterpenoids were isolated from the secondary metabolites of *Penicillium* sp. HFF16 and evaluated their anti-inflammatory and hypoglycemic activities. The results showed that encindolene C had the best anti-inflammatory activity compared with other compounds in RAW.2647 cells stimulated by LPS. Through simple structural analysis, it was speculated that the existence of prenyl group was beneficial to the improvement of anti-inflammatory activity. In HepG2 cells stimulated by glucagon, encindolene L showed the best inhibitory activity on hepatic glycogen export compared with other compounds. Structural analysis showed that encindolene L also had a prenyl group and indole and diterpene did not form a fused ring structure, again suggesting the importance of prenyl group in improving the biological activity of compounds. In consideration of such valuable work and the fact that the compound belongs to the tryptophan pathway of biosynthesis, the strain is subjected to secondary fermentation after a small amount

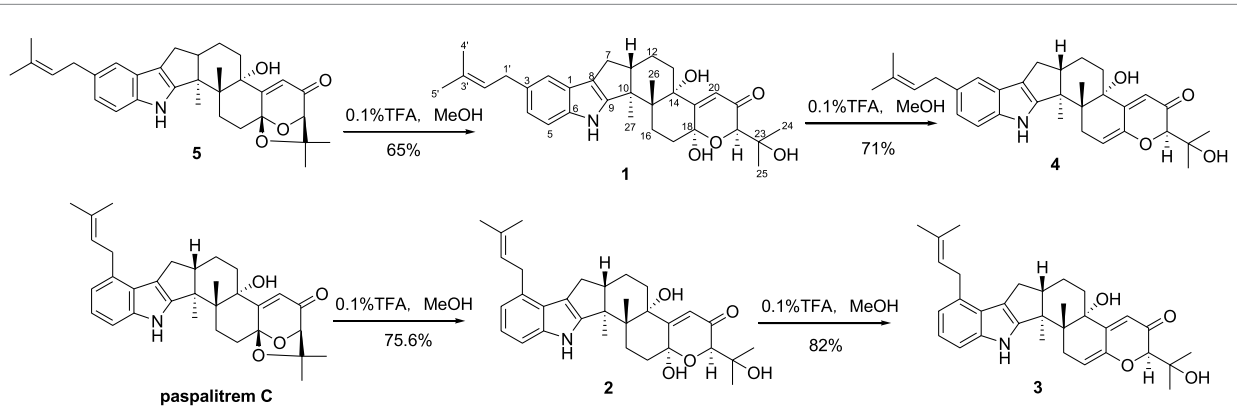

SCHEME 1
The transformation of **5** to **1** and **4** and paspalitrem C to **2** and **3** in acidic reaction condition.

10.3389/fmicb.2023.1099103

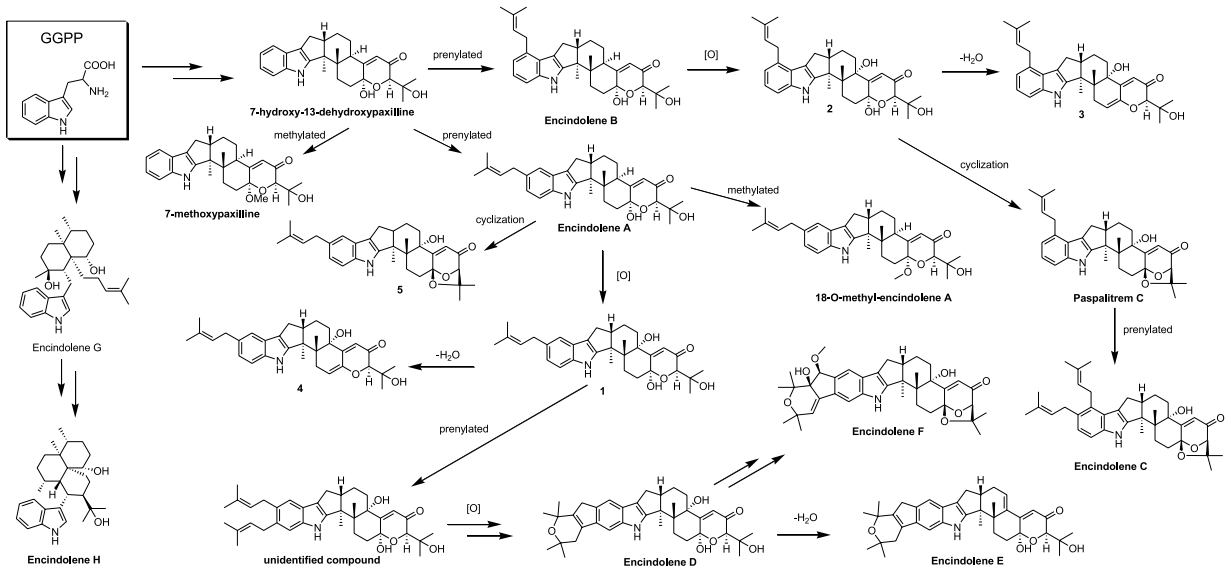

SCHEME 2
Hypothetical biosynthetic pathway for the skeletons of the indole-terpenoids isolated from *Penicillium sp.* HFF16.

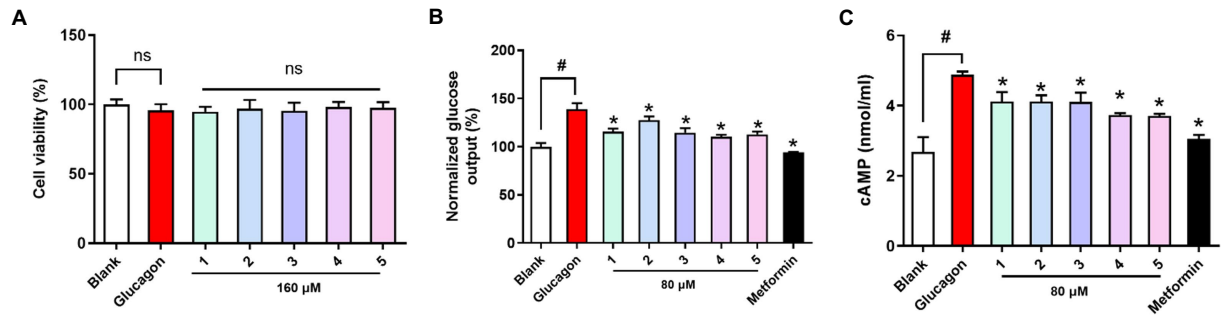

FIGURE 5
Viability and antidiabetic effects of compounds **1**–**5** against primary hepatocytes. **(A)** Cell viability **(B)** hepatic glucose output level; **(C)** cAMP contents in primary hepatocytes treated with glucagon (100nM). Metformin (1mM) as the positive control. ^{ns}p >0.05 vs. Blank, $^{*}p$<0.05 vs. Glucagon, $^{\#}p$<0.05 vs. Blank.

of tryptophan is added to a rice culture medium. Four new indole-diterpenoid encindolenes I-L containing prenyl moieties were isolated and identified. Hypoglycemic activity was evaluated by mouse primary hepatocytes, and the results showed that encindolenes I-L could inhibit the increase of cAMP production induced by glucagon and reduce hepatic glucose output, thus exerting hypoglycemic effect. From the structural analysis, it was found that the compounds containing semi-acetal group had the worst hypoglycemic activity and the dehydration compound had the best activity, suggesting that semi-acetal group was harmful to biological activity. The comparison of the structure and activity results of encindolenes I and J suggests that the different substitution positions of the prenyl group have a significant effect on the activity.

Data availability statement

The original contributions presented in the study are included in the article/Supplementary material, further inquiries can be directed to the corresponding author.

Ethics statement

The animal study was reviewed and approved by All experiments and animal care conducted in accordance with the Provision and General Recommendation of Chinese Experimental Animals Administration Legislation and were approved by the Animal Ethics Committee of Shandong Agriculture University.

Author contributions

NX and LZ contributed to bioactivity assay and revised the manuscript. GP conceived and designed the experiments and was involved in isolation of compounds. XjL, XyL, MZ, FL, and XlL contributed to isolation and collection of the NMR data of compounds. XK, JB, XyL, DK, and GH performed strain fermentation and extraction. FK supervised the study and prepared the manuscript. All authors contributed to the article and approved the submitted version.

Funding

This study was financially supported by the Natural Science Foundation of Shandong Province (ZR2021MB087), the National Natural Science Foundation of China (82004014), the Shandong traditional Chinese Medicine Science and Technology Project (2021Q083), the Innovation and entrepreneurship training program for college students in Shandong Province (202210439005, 202214039008), the Specific research project of Guangxi for research bases and talents (AD18126005), and the Natural Science Foundation of Guangxi (2021GXNSFBA075036).

Conflict of interest

The authors declare that the research was conducted in the absence of any commercial or financial relationships that could be construed as a potential conflict of interest.

Publisher's note

All claims expressed in this article are solely those of the authors and do not necessarily represent those of their affiliated organizations, or those of the publisher, the editors and the reviewers. Any product that may be evaluated in this article, or claim that may be made by its manufacturer, is not guaranteed or endorsed by the publisher.

Supplementary material

The Supplementary material for this article can be found online at: https://www.frontiersin.org/articles/10.3389/fmicb.2023.1099103/full#supplementary-material

References

Ariantari, N. P., Ancheeva, E., Wang, C., Mándi, A., Knedel, T. O., Kurtán, T., et al. (2019). Indole Diterpenoids from an *Endophytic Penicillium* sp. *J. Nat. Prod.* 82, 1412–1423. doi: 10.1021/acs.jnatprod.8b00723

Cole, R. J., Dorner, J. W., Lansden, J. A., Cox, R. H., Pape, C., Cunfer, B., et al. (1977). Paspalum staggers: isolation and identification of tremorgenic metabolites from sclerotia of *Claviceps paspali*. *J. Agric. Food Chem.* 25, 1197–1201. doi: 10.1021/jf60213a061

Dorner, J. W., Cole, R. J., Cox, R. H., and Cunfer, B. M. (1984). Paspalitrem C, a new metabolite from sclerotia of *Claviceps paspali*. *J. Agric. Food Chem.* 32, 1069–1071. doi: 10.1021/jf00125a033

Kong, F. D., Fan, P., Zhou, L. M., Ma, Q. Y., Xie, Q. Y., Zheng, H. Z., et al. (2019). Penerpenes A-D, four indole terpenoids with potent protein tyrosine phosphatase inhibitory activity from the marine-derived fungus *Penicillium* sp. KFD28. *Org. Lett.* 21, 4864–4867. doi: 10.1021/acs.orglett.9b01751

Lewis, G. F., Carpentier, A. C., Pereira, S., Hahn, M., and Giacca, A. (2021). Direct and indirect control of hepatic glucose production by insulin. *Cell Metab.* 33, 709–720. doi: 10.1016/j.cmet.2021.03.007

Liao, W., Yang, W., Shen, Z., Ai, W., Pan, Q., Sun, Y., et al. (2021). Heme Oxygenase-1 regulates ferrous iron and Foxo1 in control of hepatic gluconeogenesis. *Diabetes* 70, 696–709. doi: 10.2337/db20-0954

Pan, G. J., Li, Y. L., Che, X. Y., Tian, D., Han, W. J., Wang, Z. M., et al. (2021). New Thio-compounds and Monoterpenes with anti-inflammatory activities from the fungus *Aspergillus* sp. CYH26. *Front. Microbiol.* 12:668938. doi: 10.3389/fmicb.2021.668938

Pan, G., Zhao, Y., Ren, S., Liu, F., Xu, Q., Pan, W., et al. (2021). Indole-Terpenoids with anti-inflammatory activities from *Penicillium* sp. HFF16 associated with the Rhizosphere soil of *Cynanchum bungei* Decne. *Front. Microbiol.* 12:710364. doi: 10.3389/fmicb.2021.710364

Peter, G. M., and Christopher, M. W. (1994). Biosynthesis and transformation of tremorgenic indolediterpenoids by *Penicillium paxilli* and *Acremonium lolii*. *Phytochemistry* 36, 1209–1217. doi: 10.1016/S0031-9422(00)89639-9

Shankar, A., and Sharma, K. K. (2022). Fungal secondary metabolites in food and pharmaceuticals in the era of multi-omics. *Appl. Microbiol. Biotechnol.* 106, 3465–3488. doi: 10.1007/s00253-022-11945-8

Unger, R. H., and Cherrington, A. D. (2012). Glucagonocentric restructuring of diabetes: a pathophysiologic and therapeutic makeover. *J. Clin. Invest.* 122, 4–12. doi: 10.1172/JCI60016

Xiao, N., Lou, M. D., Lu, Y. T., Yang, L. L., Liu, Q., Liu, B., et al. (2017). Ginsenoside Rg5 attenuates hepatic glucagon response via suppression of succinate-associated HIF-1α induction in HFD-fed mice. *Diabetologia* 60, 1084–1093. doi: 10.1007/s00125-017-4238-y

Xiao, N., Xu, Y., Zhang, X., Li, H., Zhang, S., Xiao, A., et al. (2022). Anti-diabetic Indole-Terpenoids from *Penicillium* sp. HFF16 isolated from the Rhizosphere soil of *Cynanchum bungei* Decne. *Front. Chem.* 9:792810. doi: 10.3389/fchem.2021.792810

Zhang, R., Liu, W., Zeng, J., Meng, J., Jiang, H., Wang, J., et al. (2022). Niemann-pick C1-like 1 inhibitors for reducing cholesterol absorption. *Eur. J. Med. Chem.* 230:114111. doi: 10.1016/j.ejmech.2022.114111

Zhang, W. S., Pan, A., Zhang, X., Ying, A., Ma, G., Liu, B. L., et al. (2019). Inactivation of NF-κB2 (p52) restrains hepatic glucagon response via preserving PDE4B induction. *Nat. Commun.* 10:4303:4303. doi: 10.1038/s41467-019-12351-x

frontiers | Frontiers in Microbiology

TYPE Review
PUBLISHED 17 April 2023
DOI 10.3389/fmicb.2023.1177123

OPEN ACCESS

EDITED BY
Dewu Zhang,
Chinese Academy of Medical Sciences, China

REVIEWED BY
Gang Li,
Qingdao University, China
Bin Wei,
Zhejiang University of Technology, China

*CORRESPONDENCE
Xinli Wei
✉ weixl@im.ac.cn

RECEIVED 01 March 2023
ACCEPTED 24 March 2023
PUBLISHED 17 April 2023

CITATION
Ren M, Jiang S, Wang Y, Pan X, Pan F and Wei X (2023) Discovery and excavation of lichen bioactive natural products.
Front. Microbiol. 14:1177123.
doi: 10.3389/fmicb.2023.1177123

Discovery and excavation of lichen bioactive natural products

Meirong Ren[1], Shuhua Jiang[2], Yanyan Wang[2], Xinhua Pan[3], Feng Pan[3] and Xinli Wei[2]*

[1]Key Laboratory of Biodiversity Conservation in Southwest China, State Forestry Administration, Southwest Forestry University, Kunming, China, [2]State Key Laboratory of Mycology, Institute of Microbiology, Chinese Academy of Sciences, Beijing, China, [3]Jiangxi Xiankelai Biotechnology Co., Ltd., Jiujiang, China

Lichen natural products are a tremendous source of new bioactive chemical entities for drug discovery. The ability to survive in harsh conditions can be directly correlated with the production of some unique lichen metabolites. Despite the potential applications, these unique metabolites have been underutilized by pharmaceutical and agrochemical industries due to their slow growth, low biomass availability, and technical challenges involved in their artificial cultivation. At the same time, DNA sequence data have revealed that the number of encoded biosynthetic gene clusters in a lichen is much higher than in natural products, and the majority of them are silent or poorly expressed. To meet these challenges, the one strain many compounds (OSMAC) strategy, as a comprehensive and powerful tool, has been developed to stimulate the activation of silent or cryptic biosynthetic gene clusters and exploit interesting lichen compounds for industrial applications. Furthermore, the development of molecular network techniques, modern bioinformatics, and genetic tools is opening up a new opportunity for the mining, modification, and production of lichen metabolites, rather than merely using traditional separation and purification techniques to obtain small amounts of chemical compounds. Heterologous expressed lichen-derived biosynthetic gene clusters in a cultivatable host offer a promising means for a sustainable supply of specialized metabolites. In this review, we summarized the known lichen bioactive metabolites and highlighted the application of OSMAC, molecular network, and genome mining-based strategies in lichen-forming fungi for the discovery of new cryptic lichen compounds.

KEYWORDS

lichen, natural products, bioactivity, PKS, OSMAC strategy, genome mining

Introduction

Plant-derived natural products or their derivatives were a valuable source of therapeutic agents and played a key role in the treatment of various diseases, e.g., cancer chemotherapy, infectious diseases, cardiovascular diseases, and lipid metabolism disorders (Mann, 2002; Newman and Cragg, 2012; Atanasov et al., 2015; Waltenberger et al., 2016). However, natural plant product-based drug discovery has some difficulties because of technical barriers to screen natural products in high-throughput assays against molecular targets and synthetic compounds not meeting the expectations of an increasing number of new drugs reaching the market (Atanasov et al., 2015), thus scientists have had to turn their attention to other

organisms. Microbes have proven to be a bountiful source of secondary metabolites that have been successfully developed as crucial drug leads. We have already known that the structures of over 80,000 natural products from microbes (Demain, 2014) and over 80% of the antibiotics are produced by microbes (de Lima Procópio et al., 2012) since the discovery of penicillin in 1928 (Demain, 2014). Due to the extensive use of antibiotics for common infections, pathogens are showing high resistance (Harikumar and Krishanan, 2022); therefore, there is an urgent need for finding novel drugs. Grube made a point of view that microbial symbioses have a high potential leading to a wide variety of unique structures and metabolic activities (Grube and Berg, 2009).

Several studies have shown that lichens are productive organisms for the synthesis of a broad range of secondary metabolites. Lichen is a stable community in the ecosystem of the Earth's biosphere, which is composed of a mutualistic relationship between fungi and algae or between fungi and cyanobacteria (Figure 1). However, the identity of lichens is considered based on the fungal partner, and to date, the predominant records of lichens that have been identified are ascomycetes in nature. Thus, the term "lichen-forming fungi (LFF)" refer to the fungi that live in lichen thallus throughout the entire life cycle by establishing a co-benefit symbiotic relationship without causing any adverse effect and are different from those endolichenic fungi (Muggia et al., 2009).

Evidence from lichen fossils indicated that the interactions between fungi and algae have existed for at least 400 million years (Lücking and Nelsen, 2018), and studies have shown that lichen occurs over 10% of the terrestrial surface, especially extreme and aggressive environmental conditions that are not conducive to individual survival, such as extreme cold Arctic and Antarctic regions (Lee et al., 2014), hot and arid deserts (Kranner et al., 2008), alpine areas with strong UV irradiation, and on rocks or non-fertile soils (de Vera et al., 2003; Seymour et al., 2005; Boustie et al., 2010; Nguyen et al., 2013). This tendency of lichens to tolerate the extreme environment can be correlated with the production of both a unique and diverse range of metabolites known as lichen substances (Schweiger et al., 2022). Fungi and algae co-evolved unique biosynthetic pathways and metabolic mechanisms to synthesize these complex metabolites over a long period of time. Primary and secondary metabolisms are the two main groups of lichen compounds. Primary metabolism is the basic substance constituting the structure of lichen and includes proteins, amino acids, carotenoids, polysaccharides, and vitamins (Goga et al., 2020; Packiam and Perumal, 2022). The fungal filaments provide small, structurally complex, water-insoluble, and crystalline secondary metabolism, which can comprise up to 20% of the dry mass of thallus weight (Nguyen et al., 2013; González-Burgos et al., 2019; Zhao et al., 2021). Unlike primary metabolites, lichen secondary metabolism is not directly involved in growth but synthesized for algae or cyanobacteria protection (Muggia et al., 2009).

Lichens are known to produce small molecular compounds such as aliphatic and aromatic compounds, thus far, over 1,000 compounds have been identified (Shrestha and St. Clair, 2013). According to biosynthetic origins and chemical structures, lichen compounds were classified (Culberson and Elix, 1989), which were synthesized by acetyl-malonate, mevalonate, and shikimate pathways existing in all organisms as key routes for natural metabolism. The biosynthesis of lichen depsides, depsidones, dibenzofurans, chromones, xanthones, and anthraquinones occurs via the acetyl-malonate pathway, by which most bioactive compounds are synthesized, with coenzyme A as the precursor and polyketide synthase (PKS) as the responsible enzyme (Ibrahim et al., 2018). The most common lichen compounds synthesized by this pathway include evernic acid (Muggia et al., 2009), lecanoric acid (Lawrey, 1986), gyrophoric acid (Garima et al., 2022a), atranorin (Lawrey, 1986; Majchrzak-Celinska et al., 2022), thamnolic acid (Culberson et al., 1986; Jeong et al., 2021), umbilicaric acid (Posner et al., 1991; Yoshimura et al., 1994), protocetraric acid (Nishanth et al., 2015), fumarprotocetraric acid (Igoli et al., 2014; Ranković and Mišić, 2014), stictic acid (Bellio et al., 2017; Pejin et al., 2017), usnic acid (Moreira et al., 2015; Sepahvand et al., 2021), lepraric acid (Aberhart et al., 1969; Murugan et al., 2021), and thiophanic acid (Arshad et al., 1968; Dayan and Romagni, 2001). Usnic acid, one of the most common, isolated, and discussed lichen compounds, is well-known as an antibiotic with many pharmacological activities including antibacterial, antiprotozoal, anti-cytotoxic, anti-proliferative, antioxidant, and anti-inflammatory (Cocchietto et al., 2002). The mechanisms of bioactivity of usnic acid modify the structures of proteins causing irreversible changes and may even produce apoptosis. Lichen also produces an array of secondary metabolites derived from the mevalonate pathway, which play essential roles in the regulation of cell growth and development, and the products appear to be potentially interesting therapeutic targets for many areas of research such as oncology, autoimmune disorder, atherosclerosis, and Alzheimer disease (Buhaescu and Izzedine, 2007). The mevalonate pathway is mainly associated with the production of terpenes, steroids, and carotenoids (Goga et al., 2020). Until now, more than 20 different triterpene compounds from lichens have been reported. The shikimic acid pathway, ubiquitous in microorganisms and plants, provides precursors for the biosynthesis of primary metabolites such as aromatic amino acids and folic acid (Wilson et al., 1998). This pathway is mainly related to pulvinic acid and terphenylquinone pigments (Edwards et al., 2003), which help lichen adapt to UV stress by absorption and re-emitting the UV radiation as fluorescence or heat (Nguyen et al., 2013). The representative structures of lichen natural products are shown in Figure 2.

Lichen cells contain many types of natural metabolites and other bioactive molecules, receiving increased attention due to their industrial, pharmaceutical, biotechnological, medical, and cosmetics applications (Elkhateeb and Daba, 2019). Many studies have supported the potentiality of different lichen species to produce unique natural compounds with different physicochemical and biological activities (Hamida et al., 2021). Their utilization in folklore as medicines in the treatment of diverse diseases, such as arthritis, alopecia, constipation, kidney diseases, leprosy, pharyngitis rabies, infection, worm, and infestation for several centuries, has been recorded in different pharmacopeias by native Americans, Haitian, Indians, Chinese, and Europeans (Romagni and Dayan, 2002; Elkhateeb and Daba, 2019). In Table 1, the known lichen natural products with different bioactivities were

10.3389/fmicb.2023.1177123

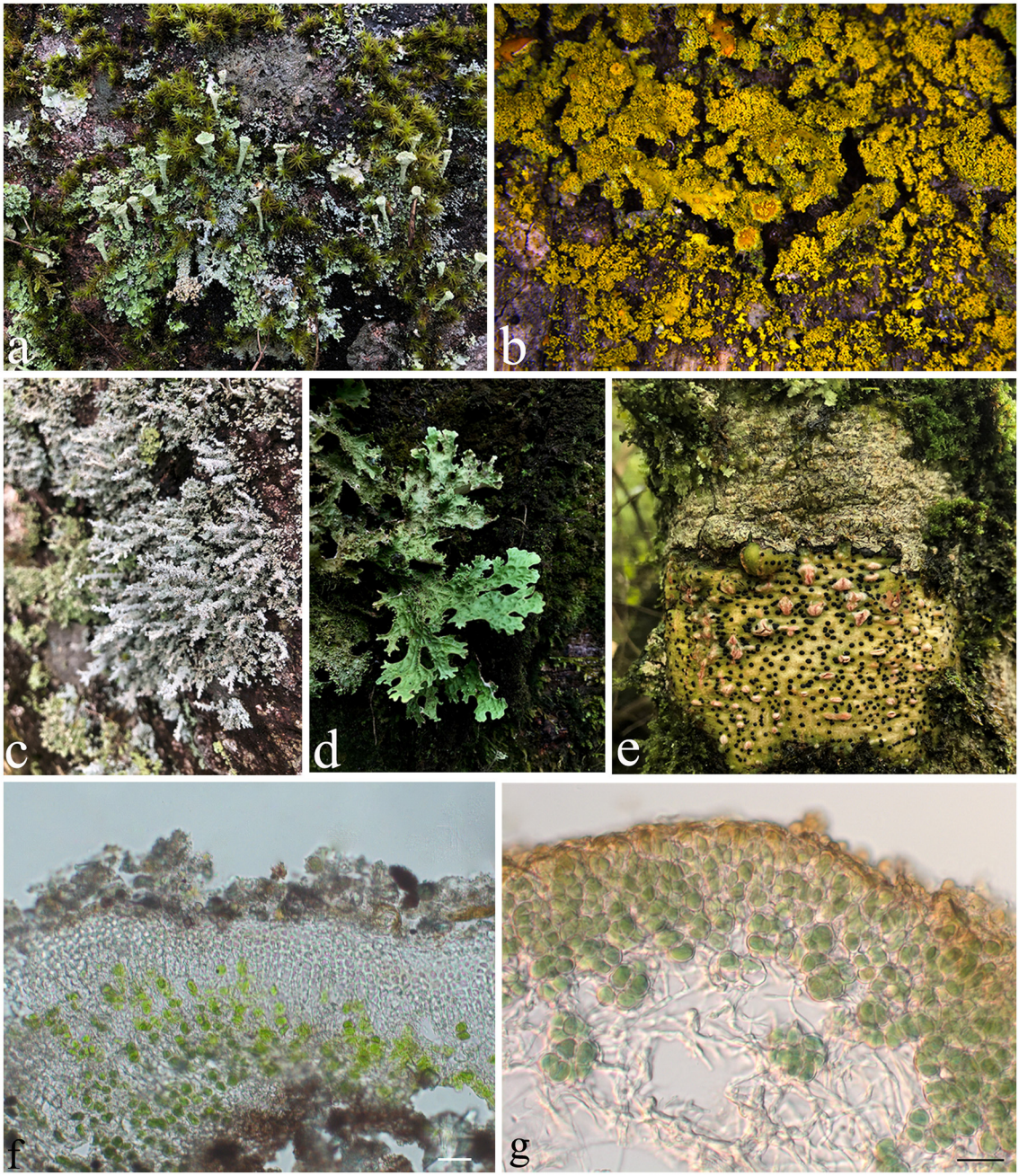

FIGURE 1
The diversity of lichens. **(a)** *Cladonia* sp.; **(b)** *Candelaria* sp.; **(c)** *Stereocaulon* sp.; **(d)** *Sticta* sp.; **(e)** *Pyrenula* sp.; **(f)** Thallus of *Endocarpon pallidulum* in vertical section, with green algae *Diplosphaera chodatii* as the photobiont; **(g)** Thallus of *Peltula submarginata* in vertical section, with cyanobacteria Chroococcales as the photobiont. Photos **(b, f)** were taken by Xue XD and Zhang TT, respectively, and photos **(a, c–e)** were taken by Yang QX. Scale bars: **(f)** = 20 μm, **(g)** = 10 μm.

summarized, among which most were isolated from the natural lichen thallus.

Strategy to discover lichen natural products

Despite the great potential of lichen bioactivity, lichens have been long neglected by mycologists and overlooked by the pharmaceutical industry. One reason is their slow growth in nature and difficult culture in either fermenters or glasshouses, or even cultivated in the open air, and has scarcely been studied from a biochemical perspective; another reason is due to difficulties in obtaining them in sufficient quantities and purities for structural elucidation and pharmacological research. These circumstances prompted lichenologists to develop more suitable strategies to look for more lichen compounds in categories and activities.

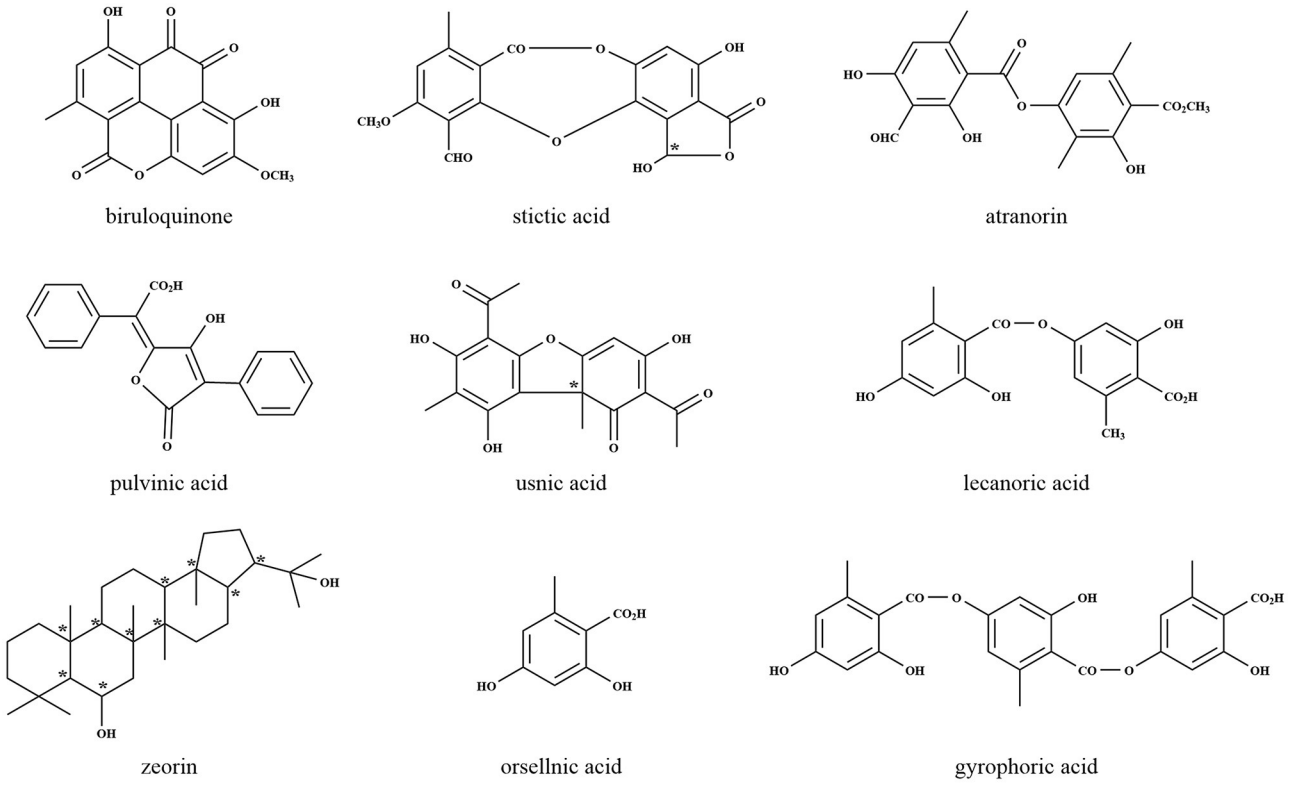

FIGURE 2
Representative lichen metabolites derived by LFF. *Indicates the chiral centers.

OSMAC strategy

To improve the production of a wider range of natural products from a microorganism, different culturing conditions are generally used. Bode et al. refer to the fact that a single strain is capable of producing a diverse array of structural compounds under specific growth conditions (Zahroh et al., 2022), however, never produces the entire compounds at the same time under one set of environmental conditions because it is not matching with a cost between energetic and metabolism (Zarins-Tutt et al., 2016). Very small changes in the cultivation parameters, such as culture medium composition, pH, temperature of growth, salinity, aeration, and even the shape of culture vessel used, can completely alter, induce, or optimize the physiology of a microbial strain and in turn significantly affect the biosynthesis of such metabolites (Bode et al., 2002). For example, bioactivity-guided isolation of the fungus *Aspergillus versicolor* KU258497 yielded two new and six known cryptic metabolites when co-cultivated with the bacterium *Bacillus subtilis* 168 trpC2 on solid rice medium, among which one new compound showed strong cytotoxic activity against the mouse lymphoma cell line L5178Y (Abdelwahab et al., 2018). A corresponding strategy named OSMAC (one strain of many compounds) opened up a new industrial production avenue for compounds needed. For lichens, the majority of the bioactive compounds are exclusively produced by the LFF; however, there are some instances where the symbiotic photobiont, particularly cyanobacteria also engaged in the production of some key secondary metabolites (Cox et al., 2005).

It has been indicated that there is a strong application basis of OSMAC in discovering lichen natural products. Especially, lichenologists from all over the world are becoming more and more interested in not only physiology but also metabolite production (Crittenden and Porter, 1991), thus, they hoped that mycelium from the lichen thallus may be free-grown on artificial medium and produced lichen compounds without the algal or cyanobacterial partners. The tissue culture method invented by Yoshimura et al. (1993), a technique for the separation of the LFF from lichen thallus and culturing it alone, greatly pushed the fulfillment of this process.

However, growth rate and metabolite yield in LFF are inverse relationships (Timsina et al., 2013) and are influenced by culturing conditions, such as the availability and type of carbon and nitrogen source (Calvo et al., 2002; Behera et al., 2006; Verma et al., 2012). Simple sugar such as glucose, sucrose, and polyethylene glycol as sole carbon sources supported high LFF growth and production of usnic acid in *Usnea ghattensis* culture, in contrast, nitrogen sources such as amino acids (glycine, asparagine, alanine, or vitamins), especially glycine, supported the LFF growth but did not well-support usnic acid production (Behera et al., 2006). A strain of LFF isolated from a thallus of *Parmotrema reticulatum* was cultured on different culture media, and all the colonies developed well; however, atranorin, the major cortical lichen depside, was only

TABLE 1 The known lichen bioactive natural products from a thallus or LFF cultures.

Class of compound	Natural compound	Bioactivity	Lichen species	References
Aliphatic and cycloaliphatic compound	D-protolichesterinic acid/nephrosterinic acid	Anticancer	*Ramalina almquistii/Usnea longissima*	Bessadottir et al., 2015; Reddy et al., 2019
	Protolichesterinic acid	Anti-bacterial/inflammatory proliferation/antimicrobial/anticancer	*Hypotrachyna cirrhata/Cornicularia aculeata/Cetraria islandica*	Bessadottir et al., 2014; Furmanek et al., 2021
	Roccellic acid	Antimicrobial	*Roccella montagnei*	Mishra et al., 2017
Anthraquinones	Emodin	Antifungal	*Xanthoria parietina/Caloplaca aurantia/Nephroma laevigatum*	Manojlovic et al., 1998
	Fallacinal	Antifungal	*Xanthoria parietina*	Manojlovic et al., 1998
	Parietin	Cytotoxicity/antimicrobial	*Xanthoria parietina*	Pichler et al., 2021
Depside	Nordivaricatic acid	Human leukocyte elastase inhibitor	*Parmelia saxatilis**	Zheng et al., 2012; Díaz et al., 2020
	Atranorin and derivatives	Anti-hepatitis C virus/anticancer/antimicrobial	*Stereocaulon evolutum/Cladonia rangiferina/Parmotrema austrosinense*	Lawrey, 1986; Kumar et al., 2018; Tekiela et al., 2021; Majchrzak-Celinska et al., 2022
	Baeomycesic acid	Anticancer	*Thamnolia vermicularis* var *subuliformis/T. subuliformis*	Ingolfsdottir et al., 1997
	Chloroatranorin	Antimicrobial	*Pseudevernia furfuracea/Hypotrachyna cirrhata/Parmotrema austrosinense*	Türk et al., 2006; Kumar et al., 2018; Furmanek et al., 2021
	Erythrin	Antioxidant	*Parmotrema grayana*	Thadhani et al., 2011
	Evernic acid	Antibiotics/antioxidant/cytotoxic	*Evernia prunastri/E. divaricata/Pseudoevernia furfuraceae/Roccella montagnei*	Lawrey, 1986; Kosanic et al., 2013; Mishra et al., 2017
	Isidiphorin	Antioxidant	*Usnea longissima/Lobaria pulmonaria*	Atalay et al., 2011
	Isodivaricatic acid	Antifungal/antiprotozoal	*Protousnea poeppigii*	Schmeda-Hirschmann et al., 2008
	Lecanoric acid	Anticancer/antioxidant/inhibitor of histidine decarboxylase/antifungal	*Umbilicaria antarctica/Parmotrema tinctorum/Roccella montagnei/Parmelina tiliacea**	Umezawa et al., 1974; Lopes et al., 2008; Luo et al., 2009; Tatipamula et al., 2019; Díaz et al., 2020; Majchrzak-Celinska et al., 2022
	Lepraric acid	Antibacterial	*Roccella phycopsis*	Parrot et al., 2015
	Olivertoric acid	Antimicrobial	*Pseudevernia furfuracea*	Türk et al., 2006
	Perlatolic acid	Anti-inflammatory	*Cetrelia monachorum*	Oettl et al., 2013
	Squamatic acid	Anticancer	*Cladonia. unclalis*	Majchrzak-Celinska et al., 2022
Depsidone	α-Collatolica acid	Antimicrobial	*Lecanora atra/Arctoparmelia centrifuga**	Neeraj et al., 2011; Pierangelo et al., 2015; Bellio et al., 2017; Díaz et al., 2020
	Lobaric acid	Cytotixic/anti-inflammatory/antimicrobial/enzyme inhibition/muscle relaxant/antioxidant/	*Stereocaulon alpinum/S. paschale/Usnea longissima/Cladonia* sp./*Parmelia saxatilis**	Gissurarson et al., 1997; Seo et al., 2009; Thadhani et al., 2011; Pierangelo et al., 2015; Joo et al., 2016; Kwon et al., 2016; Bellio et al., 2017; Claudia et al., 2018; Hong et al., 2018; Kim, 2018; Emsen et al., 2019; Lee et al., 2019; Díaz et al., 2020

(Continued)

TABLE 1 (Continued)

Class of compound	Natural compound	Bioactivity	Lichen species	References
	Norstictic acid	Antimicrobial/cytotoxic/antioxidant	*Toninia candida/Ramalina farinacea/Stereocaulon montagneanum/Usnea strigose/Xanthoparmelia tinctina**	Tay et al., 2004; Rankovic et al., 2012; Ebrahim et al., 2016; Ismed et al., 2017; Díaz et al., 2020
	Stictic acid	Cytotoxic/antibiotics/antioxidant	*Lobaria pulmonaria/Rhizoplaca aspidophora/Xanthoparmelia camtschadalis/S. montagneanum/Hypotrochyna revolute/Usnea longissima*	Papadopoulou et al., 2007; Atalay et al., 2011; McGillick et al., 2016; Bellio et al., 2017; Ismed et al., 2017; Pejin et al., 2017
	Fumarprotocetrari acid	Antimicrobial/antioxidant expectorant/photoprotection	*Cladonia foliacea/Cetraria islandica/Cladonia verticillaris/Lasallia pustulata/Evernia prunastri*	Lawrey, 1986; Dévéhat et al., 2013; de Barros Alves et al., 2014; Igoli et al., 2014; Ranković and Mišić, 2014; Tekiela et al., 2021
	Physodic acid	Anticancer/antioxidant/antimicrobial	*Hypogymnia physodes/Evernia prunastri/Pseudevernia furfuracea*	Kosanic et al., 2013; Majchrzak-Celinska et al., 2022
	Salazinic acid	Anti-Alzheimer/antioxidant/anticancer/antibacteria	*Parmelia sulcata/P. saxatilis/Everniastrum cirrhatum/Rimelia cetrata/Leucodermia leucomelos/Xanthoparmelia camtschadalis*	Manojlovic et al., 1998; Gaikwad et al., 2014; Bellio et al., 2017; Paluszczak et al., 2018; Furmanek et al., 2021; Majchrzak-Celinska et al., 2022
	α/β-Alectoronic acid	Antimicrobial/anticancer	*Alectoria sarmentosa*/Parmelia tiliacea*/Xanthoparmelia tinctina*/Arctoparmelia centrifuga**	Gollapudi et al., 1994; Díaz et al., 2020
	Physodic acid	Anticancer/antioxidant/antimicrobial	*Parmelia saxatilis**	Díaz et al., 2020
	Neuropogonines A-C	Antimicrobial	*Neuropogon* sp.	Ivanova et al., 2002
	Pannarin	Anticancer	*Psoroma reticulatum*	Russo et al., 2006, 2008
	Pseudodepsidones 1 and 2	Anti-diabetes	*Stereocaulon alpinum*	Seo et al., 2009
	Psoromic acid	Antibiotics/antivirus	*Usnea* spp./*Psoroma* spp./*Alectoria* spp.	Lawrey, 1986
	Pulmonarianin	Lipid peroxidation inhibition/antioxidant	*Usnea longissima/Lobaria pulmonaria/Xanthoparmelia tinctina**	Atalay et al., 2011; Díaz et al., 2020
Dibenzofuranes	Usnic acid and derivatives	Antimicrobial/analgesic/antipyrietic/anti-inflammatory, anti-cancer/antimutagrnic activity/enzyme inhibitor/anti-allergies/antivirus/plant growth inhibitor	*Usnea* spp./*Ramalina* spp.*/*U. longissima**	Lawrey, 1986; Wang et al., 2014; Moreira et al., 2015; Sepahvand et al., 2021
Didepsides	Barbatic acid	Anticancer	*Usnea longissima*	Reddy et al., 2019
	Divaricatic acid	Antimicrobial	*Evernia divaricata*	Çobanglu et al., 2010
	Diffractaic acid	Antioxidant/anti-inflammatory	*Usnea longissima/Lobaria pulmonaria*	Bayir et al., 2006; Atalay et al., 2011
	Sekikaic acid	Anticancer/antivirus	*Ramalina farinacea*	Yousuf et al., 2014
Dimeric tetrahydroxanthone	Hirtusneanoside	Antibacterial	*Usnea hirta/Ramalina farinaceae/Peltigera polydactyla*	Rezanka and Sigler, 2007
Lichenan	β-D-1,3/1,4-glucan	Wound healing	*Cetraria islandica*	Zacharski et al., 2018
Monocyclic aromatic compound	Atranol	Antimicrobial	*Roccella montagnei*	Tatipamula et al., 2019
	Orcinol	Antimicrobial	*Roccella montagnei*	Tatipamula et al., 2019
	Orsellinic acid	Antimicrobial	*Parmotrema austrosinense*	Kumar et al., 2018

(Continued)

TABLE 1 (Continued)

Class of compound	Natural compound	Bioactivity	Lichen species	References
Phenanthrenequinones	Biruloquinone	Achtylcholine inhibitor	*Cladonia macilenta*∗	Luo et al., 2013
		Acetylcholinesterase inhibitor		Luo et al., 2013
Poly-carboxylic fatty acid	Caperatic acid	Anti-inflammatory/cytotoxity/central nervous system therapeutics	*Platiamatia glauca*	Majchrzak-Celinska et al., 2022; Studzinska-Sroka et al., 2022
Polysaccharides	Polysaccharides	Antioxidant/anticancer/antiviral	*Umbilicaria esculenta/Parmelia perlata*	Olaleye et al., 2007; Sun et al., 2018; Wang et al., 2018
Pulvinic acid derivatives	Vulpinic acid	Antibiotics	*Letharia columbiana/L. vulpina/Pseudocyphellaria flacicans/Vulpicida pinastri*∗	Lawrey, 1986; Kowalski et al., 2011
Terphenylquinine	Polyporic acid	Anticancer	*Sticta coronata*	Goga et al., 2020
	Thelephoric acid	Antioxidant/anti-alzheimer	*Lobaria isidiosa*	Rao et al., 1965; Kwak et al., 1999; Chon et al., 2016
Tridepsides	Gyrophoric acid	Anticancer	*Umbilicaria* sp./*U. freyi*∗	Burlando et al., 2009; Garima et al., 2022a
	Tenuiorin	Anticancer	*Peltigera aphthosa/Lobaria linita/Pseudocyphellaria crocata*	Ingolfsdottir et al., 2002
Triterpenoids	Zeorin	Antimicrobial	*Leucodermia leucomelos*	Furmanek et al., 2021

*Represents the lichen compounds from LFF cultures besides lichen thallus in this species.

detected when the colonies were grown over 5 and 10 months on solid LB medium. By comparison, colonies grown on MEYE and MY10 with a gradually dry treatment did not synthesize any lichen secondary metabolite of polyketides but primary triacylglycerides and fatty acids as the major metabolites (Fazio et al., 2009).

Bu'Lock proposed that mycelial growth was slow under conditions of poor nutrition, but secondary metabolism could be induced (Bu'Lock et al., 1974), which is related to the carbon-nutrient balance hypothesis (Bryant et al., 1983). From LFF of *Endocarpon pusillum* cultured on the optimized PDB, nine secondary metabolites including two new isoindolin-1-ones were detected, while three known compounds and a new naphthoquinone were isolated from the rice culture (Liu R. D. et al., 2022). Temperature is another important factor influencing LFF cultivation and chemical diversity in secondary metabolism. It is due to higher or lower temperatures that will inhibit the enzyme secretion of LFF (Feller et al., 1994).

Therefore, it is greatly deserved to expect more lichen natural products will be discovered by OSMAC strategy after changing and improving a series of cultural conditions. However, there is an inevitable problem existing in this process, that is, what is the relationship between more lichen products and the valuable bioactivity of these products because lichen secondary metabolism mainly originates from the fungal partner, i.e., LFF, but is produced when the organisms are in symbiotic association (Moreira et al., 2015). Poor nutrition sources and slow growth rate are the natural factors in LFF decided by the characteristics of lichen symbiosis. *Heterodea muelleri* in the field produced diffractaic and barbatic acids, whereas the LFF cultures did not contain any detectable secondary metabolites (Hager et al., 2008). The study of temperature by Hamada in LFF and lichen thallus of *Ramalina siliquosa* examined changing of polyketides, that is, the quantity of depside produced by LFF of *Ramalina siliquosa* was the highest at optimal culture conditions (Hamada, 1989), on the contrary, depsidone was increased in *R. siliquosa* thallus (Hamada, 1981). Brunauer showed that the LFF of *Xanthoria elegans* produces secondary metabolism that is not present in the naturally collected lichen thallus by HPLC examination because the presence of gene clusters enables LFF to produce a potentially larger variety of polyketides than thallus (Brunauer et al., 2007). Another example, two new dibenzofurans, isostrepsilic acid and hypostrepsilic acid, are synthesized in large quantities by LFF culture of *Umbilicaria orientalis* on malt-yeast extract medium containing sugar alcohols, but they have not been produced by this lichen in the field (Kon et al., 1997). The production of lichen compounds is based on the resistance to extreme environments, and if the environment changes, the interactions between lichen and the environment will change, similarly, LFF is out of symbiosis when they grow on the culture medium and equal to the environment change; thus, the compounds of LFF are different from lichen symbiont, and correspondingly, some lichen bioactive compounds cannot be detected in the LFF cultures (Dayan and Romagni, 2001).

However, when quantitatively and variously LFF metabolites were obtained after more focusing on fermentation broth and mycelium, they were often found different from those contained in the natural lichen thallus (Miyagawa et al., 1993), while the reason why we are interested in the lichen natural products is due to the bioactive metabolites produced by the symbiotic lichen thallus. Whether the bioactivity of more and different lichen natural products produced in the LFF by OSMAC strategy is much better than those less in the lichen thallus is not fully understood. Anyway, there would be a long way to go on well balancing this current conflict. Well understanding and solving this problem still need to establish on the more and more discovering of lichen natural products through OSMAC under

breaking the lichen symbiosis, which is also closely related to the requirement of increasing the growth rate of LFF. Here, we present Table 2 to show some optimized media and cultural conditions being reported.

MS-based spectrometry as the core technology—Molecular network strategy

In the search for secondary metabolisms, analytical methods must be determined to use for the detection of the compounds (Scherlach and Hertweck, 2009; Tarkka et al., 2009; Palazzotto and Weber, 2018; Manish and Yogesh, 2019). The methods for identification and determining lichen metabolites in the liquid or solid medium are traditionally chemical empirical processes, which include classic spot tests, micro-crystallography, TLC, and HPLC. Kim confirmed the metabolite of *Cladonia rangiferina* by using HPLC and reported that usnic acid could not be found in *C. rangiferina* despite the gene cluster producing usnic acid being observed in the genome (Kim et al., 2021). However, these cheap but not sensitive enough methods will fail when the quantities of metabolites are below the detection limit or when the similar retention time of other metabolites overlaps (Egbert et al., 2022).

Mass spectrometry (MS) is a fast, modern, and simple tool for the structure identification of chemical substances (Wambui et al., 2021), and many lichen compounds and functional groups have been identified using MS (Huneck, 1999). In recent years, several studies focusing on lichen chemistry highlighted the use of a range of hyphenated technology. Mass spectrometry (MS), due to its sensitivity and Nuclear Magnetic Resonance (NMR) spectroscopy coupled with chromatographic techniques, has been recognized as a key technology to study metabolomics (Krug and Muller, 2014). It has been well-demonstrated that liquid chromatography (LC)–MS/MS is considerably more sensitive for the analysis of usnic acid (Cansaran et al., 2006; Sveshnikova et al., 2019; Xu et al., 2022).

Mass spectrometry (MS)/MS-based molecular networking and extensive spectroscopic analyses involving GIAO (Gauge-Independent Atomic Orbital) NMR shift calculation led to the isolation and identification of novel quinoid lichen pigments (Lagarde et al., 2021). However, although MS is the most sensitive and powerful method which detects and elucidates extremely low-abundance metabolites occurring in natural product research, it does not provide any information concerning the spatial and temporal distribution of metabolites. Mass Spectrometry Imaging (MSI) visualizes the production, location, and distribution of metabolites, which is newly used in lichens to visualize the accumulation of various polyketides such as parietin, physodic acid, atranorin, and pinastric acid in different tissues of the lichen and localize the phenolic compounds (Gadea et al., 2020). Desorption electrospray ionization-imaging mass spectrometry (DESI-IMS) realized the spatial distribution of usnic acid in cross-sections of the lichen thallus (Xu et al., 2022).

Some other MS-based metabolomics tools, such as electron ionization-mass spectrometry (EI-MS) (Kai et al., 2017), high performance liquid chromatography-diode array detector-mass spectrometry (HPLC-DAD-MS) (Castro et al., 2017), electron spray ionization-mass spectrometry (HESI-MS/MS) fragmentation patterns (Castro et al., 2017), and liquid chromatography-diode array detector-tandem mass spectrometry (UPLC-PDA-MS/MS) (Kumar et al., 2018), also help to identify various novel lichen metabolites and increase the understanding on a complex biological system.

To facilitate the lichen chemistry, an open-access MS/MS-based library with 250 metabolites known as the Lichen DataBase (LDB) was published by Olivier–Jimenez team. To aid this area of research, the MetaboLights database was generated containing the MS spectra of metabolites. Complementing this, the GNPS platform (CCMSLIB00004751209 to CCMSLIB00004751517) contains the merged spectra of these metabolites within a metadata file. Such a fundamental database empowers research on lichen chemistry by prioritizing novel metabolites (Olivier-Jimenez et al., 2019).

In addition to MS, NMR spectroscopy has also been widely used to determine the structure of organic molecules, which is typically coupled with LC/GC for quantitative analysis of low molecular weight compounds. Metabolite profiles in crude extracts of *Xanthoria elegans* thalli during hydration and dehydration were assessed by using ^{31}P- and ^{13}C-NMR, and approximately 30 metabolites were identified and quantified (Aubert et al., 2007). The ^{1}H-NMR spectra of *Xanthoria parietina* and *Peltigera horizontalis* crude extract displayed lichen-specific features with strong signals and confirmed untargeted analysis on a quantitative basis (Eisenreich et al., 2011). Moreover, NMR demonstrates which atoms are present in neighboring groups. Ultimately, NMR can provide information on how many atoms are present in each of these environments (Altemimi et al., 2017). Other imaging techniques such as Raman microscopic analysis can provide time-resolved information about the distribution of major compounds in lichens (Edwards et al., 1997; Liao et al., 2010; Gadea et al., 2020; Xu et al., 2022). FTIR imaging and Raman microscopy were used to localize the presence of usnic acid in *Cladonia arbuscular*, *C. Uncialis,* and *C. sulphurina* (Liao et al., 2010).

Genome mining-based strategy

If it is the common fact that is not easily solved now about the conflict between more lichen natural products by OSMAC from LFF cultures and uncertain or not very well bioactivity compared with those isolated from lichen thallus, genome mining-based strategy will be a more explicit way to discover lichen natural products. With the development of bioinformatics and the applying next-generation sequencing data, there has indeed been more focus on natural product discovery based on genomics (Garima et al., 2022b; Luo et al., 2022). Genome mining has become a powerful tool to discover compounds, identify cryptic biosynthetic gene clusters, characterize the potential biosynthetic pathways, and predict the skeletal structure of the relative products (Liu Q. et al., 2022; Liu T. et al., 2022; Kalra et al., 2023). An increasing understanding of high-quality genome sequencing and genome mining techniques coupled with the introduction of powerful computational toolkits facilitates the process of connecting these gene clusters with key compounds (Li et al., 2016). Comparing the traditional method for the identification of

TABLE 2 Optimized media and culture conditions for lichen-forming fungi (LFF).

LFF species	Medium	Culture condition	Note	References
Usnea ghattensis	MY + 10 mM Sucrose + 10 mM Polyethylglycol	18°C, 8 h light (400 lux)/16 h dark and 50–80% relative humidity, 3 months	Accelerated the growth via activating the cytochrome respiratory system	Verma et al., 2011
Haematomma sp. *Graphis proserpens*	MY + 10% sucrose	−18°C in the dark for 11 months	Promote the production of new compounds	Takenaka et al., 2011; Tanahashi et al., 2017
Endocarpon pusillum	Optimized PDA: 2 g/L yeast extract, 2 g/L soy peptone, 40 g/L sucrose, 200 g/L boiled potato juice	19°C on a rotary shaker at 120 rpm for 100 days	Accelerated the growth	Zhang and Wei, 2011
Usnea longissima	MY + 2% or 10% (w/v) inositol, annitol, sorbitol, sucrose, glucose, or fructose.	Aer 2 months of culture on MY basal medium 15°C, the mycelia were transferred into optimized MY medium	Accelerated the growth	Wang et al., 2011
Evernia divaricata	LB + 20 ml bark extreact	–	Promote the production of polyketides compounds	Stocker-Wörgötter and Hager, 2008
Heterodea muelleri	LB + 20 ml soil extract	–	Promote the production of polyketides compounds	Stocker-Wörgötter and Hager, 2008
Cryptothecia rubrocincta	LB + 4% erythriol		Promote the production of polyketides compounds	Stocker-Wörgötter and Hager, 2008
Cladonia furcata	LB + 4% ribitol		Promote the production of polyketides compounds	Stocker-Wörgötter and Hager, 2008
Bunodophoron patagonicum	MS + 4% sucrose		Promote the production of polyketides compounds	Stocker-Wörgötter and Hager, 2008
Stereocaulon ramulosum	Sabouraud 4% glucose agar		Promote the production of polyketides compounds	Stocker-Wörgötter and Hager, 2008
Peltigera aphthosa	Mix medium: (8 g/L) Peptone from meat, (8 g/L) Peptone from caseine, (20 g/L) Malt extract, (3 g/L) yeast extract, (5 g/L) Nacl, (40 g/L) Glucose, (15 g/L) Agar		Promote the production of polyketides compounds	Stocker-Wörgötter and Hager, 2008

biosynthetic gene clusters by using MS and NMR-based, *in silico* genome mining has become a crucial strategy for the discovery and characterization of gene clusters (Alam et al., 2022). Many web portals contain databases and tools to identify the metabolites by using BLAST, Diamond, and HMMer alignment tools. After uploading the genome to websites, the results of the detection and characterization of secondary metabolites are achieved soon. AntiSMASH (Medema et al., 2011), PRISM (Skinnider et al., 2017), and MIBiG (Kautsar et al., 2020) are representative *in silico* tools for predicting various types of gene clusters, and they were developed to automate biosynthetic gene clusters instead of much manual intervention in genome sequences (Kenshole et al., 2021). Among those three tools, antiSMASH is the largest database of biosynthetic gene cluster analysis, PKS, and non-ribosomal peptide synthase (NRPS) substrate specificity prediction, as well as known and unknown biosynthetic gene clusters comparison (Medema et al., 2011). In addition, antiSMASH was used to predict the molecular structure sequence database. *In silico* genome tool with antiSMASH and BLAST2GO programs investigated the type I-PKS module candidates in nine publicly available LFF genomes (Erken et al., 2021). In addition, rule-based tools such as antiSMASH, ClusterFinder, and RNNs, and machine learning tools have been developed to allow the identification of unknown biosynthetic gene clusters (Cimermancic et al., 2014; Hannigan et al., 2019). However, a much higher false-positive rate than the rule-based tools is the weakness of machine learning-based genome mining tools. Open sources such as Prodigal and automated annotation help reduce false-positive identification. All these softwares are powerful tools that help to make genome mining *in silico* of the interesting LFF.

The genome mining study of a few publicly available LFF genomes suggested the importance of genome mining at the strain level, as it increases the likelihood that researchers discover useful derivatives of known secondary metabolites. An integrated approach utilizing genomics and metabolomics is needed to study the lichen complex systems. Recently, genome mining and

comparative genomics strategy were used to assess biosynthetic gene clusters and putative regulators of LFF *Evernia prunastri* and *Pseudevernia furfuracea*. The results showed that the NR-PKS from LFF *Pseudevernia furfuracea* produces depside lecanoric acid, which has never been detected from lichen thallus in nature (Calchera et al., 2019). Genome mining analysis based on a homology searching approach revealed that enzymes of grayanic acid, patulin, and betaenones A-C biosynthesis are encoded by *Cladonia uncialis* genome (Bertrand et al., 2018), and the result corresponds with Shishido et al. (2021). The uptake of advanced analytical techniques and next-generation computational tools brought a breakthrough in lichen chemistry and resulted in the identification of various novel compounds. Moreover, understanding the genetic components leading to the biosynthesis of these metabolites provides an opportunity to exploit their commercial utilization by employing synthetic biology approach.

In LFF, polyketides are the most common class of secondary metabolites. With the help of gene knockout studies, it has been observed that cryptic PKS gene codes for PKS required for the biosynthesis of the representative polyketide orsellinic acid. Polyketides synthesized by three types of multidomain polyketide synthases in the sequential acyl acetyl-polymalonyl pathway are major, structurally diverse classes of natural products (Lin and Qu, 2022; Liu Q. et al., 2022). In the case of bacteria and fungi, PKSs belong to types I and II, while type III is present in higher plants. Despite structural differences, almost all PKSs biosynthesize polyketides via sequential decarboxylative Claisen condensation of acyl-coenzyme A (CoA) precursors and use ketoacyl synthase to catalyze the C–C bond formed during carbon chain assembly, and this process is as similar as fatty acid synthases (Lin and Qu, 2022). From the ecological perspective, these polyketide-based secondary metabolites afford a large amount of cytotoxic or antibiotic compounds to adapt to the competitive living environment. Many of these compounds or their derivatives have emerged as clinically useful drugs or are promising drug candidates. Genetic regulation study of lichen or LFF secondary metabolism is at an early stage, and as time passes and technology advances, more and more research will be covered in this field (Valarmathi et al., 2009; Calchera et al., 2019; Singh et al., 2021). Recently, several LFF PKS genes have been cloned, such as type I NR-PKS gene *XsmPKSI* from *Xanthoria substrigosa* (Hametner and Stocker-Wörgötter, 2015); three new NR-PKS genes such as *UlPKS2, UlPKS4,* and *UlPKS6* from *Usnea longissima* (Wang et al., 2014); and *XsePKS1* from *Xanthoria semiviridis* (Chooi et al., 2008). In addition, some studies of polyketide synthase genes have also focused on phylogenomic analysis (Proctor et al., 2007; Wang et al., 2018; Kealey et al., 2021). The increasing number of phylogenomic analyses shows that a single fungal genome may contain more than one PKS gene, and each species of fungi can produce more than one polyketide or polyketide family (Stocker-Wörgötter, 2008). For example, 12 PKS genes have been identified in *Cladonia grayi* (Shukla et al., 2010). Armaleo et al. (2011) identified a likely orcinol decided PKS and other pathway genes in its metabolic cluster, and it was the first genetic evidence for a complete depside/depsidone biosynthetic pathway. Experimental data that seven complete non-reducing and nine highly-reducing PKS genes indicated *Nppks7* was a new PKS that participated in usnic acid biosynthesis in LFF *Nephromopsis pallescens* (Wang et al., 2018).

The complex lichen biology as filamentous fungi, transcriptionally silent, and trace expression make an artificial synthesis of interesting secondary metabolites difficult (Harvey et al., 2018). Heterologous expression of biosynthetic gene clusters in a non-natural host or model system expedites natural product discovery, elucidation, and mass production. The apposite choice of host is one of the keys to successful heterologous expression. Due to many advantages, such as fast growth, high cell density, low cost, simple cultivation medium, fast transformation procedure, and ability to process and correctly splice introns, *Saccharomyces cerevisiae* (Kealey et al., 2021), *Fusarium venenatum* (Sinnemann et al., 2000), *Aspergillus nidulans* (Sinnemann et al., 2000), *A. niger* (Sinnemann et al., 2000), *A. oryzae* (Gagunashvili et al., 2009), and *Neurospora crassa* are the experimentally well-developed strains and are considered as the potential hosts for the expression of lichen DNA (Qiao et al., 2019). In other expression systems, to avoid the influence of the surrogate host's metabolism on heterologous biosynthesis, *Ascochyta rabiei*, chosen as the host, is a genetically tractable, wild-type plant-pathogenic fungus without the biosynthetic gene cluster of phytotoxic solanapyrones (Kim et al., 2021).

Using PKS genes as a heterologous expression of genes for filamentous fungal secondary metabolites has been widely reported (Gressler et al., 2011; Sakai et al., 2012; Qian et al., 2020). Although PKS genes of lichen and filamentous fungi showed the greatest homology, only a few PKS genes have been isolated and characterized functionally from lichen or LFF. As the first PKS gene from *Solorina crocea* LFF, *PyrG* encoding decarboxylase was functionally expressed under its own promoter in *A. nidulans* (Sinnemann et al., 2000). The result indicated that a heterologous expression system is a useful tool for the functional characterization of genes. Another example is that two pairs of degenerated primers have been used to locate and clone PKS genes containing a CMeT domain from *Xanthoparmelia semiviridis* (Chooi et al., 2008). Early functional research of lichen PKS genes mainly focused on symbiosis, physiology, and biochemistry because all the studies that attempted to express the PKS gene of unique lichen compounds failed (Chooi et al., 2008). Until recently, *de novo* biosynthetic PKS genes of atranorin and lecanoric acid have been successfully heterologously expressed (Kealey et al., 2021; Kim et al., 2021). Atranorin is one of the most concerned lichen compounds. The results from lichens such as *Cladonia*, *Stereocaulon alpinum* (Kim et al., 2021), and *Bacidia rubella* (Gerasimova et al., 2022) revealed that the PKS23 gene (*atr1*), a cytochrome P450 gene (*art2*) for oxidation, an O-methyltransferase (OMT) gene (*atr3*), and transporter gene (*atr4*) were involved in producing atranorin.

Conclusion and future perspectives

Lichen secondary metabolites are of major interest due to their applicability as therapeutic agents. However, a special way of symbiosis, extreme living environment, and slow growth of lichen limit the constant need for lichen compounds in industry and pharmacy. The analysis of genome sequence revealed that

there exist silent biosynthetic gene clusters, which are usually not expressed until being activated, leading to the discovery of lichen compounds much inadequate. OSMAC strategy is a powerful and mature method for enhancing the chemodiversity of LFF natural compounds, under which new drugs could be obtained by manipulating nutritional or environmental factors of fermentation to activate silent gene clusters. However, sometimes, the results of the OSMAC strategy are not very satisfying because it has a limited capacity to mimic the complexities of natural environmental changes. MS-based molecular network strategy further facilitates lichen chemistry, especially linked to a series of databases such as LDB and MetaboLights. Genome- and bioinformatics-based genome mining strategy not only makes up for the difficulties and shortcomings of the OSMAC strategy but also strongly pushes the identification of biosynthetic gene clusters and increases the rate of discovery of new products. Genome mining strategy, covering several different usage cases in animal, plant, and microbe, shows diverse ways, in which genomic data can be used to uncover new secondary metabolites, improves our understanding of their biosynthesis, and uncovers long-term biosynthetic mysteries, but for lichen, it is just the beginning. Nowadays, various strategies for inducing the expression of silent biosynthetic gene clusters have been developed. However, each strategy has its own limitations, and no strategy could be universal for all strains. Furthermore, significant advances are needed in terms of the enrichment of the database for lichen metabolites together with the general standardization of different generations of data. A combination of OSMAC, molecular network, and genome mining-based strategies will be greatly helpful to predict the biosynthesis and accumulation of specific natural products, discover numerous novel secondary metabolites with a range of attractive bioactivities, and pursue the establishment and maintenance of the lichen symbiosis.

Author contributions

XW: conceptualization. MR: writing—original draft preparation. SJ, YW, XP, FP, and XW: writing—reviewing and editing. All authors read and approved the manuscript.

Funding

This study was supported by the National Natural Science Foundation of China (grant numbers 32070096, 32170082, and 32270007) and the Space Application System of China Manned Space Program (KJZ-YY-WSM05).

Conflict of interest

XP and FP were employed by Jiangxi Xiankelai Biotechnology Co., Ltd.

The remaining authors declare that the research was conducted in the absence of any commercial or financial relationships that could be construed as a potential conflict of interest.

Publisher's note

References

Abdelwahab, M. F., Kurtán, T., Mándi, A., Müller, W. E. G., Fouad, M. A., Kamel, M. S., et al. (2018). Induced secondary metabolites from the endophytic fungus *Aspergillus versicolor* through bacterial co-culture and OSMAC approaches. *Tetrahedron Lett.* 59, 2647–2652. doi: 10.1016/j.tetlet.2018.05.067

Aberhart,.D. J., Overton, K. H., and Huneck, S. (1969). Studies on lichen substances. Part LXII. Aromatic constituents of the lichen Roccella fuciformis DC. A revised structure for lepraric acid. *J. Chem. Soc.* 5, 704–707. doi: 10.1039/j39690000704

Alam, K., Hao, J., Zhong, L., Fan, G., Ouyang, Q., Islam, M. M., et al. (2022). Complete genome sequencing and *in silico* genome mining reveal the promising metabolic potential in *Streptomyces* strain CS-7. *Front. Microbiol.* 13, 939919. doi: 10.3389/fmicb.2022.939919

Altemimi, A., Lakhssassi, N., Baharlouei, A., Watson, D. G., and Lightfoot, D. A. (2017). Phytochemicals: extraction, isolation, and identification of bioactive compounds from plant extracts. *Plants* 6, 42. doi: 10.3390/plants6040042

Armaleo, D., Sun, X., and Culberson, C. (2011). Insights from the first putative biosynthetic gene cluster for a lichen depside and depsidone. *Mycologia* 103, 741–754. doi: 10.3852/10-335

Arshad, M., Devlin, J. P., Olli, W. D., and Wheele, R. E. (1968). The constitution of sordidone and its relation to thiophanic acid. *Chem. Commun.* 3, 154–155. doi: 10.1039/c19680000154

Atalay, F., Halici, M. B., Mavi, A., Cakir, A., Odabasoglu, F., Kazaz, C., et al. (2011). Antioxidant phenolics from *Lobaria pulmonaria* (L.) Hoffm. and *Usnea ongissima* Ach. lichen species. *Turk. J. Chem.* 35, 647–661. doi: 10.3906/kim-1008-847

Atanasov, A. G., Waltenberger, B., Pferschy-Wenzig, E. M., Linder, T., Wawrosch, C., Uhrin, P., et al. (2015). Discovery and resupply of pharmacologically active plant-derived natural products: a review. *Biotechnol. Adv.* 33, 1582–1614. doi: 10.1016/j.biotechadv.2015.08.001

Aubert, S., Juge, C., Boisson, A. M., Gout, E., and Bligny, R. (2007). Metabolic processes sustaining the reviviscence of lichen *Xanthoria elegans* (Link) in high mountain environments. *Planta* 226, 1287–1297. doi: 10.1007/s00425-007-0563-6

Bayir, Y., Odabasoglu, F., Cakir, A., Aslan, A., Suleyman, H., Halici, M., et al. (2006). The inhibition of gastric mucosal lesion, oxidative stress and neutrophil-infiltration in rats by the lichen constituent diffractaic acid. *Phytomedicine* 13, 584–590. doi: 10.1016/j.phymed.2005.07.002

Behera, B. C., Verma, N., Sonone, A., and Makhija, U. (2006). Experimental studies on the growth and usnic acid production in "lichen" *Usnea ghattensis in vitro*. *Microbiol. Res.* 161, 232–237. doi: 10.1016/j.micres.2005.08.006

Bellio, P., Di Pietro, L., Mancini, A., Piovano, M., Nicoletti, M., Brisdelli, F., et al. (2017). SOS response in bacteria: Inhibitory activity of lichen secondary metabolites against *Escherichia coli* RecA protein. *Phytomedicine* 29, 11–18. doi: 10.1016/j.phymed.2017.04.001

Bertrand, R. L., Abdel-Hameed, M., and Sorensen, J. L. (2018). Lichen biosynthetic gene clusters part II: homology mapping suggests a functional diversity. *J. Nat. Prod.* 81, 732–748. doi: 10.1021/acs.jnatprod.7b00770

Bessadottir, M., Eiriksson, F. F., Becker, S., Ogmundsdottir, M. H., Omarsdottir, S., Thorsteinsdottir, M., et al. (2015). Anti-proliferative and pro-apoptotic effects of lichen-derived compound protolichesterinic acid are not mediated by its lipoxygenase-inhibitory activity. *Prostaglandins Leukot. Essent. Fatty Acids* 98, 39–47. doi: 10.1016/j.plefa.2015.04.009

Bessadottir, M., Skuladottir, E. A., Gowan, S., Eccles, S., Ogmundsdottir, S., Ogmundsdottir, H. M., et al. (2014). Effects of anti-proliferative lichen metabolite, protolichesterinic acid on fatty acid synthase, cell signalling and drug response in breast cancer cells. *Phytomedicine* 21, 1717–1724. doi: 10.1016/j.phymed.2014.08.006

Bode, H., Bethe, B., Hofs, R., and Zeeck, A. (2002). Big effects from small changes: possible ways to explore nature's chemical diversity. *Chem. BioChem.* 3, 619–627. doi: 10.1002/1439-7633(20020703)3:7<619::AID-CBIC619>3.0.CO;2-9

Boustie, J., Tomasi, S., and Grube, M. (2010). Bioactive lichen metabolites: alpine habitats as an untapped source. *Phytochem. Rev.* 10, 287–307. doi: 10.1007/s11101-010-9201-1

Brunauer, G., Hager, A., Grube, M., Türk, R., and Stocker-Wörgötter, E. (2007). Alterations in secondary metabolism of aposymbiotically grown mycobionts of *Xanthoria elegans* and cultured resynthesis stages. *Plant Physiol. Biochem.* 45, 146–151. doi: 10.1016/j.plaphy.2007.01.004

Bryant, J. P., Stuart Chapin, F., and Klein, D. R. (1983). Carbon nutrient balance of boreal plants in relation to vertebrate herbivory. *Oikos* 40, 357–368. doi: 10.2307/3544308

Buhaescu, I., and Izzedine, H. (2007). Mevalonate pathway: a review of clinical and therapeutical implications. *Clin. Biochem.* 40, 575–584. doi: 10.1016/j.clinbiochem.2007.03.016

Bu'Lock, J. D., Detroy, R. W., Hoštálek, Z., and Munim-Al-Shakarchi, A. (1974). Regulation of secondary biosynthesis in *Gibberella fujikuroi*. *Trans. Br. Mycol. Soc.* 62, 377–389. doi: 10.1016/S0007-1536(74)80046-X

Burlando, B., Ranzato, E., Volante, A., Appendino, G., Pollastro, F., Verotta, L., et al. (2009). Antiproliferative effects on tumour cells and promotion of keratinocyte wound healing by different lichen compounds. *Planta Med.* 75, 607–613. doi: 10.1055/s-0029-1185329

Calchera, A., Dal Grande, F., Bode, H. B., and Schmitt, I. (2019). Biosynthetic gene content of the 'perfume lichens' *Evernia prunastri* and *Pseudevernia furfuracea*. *Molecules* 24, 203. doi: 10.3390/molecules24010203

Calvo, A. M., Wilson, R. A., Bok, J. W., and Keller, N. P. (2002). Relationship between secondary metabolism and fungal development. *Microbiol. Mol. Biol. Rev.* 66, 447–459. doi: 10.1128/MMBR.66.3.447-459.2002

Cansaran, D., Kahya, D., Yurdakulola, E., and Atakol, O. (2006). Identification and quantitation of usnic acid from the lichen *Usnea* species of Anatolia and antimicrobial activity. *Z. Naturforsch. C. J. Biosci.* 61, 773–776. doi: 10.1515/znc-2006-11-1202

Castro, O. N., Benites, J., Rodilla, J., Santiago, J. C., Simirgiotis, M., Sepulveda, B., et al. (2017). Metabolomic analysis of the lichen *Everniopsis trulla* using ultra high performance liquid chromatography-quadrupole-orbitrap mass spectrometry (UHPLC-Q-OT-MS). *Chromatographia* 80, 967–973. doi: 10.1007/s10337-017-3304-4

Chon, S. H., Yang, E. J., Lee, T., and Song, K. S. (2016). ß-secretase (BACE1) inhibitory and neuroprotective effects of p-terphenyls from Polyzellus multiplex. *Food Funct.* 7, 3834–3842. doi: 10.1039/c6fo00538a

Chooi, Y. H., Stalker, D. M., Davis, M. A., Fujii, I., Elix, J. A., Louwhoff, S. H., et al. (2008). Cloning and sequence characterization of a non-reducing polyketide synthase gene from the lichen *Xanthoparmelia semiviridis*. *Mycol. Res.* 112, 147–161. doi: 10.1016/j.mycres.2007.08.022

Cimermancic, P., Medema, M. H., Claesen, J., Kurita, K., Wieland Brown, L. C., Mavrommatis, K., et al. (2014). Insights into secondary metabolism from a global analysis of prokaryotic biosynthetic gene clusters. *Cell* 158, 412–421. doi: 10.1016/j.cell.2014.06.034

Claudia, C., Xavier, B., Jabrane,.A., Katy, V., Daniel, G., Patrick, L., et al. (2018). Lobaric acid and pseudodepsidones inhibit NF-κB signaling pathway by activation of PPAR-γ. *Bioorg. Med. Chem. Lett.* 26, 5845–5851. doi: 10.1016/j.bmc.2018.10.035

Çobanglu, G., Sesal, C., Gölmen, B., and Çakar, S. (2010). Evaluation of the antimicrobial properties of some lichens. *South West J. Hortic. Biol. Environ.* 1, 153–158.

Cocchietto, M., Skert, N., Nimis, P. L., and Sava, G. (2002). A review on usnic acid, an interesting natural compound. *Naturwissenschaften* 89, 137–146. doi: 10.1007/s00114-002-0305-3

Cox, P. A., Banack, S. A., Murch, S. J., Rasmussen, U., Tien, G., Bidigare, R. R., et al. (2005). Diverse taxa of cyanobacteria produce beta-N-methylamino-L-alanine, a neurotoxic amino acid. *Proc. Natl. Acad. Sci. U. S. A.* 102, 5074–5078. doi: 10.1073/pnas.0501526102

Crittenden, P. D., and Porter, N. (1991). Lichen-forming fungi: potential sources of novel metabolites. *Trends Biotechnol.* 9, 409–414. doi: 10.1016/0167-7799(91)90141-4

Culberson, C. F., Culberson, W. L., and Johnson, A. (1986). Two new lichen products, elatinic acid and methyl barbatate, from the genus *Haematomma* (Ascomycotina, Haematommataceae). *Mycologia* 78, 888–891. doi: 10.1080/00275514.1986.12025345

Culberson, C. F., and Elix, J. A. (1989). "Lichen substances," in *Methods in Plant Biochemistry*, ed J. B. Harborne (London: Academic Press), 509–535.

Dayan, F. E., and Romagni, J. G. (2001). Lichens as a potential source of pesticides. *Pestic. Outlook* 12, 229–232. doi: 10.1039/b110543b

de Barros Alves, G. M., de Sousa Maia, M. B., de Souza Franco, E., Galvão, A. M., da Silva, T. G., Gomes, R. M., et al. (2014). Expectorant and antioxidant activities of purified fumarprotocetraric acid from *Cladonia verticillaris* lichen in mice. *Pulm. Pharmacol. Ther.* 27, 139–143. doi: 10.1016/j.pupt.2013.07.002

de Lima Procópio, R. E., da Silva, I. R., Martins, M. K., de Azevedo, J. L., and de Araújo, J. M. (2012). Antibiotics produced by Streptomyces. *Braz. J. Infect. Dis.* 16, 466–471. doi: 10.1016/j.bjid.2012.08.014

de Vera, J. P., Horneck, G., Rettberg, P., and Ott, S. (2003). The potential of the lichen symbiosis to cope with extreme conditions of outer space – I. Influence of UV radiation and space vacuum on the vitality of lichen symbiosis and germination capacity. *Int. J. Astrobiol.* 1, 285–293. doi: 10.1017/S1473550403001216

Demain, A. L. (2014). Importance of microbial natural products and the need to revitalize their discovery. *J. Ind. Microbiol. Biotechnol.* 41, 185–201. doi: 10.1007/s10295-013-1325-z

Dévéhat, F. L. L., Legouin, B., Couteau, C., Boustie, J., and Coiffard, L. (2013). Lichenic extracts and metabolites as UV filters. *J. Photochem. Photobiol. B* 120, 17–28. doi: 10.1016/j.jphotobiol.2013.01.009

Díaz, E. M., Zamora, J. C., Ruibal, C., Divakar, P. K., González-Benítez, N., Devehat, F. L., et al. (2020). Axenic culture and biosynthesis of secondary compounds in lichen symbiotic fungi, the Parmeliaceae. *Symbiosis* 82, 79–93. doi: 10.1007/s13199-020-0071903

Ebrahim, H. Y., Elsayed, H. E., Mohyeldin, M. M., Akl, M. R., Bhattacharjee, J., Egbert, S., et al. (2016). Norstictic acid inhibits breast cancer cell proliferation, migration, invasion, and *in vivo* invasive growth through targeting C-Met. *Phytother. Res.* 30, 557–566. doi: 10.1002/ptr.5551

Edwards, H. G. M., Newton, E. M., Wynn-Williams, D. D., and Coombes, S. R. (2003). Molecular spectroscopic studies of lichen substances 1: parietin and emodin. *J. Mol. Struct.* 648, 49–59. doi: 10.1016/S0022-2860(02)00384-8

Edwards, H. G. M., Russell, N. C. D., and Wynn-Williams, D. (1997). Fourier transform raman spectroscopic and scanning electron microscopic study of cryptoendolithic lichens from Antarctica. *J. Raman Spectrosc.* 28, 685–690. doi: 10.1002/(SICI)1097-4555(199709)28:9<685::AID-JRS160>3.0.CO;2-X

Egbert, S., Hoffman, J. R., McMullin, R. T., Lendemer, J. C., and Sorensen, J. L. (2022). Unraveling usnic acid: a comparison of biosynthetic gene clusters between two reindeer lichen (*Cladonia rangiferina* and *C. uncialis*). *Fungal Biol.* 126, 697–706. doi: 10.1016/j.funbio.2022.08.007

Eisenreich, W., Knispel, N., and Beck, A. (2011). Advanced methods for the study of the chemistry and the metabolism of lichens. *Phytochem. Rev.* 10, 445–456. doi: 10.1007/s11101-011-9215-3

Elkhateeb, W. A., and Daba, G. M. (2019). Lichens, an alternative drugs for modern diseases. *Int. J. Res. Pharm. Biosci.* 6, 5–9.

Emsen, B., Ozdemir, O., Engin, T., Togar, B., Cavusoglu, S., Turkez, H., et al. (2019). Inhibition of growth of U87MG human glioblastoma cells by *Usnea longissima* Ach. *An. Acad. Bras. Cienc.* 91, e20180994. doi: 10.1590/0001-3765201920180994

Erken, M. T., Cansaran-Duman, D., and Tanman, U. (2021). *In silico* prediction of type I PKS gene modules in nine lichenized fungi. *Biotechnol. Biotechnol. Equip.* 35, 358–365. doi: 10.1080/13102818.2021.1879679

Fazio, A. T., Bertoni, M. D., Adler, M. T., Ruiz, L. B., Rosso, M. L., Muggia, L., et al. (2009). Culture studies on the mycobiont isolated from *Parmotrema reticulatum* (Taylor) Choisy: metabolite production under different conditions. *Mycol. Prog.* 8, 359–365. doi: 10.1007/s11557-009-0609-1

Feller, G., Narinx, E., Arpigny, J. L., Zekhnini, Z., Swings, J., Gerday, C., et al. (1994). Temperature dependence of growth, enzyme secretion and activity of psychrophilic Antarctic bacteria. *Appl. Microbiol. Biotechnol.* 41, 477–479. doi: 10.1007/BF00939039

Furmanek, L., Czarnota, P., and Seaward, M. R. D. (2021). The effect of lichen secondary metabolites on *Aspergillus* fungi. *Arch. Microbiol.* 204, 100. doi: 10.1007/s00203-021-02649-0

Gadea, A., Fanuel, M., Le Lamer, A. C., Boustie, J., Rogniaux, H., Charrier, M., et al. (2020). Mass spectrometry imaging of sspecialized metabolites for predicting lichen fitness and snail foraging. *Plants* 9, 70. doi: 10.3390/plants9010070

Gagunashvili, A. N., Davidsson, S. P., Jonsson, Z. O., and Andresson, O. S. (2009). Cloning and heterologous transcription of a polyketide synthase gene from the lichen *Solorina crocea*. *Mycol. Res.* 113, 354–363. doi: 10.1016/j.mycres.2008.11.011

Gaikwad, S., Verma, N., Sharma, B. O., and Behera, B. C. (2014). Growth promoting effects of some lichen metabolites on probiotic bacteria. *J. Food Sci. Technol.* 51, 2624–2631. doi: 10.1007/s13197-012-0785-x

Garima, S., Anjuli, C., Dominik, M., Henrique, V., Jürgen, O., Imke, S., et al. (2022a). A candidate gene cluster for the bioactive natural product gyrophoric acid in lichen-forming fungi. *Microbiol. Spectr.* 10, e0010922. doi: 10.1128/spectrum.00109-22

Garima, S., Grande, F. D., and Schmitt, I. (2022b). Genome mining as a biotechnological tool for the discovery novel biosynthetic genes in lichens. *Front. Fungal Biol.* 3, 993171. doi: 10.1101/2022.05.04.490581

Gerasimova, J. V., Beck, A., Werth, S., and Resl, P. (2022). High diversity of type I polyketide genes in *Bacidia rubella* as revealed by the comparative analysis of 23 lichen genomes. *J. Fungi* 8, 449. doi: 10.3390/jof8050449

Gissurarson, S. R., Sigurdsson, S. B., Wagner, H., and Ingolfsdottir, K. (1997). Effect of lobaric acid on cysteinyl-leukotriene formation and contractile activity of guinea pig taenia coli. *J. Pharmacol. Exp. Ther.* 280, 770–773.

Goga, M., Elečko, J., Marcinčinová, M., Ručová, D., Bačkorová, M., and Bačkor, M. (2020). "Lichen metabolites: an overview of some secondary metabolites and their biological potential," in *Co-Evolution of Secondary Metabolites*, eds J. M. Mérillon, and K. G. Ramawat (Switzerland: Springer Nature), 1–36.

Gollapudi, S. R., Telikepalli, H., Jampani, H. B., Mirhom, Y. W., Drake, S. D., Bhattiprolu, K. R., et al. (1994). Alectosarmentin, a new antimicrobial dibenzofuranoid lactol from the lichen, Alectoria sarmentosa. *J. Nat. Prod.* 57, 934–938.

González-Burgos, E., Fernández-Moriano, C., and Gómez-Serranillos, M. P. (2019). Current knowledge on Parmelia genus: ecological interest, phytochemistry, biological activities and therapeutic potential. *Phytochemistry* 165, 112051. doi: 10.1016/j.phytochem.2019.112051

Gressler, M., Zaehle, C., Scherlach, K., Hertweck, C., and Brock, M. (2011). Multifactorial induction of an orphan PKS-NRPS gene cluster in *Aspergillus terreus*. *Chem. Biol.* 18, 198–209. doi: 10.1016/j.chembiol.2010.12.011

Grube, M., and Berg, G. (2009). Microbial consortia of bacteria and fungi with focus on the lichen symbiosis. *Fungal Biol. Rev.* 23, 72–85. doi: 10.1016/j.fbr.2009.10.001

Hager, A., Brunauer, G., Turk, R., and Stocker-Worgotter, E. (2008). Production and bioactivity of common lichen metabolites as exemplified by *Heterodea muelleri* (Hampe) Nyl. *J. Chem. Ecol.* 34, 113–120. doi: 10.1007/s10886-007-9408-9

Hamada, N. (1981). The effect of temperature on the content of the medullary depsidone salazinic acid in *Ramalina siliquosa* (lichens). *Can. J. Bot.* 60, 383–385. doi: 10.1139/b82-053

Hamada, N. (1989). The effect of various culture conditions on depside production by an isolated lichen mycobiont. *Bryologist* 92, 310–313. doi: 10.2307/3243399

Hametner, C., and Stocker-Wörgötter, E. (2015). "Type I NR-PKS gene characterization of the cultured lichen mycobiont *Xanthoparmelia substrigosa* (Ascomycota)," in *Recent Advances in Lichenology*, eds D. K. Upreti, P. K., Divakar, V. Shukla, and R. Bajpai (Berlin: Springer), 95–110.

Hamida, R. S., Ali, M. A., Abdelmeguid, N. E., Al-Zaban, M. I., Baz, L., and Bin-Meferij, M. M. (2021). Lichens-a potential source for nanoparticles fabrication: a review on nanoparticles biosynthesis and their prospective applications. *J. Fungi* 7, 291. doi: 10.3390/jof7040291

Hannigan, G. D., Prihoda, D., Palicka, A., Soukup, J., Klempir, O., Rampula, L., et al. (2019). A deep learning genome-mining strategy for biosynthetic gene cluster prediction. *Nucleic Acids Res.* 47, 110. doi: 10.1093/nar/gkz654

Harikumar, G., and Krishanan, K. (2022). The growing menace of drug resistant pathogens and recent strategies to overcome drug resistance: a review. *J. King Saud. Univ. Sci.* 34, 101979. doi: 10.1016/j.jksus.2022.101979

Harvey, C. J. B., Tang, M., Schlecht, U., Horecka, J., Fischer, C. R., Lin, H. C., et al. (2018). HEx: a heterologous expression platform for the discovery of fungal natural products. *Sci. Adv.* 4, eaar5459. doi: 10.1126/sciadv.aar5459

Hong, J. M., Suh, S. S., Kim, T. K., Kim, J. E., Han, S. J., Youn, U. J., et al. (2018). Anti-cancer activity of lobaric acid and lobarstin extracted from the Antarctic lichen *Stereocaulon alpnum*. *Molecules* 23, 658. doi: 10.3390/molecules23030658

Huneck, S. (1999). The significance of lichens and their metabolites. *Naturwissenschaften* 86, 559–570. doi: 10.1007/s001140050676

Ibrahim, S. R. M., Mohamed, G., Al Haidari, R. A., El-Kholy, A. A., Zayed, M. F., and Khayat, M. T. (2018). Biologically active fungal depsidones: chemistry, biosynthesis, structural characterization, and bioactivities. *Fitoterapia* 129, 317–365. doi: 10.1016/j.fitote.2018.04.012

Igoli, J. O., Gray, A. I., Clements, C. J., Kantheti, P., and Singla, R. K. (2014). Antitrypanosomal activity & docking studies of isolated constituents from the lichen *Cetraria islandica*: possibly multifunctional scaffolds. *Curr. Top. Med. Chem.* 14, 1014–1021. doi: 10.2174/1568026614666140324122323

Ingolfsdottir, K., Gudmundsdottir, G. F., Ogmundsdottir, H. M., Paulus, K., Haraldsdottir, S., Kristinsson, H., et al. (2002). Effects of tenuiorin and methyl orsellinate from the lichen *Peltigera leucophlebia* on 5-/15-lipoxygenases and proliferation of malignant cell lines *in vitro*. *Phytomedicine* 9, 654–658. doi: 10.1078/094471102321616481

Ingolfsdottir, K., Wiedemann, B., Birgisdottir, M., Nenninger, A., Jonsdottir, S., and Wagner, H. (1997). Inhibitory effects of baeomycesic acid from the lichen *Thamnolia subuliformis* on 5-lipoxygenase *in vitro*. *Phytomedicine* 4, 125–128. doi: 10.1016/S0944-7113(97)80056-6

Ismed, F., Devehat, F. L., Rouaud, I., Ferron, S., Bakhtiar, A., and Boustie, J. (2017). NMR reassignment of stictic acid isolated from a Sumatran lichen *Stereocaulon montagneanum* (Stereocaulaceae) with superoxide anion scavenging activities. *Z. Naturforsch. C. J. Biosci.* 72, 55–62. doi: 10.1515/znc-2016-0148

Ivanova, V., Aleksieva, K., Kolarova, M., Chipeva, V., Schlegel, R., Schlegel, B., et al. (2002). Neuropogonines A, B and C, new depsidon-type metabolites from *Neuropogon* sp., an Antarctic lichen. *Pharmazie* 57, 73–74.

Jeong, M. H., Park, C. H., Kim, J. A., Choi, E. D., Kim, S., Hur, J. S., et al. (2021). Production and activity of cristazarin in the lichen-forming fungus *Cladonia metacorallifera*. *J. Fungi* 7, 601. doi: 10.3390/jof7080601

Joo, Y. A., Chung, H., Yoon, S., Park, J. I., Lee, J. E., Myung, C. H., et al. (2016). Skin barrier recovery by protease-activated receptor-2 antagonist lobaric acid. *Biomol. Ther.* 24, 529–535. doi: 10.4062/biomolther.2016.011

Kai, H., Kinoshita, K., Harada, H., Uesawa, Y., Maeda, A., Suzuki, R., et al. (2017). Establishment of a direct-injection electron ionization-mass spectrometry metabolomics method and Its spplication to lichen profiling. *Anal. Chem.* 89, 6408–6414. doi: 10.1021/acs.analchem.7b00077

Kalra, R., Conlan, X. A., and Goel, M. (2023). Recent advances in research for potential utilization of unexplored lichen metabolites. *Biotechnol. Adv.* 62, 108072. doi: 10.1016/j.biotechadv.2022.108072

Kautsar, S. A., Blin, K., Shaw, S., Navarro-Munoz, J. C., Terlouw, B. R., van der Hooft, J. J. J., et al. (2020). MIBiG 2.0: a repository for biosynthetic gene clusters of known function. *Nucleic Acids Res.* 48, 454–458. doi: 10.1093/nar/gkz882

Kealey, J. T., Craig, J. P., and Barr, P. J. (2021). Identification of a lichen depside polyketide synthase gene by heterologous expression in *Saccharomyces cerevisiae*. *Metab. Eng. Commun.* 13, e00172. doi: 10.1016/j.mec.2021.e00172

Kenshole, E., Herisse, M., Michael, M., and Pidot, S. J. (2021). Natural product discovery through microbial genome mining. *Curr. Opin. Chem. Biol.* 60, 47–54. doi: 10.1016/j.cbpa.2020.07.010

Kim, T. K. (2018). Total syntheses of lobaric acid and its derivatives from the Antarctic lichen *Stereocaulon alpinum*. *J. Nat. Prod.* 81, 1460–1467. doi: 10.1021/acs.jnatprod.8b00227

Kim, W., Liu, R., Woo, S., Kang, K. B., Park, H., Yu, Y. H., et al. (2021). Linking a gene cluster to atranorin, a major cortical substance of lichens, through genetic dereplication and heterologous expression. *MBio* 12, e0111121. doi: 10.1128/mBio.01111-21

Kon, Y., Adanil, H. K., Wardlaw, J. H., and Elix, J. A. (1997). Effects of culture conditions on dibenzofuran production by cultured mycobionts of lichens. *Symbiosis* 23, 97–106.

Kosanic, M., Manojlovic, N., Jankovic, S., Stanojkovic, T., and Rankovic, B. (2013). *Evernia prunastri* and *Pseudoevernia furfuraceae* lichens and their major metabolites as antioxidant, antimicrobial and anticancer agents. *Food Chem. Toxicol.* 53, 112–118. doi: 10.1016/j.fct.2012.11.034

Kowalski, M., Hausner, G., and Piercey-Normore, M. D. (2011). Bioactivity of secondary metabolites and thallus extracts from lichen fungi. *Mycoscience* 52, 413–418. doi: 10.1007/s10267-011-0118-3

Kranner, I., Beckett, R., Hochman, A. N., and Thomas, H. (2008). Desiccation-tolerance in lichens: a review. *Bryologist* 111, 576–593. doi: 10.1639/0007-2745-111.4.576

Krug, D., and Muller, R. (2014). Secondary metabolomics: the impact of mass spectrometry-based approaches on the discovery and characterization of microbial natural products. *Nat. Prod. Rep.* 31, 768–783. doi: 10.1039/c3np70127a

Kumar, K., Siva, B., Sarma, V. U. M., Mohabe, S., Reddy, A. M., Boustie, J., et al. (2018). UPLC-MS/MS quantitative analysis and structural fragmentation study of five Parmotrema lichens from the Eastern Ghats. *J. Pharm. Biomed. Anal.* 156, 45–57. doi: 10.1016/j.jpba.2018.04.017

Kwak, J. Y., Rhee, I. K., Lee, K. B., Hwang, J. S., Yoo, I. D., and Song, K. S. (1999). Thelephoric acid and kynapcin-9 in mushroom polyozellus multiflex Inhibit prolyl endopeptidase *in vitro*. *J. Microbiol. Biotechnol.* 9, 798–803.

Kwon, I. S., Yim, J. H., Lee, H. K., and Pyo, S. N. (2016). Lobaric acid inhibits VCAM-1 expression in TNF-α-stimulated vascular smooth muscle cells via modulation of NF-κB and MAPK signaling pathways. *Biomol. Ther.* 24, 25–32. doi: 10.4062/biomolther.2015.084

Lagarde, A., Mambu, L., Mai, P. Y., Champavier, Y., Stigliani, J. L., Beniddir, M. A., et al. (2021). Chlorinated bianthrones from the cyanolichen *Nephroma laevigatum*. *Fitoterapia* 149, 104811. doi: 10.1016/j.fitote.2020.104811

Lawrey, J. D. (1986). Biological role of lichen substances. *Bryologist* 89, 111–122. doi: 10.2307/3242751

Lee, H. W., Kim, J. W., Yim, J. H., Lee, H. K., and Pyo, S. N. (2019). Anti-Inflammatory activity of lobaric acid via suppressing NF-κB/MAPK pathways or NLRP3 inflammasome activation. *Planta Med.* 85, 302–311. doi: 10.1055/a-0777-2420

Lee, Y. M., Kim, E. H., Lee, H. K., and Hong, S. G. (2014). Biodiversity and physiological characteristics of Antarctic and Arctic lichens-associated bacteria. *World J. Microbiol. Biotechnol.* 30, 2711–2721. doi: 10.1007/s11274-014-1695-z

Li, Y. F., Tsai, K. J. S., Harvey, C. J. B., Li, J. J., Ary, B. E., Berlew, E. E., et al. (2016). Comprehensive curation and analysis of fungal biosynthetic gene clusters of published natural products. *Fungal Genet. Biol.* 89, 18–28. doi: 10.1016/j.fgb.2016.01.012

Liao, C., Piercey-Normore, M. D., Sorensen, J. L., and Gough, K. (2010). *In situ* imaging of usnic acid in selected *Cladonia* spp. by vibrational spectroscopy. *Analyst* 135, 3242–3248. doi: 10.1039/c0an00533a

Lin, Z., and Qu, X. D. (2022). Emerging diversity in polyketide synthase. *Tetrahedron Lett.* 110, 154183. doi: 10.1016/j.tetlet.2022.154183

Liu, Q., Zhang, D., Xu, Y., Gao, S., Gong, Y., Cai, X., et al. (2022). Cloning and functional characterization of the polyketide synthases based on genome mining of *Preussia isomera* XL-1326. *Front. Microbiol.* 13, 819086. doi: 10.3389/fmicb.2022.819086

Liu, R. D., Jiang, S. H., Chen, B. S., Paguirigan, J. A., Li, E. W., and Wei, J. C. (2022). Diversity of secondary metabolites from the lichen-forming fungus *Endocarpon pusillum* (Verrucariaceae, Ascomycota). *Mycosystema* 41, 1992–2003. doi: 10.13346/j.mycosystema.220118t

Liu, T., Ren, Z., Chunyu, W. X., Li, G. D., Chen, X., Zhang, Z. T. L., et al. (2022). Exploration of diverse secondary metabolites from *Streptomyces* sp. YINM00001, using genome mining and one strain many compounds approach. *Front. Microbiol.* 13, 831174. doi: 10.3389/fmicb.2022.831174

Lopes, T. I. B., C. R. G., Yoshida, N. C., and Honda N, K. (2008). Radical-scavenging activity of orsellinates. *Chem. Pharm. Bull.* 56, 1551–1554. doi: 10.1248/cpb.56.1551

Lücking, R., and Nelsen, M. P. (2018). "Ediacarans, protolichens, and lichen-derived *Penicillium* a critical reassessment of the evolution of lichenization in fungi," in *Transformative Paleobotany*, eds M. Krings, C. J. Harper, N. R. Cúneo, and G. W. Rothwell (London: Academic Press), 551–590.

Luo, H., Li, C. T., Kim, J. C., Liu, Y. P., Jung, J. S., Koh, Y. J., et al. (2013). Biruloquinone, an acetylcholinesterase inhibitor produced by lichen-forming fungus *Cladonia macilenta*. *J. Microbiol. Biotechnol.* 23, 161–166. doi: 10.4014/jmb.1207.07016

Luo, H., Yamamoto, Y., Kim, J. A., Jung, J. S., Koh, Y. J., and Hur, J. S. (2009). Lecanoric acid, a secondary lichen substance with antioxidant properties from *Umbilicaria antarctica* in maritime Antarctica (King George Island). *Polar Biol.* 32, 1033–1040. doi: 10.1007/s00300-009-0602-9

Luo, M., Wang, M., Chang, S., He, N., Shan, G., Xie, Y., et al. (2022). Halogenase-targeted genome mining leads to the discovery of (+/-) pestalachlorides A1a, A2a, and their atropisomers. *Antibiotics* 11, 1304. doi: 10.3390/antibiotics11101304

Majchrzak-Celinska, A., Kleszcz, R., Studzinska-Sroka, E., Lukaszyk, A., Szoszkiewicz, A., Stelcer, E., et al. (2022). Lichen secondary metabolites inhibit the wnt/beta-catenin pathway in glioblastoma cells and improve the anticancer effects of temozolomide. *Cells* 11, 1084. doi: 10.3390/cells11071084

Manish, T., and Yogesh, J. (2019). "Future perspectives and challenges," in *Endolichenic Fungi: Present and Future Trends*, eds T. Manishand J. Yogesh (Singapore: Springer), 171–180. doi: 10.1007/978-981-13-7268-1_8

Mann, J. (2002). Natural products in cancer chemotherapy:past, present and future. *Cancer* 2, 143–148. doi: 10.1038/nrc723

Manojlovic, N. T., Solujic, S., Sukdolak, S., and Krstic, L. J. (1998). Anthraquinones from the lichen *Xanthoria parietina*. *J. Serb. Chem. Soc.* 63, 7–11.

McGillick, B. E., Kumaran, D., Vieni, C., and Swaminathan, S. (2016). β-Hydroxyacyl-acyl carrier protein dehydratase (FabZ) from *Francisella tularensis* and *Yersinia pestis*: structure determination, enzymatic characterization, and cross-Inhibition studies. *Biochemistry* 55, 1091–1099. doi: 10.1021/acs.biochem.5b00832

Medema, M. H., Blin, K., Cimermancic, P., de Jager, V., Zakrzewski, P., Fischbach, M. A., et al. (2011). AntiSMASH: rapid identification, annotation and analysis of secondary metabolite biosynthesis gene clusters in bacterial and fungal genome sequences. *Nucleic Acids Res.* 39, 339–346. doi: 10.1093/nar/gkr466

Mishra, T., Shukla, S., Meena, S., Singh, R., Pal, M., Upreti, D. K., et al. (2017). Isolation and identification of cytotoxic compounds from a fruticose lichen *Roccella montagnei*, and it's in silico docking study against CDK-10. *Braz. J. Pharmacogn.* 27, 724–728. doi: 10.1016/j.bjp.2017.07.006

Miyagawa, H., Hamada, N., and Tamio Ueno, M. S. (1993). Hypostrepsilic acid, a new dibenzofuran from the culturei lichen mycobiont of *Evernia esorediosa*. *Phytochem. Rev.* 34, 589–591. doi: 10.1016/0031-9422(93)80057-Y

Moreira, A. S., Braz-Filho, R., Mussi-Dias, V., and Vieira, I. J. (2015). Chemistry and biological activity of *Ramalina* lichenized fungi. *Molecules* 20, 8952–8987. doi: 10.3390/molecules20058952

Muggia, L., Schmitt, I., and Grube, M. (2009). Lichens as treasure chests of natural products. *SIM News* 59, 85–97.

Murugan, M., Muthu, S., Rajendran, K., and Ponnusamy, P. (2021). Review: UV protection and anticancer properties of lichen secondary metabolites. *Sci. Acad.* 2, 1–29.

Neeraj, V., Behera, B., Parizadeh, H., and Sharma, B. O. (2011). Bactericidal activity of some lichen secondary compounds of Cladonia ochrocholra, Parmotrema nilgherrensis & Parmotrema sancti-angelii. *Intl. J. Drug Dev. Res.* 3, 222–232.

Newman, D. J., and Cragg, G. M. (2012). Natural products as sources of new drugs over the 30 years from 1981 to 2010. *J. Nat. Prod.* 75, 311–335. doi: 10.1021/np200906s

Nguyen, K. H., Chollet-Krugler, M., Gouault, N., and Tomasi, S. (2013). UV-protectant metabolites from lichens and their symbiotic partners. *Nat. Prod. Rep.* 30, 1490–1508. doi: 10.1039/c3np70064j

Nishanth, K. S., Sreerag, R. S., Deepa, I., Mohandas, C., and Nambisan, B. (2015). Protocetraric acid: an excellent broad spectrum compound from the lichen Usnea albopunctata against medically important microbes. *Nat. Prod. Res.* 29, 574–577. doi: 10.1080/14786419.2014.953500

Oettl, S. K., Gerstmeier, J., Khan, S. Y., Wiechmann, K., Bauer, J., Atanasov, A. G., et al. (2013). Imbricaric acid and perlatolic acid: multi-targeting anti-inflammatory depsides from *Cetrelia monachorum*. *PLoS ONE* 8, e76929. doi: 10.1371/journal.pone.0076929

Olaleye, D. O., Odaibo, G. N., Abonyi, D. O., Ibezim, E. C., Adikwu, M. U., Ofokansi, K. C., et al. (2007). *In vitro* evaluation of the antiviral activity of extracts from the lichen *Parmelia perlata* (L.) Ach. against three RNA viruses. *J. Infect. Dev. Ctries.* 1, 315–320. doi: 10.3855/jidc.370

Olivier-Jimenez, D., Chollet-Krugler, M., Rondeau, D., Beniddir, M. A., Ferron, S., Delhaye, T., et al. (2019). A database of high-resolution MS/MS spectra for lichen metabolites. *Sci. Data* 6, 294. doi: 10.1038/s41597-019-0305-1

Packiam, M., and Perumal, M. S. (2022). "Culture-independent and culture-dependent approaches in symbiont analysis: in Proteobacteria," in *Microbial Symbionts: Functions and Molecular Interactions on Host*, ed D. Dharumadurai (San Diego, CA: Academic Press), 743–763.

Palazzotto, E., and Weber, T. (2018). Omics and multi-omics approaches to study the biosynthesis of secondary metabolites in microorganisms. *Curr. Opin. Microbiol.* 45, 109–116. doi: 10.1016/j.mib.2018.03.004

Paluszczak, J., Kleszcz, R., Studzinska-Sroka, E., and Krajka-Kuzniak, V. (2018). Lichen-derived caperatic acid and physodic acid inhibit Wnt signaling in colorectal cancer cells. *Mol. Cell. Biochem.* 441, 109–124. doi: 10.1007/s11010-017-3178-7

Papadopoulou, P., Tzakou, O., Vagias, C., Kefalas, P., and Roussis, V. (2007). Beta-orcinol metabolites from the lichen *Hypotrachyna revoluta*. *Molecules* 12, 997–1005. doi: 10.3390/12050997

Parrot, D., Peresse, T., Hitti, E., Carrie, D., Grube, M., and Tomasi, S. (2015). Qualitative and spatial metabolite profiling of lichens by a LC-MS approach combined with optimised extraction. *Phytochem. Anal.* 26, 23–33. doi: 10.1002/pca.2532

Pejin, B., Iodice, C., Bogdanović, G., Kojić, V., and Tešević, V. (2017). Stictic acid inhibits cell growth of human colon adenocarcinoma HT-29 cells. *Arab. J. Chem.* 10, 1240–1242. doi: 10.1016/j.arabjc.2013.03.003

Pichler, G., Candotto Carniel, F., Muggia, L., Holzinger, A., Tretiach, M., and Kranner, I. (2021). Enhanced culturing techniques for the mycobiont isolated from the lichen *Xanthoria parietina*. *Mycol. Prog.* 20, 797–808. doi: 10.1007/s11557-021-01707-7

Pierangelo, B., Bernardetta, S., Alisia, M., Pietro, D., Bottoni, L., Sabatini, C., et al. (2015). Interaction between lichen secondary metabolites and antibiotics against clinical isolates methicillin-resistant *Staphylococcus aureus* strains. *Phytomedicine* 22, 223–230. doi: 10.1016/j.phymed.2014.12.005

Posner, B., Feige, G. B., and Huneck, S. (1991). Studies on the chemistry of the lichen genus *Umbilicaria* Hoffm. *Z. Nat.* 47, 1–9. doi: 10.1515/znc-1992-1-202

Proctor, R. H., Butchko, R. A. E., Brown, D. W., and Moretti, A. (2007). Functional characterization, sequence comparisons and distribution of a polyketide synthase gene required for perithecial pigmentation in some *Food Addit. Contam.* 24, 1076–1087. doi: 10.1080/02652030701546495

Qian, Z., Bruhn, T., D'Agostino, P. M., Herrmann, A., Haslbeck, M., Antal, N., et al. (2020). Discovery of the streptoketides by direct cloning and rapid heterologous expression of a cryptic PKS II gene cluster from *Streptomyces* sp. Tu 6314. *J. Org. Chem.* 85, 664–673. doi: 10.1021/acs.joc.9b02741

Qiao, Y. M., Yu,.R. L., and Zhu, P. (2019). Advances in targeting and heterologous expression of genes involved in the synthesis of fungal secondary metabolites. *RSC Adv.* 9, 35124–35134. doi: 10.1039/C9RA06908A

Rankovic, B., Kosanic, M., Stanojkovic, T., Vasiljevic, P., and Manojlovic, N. (2012). Biological activities of *Toninia candida* and *Usnea barbata* together with their norstictic acid and usnic acid constituents. *Int. J. Mol. Sci.* 13, 14707–14722. doi: 10.3390/ijms131114707

Ranković, B., and Mišić, M. (2014). The antimicrobial activity of the lichen substances of the lichens *Cladonia furcata*, *Ochrolechia androgyna*, *Parmelia caperata* and *Parmelia conspresa*. *Biotechnol. Biotechnol. Equip.* 22, 1013–1016. doi: 10.1080/13102818.2008.10817601

Rao, P. S., Sarma, K. G., and Seshadri, T. R. (1965). Chemical components of the *Lobaria* lichens from the weatern Himalayas. *Curr. Sci.* 34, 9–11.

Reddy, S. D., Silva, B., Kumar, K., Babu, V. S. P., Sravanthi, V., Boustie, J., et al. (2019). Comprehensive analysis of secondary metabolites in *Usnea longissima* (Lichenized Ascomycetes, Parmeliaceae) using UPLC-ESI-QTOF-MS/MS and pro-apoptotic activity of brbatic acid. *Molecules* 24, 2270. doi: 10.3390/molecules24122270

Rezanka, T., and Sigler, K. (2007). Hirtusneanoside, an unsymmetrical dimeric tetrahydroxanthone from the lichen *Usnea hirta*. *J. Nat. Prod.* 70, 1487–1491. doi: 10.1021/np070079m

Romagni, J. G., and Dayan, F. E. (2002). "Structural diversity of lichen metabolites and their potential use," in *Advances in Microbial Toxin Research and Its Biotechnological Exploitation*, ed R. K. Upadhyay (New York, NY: Kluwer Academic/Plenum Publishers), 151–169.

Russo, A., Piovano, M., Lombardo, L., Garbarino, J., and Cardile, V. (2008). Lichen metabolites prevent UV light and nitric oxide-mediated plasmid DNA

damage and induce apoptosis in human melanoma cells. *Life Sci.* 83, 468–474. doi: 10.1016/j.lfs.2008.07.012

Russo, A., Piovano, M., Lombardo, L., Vanella, L., Cardile, V., and Garbarino, J. (2006). Pannarin inhibits cell growth and induces cell death in human prostate carcinoma DU-145 cells. *Anticancer Drugs* 17, 1163–1169. doi: 10.1097/01.cad.0000236310.66080.ed

Sakai, K., Kinoshita, H., and Nihira, T. (2012). Heterologous expression system in *Aspergillus oryzae* for fungal biosynthetic gene clusters of secondary metabolites. *Appl. Microbiol. Biotechnol.* 93, 2011–2022. doi: 10.1007/s00253-011-3657-9

Scherlach, K., and Hertweck, C. (2009). Triggering cryptic natural product biosynthesis in microorganisms. *Org. Biomol. Chem.* 7, 1753–1760. doi: 10.1039/b821578b

Schmeda-Hirschmann, G., Tapia, A., Lima, B., Pertino, M., Sortino, M., Zacchino, S., et al. (2008). A new antifungal and antiprotozoal depside from the Andean lichen *Protousnea poeppigii*. *Phytother. Res.* 22, 349–355. doi: 10.1002/ptr.2321

Schweiger, A. H., Ullmann, G. M., Nurk, N. M., Triebel, D., Schobert, R., and Rambold, G. (2022). Chemical properties of key metabolites determine the global distribution of lichens. *Ecol. Lett.* 25, 416–426. doi: 10.1111/ele.13930

Seo, C., Sohn, J. H., Ahn, J. S., Yim, J. H., Lee, H. K., and Oh, H. (2009). Protein tyrosine phosphatase 1B inhibitory effects of depsidone and pseudodepsidone metabolites from the Antarctic lichen *Stereocaulon alpinum*. *Bioorg. Med. Chem. Lett.* 19, 2801–2803. doi: 10.1016/j.bmcl.2009.03.108

Sepahvand, A., Studzinska-Sroka, E., Ramak, P., and Karimian, V. (2021). *Usnea* sp.: antimicrobial potential, bioactive compounds, ethnopharmacological uses and other pharmacological properties; a review article. *J. Ethnopharmacol.* 268, 113656. doi: 10.1016/j.jep.2020.113656

Seymour, F. A., Crittenden, P. D., Dickinson, M. J., Paoletti, M., Montiel, D., Cho, L., et al. (2005). Breeding systems in the lichen-forming fungal genus *Cladonia*. *Fungal Genet. Biol.* 42, 554–563. doi: 10.1016/j.fgb.2005.03.006

Shishido, T. K., Wahlsten, M., Laine, P., Rikkinen, J., Lundell, T., and Auvinen, P. (2021). Microbial communities of *Cladonia* lichens and their biosynthetic gene clusters potentially encoding natural products. *Microorganisms* 9, 1347. doi: 10.3390/microorganisms9071347

Shrestha, G., and St. Clair, L. L. (2013). Lichens: a promising source of antibiotic and anticancer drugs. *Phytochem. Rev.* 12, 229–244. doi: 10.1007/s11101-013-9283-7

Shukla, V., Joshi, G. P., and Rawat, M. S. M. (2010). Lichens as a potential natural source of bioactive compounds: a review. *Phytochem. Rev.* 9, 303–314. doi: 10.1007/s11101-010-9189-6

Singh, G., Armaleo, D., Dal Grande, F., and Schmitt, I. (2021). Depside and depsidone synthesis in lichenized fungi comes into focus through a genome-wide comparison of the olivetoric acid and physodic acid chemotypes of *Pseudevernia furfuracea*. *Biomolecules* 11, 1445. doi: 10.3390/biom11101445

Sinnemann, S. J., Andresson, O. S., Brown, D. W., and Miao, V. P. W. (2000). Cloning and heterologous expression of *Solorina crocea pyrG*. *Curr. Genet.* 37, 333–338. doi: 10.1007/s002940050536

Skinnider, M. A., Merwin, N. J., Johnston, C. W., and Magarvey, N. A. (2017). PRISM 3: expanded prediction of natural product chemical structures from microbial genomes. *Nucleic Acids Res.* 45, W49–W54. doi: 10.1093/nar/gkx320

Stocker-Wörgötter, E. (2008). Metabolic diversity of lichen-forming ascomycetous fungi: culturing, polyketide and shikimate metabolite production, and PKS genes. *Nat. Prod. Rep.* 25, 188–200. doi: 10.1039/B606983P

Stocker-Wörgötter, E., and Hager, A. (2008). "Appendix: culture methods for lichens and lichen symbionts," in *Lichen Biology*, ed T. H. Nash III (Cambridge: Cambridge University Press).

Studzinska-Sroka, E., Majchrzak-Celinska, A., Bandurska, M., Rosiak, N., Szwajgier, D., Baranowska-Wojcik, et al. (2022). Is caperatic acid the only compound responsible for activity of lichen *Platismatia glauca* within the nervous system? *Antioxidants* 11, 2069. doi: 10.3390/antiox11102069

Sun, Y. H., Li, J., Zhang, Y., Tu, Y. T., Huang, C. Z., Tao, J., et al. (2018). The polysaccharide extracted from *Umbilicaria esculenta* inhibits proliferation of melanoma cells through ROS-activated mitochondrial apoptosis pathway. *Biol. Pharm. Bull.* 41, 57–64. doi: 10.1248/bpb.b17-00562

Sveshnikova, N., Yuan, T., Warren, J. M., and Piercey-Normore, M. D. (2019). Development and validation of a reliable LC-MS/MS method for quantitative analysis of usnic acid in *Cladonia uncialis*. *BMC Res. Notes* 12, 550. doi: 10.1186/s13104-019-4580-x

Takenaka, Y., Morimoto, N., Hamada, N., and Tanahashi, T. (2011). Phenolic compounds from the cultured mycobionts of *Graphis proserpens*. *Phytochemistry* 72, 1431–1435. doi: 10.1016/j.phytochem.2011.04.017

Tanahashi, T., Takenaka, Y., Mizushina, Y., and Hamada, N. (2017). A cytotoxic pyranonaphthoquinone from cultured lichen mycobionts of *Haematomma* sp. *Heterocycles* 94, 1728. doi: 10.3987/COM-17-13704

Tarkka, M. T., Sarniguet, A., and Frey-Klett, P. (2009). Inter-kingdom encounters: recent advances in molecular bacterium-fungus interactions. *Curr. Genet.* 55, 233–243. doi: 10.1007/s00294-009-0241-2

Tatipamula, V. B., Vedula, G. S., and Sastry, A. V. S. (2019). Chemical and pharmacological evaluation of manglicolous lichen Roccella montagnei Bel em. D. D. Awasthi. *Future. J. Pharm. Sci.* 5, 8. doi: 10.1186/s43094-019-0009-6

Tay, T., Turk, A. O., Yilmaz, M., Turk, H., and Kivanc, M. (2004). Evaluation of the antimicrobial activity of the acetone extract of the lichen *Ramalina farinacea* and its (+)-usnic acid, norstictic acid, and protocetraric acid constituents. *Z. Naturforsch. C. J. Biosci.* 59, 384–388. doi: 10.1515/znc-2004-5-617

Tekiela, A., Furmanek, L., Andrusiewicz, M., Bara, G., Seaward, M. R. D., Kapusta, I., et al. (2021). Can lichen secondary compounds impact upon the pathogenic soil fungi *Fusarium oxysporum* and *F. avenaceum*? *Folia Cryptog. Estonica. Fasc.* 58, 165–181. doi: 10.12697/fce.2021.58.18

Thadhani, V. M., Choudhary, M. I., Ali, S., Omar, I., Siddique, H., and Karunaratne, V. (2011). Antioxidant activity of some lichen metabolites. *Nat. Prod. Res.* 25, 1827–1837. doi: 10.1080/14786419.2010.529546

Timsina, B. A., Sorensen, J. L., Weihrauch, D., and Piercey-Normore, M. D. (2013). Effect of aposymbiotic conditions on colony growth and secondary metabolite production in the lichen-forming fungus *Ramalina dilacerata*. *Fungal Biol.* 117, 731–743. doi: 10.1016/j.funbio.2013.09.003

Türk, H., Yilmaz, M., Tay, T., Türk, A. Ö., and Kivanç, M. (2006). Antimicrobial activity of extracts of chemical races of the lichen Pseudevernia furfuracea and their physodic acid, chloroatranorin, atranorin, and olivetoric acid. *Zeitschrift Naturforschung* C6, 499–507. doi: 10.1515/znc-2006-7-806

Umezawa, H., Shibamoto, N., Naganawa, H., Ayukawa, S., Matsuzaki, M., and Takeuchi, T. (1974). Isolation of lecanoric acid, an inhibitor of histidine decarboxylase from a fungus. *J. Antibiot.* 27, 587–596. doi: 10.7164/antibiotics.27.587

Valarmathi, R., Hariharan, G. N., Venkataraman, G., and Parida, A. (2009). Characterization of a non-reducing polyketide synthase gene from lichen *Dirinaria applanata*. *Phytochemistry* 70, 721–729. doi: 10.1016/j.phytochem.2009.04.007

Verma, N., Behera, B. C., and Joshi, A. (2012). Studies on nutritional requirement for the culture of lichen *Ramalina nervulosa* and *Ramalina pacifica* to enhance the production of antioxidant metabolites. *Folia Microbiol.* 57, 107–114. doi: 10.1007/s12223-012-0100-2

Verma, N., Behera, B. C., and Makhija, U. V. (2011). Studies on cytochromes of lichenized fungi under optimized culture conditions. *Mycoscience* 52, 65–68. doi: 10.47371/S10267-010-0070-7

Waltenberger, B., Mocan, A., Smejkal, K., Heiss, E. H., and Atanasov, A. G. (2016). Natural products to counteract the epidemic of cardiovascular and metabolic disorders. *Molecules* 21, 807. doi: 10.3390/molecules21060807

Wambui, J., Stevens, M. J. A., Sieber, S., Cernela, N., Perreten, V., and Stephan, R. (2021). Targeted genome mining reveals the psychrophilic clostridium estertheticum complex as a potential source for novel bacteriocins, including cesin A and estercticin A. *Front. Microbiol.* 12, 801467. doi: 10.3389/fmicb.2021.801467

Wang, Y., Geng, C. A., Yuan, X. L., Hua, M., Tian, F. H., and Li, C. T. (2018). Identification of a putative polyketide synthase gene involved in usnic acid biosynthesis in the lichen *Nephromopsis pallescens*. *PLoS ONE* 13, e0199110. doi: 10.1371/journal.pone.0199110

Wang, Y., Kim, J. A., Cheong, Y. H., Joshi, Y., Koh, Y. J., and Hur, J. S. (2011). Isolation and characterization of a reducing polyketide synthase gene from the lichen-forming fungus *Usnea longissima*. *J. Microbiol.* 49, 473–480. doi: 10.1007/s12275-011-0362-4

Wang, Y., Wang, J., Cheong, Y. H., and Hur, J. S. (2014). Three new non-reducing polyketide synthase genes from the lichen-forming fungus *Usnea longissima*. *Mycobiology* 42, 34–40. doi: 10.5941/MYCO.2014.42.1.34

Wilson, D. J., Patton, S., Florova, G., Hale, V., and Reynolds, K. A. (1998). The shikimic acid pathway and polyketide biosynthesis. *J. Ind. Microbiol. Biotechnol.* 20, 299–303. doi: 10.1038/sj.jim.2900527

Xu, M., Oppong-Danquah, E., Wang, X., Oddsson, S., Abdelrahman, A., Pedersen, S. V., et al. (2022). Novel methods to characterise spatial distribution and enantiomeric composition of usnic acids in four Icelandic lichens. *Phytochemistry* 200, 113210. doi: 10.1016/j.phytochem.2022.113210

Yoshimura, I., Kinoshita, Y., Yamamoto, Y., Huneck, S., and Yamada, Y. (1994). Analysis of secondary metabolites from lichen by high performance liquid chromatography with a photodiode array detector. *Phytochem. Anal.* 5, 197–205. doi: 10.1002/pca.2800050405

Yoshimura, I., Kurokawa, T., Yamamoto, Y., and Kinoshita, Y. (1993). Development of lichen thalli in vitro. *Bryologist* 96, 412–421. doi: 10.2307/3243871

Yousuf, S., Choudhary, M. I., and Rahman, A. U. (2014). Lichens: chemistry and biological activities. *Nat. Prod. Chem.* 43, 223–259. doi: 10.1016/B978-0-444-63430-6.00007-2

Zacharski, D. M., Esch, S., Konig, S., Mormann, M., Brandt, S., Ulrich-Merzenich, G., et al. (2018). beta-1,3/1,4-Glucan Lichenan from *Cetraria islandica* (L.) ACH induces cellular differentiation of human keratinocytes. *Fitoterapia* 129, 226–236. doi: 10.1016/j.fitote.2018.07.010

Zahroh, E. W., Ningsih, F., and Sjamsuridzal, W. (2022). Detection of antimicrobial compounds from thermophilic actinomycetesusing one strain many compounds(OSMAC) approach. *J. Biol. Lingkungan* 9, 76–94. doi: 10.31289/biolink.v9i1.6438

Zarins-Tutt, J. S., Barberi, T. T., Gao, H., Mearns-Spragg, A., Zhang, L. X., Newman, D. J., et al. (2016). Prospecting for new bacterial metabolites_ a glossary of approaches for inducing, activating and upregulating the biosynthesis of bacterial *cryptic* or *silent* Natural Products. *Nat.Prod. Rop.* 33, 54–72. doi: 10.1039/C5NP 00111K

Zhang, T., and Wei, J. (2011). Survival analyses of symbionts isolated from *Endocarpon pusillum* Hedwig to desiccation and starvation stress. *Sci. China Life Sci.* 54, 480–489. doi: 10.1007/s11427-011-4164-z

Zhao, Y. S., Wang, M. F., and Xu, B. J. (2021). A comprehensive review on secondary metabolites and health-promoting effects of edible lichen. *J. Funct. Foods* 80, 104283. doi: 10.1016/j.jff.2020.104283

Zheng, A. H., Zhang, S., Lu, X. H., Ma, Y., Fan, Y. L., Shi, Y., et al. (2012). Trivaric acid, a pentent depside human leukocyte elastase inhibitor. *Biol. Pharm. Bull.* 35, 2247–2251. doi: 10.1248/bpb.b12-00642

frontiers | Frontiers in Microbiology

TYPE Original Research
PUBLISHED 20 April 2023
DOI 10.3389/fmicb.2023.1130018

OPEN ACCESS

EDITED BY
Kalindi Morgan,
University of Northern British Columbia, Canada

REVIEWED BY
Gang Li,
Qingdao University, China
Andrei I. Khlebnikov,
Tomsk Polytechnic University, Russia

*CORRESPONDENCE
Yannik K.-H. Schneider
✉ yannik.k.schneider@uit.no

SPECIALTY SECTION
This article was submitted to Microbial Physiology and Metabolism, a section of the journal Frontiers in Microbiology

RECEIVED 22 December 2022
ACCEPTED 24 March 2023
PUBLISHED 20 April 2023

CITATION
Schneider YK-H, Liaimer A, Isaksson J, Wilhelmsen OSB, Andersen JH, Hansen KØ and Hansen EH (2023) Four new suomilides isolated from the cyanobacterium *Nostoc* sp. KVJ20 and proposal of their biosynthetic origin. *Front. Microbiol.* 14:1130018. doi: 10.3389/fmicb.2023.1130018

Four new suomilides isolated from the cyanobacterium *Nostoc* sp. KVJ20 and proposal of their biosynthetic origin

Yannik K.-H. Schneider[1]*, Anton Liaimer[2], Johan Isaksson[3], Oda S. B. Wilhelmsen[2], Jeanette H. Andersen[1], Kine Ø. Hansen[1] and Espen H. Hansen[1]

[1]Marbio, Faculty of Biosciences, Fisheries and Economics, UiT—The Arctic University of Norway, Tromsø, Norway, [2]Department of Arctic and Marine Biology, Faculty of Biosciences, Fisheries and Economics, UiT—The Arctic University of Norway, Tromsø, Norway, [3]Department of Chemistry, Faculty of Natural Sciences, UiT—The Arctic University of Norway, Tromsø, Norway

The suomilide and the banyasides are highly modified and functionalized non-ribosomal peptides produced by cyanobacteria of the order Nostocales. These compound classes share several substructures, including a complex azabicyclononane core, which was previously assumed to be derived from the amino acid tyrosine. In our study we were able to isolate and determine the structures of four suomilides, named suomilide B – E (**1**–**4**). The compounds differ from the previously isolated suomilide A by the functionalization of the glycosyl group. Compounds **1**–**4** were assayed for anti-proliferative, anti-biofilm and anti-bacterial activities, but no significant activity was detected. The sequenced genome of the producer organism *Nostoc* sp. KVJ20 enabled us to propose a biosynthetic gene cluster for suomilides. Our findings indicated that the azabicyclononane core of the suomilides is derived from prephenate and is most likely incorporated by a proline specific non-ribosomal peptide synthetase-unit.

KEYWORDS

***Nostoc*, cyanobacteria, natural products, protease inhibitor, biosynthesis, secondary metabolites, aeruginosin, suomilide**

1. Introduction

Cyanobacteria are well known for being prolific producers of a broad range of bioactive secondary metabolites, some of which are unique to cyanobacteria (Nunnery et al., 2010). Some cyanobacteria have been recognized for the toxins they produce, which are capable of causing severe intoxications in humans and animals (Dittmann and Wiegand, 2006). One of the most prominent groups of such toxins is the microcystins, a group of phosphatase inhibitors, which are problematic when they enter drinking water supplies during dense cyanobacterial blooms (Namikoshi and Rinehart, 1996). The diverse cyanobacterial secondary metabolites are products of different biosynthetic machineries such as non-ribosomal peptide synthetases (NRPS) and polyketide synthases (PKS), but there are also peptides that are ribosomally synthesized and posttranslationally modified, the so called ribosomally synthetized and post-translationally modified peptides (RiPP) (Kehr et al., 2011; Li and Rebuffat, 2020). For the investigation of the biosynthesis of microbial metabolites, genome mining tools have been extensively used in the

field of natural products in general and cyanobacterial natural products in particular (Micallef et al., 2015). A very powerful strategy to identify new secondary metabolites and their biosynthetic pathways is the integration of metabolomic and genomic studies combining the strengths of both techniques (Kleigrewe et al., 2015; Caesar et al., 2021).

In 1997, a new glycoside was isolated from the non-toxic cyanobacterium *Nodularia spumigena*. The structure of the compound was elucidated and named suomilide (**7**) (Figure 1A; Fujii et al., 1997), but its bioactivity was not investigated until 2021 when its potent trypsin inhibiting activity, the putative biosynthetic gene cluster (BGC) and biosynthesis were described by Ahmed et al. (2021) revealing a close similarity to aeruginoside and dysinosin BGCs, reflecting the apparent structural similarity of the compounds (see Figure 2). In 2005, two compounds with high structural similarity to suomilide, banyasides A and B (**5** and **6**) (Figure 1B), were isolated from a bloom of the cyanobacterium *Nostoc* sp. (Pluotno and Carmeli, 2005). When comparing the aglycon of **7** to the aglycon of **5** and **6**, they differ in one amino acid residue; leucine in **5** and **6** and isoleucine in **7**. The configuration of the leucine has been shown to be D in **5** and **6**, in which was also the case for **7** (Fujii et al., 1997; Pluotno and Carmeli, 2005). The difference between **5** and **6** is the modification of the glycosyl unit; **5** is esterified with hexanoic acid and carbamic acid, whereas **6** is esterified with hexanoic acid at different positions (Figure 1B).

Beside their potential for production of secondary metabolites, cyanobacteria have the capability of fixating atmospheric nitrogen. This feature is utilized by several land plants, ranging from mosses to angiosperms, which have developed the ability to attract diazotrophic *Nostoc* as their symbiotic partners (Nilsson et al., 2000). In a study from Liaimer et al. (2016) isolated a number of diverse *Nostoc* sp. strains, including KVJ20 from the symbiotic organs of the liverwort *Blasia pusilla* found at two different habitats in northern Norway. Mass spectrometric analysis of extracts from KVJ20 cultures indicated that they contained previously undescribed banyaside and suomilide like (bsl) molecules.

The crude extracts of KVJ20 showed anti-proliferative activity against a human melanoma cell line (A2058) and a human lung fibroblast cell line (MRC5) (Liaimer et al., 2016). These observations prompted a chemical investigation on the extract, which in turn led to the isolation of four bsl compounds. The draft genome of KVJ20 was published in 2019 (Halsør et al., 2019), and this enabled us to combine chemical analysis of the culture extracts with genome mining for biosynthetic gene clusters. In this study, we present the chemical and biological characterization of four novel suomilide-like compounds, suomilide B – E (**1**–**4**, Figure 1A). In addition, we investigated the *bsl* gene cluster coding for biosynthetic enzymes involved in the suomilide biosynthesis.

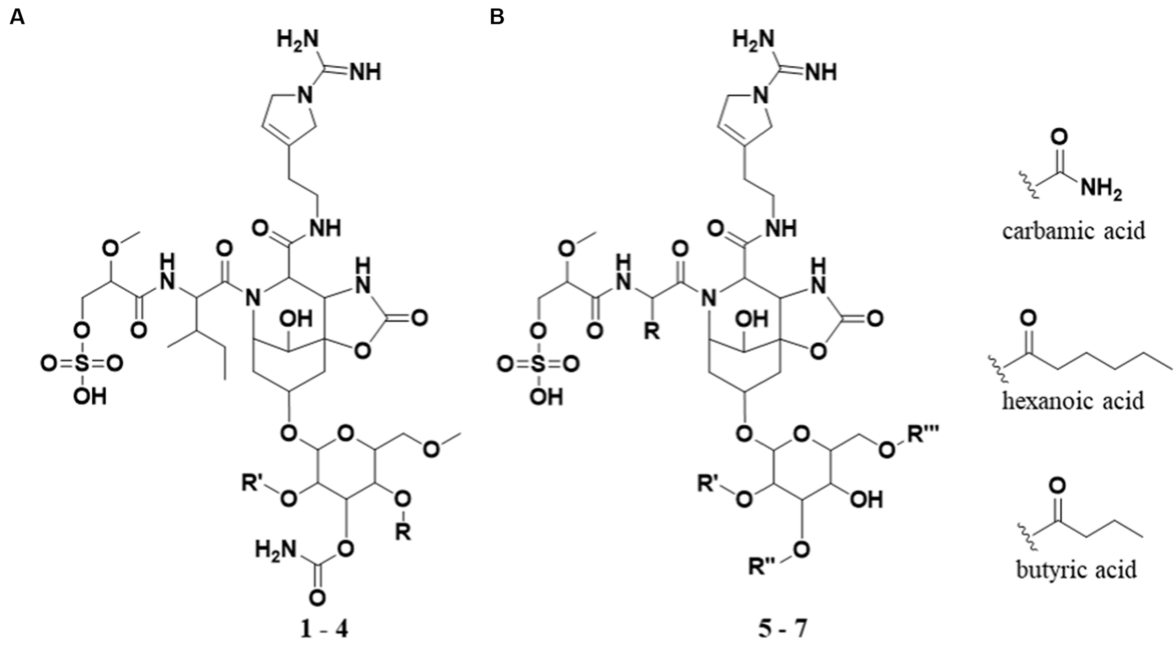

FIGURE 1
(A) Structures of suomilide B – E (**1**–**4**). **(B)** The previously isolated molecules banyasides A and B (**5** and **6**) and suomilide (**7**). All molecules share an Abn (azobicyclononane) core and an Aeap-moiety [1-amino-2-(N-amidino-Δ3-pyrrolinyl)ethyl], which also can be observed in the aeruginosins, as well as leucine and glycosylation. Suomilide differs from the banyasides by incorporation of isoleucine instead of leucine. The banyasides differ in the modification of their glycons (α-glucose for **4**, **5**, and **6**).

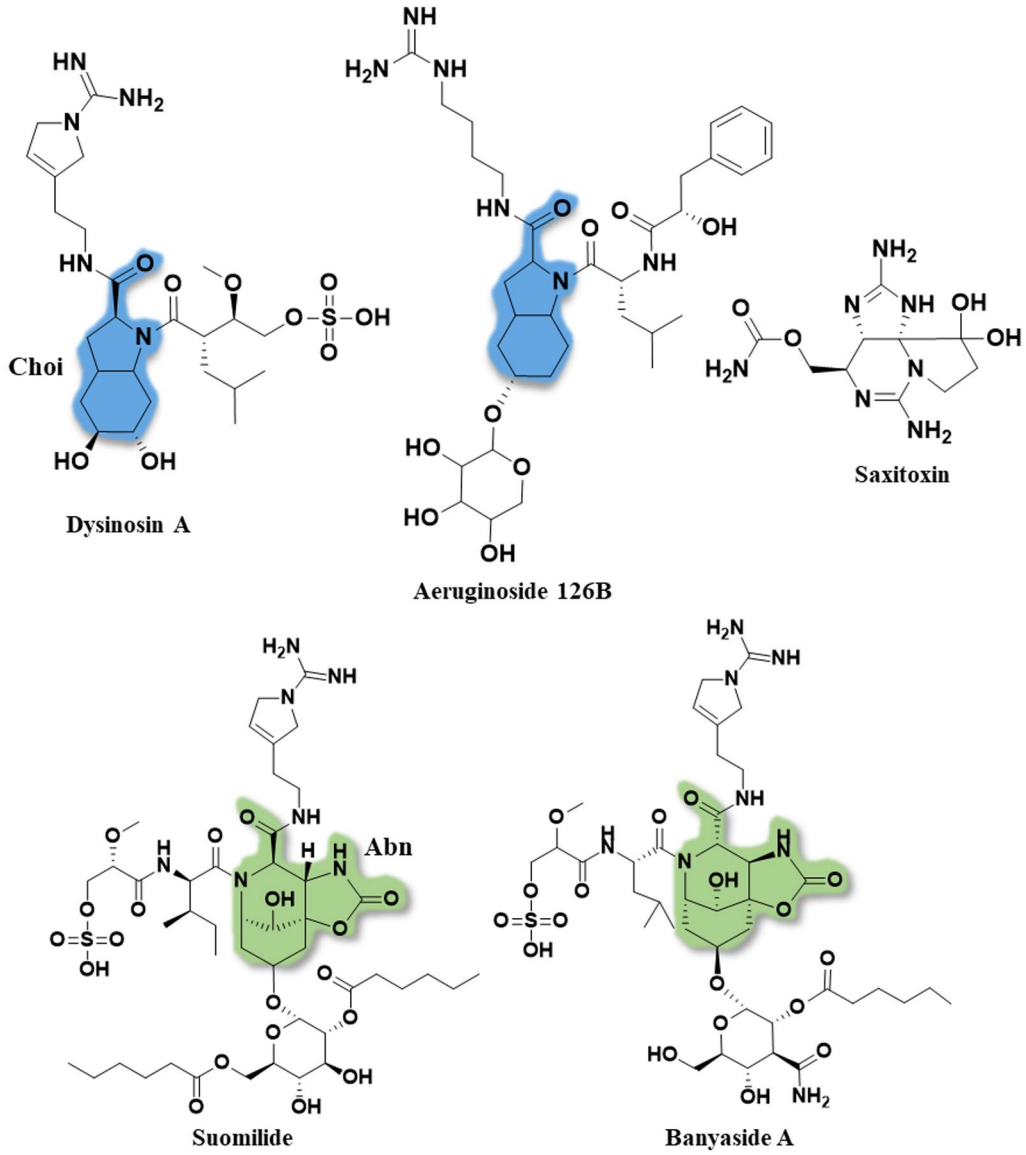

FIGURE 2
The full structures of dysinosin A, aeruginoside 126B, saxitoxin, suomilide (**7**) and banyaside A (**5**). The 2-carboxyl-6-hydroxyoctahydroindole (Choi) is marked in blue and the azabicyclononane (Abn) is highlighted in green. Note the structural similarities between the cyanobacterial metabolites, consisting of a bi-, or tri-cyclic core unit decorated with Aeap or 2-O-methylglyceric acid 3-O-sulfate (MgS).

2. Materials and methods

2.1. General experimental procedures

UPLC-ESI-HR-MS/MS-analysis of the samples was done using an Acquity I-class UPLC (Waters, Milford, MA, United States) coupled to a PDA detector and Vion® IMS QToF (Waters), UPLC-ESI-IMS-MS analysis was done using the same Vion® IMS QToF in IMS (ion mobility spectrometry)-mode. For the purification of compounds via preparative HPLC a 600 HPLC pump, a 3,100 mass spectrometer, a 2,996 photo diode array detector and a 2,767 sample manager were used with as election of columns (all Waters). NMR spectra were recorded using a Bruker Avance III HD spectrometer (Bruker, Billerica, MA, United States) operating at 599.90 MHz for ^{1}H and 150.86 MHz for ^{13}C. For the readout of bioassays in 96-well plates a 1,420 Multilabel Counter VICTOR3™ (Perkin Elmer, Waltham, MA, United States) was used.

2.2. Origin of isolate and genome sequencing

The isolate was collected at 69,64° N 18,73°E, Kvaløya island, Northern Norway and has been termed KVJ20 (Liaimer et al., 2016), its draft genome was sequenced and published in 2019 (Halsør et al., 2019).

2.3. Cultivation and extraction of *Nostoc* sp. KVJ20

The subject of this investigation, the cyanobacteria *Nostoc* sp. KVJ20, was maintained as described previously (Nilsson et al., 2000; Mihali et al., 2009). The scale-up cultures were grown for 5 weeks in 1 L bottles with constant aeration. The cultures were illuminated with 30 µmol/m^2/s using a 36 W/77 Osram Fluora light source. Following

cultivation, the cells were harvested by centrifugation, the pellet was freeze dried and sonicated in 100% methanol (MeOH), centrifuged again and the methanol supernatant was collected. The pellet was re-extracted with 50% MeOH *aq*. and 100% ddH_2O, without additional sonification. The extracts were pooled and reduced to dryness at 40°C *in vacuo*.

2.4. Compound identification and dereplication

UPLC-HR-MS/MS data for dereplication and structure elucidation was recorded. The chromatographic separation was performed using an Acquity C18 UPLC column (1.7 µm, 2.1 mm × 100 mm) (Waters). Mobile phases consisted out of ddH_2O produced by the in-house Milli-Q system for mobile phase A and acetonitrile (HiPerSolv, VWR) as mobile phase B, both containing 0.1% formic acid (v/v) (33,015, Sigma). The gradient was run from 10 to 90% B over 12 min at a flow rate of 0.45 mL/min. Samples were run in ESI+ and ESI- ionization modes. The data was processed and analyzed using UNIFI 1.9.4 (Waters). Calculation of exact ion masses was done by using ChemCalc (Patiny and Borel, 2013).

2.5. Isolation of compounds 1–4

2.5.1. Isolation protocol

Isolation of the molecules from the extract was done using a semi preparative HPLC system. The columns used for isolation were Sunfire RP-18 preparative column (10 µm, 10 mm × 250 mm) and XSelect CSH preparative Fluoro-Phenyl column (5 µm, 10 mm × 250 mm), both columns were purchased from Waters. The mobile phases for the gradients were A [ddH_2O with 0.1% (v/v) formic acid] and B [acetonitrile with 0.1% (v/v) formic acid], flow rate was set to 6.0 mL/min for both columns. Acetonitrile (Prepsolv®, Merk KGaA, Darmsatdt, Germany) and formic acid (33,015, Sigma) were purchased in appropriate quality, ddH_2O was produced with the in-house Milli-Q® system. For the MS-detection of the eluting compounds 1% of the flow was split and blended with 80% MeOH in ddH_2O (v/v) acidified with 0.2% formic acid (Sigma) and directed to the ESI-quadrupole-MS. The fractions were collected by mass triggered fraction collection and the respective fractions were reduced to dryness under reduced pressure and by vacuum centrifugation, both at 40°C. The gradient for the first purification using the RP-18 column was 20 to 100%B in 10 min, retention times for the compounds were: **1**: 7.58 min; **2**: 5.65 min; **3**: 6.42 min; **4**: 6.90 min. For the second purification using the fluoro-phenyl column a gradient from 10 to 100%B in 15 min was used. Retention times of the respective compounds were: **1**: 11.36 min; **2**: 9.11 min; **3**: 10.21 min; **4**: 10.54 min.

2.5.2. NMR spectroscopy

Structure Elucidation. NMR data of the compounds was recorded on a Bruker Avance III HD spectrometer equipped with an inverse detected TCI probe with cryogenic enhancement on ^{1}H, ^{2}H and ^{13}C. Operating frequencies were 599.90 MHz for ^{1}H and 150.86 MHz for ^{13}C. For taking up the spectra the samples were dissolved in DMSO-d_6 (NMR grade, Sigma) and recorded at 298 K. All experiments were recorded using standard pulse sequences for Proton, Presat, Carbon, DQF-COSY, HSQC, HMBC, H2BC, NOESY and ROESY (gradient selected and adiabatic versions, with matched sweeps where applicable) in Topspin 3.5pl7 and processed in Mnova 12.0.0. The solvent peak of DMSO-d_6 was used to reference the spectra. HR-MS data were recorded on the same instrument detailed in the "Compound identification and dereplication" section.

2.6. Biological characterization of 1–4

2.6.1. Antibacterial assay

To determine and quantify potential anti-microbial activity, a bacterial growth inhibition assay in liquid media was used. The samples were tested against *Staphylococcus aureus* (ATCC 25923), *Escherichia coli* (ATCC 259233), *Enterococcus faecalis* (ATCC 29122), *Pseudomonas aeruginosa* (ATCC 27853), *Streptococcus agalactiae* (ATCC 12386) and Methicillin resistant *Staphylococcus aureus* (MRSA) (ATCC 33591). *S. aureus*, MRSA, *E. coli* and *P. aeruginosa* were grown in Muller Hinton broth (275730, Becton, Dickinson and Company). *E. faecalis* and *S. agalactiae* were cultured in brain hearth infusion broth (53286, Sigma). Fresh bacteria colonies were transferred to the respective medium and incubated at 37°C overnight. The bacterial cultures were diluted to a culture density representing the log phase and 50 µL/well were pipetted into a 96-well microtiter plate (734–2097, Nunclon™, Thermo Scientific, Waltham, MA, United States). The final cell density was 1500–15,000 CFU/well. The compound was diluted in 2% (v/v) DMSO in ddH_2O, the final assay concentration was 50% of the prepared sample, since 50 µL of sample in DMSO/water were added to 50 µL bacterial culture. After adding the samples to the plates, they were incubated over night at 37°C and the growth was determined by measuring the optical density at $\lambda = 600$ nm (OD600) with a 1420 Multilabel Counter VICTOR3™ (Perkin Elmer). A water sample was used as reference control, growth medium without bacteria was used as a negative control and a dilution series of gentamycin (A2712, Merck) from 32 to 0.01 µg/mL was used as positive control and visually inspected for bacterial growth. The positive control was used as system suitability test and the results of the antimicrobial assay were only considered valid when positive control was passed. The final concentration of DMSO in the assays was ≤2% (v/v) known to have no effect in the tested bacteria.

2.6.2. Antibiofilm assay

For testing the inhibition of biofilm formation *Staphylococcus epidermidis* (ATCC 35984) was grown in Tryptic Soy Broth (TSB, 105459, Merck, Kenilworth, NJ, United States) overnight at 37°C. The overnight culture was diluted in fresh medium with 1% glucose (D9434, Sigma-Aldrich) (glucose was added for the induction of biofilm formation by *Staphylococcus epidermidis*) before being transferred to a 96-well microtiter plate; 50 µL/well were incubated overnight with 50 µL of the test compound dissolved in 2% (v/v) DMSO aq. added in duplicates. During the over-night culture, *S. epidermidis* was allowed to form a bacterial biofilm within the wells. The bacterial culture was removed from the plate and the plate was washed with ddH_2O to remove remaining culture. The biofilm adhering within the wells of the 96 well plates was fixed at 65°C for 1 h before 70 µL 0.1% crystal violet (115,940, Merck Millipore) was added to the wells for 10 min of incubation to stain the biofilm. Excess crystal violet solution was then removed and the plate dried for 1 h at

65°C. Seventy microliters of 70% EtOH were then added to each well and the plate incubated on a shaker for 5–10 min to dissolve the stain carried by the biofilm. Inhibition of biofilm formation was assessed by the presence of violet color from the stained biofilm and was measured at 600 nm absorbance using a 1,420 Multilabel Counter VICTOR3 TM. Fifty microliters of a non-biofilm forming *Staphylococcus haemolyticus* (clinical isolate 8-7A, University hospital, UNN, Tromsø, Norway) mixed in 50 µL autoclaved ddH_2O water was used as a control; 50 µL *S. epidermidis* mixed in 50 µL autoclaved ddH_2O water was used as the control for biofilm formation; and 50 µL TSB with 50 µL autoclaved ddH_2O water was used as a medium blank control.

2.6.3. Cytotoxicity assays

The inhibitory effect of compounds was tested using MTS *in vitro* cell proliferation assays against two malignant and one non-malignant cell line. The malignant cell lines were human melanoma A2058 (ATCC, CLR-1147™) and acute myeloid leukemia MOLM 13 (Matsuo et al., 1997), as cell line for the general cytotoxicity assessment, non-malignant MRC5 lung fibroblast cells (ATCC CCL-171™) were used. The cells were cultured and assayed in Roswell Park Memorial Institute medium (RPMI-16040, FG1383, Merck) containing 10% (v/v) Fetal Bovine serum (FBS, 50115, Biochrom, Cambridge, United Kingdom). The cell-concentration was 4,000 cells/well for the lung fibroblast cells and 2,000 cells/well for the cancer cells. After seeding, the cells were incubated 24 h at 37°C and 5% CO_2. The medium was then replaced with fresh RPMI-1640 medium supplemented with 10% (v/v) FBS and gentamycin (10 µg/mL, A2712, Merck). After adding 10 µL of sample diluted in 2% (v/v) DMSO in ddH2O the cells were incubated for 72 h at 37°C and 5% CO2. For assaying the viability of the cells 10 µL of CellTiter 96AQueous One® Solution Reagent (G3581, Promega, Madison, WI, United States) containing tetrazolium [3-(4,5-dimethylthiazol-2-yl)-5-(3-carboxymethoxyphenyl)-2-(4-sulfophenyl)-2H-tetrazolium, inner salt] and phenazine ethosulfate was added to each well and incubated for 1 h. The tests were executed with three technical replicates and were repeated twice. The plates were read using a DTX 880 plate reader by measuring the absorbance at $\lambda = 485$ nm. The cell viability was calculated using the media control. As a negative control RPMI-1640 with 10% (v/v) FBS was used and 0.5% Triton™ X-100 (Sigma-Aldrich) was used as a positive control. The data was processed and visualized using GraphPad Prism 8.

2.7. Genome and gene-cluster analysis

The recently published genome of *Nostoc* KVJ20 (Halsør et al., 2019) was submitted to antiSMASH (Medema et al., 2011). Genes predicted to belong to the aeruginosin biosynthetic gene clusters were found at the edges of several contigs. Therefore, we have undertaken analysis of additional data acquired in connection to the previous genome study and processed in the same way (Halsør et al., 2019). We were able to find a contig containing the entire operon which was verified again by antiSMASH. The *bsl*-operon was deposited within GenBank and can be retrieved under the following accession number: MT269816.

2.8. RNA isolation and gene expression studies

As an addition to the genome-wide BGC survey we have conducted a gene expression study described in detail within the Supplementary Information S30. Along with *bslA* gene, we investigated expression patterns for all other 18 BGCs as well as *nifH*, *avaK* and *gvpC* indicative of diazotrophic growth, akinete and hormogonia differentiation, respectively. In addition to the standard cultivation condition, the cultures were subjected to nitrogen, phosphate or iron depletion, and to the presence of competitor strains. The comprehensive data is given in the Supplementary material.

3. Results and discussion

3.1. Compound identification and dereplication

Investigation of the methanol–water extract of KVJ20 cells using UHPLC-IMS-MS led to the identification of four compounds with a common fragment at *m/z* 610.3203 $[M+H]^+$ ($C_{27}H_{44}N_7O_9$, calcd. *m/z* = 610.3201, mass error: 0.33 ppm, see Supplementary material S1.1). This mass and calculated elemental composition, are identical to the desulfo-aglycon moiety of **5**–**7** (see Supplementary material S1.6), which indicates that the compounds belong to the bsl family of molecules. The tentative identification of the new compounds' structural relationship to the banyasides was supported by comparing their obtained MS spectra to the published MS spectrum of synthetic **6** (Schindler et al., 2010). Signals of a neutral loss of 80 u in ESI+ (see Supplementary material S1.1) indicated that the molecules were carrying a sulfate group. The supernatants of the bacterial cultures were analyzed for the presence of the compounds described above, but none of them were detected, indicating that they were not excreted by the cells to the growth medium. In addition to compounds **1**–**4**, dereplication of the cyanobacterial extract gave a hit in the ChemSpider database for elemental composition and one common fragment of the anabeanopeptin-like cyclic peptide schizopeptin at m/z 792.46506 $[M+H]^+$ (calcd. m/z = 792.46599, $C_{42}H_{62}N_7O_8$), fragmentation and elemental compositions fitted schizopeptin 791 (see Supplementary materials S2, S3; Reshef and Carmeli, 2002). Schizopeptin has not been reported for this strain previously, but as schizopeptin is well described in literature, the peptide was not selected for isolation in this study.

3.2. Isolation and chemical characterization of the compounds 1–4

Compounds **1**–**4** were isolated using mass-guided fractionation on preparative HPLC from 29.4 g dry mass of lyophilized cyanobacteria from 10 L of culture. For the first purification step, the compounds were separated using a C18 reversed phase column. The collected fractions were reduced to dryness at 40°C *in vacuo*. The fractions were dissolved in DMSO or methanol (**1** dissolved poorly in methanol, but well in DMSO after extensive shaking, **2**–**4** dissolved well in methanol), and isolated in a second step using a fluoro-phenyl reversed phase column. The yields were: **1**: 9.8 mg; **2**: 4.1 mg; **3**: 5.9 mg; **4**: 2.6 mg.

3.2.1. Isolated compounds

Suomilide B (**1**): white powder (9.8 mg); HRESIMS *m/z* 1075.4496 $[M-H]^-$ (calcd. for $C_{45}H_{71}N_8O_{20}S$, 1075.4510) Mass error: 1.30 ppm.

Retention Time$_{UPLC}$: 4.14 min; CCS values for the respective adducts (N_2 as drift gas) $[M+H]^+$: 325.25 Å^2; $[M\text{-}H]^-$: 332.58 Å^2.

Suomilide C (**2**): white powder (4.1 mg); HRESIMS *m/z* 977.3781 $[M-H]^-$ (calcd. for $C_{39}H_{61}N_8O_{19}S$, 977.3774) Mass error: 0.72 ppm. Retention Time$_{UPLC}$: 2.10 min; CCS values for the respective adducts (N_2 as drift gas) $[M+H]^+$: 297.83 Å^2; $[M\text{-}H]^-$: 296.73 Å^2.

Suomilide D (**3**): white powder (5.9 mg); HRESIMS *m/z* 1005.4089 $[M-H]^-$ (calcd. for $C_{41}H_{65}N_8O_{19}S$, 1005.4087) Mass error: 0.20 ppm. Retention Time$_{UPLC}$: 2.93 min; CCS values for the respective adducts (N_2 as drift gas) $[M+H]^+$: 309.25 Å^2; $[M\text{-}H]^-$: 308.06 Å^2.

Suomilide E (**4**): white powder (2.6 mg); HRESIMS *m/z* 1047.4171 $[M-H]^-$ (calcd. for $C_{43}H_{67}N_8O_{20}S$, 1047.4192) Mass error: 2.01 ppm. Retention Time$_{UPLC}$: 3.30 min; CCS values for the respective adducts (N_2 as drift gas) $[M+H]^+$: 317.28 Å^2; $[M\text{-}H]^-$: 320.59 Å^2.

3.2.2. Structure elucidation

Suomilide B (**1**) (Figure 1A) was isolated as white crystalline substance. The molecular formula was calculated to be $C_{45}H_{72}N_8O_{20}S$ by HRESIMS, suggesting a presence of 14 degrees of unsaturation. 1D (^{1}H and ^{13}C, Tables 1, 2 and Supplementary Figures S4, S5) and 2D (HSQC, HMBC, COSY, ROESY, Supplementary Figures S6–S8) NMR data resembled those reported for **7** (Supplementary Table S9) and allowed seven substructures of **1** to be assigned. The substructures were isoleucine (Ile), 1-amidino-3-(2-aminoethyl)-3-pyrroline (Aaep), azabicyclononane (Abn), glycolipid with a methylated hexose core decorated with the subunits butyric acid (BA), carbamic acid (CA) and hexanoic acid (HA) (Figure 3A). An additional substructure, 2-O-methylglyceric acid 3-O-sulfate (MgS), was partially assigned, the sulfate group at C-1 was finally assigned based on elimination of every other possible binding site for the group (Figure 3B).

The Abn substructure was assigned based on COSY and HMBC correlations, and by comparing our data to previously published data (Fujii et al., 1997). A COSY spin system was observed from H-17 (δH 3.72) to H-21a (δH 2.14)/H-21b (δH 1.99). The shift value of the tertiary C-17 (δC 65.7) suggested hydroxylation in this position. HMBC correlations furthermore linked both H-17 and H-21a to the quaternary C-16 (δC 80.5) carbon atom, which was further linked to H-13 (δH 4.22) through an HMBC correlation. The downfield shift value of C-16 (δC 80.5) suggested that it was linked to an oxygen. H-13 was linked to H-12 (δH 4.52) through a COSY correlation. A HMBC correlation was observed between NH-14 (δH 7.98) and carbon atoms C-13 (δC 58.3) and C-15 (δC 156.7). The de-shielded shift value of C-15 (δC 156.7) was characteristic for a carboxyl carbon, placing an oxygen atom at this position, and attached C-15 to C-16 via an ester linkage. Our 1D NMR data closely resembles that of the previously published data for the Abn subunit. When comparing 1D NMR data for protons and carbons 12–22 to the same data recorded for **7** (Fujii et al., 1997), the ΔδC shift values varies on average 0.12 ppm and ΔδH shift values varies on average 0.03 ppm (data recorded in DMSO-d_6, Supplementary Table S9). This confirmed that **1** had the Abn moiety, which is a collective feature of the bsl family of compounds.

The Ile subunit was assigned based on typical proton and carbon chemical shifts and correlations in HMBC and COSY spectra and was found to be attached from C-10 (δC 171.9) to position 11 of the Azbn subunit through a weak HMBC correlation between H-12 (δH 4.52) and C-10 (δC 171.9). This places a nitrogen in the 11 position and completes the tricyclic Abn subunit. The MgS subunit was assigned based on 1D NMR shift values and HMBC and COSY correlations. It was found to be attached to N-4 of the Ile group through an HMBC correlation between NH-4 (δH 7.94) and C-3 (δC 169.8). A sulfate group at C-1 based on elimination of every other possible binding site for the group. The glycosyl group of the glycolipid subunit was determined to be methylated hexose based on typical proton and carbon chemical shifts and correlations in HMBC and COSY spectra. The hexose was determined to be methylated through an HMBC correlation between H-38a (δH 3.34) and H-38b (δH 3.25) and the primary carbon atom C-39 (δC 58.5). The glucose subunit was found to be attached through an ether bond to C-20 of the Abn subunit through a weak HMBC correlation between H-33 (δH 4.97) and C-20 (δC 70.0). The CA subunit was assigned based on 1D and 2D NMR data and was found to be linked to the hexose subunit through an ester bond determined by a weak HMBC correlation between H-35 (δH 5.02) and the quaternary C-46 carbon atom (δC 115.4). The HA and BA subunits were identified by correlations in the HMBC and COSY spectra. The HA and BA subunits were linked to the hexose subunit through ester bonds. The HA subunit was placed at C-36-O through an HMBC correlation between H-36 (δH 5.34) and C-40 (δC 172.9). The BA subunit was found to be linked to C-34 through an ether bond through weak ROESY correlations between H-34 (δH 4.83) and the BA protons H-49 (δH 2.41–2.24) and H-50 (δH 1.54). Consequently, the structure of **1** was assigned.

Suomilide C (**2**) (Figure 1A) was isolated as white crystalline substance. The molecular formula was calculated to be $C_{39}H_{62}N_8O_{19}S$ by HRESIMS, suggesting a presence of 13 degrees of unsaturation. The mass and elemental composition of **2** indicated that its structure was closely related to that of **1**. By close inspection of 1D (^{1}H, ^{13}C, Tables 1, 2 and Supplementary Figures S10, S11) and 2D (HSQC, HMBC, COSY, TOCSY and ROESY, Supplementary Figures S12–S15) NMR data, the structure of 2 was elucidated in a similar manner as described above for **1**. In the ^{13}C spectra, only 22 of the carbon atoms gave prominent peaks. The remaining carbon atom shift values were extracted from the HSQC spectra. When comparing the ^{1}H and ^{13}C chemical shift values of **1** and **2** for the MgS, Ile, Abn, Aaep, CA and BA substructures, the values were found to conform well (ΔδC average: 0.2 ppm, ΔδH average: 0.013 ppm). The most noticeable difference between the ^{1}H-NMR datasets of **1** and **2**, was the lack of a proton resonance for H-36 at 5.34 ppm in the ^{1}H spectrum of **2**. Instead, H-36 was found to have a shift value of 3.86 ppm. The shift value of C-36 had also changed from 68.4 ppm in **1** to 66.4 in **2**. The shielding of CH-36 could be explained by elimination of the HA subunit, causing C-36 to be attached to a hydroxyl group rather than, as in **1**, an ester. Elimination of HA was in line with the difference in the calculated elemental compositions of **1** and **2**. Signals from the HA subunit were however still visible but were significantly less prominent in the spectra recorded for **2**. Thus, the structure of **2** was confirmed and **1** was confirmed to be present in the sample of **2** as a minor component.

Suomilide D (**3**) (Figure 1A) was isolated as white crystalline substance. The molecular formula was calculated to be $C_{41}H_{66}N_8O_{19}S$ by HRESIMS, suggesting a presence of 13 degrees of unsaturation. Compared to **1**, the calculated elemental composition of **3** indicated the compound as a variant of **1** lacking BA on the methylated hexose subunit. 1D (^{1}H and ^{13}C, Tables 1, 2 and Supplementary Figures S16, S17) and 2D (HSQC, HMBC, COSY and ROESY, Supplementary Figures S18–S20) NMR analysis,

10.3389/fmicb.2023.1130018

TABLE 1 ^{1}H NMR assignments for suomilides B – E (1–4) (^{1}H 600MHz, DMSO-d_6).

	δ_H (*J* in Hz)			
Position	1	2	3	4
1a	3.96–3.90, m*	3.97–3.85, m*	3.94, m	3.92, m*
1b	3.76, dt (11.9, 7.7)	3.76, dd (11.6, 7.8)	3.74, m	3.76, m*
2	3.96–3.90, m*	3.97–3.85, m*	3.92, m	3.92, m*
4	7.94, d (6.9)	8.00–7.92, m*	7.92, d (7.1)	7.88, d (7.2)
5	4.62, t (6.9)	4.62, t (7.0)	4.63, t (6.8)	4.63, t (7.0)
6	1.72, m*	1.71, m*	1.71, s*	1.70, m*
7	0.92–0.83, m*	0.92–0.79, m*	0.92–0.85, m*	0.96–0.78, m
8a	1.29, m*	1.29, m	1.29, m	1.29, m
8b	1.19, m	1.17, m	1.17, m	1.16, m
9	0.92–0.83, m*	0.92–0.79, m*	0.92–0.85, m*	0.96–0.78, m
12	4.52, d (2.4)	4.54, m	4.56, dd (7.4, 2.2)	4.52, d (2.4)
13	4.22, s	4.23, m	4.24, s*	4.20, d (2.4)
14	7.98, s	8.00–7.92, m*	8.10, s	8.09, s
17	3.72, s*	3.71, m	3.71, m	3.72, m*
18	4.28, s	4.27, m	4.24, s*	4.26, d (13.6)
19a	2.14, d (11.1, 5.4)	2.12, d (12.9)	2.15, d (11.8)	2.13, t (7.4)
19b	1.72, m*	1.71, m*	1.71, s*	1.72, m*
20	3.72, m*	3.69, m	3.72, m*	3.75, m*
21a	2.41–2.24, m*	2.30, m*	2.29, m*	2.32–2.23, m*
21b	1.99, dd (11.1, 5.4)	1.96, m	1.94, m	1.98, m
23	7.59, s	7.61, s	7.73, s	7.73, d (6.0)
24	3.18, m	3.18, m	3.19, m	3.19, m
25	2.41–2.24, m*	2.32–2.23, m*	2.26, m*	2.32–2.23, m*
27	5.64, s	5.64, s	5.63, s	5.64, s
28	4.17–4.11, m*	4.12, m	4.10, m*	4.12, m*
30	4.17–4.11, m*	4.12, m	4.11, m*	4.11, m*
32′/32″	7.25, s	7.23, s	7.20, s	7.66, s
33	4.97, d (3.8)	4.90–4.80, m	4.85, d (3.8)	4.96, d (3.8)
34	4.83, dd (11.0, 3.7)	4.90–4.80, m	4.49, dd (10.4, 3.7)	4.84, dd (11.0, 3.7)
35	5.02, dd (11.0, 3.5)	4.95, dd (10.7, 3.9)	4.95, dd (11.2, 8.4)	5.02, dd (11.0, 3.4)
36	5.34, d (3.3)	3.89, m	3.33, m*	5.35, m
37	4.17–4.11, m*	3.88, m	3.67, m	4.14, m
38a	3.34, m	3.44, m	3.50, m	3.34, m
38b	3.25, dd (10.0, 6.0)	3.38, m	3.38, m*	3.25, m
39	3.21, s	3.25, s	3.25, s	3.21, s
41	2.41–2.24, m*	–	2.27, m*	2.32–2.23, m*
42	1.54, m*	–	1.51, *p* (7.3)	1.60–1.49, m*
43	1.28, m*	–	1.24, m*	0.96–0.78, m
44	1.28, m*	–	1.26, m*	–
45	0.92–0.83, m*	–	0.92–0.85, m*	–
47	6.56, s	6.50, s	6.44, m	6.56, s
49	2.41–2.24, m*	2.32–2.23, m*	–	2.32–2.23, m*

(Continued)

TABLE 1 (Continued)

	δ_H (*J* in Hz)			
Position	1	2	3	4
50	1.54, m*	1.53, m	–	1.60–1.49, m*
51	0.92–0.83, m*	0.92–0.79 (m)*	–	0.96–0.78, m
2me	3.30, s	3.30, s	3.30, s	3.30, s

* Peaks are overlapped; n.d., not detected; –, protons not part of the structure.

TABLE 2 ^{13}C NMR assignments for suomilides B – E (1–4) (^{13}C 150MHz, DMSO-d_6).

	δ_C, type					δ_C, type			
Position	1	2	3	4	Position	1	2	3	4
1	66.2, CH_2	65.9, CH_2	66.2, CH_2	66.2, CH_2	28	55.4, CH	55.4, CH	55.3, CH_2	55.3, CH_2
2	80.2, CH	79.9, CH	80.3 CH	80.3, CH	30	54.2, CH	54.2, CH	54.1, CH_2	54.1, CH_2
3	169.8, C	169.7, C	169.7, C	169.7, C	31	154.2, C	154.0, C	154.5, C	154.5, C
5	53.1, CH	52.9, CH	53.0, CH	52.9, CH	33	94.7, CH	94.6, CH	94.2, CH	94.0, CH
6	36.5, CH	36.3, CH	36.5, CH	36.5, CH	34	68.0, CH	68.8, CH	71.0, CH	68.0, CH
7	14.5, CH_3	14.1, CH_3	14.5, CH_3	14.5, CH_3	35	66.6, CH	67.7, CH	71.5, CH	66.6, CH
8	25.4, CH_2	25.3, CH_2	25.5, CH_2	25.4, CH_2	36	68.4, CH	66.4, CH	68.0, CH	68.4, CH
9	11.8, CH_3	11.5, CH_3	11.8, CH_3	11.8, CH_3	37	67.0, CH	68.7, CH	71.4, CH	67.0, CH
10	171.9, C	171.2, C	171.8, C	171.8, C	38	70.0, CH_2	70.4, CH_2	70.8, CH_2	70.0, CH_2
12	56.9, CH	56.6, CH	56.8, CH	57.0, CH	39	58.5, CH_3	58.4, CH_3	58.5, CH_3	58.6, CH_3
13	58.3, CH	57.9, CH	58.2, CH	58.2, CH	40	172.0, C	–	172.6, C	171.8, C
15	156.7, C	156.7, C	156.6, C	156.7, C	41	33.3, CH_2	–	33.5, CH_2	35.3, CH_2
16	80.5, C	80.3, C	80.5, C	80.5, C	42	24.1, CH_2	–	24.1, CH_2	18.0, CH_2
17	65.7, CH	65.6, CH	65.8, CH	65.7, CH	43	30.6, CH_2	–	30.5, CH_2	13.4, CH_3*
18	53.4, CH	53.2, CH	53.5, CH	53.4, CH	44	21.8, CH_2	–	21.8, CH_2	-
19	28.8, CH_2	28.6, CH_2	28.8, CH_2	28.9, CH_2	45	13.8, CH_3	–	13.8, CH_3	–
20	70.0, CH	69.1, CH	69.3, CH	70.0, CH	46	155.4, C	156.3, C	156.3, C	155.4, C
21	34.4, CH_2	34.4, CH_2	34.4, CH_2	34.5, CH_2	48	172.6, C	172.3, C	–	172.6, C
22	168.8, C	168.7, C	168.8, C	168.9, C	49	35.3, CH_2	35.2, CH_2	–	35.5, CH_2
24	37.2, CH_2	36.9, CH_2	37.2, CH_2	37.2, CH_2	50	18.0, CH_2	17.8, CH_2	–	18.0, CH_2
25	27.8, CH_2	27.6, CH_2	27.8, CH_2	27.8, CH_2	51	13.4, CH_3	14.1, CH_3	–	13.4, CH_3*
26	135.9, C	135.9, C	136.0, C	136.0, C	2me	57.3, CH_3	57.07, CH_3	57.3, CH_3	57.4, CH_3
27	119.0, CH	118.8, CH	119.0, CH	119.0, CH					

*Peaks are overlapped; –, carbon atoms not part of the structure.

confirmed that **3** consisted of the Ile, Abn, Aaep, CA and HA subunits. The positions of the Ile, Abn and Aaep subunits were confirmed in a similar manner as described for **1**. In the COSY spectrum (Supplementary Figure S19), H-36 (δH 3.36) coupled to a hydrogen atom at 5.32 ppm. This shift value is comparable to the shift values for the hydroxyl hydrogens on the hexosesubstructure of suomilide (δH 36-OH 5.23, δH 35-OH 5.31) (Fujii et al., 1997), confirming that **3** had an unsubstituted hydroxyl group on C-36 (δC 68.0). The CA subunit was linked to C-35 (δC 71.3) through a HMBC correlation from H-35 (δH 4.96) to C-46 (δC 156.3) (Supplementary Figure S22). The HA subunit was linked C-34 (δC 70.8) through a weak ROESY correlation between H-34 (δH 4.48) and H-41 (δH 2.27) (Supplementary Figure S20). Finally, the structure of the MgS subunit was determined in a similar manner as described for **1**, and the sulfate group was placed at C-1 (δC 65.9) after elimination of every other possible binding site for the group.

Suomilide E (**4**) (Figure 1A) was isolated as white crystalline substance. The molecular formula was calculated to be $C_{43}H_{68}N_8O_{20}S$ by HRESIMS, suggesting a presence of 14 degrees of unsaturation. The structure of **4** was assigned by 1D (^{1}H and ^{13}C, Tables 1, 2 and Supplementary Figures S21, S22) and 2D (HSQC, HMBC, COSY, TOCSY, ROESY and HSQC-HSQCTOCSY, Supplementary Figures S23–S28) NMR experiments. In a similar matter as described above, **4** was confirmed to contain the MgS, Ile, Abn, Aaep and methylated hexose subunits. The decoration of the methylated hexose was determined to be two BA subunits and a CA

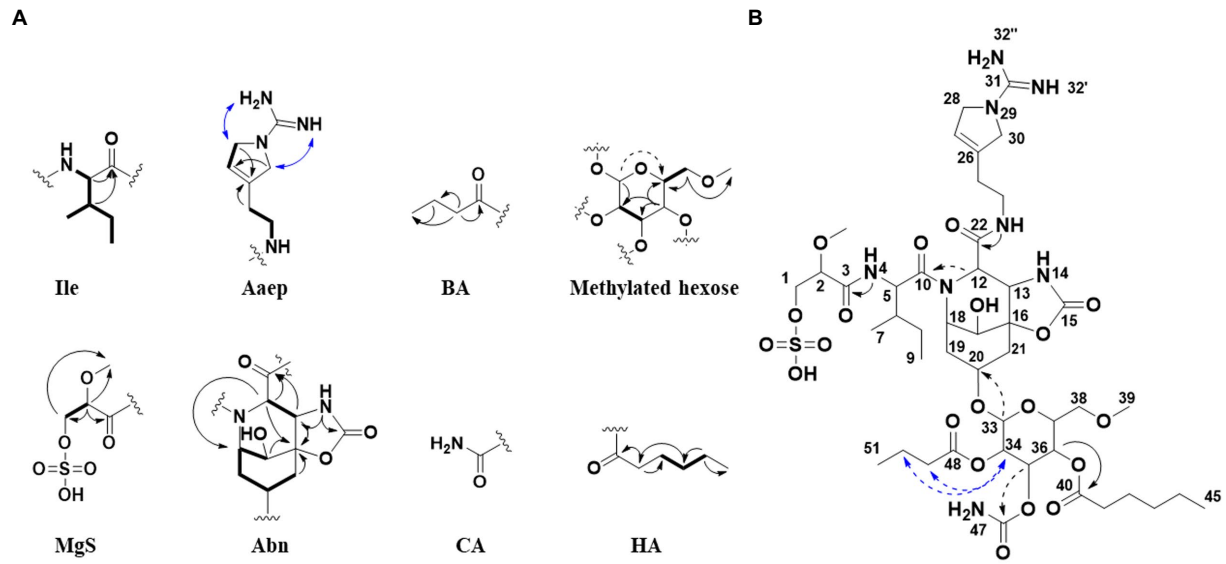

FIGURE 3
(A) Selected 2D NMR correlations obtained for substructures of **1**. **(B)** Key 2D NMR correlations used to connect the substructures and elucidate the complete structure of **1**. HMBC (black arrows), COSY (bold), ROESY (blue arrows). Weak correlations are indicated with dashed arrows. Ile, isoleucine; Aaep, 1-amidino-3-(2-aminoethyl)-3-pyrroline; BA, butyric acid; MgS, 2-O-methylglyceric acid 3-O-sulfate; Abn, azabicyclononane; CA, carbamic acid; HA, hexanoic acid.

subunit. One BA subunit was attached to C-34 (δC 68.0) through a HMBC between H-34 (δH 4.84) to C-48. The second BA subunit was placed at C-36 (δC 66.6) through a HMBC between H-36 (δH 5.35) to C-40 (δC 171.8). The placement of the CA subunit was, as for **1**–**3**, determined to be at C-35 (δC 66.6) through a weak HMBC between H-35 (δH 5.02) and C-46 (δC 155.4). The sulfate group placed at C-1 (δC 66.2) after elimination of every other possible binding site for the group. Thus, the structure of **4** was elucidated.

3.3. Biological evaluation of compounds 1–4

With the isolated compounds **1**–**4** at hand, it was possible to investigate the bioactivity of all four compounds. Since the production of secondary metabolites represents a metabolic and energetic effort, they are likely to give a selective advantage to the producing organism (Maplestone et al., 1992) or have a function within the organism. Were therefore tested to see if **1**–**4** had any effect on the survival of bacterial cells as well as on formation of bacterial biofilm. In addition, the compounds were screened for potential anti-proliferative effects on malignant and non-malignant human cells. We also wanted to investigate if the previously observed bioactivity of this strain (Liaimer et al., 2016) is related to the isolated suomilides, by assaying the ability of **1**–**4** to act as protease inhibitors. For the bioassays, **1**–**4** were dissolved in DMSO and further diluted in ddH_2O.

3.3.1. Antibacterial and antibiofilm activity

There were no significant effects of **1**–**4** when tested at concentrations up to 100 μM against *Staphylococcus aureus*, *Escherichia coli*, methicillin resistant *S. aureus*, *Pseudomonas aeruginosa*, *Enterococcus faecalis* and *Streptococcus agalactiae*. There were also no effects on biofilm formation by *Staphylococcus epidermidis* at concentrations up to 100 μM.

3.3.2. Cytotoxicity against malignant and non-malignant cell lines

The crude extract of KVJ20 was initially assayed against a panel of human cell lines showing anti-proliferative effects against the human non-malignant cell line MRC5 (lung fibroblast) and the human malignant cell line A2058 (melanoma), but the previous study did not show that the extract had any effect against the human malignant cell line HT29 (colon carcinoma) (Liaimer et al., 2016). Therefore, we investigated the bioactivity of **1**–**4** against MRC5 and A2058 as well as the human malignant cell line MOLM13 (acute myeloid leukemia). Compounds **1**–**4** were assayed at concentrations up to 100 μM. No effects were observed.

Compounds 5 and 6 were originally isolated via bioassay guided purification using a serine-protease inhibition assay when they were discovered in 2005 (Pluotno and Carmeli, 2005). The two banyasides were reported to inhibit the catalytic activity of trypsin. As far as we know, anti-bacterial activity of suomilide have not been reported previously, and the *Nostoc* sp. strain it has been isolated from was reported as non-toxic. This complies with our results, as no activity could be detected for **1**–**4** against bacteria or cell lines at high concentrations. Suomilide A has recently been investigated for serine protease inhibition and has been shown to inhibit trypsin-1, −2 and −3 with IC_{50} values of 104, 4.7 and 11.5 nM, respectively (Ahmed et al., 2021). Molecular docking studies of suomilide A revealed that the Aeap and Mgs moieties are responsible for the compound-target interaction with trypsine, confirmed by surface plasmon resonance spectroscopy the revealing residence time of 57 min for trypsin-3 was determined (Ahmed et al., 2021). A concentration of 3.3 μM of suomilide A was shown to inhibit the invasion of prostate cancer cells

in a cell invasion assay while it had no effect on cancer cell proliferation (Ahmed et al., 2021), which is in accordance with our results. Taking a closer look on the structure of other cyanobacterial protease inhibitors, such as cyanopeptolins, microviridins and others, it appears that they are cyclic peptides in contrast to the rigid modified core of the suomilides and banyasides (Singh et al., 2011; Gallegos et al., 2018; Mazur-Marzec et al., 2018; Sieber et al., 2020). The suomilides on the other hand clearly belong to the aeruginosin family of protease inhibitors (Ersmark et al., 2008).

3.4. Biosynthesis of the suomilides

A previous study predicted the presence of 19 gene clusters in KVJ20 containing genes involved in the biosynthesis of nonribosomal peptides, polyketides, and ribosomally synthesized and posttranslational modified peptides (Halsør et al., 2019). In addition to the well-defined anabaenopeptin and nostocyclopeptide gene clusters, we were able to identify genes associated with aeruginosin production and assemble the entire *bsl* gene cluster. The reassembled *bsl* cluster can be retrieved under the gene bank accession number: MT269816 (Figure 4). The cluster consists predominantly of genes that are also present in aeruginosin and saxitoxin (molecular structure in Figure 2) gene clusters. For aeruginosin, the most similar clusters are aeruginosin 126B (BGC0000297) where 41% of the genes show similarity and aeruginosin 98-A (BGC0000298, 42% of genes show similarity).

For saxitoxin, the clusters BGC0000887, BGC0000188 and BGC0000928 show a similarity of 14%. The genes and the respective clusters they originate from are given in Supplementary Table S32 and illustrated in Figure 4. We propose the cluster described here (Figure 4 and Supplementary Table S32) is the biosynthetic gene cluster responsible for the production of the suomilides. The proposed functions for the respective genes are given in Supplementary Table S32. For the banyasides, the biosynthesis of the Abn moiety was proposed to start from L-tyrosine (Pluotno and Carmeli, 2005). The present cluster, however, possesses prephenate decarboxylase (*bslG*), as predicted via anti-smash. We therefore propose an alternative biosynthesis starting from prephenate instead of tyrosine as shown in Figure 5. The biosynthesis of secondary metabolites from prephenate involving prephenate decarboxylases has been observed for bacilysin, salinosporamide A and aeruginoside 126A as well (Mahlstedt et al., 2010). Ahmed et al. (2021) suggested the synthesis of Abn from the Choi moiety (highlighted in Figure 2), starting off from prephenate as well and proposed a similar cluster. They have also identified the presence of the *sxtJ* and *sxtK* genes (see Ahmed et al., 2021; Supplementary Table S2). We have identified *sxtJ,K,L* and *O*-like genes (see Figure 4 and Supplementary Table S29). Another group of protease inhibiting natural products bearing the 2-carboxyl-6-hydroxyoctahydroindole (Choi) moiety are the dysinosins (see Figure 2) that were originally isolated from sponges but are likely to be produced by a cyanobacterial symbiont (Carroll et al., 2002, 2004; Schorn et al., 2019). Also Ahmed et al. compared their cluster, among others, to those of Dysinosin B and Aeruginoside 126A which are related. Based on our findings we hypothesize that the Suomilide BGC shows genes that originate from two "parent" BGCs, one saxitoxin-like and one aeruginoside-like. Interestingly, within our assembly, the genes *sxtJ,K* and *L* cluster together within the BGC as well. The gene *bslJ* is coding a NRPS subunit predicted to incorporate isoleucine which is apparently present in the suomilides. However, *bslA* is predicted to code for a NRPS incorporating proline, we hypothesize that the NRPS-subunit is binding the Abn moiety due to its distant structural similarity to proline (see Figure 5, VII). The proposed cluster and its genes can be related to the structural properties of suomilides.

Potential ecological functions of the suomilides may be related to their serine-protease inhibition, such as anti-grazing activity (Ferrão-Filho and Kozlowsky-Suzuki, 2011; Sieber et al., 2020). This is supported by the fact that the bacteria accumulate suomilides within the cells, and do not release notable amounts to the growth media (Liaimer et al., 2016). In a gene-expression study we investigated the expression of the *bslA* gene and differentiation marker genes under phosphate, iron and nitrogen depletion as well as solid/liquid media. Gene expression patterns in presence of two other cyanobacterial strains (KVJ2 and KVJ10) were also investigated. *bsl* genes showed higher relative expression levels in the cultures under nitrogen limitation. No up-regulation in response to phosphate and iron removal was observed, neither did the presence of competitor strains induce higher transcript levels (see Figure 6 and for a detailed discussion of the results of the gene-expression studies Supplementary material S30). Therefore, it is feasible to suggest that suomilides are in one way or another related to the diazotrophic growth of the producer strain.

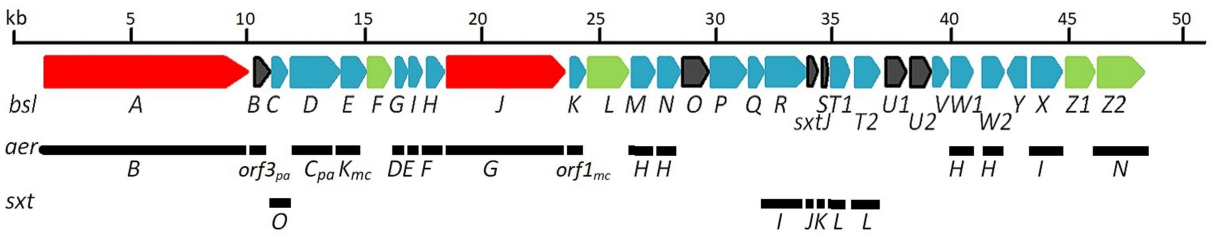

FIGURE 4
bsl-biosynthetic cluster proposed for suomilides: At the top the *bsl*-gene cluster. Below the indication of which genes are similar to those in the respective gene clusters of aeruginosin (*aer*) and saxitoxin (*sxt*). A detailed description is given in Supplementary Table S29. NRPS genes are given in red, other biosynthetic genes in blue and transporters/transport related genes in green. Open reading frames/hypothetical genes are colored black. Genes found only in *Microcystis aeruginosa* or *Planctothrix aghardii* are marked with $_{mc}$ and $_{pa}$, respectively.

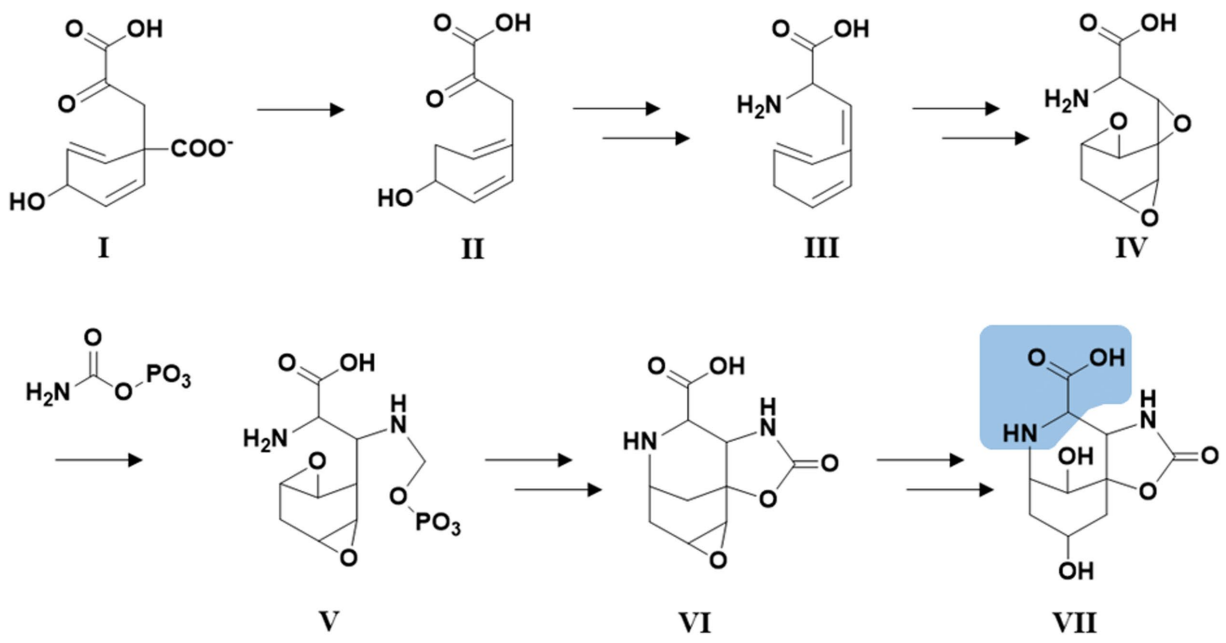

FIGURE 5
Hypothetical biosynthetic pathway for the Abn moiety (VII) based on Pluotno and Carmeli (2005) but starting from prephenate (I). Structural feature highlighted in blue: The structural features of VII which are distantly similar to proline.

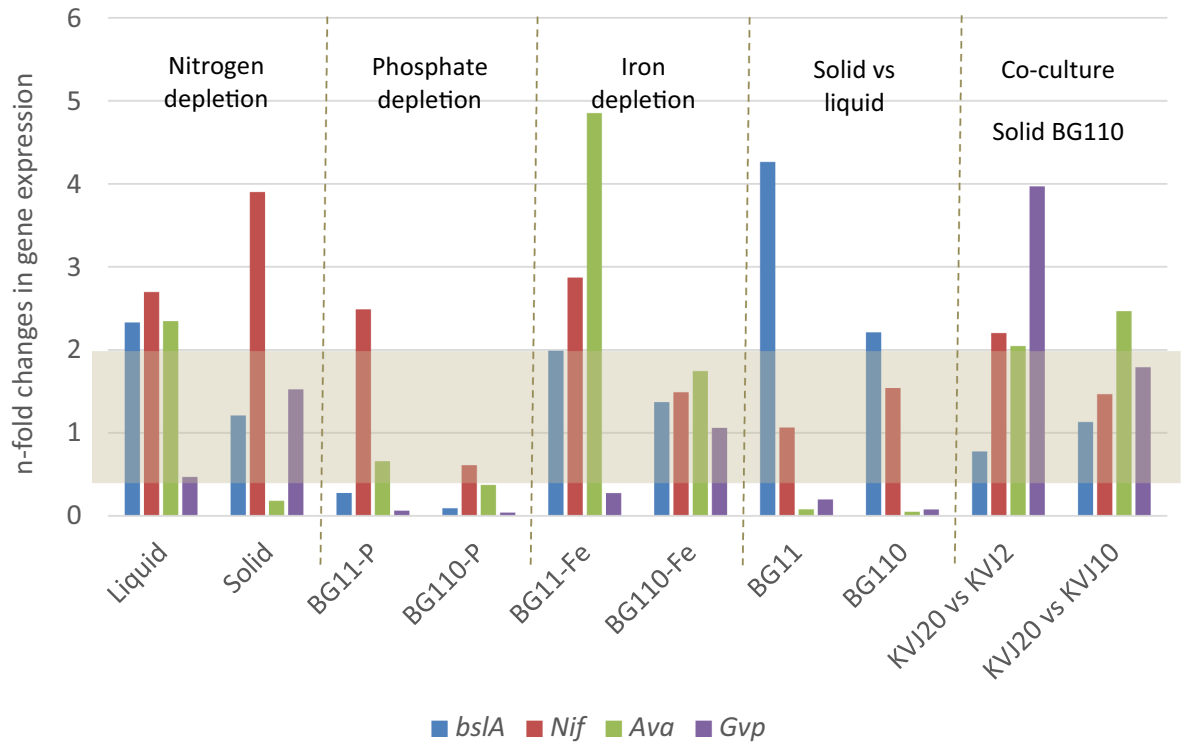

FIGURE 6
Results of the gene expression studies. The results are given as gene expression n-fold change in *Nostoc* sp. KVJ20 for the NRPS gene *bslA*, marker for nitrogen fixation nitrogenase (*nifH*), akinete formation marker (*avaK*), and hormogonia differentiation marker (*gvpC*). The fold changes were calculated as follows. For nitrogen depletion liquid cultures in BG110 medium were compared to liquid cultures in BG11 medium; similarly, the cultures on solid BG110 were compared to cultures on solid BG11. For iron and phosphate depletions, as well as solid vs. liquid grown, the nitrogen regime was the same in mutually compared cultures. The gene expression in colonies grown aside another strain (co-culture) on BG110 agar were compared to cultures on solid BG110 medium with another *Nostoc* sp. KVJ10 or KVJ2 colony as neighbor (Liaimer et al., 2016). The gray area covers the values with less than two-fold change in expression.

4. Conclusion

We were able to isolate four suomilide variants and to elucidate their structures. The compounds did not show any bioactivity against bacteria, bacterial biofilm-generation or against human cell lines, which is in accordance with previous studies demonstrating that suomilide A stops the infiltration of prostate cancer cells but not their proliferation. The suomilides A-E differ among each other in the decoration of their glycon. The biosynthetic gene-cluster we propose for the suomilides suggests that the biosynthesis of azabizyclononane starts from prephenate and the cluster comprises genes from both, aeruginosin and saxitoxin gene clusters.

Data availability statement

The datasets presented in this study can be found in online repositories. The names of the repository/repositories and accession number(s) can be found in the article/Supplementary material.

Author contributions

YS: extraction, isolation, bioactivity testing, HPLC-MS analysis, and preparation of the manuscript. AL and OW: dereplication, cultivation of biomass, genome mining, molecular biology, and preparation of the manuscript. KH: structure elucidation and preparation of the manuscript. JI: NMR spectroscopy and structure elucidation. JA and EH: preparation of the manuscript and review. All authors contributed to the article and approved the submitted version.

Funding

This project was received from the Marie Skłodowska-Curie Action MarPipe, grant agreement GA 721421 H2020-MSCA-ITN-2016, and from UiT – The Arctic University of Norway.

Acknowledgments

We gratefully acknowledge Kirsti Helland and Marte Albrigtsen from Marbio, UiT, for performing the bioactivity assays.

Conflict of interest

The authors declare that the research was conducted in the absence of any commercial or financial relationships that could be construed as a potential conflict of interest.

Publisher's note

All claims expressed in this article are solely those of the authors and do not necessarily represent those of their affiliated organizations, or those of the publisher, the editors and the reviewers. Any product that may be evaluated in this article, or claim that may be made by its manufacturer, is not guaranteed or endorsed by the publisher.

Supplementary material

The Supplementary material for this article can be found online at: https://www.frontiersin.org/articles/10.3389/fmicb.2023.1130018/full#supplementary-material

References

Ahmed, M. N., Wahlsten, M., Jokela, J., Nees, M., Stenman, U.-H., Alvarenga, D. O., et al. (2021). Potent inhibitor of human trypsins from the aeruginosin family of natural products. *ACS Chem. Biol.* 16, 2537–2546. doi: 10.1021/acschembio.1c00611

Caesar, L. K., Montaser, R., Keller, N. P., and Kelleher, N. L. (2021). Metabolomics and genomics in natural products research: Complementary tools for targeting new chemical entities. *Nat. Prod. Rep.* 38, 2041–2065. doi: 10.1039/D1NP00036E

Carroll, A. R., Buchanan, M. S., Edser, A., Hyde, E., Simpson, M., Quinn, R. J., et al. (2004). Dysinosins B-D, inhibitors of factor VIIa and thrombin from the Australian sponge *Lamellodysidea chlorea*. *J. Nat. Prod.* 67, 1291–1294. doi: 10.1021/np049968p

Carroll, A. R., Pierens, G. K., Fechner, G., De Almeida Leone, P., Ngo, A., Simpson, M., et al. (2002). Dysinosin A: A novel inhibitor of factor VIIa and thrombin from a new genus and species of Australian sponge of the family Dysideidae. *J. Am. Chem. Soc.* 124, 13340–13341. doi: 10.1021/ja020814a

Dittmann, E., and Wiegand, C. (2006). Cyanobacterial toxins – occurrence, biosynthesis and impact on human affairs. *Mol. Nutr. Food Res.* 50, 7–17. doi: 10.1002/mnfr.200500162

Ersmark, K., Del Valle, J. R., and Hanessian, S. (2008). Chemistry and biology of the aeruginosin family of serine protease inhibitors. *Angew. Chem. Int. Ed.* 47, 1202–1223. doi: 10.1002/anie.200605219

Ferrão-Filho, A. D. S., and Kozlowsky-Suzuki, B. (2011). Cyanotoxins: Bioaccumulation and effects on aquatic animals. *Mar. Drugs* 9, 2729–2772. doi: 10.3390/md9122729

Fujii, K., Sivonen, K., Adachi, K., Noguchi, K., Shimizu, Y., Sano, H., et al. (1997). Comparative study of toxic and non-toxic cyanobacterial products: A novel glycoside, suomilide, from non-toxic *Nodularia spumigena* HKVV. *Tetrahedron Lett.* 38, 5529–5532. doi: 10.1016/S0040-4039(97)01193-3

Gallegos, D. A., Saurí, J., Cohen, R. D., Wan, X., Videau, P., Vallota-Eastman, A. O., et al. (2018). Jizanpeptins, cyanobacterial protease inhibitors from a *Symploca* sp. cyanobacterium collected in the Red Sea. *J. Nat. Prod.* 81, 1417–1425. doi: 10.1021/acs.jnatprod.8b00117

Halsør, M.-J. H., Liaimer, A., Pandur, S., Ræder, I. L. U., Smalås, A. O., and Altermark, B. (2019). Draft genome sequence of the symbiotically competent cyanobacterium *Nostoc* sp. strain KVJ20. *Microbiol. Resour. Announc.* 8:e01190-19. doi: 10.1128/MRA.01190-19

Kehr, J., Picchi, D. G., and Dittmann, E. (2011). Natural product biosyntheses in cyanobacteria: A treasure trove of unique enzymes. *Beilstein J. Org. Chem.* 7, 1622–1635. doi: 10.3762/bjoc.7.191

Kleigrewe, K., Almaliti, J., Tian, I. Y., Kinnel, R. B., Korobeynikov, A., Monroe, E. A., et al. (2015). Combining mass spectrometric metabolic profiling with genomic analysis: A powerful approach for discovering natural products from cyanobacteria. *J. Nat. Prod.* 78, 1671–1682. doi: 10.1021/acs.jnatprod.5b00301

Li, Y., and Rebuffat, S. (2020). The manifold roles of microbial ribosomal peptide-based natural products in physiology and ecology. *J. Biol. Chem.* 295, 34–54. doi: 10.1074/jbc.REV119.006545

Liaimer, A., Jensen, J. B., and Dittmann, E. (2016). A genetic and chemical perspective on symbiotic recruitment of cyanobacteria of the genus Nostoc into the host plant *Blasia pusilla* L. (brief article). *Front. Microbiol.* 7:1693. doi: 10.3389/fmicb.2016.01693

Mahlstedt, S., Fielding, E. N., Moore, B. S., and Walsh, C. T. (2010). Prephenate decarboxylases: A new prephenate-utilizing enzyme family that performs nonaromatizing decarboxylation en route to diverse secondary metabolites. *Biochemistry* 49, 9021–9023. doi: 10.1021/bi101457h

Maplestone, R. A., Stone, M. J., and Williams, D. H. (1992). The evolutionary role of secondary metabolites — a review. *Gene* 115, 151–157. doi: 10.1016/0378-1119(92)90553-2

Matsuo, Y., MacLeod, R., Uphoff, C. C., Drexler, H. G., Nishizaki, C., Katayama, Y., et al. (1997). Two acute monocytic leukemia (AML-M5a) cell lines (MOLM-13 and MOLM-14) with interclonal phenotypic heterogeneity showing MLL-AF9 fusion

resulting from an occult chromosome insertion, ins(11;9)(q23;p22p23). *Leukemia* 11, 1469–1477. doi: 10.1038/sj.leu.2400768

Mazur-Marzec, H., Fidor, A., Cegłowska, M., Wieczerzak, E., Kropidłowska, M., Goua, M., et al. (2018). Cyanopeptolins with trypsin and chymotrypsin inhibitory activity from the cyanobacterium Nostoc edaphicum CCNP1411. *Mar. Drugs* 16:220. doi: 10.3390/md16070220

Medema, M. H., Blin, K., Cimermancic, P., De Jager, V., Zakrzewski, P., Fischbach, M. A., et al. (2011). antiSMASH: Rapid identification, annotation and analysis of secondary metabolite biosynthesis gene clusters in bacterial and fungal genome sequences. *Nucleic Acids Res.* 39, W339–W346. doi: 10.1093/nar/gkr466

Micallef, M. L., D'agostino, P. M., Sharma, D., Viswanathan, R., and Moffitt, M. C. (2015). Genome mining for natural product biosynthetic gene clusters in the subsection V cyanobacteria. *BMC Genomics* 16:669. doi: 10.1186/s12864-015-1855-z

Mihali, T. K., Kellmann, R., and Neilan, B. A. (2009). Characterisation of the paralytic shellfish toxin biosynthesis gene clusters in *Anabaena circinalis* AWQC131C and *Aphanizomenon* sp. NH-5. *BMC Biochem.* 10:8. doi: 10.1186/1471-2091-10-8

Namikoshi, M., and Rinehart, K. (1996). Bioactive compounds produced by cyanobacteria. *J. Ind. Microbiol.* 17, 373–384. doi: 10.1007/BF01574768

Nilsson, M., Bergman, B., and Rasmussen, U. (2000). Cyanobacterial diversity in geographically related and distant host plants of the genus Gunnera. *Arch. Microbiol.* 173, 97–102. doi: 10.1007/s002039900113

Nunnery, J. K., Mevers, E., and Gerwick, W. H. (2010). Biologically active secondary metabolites from marine cyanobacteria. *Curr. Opin. Biotechnol.* 21, 787–793. doi: 10.1016/j.copbio.2010.09.019

Patiny, L., and Borel, A. (2013). ChemCalc: A building block for tomorrow's chemical infrastructure. *J. Chem. Inf. Model.* 53, 1223–1228. doi: 10.1021/ci300563h

Pluotno, A., and Carmeli, S. (2005). Banyasin A and banyasides A and B, three novel modified peptides from a water bloom of the cyanobacterium *Nostoc* sp. *Tetrahedron* 61, 575–583. doi: 10.1016/j.tet.2004.11.016

Reshef, V., and Carmeli, S. (2002). Schizopeptin 791, a new anabeanopeptin-like cyclic peptide from the cyanobacterium *Schizothrix* sp. *J. Nat. Prod.* 65, 1187–1189. doi: 10.1021/np020039c

Schindler, C. S., Bertschi, L., and Carreira, E. M. (2010). Total synthesis of nominal banyaside B: Structural revision of the glycosylation site. *Angew. Chem. Int. Ed.* 49, 9229–9232. doi: 10.1002/anie.201004047

Schorn, M. A., Jordan, P. A., Podell, S., Blanton, J. M., Agarwal, V., Biggs, J. S., et al. (2019). Comparative genomics of cyanobacterial symbionts reveals distinct, specialized metabolism in tropical dysideidae sponges. *mBio* 10:e00821-19. doi: 10.1128/mBio.00821-19

Sieber, S., Grendelmeier, S. M., Harris, L. A., Mitchell, D. A., and Gademann, K. (2020). Microviridin 1777: A toxic chymotrypsin inhibitor discovered by a metabologenomic approach. *J. Nat. Prod.* 83, 438–446. doi: 10.1021/acs.jnatprod.9b00986

Singh, R. K., Tiwari, S. P., Rai, A. K., and Mohapatra, T. M. (2011). Cyanobacteria: An emerging source for drug discovery. *J. Antibiot.* 64, 401–412. doi: 10.1038/ja.2011.21

frontiers | Frontiers in Microbiology

TYPE Correction
PUBLISHED 07 June 2023
DOI 10.3389/fmicb.2023.1221368

OPEN ACCESS

APPROVED BY
Frontiers Editorial Office,
Frontiers Media SA, Switzerland

*CORRESPONDENCE
Yannik K.-H. Schneider
✉ yannik.k.schneider@uit.no

RECEIVED 12 May 2023
ACCEPTED 26 May 2023
PUBLISHED 07 June 2023

CITATION
Schneider YK-H, Liaimer A, Isaksson J, Wilhelmsen OSB, Andersen JH, Hansen KØ and Hansen EH (2023) Corrigendum: Four new suomilides isolated from the cyanobacterium *Nostoc* sp. KVJ20 and proposal of their biosynthetic origin.
Front. Microbiol. 14:1221368.
doi: 10.3389/fmicb.2023.1221368

Corrigendum: Four new suomilides isolated from the cyanobacterium *Nostoc* sp. KVJ20 and proposal of their biosynthetic origin

Yannik K.-H. Schneider[1]*, Anton Liaimer[2], Johan Isaksson[3], Oda S. B. Wilhelmsen[2], Jeanette H. Andersen[1], Kine Ø. Hansen[1] and Espen H. Hansen[1]

[1]Marbio, Faculty of Biosciences, Fisheries and Economics, UiT—The Arctic University of Norway, Tromsø, Norway, [2]Department of Arctic and Marine Biology, Faculty of Biosciences, Fisheries and Economics, UiT—The Arctic University of Norway, Tromsø, Norway, [3]Department of Chemistry, Faculty of Natural Sciences, UiT—The Arctic University of Norway, Tromsø, Norway

KEYWORDS

***Nostoc*, cyanobacteria, natural products, protease inhibitor, biosynthesis, secondary metabolites, aeruginosin, suomilide**

A corrigendum on
Four new suomilides isolated from the cyanobacterium *Nostoc* sp. KVJ20 and proposal of their biosynthetic origin

by Schneider, Y. K.-H., Liaimer, A., Isaksson, J., Wilhelmsen, O. S. B., Andersen, J. H., Hansen, K. Ø., and Hansen, E. H. (2023). *Front. Microbiol.* 14:1130018. doi: 10.3389/fmicb.2023.1130018

In the published article, there was an error in Figure 1 as published. In Figure 1, the list of compounds was incorrectly presented, such that six compounds were listed rather than seven and the order of compounds was not correct. The corrected Figure 1 and its caption appear below.

The authors apologize for this error and state that this does not change the scientific conclusions of the article in any way. The original article has been updated.

Publisher's note

All claims expressed in this article are solely those of the authors and do not necessarily represent those of their affiliated organizations, or those of the publisher, the editors and the reviewers. Any product that may be evaluated in this article, or claim that may be made by its manufacturer, is not guaranteed or endorsed by the publisher.

10.3389/fmicb.2023.1221368

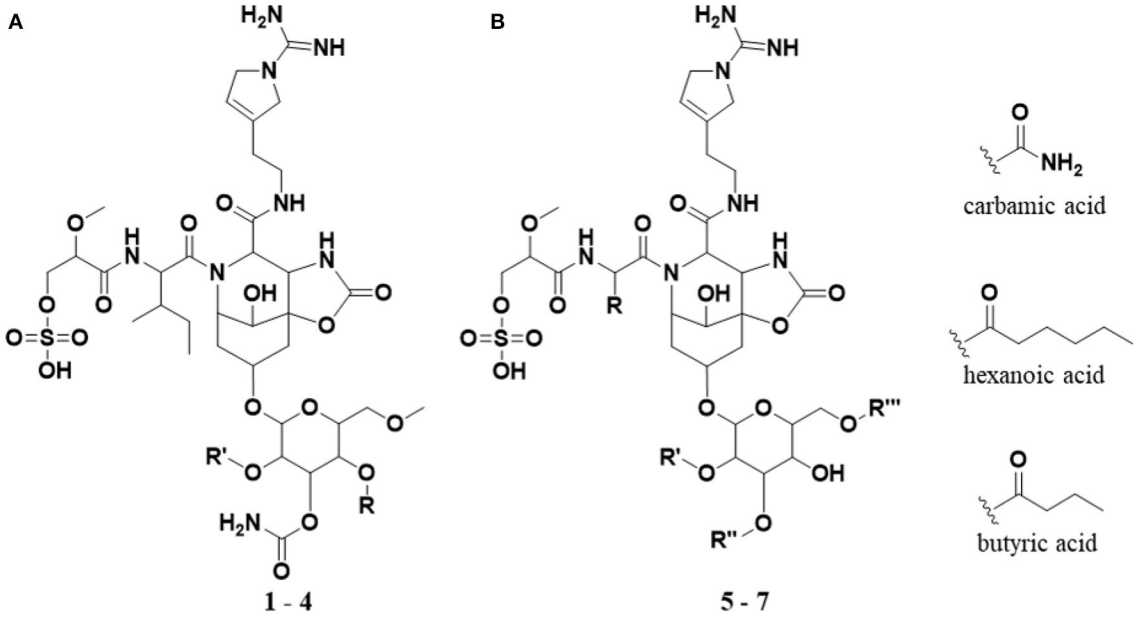

1: R= hexanoic acid, R'= butyric acid
2: R= -H, R'= butyric acid
3: R= -H, R'= hexanoic acid
4: R and R'= butyric acid
5: R= leucine, R'= hexanoic acid, R''= carbamic acid, R'''= -H
6: R= leucine, R'= -H, R''= H. R'''= hexanoic acid
7: R= isoleucine, R'= hexanoic acid , R''= -H, R'''= hexanoic acid

FIGURE 1
(A) Keep bold structures of suomilide B – E (**1–4**). **(B)** The previously isolated molecules banyasides A and B (**5** and **6**) and suomilide (**7**). All molecules share an Abn (azobicyclononane) core and an Aeap-moiety [1-amino-2-(N-amidino-Δ3-pyrrolinyl)ethyl], which also can be observed in the aeruginosins, as well as leucine and glycosylation. Suomilide differs from the banyasides by incorporation of isoleucine instead of leucine. The banyasides differ in the modification of their glycons (α-glucose for **4**, **5**, and **6**.

frontiers | Frontiers in Microbiology

TYPE Original Research
PUBLISHED 03 May 2023
DOI 10.3389/fmicb.2023.1144328

OPEN ACCESS

EDITED BY
Dewu Zhang,
Chinese Academy of Medical Sciences, China

REVIEWED BY
Fuguo Xing,
Chinese Academy of Agricultural Sciences, China
Xiaoyan Pang,
Chinese Academy of Sciences (CAS), China

*CORRESPONDENCE
Yi Zhang
✉ hubeizhangyi@163.com;
✉ zhangyi@gdou.edu.cn

†These authors have contributed equally to this work

RECEIVED 14 January 2023
ACCEPTED 03 April 2023
PUBLISHED 03 May 2023

CITATION
Lu T, Liu Y, Zhou L, Liao Q, Nie Y, Wang X, Lei X, Hong P, Feng Y, Hu X and Zhang Y (2023) The screening for marine fungal strains with high potential in alkaloids production by *in situ* colony assay and LC-MS/MS based secondary metabolic profiling. *Front. Microbiol.* 14:1144328. doi: 10.3389/fmicb.2023.1144328

The screening for marine fungal strains with high potential in alkaloids production by *in situ* colony assay and LC-MS/MS based secondary metabolic profiling

Tiantian Lu[1†], Yayue Liu[1,2,3†], Longjian Zhou[1,2,3], Qingnan Liao[1], Yingying Nie[1], Xingyuan Wang[1], Xiaoling Lei[1,2,3], Pengzhi Hong[1,2,3], Yan Feng[1], Xueqiong Hu[1,2,3] and Yi Zhang[1,2,3]*

[1]Guangdong Provincial Key Laboratory of Aquatic Product Processing and Safety, Guangdong Provincial Engineering Technology Research Center of Seafood, Shenzhen Institute of Guangdong Ocean University, College of Food Science and Technology, Guangdong Ocean University, Zhanjiang, China, [2]Southern Marine Science and Engineering Guangdong Laboratory (Zhanjiang), Zhanjiang, China, [3]Provincial Ministry Collaborative Innovation Center for Key Technologies of Marine Food Finishing and Deep Processing, Dalian Polytechnic University, Dalian, China

Background: Alkaloids are the second primary class of secondary metabolites (SMs) from marine organisms, most of which have antioxidant, antitumor, antibacterial, anti-inflammatory, and other activities. However, the SMs obtained by traditional isolation strategies have drawbacks such as highly reduplication and weak bioactivity. Therefore, it is significantly important to establish an efficient strategy for screening strains and mining novel compounds.

Methods: In this study, we utilized *in situ* colony assay combined with liquid chromatography-tandem mass spectrometry (LC-MS/MS) to identify the strain with high potential in alkaloids production. The strain was identified by genetic marker genes and morphological analysis. The secondary metabolites from the strain were isolated by the combine use of vacuum liquid chromatography (VLC), ODS column chromatography, and Sephadex LH-20. Their structures were elucidated by 1D/2D NMR, HR-ESI-MS, and other spectroscopic technologies. Finally, these compounds bioactivity were assay, including anti-inflammatory and anti-β aggregation.

Results: Eighteen marine fungi were preliminarily screened for alkaloids production by *in situ* colony assay using Dragendorff reagent as dye, and nine of them turned orange, which indicated abundant alkaloids. By thin-layer chromatography (TLC), LC-MS/MS, and multiple approaches assisted Feature-Based Molecular Networking (FBMN) analysis of fermentation extracts, a strain ACD-5 (*Penicillium mallochii* with GenBank accession number OM368350) from sea cucumber gut was selected for its diverse alkaloids profiles especially azaphilones. In bioassays, the crude extracts of ACD-5 in Czapek–dox broth and brown rice medium showed moderate antioxidant, acetylcholinesterase inhibitory, anti-neuroinflammatory, and anti-β aggregation activities. Three

chlorinated azaphilone alkaloids, **compounds 1–3** (sclerotioramine, isochromophilone VI, and isochromophilone IX, respectively), were isolated from the fermentation products of ACD-5 in brown rice medium guided by bioactivities and mass spectrometry analysis. **Compound 1** had shown remarkable anti-neuroinflammatory activity in liposaccharide induced BV-2 cells.

Conclusion: In summary, *in situ* colony screening together with LC-MS/MS, multi-approach assisted FBMN can act as an efficient screening method for strains with potential in alkaloids production.

KEYWORDS

alkaloids, *in situ* colony screening, LC-MS/MS, *Penicillium mallochii*, azaphilone, anti-neuroinflammatory

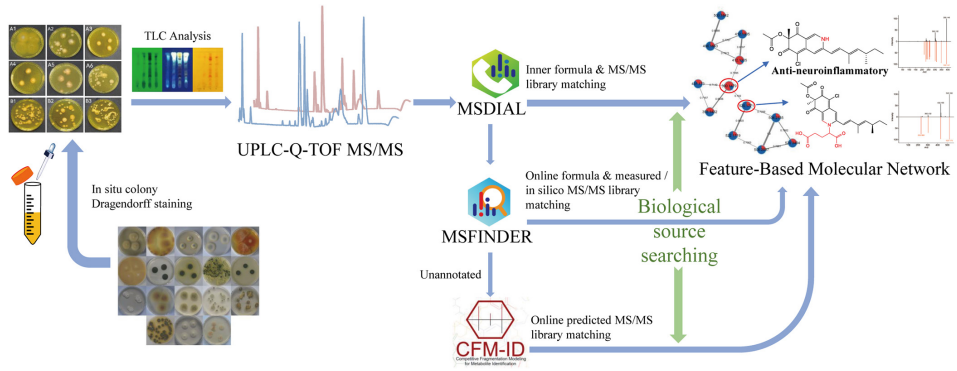

GRAPHICAL ABSTRACT
A comprehensive strategy "multi-approach assisted FBMN" for secondary metabolomic annotation combining FBMN, MSDIAL, MSFINDER, CFM-ID 3.0, and biological sources retrievement.

1. Introduction

With the depletion of terrestrial resources and the lack of inspiration in synthesizing effective novel drugs, marine-originated drugs attract more researchers' attention based on their novel structures and biological activities (Haque et al., 2022). Particularly, discovering new marine natural products (MNPs) from fungi have outpaced discoveries from all the other marine phyla in the last few years (Carroll et al., 2021). Sourced from diverse habitats, fungi are "talented" organisms with the capacity to produce compounds with unique physiological activities. Fungal MNPs mainly include polyketones, peptides, alkaloids, terpenoids, etc. Among these classes, alkaloids are one of the most diverse groups (Yin et al., 2023). The current research on marine fungal alkaloids is mainly focused on the discovery of novel structures and their versatile biological activities. Despite the remarkable progress in marine alkaloids research, the emergence of new bioactive molecules still cannot fulfill the demand for drug discovery using traditional methods. New mining techniques for alkaloids from marine fungi will likely lead to new space for marine alkaloids chemical diversity.

Qualitative screening methods directly performed on microbial colonies are always favored because they can intuitionally reflect the potential of microorganisms in producing specific substances. Quite a few methods have been reported for such *in situ* studies using plate assays. Sawant reported a method using Gram's iodine assay solution on fucoidan plates to observe the transparent circles to screen the alginate degrading enzymes-producing strains (Sawant et al., 2015). Except for the detection of alginate lyase, *in situ* colony assay was also reported that could be used to screen the fungi with antibacterial activity (Guan, 2019). However, *in situ* colony screening of alkaloid-producing strains has not been reported. The traditional screening of alkaloid-producing strains is performed by fermentation of all the tested strains, metabolites extraction, preliminary thin-layer chromatographic (TLC) colorization analysis using dyes like Dragendorff reagent, and in-depth diversity analysis using high performance liquid chromatography (HPLC), liquid chromatography-mass spectrometry (LC-MS), or direct compound isolation and structural elucidation (Yin and Sun, 2011; Han et al., 2015; Munakata et al., 2022). This pipeline is laborious, time-consuming, long-period, and unpredictable to the structural information. Inspired by the other plate assays, we attempted to develop an *in situ* colony screening method performed directly on agar plates for marine fungal alkaloid producers. This strategy could quickly identify the potential strains, slash workload from the begin and elevate the efficiency compared with the traditional screening pipeline.

To reliably recognize the alkaloids (or nitrogen-containing molecules) in crude extracts, LC-MS/MS instruments with high mass resolution like ultra-high-performance liquid chromatography quadrupole time-of-flight mass spectrometry (UPLC-QTOF-MS) are usually adopted due to its sensitivity and the ability to provide molecular formula and fragmentation

information. For example, Li set up a mining strategy for rapid discovery and identification of lycorine-type alkaloids (Li et al., 2019). However, such a strategy relies on an in-depth understanding for the specific type of alkaloids and is not suitable for microbial strains with unclear background of metabolites. As a rising tool, Global Natural Products Social Molecular Networking (GNPS) allows the visualization of all the molecular ions detected in LC-MS/MS, and reveals their structural relationships based on MS/MS similarity. Besides, it also can present possible annotations by comparison with the MS/MS spectral records in metabolite databases even the researchers have little information on the strain metabolite background and fragmentation rules (Wang et al., 2016, 2022; Nie et al., 2020). Guided by GNPS, many new alkaloids like lipopeptides microcolins E–M and pyrrole-derived alkaloids phallusialides A–E have been reported to be isolated from different marine microorganisms (Yu et al., 2019; Zhang et al., 2019).

On the basis of classic GNPS, an updated version called Feature-Based Molecular Networking (FBMN) has been developed to enhance its ability to recognize different adduct ion forms for the same compound and discriminate isomers with different retention times (Nothias et al., 2020). Besides, the formula and MS^2 information obtained from LC-MS/MS for FBMN construction can also be used to annotate the possible metabolites by automated MSDIAL-MSFINDER searching in multi-databases such as HDMB, YMDB, COCONUT, KNApSAcK, Natural Product Atlas, Drug Bank, PubChem, etc., through formula matching and comparison between measured MS/MS spectra and reference MS/MS (or even *in silico* calculated MS/MS spectra) (Lai et al., 2018; Tsugawa et al., 2019). Some new tools like CFM-ID version 3.0 (or 4.0) can assist in manually identifying structures via similar ways but with stronger ability to compare measured/predicted MS/MS spectra under multiple collision energies and annotate ion fragments (Djoumbou-Feunang et al., 2019; Wang et al., 2021). However, the above-mentioned tools also have their shortcomings if applied individually. For example, FBMN is not easy to compare with compounds without experimental MS/MS, MSDIAL is not convenient to match multiple databases, MSFINDER annotation does not consider the internal relationships between the metabolites in the sample, and all these tools do not give direct biological source annotations to the candidates. Thus, it is common for compounds to be annotated inappropriately.

In the present study, to screen fungal alkaloid producers intuitively and efficiently, the authors established an *in situ* colony screening method using Dragendorff reagent as dye in combined use with LC-MS/MS and FBMN assisted by multiple approaches (MSDIAL-MSFINDER, biological source annotation, and CFM-ID). This pipeline can quickly identify the potential alkaloid producer strains at the early step, greatly reduce the workload of fermentation-extraction, and display the diversity of alkaloid metabolite for background unclear strains. In this paper, we reported the *in situ* colony dyeing screening on marine fungal strains, diversity displaying of alkaloids by TLC colorization, LC-MS/MS profile, and multi-approach assisted FBMN networking, and the biological identification of the most fertile alkaloid producer strain ACD-5. The isolation and elucidation of three representative metabolites chlorinated azaphilones from this strain, as a proof for the effectiveness of this method, was also reported with related bioactivity study.

TABLE 1 Strains information used in this study.

Strain	Host	Collection place
S5-2-1	*Codium fragile*	Yangmeikeng, Shenzhen
S5-2-2	*Codium fragile*	Yangmeikeng, Shenzhen
S5-3	*Codium fragile*	Yangmeikeng, Shenzhen
S5-5-1	*Codium fragile*	Yangmeikeng, Shenzhen
S5-5-2	*Codium fragile*	Yangmeikeng, Shenzhen
S6-3 Y	*Sargassum henslowianum*	Yangmeikeng, Shenzhen
S6-3 Y2	*Sargassum henslowianum*	Yangmeikeng, Shenzhen
S7-1	*Grateloupia turuturu*	Yangmeikeng, Shenzhen
S7-1-1	*Grateloupia turuturu*	Yangmeikeng, Shenzhen
S7-3	*Grateloupia turuturu*	Yangmeikeng, Shenzhen
C23-1	*Pavona lamarck*	Coral reserve, Zhanjiang
C23-3	*Pavona lamarck*	Coral reserve, Zhanjiang
CD-1	*Holothuria scabra*	Meizhen sea cucumber breeding factory, Zhanjiang
NY-8	*Holothuria scabra*	Meizhen sea cucumber breeding factory, Zhanjiang
ACD-2	*Holothuria scabra*	Meizhen sea cucumber breeding factory, Zhanjiang
ACD-5	*Holothuria scabra*	Meizhen sea cucumber breeding factory, Zhanjiang
ACD-6	*Holothuria scabra*	Meizhen sea cucumber breeding factory, Zhanjiang
ACD-12	*Holothuria scabra*	Meizhen sea cucumber breeding factory, Zhanjiang

2. Materials and methods

2.1. Materials

Eighteen fungal strains from different hosts (seaweeds, coral, and sea cucumber) were previously isolated by our team and used for this study (**Table 1**). Four culture mediums were used for fermentation including Czapek–Dox Broth (CDB), Potato Sucrose Broth (PSB), Malt Extract Broth (MEB), and Brown Rice Medium (BRM). The mediums used for morphological identification of the strain ACD-5 included Potato Dextrose Agar (PDA), Blakeslee's Malt Extract Agar (MEA), Czapek Yeast Agar (CYA), and Yeast Extract Sucrose Agar (YES). Czapek–Dox Agar (CDA) was used for the *in situ* colony screening experiment. 20.0 g/L sea salts were added to all the above culture media. The details of all the cultural mediums involved in this study were listed in **Supplementary Table 1**.

The 1D/2D Nuclear Magnetic Resonance (NMR) spectra were recorded on a Bruker Advance 700 MHz spectrometer ($^1H/^{13}C$, 700/175 MHz). LC-MS/MS data were recorded on a Waters Acquity UHPLC-DAD-Xevo G2-XS Q-Tof liquid chromatography-mass spectrometer. High resolution electron spray ionization mass

spectrometry (HR-ESI-MS) data for pure compound were recorded on a Bruker Daltonics maXis impact mass spectrometer. Circular dichroism (CD) spectrum was recorded on a Chirascan spectropolarimeter (Applied Photophysics). Optical rotation was measured using an Anton Paar MCP–500 (Anton Paar, Graz, Austria). A 96-well microplate reader (Bio-Tek Epoch 2) was used for spectrophotometric measurements. A Di B60F microscope and a TESCAN MIRA 3 scanning electron microscope were used for fungal morphological observation. Solvent was evaporated through a EYELA rotary evaporator with a vacuum pump. Column chromatographies (CC) were performed on 200–300 mesh silica gel purchased from Qingdao Marine Chemical Factory and Sephadex LH-20 (Amersham Pharmacia). Precoated silica gel plates purchased from Qingdao Kai Bang Chemical Group Co (G60, F-254) were used for TLC analysis.

2.2. *In situ* colony assay

The activated fungal strains on slants were inoculated onto the CDA petri dishes with diameter of 9 cm at 28°C for 4 days. And then the strains were dyed with Dragendorff reagent to cover the surface of the strain colonies for 10 min. The formula and preparation of the Dragendorff reagent was [liquid A: bismuth nitrate 0.52 g, glacial acetic acid 6 mL, and pure water 24 mL. liquid B: potassium iodide 12 g and pure water 30 mL. After mixing liquid A and B, pure water 120 mL and glacial acetic acid 160 mL were added]. After the dyeing, the chromogenic agent was poured out and the color change of the colonies was observed. The colonies turned orange were selected as positive ones since Dragendorff reagent can form orange complex with alkaloids (Rubia and Gomez, 1977). Blank agar plates were used to monitor the sterile condition. All experiments were carried out in two repeats after a pilot study.

2.3. Preparation of strain fermentation crude extracts

The positive strains which had shown obvious yellow to orange colored colonies in the above *in situ* dyeing screening were picked out for further fermentation. They were inoculated into CDB, PSB, MEB, and BRM for a 3 weeks static fermentation, respectively. The fermentation was performed in 150 mL conical flasks filled with 30 mL of liquid or solid culture medium. The contaminated cultures would be replaced in time and a blank control was set to prevent the loss caused by fungal contamination. When the cultivation was finished, the fermentation broth was extracted with equal volume of ethyl acetate. Then, the broth extracts were concentrated under vacuum. Mycelium was extracted using 30 mL ethyl acetate: methanol (v/v = 1:1) assisted with ultrasonic for 30 min, and then concentrated. The broth and mycelium extracts for each culture were combined and evaporated to dryness. As for the solid cultures on BRM, 30 mL of methanol was used for 30 min ultrasonic assisted extraction, and the extraction was repeated for three times to collect filtrate which was concentrated to dryness. The crude extracts were dissolved with methanol to a concentration of 10 mg/mL and kept in a refrigerator at 4°C until use.

2.4. TLC analysis

The mobile phase for TLC was dichloromethane: methanol (v/v = 5:1) and the sample volume was 10 μL. The plates were observed under 254 and 365 nm UV lamps. Then, the plates were evenly sprayed with Dragendorff reagent and observed for the colorization of the spots. All experimental results were recorded by photography. Two known fungal products butyrolactone-I and epi-aszonalenin A were used as quality controls for non-alkaloids and alkaloids, respectively.

2.5. LC-MS/MS analysis

The selected extract samples were prepared as solutions with the concentration of 50 μg/mL using LC-MS pure methanol and pretreated with Agilent SPE column before LC-MS/MS analysis.

The LC-MS/MS analyses were run on a Waters Acquity UHPLC-DAD-Xevo G2-XS Q-Tof liquid chromatography-mass spectrometer. Waters ACQUITY UPLC BEH RP18 (2.1 × 50 mm, 1.7 μm) column was used for the analysis. The sample injection volume was 1.0 μL. The aqueous solution containing 0.1% formic acid was used as mobile phase A, and mobile phase B was acetonitrile. The gradient elution condition was as follows: 30% B (0–0.5 min), 30–80% B (0.5–4.0 min), 80% B (4.0–7.0 min), 80–30% B (7.0–7.2 min), 30% B (7.2–8.5 min) at a flow rate of 0.3 mL/min. The range of MS scan was set to *m/z* 50–2,000, electrospray ionization, and positive ion mode. The MS parameters were as follows: ion source temperature, 120°C; Capillary, 2 KV; Sampling Cone, 40 V; Source Offset, 80 V; Desolvation temperature, 450°C; Cone Gas, 50 L/h; Desolvation Gas, 700 L/h.

2.6. Multi-approach assisted FBMN analyses

After LC-MS/MS data acquisition, compounds feature table in the crude extracts was exported by upload converted raw data to MSDIAL Version 4.80 (The table information for features: Retention time; Precursor *m/z*; Adduct ion type; MS type; MS^1 isotopic patterns; MS^2 spectra). During the MSDIAL alignment running, an inner authentic standards database "MSMS_Public_EXP_Pos_VS17" from MSDIAL platform[1] was also matched based on precursor mass and MS/MS similarity. The feature table was then automatically compared with different databases such as Drug Bank, PubChem, NANPDB, COCONUT, KNApASck, ChEBI, and UNPD by MSFINDER Version 3.52 to annotate compounds that each feature may represent. Furthermore, the alkaloids production in different culture mediums were analyzed and compared by FBMN using the above mentioned feature table and following the workflow on GNPS platform (Nothias et al., 2020). When the job was done, exported the result and visualized it using Cytoscape Version 3.70. All annotations from MSDIAL, MSFINDER, and FBMN were traced for their biological sources in important natural product databases (PubChem, COCONUT, LOTUS, NPA, DNP, CMNPD,

1 http://prime.psc.riken.jp/compms/msdial/main.html

NMRDATA, and others from which the candidates were matched) or original literature to verify their reasonability. If the candidates were from unreasonable organisms (e.g., structures typically from plants or animals but not from fungi) or the above three tools failed to annotate the metabolites, the MS^1 and MS^2 information will be submitted for structure identification onto CFM-ID 3.0 online platform[2] (since its 4.0 version is yet not stable enough to visit) by comparison with the predicted MS^2 spectra in 11 small molecule databases (HMDB, KEGG, MassBank, NIST, DrugBank, PhytoHub, FiehnLib, ContaminantDB, iTree, CASMI2016, and MetaboBASE). The resulting candidates were then traced for biological source again. Finally, the metabolites in the FBMN clusters were annotated on comprehensive account of the above approaches.

2.7. Bioassay

The crude extracts of the selected strain, or the metabolites that were subsequently isolated, were screened for the following activities.

2.7.1. DPPH free radicals scavenging assay

The 1,1-diphenyl-2-picrylhydrazyl (DPPH) free radical scavenging potentials of crude extracts were evaluated in 96-well plates according to the manufacturer's kit instruction. A total of 200 μL of the reaction mixture was composed of 100 μL DPPH and 100 μL sample with different concentrations in methanol (A_{sample}). The reaction mixture was incubated for 30 min in darkness at room temperature and the absorbance was measured at 517 nm on the microplate reader. Meanwhile, $A_{control}$ represented control group consisting of 100 μL samples and 100 μL methanol, A_{blank} represented blank group consisting of 100 μL DPPH and 100 μL methanol. Vitamin C was taken as a positive control. DPPH free radicals scavenging capacity was calculated by the formula:

$$\text{Scavenging capacity (\%)} = \left(1 - \frac{A_{sample} - A_{control}}{A_{blank}}\right) \times 100\%$$

Besides, an antioxidant TLC bioautography using DPPH as dye was also performed to display the diversity of antioxidant constituents in the extracts following our previously reported method (Nie et al., 2020; Wang et al., 2022).

2.7.2. Acetylcholinesterase inhibition assay

The electric eel acetylcholinesterase (AChE) (Sigma-Aldrich, St. Louis, MO, USA) inhibitory activities were measured in 96-well plates by modified Ellman's et al., 1961 methods. The concentration range of the positive control (donepezil) and the tested samples were set to be 0.01, 0.10, 0.25, 0.50, and 1.00 mg/mL (in DMSO). Likewise, an AChE inhibitory TLC bioautography was performed to show the diversity of AChE inhibitors following our previous reports (Nie et al., 2020; Wang et al., 2022).

2.7.3. Cell viability assay

BV-2 cells were cultured in dulbecco's modified eagle's medium (DMEM) (GIBCO, Billings, MT, USA) supplemented with 1% of penicillin/streptomycin and 5% fetal bovine serum (FBS) (ZETA, Spring House, PA, USA) at 37°C in a moist 5% CO_2 incubator. The cytotoxicity of the samples in different concentrations on cells were measured after 24 h incubation by MTT assay as previously described (Qian et al., 2012; Zhang et al., 2018).

2.7.4. Nitric oxide (NO) production determination

To examine the inhibitory effect of the samples on the production of NO, BV-2 cells were seeded at density 2×10^4 cells/well in 96-well plates. The cells were pre-treated with samples in different concentrations for 1 h and were subsequently activated by lipopolysaccharide (LPS) (Sigma-Aldrich, St. Louis, MO, USA) (1 μg/mL) for 24 h. The production of NO was measured using the Griess Reagent System according to the previous study (Ryu et al., 2010). The absorbance was measured at 540 nm by microplate reader.

2.7.5. Gold nanoparticle-mediated anti-aggregation of amyloid-β

The preparation of gold nanoparticles (GNPs) was using Chah's et al., 2005 method. Briefly, the particles were prepared by boiling 100 mL of aqueous 0.03% (w/w) hydrogen tetrachloroaurate (III) trihydrate ($HAuCl_4 \cdot 3H_2O$) in a flask with constant vigorous stirring and then adding 3 mL of 3% (w/w) sodium citrate ($Na_3C_6H_5O_7 \cdot 2H_2O$). When the solution became almost opaque, heating was stopped and the solution was let cool to room temperature for 30 min. This GNPs solution was stored at 4°C for 24 h before use.

10 μL of Aβ solution consisting of 10 μM $A\beta_{1-40}$ (Rhawn, China) and 10 μM $A\beta_{1-42}$ (Yuanye, China) with a ratio of 9:1 (v/v) was first incubated with 10 μL of samples (20, 100, and 500 μg/mL) for 10 min. Then, this 20 μL solution was mixed with 90 μL of GNPs together with 10 μL of 5 mM Cu^{2+} and 10 μL of 30 mM HCl. After 5 min's incubation, the absorbances were measured at 520 nm (as an intrinsic GNPs peak) and 650 nm (as an indicator peak of large fibrillar aggregation), respectively using a microplate reader (Kim et al., 2017). For sample testing, the final concentration of DMSO (co-solvent) was 5% in the testing system.

2.8. Strain identification by genetic marker genes

The genomic DNA was extracted from the strain grown on PDA using the Genomic DNA Extraction Kit (Solarbio, Beijing, China) following the manufacturer's protocol. The internal transcribed spacer (ITS) was amplified and sequenced with primers ITS1 (5′-TCCGTAGGTGAACCTGCGG–3′) and ITS4 (5′-TCCTCCGCTTATTGATATGC–3′), while *BenA* (β-tubulin gene) with primers Bt2a (5′- GGTAACCAAATCGGTGCTGCTTTC –3′) and Bt2b (5′- ACCCTCAGTGTAGTGACCCTTGGC -3′). The PCR reactions were performed in 50 μL reaction mixtures containing 5 μL genomic DNA, 25 μL 2 × Phanta Max Buffer, 1 μL dNTP Mix (10 mM each), 1 μL Phanta Max Super-Fidelity DNA Polymerase, 2 μL each of the upstream and downstream primers and ddH_2O using reagents from Vazyme (China) and primers from Sangon Biotech (China). The PCR parameters for ITS and *BenA* were pre-denaturation at 95°C for 3 min; denaturation at 95°C for

2 https://cfmid.wishartlab.com/

15 s, annealing at 56°C for 15 s, extension at 72°C for 90 s, 30 cycles, and complete extension at 72°C for 5 min. The PCR products were visualized by gel electrophoresis in a 1% agarose gel containing Ultra GelRed. The PCR amplification products were purified by gel cutting and ligated with T4 DNA ligase to pGM-T vector (Tiangen, China) overnight at 16°C. The pGM-T vector containing the target fragment was heat-stripped into sensitive *E. coli* TOP10 and incubated at 37°C for 45 min. The bacterial solution was spread onto LB agar plates containing ampicillin supplemented with X-gal and IPTG and incubated for 12-16 h at 37°C. The white clones were picked to identify whether the recombination was successful by direct PCR, and the positive PCR products were sequenced by Beijing Liuhe Huada Gene Technology Co., Ltd. (Beijing, China).

The sequencing results were compared with other known strains on the NCBI[3] for gene sequence alignment to determine the strain genus. A phylogenetic tree was constructed by the neighbor-joining method using MEGA Version 11.0. The confidence value of each clade was assessed using bootstrap analyses based on 1,000 replications. The sequence was finally deposited in the GenBank database.

2.9. Morphological analysis

The strain ACD-5 was cultured on MEA, CYA, CDA, YES, and PDA agar plates, respectively, at 25°C for 7 days, with two parallels for each plate after a pilot study. Blank agar plates were used to monitor the sterile condition. The colony morphology of the strains was observed and recorded by camera. For microscopic observation, the strain was additionally inoculated on the PDA plates inserted with sterile coverslips at 45° obliquely near the inoculation spots at 25°C for 7 days. The coverslips with mycelium growth were pulled out after 4 days, fixed in 2.5% glutaraldehyde at 4°C for 2 h, rinsed in PBS for 15 min, dehydrated in gradients of 30, 50, 70, 90, and 100% ethanol for 15 min each, and dried naturally. The sample slides were placed in patches, sprayed with gold at 1.5 kV and 10 mA for 400 s. Finally, the fungal morphological structures were observed under the scanning electron microscope, photographed, and recorded. Besides, the coverslips with fresh mycelia were directly observed under optical microscope.

2.10. Fungal fermentation and characterization of the main products

The fungus ACD-5 was cultured on the PDA plate at 28°C for 4 days as seed culture. Then, the mycelium was inoculated into sixty–five 1 L-Erlenmeyer flasks, each containing 120 g of brown rice and 120 mL 2% artificial seawater. The culture was incubated at room temperature for 30 days. After culture, the rice with mycelium was extracted with ultrasonic for 30 min in methanol for three times, and the filtrate was collected and concentrated to dryness. A total of 80 g crude extracts were obtained.

Then the crude extracts were subjected to silica gel vacuum liquid chromatography (VLC) column, eluting with a gradient of *n*-hexane: ethyl acetate: methanol (v/v/v, 1:0:0, 1:1:0, 0:1:0, 0:1:1, 0:0:1, and successively) to obtain 5 fractions (Fr.1–Fr.5). Fr.3 was further purified by a silica gel VLC column eluted with *n*-hexane: ethyl acetate: methanol (v/v/v, 15:1:0 to 1:5:0 gradually, 0:1:0, 0:1:1, 0:0:1, and successively) to give 9 sub-fractions (SFr.3-1–SFr.3-9). SFr.3-5 was subjected to VLC eluted with dichloromethane: methanol (v/v, 80:1, 40:1) to give 9 subfractions (SFr.3-5-1–SFr.3-5-9). SFr.3-5-4 was recrystallized and repurified with ODS column chromatography eluted with 80% methanol/H_2O to yield **compound 1** (35 mg). SFr.3-6 was purified by Sephadex LH-20 (dichloromethane-methanol, v/v, 1:1) to give 4 sub-fractions (SFr.3-6-1–SFr.3-6-4). SFr.3-6-3 was separated using ODS column (methanol/H_2O, v/v, 4:1) and Sephadex LH-20 (dichloromethane-methanol, v/v, 1:1) to yield **compound 2** (13.6 mg). SFr3-7 was purified by VLC eluted with dichloromethane: methanol (v/v, 40:1 to 5:1 gradually) to give 5 sub-fractions (SFr.3-7-1–SFr.3-7-5). SFr3-7-3 was separated sequentially using ODS column (methanol/H_2O, v/v, 7:3), Sephadex LH-20 (dichloromethane-methanol, v/v, 1:1), and ODS column (methanol/H_2O, v/v, 4:1) to yield **compound 3** (12 mg).

The planar structures of **compounds 1–3** were elucidated by comparison of ^1H and/or ^{13}C NMR spectra with the report data in literature, and supported by high resolution mass spectrometry. And the stereo-structures were defined by comparison of the specific optical rotation and CD spectrum with the literature data.

2.11. Statistical analysis

The data were expressed by the GraphPad Prism Version 8.0.1 as the means ± SD ($n = 3$). A value of $p < 0.05$ was considered statistically significant. Differences between groups were calculated by One-way analysis of variance (ANOVA). For DPPH scavenging and AChE inhibitory assays, $^{****}p < 0.0001$ compared with positive control of the same concentration. For NO production determination, $^{**}p < 0.01$, $^{****}p < 0.0001$ compared with the LPS group. For cell viability assay, $^{****}p < 0.0001$, compared with the control group.

3. Results

3.1. *In situ* colony assay

This study focused on establishing an efficient alkaloid screening pipeline, of which the first step was an *in situ* colony dyeing screening. The ingredients of culture medium Czapek–Dox Agar (CDA) were mainly inorganic salts such as sodium nitrate, dipotassium hydrogen phosphate, and magnesium sulfate. It was free of alkaloid-like substances that may interfere with the results. Besides, the colorless and transparent plate made of CDA was conductive to the observation of color change. Thus, CDA was selected for *in situ* screening of strain producing alkaloids.

When the individual colony diameter reached 2–3 cm after 4 days, the colonies were dyed with Dragendorff reagent to discriminate the alkaloid producers. Among the 18 tested marine fungal strains, 9 strains (S5-2-1; S5-2-2; S5-3; S5-5-1; S6-3 Y; S7-3; CD-1; ACD-2 and ACD-5) showed obvious orange color on

3 https://www.ncbi.nlm.nih.gov/guide/all/

colonies surface compared with other strains, which indicated presumable alkaloids production (**Figure 1** and **Supplementary Figure 1**). To perform this *in situ* colony screening, it is important to dye the colonies before they grow too old, otherwise some colonies would produce pigments that may interfere with the judgment.

3.2. TLC analysis

To confirm the alkaloid producing ability of the positive strains selected by *in situ* colony screening, they were cultivated in four different media including CDB, PSB, MEB, and BRM, respectively. After 3 weeks of cultivation, their metabolites were extracted by organic solvents and analyzed on TLC plates stained with Dragendorff reagents to observe the presence of typical orange spots caused by alkaloids (Rubia and Gomez, 1977). As shown in **Figure 2**, two previously isolated compounds Butyrolactone I (BL-I, non-alkaloid) (Zhang et al., 2018) and epi-aszonalenin A (LJY-6, alkaloid) (Liu et al., 2022) from our laboratory were used as the controls and their respective negative and positive colorizations ensured the reliability of the TLC staining results. The crude extracts S5-3-PSB (means the fermentation extract of strain S5-3 in culture medium PSB, the next sample numbers follow the same rule), S5-3-BRM, S5-5-1-PSB, S5-5-1-BRM, S6-3Y-BRM, S7-3-BRM, CD-1-BRM, CD-1-MEB, ACD-2-BRM, ACD-2-MEB, ACD-5-BRM, and ACD-5-CDB presented significant alkaloid spots on TLC plates. Among them, ACD-5-BRM and ACD-5-CDB displayed the most abundant alkaloids. To have an insight to the alkaloid metabolites of the strain ACD-5 and their biological potential, this strain was selected for further secondary metabolic profile investigation by LC-MS/MS.

3.3. LC-MS/MS analysis of ACD-5

To investigate the metabolites diversity especially for alkaloids, the extract samples ACD-5-BRM and ACD-5-CDB were analyzed by LC-MS/MS and successive multi-approach assisted FBMN networking.

Firstly, MSDIAL-generated 2D peak spot heatmaps (**Figure 3**) showed the metabolic profiles of the two samples including the precursor *m/z* values, retention times, and peak areas of all the features and they were annotated primarily by matching the internally loaded database. The exported aligned feature information was then used for FBMN networking and MSFINDER multi-database searching, respectively. Their annotations were successively checked for biological source reasonability in several important natural product databases as described above in the (section of "2. Materials and methods"). The features unannotated by MSDIAL/FBMN/MSFINDER or the ones with obviously unreasonable biological resource were individually submitted to CFM-ID 3.0 for more opportunity of annotation by matching the plenty of *in silico* MS/MS spectra in databases. These CFM-ID annotations were then checked for biological source again. The final annotations to the FBMN network were synthetically determined on the basis of the above MSDIAL/FBMN/MSFINDER/CFM-ID—Biological Source Investigation pipeline, during which the

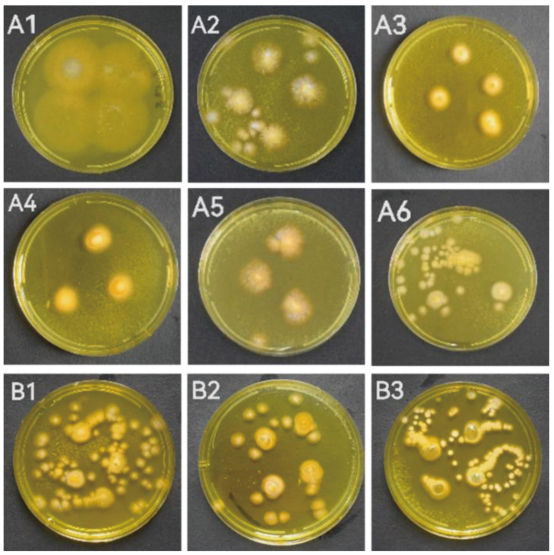

FIGURE 1
The strains showed alkaloid positive reaction in the *in situ* colony screening by Dragendorff reagent. **(A1–A6)** Strains from seaweeds; **(B1–B3)**: Strains from sea cucumber. (**A1**, S5-2-1; **A2**, S5-2-2; **A3**, S5-3; **A4**, S5-5-1; **A5**, S6-3 Y; **A6**, S7-3; **B1**, CD-1; **B2**, ACD-2; **B3**, ACD-5).

structural relationships between features revealed by FBMN were also taken into crucial account.

Totally, 661 features were recognized by MSDIAL including 580 from ACD-5-BRM and 447 from ACD-5-CDB and 366 from both conditions (**Figure 4A**). In FBMN molecular networking, these 661 features from the two conditions formed 372 networks including 81 ones with more than 2 nodes (features) inside (**Figure 5**). By the above-mentioned multi-approach assisted FBMN annotation strategy, 227 metabolites including 106 alkaloids (or nitrogen-containing compounds) from ACD-5-CDB and 273 metabolites including 152 alkaloids from ACD-5-BRM were annotated, and 220 and 307 remained as unknown ones for the two conditions, respectively, (**Figure 4B**). Thus, this strain was confirmed as a fertile producer of alkaloids.

Intriguingly, a series of features (a total of 13 compounds) were annotated as plausible azaphilones most of which were nitrogenated ones as highlighted in Networks 5, 7, 9, 12, and 13 in the FBMN map (**Figure 5** and **Supplementary Table 1**). They all showed high MSFINDER scores usually close to or even higher than 5 with fungal origins, and were mutually annotated by MSDIAL and FBMN (GNPS platform). As a sound proof, the ongoing isolation work has already yielded three **compounds 1–3** from ACD-5-BRM and their structures were elucidated by NMR, HR-ESI-MS, and CD (see detailed below in "Section 3.7. Isolation and identification of azaphilones"), which confirmed the result of LC-MS/MS based metabolic investigation. Judged from the parent ion intensity as indicated by the sector proportions in the nodes, the most of the azaphilones present higher yields in culture medium BRM than in CDB.

In addition to these azaphilones, this fungus can also produce a number of other types of alkaloids containing diverse nitrogenated moieties like diketopiperazines, tetrazoles, thiazoles,

thiadiazolo, indoles, amines and acyl amines, purines, pyrimidines, isoquinolines, quinolines, quinazoline, pyridines, piperidines, amino acid residues, carbapenems, plumerans, pyrrolizine, diazepine, naphthyridine, sphingosine, cytisine, etc., and various molecular scaffolds (**Supplementary Figure 2** and **Supplementary Tables 1**, **2**). Similar to the distribution of azaphilones, this fungus also produced more alkaloids species in culture medium BRM than in CDB (**Figure 4C**).

Besides, this strain also produced other types of non-nitrogenated compounds, for example, high yields of long-chain lipids, steroids, phenols, and glycosides (**Supplementary Tables 1**, **2**).

3.4. Bioactivities of the strain ACD-5's fermentation extracts

As Alzheimer's disease (AD) is among the most severe threats to human health and alkaloids usually cover related bioactivities, the fermentation extracts of strain ACD-5 were screened for related antioxidant, AChE inhibitory, anti-neuroinflammatory, and anti-Aβ aggregation activities.

The antioxidant effect of crude extracts was evaluated by their DPPH free radical scavenging ability. As shown in **Figure 6A**, the antioxidant effect of ACD-5-CDB was better than ACD-5-BRM. ACD-5-CDB scavenged DPPH free radicals in a dose dependent manner, and with 90% clearance rate in a concentration of 0.25 mg/mL. In the DPPH scavenging TLC bioautographic image, strong and rich active spots in ACD-5-CDB were observed to show clearing zone on the purple background stained by DPPH. By comparing the plates stained by DPPH and Dragendorff reagent, respectively, some of the antioxidant spots may be linked to alkaloids (**Figure 6B**).

Low levels of acetylcholine are one of the molecular characteristics of AD. Thus, AChE inhibitors have been traditionally valued as an important source of anti-AD drugs. As shown in **Figure 6C**, both the two extracts possess moderate AChE inhibitory activity with the highest inhibition rate of 45% for ACD-5-BRM and 33% for ACD-5-CDB. The AChE inhibitory TLC bioautography image also located the inhibitory compounds as white spots with Rf value of 0.82 in ACD-5-BRM and 0.79 in ACD-5-CDB, respectively, (**Figure 6D**).

The inhibitory to bacterial LPS induced NO production in microglial cells (BV-2) was tested for the two extracts. As shown in **Figures 7A, B**, when the BV-2 cells were pre-treated with increasing concentrations of the two crude extracts, the levels of NO were decreased significantly by ACD-5-BRM in 100 μg/mL. Furthermore, ACD-5-BRM did not exhibited obvious cytotoxicity to BV-2 cells in the concentration range of 0–100 μg/mL (**Figure 7C**). These results indicated that the crude extract ACD-5-BRM has potential anti-neuroinflammatory effect.

Oligomerization and fibrillation of Aβ are thought to be key steps in the pathogenesis of AD (Jucker and Walker, 2013). Aβ monomers and crude extracts with various concentrations were pre-incubated for 10 min and then GNPs were added as indicator to screen the anti-aggregation effects of ACD-5-CDB and ACD-5-BRM (**Figure 7D**). The anti-aggregation effect was negatively correlated to the ratio of absorbance at 650 nm to that at 520 nm (A_{650nm}/A_{520nm}) (Kim et al., 2017). The results indicated the anti-aggregation ability of ACD-5-BRM and ACD-5-CDB are much weaker than the positive control albumin.

3.5. Analysis of morphological characteristics

After strain ACD-5 was cultured on MEA, CYA, CDA, YES, and PDA for 1 week at 25°C (**Figure 8A**), characteristics including colony morphology and growth rate were recorded (**Table 2**). The scanning electron microscope (SEM) and optical microscope analysis revealed that strain ACD-5 produced conidiophores

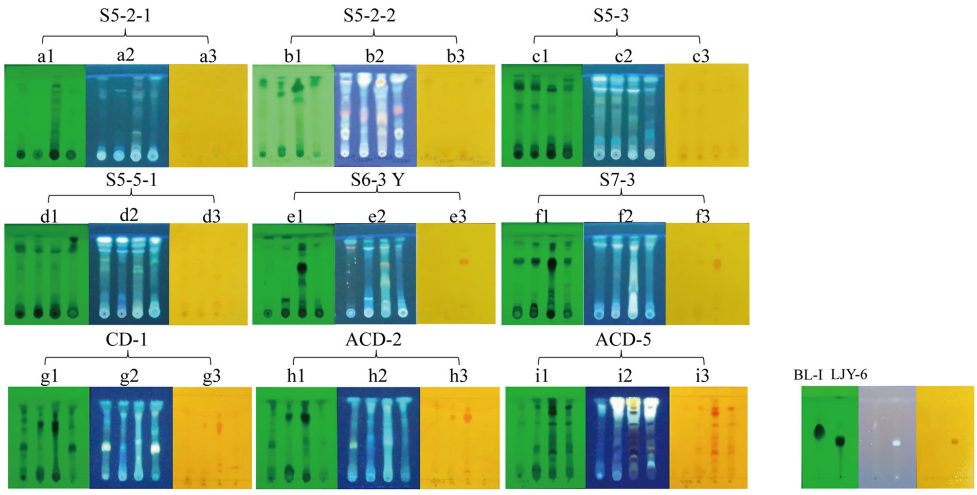

FIGURE 2
The TLC analysis of the positive strains. **(A1–I1)** UV pattern at 254 nm; **(A2–I2)** fluorescence pattern at 365 nm; **(A3–I3)** the results of Dragendorff reagent staining. The order of spotting on each plate from left to right is PSB, MEB, BRM, and CDB (representing different cultural medium used). BL-I was as a negative result and LJY-6 was as a positive result in TLC analysis.

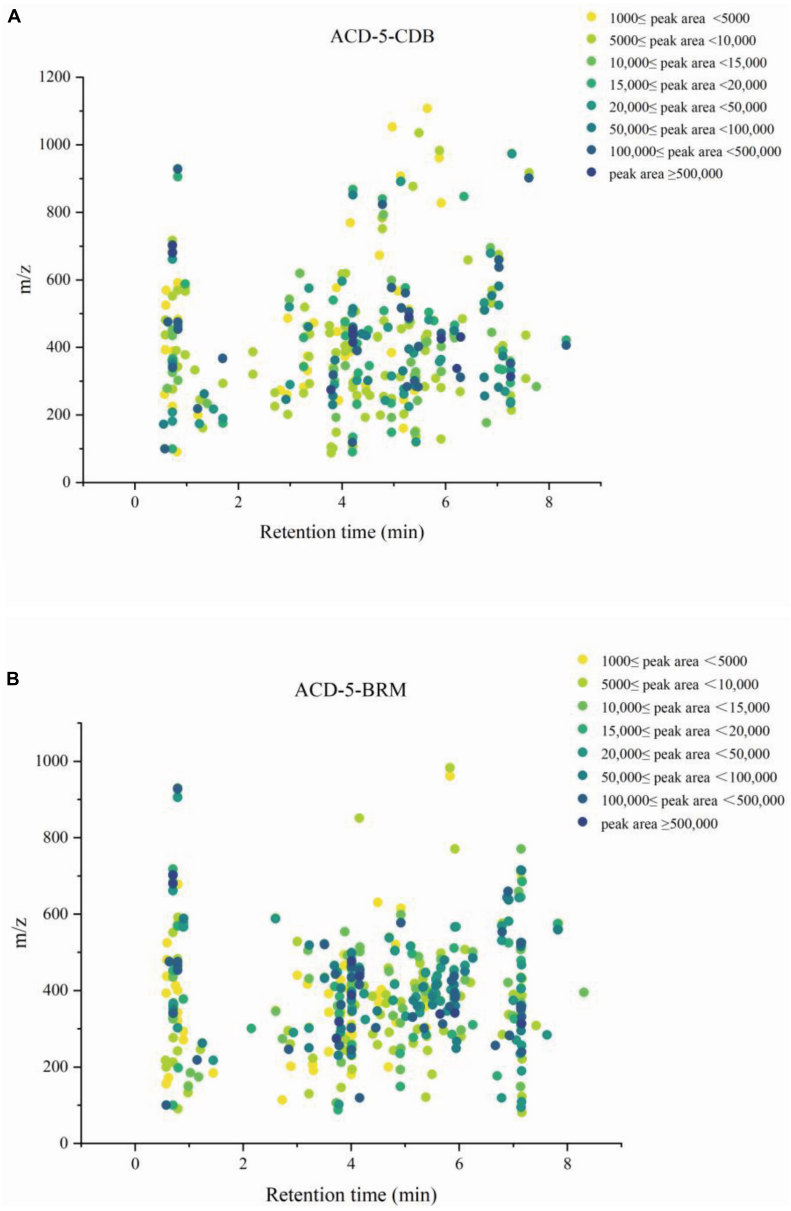

FIGURE 3
The metabolic profile of the features in extracts ACD-5-CDB **(A)** and ACD-5-BRM **(B)** showing their retention times, precursor ion *m/z* values, and intensities (exported from MSDIAL).

monoverticillate, stipes septate, mostly unbranched, phialides 6–7.2 × 1.6–2.8 μm, ampulliform with a collula, conidia ellipsoidal, fine and rough, 2.3–3.8 × 1.6–2 μm, and mean L/W ratio 1.7: 1 (**Figure 8B**; Rivera and Seifert, 2011; Rivera et al., 2012).

3.6. Identification by phylogenetic analysis

The ITS and *BenA* sequences of strain ACD-5 were amplified and sequenced. After alignment, the ITS sequence showed the highest similarity (100%) to *Penicillium mallochii* DAOM 2,39,917 and the *BenA* sequence showed the highest similarity (100%) to *P. johnkrugii* DAOM 239943. It was supported by the phylogenetic trees constructed by the neighbor-joining approach (**Figure 9**). Combined with the morphological analysis, ACD-5 was identified as *P. mallochii*. Subsequently, the ITS sequence of ACD-5 had been submitted to the GenBank database of NCBI with the accession number OM368350. This strain is deposited in Guangdong Microbial Culture Collection Center with the deposit number of GDMCC62411.

3.7. Isolation, identification, and bioassay of azaphilones

In the above chemical analysis and bioassay, ACD-5-BRM showed generally richer alkaloids and better activities than those

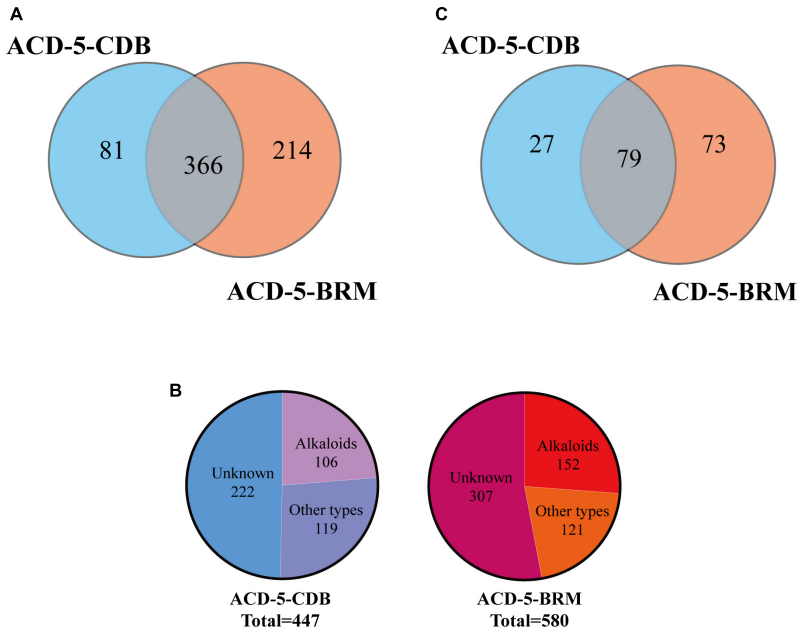

FIGURE 4
The statics of the numbers of the total features **(A)**, the annotated and unknown features **(B)**, and the alkaloids **(C)** detected in the two crude extracts of strain ACD-5.

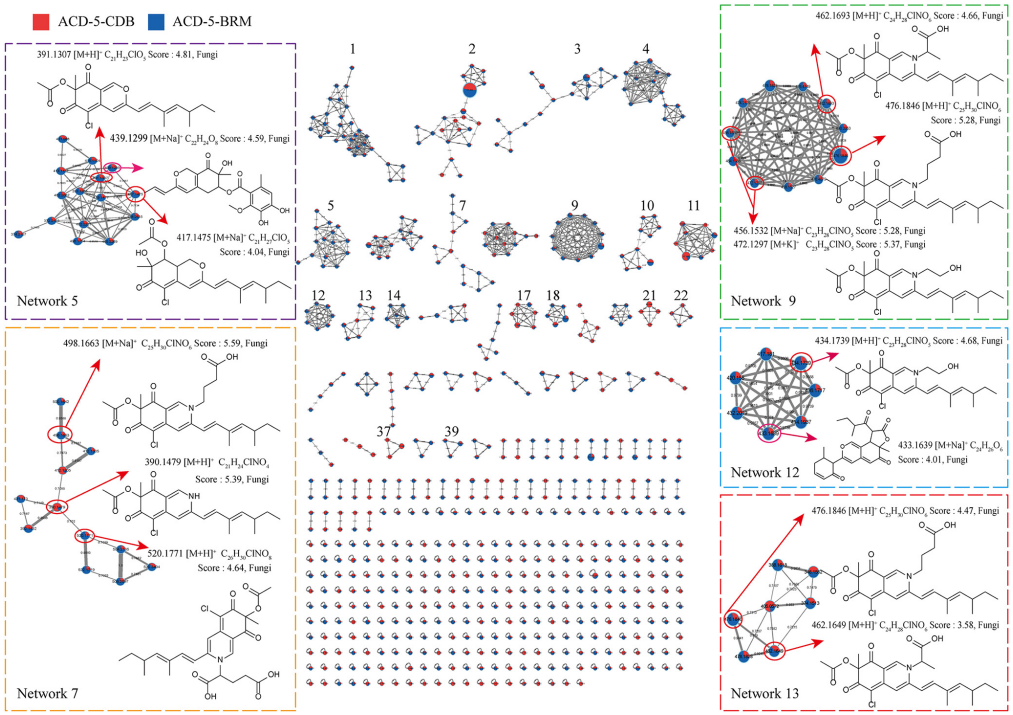

FIGURE 5
The FBMN molecular network based on positive ion MS/MS spectral similarity, showing a selection of amplified clusters. In the FBMN network, each node represents a feature marked with the mean *m/z* value of the parent ion, and the similarity of the secondary mass spectra between compounds was expressed by the cosine value, which was proportional to the similarity. The different colors of sections in the nodes represent different samples, i.e., 1 2 : respectively, ACD-5-BRM and ACD-5-CDB. The thickness of the connecting lines between nodes was positively correlated with the cosine value. The node size reflects the feature abundance (ion intensity).

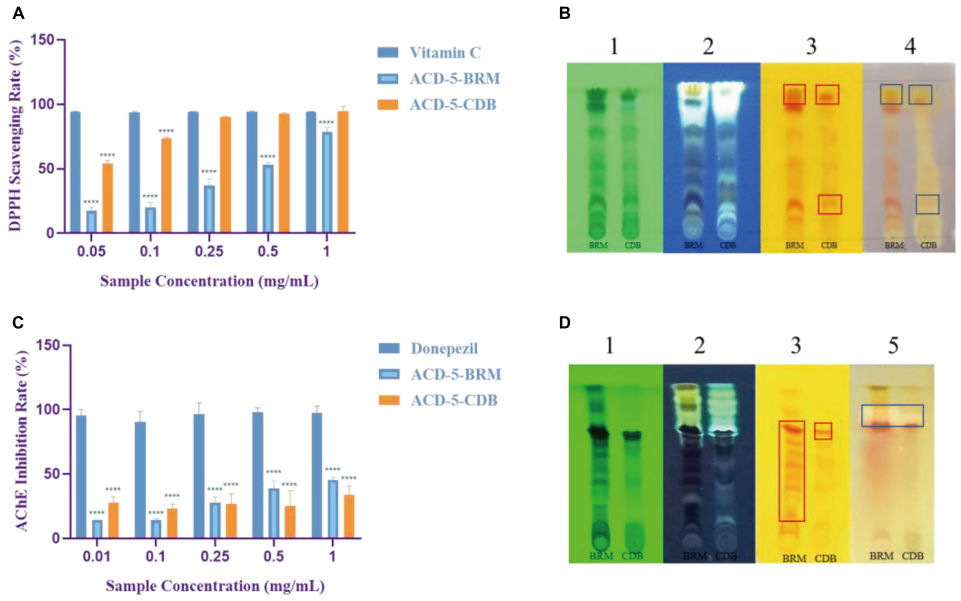

FIGURE 6
The DPPH scavenging and AChE inhibitory assays of the two crude extracts of strain ACD-5. **(A)** DPPH scavenging rate of ACD-5-BRM and ACD-5-CDB. Vitamin C was taken as a positive control. **(B)** The TLC-bioautography of the two extracts: (1) UV, (2) fluorescence, (3) Dragendorff reagent staining, (4) DPPH staining. **(C)** AChE inhibitory effect of ACD-5-BRM and ACD-5-CDB. The positive control was donepezil. **(D)** The TLC-bioautography of the two extracts: (1) UV, (2) fluorescence, (3) Dragendorff reagent staining, (5) AChE bioautography. The TLC developing system was dichloromethane: methanol = 5:1 (v/v). The results were expressed as the means ± SD (n = 3), ****: $p < 0.0001$ compared with positive control of the same concentration. A value of $p < 0.05$ was considered statistically significant.

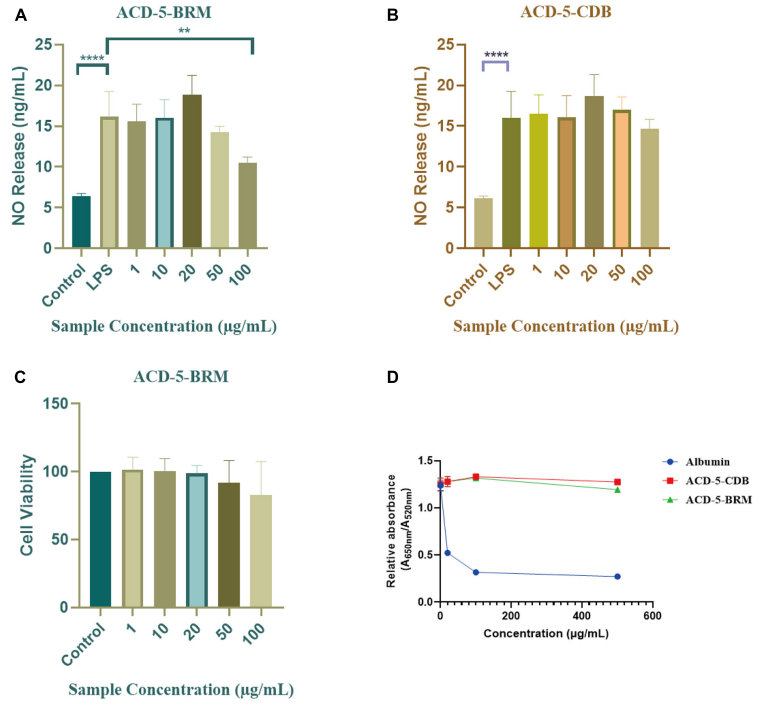

FIGURE 7
The anti-neuroinflammatory, cytotoxic, and anti-Aβ aggregation effects of the extracts ACD-5-BRM and ACD-5-CDB. **(A,B)** Inhibition to liposaccharide induced nitric oxide (NO) production of BV-2 cells of ACD-5-BRM **(A)** and ACD-5-CDB **(B)**, respectively. The results were expressed as the mean ± SD (n = 3). **$p < 0.01$, ****$p < 0.0001$, compared with the LPS group. A value of $p < 0.05$ was considered statistically significant. **(C)** The effect of ACD-5-BRM on the viability of BV-2 cells. Since the quantity of ACD-5-CDB was insufficient, no cytotoxicity test was conducted. **(D)** The Anti-Aβ aggregation effect of ACD-5-CDB and ACD-5-BRM in gold nanoparticle-mediated anti-Aggregation test. Albumin was taken as a positive control.

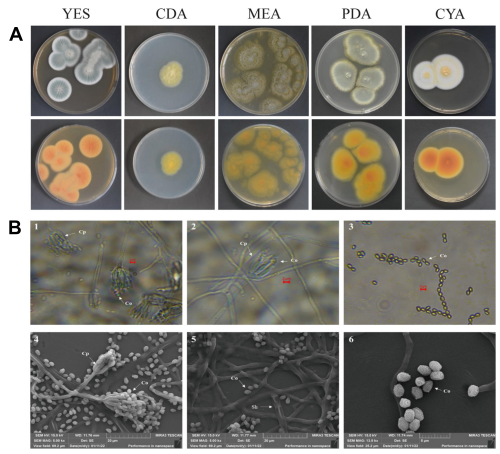

FIGURE 8
The colonial and microscopic morphology of ACD-5. **(A)** The 7-day old cultures of ACD-5 on CYA, CDA, MEA, YES, and PDA, showing variation in colony characters. The front view of colony on the left and the back view of colony on the right. **(B)** The microscopic morphology of strain ACD-5. 1–3 were morphologies observed under light microscope at 100 x magnification, scale bar = 2 μm; 4–6 were the morphologies observed under scanning electron microscope, the scale bar of 4 and 5 was 20 μm while the 6 was 5 μm. Co, Conidium; Cp, Conidiophore; Sh, Septa hypha.

of ACD-5-CDB. Therefore, BRM was chosen for bulk fermentation of strain ACD-5, and a total of 80 g crude extracts were obtained after fermentation for metabolite isolation.

The extract was subjected to a silica gel vacuum liquid chromatography (VLC), which was eluted with a gradient of *n*-hexane/ethyl acetate/methanol to obtain 5 fractions (Fr.1–Fr.5). In the anti-Aβ aggregation assay, Fr.3 to Fr.5 demonstrated increased anti-aggregation activities (Figure 10A). Analysis of them using LC-MS/MS revealed the presence of rich azaphilone alkaloids. Further separation of Fr.3 had led to the isolation of **compounds 1–3**.

Compound 1 was obtained as a red powder. Its molecular formula was determined to be $C_{21}H_{24}ClNO_4$ by the positive HR-ESI-MS with the quasimolecular ion peak at *m/z* 390.1471 $[M + H]^+$ (calcd. 390.1467 for $C_{21}H_{25}ClNO_4^+$) and the typical 3:1 isotopic pattern for monochlorinated molecules. The $^1H/^{13}C$ NMR data were listed as follows.^1H NMR (DMSO-d_6, 700 MHz): δ_H 7.96 (1 H, s, H-1), 6.95 (1 H, s, H-4), 6.47 (1 H, d, J = 16.3 Hz, H-9), 7.24 (1 H, d, J = 16.3 Hz, H-10), 5.71 (1 H, d, J = 9.7 Hz, H-12), 2.49 (1 H, m, H-13), 1.30∼1.41 (2 H, m, H-14), 0.84 (3 H, t, J = 7.4 Hz, H-15), 0.98 (3 H, d, J = 6.6 Hz, H-16), 1.83 (3 H, s, H-17), 1.40 (3 H, s, H-18), and 2.07 (3 H, s, H-20). ^{13}C NMR (DMSO-d_6, 175 MHz): δ_C 139.1 (C–1), 146.2 (C–3), 110.6 (C–4), 146.1 (C–4a), 100.3 (C–5), 183.0 (C–6), 85.3 (C–7), 193.5 (C–8), 113.5 (C–8a), 118.5 (C–9), 141.5 (C–10), 132.8 (C–11), 146.8 (C–12), 34.7 (C–13), 30.0 (C–14), 12.3 (C–15), 20.6 (C–16), 12.7 (C–17), 20.5 (C–18), 169.6 (C–19), and 20.6 (C–20). Its specific optical rotation was $[\alpha]_D^{25}$+408° (*c* 0.01, MeOH). CD (*c* 0.02, MeOH) λmax (Δε) 215 (−6.66), 246 (+4.87), 309 (−4.64) and 381 (+8.24) nm. By comparison of its ^1H and ^{13}C NMR data as well as CD spectrum with the reported data in literature (Jia et al., 2019), **compound 1** was elucidated to be sclerotioramine with the same stereochemistry (7*R*, 13*S*) (Figure 10B).

Compound 2 was obtained as a red powder. The molecular formula of **compound 2** was determined to be $C_{23}H_{28}ClNO_5$ by the HR-ESI-MS peak at *m/z* 433.17 $[M + H]^+$, with the 3:1 chlorine isotope peaks. The ^1H NMR data was listed as follows. ^1H NMR (DMSO-d_6, 700 MHz): δ_H 8.09 (1 H, s, H-1), 6.95 (1 H, s, H-4), 6.53 (1 H, d, J = 15.5 Hz, H-9), 7.10 (1 H, d, J = 15.5 Hz, H-10), 5.83 (1 H, d, J = 9.70 Hz, H-12), 2.47 (1 H, m, H-13), 1.30∼1.41 (1 H, m, H-14), 0.84 (3 H, t, J = 7.0 Hz, H-15), 0.98 (3 H, d, J = 6.7 Hz, H-16), 1.85 (3 H, s, H-17), 1.40 (3 H, s, H-18), 2.07 (3 H, s, H-20), 4.21 (2 H, m, H-21), and 3.66 (2 H, m, H-22). Its specific optical rotation was $[\alpha]_D^{25}$+590° (*c* 0.01, MeOH). CD (*c* 0.02, MeOH) λmax (Δε) 226 (+0.55), 244 (+4.04), 304 (-5.48) and 380 (+4.44) nm. By comparison of its ^1H NMR data with **compound 1** and the reported data in literature (Jia et al., 2019), **compound 2** was elucidated to be isochromophilone VI with the same stereochemistry (7*R*, 13*S*) (Figure 10B).

Compound 3 was obtained as a red powder. The peak *m/z* 475.18 $[M + H]^+$ and the chlorine isotope peaks in HR-ESI-MS spectrum indicated the molecular formula was $C_{25}H_{30}ClNO_6$. The ^1H NMR data was listed as follows. ^1H NMR (DMSO-d_6, 700 MHz): δ_H 8.18 (1 H, s, H-1), 6.97 (1 H, s, H-4), 6.54 (1 H, d, J = 15.5 Hz, H-9), 7.17 (1 H, d, J = 15.5 Hz, H-10), 5.85 (1 H, d, J = 9.7 Hz, H-12), 2.49 (1 H, m, H-13), 1.31 ∼ 1.44 (1 H, m, H-14),

TABLE 2 Cultural characteristics of strain ACD-5 after 1 week growth at 25°C.

Medium	Diameter (mm)	Colony characteristics	
		Front	Reverse
CYA	32–42	Dense and velutinous, sometimes with aerial mycelium in the center; conidia white to orange; produce clear orange exudate droplets; mycelium edges white.	Red-orange, light to pastel yellow at the margins.
CDA	27–30	Sparsely downy with aerial mycelium; conidia white to yellow; no exudate and soluble pigment.	Yellow.
MEA	25–38	Planar, with no aerial mycelium; conidia greyish green to dull green; no exudates or soluble pigments.	Yellow, deep yellow or orange, with lighter shades of these colors near the edges.
YES	27–38	Dense, velutinous; conidia white to greyish green; moderately sulcate, often wrinkled in the center; produce clear orange-yellow exudate droplets, yellowish exudate droplets.	Reddish-orange on the center.
PDA	40–42	Planar, with aerial mycelium in the center; conidia are greyish green to dull green with light yellow marginal spores; no exudate.	Yellow or red-orange.

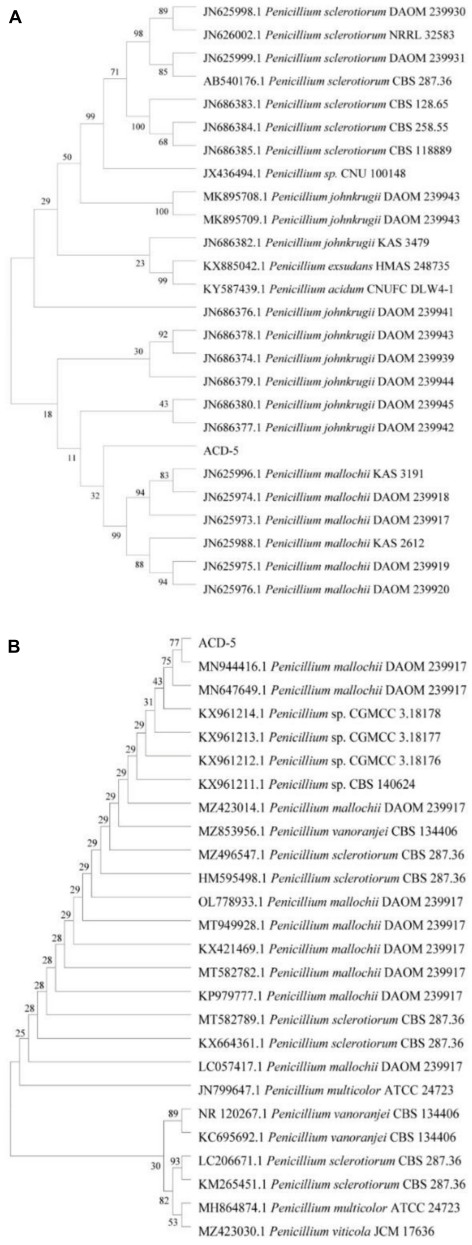

FIGURE 9
Neighbor-jointing trees based on β-tubulin **(A)** and ITS rDNA **(B)** of ACD-5 and adjacent areas of the dominant fungal groups (Bootstrap values were calculated using 1,000 replications).

0.84 (3 H, t, J = 7.4 Hz, H-15), 0.98 (3 H, d, J = 6.6 Hz, H-16), 1.90 (3 H, s, H-17), 1.40 (3 H, s, H-18), 2.07 (3 H, s, H-20), 4.13 (2 H, m, H-21), 1.93 (2 H, m, H-22), and 2.32 (2 H, t, J = 6.7 Hz, H-23). Its specific optical rotation was $[\alpha]_D^{25}$ + 1240° (c 0.01, MeOH). CD (c 0.02, MeOH) λmax (Δε) 231 (+0.35), 244 (+2.89), 305 (-3.45), and 378 (+2.98) nm. By comparison of its ^{1}H NMR data with the above two azaphilones and the reported data in literature (Jia et al., 2019), **Compound 3** was elucidated to be isochromophilone IX with the same stereochemistry (7*R*, 13*S*) (**Figure 10B**).

In the bioassays, **compound 1** displayed remarkable inhibition to LPS induced NO release in microglial BV-2 cells at the dose of 10–100 μg/mL without toxicity to this cell within the same concentration range (**Figures 10C, D**). **Compound 2** also exhibited inhibition to NO release without cytotoxicity at 1 and 10 μg/mL; however, it produced toxicity to the cell at higher concentrations. **Compound 3** only showed weak inhibition to NO release at 20 μg/mL. This suggested the potential of **compound 1** as anti-neuroinflammatory agent. Judged from their structures, the too long side chain on N-2 position seems to weaken their anti-neuroinflammatory activity or increase cytotoxicity. In the anti-Aβ aggregation activity assay, no significant effect comparable to the control albumin was observed for these three compounds. **Compounds 2** and **3** displayed relatively higher anti-aggregation effect than **compound 1** at 20 and 100 μg/mL. However, their low solubility in the test system, hampered their testing at higher concentration. Considering the anti-aggregation effect of Fr.3 to Fr.5, we speculate that more azaphilones with strong activity may be found later from these fractions.

4. Discussion

In this study, a *Penicillium mallochii* strain derived from sea cucumber with diverse alkaloid metabolites was screened out from marine fungal collection by *in situ* colony dyeing and multi-approach assisted FBMN and identified by genetic markers and morphology. Intriguingly, it is capable of producing rich azaphilones, most of which belong to alkaloids. This ability was confirmed by the isolation and elucidation of three representative **compounds 1** (sclerotioramine), **2** (isochromophilone VI), and **3** (isochromophilone IX). Its crude extracts, fractions, and/or isolated compounds exhibited antioxidant, AChE inhibitory, anti-Aβ aggregation, and anti-neuroinflammatory effects.

The traditional screening of alkaloid-producing strains is usually carried out via alkaloids detecting in culture extracts by chromogenic reactions in liquid or on TLC plate and by HPLC, LC-MS, or direct ESI-MS (Yin and Sun, 2011; Han et al., 2015; da Silva et al., 2021; Munakata et al., 2022). However, these methods usually require a term of fermentation before extraction of metabolites from all the tested strains in the first step. It is usually time-consuming and laborious, though sometimes the extraction can be skipped. While *in situ* colony assay in our study has proven to be a more convenient and effective method as it was performed by direct color development of the strain to determine whether it can produce alkaloids, which can help us shorten the range and find the target strains quickly. LC-MS/MS is well known for its wide analytical range, reliable qualitative analysis results and low detection limits. *In situ* colony assay combined with high-resolution LC-MS/MS enabled us to quickly find the alkaloid producing strains in the screening. Although some new technologies like DESI-MS (desorption electrospray ionization mass spectrometry) and DART-MS (direct analysis in real-time mass spectrometry) may be used for direct MS analysis on colonies (Tata et al., 2015; Gross, 2014), the minute contents of secondary metabolites (SMs) in colony may limit the completeness of information and much more accurate instruments are needed.

Mass spectrometry-based molecular networks are established on the similar MS/MS fragmentation for the structurally similar molecules. To discover potential SMs, molecular networking tools like GNPS can provide useful information to annotate

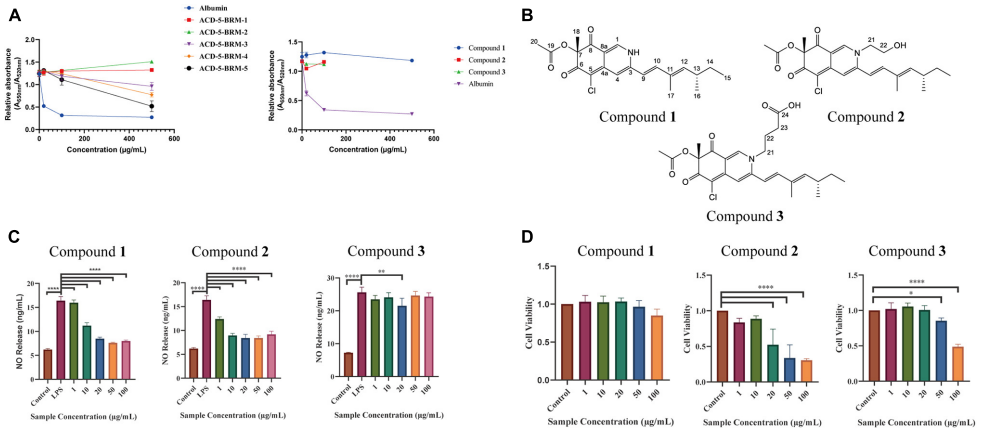

FIGURE 10
The anti-Aβ aggregation, anti-neuroinflammatory and cytotoxic effects of the primary fractions of ACD-5-BRM and the isolated **compounds 1–3**. **(A)** The anti-Aβ aggregation effects of the primary fractions of ACD-5-BRM and compounds. Since **compounds 2** and **3** were not soluble in methanol at high concentrations, anti-Aβ aggregation assay was not performed on 500 μg/mL. Albumin was taken as a positive control. **(B)** The structure of **compounds 1–3**. **(C)** The inhibitory effect of compounds on LPS induced nitric oxide (NO) production of BV-2 cells. **(D)** The effect of **compounds 1–3** on the viability of BV-2 cells. The results were expressed as the mean ± SD (n = 3). *p < 0.05, **p < 0.01, ****p < 0.0001, compared with the control group. A value of p < 0.05 was considered statistically significant.

possibly known natural products and find novel compounds in the dereplication of strains. The updated version of GNPS, i.e., FBMN can make use of data containing molecular formula and retention time information collected from high-resolution mass spectrometry and thus enhances the annotation function to discriminate isomers (Nothias et al., 2020). MSDIAL, MSFINDER, and CFM-ID are also practical tools for metabolites annotation. However, GNPS or FBMN usually provides very limited hits due to the capacity of the measured MS/MS spectral databases. While MSDIAL, MSFINDER, and CFM-ID merely annotate compounds separately without considering the internal relationship between metabolites. And a mutual shortcoming of these approaches is that the reasonable biological sources of compounds have not been taken into account during annotation.

In the present study, we developed a comprehensive strategy named "multi-approach assisted FBMN" to annotate the metabolites in the extracts of the strain ACD-5 (**Graphical Abstract**). This strategy could fully utilize the advantages of FBMN (networking view, multiple measured MS/MS spectral libraries), MSDIAL (inner set measured MS/MS library), MSFINDER (multiple measured and *in silico* MS/MS spectral libraries), and CFM-ID 3.0 (rich *in silico* MS/MS spectra with different collision energies predicted for natural product libraries). In addition, the biological sources of the hits were investigated by manual retrieving in quite a few important natural product libraries. The final annotations were made on the basis of comprehensive consideration of these results. With this strategy, diverse alkaloids together with other compounds were annotated for strain ACD-5. Particularly, a series of azaphilones were found in the extracts and their high scores and fungal origin in literatures demonstrated the effectiveness of this metabolic annotation strategy. However, it is reminded that the consideration of the biological source should be cautiously given priority since some natural products are evolutionarily conservative between different taxa and it is not excludable the residue of plant-derived ingredients in cultural medium.

Marine fungi are one of the important sources of MNPs due to their ability to produce abundant SMs and the potential for sustainable utilization. ACD-5 was isolated from the sea cucumber *Holothuria scabra* intestine and was identified as *P. mallochii* by gene sequencing and morphology. Little is known about this fungal species up to now. *P. mallochii* has been first isolated from *Rothschildia lebeau* and *Citheronia lobesis* larvae in Costa Rica and is monoverticillate with greenish globose to sub-globose conidia, smooth-walled conidiophores, and an orange-red extracellular pigment in agar culture (Rivera et al., 2012). There are fewer reports on its SMs and activities. The chlorinated azaphilone sclerotiorin is the first secondary metabolite reported from this species (Maccurin and Relly, 1940). Herein, we discover the great potential of *P. mallochii* strain ACD-5 in the production of alkaloids, including diverse azaphilones, by *in situ* colony screening and LC-MS/MS.

Azaphilones have been found with versatile bioactivities and structures. A previous report showed that azaphilones produced by *P. mallochii* exhibited an inhibitory effect on glioblastoma and the effective dose showed no lethal properties in healthy cells (Bouhri et al., 2020). Furthermore, sclerotiorin was reported to potently delay both seeded and non-seeded $A\beta_{42}$ polymerization in cell-free assays. The azaphilones also have antioxidant and anti-inflammatory properties (Tang et al., 2019; Ayyolath et al., 2020) and have been described as modulators of tau aggregation *in vitro* (Paranjape et al., 2015). Thus, this type of compound has great potential as drug candidates for the treatment of AD (Wiglenda et al., 2020). In addition, azaphilones from different fungi were reported for their cytotoxic, antimicrobial, antitumoral, and antiviral (including inhibition to SARS-CoV-2, the pathogen of COVID-19) properties (Ayyolath et al., 2020; Pimenta et al., 2021; Youssef et al., 2021). Some azaphilones like sclerotiorin have no nitrogen atoms in structures while others like sclerotioramine contain nitrogen. Previous reports indicated that the pyranyl oxygens in their structures are readily converted to nitrogens with ammonia (Maccurin and Relly, 1940; Arai et al., 1995), which enhances their structural and bioactivity diversities.

In strain ACD-5, a total of thirteen azaphilones including nitrogenated and non-nitrogenated were annotated (Figure 5), most of them contain chlorin as well, and their structural scaffold or side-chain substitution are also quite different. Moreover, some other unannotated nodes were also observed to have high structural similarities with the annotated ones in the same networks as shown by their cosine values (higher than 0.8 and even close to 1.0). In anti-neuroinflammatory and anti-Aβ aggregation assays, the extracts and fractions of ACD-5 exhibited bioactivities, which need further investigation of their bioactive compounds especially azaphilones. Promisingly, **compound 1** (sclerotioramine) from fraction Fr.3 showed potent anti-neuroinflammatory activity without apparent toxicity to BV-2 cells. Therefore, ACD-5 is considered as a strain with great potential to be explored and we believe more azaphilones will be continuously contributed by this strain with in-depth isolation and application of metabolomic and genomic mining.

In summary, this study reported the discovery of a marine fungus *P. mallochii* ACD-5 from sea cucumber with high potential in alkaloids production through an integrated pipeline consisting of an efficient *in situ* colony assay, TLC chemical colorization and LC-MS/MS based metabolomics profiling. During this, a comprehensive metabolic annotation strategy named "multi-approach assisted FBMN" was established by combining MSDIAL, MSFINDER, FBMN, CFM-ID, and manual biological source annotation for metabolomics investigation. Using this strategy, diverse alkaloids especially azaphilones were annotated in the extracts of this strain. Its fermentation extracts, fractions and/or the isolated compounds displayed good antioxidant ability, inhibited Aβ aggregation and had anti-neuroinflammatory effect. The isolation and elucidation of the azaphilone alkaloids sclerotioramine, isochromophilone VI, and isochromophilone IX verified the effectiveness of our alkaloids "hunting" pipeline. As a fertile producer of potential alkaloids, the bioactive azaphilones and other metabolites are deserved to be mined from strain ACD-5 by further metabonomic, genomic, and pharmacological approaches.

Data availability statement

The datasets presented in this study can be found in online repositories. The names of the repository/repositories and accession number(s) can be found in this article/ Supplementary material.

Author contributions

YZ and YL designed the research plan. TL mainly performed most of the experiments and prepared the draft. YN and XL participated in the experiments on sampling, isolation, culture of seaweeds, sea cucumbers, and corals. YF and LZ participated in the strain identification. QL was responsible for the assay of anti-inflammatory activity. XW was responsible for the assay of anti-aggregation of Aβ. PH and XH provided advice on the research. YZ supervised the work. YL, LZ, and YZ reviewed the manuscript. All authors contributed to the article and approved the submitted version.

Funding

This study was supported by the Guangdong Provincial Natural Science Foundation (Grant Number: 2022A1515010783), the Guangdong Provincial Special Project in Science and Technology (Grant Number: 2021A05240), the National Natural Science Foundation (Grant Number: 21807015), the Special project in key fields of Guangdong provincial higher education institutions (Biomedicine and health care) (Grant Number: 2021ZDZX2064), the Basic Research Project of Shenzhen Science and Technology Innovation Commission (Grant Numbers: JCYJ20220530162014032 and JCYJ20190813105005619), the Zhanjiang Marine Youth Talent Innovation Project (Grant Number: 2022E05010), the Shenzhen Dapeng New District Scientific and Technological Research and Development Fund (Grant Number: KJYF202001–07), the Science and Technology Development Special Fund Competitive Allocation Project of Zhanjiang City (Grant Number: 2020A01030), the Program for Scientific Research Start-up Funds of Guangdong Ocean University (Grant Numbers: R18008 and 060302042201), the Innovation and Development Project about Marine Economy Demonstration of Zhanjiang City (Grant Number: Zhan–Hai–Chuang XM–202008–01B1), and the Graduate Student Education Innovation Project of Guangdong Ocean University (Grant Number: 202232).

Acknowledgments

We thank Mr. Weiming Su in the Key Laboratory of Guangdong Province Aquatic Products Processing and Safety for providing LC-MS/MS technical support.

Conflict of interest

The authors declare that the research was conducted in the absence of any commercial or financial relationships that could be construed as a potential conflict of interest.

Publisher's note

Supplementary material

The Supplementary Material for this article can be found online at: https://www.frontiersin.org/articles/10.3389/fmicb.2023.1144328/full#supplementary-material

References

Arai, N., Shiomi, K., Tomoda, H., Tabata, N., Yang, D. J., Masuma, R., et al. (1995). Isochromophilones III–VI, inhibitors of acyl-CoA: Cholesterol acyltransferase produced by *Penicillium multicolor* FO-3216. *J. Antibiot.* 48, 696–702. doi: 10.7164/antibiotics.48.696

Ayyolath, A., Kallingal, A., Kundil, V. T., and Variyar, E. J. (2020). Studies on the bioactive properties of *Penicillium mallochi* ARA-1 pigment isolated from coffee plantation. *Biocatal. Agric. Biotechnol.* 30:101841. doi: 10.1016/j.bcab.2020.101841

Bouhri, Y., Askun, T., Tunca, B., Deniz, G., Aksoy, S., and Mutlu, M. (2020). The orange-red pigment from *Penicillium mallochii*: Pigment production, optimization, and pigment efficacy against glioblastoma cell lines. *Biocatal. Agric. Biotechnol.* 23:101451. doi: 10.1016/j.bcab.2019.101451

Carroll, A. R., Copp, B. R., Davis, R. A., Keyzers, R. A., and Prinsep, M. R. (2021). Marine natural products. *Nat. Prod. Rep.* 38, 362–413. doi: 10.1039/d0np00089b

Chah, S., Hammond, M. R., and Zare, R. N. (2005). Gold nanoparticles as a colorimetric sensor for protein conformational changes. *Chem. Biol.* 12, 323–328. doi: 10.1016/j.chembiol.2005.01.013

da Silva, F. A., de Souza, M. M. M., Rezende, G. O., da Silva, F. M. A., da Cruz, J. C., da Silva, G. F., et al. (2021). Screening of alkaloid-producing endophytic *Penicillium* strains from amazon medicinal plants by electrospray ionization mass spectrometry (ESI-MS) and principal component analysis (PCA). *J. Brazil. Chem. Soc.* 32, 1832–1839. doi: 10.21577/0103-5053.20210074

Djoumbou-Feunang, Y., Pon, A., Karu, N., Zheng, J. M., Li, C., Arndt, D., et al. (2019). CFM-ID 3.0: Significantly improved ESI-MS/MS prediction and compound identification. *Metabolites* 9:72. doi: 10.3390/metabo9040072

Ellman, G. L., Courtney, K. D., Andres, V., and Featherstone, R. M. (1961). A new and rapid colorimetric determination of acetylcholinesterase activity. *Biochem. Pharmacol.* 7, 88–95. doi: 10.1016/0006-2952(61)90145-9

Gross, J. H. (2014). Direct analysis in real time-a critical review on DART-MS. *Anal. Bioanal. Chem.* 406, 63–80. doi: 10.1007/s00216-013-7316-0

Guan, X. (2019). *Screening of antibacterial active strains in marine fungi and overexpression of eqxR gene in Fusarium equiseti*. Ph.D. thesis. Harbin: Harbin University of Commerce.

Han, W. X., Song, T., Yang, S. Z., Li, X. F., Zhang, H., Wu, Y. H., et al. (2015). Identification of alkaloids and huperzine A-producing endophytic fungi isolated from wild *Huperzia serrata*. *J. Int. Pharm. Res.* 42, 507–512. doi: 10.13220/j.cnki.jipr.2015.04.014

Haque, N., Parveen, S., Tang, T. T., Wei, J. E., and Huang, Z. N. (2022). Marine natural products in clinical use. *Mar. Drugs* 20:528. doi: 10.3390/md20080528

Jia, Q., Du, Y. Q., Wang, C., Wang, Y., Zhu, T. H., and Zhu, W. M. (2019). Azaphilones from the marine sponge-derived fungus *Penicillium sclerotiorum* OUCMDZ-3839. *Mar. Drugs* 17:260. doi: 10.3390/md17050260

Jucker, M. and Walker, L. C. (2013). Self-propagation of pathogenic protein aggregates in neurodegenerative diseases. *Nature* 501, 45–51. doi: 10.1038/nature12481

Kim, H. Y., Lee, D., Ryu, K. Y., and Choi, I. (2017). A gold nanoparticle-mediated rapid in vitro assay of anti-aggregation reagents for amyloid beta and its validation. *Chem. Commun.* 53, 4449–4452. doi: 10.1039/c7cc00358g

Lai, Z. J., Tsugawa, H., Wohlgemuth, G., Mehta, S., Mueller, M., Zheng, Y. X., et al. (2018). Identifying metabolites by integrating metabolome databases with mass spectrometry cheminformatics. *Nat. Methods* 15, 53–56. doi: 10.1038/nmeth.4512

Li, A. Q., Du, Z. F., Liao, M., Feng, Y. L., Ruan, H. L., and Jiang, H. L. (2019). Discovery and characterisation of lycorine-type alkaloids in *Lycoris* spp. (*Amaryllidaceae*) using UHPLC-QTOF-MS. *Phytochem. Anal.* 30, 268–277. doi: 10.1002/pca.2811

Liu, Y., Li, Y. M., Chen, M. Q., Liu, Y. Y., Liang, J. Y., Zhang, Y., et al. (2022). Mechanism of two alkaloids isolated from coral endophytic fungus for suppressing angiogenesis in atherosclerotic plaque in HUVEC. *Int. Immunopharmacol.* 109:108931. doi: 10.1016/j.intimp.2022.108931

Maccurin, T., and Relly, J. (1940). Sclerotiorine, a chlorinated metabolic product of *Penicillium sclerotiorum*, Van Beyma. *Nature* 146:335. doi: 10.1038/146335b0

Munakata, Y., Spina, R., Slezack-Deschaumes, S., Genestier, J., Hehn, A., and Laurain-Mattar, D. (2022). Screening of endophytic bacteria of *Leucojum aestivum* 'gravety giant' as a potential source of alkaloids and as antagonist to some plant fungal pathogens. *Microorganisms* 10:2089. doi: 10.3390/microorganisms10102089

Nie, Y. Y., Yang, W. C., Liu, Y. Y., Yang, J. M., Lei, X. L., Gerwick, W. H., et al. (2020). Acetylcholinesterase inhibitors and antioxidants mining from marine fungi: Bioassays, bioactivity coupled LC-MS/MS analyses and molecular networking. *Mar. Life Sci. Tech.* 2, 386–397. doi: 10.1007/s42995-020-00065-9

Nothias, L. F., Petras, D., Schmid, R., Dührkop, K., Rainer, J., Sarvepalli, A., et al. (2020). Feature-based molecular networking in the GNPS analysis environment. *Nat. Methods* 17, 905–908. doi: 10.1101/812404

Paranjape, S. R., Riley, A. P., Somoza, A. D., Oakley, C. E., Wang, C. C. C., Prisinzano, T. E., et al. (2015). Azaphilones inhibit tau aggregation and dissolve tau aggregates in vitro. *ACS. Chem. Neurosci.* 6, 751–760. doi: 10.1021/acschemneuro.5b00013

Pimenta, L. P. S., Gomes, D. C., Cardoso, P. G., and Takahashi, J. A. (2021). Recent findings in azaphilone pigments. *J. Fungi* 7:541. doi: 10.3390/jof7070541

Qian, Z. J., Kang, K. H., and Kim, S. K. (2012). Isolation and antioxidant activity evaluation of two new phthalate derivatives from seahorse, Hippocampus Kuda Bleeler. *Biotechnol. Bioproc. E.* 17, 1031–1040. doi: 10.1007/s12257-012-0115-1

Rivera, K. G., and Seifert, K. A. (2011). A taxonomic and phylogenetic revision of the *Penicillium sclerotiorum* complex. *Stud. Mycol.* 70, 139–158. doi: 10.3114/sim.2011.70.03

Rivera, K. G., Díaz, J., Chavarria-Diaz, F., Garcia, M., Urb, M., Thorn, R. G., et al. (2012). *Penicillium mallochii* and *P. guanacastense*, two new species isolated from costa rican caterpillars. *Mycotaxon* 119, 315–328. doi: 10.5248/119.315

Rubia, L. B., and Gomez, R. (1977). TLC sensitivity of six modifications of Dragendorff's reagent. *J. Pharm. Sci.* 66, 1656–1657. doi: 10.1002/jps.2600661147

Ryu, B., Qian, Z. J., and Kim, S. K. (2010). SHP-1, a novel peptide isolated from seahorse inhibits collagen release through the suppression of collagenases 1 and 3, nitric oxide products regulated by NF-kappaB/p38 kinase. *Peptides* 31, 79–87. doi: 10.1016/j.peptides.2009.10.019

Sawant, S. S., Salunke, B. K., and Kim, B. S. (2015). A rapid, sensitive, simple plate assay for detection of microbial alginate lyase activity. *Enzyme Microb. Technol.* 77, 8–13. doi: 10.1016/j.enzmictec.2015.05.003

Tang, J. L., Zhou, Z. Y., Yang, T., Yao, C., Wu, L. W., and Li, G. Y. (2019). Azaphilone alkaloids with anti-inflammatory activity from fungus *Penicillium sclerotiorum* cib-411. *J. Agric. Food Chem.* 67, 2175–2182. doi: 10.1021/acs.jafc.8b05628

Tata, A., Perez, C. J., Ore, M. O., Lostun, D., Passas, A., Morin, S., et al. (2015). Evaluation of imprint DESI-MS substrates for fungal metabolites analysis. *RSC Adv.* 5, 75458–75464. doi: 10.1039/C5RA12805F

Tsugawa, H., Nakabayashi, R., Mori, T., Yamada, Y., Takahashi, M., Rai, A., et al. (2019). A cheminformatics approach to characterize metabolomes in stable-isotope-labeled organisms. *Nat. Methods* 16, 295–298. doi: 10.1038/s41592-019-0358-2

Wang, F., Liigand, J., Tian, S. Y., Arndt, D., Greiner, R., and Wishart, D. S. (2021). CFM-ID 4.0: More accurate ESI-MS/MS spectral prediction and compound identification. *Anal. Chem.* 93, 11692–11700. doi: 10.1021/acs.analchem.1c01465

Wang, M. X., Carver, J. J., Phelan, V. V., Sanchez, L. M., Garg, N., Peng, Y., et al. (2016). Sharing and community curation of mass spectrometry data with Global Natural Products Social Molecular Networking. *Nat. Biotechnol.* 34, 828–837. doi: 10.1038/nbt.3597

Wang, Y., Glukhov, E., He, Y. F., Liu, Y. Y., Zhou, L. J., Ma, X. X., et al. (2022). Secondary metabolite variation and bioactivities of two marine *Aspergillus* strains in static co-culture investigated by molecular network analysis and multiple database mining based on LC-PDA-MS/MS. *Antibiotics* 11:513. doi: 10.3390/antibiotics11040513

Wiglenda, T., Groenke, N., Hoffmann, W., Manz, C., Diez, L., Buntru, A., et al. (2020). Sclerotiorin stabilizes the assembly of nonfibrillar Abeta42 oligomers with low toxicity, seeding activity, and beta-sheet content. *J. Mol. Biol.* 432, 2080–2098. doi: 10.1016/j.jmb.2020.01.033

Yin, H., and Sun, Y. H. (2011). Vincamine-producing endophytic fungus isolated from Vinca minor. *Phytomedicine* 18, 802–805. doi: 10.1016/j.phymed.2011.01.005

Yin, Q. Z., Liu, X. W., Zhang, Z. J., Lei, H. X., and Wu, B. (2023). Chemistry and bioactivities of alkaloids isolated from marine fungi (covering 2016–2022). *Fitoterapia* 164:105377. doi: 10.1016/j.fitote.2022.105377

Youssef, F. S., Alshammari, E., and Ashour, M. L. (2021). Bioactive alkaloids from genus *Aspergillus*: Mechanistic interpretation of their antimicrobial and potential SARS-CoV-2 inhibitory activity using molecular modelling. *Int. J. Mol. Sci.* 22:1866. doi: 10.3390/ijms22041866

Yu, H. B., Glukhov, E., Li, Y. Y., Iwasaki, A., Gerwick, L., Dorrestein, P. C., et al. (2019). Cytotoxic microcolin lipopeptides from the marine cyanobacterium Moorea producens. *J. Nat. Prod.* 82, 2608–2619. doi: 10.1021/acs.jnatprod.9b00549

Zhang, F., Braun, D. R., Chanana, S., Rajski, S. R., and Bugni, T. S. (2019). Phallusialides A–E, Pyrrole-derived alkaloids discovered from a marine-derived *Micromonospora* sp. bacterium using MS-based metabolomics approaches. *J. Nat. Prod.* 82, 3432–3439. doi: 10.1021/acs.jnatprod.9b00808

Zhang, Y. Y., Zhang, Y., Yao, Y. B., Lei, X. L., and Qian, Z. J. (2018). Butyrolactone-I from coral-derived fungus *Aspergillus terreus* attenuates neuro-inflammatory response via suppression of NF-kappaB pathway in BV-2 cells. *Mar. Drugs* 16:202. doi: 10.3390/md16060202

frontiers | Frontiers in Microbiology

TYPE Mini Review
PUBLISHED 10 May 2023
DOI 10.3389/fmicb.2023.1174591

OPEN ACCESS

EDITED BY
Sylvie Lautru,
Centre National de la Recherche Scientifique (CNRS), France

REVIEWED BY
Sonia Ilaria Maffioli,
Naicons Srl, Italy
Christophe Corre,
University of Warwick, United Kingdom

*CORRESPONDENCE
Kalindi D. Morgan
✉ kalindi.morgan@unbc.ca

RECEIVED 26 February 2023
ACCEPTED 17 April 2023
PUBLISHED 10 May 2023

CITATION
Morgan KD (2023) The use of nitrogen-15 in microbial natural product discovery and biosynthetic characterization.
Front. Microbiol. 14:1174591.
doi: 10.3389/fmicb.2023.1174591

The use of nitrogen-15 in microbial natural product discovery and biosynthetic characterization

Kalindi D. Morgan*

Department of Chemistry and Biochemistry, University of Northern British Columbia, Prince George, BC, Canada

This mini-review covers the use of nitrogen-15 in bacterial and fungal natural product discovery and biosynthetic characterization from 1970 to 2022. Nitrogen is an important element in a number of bioactive and structurally intriguing natural products including alkaloids, non-ribosomal peptides, and hybrid natural products. Nitrogen-15 can be detected at natural abundance utilizing two-dimensional nuclear magnetic resonance and mass spectrometry. Additionally, it is a stable isotope that can be added to growth media for both filamentous fungi and bacteria. With stable isotope feeding, additional two-dimensional nuclear magnetic resonance and mass spectrometry strategies have become available, and there is a growing trend to use nitrogen-15 stable isotope feeding for the biosynthetic characterization of natural products. This mini-review will catalog the use of these strategies, analyze the strengths and weaknesses of the different approaches, and suggest future directions for the use of nitrogen-15 in natural product discovery and biosynthetic characterization.

KEYWORDS

natural products, nitrogen-15, NMR-guided discovery, mass spectrometry, structure elucidation, biosynthetic characterization, biosynthetic gene clusters

1. Nitrogen-15 in natural products

Nitrogen is often found within structurally interesting and bioactive microbial natural products in varying frequencies and moieties. Natural product classes with significant nitrogen representation include alkaloids, non-ribosomal peptides, polyketide macrolactams, and ribosomally synthesized post-translationally modified peptides (RiPPs). Due to this prevalence, tools and methodologies that can detect nitrogen are of great use to those who study microbial natural products. Important tools are nuclear magnetic resonance (NMR) and mass spectrometry (MS). ^{15}N-NMR can be employed strategically for structure elucidation and discovery, while MS methodologies are pivotal for biosynthetic characterization and discovery particularly by detecting nitrogen-15 isotope ratio shifts.

2. Nitrogen-15 NMR

2.1. Nitrogen-15 NMR background

Nitrogen-15 nuclear magnetic resonance (NMR) spectroscopy is a powerful tool for elucidating natural product structures which contain nitrogen atoms. With steady instrument improvements and new techniques, valuable NMR data

can be gathered with increasingly less material (Breton and Reynolds, 2013). Of the commonly found elements in natural products—hydrogens (i.e., protons), carbon, oxygen, nitrogen, sulfur and phosphorous– experiments can be run to directly probe small variations in structural environments for ^{1}H, ^{13}C,^{14}N, ^{15}N, and ^{31}P nuclei (Parella and Sánchez-Ferrando, 2004; Martin, 2011). Nitrogen has two NMR active isotopes: ^{14}N and ^{15}N. ^{14}N is the more abundant isotope; however, ^{14}N is a spin-1 nucleus, and the signal suffers from significant line broadening due to quadrupolar relaxation (Witanowski and Webb, 1972). Alternately, nitrogen-15 is a spin-1/2 nucleus that does not experience significant line broadening, and is thus the more commonly observed nitrogen isotope (Witanowski and Webb, 1972). However, ^{15}N has a natural abundance of only 0.36%, making it less sensitive than other more abundant nuclei such as carbon-13 or proton. The ^{15}N isotope's negative gyromagnetic ratio (−2.7126) (Martin and Williams, 2010) also results in decreased sensitivity of the ^{15}N isotope in NMR experiments in comparison to isotopes with a positive gyromagnetic ratio.

Methods for overcoming both ^{15}N and ^{13}C signal insensitivities incorporate a suite of two-dimensional (2D) NMR experiments in which the sensitivity of the proton is transferred to the more insensitive nuclei, increasing the signal-to-noise ratio and permitting data analysis of lower-abundance metabolites (Marek and Lycka, 2002; Martin and Williams, 2010). In general, two phenomena are exploited to transfer sensitivity from the proton to insensitive nuclei, such as ^{13}C and ^{15}N: the nuclear Overhauser effect, and polarization transfer for scalar coupled nuclei (Morris and Freeman, 1979; Freeman, 1997). Sensitivity transfer through the nuclear Overhauser effect is directly related to the gyromagnetic ratio of the observed nuclei. Because of this relationship, the nuclear Overhauser effect is not of value for sensitivity enhancement of the ^{15}N nuclei with its negative gyromagnetic ratio (Freeman, 1997). The base experiment for non-selective sensitivity enhancement for scalar coupled nuclei is called the Insensitive Nuclei Enhanced by Polarization Transfer (INEPT) experiment (Morris and Freeman, 1979). Polarization transfer in scalar coupled nuclei is independent of the sign of the gyromagnetic ratio and, as such, is very useful for ^{15}N experiments (Morris and Freeman, 1979). One caveat is that because polarization transfer relies on scalar coupling, through-bond connectivity must occur for this enhancement. Usefully, in inverse detected 2D experiments, the ^{15}N isotope experiences significant increases in detection sensitivity (Freeman, 1997) due to the large population disparity between ^{1}H and ^{15}N, which arises from the sizeable gyromagnetic ratio difference between ^{1}H (26.7522) and ^{15}N (−2.7126) (Marek and Lycka, 2002). With experiments built off the INEPT foundation (Morris and Freeman, 1979), ^{15}N is routinely used in NMR methods for elucidating amino acids for protein structure determination (Mulder and Filatov, 2010; Williamson et al., 2014), while usage in small molecule structure determination has varied in the literature (Marek and Lycka, 2002; Martin and Williams, 2010). The low natural abundance can be circumvented by incorporating stable isotope (or labeled) precursors into natural products to increase the ^{15}N signal (Bax, 1989; Ohki and Kainosho, 2008; Chokkathukalam et al., 2014; Deev et al., 2017). However, with 2D experiments, natural abundance is usually enough to collect data from pure samples (Martin and Hadden, 2000; Marek and Lycka, 2002). Another barrier to its use has been the historical tendency to report nitrogen referenced to various internal and external references (Witanowski and Webb, 1972; Wishart et al., 1995), which has made it difficult to look to the literature for typical chemical shifts that are widely applicable. Fortunately, over the last several decades, there has been a shift to reference ^{15}N NMR spectra to either nitromethane or liquid ammonia set equal to 0 ppm (IUPAC recommendation Harris et al., 2002; Martin and Williams, 2010). Additionally, experimental work has been done to compare the shifts of nitromethane and liquid ammonia, meaning chemical shift values can be easily converted between these two ^{15}N references (Witanowski and Webb, 1972; Martin et al., 2007; Martin and Williams, 2010; Martin, 2011). Nitrogen chemical shifts referenced to liquid ammonia tend to have positive signs. Nitromethane is more deshielded than most nitrogens in natural products; this has historically been represented with shielded nitrogens possessing negative values in relation to nitromethane (IUPAC recommendation (Harris et al., 2002). Since about 2015, chemists are reversing that convention in relation to nitromethane (Martin and Williams, 2015). However, because most natural product nitrogens are more shielded than nitromethane, if a negative nitrogen chemical shift is reported, it can be generally assumed the historical conventions are being followed.

2.2. Nitrogen-15 NMR in natural product structure elucidation and discovery

Two-dimensional (2D) NMR experiments that indirectly detect nitrogen-15 improve the sensitivity limitations due to nitrogen's natural abundance. These experiments can detect one-bond couplings between nitrogen-15 and their attached protons (the sensitive ^{1}H-^{15}N HSQC/HMQC), detecting two-to-three bond couplings between tertiary nitrogen and protons in the molecule (long-range ^{1}H-^{15}N HMBC) (Martin and Hadden, 2000; Martin et al., 2007; Martin and Williams, 2010); and even detect carbon-13-nitrogen-15 correlations (^{13}C-^{15}N HSQC) with appropriate labeling. These 2D ^{15}N NMR experiments are invaluable in solving complex bioactive natural product structures (Figure 1). Examples include the taumycins A (**1**) and B (Bishara et al., 2008), hyrtioreticulin F (**2**) (Imada et al., 2013) and coibamide A (Medina et al., 2008). The structure of the polyketide, forazoline A (**3**), was solved (after stable isotope feeding) utilizing the first example of carbon-13-nitrogen-15 direct detection via ^{13}C-^{15}N HSQC (Wyche et al., 2014). This same experiment proved vital in the recent structure elucidation of the structurally-unprecedented ecteinamine after discovery using an integrated genomic-metabolomic strategy by the Bugni group (Wu et al., 2022).

These 2D nitrogen-15 experiments can also be used in the discovery process, as first exemplified in 2007 in the genomisotopic approach developed by the Gerwick lab. The genomisotopic approach used ^{15}N isotopically labeled precursors as predicted by *in silico* adenylation domain specificity of a genetically encoded non-ribosomal peptide to link orphan secondary metabolite gene clusters to the putatively produced natural product (Gross et al., 2007). In this method, use of the ^{1}H-^{15}N HMBC experiment

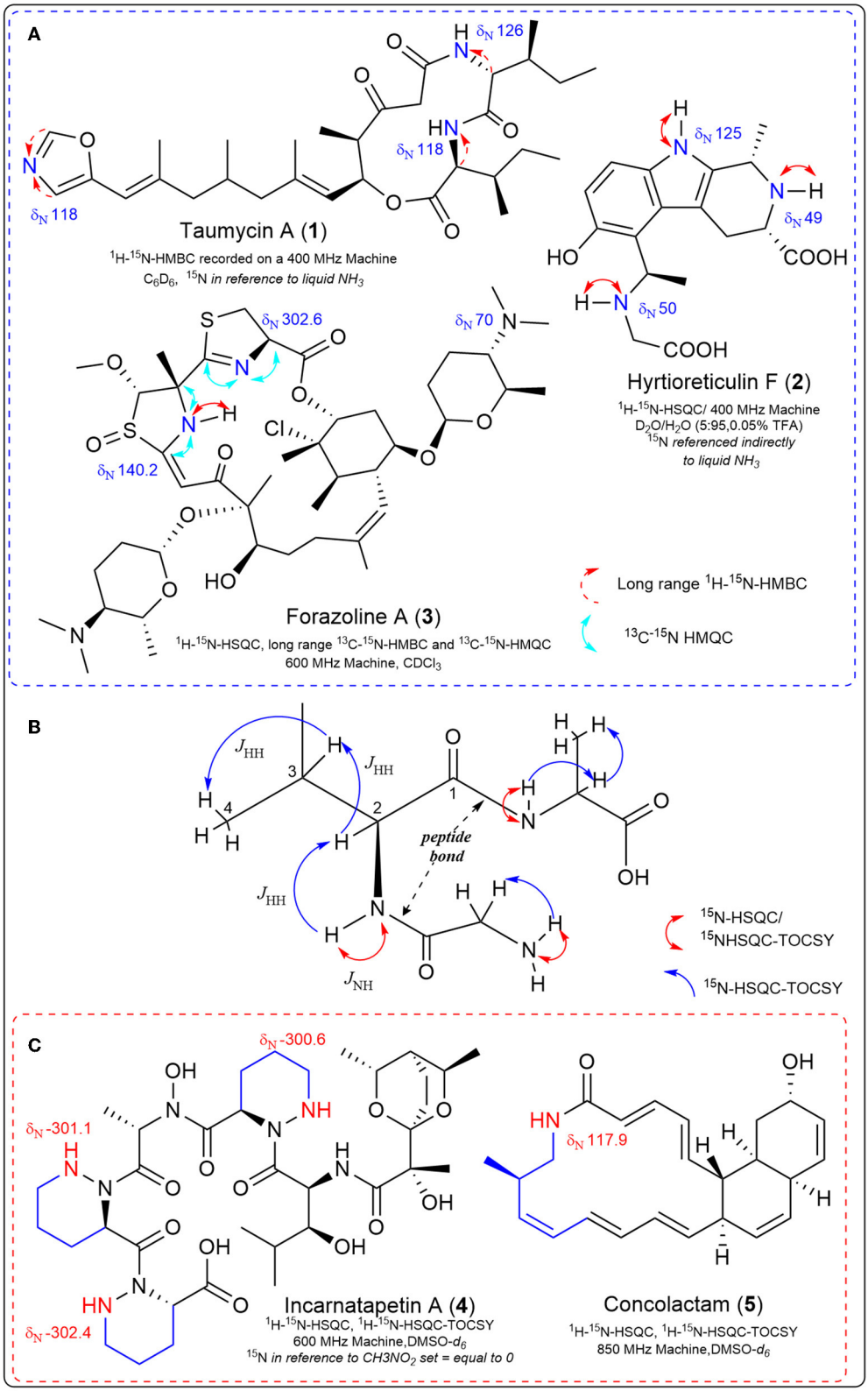

FIGURE 1
Experimentally determined nitrogen chemical shifts are provided, along with key correlations observed from various nitrogen-15 NMR experiments. **(A)** Select natural products structures that required ^{15}N NMR 2D experiments during structure elucidation. **(B)** ^{1}H-^{15}N HSQC-TOCSY is an NMR experiment that allows us to observe the proton spin system of a single amino acid embedded in a peptide, beginning with the N-H correlation. The carbonyl of the peptide bond provides an insulator functionality that constrains the observation of single amino acid spin systems in the TOCSY spectrum. **(C)** Key examples where ^{15}N NMR spectroscopy was integrated with genomic data for natural product discovery.

to identify a ^{15}N labeled isoleucine in tandem with bioassay-guided fractionation led to the successful isolation and structure elucidation of orfamide A representative of a new peptide class.

In fact, one advantage of ^{15}N NMR is the large spectral range (~900 ppm), such that different nitrogen-containing functional groups can have widely dispersed ^{15}N chemical shifts (Williamson et al., 1999). Due to fewer nitrogen atoms (compared to protons or carbons) in small molecule natural products, ^{15}N spectra tend to be less crowded. Specific experiments designed to use this larger spectral dispersion to provide a means of separating crowded proton and carbon signals include the ^{1}H-^{15}N-HSQC-TOCSY and ^{1}H-^{15}N-HSQC-NOESY (Williamson et al., 1999). The ^{1}H-^{15}N-HSQC-TOCSY experiment allows observations of proton spin systems which are ultimately connected to a ^{15}N resonance, that is, the set of scalar-coupled protons adjacent to a nitrogen-attached proton (Figure 1). ^{1}H-^{15}N HSQC experiments can be used to link a primary or secondary nitrogen with its attached proton, which, due to the large dispersion of nitrogen signals, allows observation of spin systems outside the crowded proton spectral window (Williamson et al., 1999). The TOCSY portion of the ^{1}H-^{15}N HSQC-TOCSY allows observation of magnetization transfer through scalar-coupled protons to observe a complete amino acid ^{1}H spin system in peptide natural products (Figure 1). Recently these spectroscopic experiments have been integrated with genomic information to discover piperazic acid (Piz)-containing polyketide-nonribosomal peptides (PK-NRP) (Morgan et al., 2020, 2022a,b). and macrolactams (Shin et al., 2023) (Figure 1). In both cases, the dispersion of the nitrogen signals allowed detection of the predicted genetically encoded chemical structures in crude microbial extracts, significantly speeding up the discovery process. ^{15}N NMR was the ideal tool to uncover genomically encoded Piz-containing natural products because Piz contains a unique nitrogen chemical shift and N-H correlation (Williams et al., 2011) distinct from other amides within peptides. Thus, we utilized the sensitive ^{15}N-HSQC experiment to quickly screen microbial extracts obtained from small amounts of bacterial cultures fed with the stable isotope Piz-precursor $^{15}N_2$ L-Orn (Morgan, 2021). After quickly screening through dozens of $^{15}N_2$ L-Orn labeled microbial extracts, the less sensitive ^{1}H-^{15}N-HSQC-TOCSY was applied for unequivocal detection of piperazic acid-containing extracts that aligned with genetically encoded chemical structures of interest (Morgan et al., 2020). We then conducted microbial scale-up, with efficient isolation guided by the ^{1}H-^{15}N-HSQC-TOCSY Piz signal leading to the cytotoxic incarnatapeptin B, the related incarnatapeptin A (**4**) and the piperazic-acid containing dentigerumycins G and H (Morgan et al., 2020, 2022a,b). For the discovery of the novel and cytotoxic muanlactam and antibacterial concolactam (**5**) by the Oh group, the presence and expression of genetically encoded macrolactams was detected through PCR analysis of an in-house gDNA library utilizing macrolactam-specific primers (Shin et al., 2023). Then, bacterial strains identified in the PCR experiments were fed the stable isotope $^{15}NH_4Cl$ to enrich all amide bonds in crude extracts and permit detection of the macrolactams utilizing ^{1}H-^{15}N-HSQC-TOCSY NMR experiments. After this detection, scale-up provided efficient discovery of the muanlactam, **5** and structural reassignment of salinilactam (Shin et al., 2023). The application of ^{1}H-^{15}N-HSQC-TOCSY to the discovery of polyketide macrolactams by the Oh group provides strong support for the power of this method as the novel macrolactams contain but one nitrogen each.

3. Nitrogen mass spectrometry

3.1. Nitrogen mass spectrometry background

As discussed above, nitrogen has two stable isotopes, nitrogen-14 and nitrogen-15 (^{15}N), with 99.635% and 0.365% natural abundance, respectively (Wieser and Brand, 2017). Due to the low natural abundance of ^{15}N, precursors enriched in ^{15}N have been used in biosynthetic characterization to study the metabolic pathways of living organisms for a century (Rinkel and Dickschat, 2015). The most common application of ^{15}N is in metabolic labeling experiments, in which the organism is grown in a medium containing ^{15}N-labeled compounds, such as ammonium or nitrate. These labeled compounds are then incorporated into the organism's biomass and metabolic intermediates, and the distribution of ^{15}N can be used to trace the metabolic pathways of the organism. Originally, isotope ratio mass spectrometry (IRMS) and degradation prior to mass spectrometric analysis were used to assess distribution of incorporated nitrogen-15 in metabolic pathways (Kahn et al., 2002). As mass spectrometers technology developed with increased sensitivity, techniques like ESI-MS began to be utilized for detecting isotopic ratios patterns between ^{14}N and ^{15}N to detect ^{15}N enrichment in metabolic labeling (Kahn et al., 2002; Wieser and Brand, 2017). The advantage of utilizing mass spectrometry (MS) combined with stable isotopes for biosynthetic characterization is the higher sensitivity of the MS instrumentation (Chokkathukalam et al., 2014).

3.2. Nitrogen-15 MS for biosynthetic characterization and discovery

Feeding specific ^{15}N-enriched precursors has been used in conjunction with mass spectrometry for natural product biosynthetic characterization (Feng et al., 2009; Rinkel and Dickschat, 2015). By feeding these specific stable isotope precursors enriched with ^{15}N into a natural product and then analyzing the resulting isotopomers and isotopic ratios with mass spectrometry, it is possible to determine the biosynthetic pathway of the natural product (Figure 2). Enrichment with ^{15}N typically involves the incorporation of a precursor labeled with the stable isotope. In mass spectrometry, the incorporation of a ^{15}N-enriched precursor into a molecule can be detected through the observation of isotopic peaks in the mass spectrum. When a molecule enriched with ^{15}N isotopes is ionized in the mass spectrometer, it produces a series of isotopic peaks with increased m/z values compared to the peaks of the unlabeled molecule. The number of ^{15}N atoms in the molecule determines the spacing between the isotopic peaks. For example, if a molecule with three nitrogen atoms incorporates ^{15}N into all three positions, the isotopic peaks will show an increase of three mass units higher than the corresponding peaks of the unlabeled molecule. The increased spacing between the isotopic peaks provides evidence that the molecule has incorporated ^{15}N.

Additionally, the relative abundance of the isotopic peaks can provide information about the extent of incorporation of the ^{15}N-labeled precursor. The higher the relative abundance of the isotopic peaks, the greater the extent of incorporation of the ^{15}N-labeled precursor into the molecule.

For example, the biosynthesis of aspirochlorine (**6**) was solved by feeding the stable isotope enriched $^{13}C_2$-^{15}N-Gly to the producing *Aspergillus oryzae* strain and demonstrating via liquid chromatography-mass spectrometry that only the carbon-13 was incorporated into aspirocholine. This result helped demonstrate that phenylalanine was being transformed into a glycine-like moiety and that glycine was only utilized during N-methylation (Chankhamjon et al., 2014). The Charusanti group recently established the biosynthesis of the antibiotic pyracrimycin A (**7**) in a *Streptomyces* strain utilizing the isotopic ratios in MS analysis after feeding with ^{15}N-proline and ^{15}N-$^{13}C_3$-serine, together and individually (Nielsen et al., 2022). ^{15}N-enriched precursors were utilized to demonstrate that αNH_2 nitrogen atom of glutamic acid was involved in forming the nitrogen-nitrogen bond into the rare C-nucleoside antibiotic pyrazomycin (**8**) and point to a new nitrogen-nitrogen bond forming enzyme PyrN (Zhao et al., 2020). More recently, detailed bioinformatic analysis in tandem with feeding synthesized ^{15}N-labeled Piz to the **4** producing *Streptomyces incarnatus* NRRL8089 strain followed by high resolution mass spectrometry isotopic ratio analysis demonstrated that free piperazic acid residues are most commonly incorporated into growing non-ribosomal peptide chains (Wei et al., 2022).

Another strategy that has been recently developed is utilizing ^{15}N-labeled stable isotope precursors in integrated genomic and mass spectrometry metabolomic approaches (Chokkathukalam et al., 2014). This integration of ^{15}N with genomic and metabolomic approaches has allowed the discovery of novel compounds and importantly, the linking of natural product structures with their producing biosynthetic gene clusters (Figure 2). When coupled with metabolomic data analysis methods such as multivariate statistical analyses or molecular networking, strains or extracts with potentially novel components can be prioritized for investigation (Hou et al., 2012; Covington et al., 2017). This type of approach has seen the discovery of molecules such as tambromycin (**9**) (Goering et al., 2016) and columbamides (Kleigrewe et al., 2015) and often linked them to their gene cluster using ^{15}N-labeled precursors and MS analysis. The structure of **9** was discovered using the metabologenomics approach whereby statistical analysis of the data from simultaneous bioinformatic analysis of 172 draft genomes and MS analysis of extracts from the corresponding bacteria in four media led to an *m/z* value for an unknown molecule that correlated with several bacteria carrying the same gene cluster. Scale-up allowed isolation and structure elucidation of the novel cytotoxic non-ribosomal peptide, tambromycin (**9**). Stable isotope feeding of $^{15}N_1$-Lysine (as compared to unlabeled media) was followed by MS isotopic analysis to link tambromycin with its' gene cluster. Next, the Gerwick Lab discovered both columbamides and cryptomaldamide (**10**) integrating genomic and MS analysis. The columbamides, a mild cannabinomimetic, were also discovered by matching molecular networks of MS data from cyanobacterial extracts with putative gene clusters obtained from their draft genomes (Kleigrewe et al., 2015). In the case of **10**, they used MALDI-MS after ^{15}N-Nitrate feeding and noticed a 5 dalton shift in the *m/z* value of interest after 4 days of growth. In both cases, they used MS to guide isolation and 1D and 2D NMR to solve the final structures (Kinnel et al., 2017). Building from these ideas, the Orjala lab utilized shifts in MS isotopic ratio after comparing with data from unlabeled media extracts with 99% ^{15}N-nitrate labeled media extracts to match the *m/z* value with isotopic shifts indicative of ^{15}N incorporation with predicted nitrogen rich gene clusters from sequenced cyanobacteria. Through this approach, they isolated four peptides, two known and two unknown. They named the unknown peptides anabaenopeptin UIC827 (**11**) and nostopyrrolidonamide after solving their structures with NMR and MS/MS data (May et al., 2020). Finally, the Medema and Linington labs have recently developed IsoAnalyst which can analyze MS data of extracts arising from isotope labeling, including ^{15}N-labeled precursors, and connect them with their predicted biosynthetic gene clusters. The developers used IsoAnalyst to match multiple gene clusters with their chemical phenotype and discovered lobosamide D (**12**) after structure elucidation with 1D and 2D NMR (McCaughey et al., 2022). In conclusion, using ^{15}N-labeled stable isotope precursors in integrated genomic and MS metabolomic approaches has proven to be a successful strategy for discovering novel compounds and linking natural product structures with their producing biosynthetic gene clusters.

4. Discussion

Due to their utility, both ^{15}N-NMR and MS have been incorporated into various methodologies and strategies to solve natural product structures, to uncover novel natural product structures, to reveal the biogenesis of the natural products, and to link biosynthetic gene clusters to specific natural products. Indeed, nitrogen-15 NMR is a premier tool due to nitrogen's presence in many of the most structurally interesting and bioactive natural products. Nitrogen-15 NMR experiments are inconsistently used for structure elucidation purposes, perhaps because of the historical challenges and the low natural abundance. However, experiments by Gary Martin of Merck (amongst others) demonstrate that inversely detected nitrogen-15 2D data can be collected at natural abundance for even around 1 mg of pure sample (Martin and Hadden, 2000). ^{15}N NMR as a discovery tool has produced structurally interesting and bioactive products from its first use by Gross et al. (2007), to the discovery of the incarnatapeptins (Morgan et al., 2020), to the most recent use by Oh et al. combining genomics and spectroscopic tools (Shin et al., 2023). The application of the ^{15}N-HSQC-TOCSY experiments for targeted and efficient discovery approaches for both polyketide-nonribosomal peptide hybrids and macrolactams demonstrates that these approaches are worth considering for a wide range of nitrogen-containing natural products. Moreover, the structural revision of salinilactam during the discovery process by Oh et al., demonstrates that these 2D nitrogen-15 NMR experiments are a critical tool for structure elucidation of natural products. NMR instrumentation now routinely come equipped with the ability to detect nitrogen-15. With these modern enhancements, obtaining 15N NMR 2D experiments during dataset collection for all small molecule natural products should be habitual. Furthermore, if

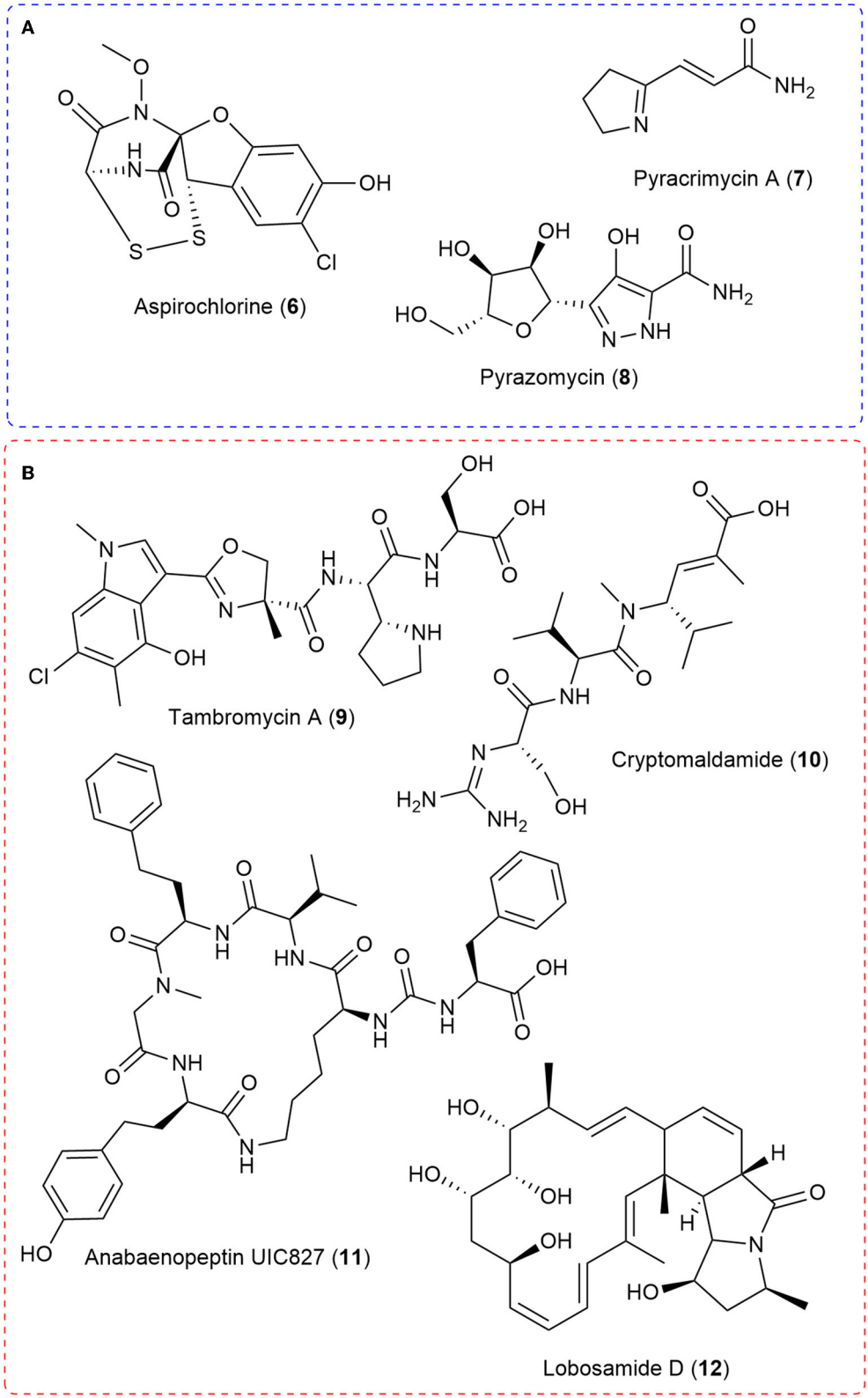

FIGURE 2
(A) Select natural products examples where stable isotope feeding of ^{15}N-labeled precursors allowed the use of MS isotopic ratios to characterize all or key components of the biosynthetic pathway. **(B)** A selection of natural products discovered through integrated genomics and MS metabolomic strategies in which ^{15}N played a crucial role.

novel structures report nitrogen, journals and editors could require 2D nitrogen-15 NMR experiments alongside the proton and carbon spectra whenever not prohibited by older equipment.

Stable isotope ^{15}N labeling combined with MS is a powerful tool for biosynthetic characterization and integrated MS-metabolomic and genomic approaches. These strategies have been useful in uncovering new chemistry with a multitude of MS instrumentation. Perhaps more importantly, ^{15}N MS is an invaluable tool in biosynthetic characterization, from how molecules like aspirocholorine are made to how the intriguing non-ribosomal piperazic acid residue is incorporated in the building of natural products. Tools such as IsoAnalyst will surely become indispensable for linking genotype to phenotype. However, there are still some significant limitations when using mass spectrometry as a discovery tool, such as varying tendencies of molecules to ionize, media interference in crude samples (Watrous et al., 2012), unpredictable fragmentation patterns of some natural product classes (Liu et al., 2009; Novák et al., 2015; Townsend et al., 2018), and the need to use NMR in order to determine the final structure usually. At the same time, NMR usually suffers from sensitivity limitations. Therefore, just as MS and NMR data are utilized together to solve natural product structure *de novo*, so could the discovery process be amplified utilizing approaches that integrate the ability of ^{15}N NMR to detect precise chemical environments with the sensitivity of MS data and the clarity of isotopic ratio shifts. As stable isotopes are increasingly included for structure elucidation, discovery, and gene cluster linking, the community could consider other tools to exploit the presence of precisely included ^{15}N and ^{13}C isotopes, such as increased usage of 2D ^{15}N NMR experiments and analysis of carbon-nitrogen NMR splitting patterns.

Author contributions

The author confirms being the sole contributor of this work and has approved it for publication.

Conflict of interest

The author declares that the research was conducted in the absence of any commercial or financial relationships that could be construed as a potential conflict of interest.

Publisher's note

References

Bax, A. (1989). Two-dimensional NMR and protein structure. *Annu. Rev. Biochem.* 58, 223–256. doi: 10.1146/annurev.bi.58.070189.001255

Bishara, A., Rudi, A., Aknin, M., Neumann, D., Ben-Califa, N., and Kashman, Y. (2008). Taumycins A and B, two bioactive lipodepsipeptides from the Madagascar sponge *Fascaplysinopsis* sp. *Org. Lett.* 10, 4307–4309. doi: 10.1021/ol801750y

Breton, R. C., and Reynolds, W. F. (2013). Using NMR to identify and characterize natural products. *Nat. Prod. Rep.* 30, 501. doi: 10.1039/c2np20104f

Chankhamjon, P., Boettger-Schmidt, D., Scherlach, K., Urbansky, B., Lackner, G., Kalb, D., et al. (2014). Biosynthesis of the halogenated mycotoxin aspirochlorine in koji mold involves a cryptic amino acid conversion. *Angewandte Chemie Int. Ed.* 53, 13409–13413. doi: 10.1002/anie.201407624

Chokkathukalam, A., Kim, D.-H., Barrett, M. P., Breitling, R., and Creek, D. J. (2014). Stable isotope-labeling studies in metabolomics: new insights into structure and dynamics of metabolic networks. *Bioanalysis* 6, 511–524. doi: 10.4155/bio.13.348

Covington, B. C., McLean, J. A., and Bachmann, B. O. (2017). Comparative mass spectrometry-based metabolomics strategies for the investigation of microbial secondary metabolites. *Nat. Prod. Rep.* 34, 6–24. doi: 10.1039/C6NP00048G

Deev, S. L., Paramonov, A. S., Shestakova, T. S., Khalymbadzha, I. A., Chupakhin, O. N., Subbotina, J. O., et al. (2017). ^{15} N-labelling and structure determination of adamantylated azolo-azines in solution. *Beilstein J. Org. Chem.* 13, 2535–2548. doi: 10.3762/bjoc.13.250

Feng, X., Ratnayake, A. S., Charan, R. D., Janso, J. E., Bernan, V. S., Schlingmann, G., et al. (2009). Probing natural product biosynthetic pathways using Fourier transform ion cyclotron resonance mass spectrometry. *Bioorganic Med. Chem.* 17, 2154–2161. doi: 10.1016/j.bmc.2008.10.073

Freeman, R. (1997). *Spin Choreography: Basic Steps in High Resolution NMR*. Oxford, Sausalito, CA: Spektrum; University Science Books.

Goering, A. W., McClure, R. A., Doroghazi, J. R., Albright, J. C., Haverland, N. A., Zhang, Y., et al. (2016). Metabologenomics: correlation of microbial gene clusters with metabolites drives discovery of a nonribosomal peptide with an unusual amino acid monomer. *ACS Cent. Sci.* 2, 99–108. doi: 10.1021/acscentsci.5b00331

Gross, H., Stockwell, V. O., Henkels, M. D., Nowak-Thompson, B., Loper, J. E., and Gerwick, W. H. (2007). The genomisotopic approach: a systematic method to isolate products of orphan biosynthetic gene clusters. *Chem. Biol.* 14, 53–63. doi: 10.1016/j.chembiol.2006.11.007

Harris, R. K., Becker, E. D., Cabral De Menezes, S. M., Goodfellow, R., and Granger, P. (2002). NMR nomenclature: Nuclear spin properties and conventions for chemical shifts (IUPAC recommendations 2001). *Concepts Magnetic Resonance* 14, 326–346. doi: 10.1002/cmr.10035

Hou, Y., Braun, D. R., Michel, C. R., Klassen, J. L., Adnani, N., Wyche, T. P., et al. (2012). Microbial strain prioritization using metabolomics tools for the discovery of natural products. *Anal. Chem.* 84, 4277–4283. doi: 10.1021/ac202623g

Imada, K., Sakai, E., Kato, H., Kawabata, T., Yoshinaga, S., Nehira, T., et al. (2013). Reticulatins A and B and hyrtioreticulin F from the marine sponge Hyrtios reticulatus. *Tetrahedron* 69, 7051–7055. doi: 10.1016/j.tet.2013.06.043

Kahn, M. L., Parra-Colmenares, A., Ford, C. L., Kaser, F., McCaskill, D., and Ketchum, R. E. (2002). A mass spectrometry method for measuring 15N incorporation into pheophytin. *Anal. Biochem.* 307, 219–225. doi: 10.1016/S0003-2697(02)00046-5

Kinnel, R. B., Esquenazi, E., Leao, T., Moss, N., Mevers, E., Pereira, A. R., et al. (2017). A Maldiisotopic approach to discover natural products: cryptomaldamide, a hybrid tripeptide from the marine cyanobacterium moorea producens. *J. Nat. Prod.* 80, 1514–1521. doi: 10.1021/acs.jnatprod.7b00019

Kleigrewe, K., Almaliti, J., Tian, I. Y., Kinnel, R. B., Korobeynikov, A., Monroe, E. A., et al. (2015). Combining mass spectrometric metabolic profiling with genomic analysis: a powerful approach for discovering natural products from cyanobacteria. *J. Nat. Prod.* 78, 1671–1682. doi: 10.1021/acs.jnatprod.5b00301

Liu, W.-T., Ng, J., Meluzzi, D., Bandeira, N., Gutierrez, M., Simmons, T. L., et al. (2009). Interpretation of tandem mass spectra obtained from cyclic nonribosomal peptides. *Anal. Chem.* 81, 4200–4209. doi: 10.1021/ac900114t

Marek, R., and Lycka, A. (2002). 15N NMR spectroscopy in structural analysis. *COC* 6, 35–66. doi: 10.2174/1385272023374643

Martin, G. E. (2011). "Chapter 5 - using 1,1- and 1,n-ADEQUATE 2D NMR data in structure elucidation protocols," in *Annual Reports on NMR Spectroscopy*, editor G. A. Webb (Academic Press), 215–291.

Martin, G. E., and Hadden, C. E. (2000). Long-range ^{1} H– ^{15} N heteronuclear shift correlation at natural abundance. *J. Nat. Prod.* 63, 543–585. doi: 10.1021/np9903191

Martin, G. E., Solntseva, M., and Williams, A. J. (2007). "Applications of 15N NMR spectroscopy in alkaloid chemistry," in *Modern Alkaloids*, eds. E. Fattorusso and O. Taglialatela-Scafati (Weinheim: John Wiley & Sons. Ltd.), 409–471.

Martin, G. E., and Williams, A. J. (2010). "Utilizing long-range 1 H−15 N 2-D NMR spectroscopy for chemical structure elucidation and confirmation," in *eMagRes*, eds. R. K. Harris and R. L. (Wasylishen: American Cancer Society).

Martin, G. E., and Williams, A. J. (2015). "Applications of 1H−15N long-range heteronuclear shift correlation and 15N NMR in alkaloid chemistry," in *Annual Reports on NMR Spectroscopy* (Elsevier), 1–76.

May, D. S., Crnkovic, C. M., Krunic, A., Wilson, T. A., Fuchs, J. R., and Orjala, J. E. (2020). 15N stable isotope labeling and comparative metabolomics facilitates genome mining in cultured cyanobacteria. *ACS Chem. Biol.* 15, 758–765. doi: 10.1021/acschembio.9b00993

McCaughey, C. S., van Santen, J. A., van der Hooft, J. J. J., Medema, M. H., and Linington, R. G. (2022). An isotopic labeling approach linking natural products with biosynthetic gene clusters. *Nat. Chem. Biol.* 18, 295–304. doi: 10.1038/s41589-021-00949-6

Medina, R. A., Goeger, D. E., Hills, P., Mooberry, S. L., Huang, N., Romero, L. I., et al. (2008). Coibamide A, a potent antiproliferative cyclic depsipeptide from the panamanian marine cyanobacterium *Leptolyngbya* sp. *J. Am. Chem. Soc.* 130, 6324–6325. doi: 10.1021/ja801383f

Morgan, K. D. (2021). *Chemical and Genetic Investigations of Marine and Terrestrial Bacteria Towards Bioactive Natural Product Discovery*. doi: 10.14288/1.0397473

Morgan, K. D., Williams, D. E., Patrick, B. O., Remigy, M., Banuelos, C. A., Sadar, M. D., et al. (2020). Incarnatapeptins A and B, nonribosomal peptides discovered using genome mining and 1H/15N HSQC-TOCSY. *Org. Lett.* 22, 4053–4057. doi: 10.1021/acs.orglett.0c00818

Morgan, K. D., Williams, D. E., Ryan, K. S., and Andersen, R. J. (2022a). Corrigendum to "dentigerumycin F and G: dynamic structures retrieved through a genome-mining/nitrogen NMR methodology" [Tetrahedron Lett. 94C (2022) 153688]. *Tetrahedron Lett.* 105, 154030. doi: 10.1016/j.tetlet.2022.154030

Morgan, K. D., Williams, D. E., Ryan, K. S., and Andersen, R. J. (2022b). Dentigerumycin F and G: dynamic structures retrieved through a genome-mining/nitrogen-NMR methodology. *Tetrahedron Lett.* 94, 153688. doi: 10.1016/j.tetlet.2022.153688

Morris, G. A., and Freeman, R. (1979). Enhancement of nuclear magnetic resonance signals by polarization transfer. *J. Am. Chem. Soc.* 101, 760–762. doi: 10.1021/ja00497a058

Mulder, F. A. A., and Filatov, M. (2010). NMR chemical shift data and ab initio shielding calculations: emerging tools for protein structure determination. *Chem. Soc. Rev.* 39, 578–590. doi: 10.1039/B811366C

Nielsen, J. B., Gren, T., Mohite, O. S., Jørgensen, T. S., Klitgaard, A. K., Mourched, A.-S., et al. (2022). Identification of the biosynthetic gene cluster for pyracrimycin A, an antibiotic produced by *Streptomyces* sp. *ACS Chem. Biol.* 17, 2411–2417. doi: 10.1021/acschembio.2c00480

Novák, J., Lemr, K., Schug, K. A., and Havlíček, V. (2015). CycloBranch: *de novo* sequencing of nonribosomal peptides from accurate product ion mass spectra. *J. Am. Soc. Mass Spectrom.* 26, 1780–1786. doi: 10.1007/s13361-015-1211-1

Ohki, S., and Kainosho, M. (2008). Stable isotope labeling methods for protein NMR spectroscopy. *Progress Nuclear Magnetic Resonance Spectrosc.* 53, 208–226. doi: 10.1016/j.pnmrs.2008.01.003

Parella, T., and Sánchez-Ferrando, F. (2004). Improved multiplicity-edited ADEQUATE experiments. *J. Magnetic Resonance* 166, 123–128. doi: 10.1016/j.jmr.2003.10.010

Rinkel, J., and Dickschat, J. S. (2015). Recent highlights in biosynthesis research using stable isotopes. *Beilstein J. Org. Chem.* 11, 2493–2508. doi: 10.3762/bjoc.11.271

Shin, Y.-H., Im, J. H., Kang, I., Kim, E., Jang, S. C., Cho, E., et al. (2023). Genomic and spectroscopic signature-based discovery of natural macrolactams. *J. Am. Chem. Soc.* 145, 1886–1896. doi: 10.1021/jacs.2c11527

Townsend, C., Furukawa, A., Schwochert, J., Pye, C. R., Edmondson, Q., and Lokey, R. S. (2018). CycLS: accurate, whole-library sequencing of cyclic peptides using tandem mass spectrometry. *Bioorganic Medicinal Chem.* 26, 1232–1238. doi: 10.1016/j.bmc.2018.01.027

Watrous, J., Roach, P., Alexandrov, T., Heath, B. S., Yang, J. Y., Kersten, R. D., et al. (2012). Mass spectral molecular networking of living microbial colonies. *Proc. Natl. Acad. Sci.* 109, E1743–E1752. doi: 10.1073/pnas.1203689109

Wei, Z.-W., Niikura, H., Morgan, K. D., Vacariu, C. M., Andersen, R. J., and Ryan, K. S. (2022). Free piperazic acid as a precursor to nonribosomal peptides. *J. Am. Chem. Soc.* 144, 13556–13564. doi: 10.1021/jacs.2c03660

Wieser, M. E., and Brand, W. A. (2017). "Isotope ratio studies using mass spectrometry," in *Encyclopedia of Spectroscopy and Spectrometry*, eds. J. C. Lindon, G. E. Tranter, and D. W. Koppenaal (Oxford: Elsevier), 488–500.

Williams, David. E., Dalisay, D. S., Patrick, B. O., Matainaho, T., Andrusiak, K., Deshpande, R., et al. (2011). Padanamides A and B, Highly Modified Linear Tetrapeptides Produced in Culture by a Streptomyces sp. Isolated from a Marine Sediment. *Org. Lett.* 13, 3936–3939. doi: 10.1021/ol2014494

Williamson, R. T., Buevich, A. V., Martin, G. E., and Parella, T. (2014). LR-HSQMBC: a sensitive NMR technique to probe very long-range heteronuclear coupling pathways. *J. Org. Chem.* 79, 3887–3894. doi: 10.1021/jo500333u

Williamson, R. T., Márquez, B. L., and Gerwick, W. H. (1999). Use of 1H-15N PEP-HSQC-TOCSY at natural abundance to facilitate the structure elucidation of naturally occurring peptides. *Tetrahedron* 55, 2881–2888. doi: 10.1016/S0040-4020(99)00081-2

Wishart, D. S., Bigam, C. G., Yao, J., Abildgaard, F., Dyson, H. J., Oldfield, E., et al. (1995). 1H, 13C and 15N chemical shift referencing in biomolecular NMR. *J. Biomol. NMR* 6, 135–140. doi: 10.1007/BF00211777

Witanowski, M., and Webb, G. A. (1972). "Nitrogen NMR spectroscopy," in *Annual Reports on NMR Spectroscopy*, ed. E. F. Mooney (Elsevier), 395–464.

Wu, Q., Bell, B. A., Yan, J.-X., Chevrette, M. G., Brittin, N. J., Zhu, Y., et al. (2022). Metabolomics and genomics enable the discovery of a new class of nonribosomal peptidic metallophores from a marine micromonospora. *J. Am. Chem. Soc.* 145, 58–69. doi: 10.1021/jacs.2c06410

Wyche, T. P., Piotrowski, J. S., Hou, Y., Braun, D., Deshpande, R., McIlwain, S., et al. (2014). Forazoline A, a novel marine-derived polyketide with antifungal *in vivo* efficacy. *Angew. Chem. Int. Ed. Engl.* 53, 11583–11586. doi: 10.1002/anie.201405990

Zhao, G., Yao, S., Rothchild, K. W., Liu, T., Liu, Y., Lian, J., et al. (2020). The biosynthetic gene cluster of pyrazomycin—A C-nucleoside antibiotic with a rare pyrazole moiety. *ChemBioChem* 21, 644–649. doi: 10.1002/cbic.201900449

Frontiers in Microbiology

Explores the habitable world and the potential of microbial life

The largest and most cited microbiology journal which advances our understanding of the role microbes play in addressing global challenges such as healthcare, food security, and climate change.

Discover the latest Research Topics

See more →

Frontiers

Avenue du Tribunal-Fédéral 34
1005 Lausanne, Switzerland
frontiersin.org

Contact us

+41 (0)21 510 17 00
frontiersin.org/about/contact